Government of Western Australia

Department of
Mines and Petroleum

REPORT
158

DEPOSIT-SCALE TARGETING FOR GOLD IN THE YILGARN CRATON: PART 3 OF THE YILGARN GOLD EXPLORATION TARGETING ATLAS

by WK Witt

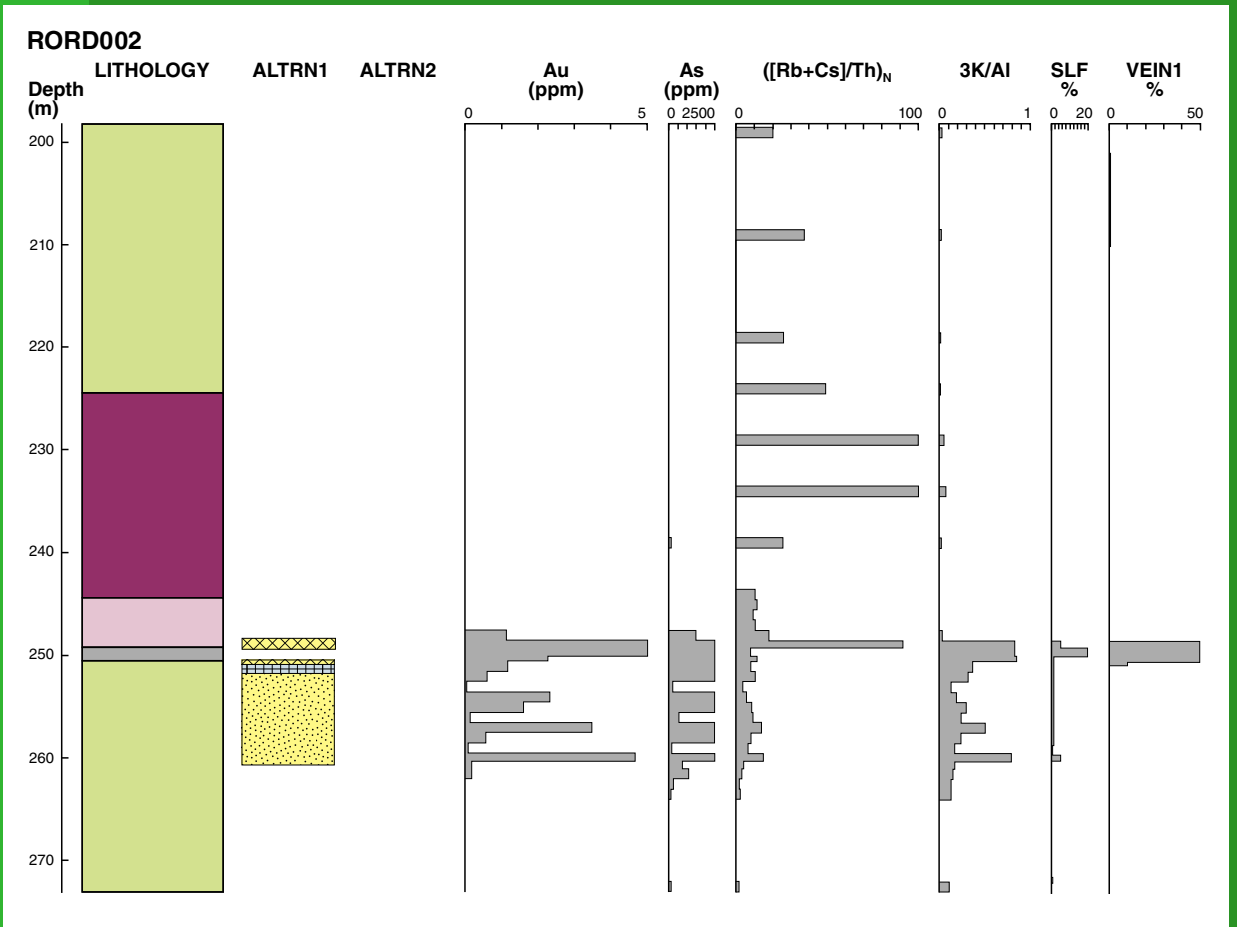

Geological Survey of Western Australia

DEPOSIT-SCALE TARGETING FOR GOLD IN THE YILGARN CRATON: PART 3 OF THE YILGARN GOLD EXPLORATION TARGETING ATLAS

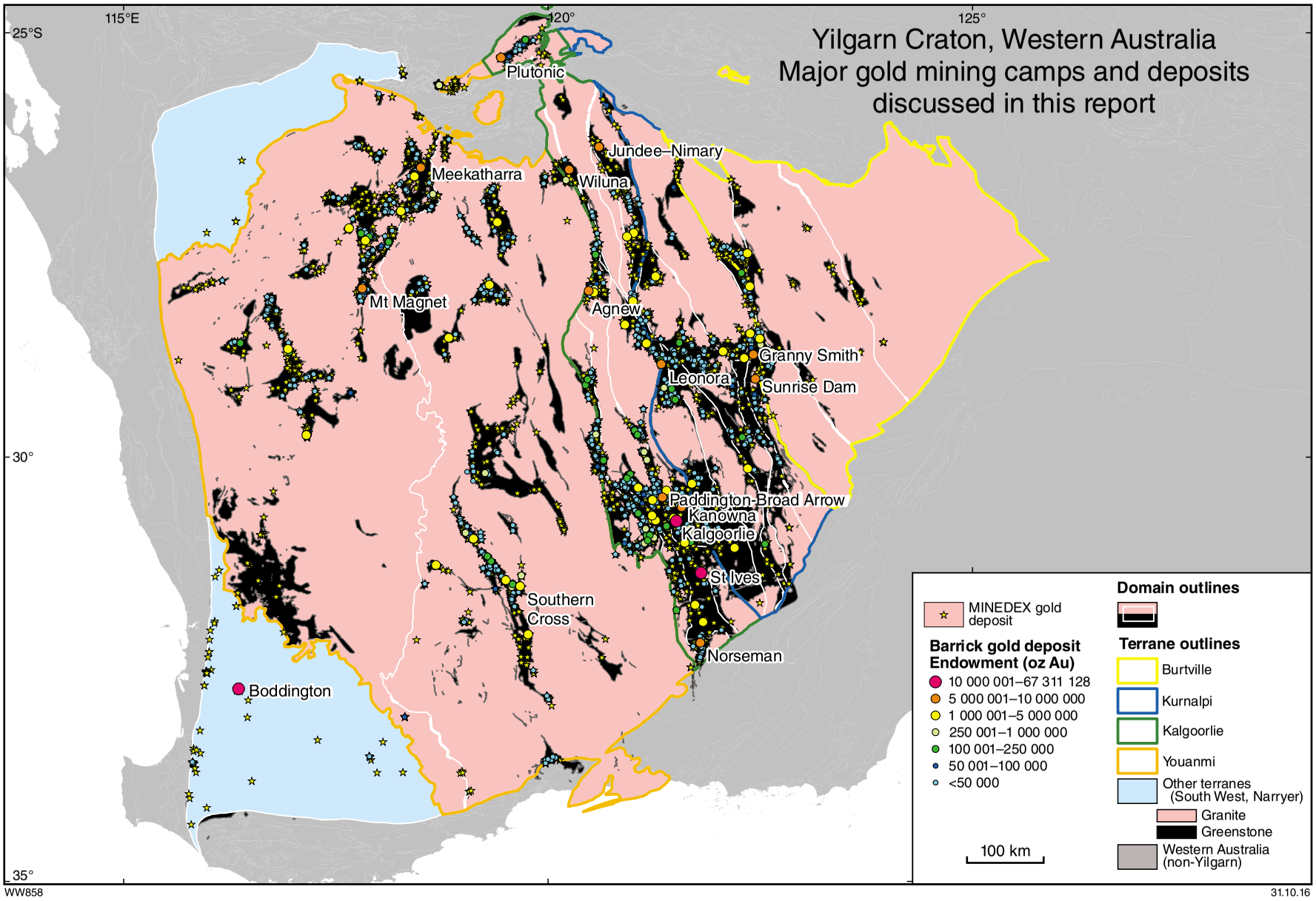
Yilgarn Craton, Western Australia
Major gold mining camps and deposits discussed in this report
115°E
120°
125°
25°S
30°
35°
Plutonic
Jundee–Nimary
Meekatharra
Wiluna
Mt Magnet
Agnew
Granny Smith
Leonora
Sunrise Dam
Paddington-Broad Arrow
Kanowna
Kalgoorlie
St Ives
Southern Cross
Norseman
Boddington
MINEDEX gold deposit
Barrick gold deposit Endowment (oz Au)
10 000 001–67 311 128
5 000 001–10 000 000
1 000 001–5 000 000
250 001–1 000 000
100 001–250 000
50 001–100 000
<50 000
Domain outlines
Terrane outlines
Burtville
Kurnalpi
Kalgoorlie
Youanmi
Other terranes (South West, Narryer)
Granite
Greenstone
Western Australia (non-Yilgarn)
100 km
WW858
31.10.16

Government of **Western Australia**
Department of **Mines and Petroleum**

REPORT 158

DEPOSIT-SCALE TARGETING FOR GOLD IN THE YILGARN CRATON: PART 3 OF THE YILGARN GOLD EXPLORATION TARGETING ATLAS

by
WK Witt[1]

1 Centre for Exploration Targeting, University of Western Australia, Nedlands WA 6009

Perth 2016

Geological Survey of Western Australia

REFERENCE
The recommended reference for this publication is:
Witt, WK 2016, Deposit-scale targeting for gold in the Yilgarn Craton: Part 3 of the Yilgarn Gold Exploration Targeting Atlas: Geological Survey of Western Australia, Report 158, 182p.

National Library of Australia Cataloguing-in-Publication entry:

Creator:	Witt, W. K., author.
Title:	Deposit-scale targeting for gold in the Yilgarn Craton: part 3 of the Yilgarn Gold Exploration Targeting Atlas / WK Witt.
ISBN:	9781741685237 (ebook)
Subjects:	Gold ores--Western Australia--Yilgarn Craton. Gold mines and mining--Western Australia--Yilgarn Craton. Geology--Western Australia--Yilgarn Craton.
Other Authors/Contributors:	Geological Survey of Western Australia, issuing body.
Dewey Decimal Classification:	553.41099416

ISSN 1834–2280

Grid references in this publication refer to the Geocentric Datum of Australia 1994 (GDA94). Locations mentioned in the text are referenced using Map Grid Australia (MGA) coordinates, Zones 49–52. All locations are quoted to at least the nearest 100 m.

Copy editor: A Forbes
Cartography: J Peng
Desktop publishing: RL Hitchings

Published 2016 by Geological Survey of Western Australia
This Report is published in digital format (PDF), as part of a digital dataset on USB, and is available online at <www.dmp.wa.gov.au/GSWApublications>.

Further details of geological publications and maps produced by the Geological Survey of Western Australia are available from:
Information Centre
Department of Mines and Petroleum
100 Plain Street | EAST PERTH | WESTERN AUSTRALIA 6004
Telephone: +61 8 9222 3459 Facsimile: +61 8 9222 3444
www.dmp.wa.gov.au/GSWApublications

Cover image: Comparison of downhole geology and geochemistry, RORD002, Red October gold mine, illustrating the broad dispersion of elevated rare alkali index $([Rb+Cs/Th])_N$ beyond the gold lode at 250–260 m depth. This dispersion is much greater than that shown by the conventional indicator of alteration based on potassic micas (3K/Al) and pathfinder element arsenic.

Frontispiece: Map of Yilgarn Craton showing major tectonic divisions, and gold camps and deposits discussed in this report.

Contents

Figures

Tables

Deposit-scale targeting for gold in the Yilgarn Craton: Part 3 of the Yilgarn Gold Exploration Targeting Atlas

by

WK Witt[1]

Abstract

Part 3 of the Yilgarn Gold Exploration Targeting Atlas presents 12 targeting criteria for deposit- or mine-scale exploration for gold lodes that are based on empirical, qualitative observations or reports from lode gold deposits in the Yilgarn Craton. These can be subdivided into structural criteria, which are largely predictive in nature, and geochemical and mineralogical criteria, which are used to directly detect evidence for the presence of ore shoots. Structural targeting includes well-established criteria such as fault intersections, fault intersections with specific lithological units, and fault bends and jogs. All three of these settings potentially provide anomalies in structurally induced permeability resulting from tensile failure of rock units and consequent focusing of ore fluid flux. Examples of deposits where hydraulic seals and constriction zones (bottlenecks) may have contributed to localization of ore shoots are also presented. As crustal level deepens and metamorphic grade increases, folds and boudins become increasingly important structural controls on the location and orientation of ore shoots. Common elements in all of these structural targeting criteria are rock rheology and steep rheological gradients. Previous studies of geochemical dispersion of gold and pathfinder elements around gold lodes indicate that their extent orthogonal to gold lodes is very limited. Similarly limited dispersion has been demonstrated where alteration indices and stable isotopes have been studied. However, application of these geochemical parameters to detect conduits between ore shoots holds some promise. The relatively recently developed rare alkali index is the most useful of these parameters as it remains anomalous for up to tens of metres beyond the visible alteration halo around gold lodes in many of the deposits where it has been applied, including Red October (a new study completed for this Atlas). Another recent technological development with potential application to deposit- and mine-scale exploration is the automated spectral identification of hydrothermal minerals associated with gold mineralization. Spectra generated in the VNIR–SWIR range have been used to develop vectors to gold ore at the Golden Mile and Kanowna. The very recent introduction of a thermal infrared (TIR) spectrometer to the automated HyLogger instrument allows identification of anhydrous minerals such as feldspars and pyroxenes, which has application in higher-temperature gold deposits such as those in the Southern Cross district. Application of combined VNIR–SWIR and TIR spectral data to six diamond cores from gold deposits at Southern Cross has allowed distinction of the main lithological groups in the greenstone sequence and identified vectors to gold lodes, including changes in mineral abundance, the composition of plagioclase, and the presence of K-feldspar, none of which are easily identified by conventional logging of the core.

KEYWORDS: economic analysis, exploration, geochemical interpretation, gold, spectral analysis, structural geology

1 Centre for Exploration Targeting, University of Western Australia, Nedlands WA 6009

Introduction

The concept of a Yilgarn Exploration Targeting Atlas (YETA) Project for gold was conceived in 2009. At that time, a wealth of pre-competitive geological, geochemical, and geophysical data had become available to explorers through government agencies, especially the Geological Survey of Western Australia (GSWA), Geoscience Australia, and the Commonwealth Scientific and Industrial Research Organisation (CSIRO). A major research effort (known as the Predictive Mineral Discovery Cooperative Research Centre, or pmd*CRC) on the geology and mineralization of the Yilgarn Craton, co-funded by government and industry, had also been recently completed. This was also a time when several new exploration targeting strategies were proposed, adding to those already established through scientific publications or time-honoured practical application. With some exceptions, the proposed exploration targeting criteria were based on work carried out at a particular gold deposit, camp, or district and purported to have possible applications in regions beyond the specific study area. Moreover, in most cases the suggested exploration criteria were only briefly proposed towards the end of a publication, as an outcome of a larger body of work.

The initial concept for the Atlas was to gather the various exploration targeting criteria and techniques into one volume and to make them the main subject of the publication rather than an afterthought. Assessment of the targeting criteria would be restricted to depths below the base of weathering because of the common conception that the Yilgarn Craton is a mature exploration province and that significant new discoveries would almost invariably be made below the relatively thin near-surface intervals of transported cover and weathered basement. Studies by CSIRO during the 1980s and 1990s, summarized by Anand and Butt (2010), had already clearly laid out recommended exploration strategies for gold and other commodities in the regolith layer, but there was no comparable publication dealing with exploration in basement rocks below the regolith layer.

During the course of the YETA Project, Guj et al. (2011) published results of application of Zipf's Law to the exploration maturity of the Yilgarn Craton. Guj et al. (2011) used the Barrick Gold Corporation gold deposit database in their analysis and this same database has been used in most of the regional- and district-scale analyses presented in Parts 1 and 2 of the YETA Atlas (Witt et al., 2013, 2015a). Guj et al. (2011) found that (in 2008) only 75% of the endowment of the Yilgarn Craton had been discovered. Based on a total Yilgarn Craton gold endowment of 324 375 897 oz (Barrick gold deposit database), the remaining undiscovered gold in the Yilgarn Craton is 108 125 299 oz. This undiscovered gold was predicted by Guj et al. (2011) to include two world-class deposits containing more gold than St Ives (13 Moz Au) but less than that at Boddington (38.6 Moz Au). Guj et al. (2011) showed that near mine-site exploration led to increases of resources of more than 10 Moz Au at five mining operations (Golden Mile, Boddington, St Ives, Leonora, Plutonic), and increases of 5–10 Moz Au at a further 13 operations (e.g. Kanowna Belle, Granny Smith, Agnew, Jundee–Nimary, Marvel Loch, Mount Magnet). These increases highlight the importance of targeting criteria at deposit scale, as addressed in Part 3 of the Atlas, for the discovery of new deposits and new ore shoots.

The substantial remaining gold endowment for the Yilgarn Craton calculated by Guj et al. (2011), and the common consensus (e.g. Griffin, 2007) that remaining major discoveries will be found below transported cover or below the base of weathered bedrock ('blind' deposits), mean that 'conceptual' exploration for gold (prediction rather than direct detection; Hronsky and Groves, 2008; McCuaig et al., 2010) will become increasingly important in the twenty-first century. It is therefore timely for publication of a volume that describes and assesses the effectiveness of a wide range of targeting criteria for gold in the Yilgarn Craton. This is the aim of the YETA Project.

From the outset, it was determined that the YETA Project would assess the effectiveness of targeting criteria based on undivided gold deposits, that is, regardless of deposit models. This means that VMS-hosted gold deposits, such as those at Golden Grove and Jaguar, have been grouped with deposits such as Mount Charlotte, which is widely regarded as belonging to the orogenic class of gold deposits. This approach also groups gold deposits formed at different times and under different geological circumstances (e.g. Czarnota et al., 2010). The decision to assess all gold deposits as one group rather than subdivide them based on genetic models reflects the ephemeral and controversial classification of many gold deposits in the Yilgarn Craton. Furthermore, recent years have seen a realisation that gold deposits belonging to several genetic models (e.g. orogenic, intrusion-related, Carlin-type) display common controls, particularly at global to regional scales (Hronsky et al., 2012; Witt et al., 2012). At deposit scale, however, controls on deposits of contrasting genetic classification are likely to differ. These differences are addressed in Part 3 of the Atlas by focusing on deposits widely regarded as orogenic. However, these deposits include examples of proximal intrusion-related and distal source-related subgroups of the orogenic class proposed by Witt et al. (2015b).

Terminology for subdivisions of the Yilgarn Craton

There have been several recent attempts to subdivide the Yilgarn Craton into component terranes and domains; the most commonly cited is that of Cassidy et al. (2006). These are the subdivisions used in the regional-scale spatial analyses of Yilgarn terranes and domains (Part 1 of the Atlas). They are also used for descriptive purposes in Part 3 of the Atlas.

Structure of the Atlas

The Atlas comprises three parts reflecting the scale of exploration (Hronsky and Groves, 2008). The regional-scale targeting section (Part 1) examines exploration criteria at the craton to superterrane scale and addresses those criteria thought to be useful when selecting a project area, the initial stage of gold exploration. The district-scale targeting section of the Atlas (Part 2) addresses those criteria thought to be useful when selecting a prospect for more detailed exploration within a project area. Part 3 of the Atlas (this volume) addresses deposit-scale targeting criteria thought to be useful when exploring for new lodes or extensions to known high-grade lodes within a gold deposit. The three scale divisions are similar to three of the four proposed by Hronsky and Groves (2008), but their global-scale exploration, which addresses search areas larger than the Yilgarn Craton, is omitted.

The explosion of freely available pre-competitive datasets has provided an opportunity for qualitative analysis of the relationship between gold mineralization and various exploration targeting criteria in and beyond the areas where those criteria were initially proposed. In some respects, this approach is similar to that advocated by Barnett and Williams (2012), although in Part 1 of this Atlas, targeting criteria were assessed individually and a fuzzy logic approach (Knox-Robinson, 2000), rather than a neural network approach, was used to synthesize some of the results and generate gold prospectivity maps of the Yilgarn Craton and Eastern Goldfields Superterrane. In contrast with Parts 1 and 2 of this Atlas, the relationships between gold mineralization and the various targeting elements presented here were determined qualitatively because spatial data suitable for quantitative spatial analyses are sparse at deposit scale. This difference reflects both the nature (e.g. regional scale) of publicly available datasets and the change of emphasis from prediction to direct detection as exploration changes from regional scale to deposit scale (Hronsky and Groves, 2008).

Both quantitative and qualitative analyses relating gold endowment to exploration targeting criteria require an accurate database of the locations and endowments of gold deposits. For regional-scale analyses (Part 1 of this Atlas), the Yilgarn component of the Barrick gold deposit database was used. For district-scale analyses (Part 2 of this Atlas), both the Barrick database and the GSWA MINEDEX database (available from <www.dmp.wa.gov.au>) were used. The limitations of these two databases are discussed in the Introduction sections of Parts 1 and 2 of this Atlas. However, these gold deposit databases were not used for the qualitative assessment of exploration criteria described in this volume (Part 3).

Targeting Criterion 3.1: Fault intersections

Fault intersections are commonly cited controls on the location and geometry of ore shoots in Yilgarn gold deposits. In some cases, the intersection of two or more faults produces a jog or bend on one of the faults, as described in section 3.2. In other cases, no jog is described and the ore shoot is attributed to increased rock permeability and consequent high fluid pressure around fault intersections (e.g. Vearncombe, 1998; Tripp and Vearncombe, 2004). Table 3.1 summarizes the structural parameters of the examples described below).

Wiluna district

Perhaps the district most frequently cited as an example in which fault intersections control gold mineralization at deposit scale is the Yandal greenstone belt in the Wiluna district, northern Eastern Goldfields Superterrane (Vearncombe, 1998; Vearncombe and Vearncombe, 1999; Kohler et al., 2000). At Jundee–Nimary in the northern Yandal greenstone belt, gold deposits are at the intersections of faults striking 115° to 150° (the Barton trend), 000° to 020° (the Nim 3 trend), and 070° to 110° (the Hughes trend). Gold mineralization forms tabular orebodies within these structures but high-grade, rod-like ore shoots form where two or more of the faults intersect (Kohler et al., 2000). At Bronzewing in the central Yandal belt, deposits and ore shoots within them reflect the intersection of northeast and east-southeasterly striking faults with north–south regional faults (or deformation zones; Fig. 3.1). In the southern Yandal belt, high-grade ore shoots at Darlot have formed adjacent to the intersection of steep east-northeasterly striking faults with the 30° northeast-dipping Darlot thrust (Gardner et al., 2001).

Laverton district

At Mount Morgans in the Laverton district, gold is hosted by banded iron-formation on the overturned western limb of the Mount Margaret anticline (Vielreicher et al., 1994). The host iron-formation, together with quartz–feldspar porphyry intrusions and carbonated mafic and ultramafic rocks, is within a north-northwesterly striking sinistral, strike-slip shear zone. Gold mineralization shows a strong spatial relationship with intersections of this shear zone with several north-northeasterly striking sinistral shear zones, some of which are intruded by lamprophyre and quartz(–feldspar) porphyry dykes (Salier et al., 2005; Vielreicher et al., 1994). Ore shoots are colinear with intersections between the two structural elements.

Kalgoorlie – Ora Banda and Agnew districts

The Kanowna Belle deposit, Kalgoorlie – Ora Banda district, is in the east-northeasterly striking Fitzroy Fault and is hosted by the Kanowna Belle porphyry (Fig. 3.2). The bulk of the gold at Kanowna Belle formed during late northeast–southwest shortening (D_5 of Blewett et al., 2010), which produced sinistral movement on the Fitzroy Fault (Davis et al., 2010). The overall 60° south-southeasterly plunge of the Kanowna Belle orebody is coincident with the intersection of a steep north-northwesterly striking structural element with the Fitzroy Fault (Davis et al., 2010), and some of the larger individual ore shoots (e.g. Lowes) are at the intersection of the Fitzroy Fault with northwesterly striking faults in the hangingwall of the Fitzroy Fault (Fig. 3.2). As at Mount Morgans, the hangingwall faults are associated with dykes of felsic and mafic intrusive rock, which may initially mask recognition of the fault structure. Tripp (2013, and pers. comm., March 2015) pointed out that there were two periods of gold mineralization at Kanowna Belle, where early, volumetrically minor, telluride-bearing mineralization in crustiform carbonate(–quartz) veins and breccias have been overprinted by telluride-free quartz–carbonate–pyrite–sericite veinlets that account for most of the gold resource. Although controls on the early gold associated with crustiform carbonate veins and breccias are not well documented, there is general agreement about the late timing (post D_3 of Blewett et al., 2010) of the main period of gold mineralization and the role of fault intersections in forming the main gold resource.

High-grade ore shoots in granite-hosted deposits at Lawlers (Agnew district) and Lady Bountiful (Kalgoorlie – Ora Banda district) are similarly located at the intersections between differently oriented vein or fault components of the ore system (Fig. 3.3). At Lawlers, near Agnew in the Agnew district, high-grade quartz veins and breccias formed at the intersections of shear zones striking 110° and 065° to 090°, whereas at Lady Bountiful ore shoots formed at the intersection of structures striking 085° and 055° (Cassidy and Bennet, 1993; Cassidy et al., 1998). Similarly, Enterprise (1.3 Moz Au; Tripp, 1998) is at the intersection of the Gimlet South – Galactica lode at Ora Banda with the Cashmans Shear Zone (Fig. 3.4). The Gimlet South lode (>1 Moz Au production plus resources; Tripp, 1998) is hosted by a fault striking 240° (70°–80° northerly dip) that has accommodated about 70 m of dextral strike-slip displacement and 20 m of reverse movement (Witt, 1992b). Within the broad gold envelope of Gimlet South, intersections between the fault striking 240° and east–west spur veins host high-grade ore shoots characterized by high fracture density and strong hydrothermal alteration, such as the Wilsons ore shoot (Fig. 3.4; Tripp and Vearncombe, 2004; Witt, 1992b).

A very good example of a gold camp where gold is controlled by fault and fracture intersections is Woodcutters, also known as Golden Cities (1.4 Moz Au, Davis et al., 2010), which is within the granitic Scotia–Kanowna dome in the Kalgoorlie – Ora Banda district (Zhou et al., 2003; Davis et al., 2010). Four main fracture sets are evident from aeromagnetic imagery in this poorly exposed area of granite (Fig. 3.5):

- fractures parallel to the margins of the dome
- northwest-striking fractures
- northeast-striking fractures
- east-southeast-striking fractures.

Table 3.1. Selected examples of Yilgarn gold deposits where ore shoots are controlled by intersecting faults

District	*Deposit*	*Fault orientations*[(a)]	*Fault intersections*	*Ore shoot orientations*[(b)]	*References*
Wiluna	Jundee–Nimary	115-150° (55° SW)			Kohler et al.(2000)
		000-020° (65° W)	c. 55° towards 250°	30–50° towards 220° (Nim 3)	
		070-110° (80° S)			
	Bronzewing	040-060° (70° SE)	c. 80° towards 135°	c. 70° SE (shoot 39)	Phillips et al. (2000)
		090-120°		c. 10° towards 200° (W zone)	Vearncombe (1998)
		000-160°			
	Darlot	067.5° (steep)	c. 28° towards 070°		Gardner et al. (2001)
		315° (30° NE)			Krcmarov et al. (2000)
Laverton	Mount Morgans	340° (82/070°)	61° towards 143°	40-60° SE	Vielreicher et al. (1994)
		025° (65/115°)			
Kalgoorlie–Ora Banda	Kanowna Belle	070° (70/160°)	c. 70° towards 140°	60° SSE	Davis et al. (2010)
		337.5° (90/227.5°)			
		315° (90/225°)			
	Lady Bountiful	085° (70/355°)	c. 60° towards 300°		Cassidy et al. (1998)
		055° (60/325°)			Cassidy and Bennet (1993)
	Gimlet South	240° (75/330°)	c. 70° towards 020°	c. 70° ENE	Witt (1992b)
		090° (70/360°)			Tripp and Vearncombe (2004)
	Havana	315° (80/045°)	c. 70 towards 340°		Witt (unpublished)
		045°(70/315°)			Davis et al. (2010)
Agnew	Lawlers	110° (70/020°)	c. 55° towards 315°		Cassidy et al. (1998)
		065-090° (55/345°)			
North Murchison	Victory United	045° (80/315°)	c. 70° towards 030°	steep to the east	
		000° (80/090°)			
	Cue	067.5° (35/337.5°)	c. 35° towards 335°	45° towards NW	
		348° (70/258°)			

NOTES: (a) Where published descriptions give non-numerical orientations (e.g. NE), they have been converted to bearings in degrees (e.g. 45°). Where dips of faults are not given, a vertical dip is assumed.
(b) Quantitative ore shoot orientations are quoted only where available from source publications; otherwise, for blank entries, qualitative colinearity between fault intersections and ore shoots is stated in the source publication.

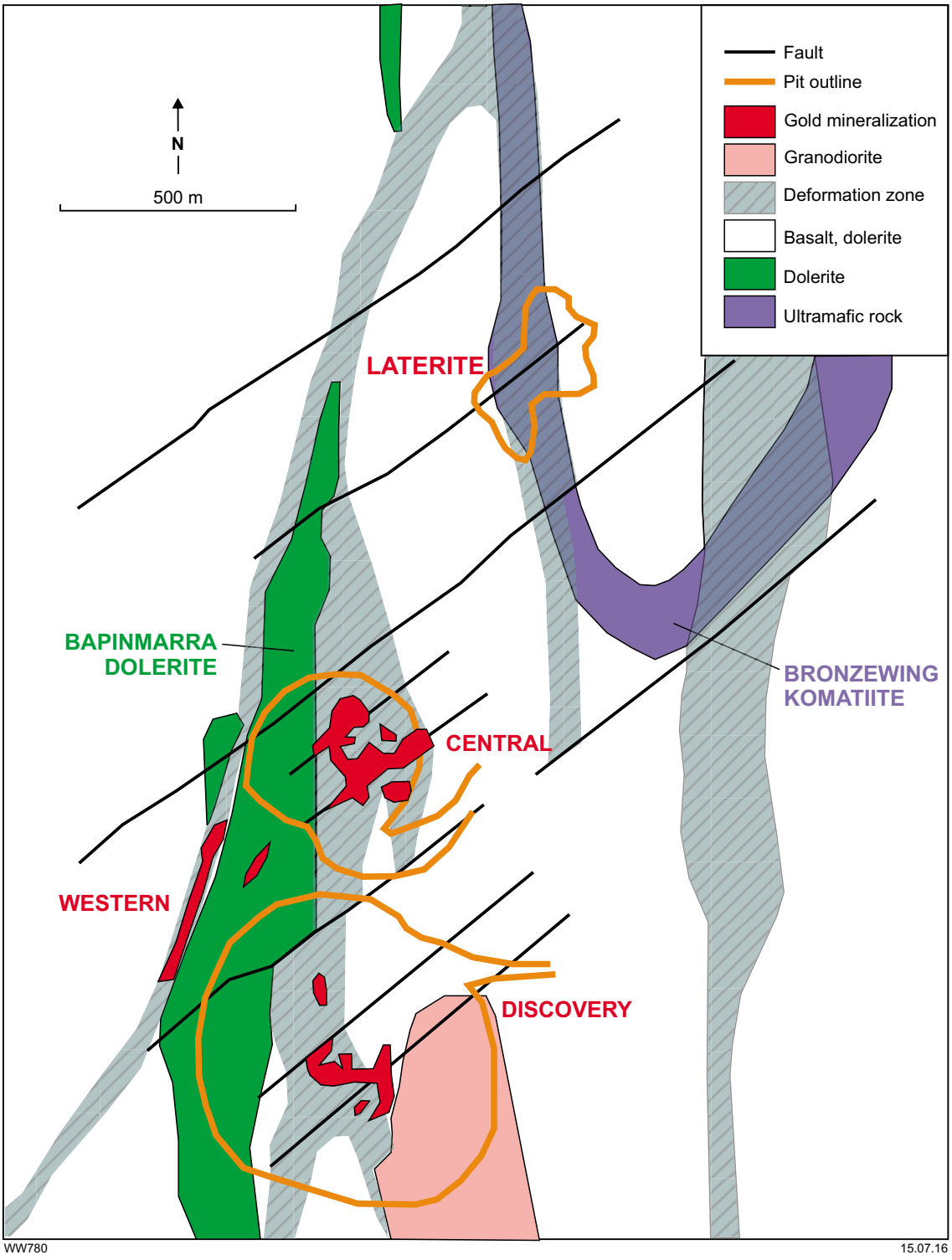

Figure 3.1. **Geological map of the Bronzewing mine area, Yandal greenstone belt, Eastern Goldfields Superterrane, showing relationships among lithology, structure, and gold mineralization (after Vearncombe, 1998)**

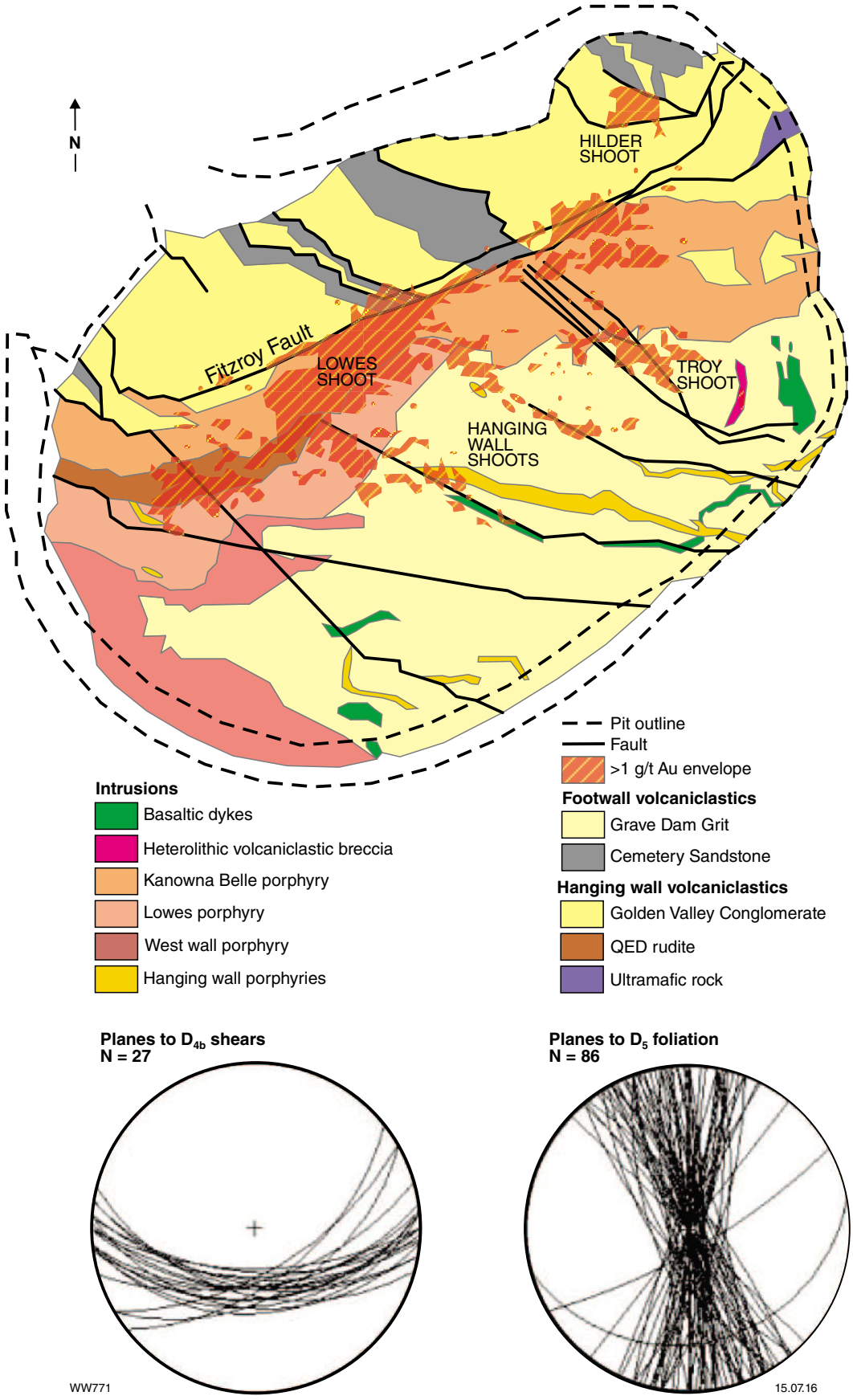

Figure 3.2. **Geology of the Kanowna Belle openpit, Kanowna gold camp, Eastern Goldfields Superterrane, showing relationship of gold mineralization to the Fitzroy Fault (within the Fitzroy Structural Zone of Davis et al., 2010) and intersecting hangingwall structures (after Davis et al., 2010)**

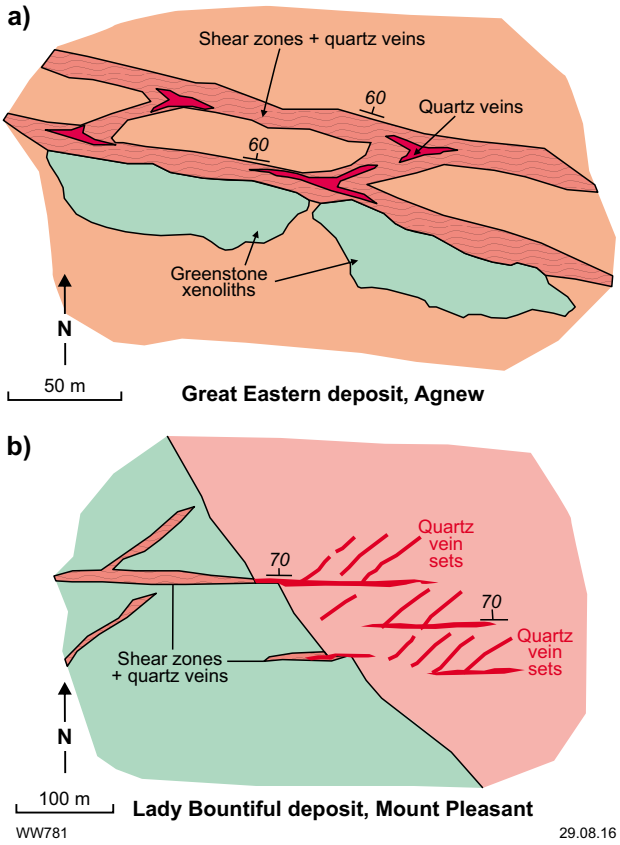

Figure 3.3. **Schematic sketches showing the relationship of gold mineralization to intersecting structures at a) Great Eastern (Lawlers) and b) Lady Bountiful gold deposits, Eastern Goldfields Superterrane (after Cassidy et al., 1998)**

Woodcutters camp is in an area of dense fracture intersections involving all four fracture sets (see also Tripp and Vearncombe, 2004). However, most descriptions of Woodcutters camp emphasize the role of northwest- and northeast-striking fracture sets. The Havana, Suva (Zhou et al., 2003; Davis et al., 2010), and Oriental deposits lie at the intersections of northwest- and northeast-striking fractures (Fig. 3.5). The Federal deposit is midway between northwest-striking fractures but the gross form of the Federal and Havana orebodies show northwest–southeast elongation. The Suva deposit is elongated in a northeasterly direction; unlike other deposits in Woodcutters camp, Suva shows no evidence of control by northwest-striking faults or fractures (Weinberg and Vanderborgh, 2008).

The Federal and Havana deposits show northwest–southeast elongation and cross the contact between intrusions of granodiorite and monzogranite (Fig. 3.6). At Havana, the sheared contact between massive granodiorite and foliated monzogranite dips shallowly to the south and southeast. Extensional movement on this contact is indicated by S–C fabrics. Weinberg and Vanderborgh (2008) also interpreted S–C fabrics in a similar zone of deformation at Suva to indicate an oblique dextral–normal sense of movement. At Havana, both intrusions are mineralized but the stronger mineralization is in the south Havana pit, immediately below the shallow southeast-dipping structural contact between the two granites. Grade-control data in the deeper and fresher southern exposures reflect northwest and northeast components of the orebody (Fig. 3.6). A swarm of closely spaced northwest-striking fractures is exposed in the southeastern end of the pit (Fig. 3.7a). However, gold is associated with quartz–biotite–pyrite in east-northeasterly to north-northeasterly striking fractures and veins (Figs 3.7b,c and 3.8) in which biotite is variably retrogressed to chlorite. These mineralizing structures range from simple fracture surfaces painted with biotite and pyrite, to a maximum vein width of about 1 cm. The east-northeasterly to north-northeasterly striking fractures are irregularly spaced and locally concentrated in zones up to about 2 m wide, but with an average spacing of about 0.2 to 1 m in the southern orebody. The intervening wallrocks show no clear hydrothermal alteration halos, but locally contain up to 5% disseminated pyrite. The fractures are best developed in the floor of the pit and persist beyond the northwest-trending orebody, but become relatively pyrite-poor and thinner in distal locations (Fig. 3.7b); they are present but not readily recognizable in the walls of the south pit. Weathering in the relatively shallow, northern pit area has highlighted some east-northeasterly to north-northeasterly striking fracture swarms by virtue of colour changes associated with oxidation of pyrite (and possibly some carbonate) to limonite (Fig. 3.7d). The structural orientations of 210 fracture surfaces within the Havana pit are shown in Figure 3.8. The plunge of the Havana orebody (steep to the north-northwest) conforms to the intersection between the two dominant (northwest-trending and northeasterly to north-northeasterly striking) fracture sets.

Northern Murchison district

Fault intersections control high-grade ore shoots in the Victory United mine and several granite-hosted deposits in the Murchison Domain (Watkins and Hickman, 1990). At Victory United in the Cuddingwarra camp, high-grade gold mineralization is partly within breccia zones at the intersection of a northeast-striking vein with a north-striking shear zone. The shoot plunges steeply to the east. Watkins and Hickman (1990) interpreted the northeast-striking quartz veins at Victory United as tension veins formed contemporaneously with dextral movement on the north-striking Cuddingwarra Shear Zone. At Cue, northeast- to east-striking faults reflect the local orientation of the regional cleavage, whereas north to north-northwesterly striking faults are interpreted as tension fractures (Watkins and Hickman, 1990). Ore shoots at individual mines plunge northwest, reflecting the intersection of the two component faults.

Fault splays that intersect master faults are another type of fault intersection that provides a focus for gold mineralization, as exemplified by the Golden Crown deposit (Cue camp) in the northern Murchison Domain (similar to Gimlet South, see above). The auriferous quartz reef at Golden Crown tends to thicken where it bifurcates, whereas individual splays diminish into chloritic shears within a few metres (Hicks, 1990).

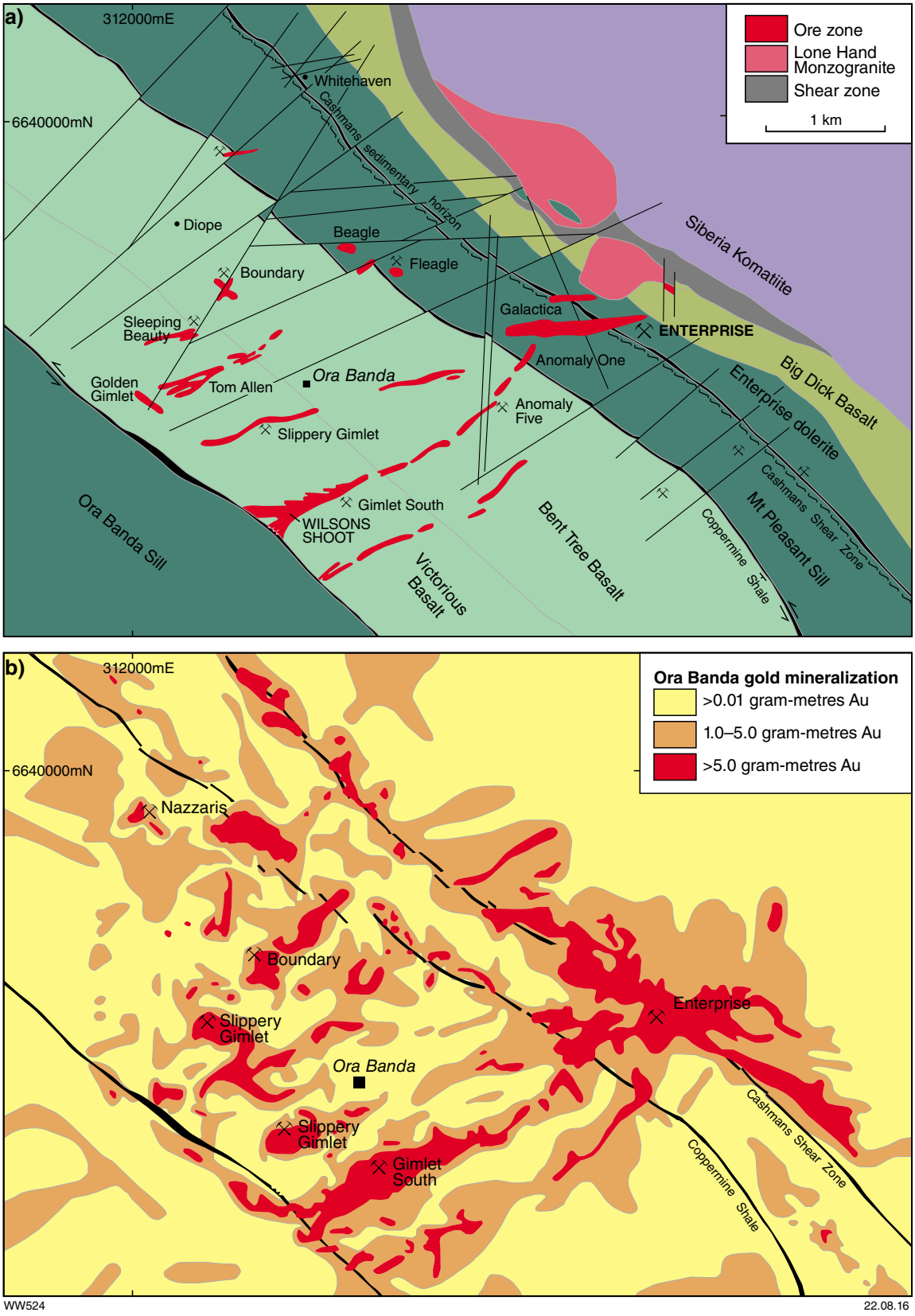

Figure 3.4. **a) Geology and gold mineralization, Ora Banda gold camp, Eastern Goldfields Superterrane; b) distribution of gold mineralization, Ora Banda gold camp, derived from exploration drilling data (after Tripp and Vearncombe, 2004)**

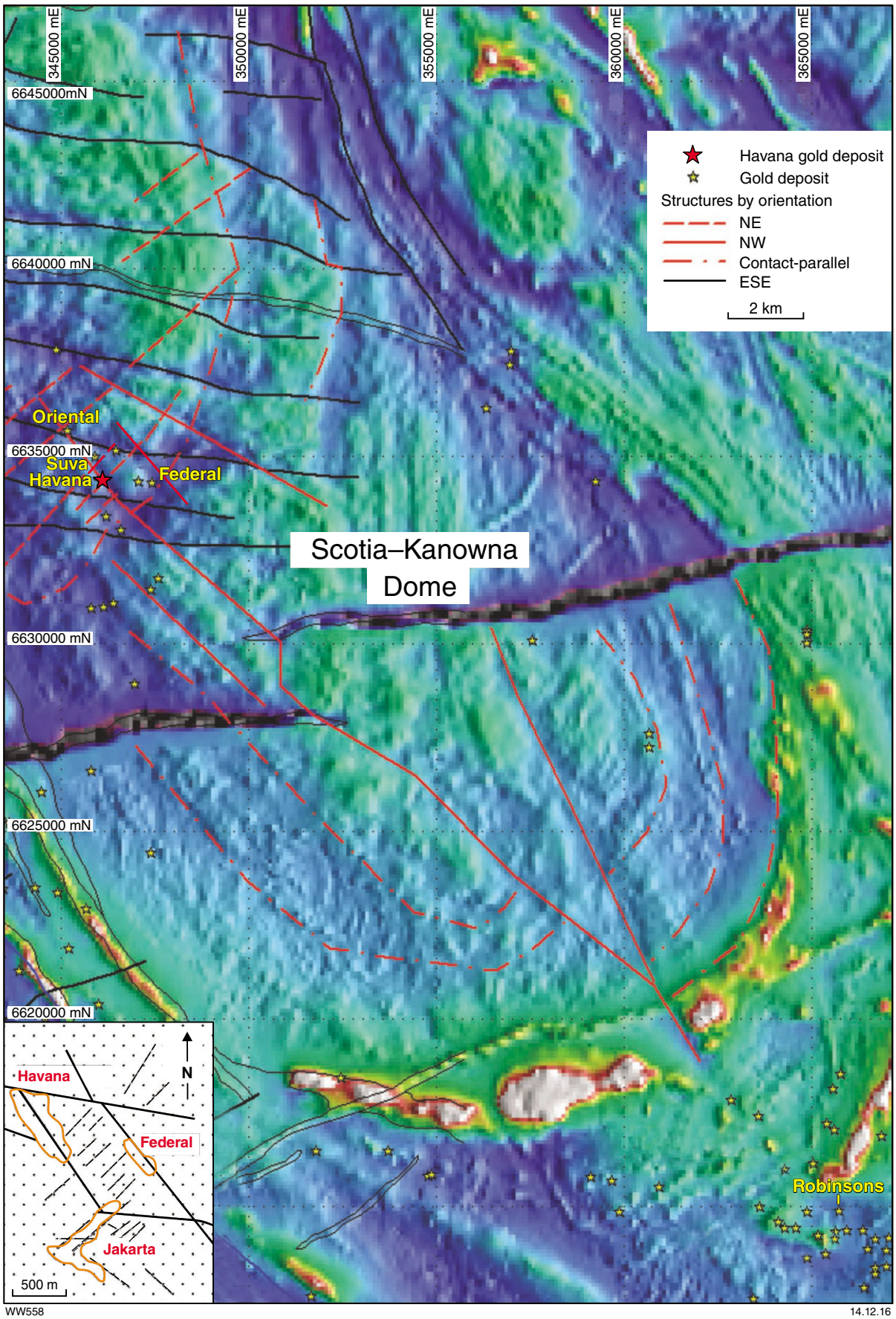

Figure 3.5. **Aeromagnetic image (reduced to pole) of the granitic Scotia–Kanowna Dome, Eastern Goldfields Superterrane, showing interpreted faults and fractures, and gold deposits. Inset (after Davis et al., 2010) shows the location of Havana with respect to other gold deposits and structures in the Woodcutters gold camp.**

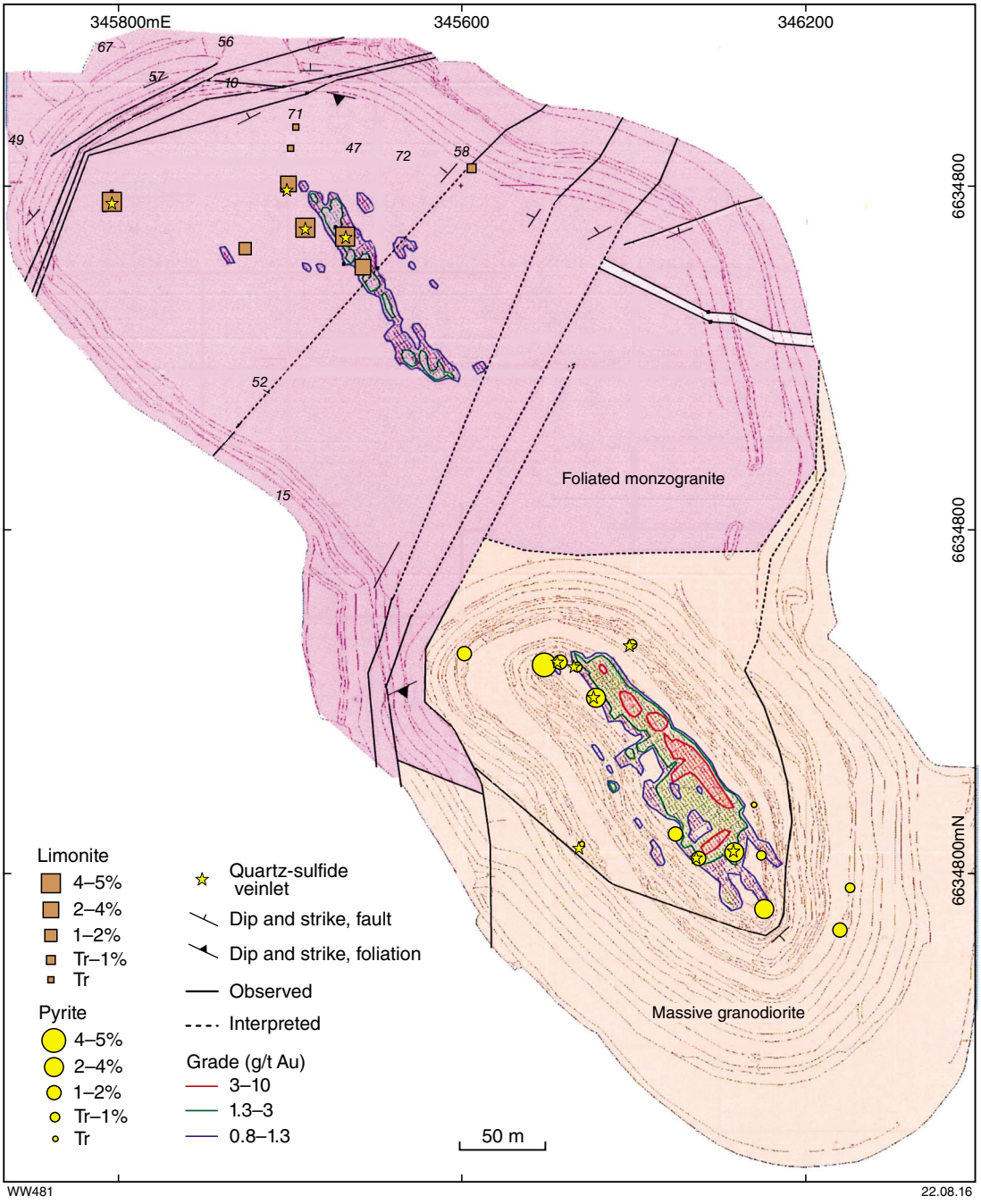

Figure 3.6. **Geology of the Havana openpit, Woodcutters camp, Eastern Goldfields Superterrane, showing distribution of gold and pyrite. Note north-northwesterly and east-northeasterly components of gold mineralization indicated by grade control data.**

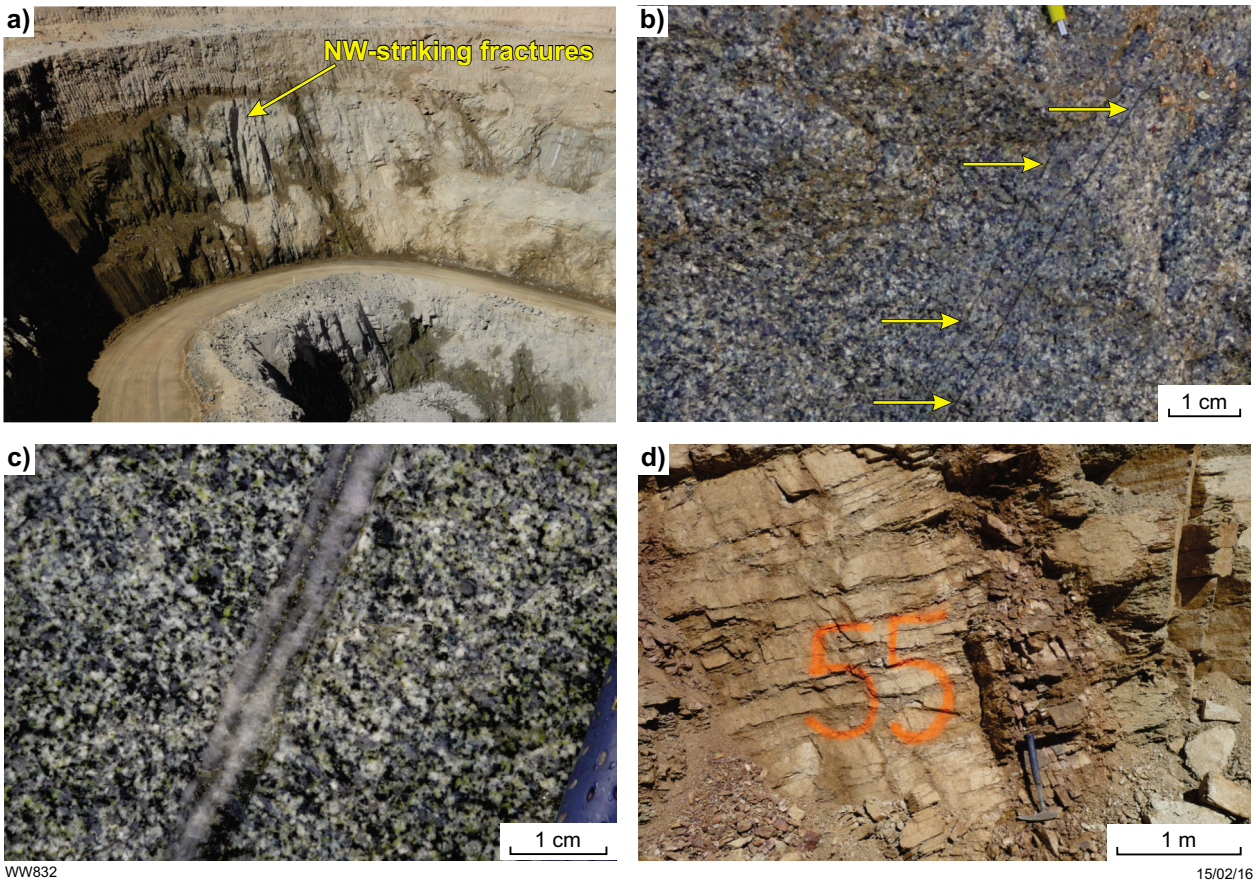

Figure 3.7. **Photos illustrating gold mineralization at Havana gold deposit. a) northwest-striking fractures exposed in the southeastern wall of south (Stage 1) pit (looking south). b) Sulfide-poor hairline veinlets in north-northeast to northeasterly striking fractures outside the auriferous ore zone, east wall of south pit. c) Centimetre-scale, laminated quartz–biotite–pyrite vein in a north-northeast to northeasterly striking fracture within the northwest-trending ore zone, floor of south pit. Note epidote after plagioclase in wallrocks and stability of biotite up to and within the vein. d) Subhorizontal fractures in monzogranite cut by steep, limonitic (dark brown) north-northeast to northeasterly striking fractures, north (Stage 3) pit.**

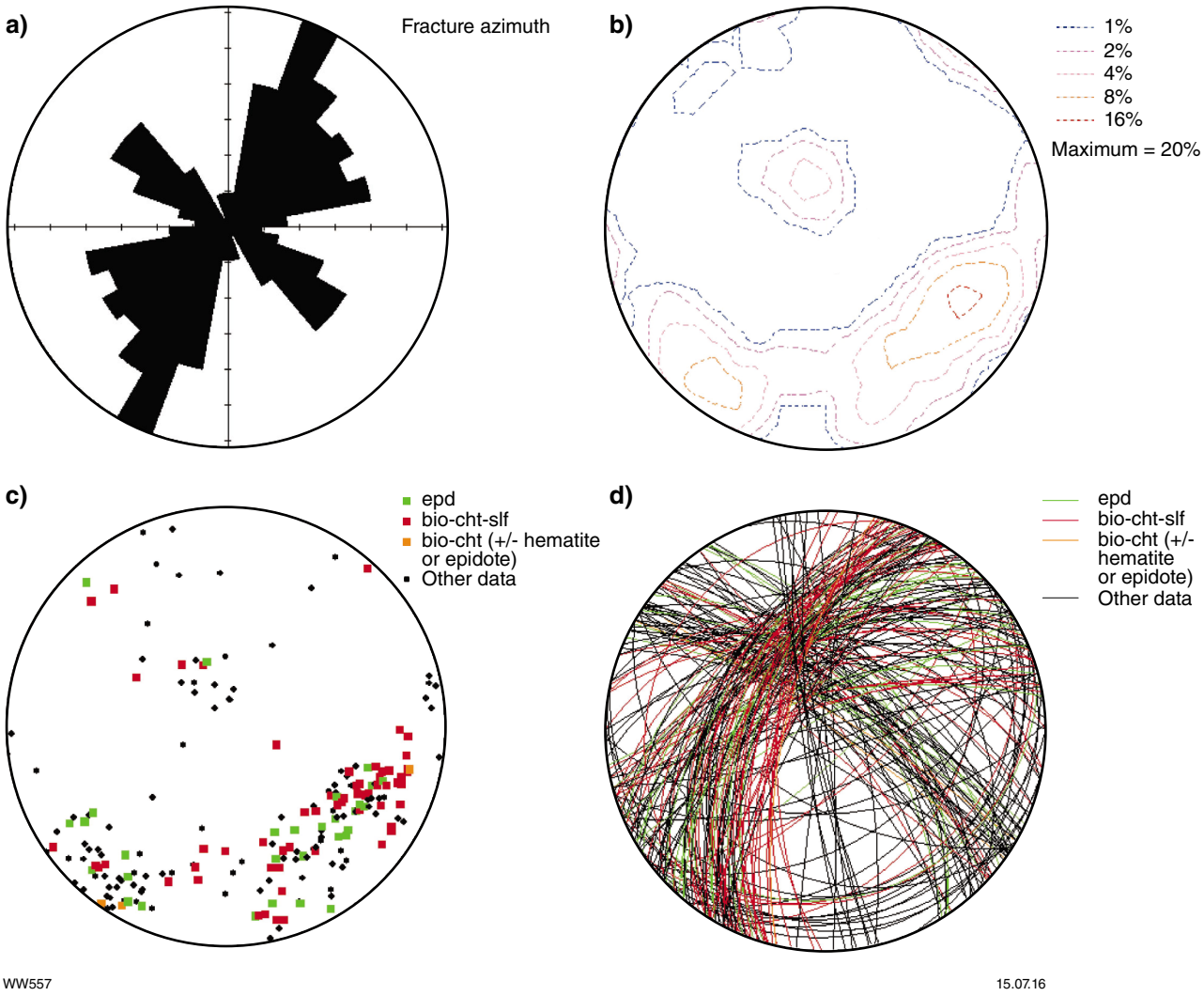

Figure 3.8. **Fracture orientations in Havana pit, Woodcutters gold camp. a) Rose diagram; b) contoured poles to fracture planes; c) poles to fracture planes coded according to mineralogy; d) great circles coded according to mineralogy. bio, biotite; cht, chlorite; epd, epidote; hem, hematite; slf, sulfide.**

Targeting Criterion 3.2: Fault bends and fault jogs

As was the case at regional and district scales (Parts 1 and 2 of this Atlas), fault jogs and fault bends at several Yilgarn gold deposits are important controls on overall deposit geometry and on the location of high-grade lodes within broader zones of lower grade mineralization. Stress heterogeneity around jogs and fault bends within fault zones leads to increased rock fracture and ore fluid focusing. At district scale, the relationship between gold mineralization and fault jogs and bends has been well demonstrated by the stress transfer modelling of Cox and Ruming (2004) and Micklethwaite and Cox (2004), but this approach has not yet been applied at deposit scale. The distinction made here between fault bends and fault jogs (see Fig. 2.72, Part 2 of this Atlas) follows that of Micklethwaite and Cox (2004) in which the former are 'hard-linked' (physically contiguous fault segments) and the latter are 'soft-linked' (fault segments either side of the jog are not physically connected).

Regional- and district-scale spatial analyses of fault jogs and fault bends (Targeting Criteria 1.10, 2.8, and 2.9 of this Atlas) mostly identified broadly equivalent gold prospectivity for dilational and compressional features. At deposit scale, however, gold mineralization in dilational settings is more common. For example, a contractional jog on the Playa Fault is viewed as the main camp-scale structural control on gold mineralization at St Ives (Targeting Criterion 2.9, Part 2 of this Atlas), but mine-scale controls on mineralization in the same camp are commonly dilational fault jogs and fault bends (e.g. Defiance, Clark et al., 1989; Revenge, Nguyen et al., 1998). The Ballarat – Last Chance deposit in the Kanowna gold camp provides an example of a deposit where a compressional jog has been suggested to control gold mineralization (Davis et al., 2010).

A well-described example where fault bends control the location and geometry of ore shoots is the 'shear–link' system at Norsemen (Campbell, 1990; Thomas et al., 1990). Production from laminated quartz veins (0.5–2 m thick) in the north–south oriented, east-dipping Mararoa, Crown, and Royal reefs constitutes 93% of total gold produced from the Norseman camp (Thomas et al., 1990). Although the reefs are stratigraphically within the Mararoa Basalt, at the base of the west-dipping Woolyeenyer Formation, high-grade ore shoots within the reefs are best developed where the basaltic rocks host subvertical dykes of varying composition (Thomas et al., 1990). The east-dipping reefs comprise the 'links' of the 'shear–link' system and join more steeply dipping shears. A reverse component of movement on the 'shears' caused dilation and quartz reef formation on the 'links' (Fig. 3.9a). High-grade ore shoots formed where the linking reef traverses dykes (Fig. 3.9b), presumably reflecting rheological differences between the dykes and their basaltic wallrocks.

Structural controls on ore shoot geometry similar to those described above at Norseman camp are known in other greenschist facies metamorphic settings. Examples include Darlot (Krcmarov et al., 2000) and the Sunrise Shear Zone at Sunrise Dam, where 'ramp–flat' terminology is substituted for 'shear–link' (Mair et al., 2000), as well as some higher grade metamorphic settings (e.g. Westonia, Cassidy et al., 1998; Yilgarn Star, Witt et al., 2001). In some cases, ore shoots are dilational bends that formed where the dip of a shear zone or fault flattens differentially against an irregular lithological contact, commonly involving a competent granitic intrusion within weaker greenstones (e.g. Granny Smith, Ojala et al., 1993; Porphyry, Cassidy et al., 1998; and possibly Tarmoola, Duuring et al., 2004 and Tower Hill, Witt, 2001). Dilational fault bends similar to those described for the Norseman camp may be formed by relatively subtle changes in the strike or dip of mineralized faults or reefs, but can be demonstrated by careful measurement and construction of Connolly diagrams (Connolly, 1936; e.g. Golden Age reef and Wiluna; Kenworthy et al., 2001).

Perhaps the best demonstration of the close relationship of gold mineralization to fault terminations, fault jogs, and fault bends comes from the Wiluna gold camp (Fig. 3.10; Hagemann et al., 1992). The Happy Jack deposit is located where the north–south Graphite Fault splays to form the Creek and Happy Jack – Bulletin Faults, but most of the mineralization at Happy Jack (and Bulletin) is on the Happy Jack – Bulletin Fault, which strikes northeast and is therefore in a favourable orientation for dilation under the east-northeast to west-southwest regional stress at the time of mineralization (Fig. 3.11b). Deposit-scale thickenings of the ore envelope are at second-order bends in the Happy Jack – Bulletin Fault, and in a fault jog at the northeastern end of the Happy Jack openpit (Fig. 3.11b). High-grade ore shoots plunge steeply south, coincident with the intersection of the Happy Jack – Bulletin Fault with the Creek Fault and with steep northwest-striking quartz reefs. The Bulletin deposit is at the northeastern termination of the Happy Jack – Bulletin Fault (Fig. 3.10).

The North Lode deposit is coincident with a fault bend on the East Lode Fault but, in this case, mineralization is on the north-striking portion of the fault bend and is best developed at a fault jog in the south central pit area (Fig. 3.11d). This jog formed where the East Lode Fault intersects northwest to west-northwesterly striking quartz reefs in the footwall and hangingwall, and hosts a steeply south-plunging, pipe-like, high-grade ore shoot. Another area of pronounced gold mineralization, at the northern end of the North Lode openpit, appears to be a fault termination at deposit scale, but is more likely an incompletely exposed jog, because the East Lode Fault is shown on the camp-scale map as persisting for another 500 m to the northeast (Fig. 3.10).

The East Lode deposit is on a major fault bend where the north-northeasterly striking East Lode Fault is intersected by the north–south East Lode Fault South, and by quartz reefs in the hangingwall and footwall (Fig. 3.11c). Ore shoots plunge steeply south and are colinear with the intersection of the East Lode Fault with northwest-striking stratigraphic contacts and quartz reefs.

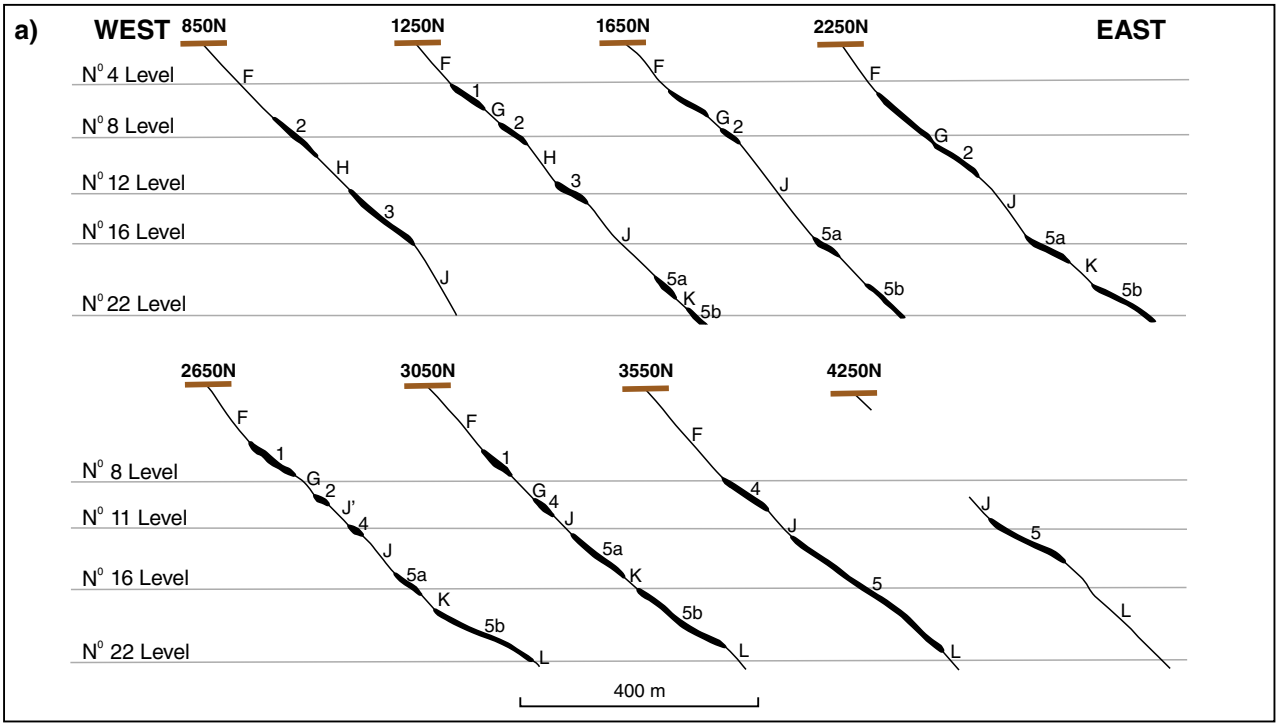

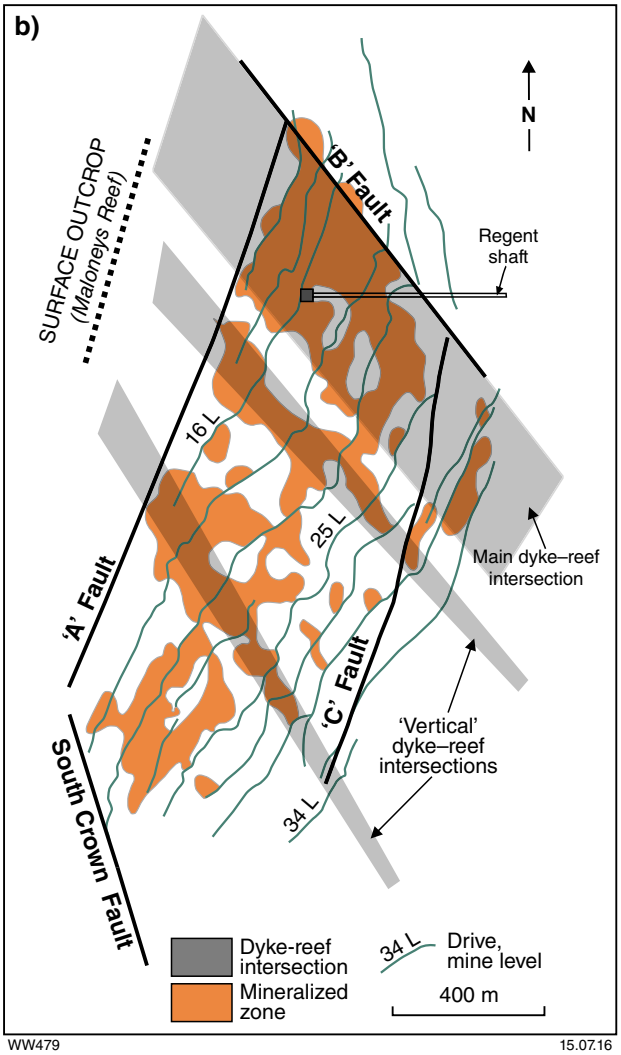

Figure 3.9. **Mineralized shear–link system, Norseman gold camp, Eastern Goldfields Superterrane. a) Serial cross sections through the shear–link system showing thickening of the structures where the dip is flatter (the 'links') (after Campbell, 1990). b) Projection onto the link (reef) showing location of higher grade ore shoots where the reef intersects dykes (after Thomas et al., 1990).**

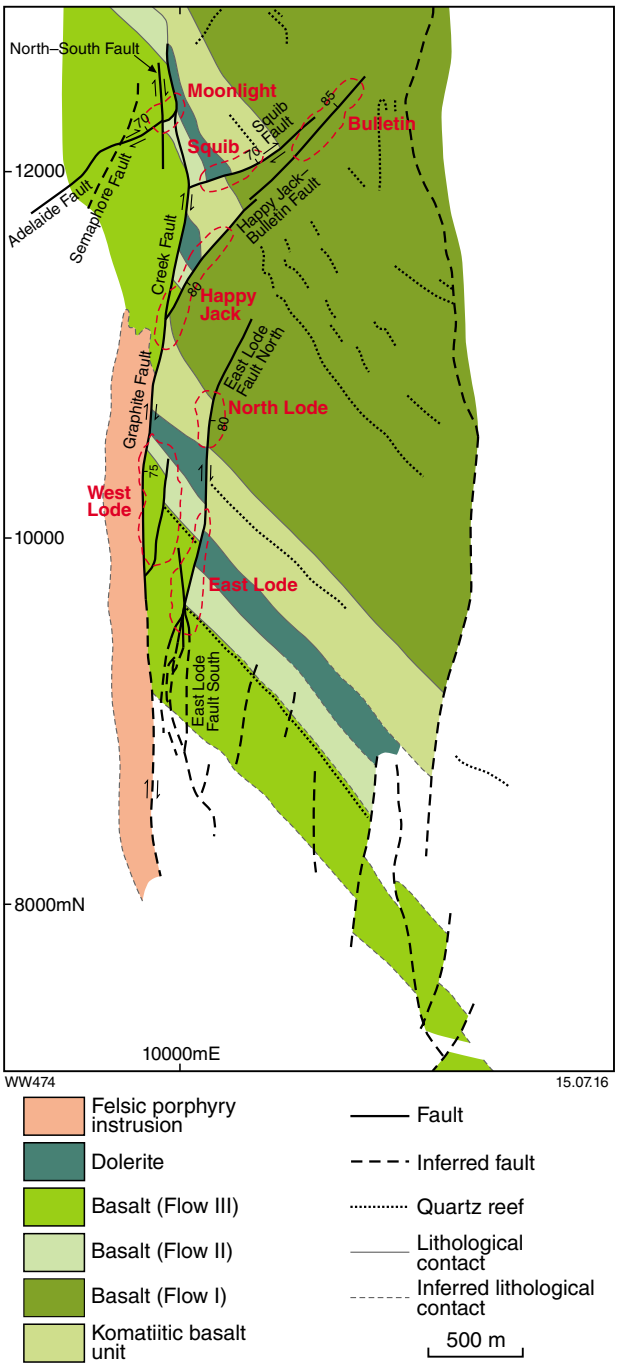

Figure 3.10. **Geological map of the Wiluna gold camp, Eastern Goldfields Superterrane, showing the Wiluna strike-slip fault system, semi-concordant (northwest-striking) quartz reefs and gold deposits (after Hagemann et al., 1992). Note: local grid shown.**

The West Lode deposit is on a splay fault that branches off the Graphite Fault. The two largest mineralization envelopes in this deposit are where the splay fault is intersected by northwest to west-northwesterly striking quartz reefs in the hangingwall of the splay fault, and at the termination of the splay fault, where the fault plane leaves a lithological contact and disperses into a branching array of smaller faults within Flow II basalt (Fig. 3.11a). Some of the intersecting northwest to west-northwesterly striking faults were intruded by dolerite, quartz porphyry, and lamprophyre, which may mask the original structural control on the lode. Intersections that control the position of high-grade ore shoots plunge moderately or steeply to the south (Hagemann et al., 1992).

The main gold orebody at the Squib deposit is also at the intersection of a strike-slip fault (the Squib Fault, subparallel to the Happy Jack – Bulletin Fault) with north-northwesterly striking porphyry and lamprophyre intrusions.

At Wiluna, mineralized fault intersections take the form of fault-hosted breccias (including implosion breccias), shear veins of laminated quartz (some of which are overprinted by a network of intense fracturing), cockade-textured extension veins (rare), and cataclasites (minor mineralization only). The most common forms of mineralization (fault-hosted breccias and shear veins) are associated with disseminated sulfides in unstrained to highly strained wallrocks; these are a major component of gold resources at Wiluna (Hagemann et al., 1992).

Although the foregoing description emphasizes fault intersections as much as fault jogs and bends, the evidence from Wiluna (and elsewhere) shows that fault jogs commonly nucleate at fault intersections, after which they may evolve with increasing strain into fault bends (Peacock, 1991). Critical intersecting faults may not be immediately recognized if they have been masked by subsequent igneous intrusions, such as porphyries and lamprophyres. Other examples where fault splays, fault jogs, and fault bends are probably genetically related to the intersection of two faults with different strike or dip orientations include Jundee–Nimary (Kohler et al., 2000), Darlot (Gardner et al., 2001), and Ballarat – Last Chance in the Kanowna district (Davis et al., 2010; GI Tripp, unpublished data; WK Witt, unpublished data).

A mineralized dilational fault jog forms the Slippery Gimlet deposit (8 t Au) at Ora Banda, where an east-northeasterly striking fault crosses a lithological contact (Tripp and Vearncombe, 2004). The lithological contact represents a rheological boundary separating different segments of the east-northeasterly striking fault (Fig. 3.12). The Ora Banda example shows that the lithological contacts on which fault jogs nucleate can be rather subtle, and may be based on grain size rather than bulk rock composition.

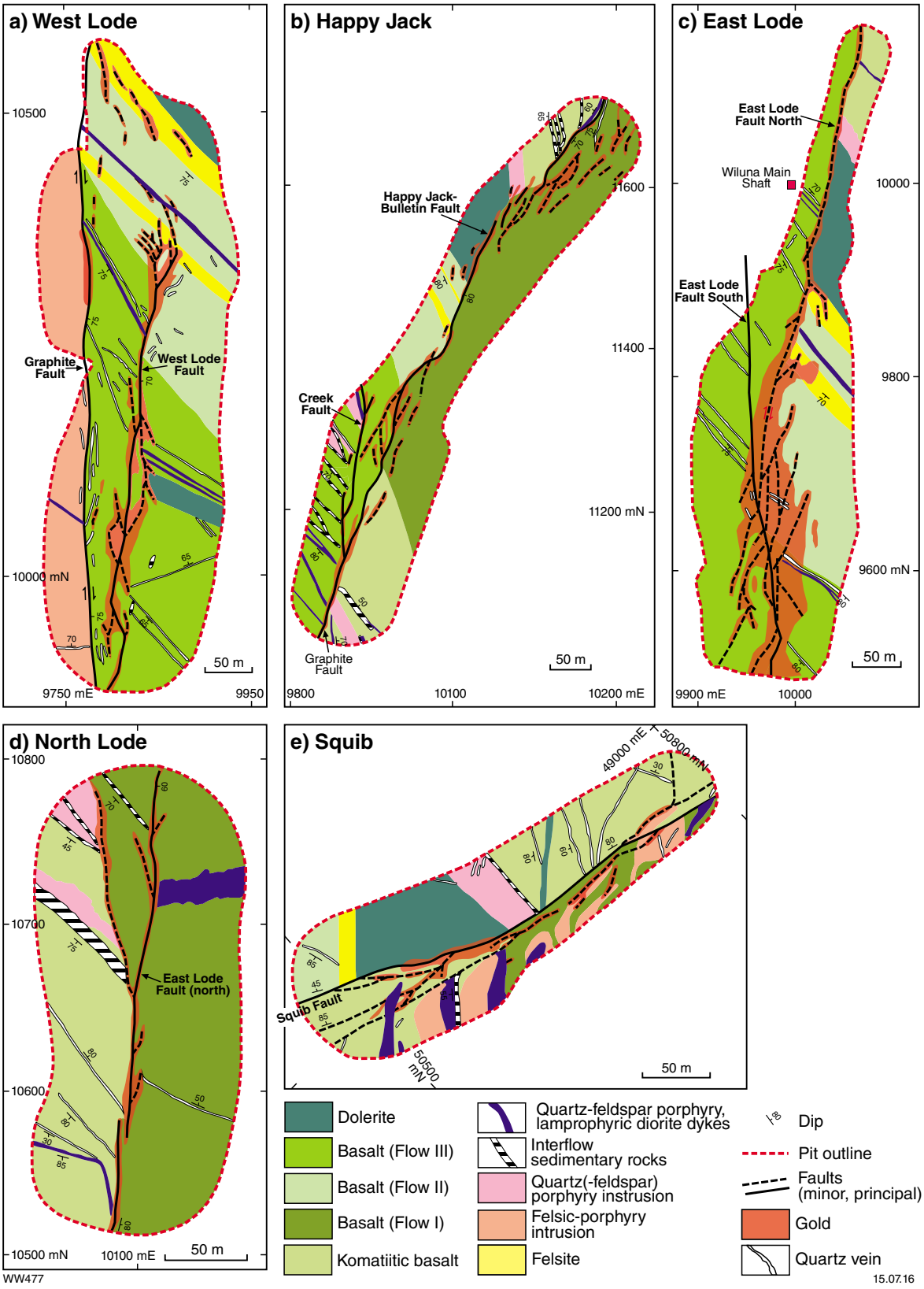

Figure 3.11. **Detailed geology of five gold deposits from the Wiluna gold camp illustrating relationships of gold lodes to fault bends, fault jogs, and fault terminations, and to the intersections of faults with quartz reefs and intrusions (after Hagemann et al., 1992). a) West Lode, b) Happy Jack, c) East Lode, d) North Lode, e) Squib.**

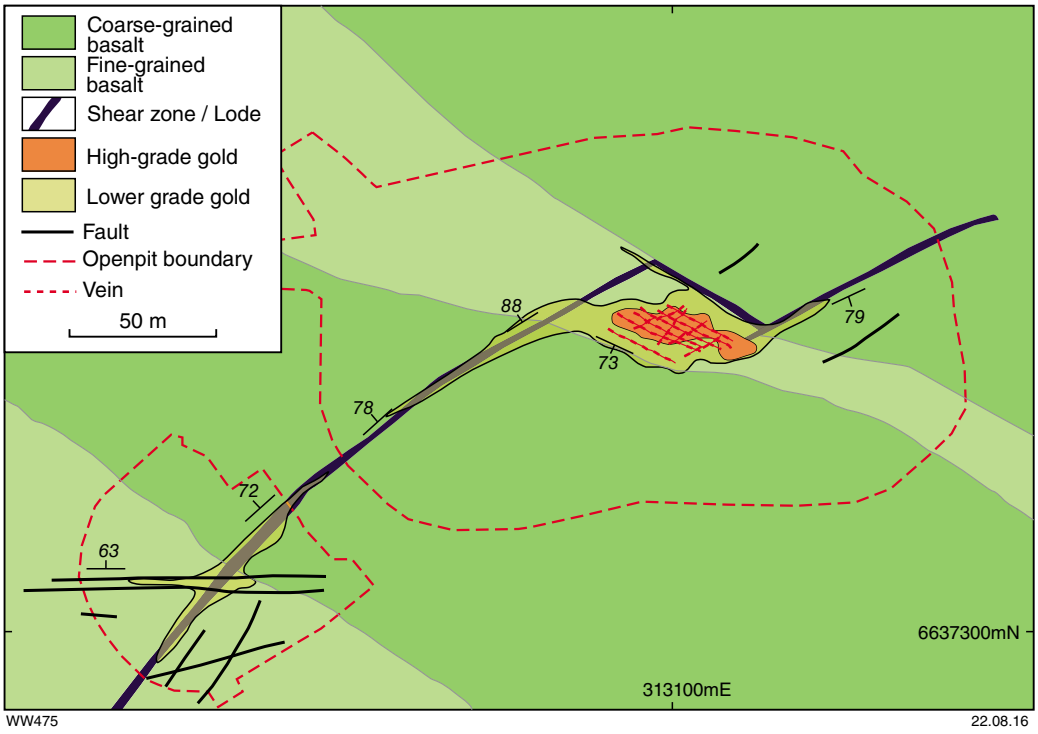

Figure 3.12. Geology of the Slippery Gimlet gold deposit, Ora Banda gold camp, Eastern Goldfields Superterrane, showing dilational jog at intersection of fault with lithological contact defined by grain size (after Tripp and Vearncombe, 2004)

The very high-grade Oroya shoot at the Golden Mile, Kalgoorlie, is also at a fault jog, which formed where reverse movement along a southwest-dipping sheared slate horizon encountered a minor asymmetric fold. The jog was created where the fault stepped across opposing limbs of the asymmetric fold (Swager, 1989; Bateman and Hagemann, 2004). Other mineralized jogs at locations where a fault crosses or encounters a fold axis, most commonly a minor asymmetric fold that is only apparent at district or deposit scale, include Twin Peaks (Carosue Dam gold camp) in the Eastern Goldfields Superterrane (Targeting Criterion 3.9) and Transvaal in the Southern Cross Domain (Targeting Criterion 3.7).

It is clear from the foregoing review that gold mineralization and high-grade ore shoots within the mineralized envelope at many deposits are controlled by irregularities in the form of hosting fault surfaces. These irregularities include fault terminations, fault splays, fault bends, and fault jogs. Predictive deposit-scale exploration for these structural sites should target locations where the mineralized fault

- crosses stratigraphic contacts, particularly contacts between lithological units of contrasting rheology
- encounters fold axes, particularly district- to deposit-scale minor asymmetric folds, along the strike of the fault
- intersects hangingwall and footwall faults or quartz reefs.

In some cases, the intersecting hangingwall and footwall faults may have been intruded by porphyry or other intrusions, which may mask the presence of an earlier fault. The northwest-striking quartz reefs in the Wiluna camp formed before the gold mineralization event and are, for the most part, barren. However, they control the formation of high-grade ore shoots where they intersect the principal displacement strike-slip faults (e.g. the Graphite Fault) of the later (syn-mineralization) Wiluna strike-slip fault system.

Targeting Criterion 3.3: Hydraulic seals

Phillips and Groves (1984) published a description of the Hunt deposit, a small gold deposit hosted by the Lunnon Basalt, the lowermost unit of the greenstone sequence at Kambalda (St Ives gold camp). They raised the possibility that certain stratigraphic horizons or contacts may have acted as hydraulic seals during the formation of some gold deposits. Hydraulic seals impede the upward movement of fluids sourced from below, thereby raising fluid pressure in the immediately underlying rock unit and increasing the capacity for hydraulic fracture of the rock, and for the fluid to deposit quartz and gold in the fractures as a result of phase separation or fluid–rock reaction. At Hunt mine, the proposed hydraulic seal was identified as the base of the ultramafic Kambalda Komatiite. A narrow, subvertical mineralized fault in the Lunnon Basalt expands into a sizeable body of hydraulic breccia immediately beneath the base of the ultramafic unit; this breccia unit is a major part of the Hunt orebody. The concept of a hydraulic seal was based on the different rheological properties of the two rock types. At the Hunt deposit, the relatively competent Lunnon Basalt, prone to deformation by brittle fracture, contrasts with the capacity of the weaker overlying ultramafic rock to deform by ductile extension and thinning. The contact between the two units can act as a detachment fault under these circumstances.

The concept of hydraulic seals was extended to district- and regional-scale exploration by Hall (2007), who identified unconformities at the base of late-stage sedimentary basins as possible aquicludes. The results of a regional-scale analysis of late-stage basins in the Eastern Goldfields Superterrane provide some support for this concept (Targeting Criterion 1.17, Part 1 of this Atlas), but a district-scale analysis of several potential hydraulic seals in the Kalgoorlie – Ora Banda district yielded mixed results (Targeting Criterion 2.3, Part 2 of this Atlas). The analysis identified the base of the ultramafic Walter Williams Formation as an effective seal at exactly the same stratigraphic level as the base of the Kambalda Komatiite (Hunt mine). However, the gold deposits underlying the base of the Walter Williams Formations capture only a very small proportion of the total gold endowment of the district. The base of the late-stage basins, the base of the metasedimentary Black Flag Group, and major thrust faults were shown not to be particularly effective seals at district scale.

Other potential hydraulic seals involving ultramafic rocks in the Kalgoorlie – Ora Banda district (but not investigated in Part 2) are the basal horizons of layered sills such as the Ora Banda Sill and the Mount Pleasant Sill; a thin carbonaceous shale unit is commonly found at these horizons (Witt, 1990, 1992b). The potential of these horizons to act as hydraulic seals is most convincingly demonstrated in the Ora Banda gold camp where east-northeasterly striking lodes broaden beneath the basal contacts of the ultramafic units and stop abruptly at the same contacts (Fig. 3.4). Although the shallower mineralization at Ora Banda is hosted by Victorious Basalt and has accumulated below the base of the overlying Ora Banda Sill, deeper exploration has shown that further gold mineralization (Ora Banda Deeps) is hosted by the underlying Bent Tree Basalt, and this deeper mineralization appears to be delimited by a thin black shale unit separating the Bent Tree and Victorious Basalts (Fig. 3.13).

At Enterprise, a recently discovered resource of almost 1 Moz Au (Reserves + Indicated + Inferred Resources; Norton Goldfields Ltd <www.nortongoldfields.com.au>, viewed 3 May 2016), gold grades are spatially related to east-northeasterly striking faults and stratigraphic zones within the differentiated Enterprise Dolerite (Tripp and Vearncombe, 2004). However, the additional role of the Cashmans Shear Zone, a deformed sedimentary horizon underlying the ultramafic base of the Mount Pleasant Sill, as a hydraulic seal is well demonstrated by the grade-distribution data (Fig. 3.14). Diamond drillholes designed to intersect the east-northeasterly striking faults at 90° similarly show that gold accumulated beneath the basal contact of the Mount Pleasant Sill in zones of intense fracturing and vein formation, locally in zones of hydraulic brecciation, and in zones of biotite–calcite–pyrite alteration (Fig. 3.15). There are two stratigraphically controlled high-grade sections within the deposit, both of which extend about 100 m along strike between the bounding east-northeasterly striking faults. The stratigraphically higher lode is in medium-grained, melanocratic dolerite in the upper part of the Enterprise Sill (directly beneath the putative seal) and the stratigraphically lower lode is in the fractionated, Fe-rich, quartz-bearing zones (U4 and U5 in Fig. 3.15) of the Enterprise Dolerite. High-grade shoots at Enterprise are colinear with the intersection of these stratigraphic units with the east-northeasterly striking faults (Tripp and Vearncombe, 2004).

The hydraulic seal concept has also been applied to at least one of the largest gold deposits in Eastern Goldfields Superterrane: Sunrise Dam. Baker et al. (2010) suggested that moderately northwest-dipping brittle–ductile shear zones (such as the Sunrise Shear Zone), although mineralized, acted as aquicludes to gold-bearing fluids ascending through subvertical faults and shear zones in the underlying rock sequence. These subvertical faults and shear zones are mineralized where they host stockwork and breccia zones with associated wallrock alteration and sulfides. Baker et al. (2010) interpreted the results of fluid inclusion microthermometry to indicate a transition from lithostatic to hydrostatic pressure conditions in the subvertical structures beneath hydraulic seals represented by the Sunrise Dam Shear Zone. These fluctuations between lithostatic and hydrostatic pressure may have been caused by periodic rupturing of the seal under high fluid pressure and subsequent healing by mineral deposition. Gold was deposited due to the combined effects of decreasing temperature, fluid immiscibility (phase separation), and the influx of a second CO_2-rich ore fluid resulting from fluid pressure fluctuations.

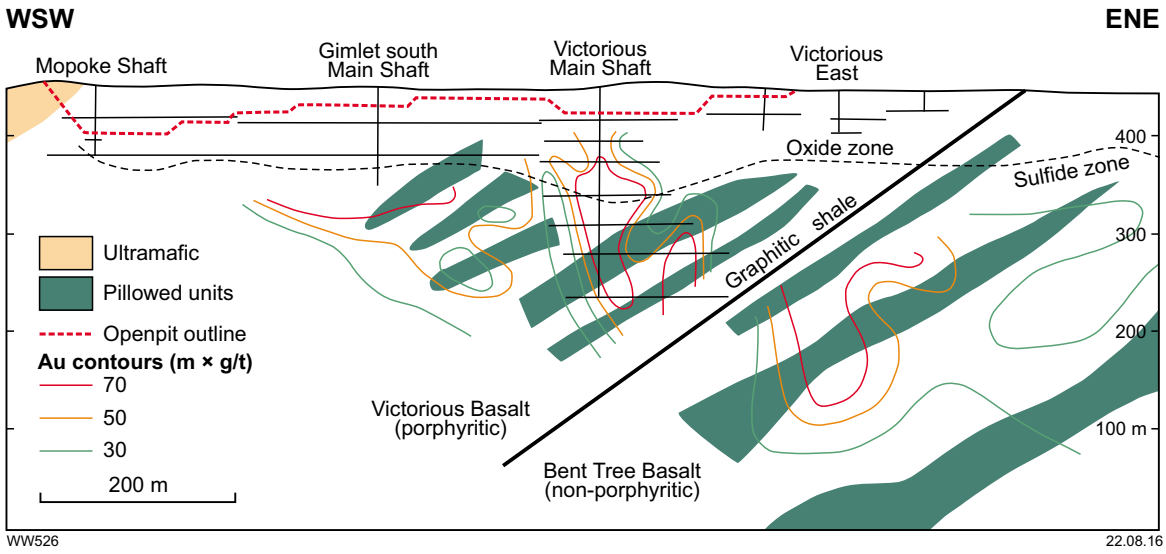

Figure 3.13. **Longitudinal cross section through the Gimlet South orebody, Ora Banda gold camp, Eastern Goldfields Superterrane, showing accumulation of gold beneath the graphitic shale horizon that separates the porphyritic Victorious Basalt and the non-porphyritic Bent Tree Basalt (after Harrison et al., 1990). Although it is possible that the distribution of gold was produced by normal fault offset along the graphitic shale unit, no such fault movement has been documented in the published literature.**

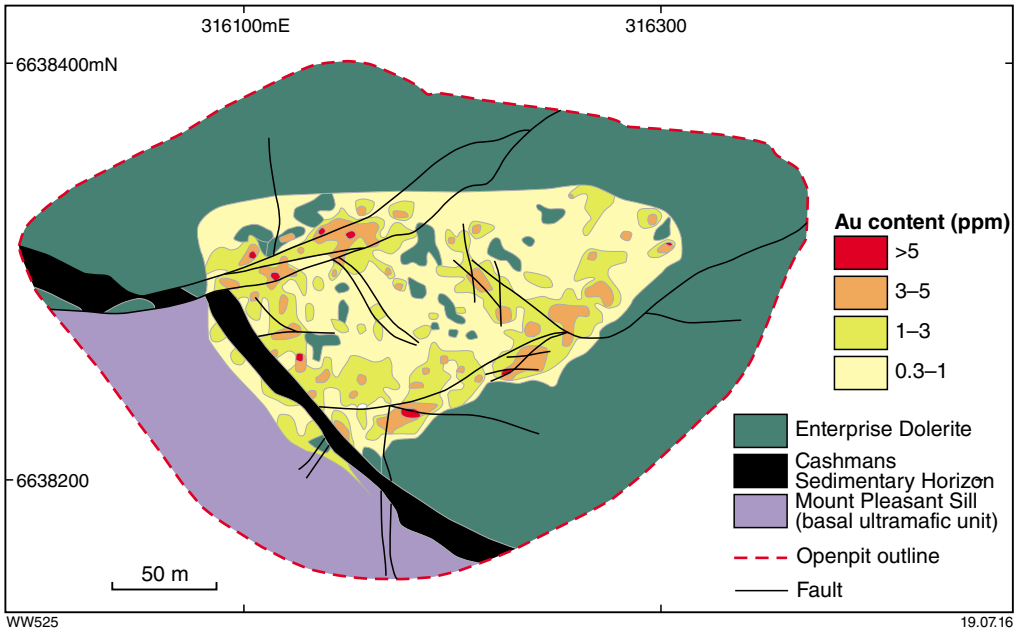

Figure 3.14. **Geology and distribution of gold at the Enterprise deposit, Ora Banda gold camp (after Tripp and Vearncombe, 2004), illustrating the accumulation of gold below the Cashmans sedimentary horizon (equivalent to Cashmans Shear Zone in Figure 3.4b)**

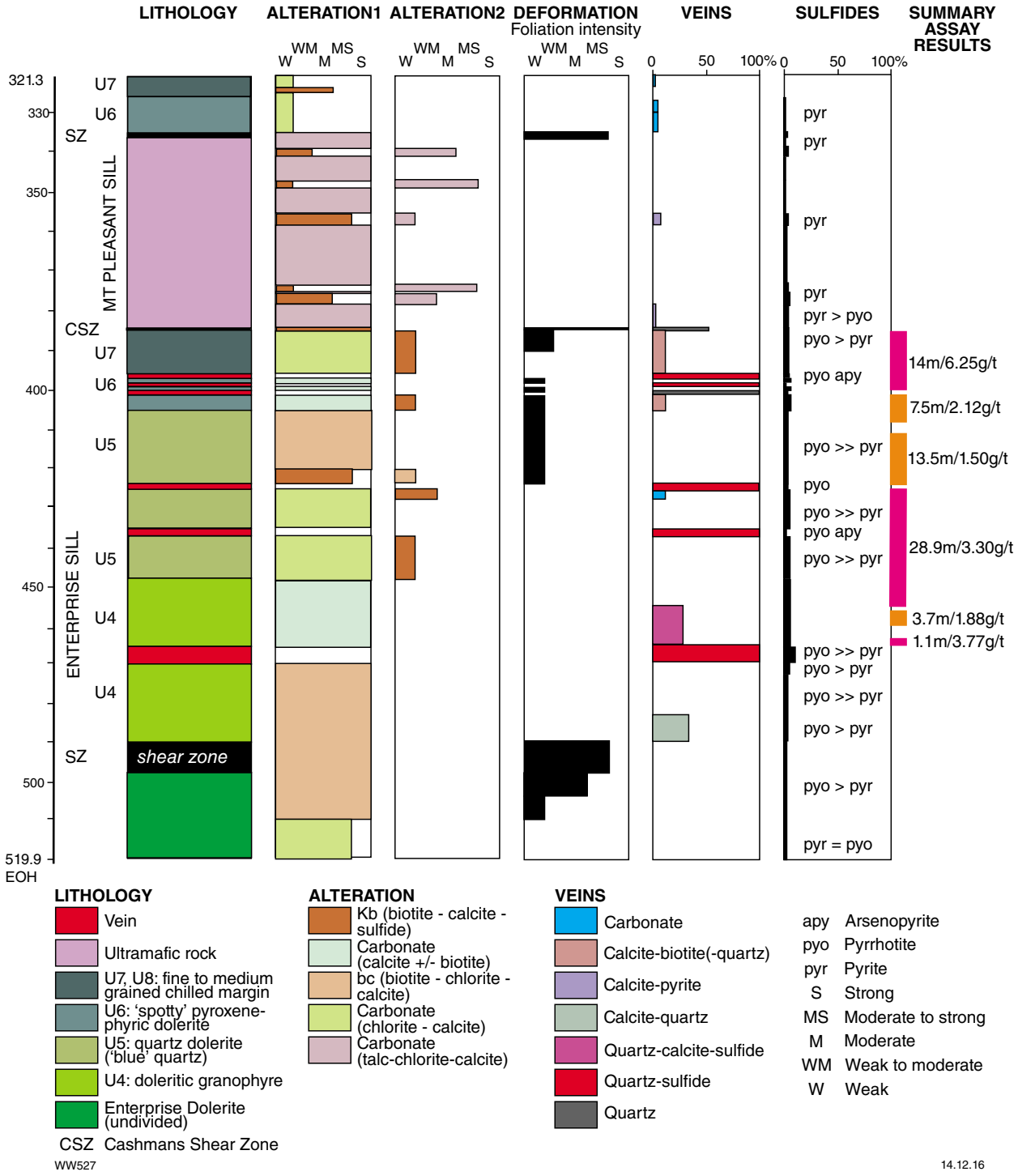

Figure 3.15. Strip log, hole POBD016, Enterprise gold deposit, showing distribution of gold, veins, deformation, and hydrothermal alteration, and illustrating the accumulation of gold directly below the Cashmans Shear Zone at the base of the Mount Pleasant Sill

Targeting Criterion 3.4: Constriction* zones (bottlenecks)

At deposit scale, constriction zones appear to be favourable sites for mineralization in some deposits. One such example is the Robinsons mine in the Kanowna camp of the Kalgoorlie – Ora Banda district. The main geological trends in the Kanowna camp are northeast to east-northeast, but at Robinsons, the greenstones are folded about an east-northeasterly axis (Fig. 3.16) that is probably the result of an early (before gold mineralization) deformation event. The gold deposit is hosted by a deformation zone that is oriented east-northeast at the southern end of the openpit, and almost north–south at its northern end (Fig. 3.17).

The greenstone sequence at Robinsons dips moderately to steeply southeast and can be subdivided into three domains (Fig. 3.17). The western (footwall) domain is formed by moderately to well-sorted, poorly bedded sandstone and grit, interpreted by Norton Goldfields Ltd as a tectonic slice of the Grave Dam Grit. The eastern (hangingwall) domain is formed by high-Mg basalt. Both domains display low strain with good preservation of primary sedimentary and igneous textures. The central (high-strain) domain comprises polymictic conglomerate and grit (Ballarat Conglomerate of Tripp, 2013, which is dominated by mafic and ultramafic clasts), ultramafic rock, and a thin lens of Grave Dam Grit. The central domain is a deformation zone, although strain is strongly partitioned around intensely carbonated ultramafic rock (dolomite/magnesite + quartz + fuchsite) at the northern and southern ends of the openpit (Fig. 3.18a,b). This intense carbonate alteration of the ultramafic unit pre-dates gold mineralization and weaker gold-related carbonate alteration, but nevertheless played an important role in the localization of gold on account of its rheological properties (see also Mulgarrie; Davis et al., 2010).

The central domain contains six strike-parallel brittle–ductile faults named, from west to east, W1 to W3 and E3 to E1, and a seventh fault on the contact between the western and central domains (Figs 3.17 and 3.18a,b). Faults E1 to W1 are up to 1 m wide and most contain prominent fault-fill laminated quartz veins that are up to about 0.5 m wide (Fig. 3.18c). These faults have taken up most of the strain in the central domain. Grade-control data indicate that economic gold mineralization is largely confined to the central, high-strain zone, and is subdivided into a western lode that is spatially associated with the lens of rheologically strong Grave Dam Grit, and an eastern lode along the eastern margin of the central domain (Fig. 3.17).

A vertical section exposed on the northern pit wall shows that faults E1 to E3 converge with depth (Fig. 3.18b). In plan view, southwards attenuation of the central domain is particularly pronounced (Figs 3.17 and 3.18a). The southern end of the central domain is therefore a constriction zone in which the greenstones have been reduced (in plan view) to a width of less than 50 m, compared to a width of more than 100 m in the north. The greater than 50% reduction in width of the central domain from north to south has been accommodated by vertical movement of greenstones across faults W1 to E1, which locally preserve downdip slickenlines (a positive flower structure; Harding, 1985). Subhorizontal centimetre-scale quartz veins in rheologically strong units of intensely carbonated ultramafic rock in the central domain, and in high-Mg basalt in the eastern domain (Figs 3.17 and 3.18b), provide further evidence for vertical extension of the greenstone sequence.

The western and eastern lodes merge to the south towards the constriction zone (bottleneck). Fault-fill veins in faults W1 to E1 are massive to laminated and are associated with carbonation of wallrocks. In the northern pit area, the central domain greenstones are weathered and strongly limonitic (after carbonate), although the veins also contain minor amounts of pyrite. Similarly strong carbonate alteration of ultramafic wallrocks also characterizes the less weathered constriction zone in the south of the pit. Lamellae in the fault-fill veins are fuchsitic and contain up to 3% coarse-grained idioblastic arsenopyrite (Fig. 3.18c). Grab samples of laminated veins from the constriction zone assayed up to 79.6 g/t and are consistently >1 g/t Au (Fig. 3.17). Wallrock samples from the constriction zone are of lower grade, but still contain up to 2 g/t Au. Selective sampling of laminated fault-fill veins and wallrock in the northern and central parts of the pit returned mostly lower gold contents, up to about 1.5 g/t, though some higher grades were found in footwall splay veins to fault E3 (Fig. 3.17).

Strain partitioning around rheologically strong bodies within the central domain is perhaps the main factor controlling the deposit-scale distribution of gold at Robinsons. Thus, the western lode envelops the lens of the rheologically strong Grave Dam Grit, and gold is concentrated at the tips of competent bodies (?boudins) of dolomite/magnesite + quartz + fuchsite rock at the northern and southern ends of the openpit (Fig. 3.17). However, the results of selective sampling in the Robinsons pit suggest that the constriction zone at the southern end of the pit contains a significant proportion of the gold resource (as a relatively high-grade ore shoot). Additional to the inherently favourable structural setting of the attenuated greenstones, the orientation of the constriction zone is probably also significant. In the constriction zone, the central domain greenstones form a thin incompetent unit between rheologically strong units in the western and eastern domains, and are oriented east-northeast (i.e. in the plane of σ_1, the principal strain axis). As discussed elsewhere (p. 188, Part 2 of this Atlas), this orientation favours dilation of thin incompetent units between thicker rheologically strong units, thus promoting focused fluid flow into the constriction zone and the formation of laminated quartz veins (cf. Ridley, 1993).

* The term constriction zone, as used here, is not the same as that applied by structural geologists to deformation zones defined by L-tectonites. Rather it denotes deformation zones caused by focussing of strain into domains of greenstone attenuation between rigid bodies such as granite intrusions. L-tectonites may or may not form in these structural environments.

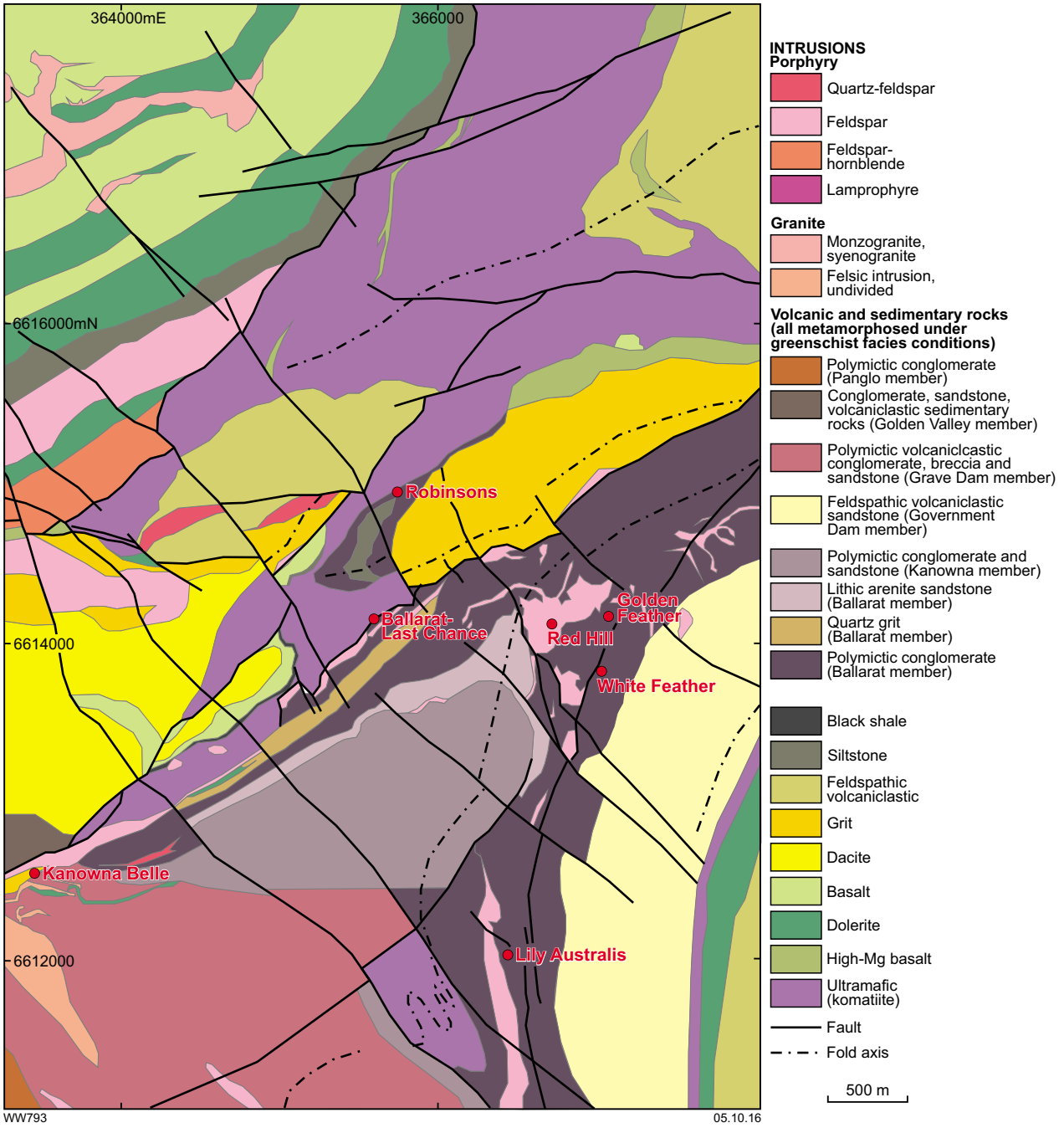

Figure 3.16. **District-scale map of the Kanowna gold camp, Kalgoorlie – Ora Banda district, Eastern Goldfields Superterrane, showing location of Robinsons deposit and several other significant gold deposits, including the world-class Kanowna Belle deposit (geology after AurionGold Ltd)**

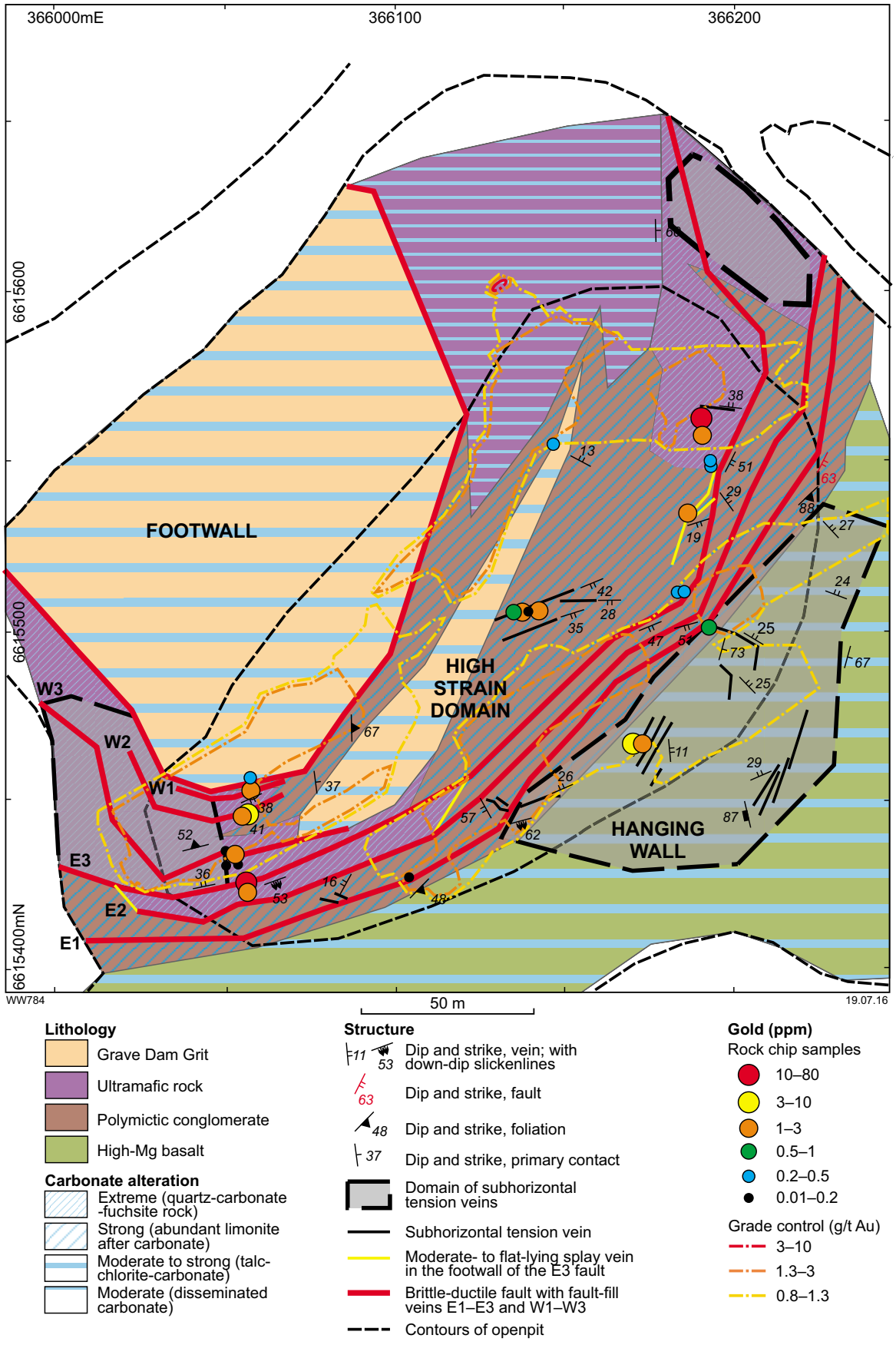

Figure 3.17. Geology of the Robinsons openpit mine, Kanowna gold camp. Note that grade-control data relate to a period before geological mapping was completed and are displaced approximately 10 to 20 m west of the east-dipping geological units exposed on the pit floor, particularly for the more moderately dipping western lodes.

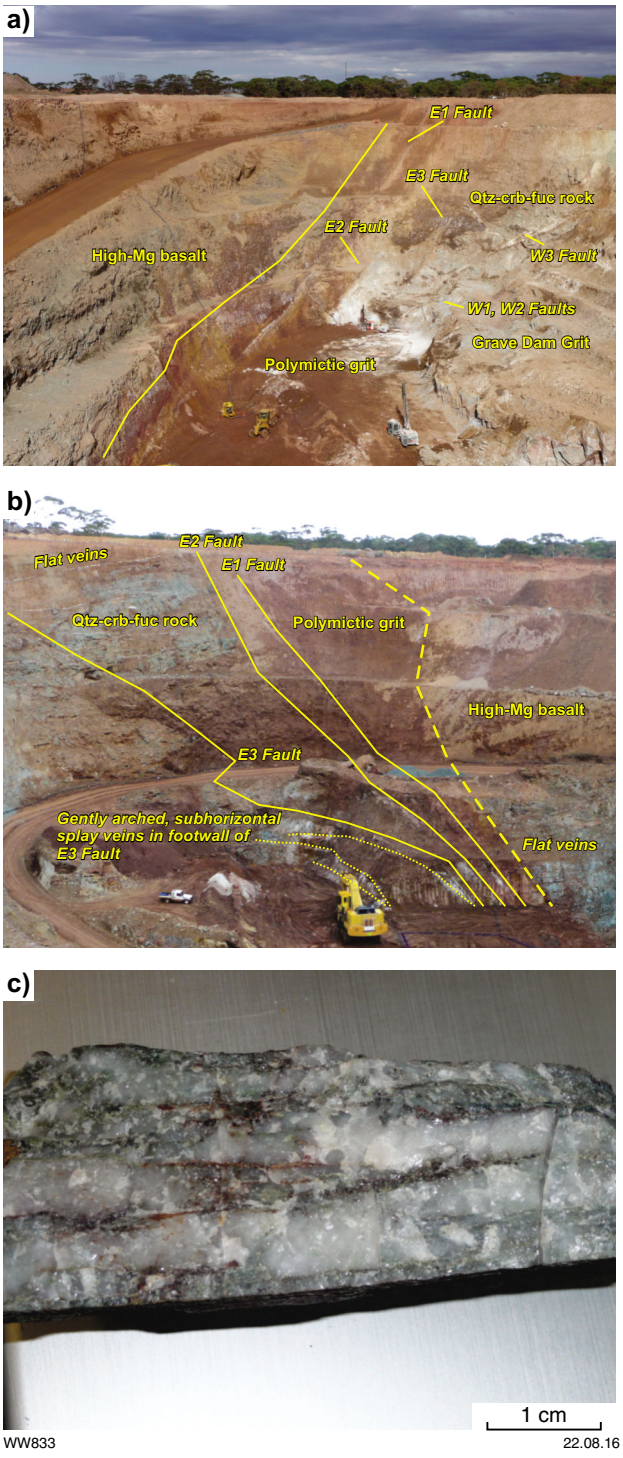

A minor component of the gold resource at Robinsons is contained in subhorizontal, centimetre-scale quartz tension veins in low-strain domains represented by the eastern high-Mg basalt and dolomite/magnesite + quartz + fuchsite rock at the northern end of the central domain (Figs 3.17 and 3.18b). These veins are associated with fuchsite and disseminated pyrite and arsenopyrite in the wallrocks and are considered to be contemporaneous with the fault-fill veins in the central domain. They represent the flat component in a flat–steep association similar to that at Sigma–Lamaque in the Abitibi greenstone belt in Canada, as described by Robert and Brown (1986).

Although the concept of constriction zones as a deposit-scale target for high-grade ore shoots is illustrated here by only one example, it finds some support from regional-scale analyses (Part 1 of this Atlas). At regional scale, greenstone constriction zones were shown to be better endowed in gold than the average for greenstones in the same terrane, but they captured only a relatively small proportion of the overall gold endowment in the terrane (Targeting Criterion 1.12, Part 1 of this Atlas). At district scale (Part 2 of this Atlas), shear-hosted gold in the Southern Cross greenstone belt were shown to be associated with constriction zones (attenuated greenstones) at the tips of a mega-boudin (Targeting Criterion 2.13, Part 2 of this Atlas).

Figure 3.18. **(left) Photos illustrating gold mineralization at Robinsons gold deposit. a) View looking south showing contact between high-Mg basalt and polymictic grit (yellow line), and some of the main faults in the Robinsons pit. Note the thin but continuous nature of the E1 Fault. b) View to north showing gently arched, subhorizontal splay veins in footwall of E3 Fault. Note the difference between these splay veins and the more planar subhorizontal (flat) veins in the quartz–carbonate–fuchsite (Qtz-crb-fuc) rock and high-Mg basalt. Yellow lines delineating faults E1 to E3 have been moved slightly to the right to allow recognition of the faults in the photo. c) Margin of laminated quartz–fuchsite vein from the E3 Fault; several percent arsenopyrite is present in the fuchsitic laminations (79.6 g/t Au).**

Targeting Criterion 3.5: Rheological units and rheological contacts

Although the principal structural control on ore shoots in the Wiluna camp are fault anomalies such as jogs, bends, and terminations (Targeting Criterion 3.2), Hagemann et al. (1992) pointed out that the high-grade sections of mineralized faults are commonly at the contacts of rheologically strong (competent) units (e.g. basalt flow II, felsites within basalt flow II, quartz porphyry intrusions, and pre-existing quartz reefs; Figs 3.10 and 3.11). The intersections of the mineralized strike-slip faults with these competent lithological units promotes stress heterogeneity, which leads to the formation of steep, pipe-like fault jogs and fault bends. This point is well illustrated by the relatively large East and West Lode deposits, where mineralized splay structures off the main strike-slip fault of the Wiluna fault system (the Graphite Fault) structurally juxtapose rheologically strong flow II basalt against weaker flow III basalt (Figs 3.10 and 3.11). This relationship is shown again, at the '450-foot level' (Fig. 3.19) in the same area, where high-grade ore shoots are preferentially localized on structural contacts between flow II basalt (and felsites within flow II basalt) and rheologically weaker flow III basalt and komatiitic basalt.

Similarly, but in a slightly different context, rheological properties were fundamental for the formation of the Homestead deposit, Mount Pleasant (WK Witt, unpublished data). The Homestead deposit is hosted by the north–south Homestead Shear Structure, a splay off the Black Flag Fault (see Fig. 2.78, Targeting Criterion 2.9, Part 2 of this Atlas). At the Homestead deposit, the strike and dip extents of mineralized laminated quartz veins within the Homestead Shear Structure are confined to the upper Bent Tree Basalt and the lower part of the overlying Victorious Basalt. The strike extents of the Black Flag Fault and Homestead Shear Structure, however, are considerably greater than that of the Homestead mineralization. The critical factor for the location of gold mineralization within the Homestead Shear Structure appears to be a massive hydrothermal carbonate(–quartz)-rich unit that lies along the western side of the dextral strike-slip Homestead Shear Structure, which is otherwise characterized by chloritic alteration (Figs 3.20 and 3.21). The rheological contrast between the competent hydrothermal carbonate unit and weak chloritic schists has caused brecciation of the former unit (Fig. 3.21g) and localization of auriferous laminated veins at or close to contacts between the two lithological units (Fig. 3.21a,b). The hydrothermal carbonate-rich unit is closely associated with carbonate-altered mafic volcanic breccia and is interpreted as a possible synvolcanic feature (e.g. sea-floor alteration), in part stratigraphically controlled by the uppermost sections of the Bent Tree Basalt. The strike extent of the Homestead mineralized vein system correlates with the strike-displaced offset of this hydrothermal unit within the Homestead Shear Structure (Fig. 3.20), but extends downdip for about 200 m below the massive to brecciated hydrothermal unit at the 1165 m RL (reduced level). In this downdip section of the mineralization, laminated veins are associated with isolated pods of strongly carbonated (± silica) basalt within chloritic schist (Fig. 3.21a,b). The contacts of these pods provided sites for thick laminated vein development during later dextral strike-slip movement (Fig. 3.21a–d), generating steeply plunging ore shoots.

At the southern end of the Homestead orebody, on and above the 1150 m RL, the massive hydrothermal unit expands from the west wall of the drives to occupy the entire width of the drives (Fig. 3.20). Here, the laminated veins that form the orebody swing sharply towards an east–west orientation and are structurally duplicated (Fig. 3.21e,f) before the system is terminated a further 10–20 m south. Similar dispersal and termination of the laminated vein system in a brecciated carbonate-rich unit is seen at deeper levels of the mine (970 m and 985 m RLs), and on the 1195 m RL at the northern end of the mine. These terminations are represented by a dispersed array of laminated veins of short strike length and diverse orientation, including horse-tail structures (Fig. 3.21h), but without the prominent east–west strike deflection seen on the 1165 m RL, South development face. These features are similar to those described at the tips of strike-slip faults (McGrath and Davison, 1995) and probably represent terminations of faults formed within the broader Homestead Shear Structure at the time of gold deposition.

Within shear zones, more generally in the Eastern Goldfields Superterrane, high strain (coaxial or non-coaxial) enhances the importance of rheological differences between adjacent units, as demonstrated in numerous examples of shear- and fault-hosted gold deposits. The Hampton–Boulder deposit in the New Celebration gold camp is a shear-hosted gold deposit in which mineralization is preferentially developed on deposit-scale rheological contacts. Brittle–ductile to ductile strike-slip movement on the Boulder–Lefroy Fault has led to fracture and vein formation on the margins of competent porphyry bodies (?boudins) in a matrix of ultramafic and mafic schist, producing steeply plunging ore shoots (Norris, 1990; Witt, 1992c; Nichols and Hagemann, 2014). Similar, but smaller, examples involving albitic porphyry units within ultramafic schist of the Zuleika Shear Zone, in the Kalgoorlie – Ora Banda district, include Hawkins Find and Anthill (Witt, 1992c).

Harbour Lights deposit, at Leonora, presents a similar rheological control on gold mineralization to that described above for New Celebration and Homestead, but in a normal shear zone. At Harbour Lights, gold is associated with laminated quartz(–carbonate) veins within a broad zone of ductile normal shear (Vearncombe, 1992). Mineralized veins and associated alteration are concentrated in and around a thin mafic unit enclosed within ultramafic schist (Fig. 3.22; Skwarnecki, 1989; Vearncombe, 1992). The veins are concentrated in the leeward (pressure shadow) sides of low-strain lithons of mafic to ultramafic rock (banded tremolite–chlorite rock). Another example, from a higher metamorphic grade (amphibolite facies) setting is Yunndaga (96 000 oz Au), which is the largest deposit in the Menzies area (Witt, 1992a; Blewett and Czarnota, 2007; Morey et al., 2007a,b). At Yunndaga, 6 km south of Menzies township

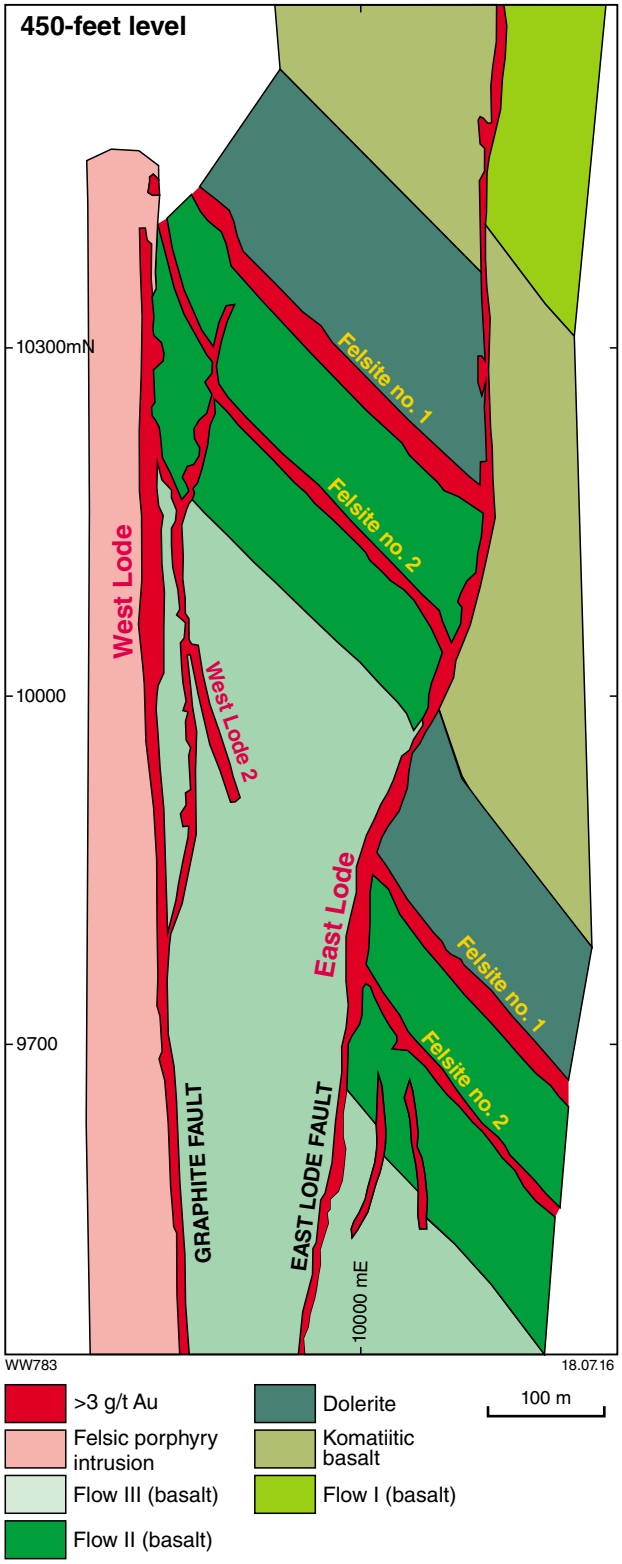

Figure 3.19. **Geological map at the '450-foot level' of the East and West Lode mine area, Wiluna camp, Eastern Goldfields Superterrane (from Hagemann et al., 1992) showing preferential development of gold mineralization on rheological contacts of flow II basalt with internal felsite units and with flow III basalt**

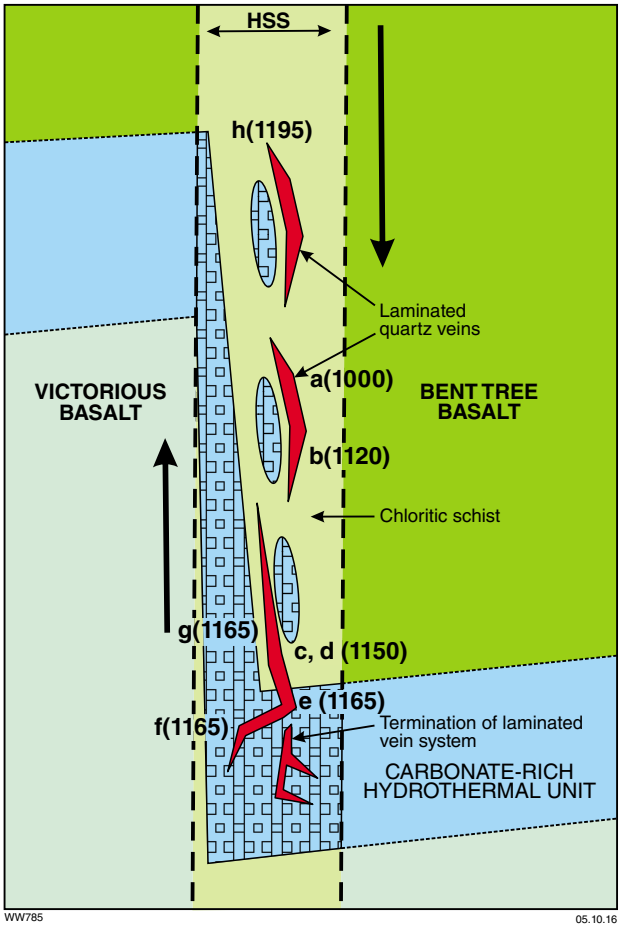

Figure 3.20. **Schematic plan showing interpreted relationships of the carbonate-rich hydrothermal unit at or near the top of the Bent Tree Basalt with the Homestead Shear Structure (HSS), and with laminated quartz–gold veins at the Homestead underground mine, Mount Pleasant. Approximate locations of photographs a to h (Fig. 3.21) are shown schematically, with RL (m) shown in parentheses. Square pattern represents fracture and brecciation of the carbonate-rich hydrothermal unit. Dotted lines outlining the hydrothermal unit outside the HSS indicate a conceptual interpretation. Although the stratigraphic contacts shown have been mapped at camp scale, the presence of the strongly carbonated horizon outside the HSS has not been verified by exploration drilling in areas of poor exposure beyond the HSS.**

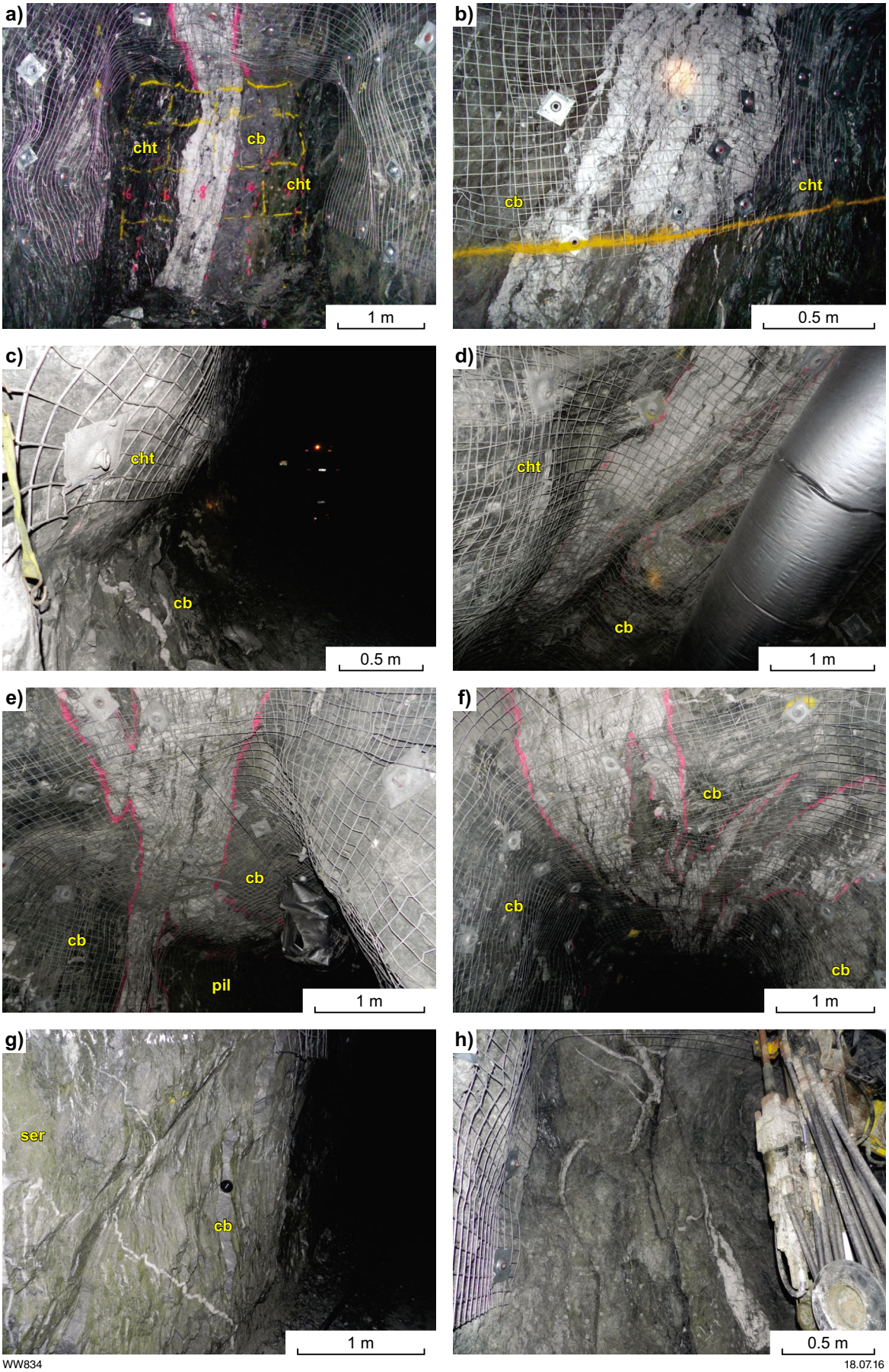
a)
cht
cb
cht
1 m
b)
cb
cht
0.5 m
c)
cht
cb
0.5 m
d)
cht
cb
1 m
e)
cb
cb
pil
1 m
f)
cb
cb
cb
1 m
g)
ser
cb
1 m
h)
0.5 m
WW834
18.07.16

Figure 3.21. **(opposite) Rheological controls, Homestead gold deposit. a) 1000 m RL, North development face, showing a metre-scale laminated quartz vein at the contact between a footwall hydrothermal unit (grey, cb) and hangingwall chloritic schist (cht). b) 1120 m RL, North development face, showing metre-scale laminated quartz vein at contact between footwall chloritic schist (cht) and brecciated hangingwall hydrothermal unit (cb). c) 1150 m RL, looking south, contact of massive hydrothermal unit (cb) against chloritic schist (cht), near floor on east wall of development drive. Note barren tension veins in hydrothermal unit. d) Two laminated veins exposed in roof of development drive above location shown in c; the eastern vein (left in photo) tapers out along strike and downdip against the eastern contact of the hydrothermal unit (cb), and the western vein (right in photo) swings sharply to the west on passing out of the chloritic schist and encountering the hydrothermal unit. e) 1165 m RL, roof (looking north), showing sharp deviation of laminated vein to east–west orientation where the Homestead Shear Structure crosses into the hydrothermal unit; the east–west oriented vein section is on the contact between a pod (or lithon) of pillow basalt (pil) within the HSS and the brecciated hydrothermal unit (cb). f) 1165 m RL, roof (looking south), showing duplication of laminated veins in the brecciated hydrothermal unit, along strike to south and west of view shown in e. g) 1165 m RL, west wall showing brecciated hydrothermal unit with sericitic infill/alteration (ser) along fractures between clasts of carbonate-altered basalt (grey, cb). The laminated vein system terminates at the far end of the drive (south). Black circular object at centre of photo is a camera lens cap. h) 1195 m RL, North development face, showing termination of laminated vein system in sericitic carbonate breccia (hydrothermal unit).**

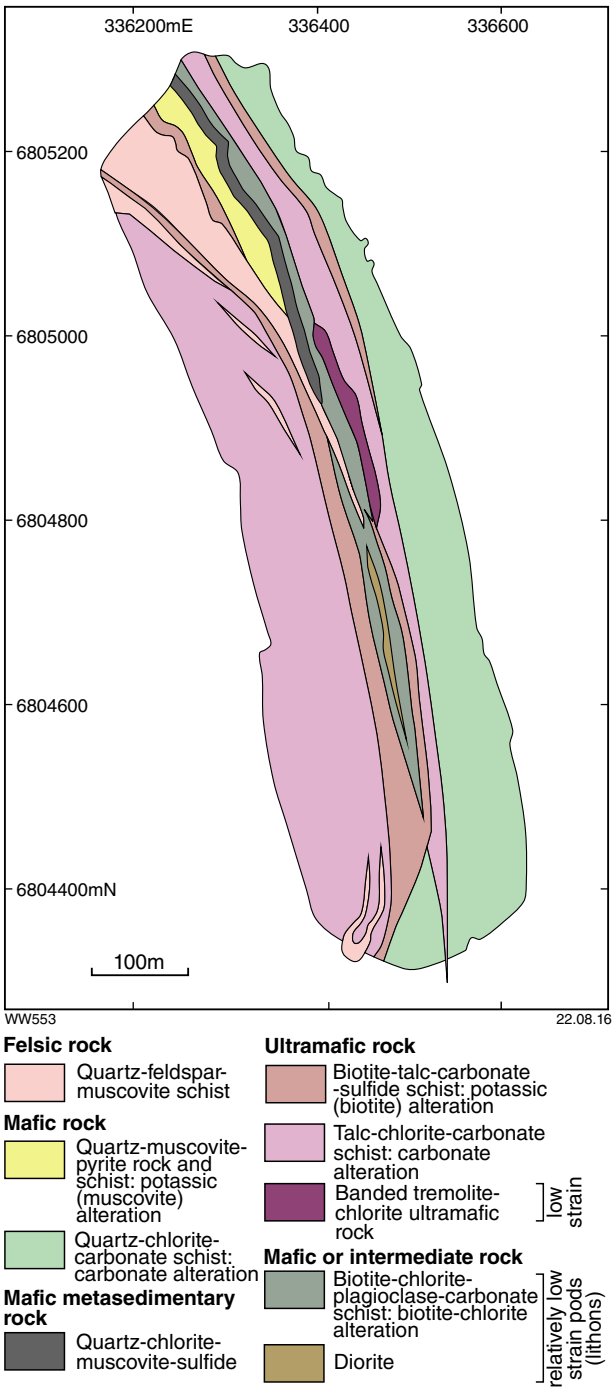

Figure 3.22. **Geological map of Harbour Lights deposit, Leonora, Eastern Goldfields Superterrane (Witt, unpublished data). Gold is closely associated with veins in biotite–talc–carbonate–sulfide schist (altered ultramafic rock), and these are at the contact between highly deformed schists and relatively low-strain and competent pods (lithons) of mafic volcanic and intermediate intrusive units.**

and within the Bardoc Tectonic Zone, gold mineralization is in laminated veins on the contact between thin dolerite (competent) and carbonaceous shale (incompetent) units; these units are themselves located within a broader, rheologically weak metasedimentary unit (Fig. 3.23).

Other rheological contacts that are not in major faults and shear zones also represent potential sites of mineralization at deposit scale; porphyry intrusions in ultramafic units are especially common examples. During regional shortening, the rheological contrast between these rock types generates localized shearing along the contacts, particularly those contacts at a high angle to the regional shortening direction. In some cases, gold mineralization has been deposited in these localized shears, and more commonly within zones of brittle fracture at the margins of the porphyry. Examples include the Bayleys, Barbara–Surprise, and Brilliant–Tindalls deposits in the Coolgardie district, Eastern Goldfields Superterrane (Knight et al., 1993), and the Paddys Flat deposits at Meekatharra in the Murchison Domain (Watkins and Hickman, 1990).

At Red Hill (50 000 oz Au) in the Kanowna gold camp, Eastern Goldfields Superterrane, gold mineralization is related to gently dipping extensional quartz veins in the Red Hill porphyry, which intruded coarse clastic sedimentary rocks of mixed provenance. The quartz veins that constitute this orebody are concentrated at the western end of the intrusion where the rheologically strong porphyry intrusion is relatively thin and cut by subvertical north-northwesterly striking structures represented by zones of foliation (Davis et al., 2010).

Other intrusions that host gold, at least partly resulting from the rheological contrast with enclosing country rock, are trondhjemites, quartz monzonites, and monzonites or syenites at Tarmoola (Duuring et al., 2004; Blewett and Czarnota, 2007), Jupiter (Duuring et al., 2000), Wallaby (Salier et al., 2004), and several deposits (Yerilla, Porphyry, Butcher Well, Tin Dog Flats) in the Kurnalpi Terrane of the Eastern Goldfields Superterrane (Roberts et al., 2004). At the largest of these deposits (Wallaby), the volume of relatively competent rocks that now host gold mineralization was increased beyond the limits of syenite intrusions by intrusion-related actinolite–magnetite–epidote–calcite (ferruginous) alteration (Salier et al., 2004). Similar hydrothermally induced rheological strengthening of country rocks probably also occurred at the Yerilla, Porphyry, Butcher Well, and Tin Dog Flats deposits.

Deposits of the Randalls gold camp (see Targeting Criterion 3.6) clearly demonstrate the role of rheological heterogeneity in gold deposition within a sedimentary basin. Less obvious lithological variations within sedimentary sequences can also provide rheological gradients capable of influencing the location of gold mineralization, as exemplified by New Holland and other gold deposits of the 'Glasgow Lass trend' in the Agnew district, Eastern Goldfields Superterrane. At New Holland, gold is associated with shear veins and shallow-dipping extension veins in and around brittle–ductile shear zones formed at the contacts between fine-grained and medium- to coarse-grained metasedimentary rocks (Ackroyd et al., 2001). Quartz veins and gold mineralization are concentrated in relatively thin, medium- to very coarse-grained sandstone units, which were rheologically stronger than the enclosing fine-grained sandstone and siltstone. A critical factor at New Holland may have been pervasive pre-mineralization hydrothermal alteration of the coarse-grained sandstone unit resulting in the destruction of metamorphic biotite and the formation of a quartz–albite–microcline assemblage of greater rheological strength (Ackroyd et al., 2001). This is certainly the case for the southern lode at Navajo Chief in the Binduli camp, Eastern Goldfields Superterrane, where gold mineralization is confined to sedimentary units that have been altered to a relatively competent albite–ankerite–pyrite assemblage (WK Witt, unpublished data). In contrast to New Holland, it is the finer-grained sedimentary units that were more prone to this hydrothermal alteration at Navajo Chief (Fig. 3.24). At Navajo Chief, it is not clear whether the albite–ankerite–pyrite (sodic) alteration was earlier than, or synchronous with gold mineralization. Even if the sodic alteration did not significantly pre-date gold mineralization, as at New Holland, progressive sodic alteration of wallrocks by gold ore fluid can still be an effective mechanism for increasing the relative rheological strength of the host rocks, leading to repeated fracturing and further influx of gold-bearing fluids (see also Karari; Witt et al., 2009). Gold deposition could take place through fluid immiscibility (phase separation) or reaction of the fluid with Fe-bearing carbonate minerals in this situation. Intense carbonate alteration can also play a role in enhancing the rheological properties of potential host rocks, particularly ultramafic rocks, as exemplified by Mulgarrie (Davis et al., 2001) and Robinsons (see Targeting Criterion 3.4), both of which are in the Kanowna camp of the Eastern Goldfields Superterrane.

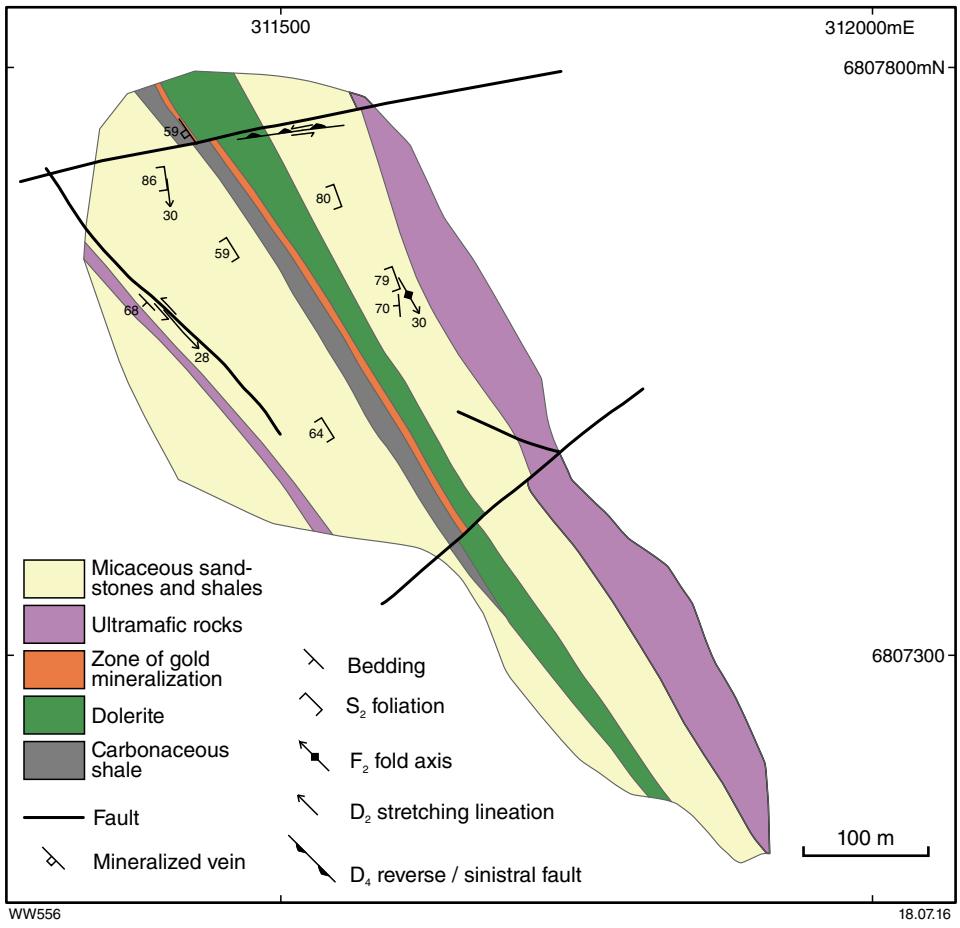

Figure 3.23. Geological map of the Yunndaga openpit, Menzies area, Eastern Goldfields Superterrane, showing localization of gold mineralization at the contact between rheologically strong dolerite and weak metasedimentary rocks (from Morey et al., 2007b)

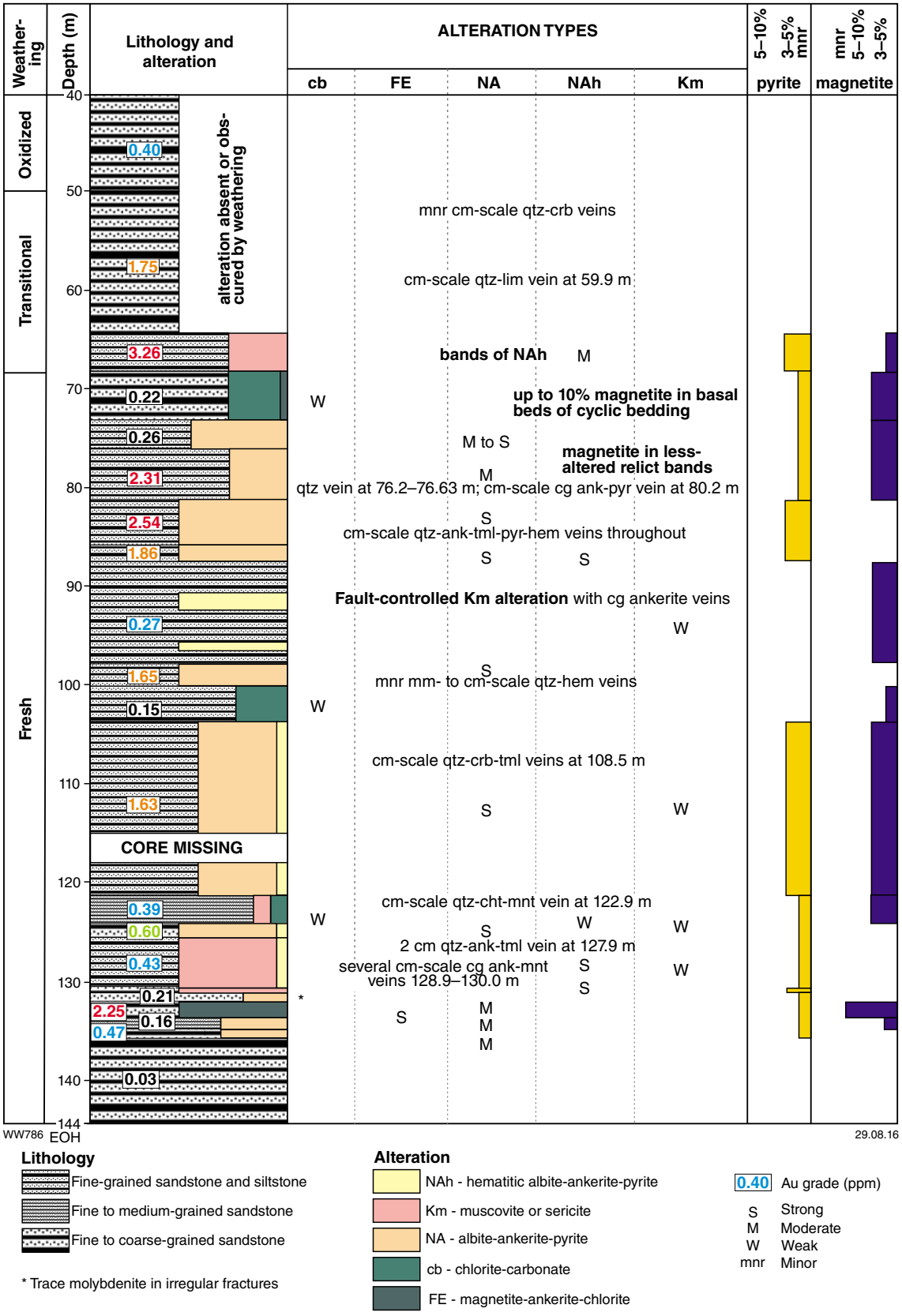

Figure 3.24. **Strip log, hole PBND008, Binduli gold camp, Eastern Goldfields Superterrane (Witt, unpublished data). Note the association of higher gold grades with sodic alteration (NA) in finer-grained metasedimentary units. Coarse-grained metasedimentary units beneath (and probably above) the NA-altered fine-grained metasediments show no evidence of hydrothermal alteration. ank, ankerite; cg, coarse-grained; cht, chlorite; crb, carbonate; hem, hematite; lim, limonite; mnr, minor; mnt, magnetite; pyr, pyrite; qtz, quartz; tml, tourmaline.**

Targeting Criterion 3.6: Structural–stratigraphic intersections

A diverse range of structural–stratigraphic relationships accounts for most gold deposits in the Yilgarn Craton. As seen in the Wiluna gold camp, the intersection of fault systems with steeply dipping volcanic or intrusive contacts (some occupied by quartz reefs) can result in steeply plunging ore shoots (see Targeting Criterion 3.2). Mineralization is preferentially developed where faults cut relatively competent lithological units (see Targeting Criterion 3.5). At Norseman, ore shoots have developed where the 'shear–link' fault system intersects relatively competent gabbro or ultramafic dykes (see Targeting Criterion 3.2). In this section, however, the emphasis is on the role of oblique faults in the isolation or partial isolation of competent units within broader units or sequences of rheologically weak rock.

Groves et al. (2000) recognized a particular structural class of gold deposit in which the most competent lithologic units are structurally isolated within a broader matrix of less-competent rock. They included the Mount Charlotte, Paddington, and Three Mile Hill gold deposits, all in the Eastern Goldfields Superterrane, in this class (Fig. 3.25). Groves et al. (2000) suggested that, in the Yilgarn Craton, the most common setting for this type of gold deposit is where northwest-striking greenstones are offset by late north-northeasterly or northeasterly striking faults. Enterprise, hosted by the Enterprise Dolerite in the Ora Banda area (Tripp and Vearncombe, 2004), and Centenary, hosted by the Mount Pickering Dolerite in the Darlot area (Krcmarov et al., 2000; Gardiner et al., 2001), may be further examples from the Eastern Goldfields Superterrane of this type of deposit. Other examples abound in the Murchison Domain (e.g. Hill 50 at Mount Magnet, Tuckanarra, and Tuckabianna; Thompson et al., 1990; Watkins and Hickman, 1990). The competent lithology in these deposits is most commonly dolerite (e.g. Mount Charlotte, Three Mile Hill, Paddington, Enterprise in the Eastern Goldfields Superterrane; Great Fingall and Day Dawn in the Murchison Domain) or magnetite-bearing chert and banded iron-formation (e.g. Randalls and Mount Morgan in the Eastern Goldfields Superterrane; Nevoria in the Southern Cross Domain; Mount Magnet and Galtee Moore in the Murchison Domain), but porphyry intrusions and massive felsic volcanic units are also effective host rocks in some cases (e.g. Orient Well at Kookynie and Mirror Magic in the Mount Monger camp of the Eastern Goldfields Superterrane; WK Witt, unpublished data; Roberts et al., 2004).

At Randalls, mineralization was generated by brittle fracture (producing quartz vein arrays) in rheologically strong banded iron-formation within a matrix of weaker metasedimentary rocks, particularly where blocks of iron-formation (especially thickened fold hinges) have been isolated by oblique faulting (Fig. 3.26; Newton et al., 1998; Roberts et al., 2004). Where differentiated or layered mafic(–ultramafic) intrusions take the role of the competent unit, the fractionated (in some cases granophyric) quartz dolerite unit is preferentially mineralized (e.g. Mount Charlotte). This preferential mineralization appears to be related to the rheological properties of quartz dolerite because auriferous quartz veins are preferentially developed or quartz reefs are thicker in these units (e.g. Mount Charlotte, Ridley and Mengler, 2000; Golden Crown, Hicks, 1990).

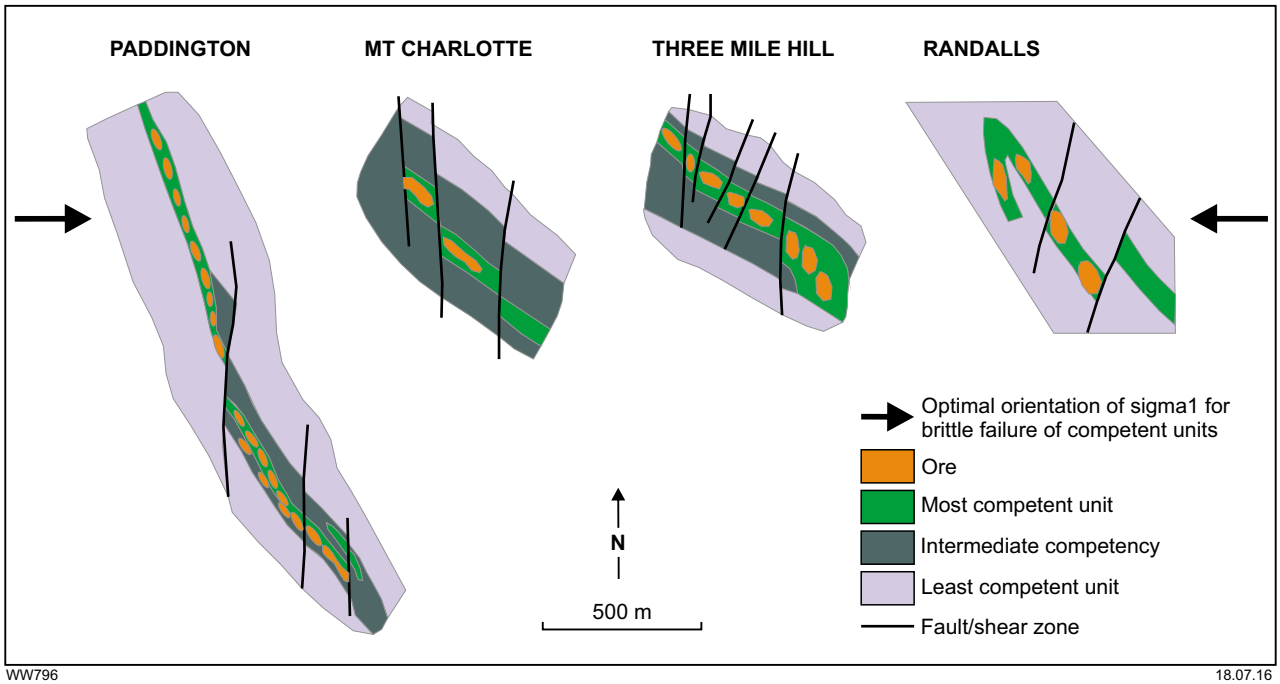

Figure 3.25. Schematic maps of gold deposits formed in rheologically competent units that have been offset and partially or completely isolated by oblique faults (after Groves et al., 2000)

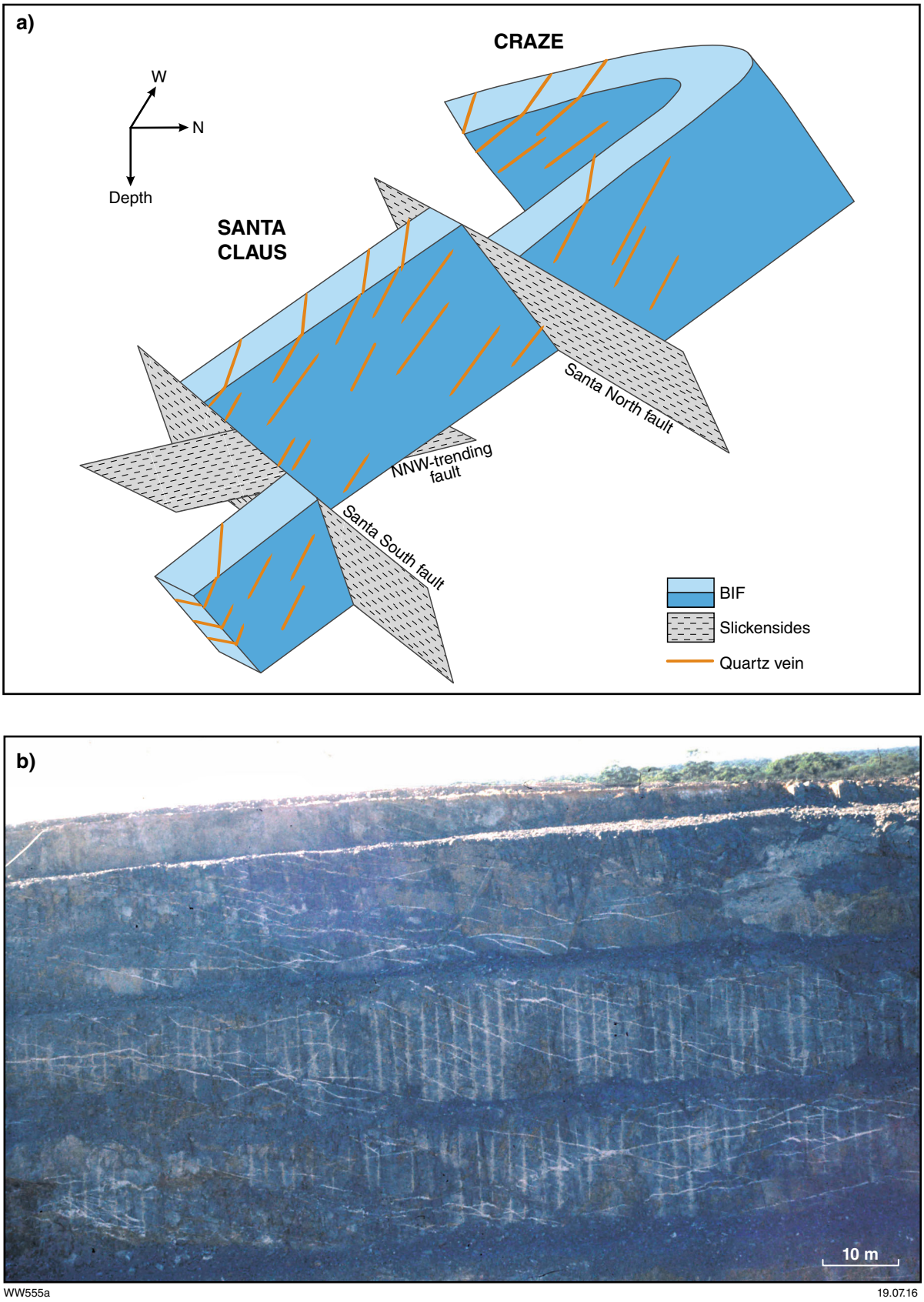

Figure 3.26. **Randalls gold deposits, Eastern Goldfields Superterrane. a) Schematic diagram showing gold-bearing veins and vein stockworks formed in isolated blocks of competent banded iron-formation within weaker metasedimentary rocks (not shown; after Newton et al., 1998). The isolated iron-formation blocks include fold hinges and fault-bound offsets. b) Photo of mineralized quartz vein stockwork hosted by iron-formation at Randalls.**

The Fe-rich composition of fractionated dolerite units is an important depositional control on gold mineralization, but ore fluid is brought into contact with the Fe-rich wallrocks only by preferential fracturing of the more competent quartz dolerite unit.

Under stress, over-pressured fluids exceed supralithostatic pressures (plus tensile strength of the host rock), leading to selective fracture and the formation of vein arrays in isolated or semi-isolated blocks of competent rock (Fig. 3.25). Shortening that is taken up by formation of schists in surrounding rheologically weak units is accommodated by fracturing and dilation in the rheologically competent unit. In some deposits, mineralized veins or vein stockworks develop in the interior of the competent block but, more commonly, they are concentrated at the margins of the block, adjacent to bounding (off-setting) faults (e.g. Randalls, Newton et al., 1998). These orebodies are pipe-like, and the plunge of the mineralized pipe is defined by the intersection of the receptive (competent) unit with the bounding faults (Fig. 3.27). Networks of fractures in some deposits are distal from regional faults and there is an absence of gold-related hydrothermal alteration in the bounding oblique faults. These observations have been interpreted (Ridley and Mengler, 2000) to imply that vertical transport of ore fluid from depth was accommodated by progressive fracturing of the competent host rock (i.e. the fluid conduit was generated by formation of the mineralized fracture network itself).

At Mount Charlotte, ore is largely confined to Unit 8 of the Golden Mile Dolerite, which is Fe-rich as well as rheologically strong (Fig. 3.28). The Fe-rich composition of fractionated dolerite host rocks is an additional controlling factor on mineralization because of the chemical reactivity of the rock with ore fluid (Phillips and Groves, 1983). A similar combined rheological–chemical reactivity model can probably be applied to some deposits hosted by banded iron-formation in the Southern Cross (e.g. Nevoria, Arnold et al., 1995) and Murchison (Mount Magnet, Thompson et al., 1990, Wilson, 1990; Galtee More, Bromley, 1990) Domains.

Where the bounding faults of these deposits are most effective, they dip steeply and strike approximately normal to the regional shortening direction (Fig. 3.25). As argued by Sibson (1990) and Ridley (1993), where the rheological contacts are normal to the principal axis of shortening, movement on the bounding faults during regional deformation is suppressed. The juxtaposition of rheologically strong and weak rocks across the immobile bounding fault maximizes the potential for fracture at the margins of the competent body, resulting in localized extension through fracture and vein formation (e.g. Ridley and Mengler, 2000). Mineralized quartz veins formed by this mechanism are most commonly gently dipping to subhorizontal, inferring vertical extension (e.g. Paddington; Witt, 1992a, Morey, 2007a). Examples of steep veins striking in the direction of the principal axis of shortening, thus implying horizontal extension, have been

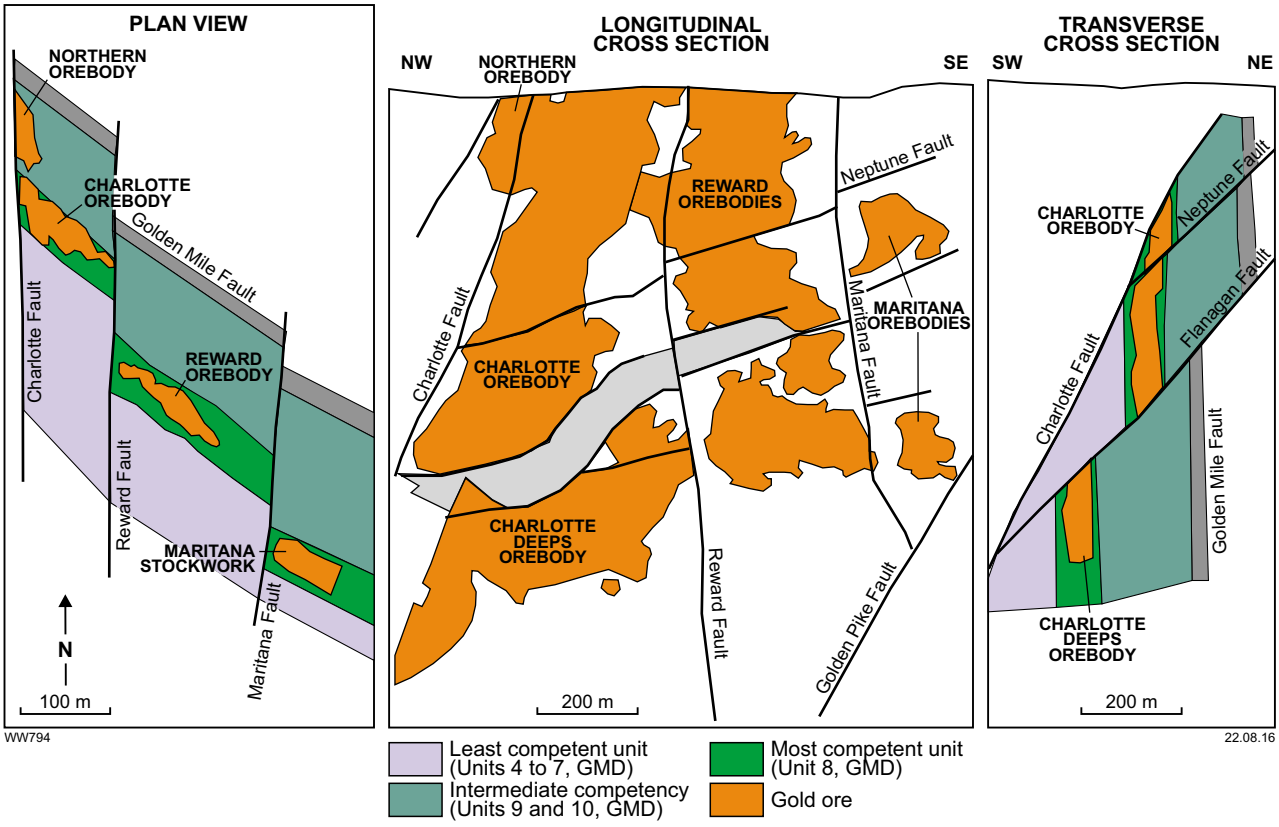

Figure 3.27. Plan view and transverse and longitudinal cross sections, Mount Charlotte gold deposit, Kalgoorlie, Eastern Goldfields Superterrane (from Ridley and Mengler, 2000), illustrating pipe-like form of orebodies controlled by intersections of oblique faults with competent Unit 8 of the Golden Mile Dolerite (GMD)

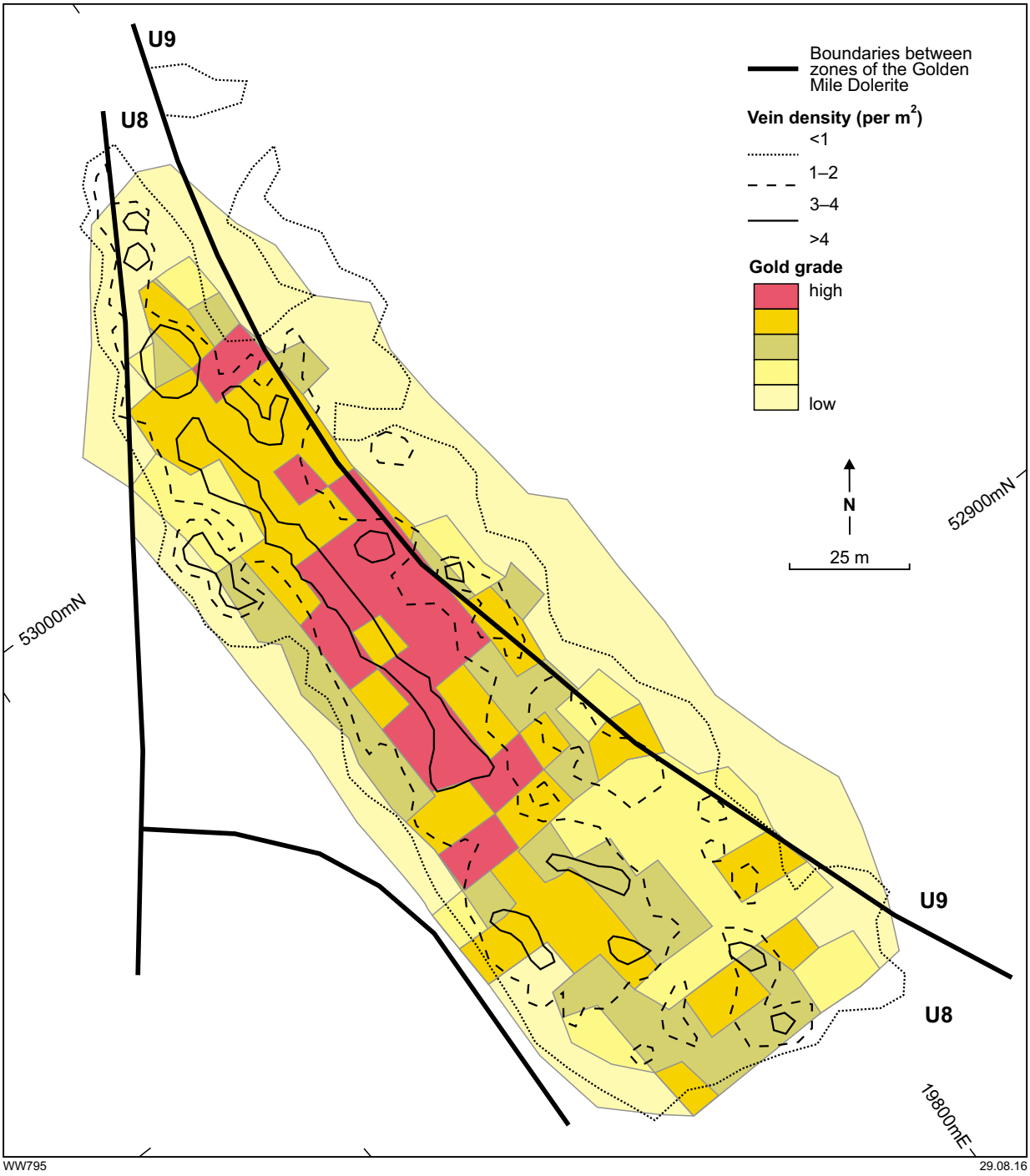

Figure 3.28. **Charlotte Deeps orebody, Mount Charlotte, 29 level, showing gold grade in 10 × 10 × 8 m ore blocks and density of quartz veins, illustrating how quartz veins and gold grade are concentrated in Fe-rich Unit 8 (U8) of the Golden Mile Dolerite (from Ridley and Mengler, 2000)**

reported from the Hampton–Boulder ore deposit at New Celebration on the Boulder–Lefroy Fault, at Hawkins Find on the Zuleika Fault (Witt, 1992c, 1993a,b), and at Castle Hill on the Kunanalling Fault (Warren et al., 2015), all in the Eastern Goldfields Superterrane. Other examples, such as Mount Charlotte and Randalls, present more complex vein arrays that may have formed conjugate fractures related to the prevailing shortening direction. It should be noted that in some deposits of this type, some vein sets may exploit suitably oriented fractures formed before the gold mineralization event (Ridley and Mengler, 2000). In these cases, the orientation of the veins does not provide information about the orientation of stress components at the time of mineralization.

Targeting Criterion 3.7: Folds and boudins

Fold hinges control the location and geometry of orebodies, and high-grade lodes within them, in a high proportion of Yilgarn gold deposits. There are two main classes of such gold deposits (Fig. 3.29):

- Class 1, in which mineralized veins or lodes formed either before or during an early stage of progressive regional shortening and/or simple shear, and have been folded, or otherwise deformed, by the superimposed deformation
- Class 2, in which mineralized veins or lodes formed after or at a late stage of folding.

In class 1 deposits, mineralized stratabound units remain broadly conformable with folded planar elements of the host rock sequence, whereas highly discordant lodes are rotated towards the axial plane orientation. Mineralized veins that formed late in the folding event or post-date folding can form in a wide range of orientations and geometries. These may be conformable (as in saddle reefs) or discordant with respect to folded planar elements, but they are commonly localized in the fold hinges as shear veins parallel to the axial plane of the fold, or more irregular stockworks (Fig. 3.29). Another example of a class 2 deposit entails the dilational or contractional jogs that may form where layer-parallel faults encounter asymmetric folds (e.g. Transvaal and Twin Peaks, see Targeting Criterion 3.2 and below).

In the Yilgarn Craton, gold-mineralized veins that have been folded as part of the deformation history of the enclosing rocks (class 1, above) include Sons of Gwalia and most shear-hosted deposits in the Southern Cross district, including Marvel Loch. These deposits generally contain ore shoots with a very consistent plunge and azimuth, reflecting the trajectory of folded ore veins. Where folding is related to strong ductile shearing (intrafolial folds), the limbs of folded ore veins or layers are likely to be boudinaged (Fig. 3.29). In this case, some shoots are controlled by the plunge and azimuth of the boudins, which are normally colinear with fold axes. In class 2 deposits, the ore shoot trajectory is less consistent and depends on the relationship between the newly formed mineralized structures and the geometry of the pre-existing fold (Fig. 3.29).

The Sons of Gwalia orebody (8 Moz Au) in the Leonora camp of the Eastern Goldfields Superterrane, is about 700 m long and 200 m wide, but extends to more than 2 km below the surface with a consistent down-plunge extent of >3 km. For mining purposes, it has been subdivided into the Main Lode, South Gwalia Series, and West Lode orebodies (Fig. 3.30). The overall form of the orebody resembles that of a southeast-plunging antiform in which the Main Lode constitutes the east limb, the South Gwalia Series is in the transposed fold hinge, and the West Lode is within the sheared and attenuated western limb. There is controversy over the timing and origin of the Sons of Gwalia deposit, but general agreement that the orebody and its component ore shoots plunge 39° towards 119° and are colinear with the plunge of minor fold axes defined

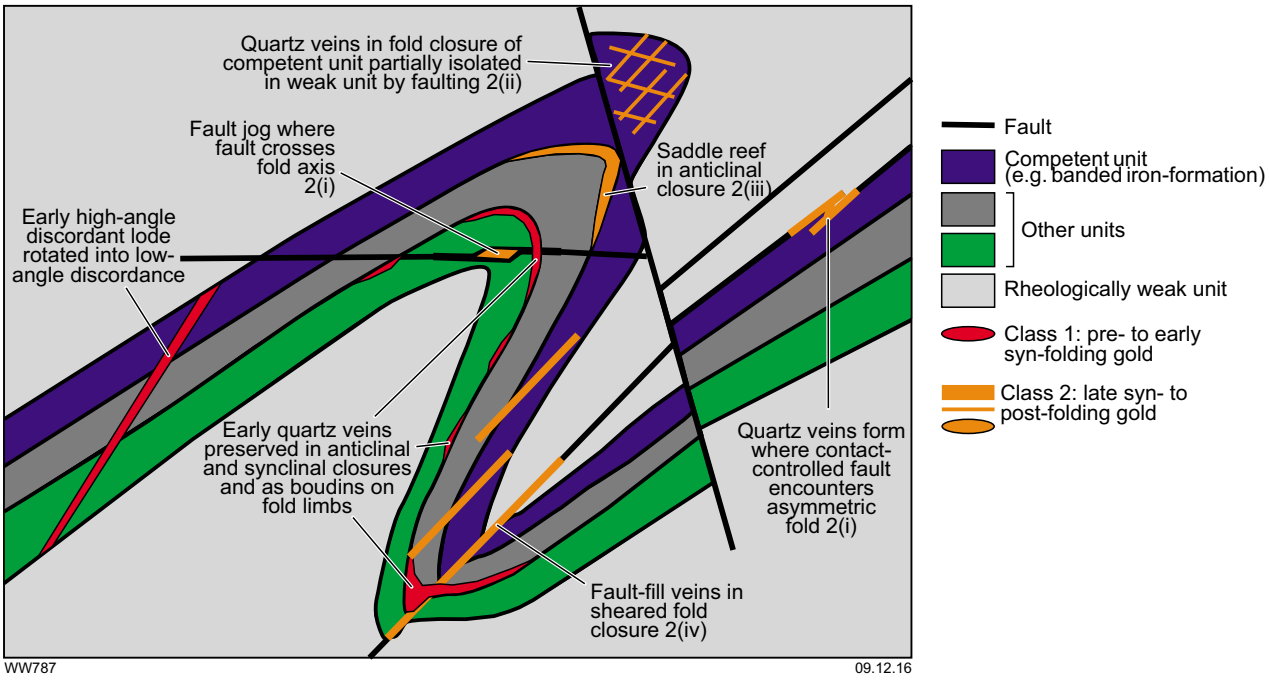

Figure 3.29. Schematic diagram illustrating the range of relationships of auriferous veins to fold geometry in deposits structurally related to folds and folding. Examples include: Class 1, Sons of Gwalia, Marvel Loch; Class 2(i), Transvaal, Oroya Shoot; Class 2(ii), Randalls, Copperhead, Golden Pig, and Cornishman.

by deformed gold-bearing quartz veins (Tattum, 1953; Finucane, 1965; Smith, 2000; Williams et al., 1989; Witt, 2001; Baggot, 2006; Jones, 2014). Williams et al. (1989), Blewett and Czarnota (2007), and Jones (2014) interpreted the fold hinges to be colinear with the stretching direction, implying that the folds are sheath folds, whereas other investigators interpreted the pervasive linear fabric as an intersection lineation. These diametrically opposed interpretations imply movement sense and regional stress orientations that are incompatible with one another. There is further controversy regarding the timing of the deposit. Some authors have interpreted the ore-bearing veins to significantly pre-date the enveloping deformation fabric (Williams et al., 1989; Witt, 2001; Jones, 2014) and others have interpreted the ore to have formed synchronously with ductile deformation in an enveloping shear zone and to have been folded during progressive strain accumulation (Smith, 2000; Baggot, 2006). Despite these competing theories, the role of fold hinges in defining the plunge of the orebody and ore shoots within Main Lode, the South Gwalia Series and West Lode (Figs 3.31 and 3.32) is not disputed.

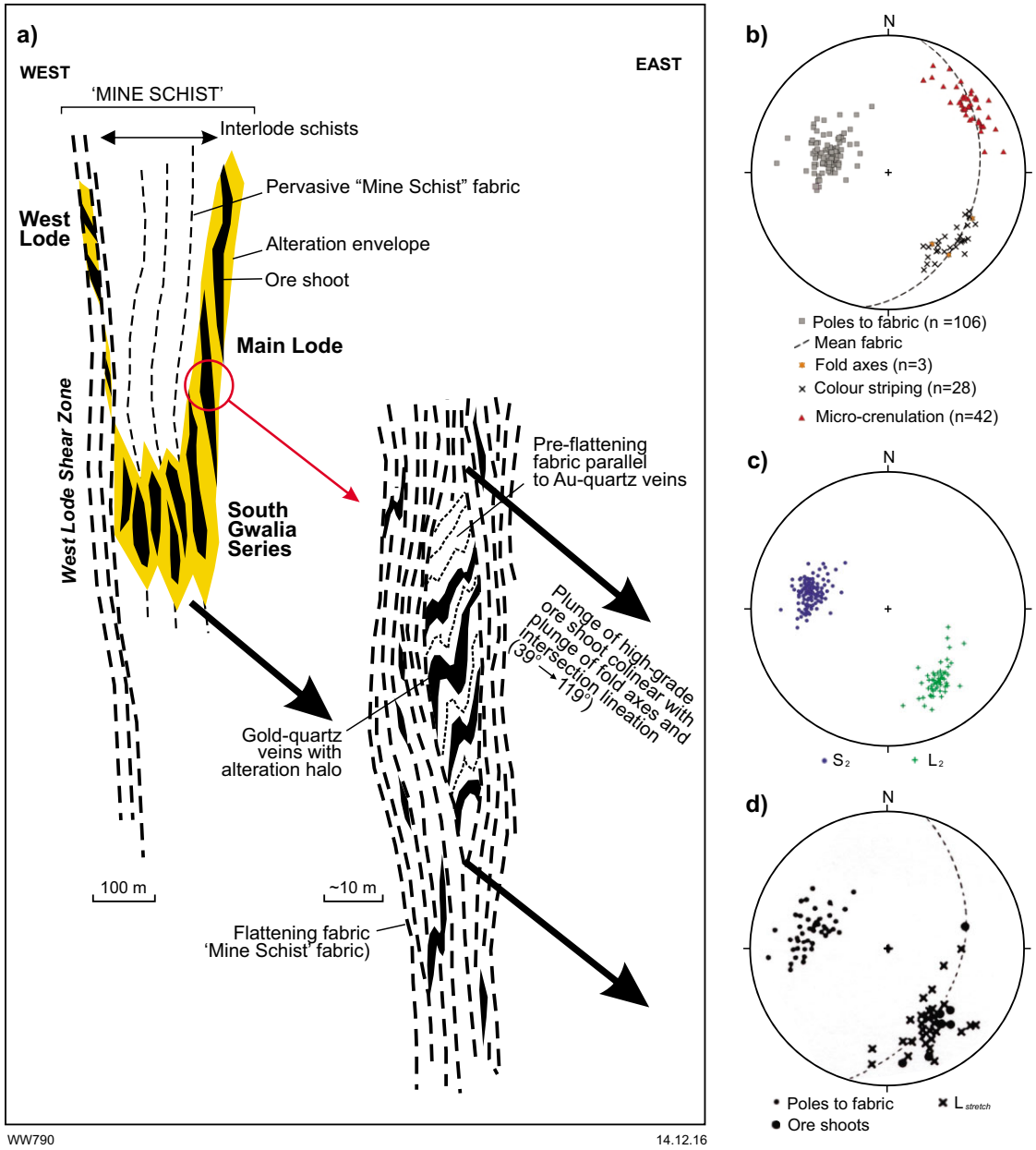

Figure 3.30. **Schematic diagram a) illustrating the geometric relationships among component lodes (Main, South Gwalia Series, West) within the Sons of Gwalia gold deposit, Leonora area, Eastern Goldfields Superterrane. b) to d) Stereographic projections of key structural elements noted by several investigators at Sons of Gwalia (provided by M Baggot). b) Baggot (2006), c) Smith (2000), d) Williams et al. (1989). 'Colour striping' in b) refers to an intersection lineation that is colinear with fold axes; micro-crenulations are approximately normal to plunge of fold axes. Fabric in b) and d) is equivalent to S2 in c) and is the main flattening fabric (pervasive 'Mine Schist' fabric in a). L2 in c) is equivalent to fold axes. Lstretch in d) is viewed by other workers as an intersection lineation colinear with fold axes.**

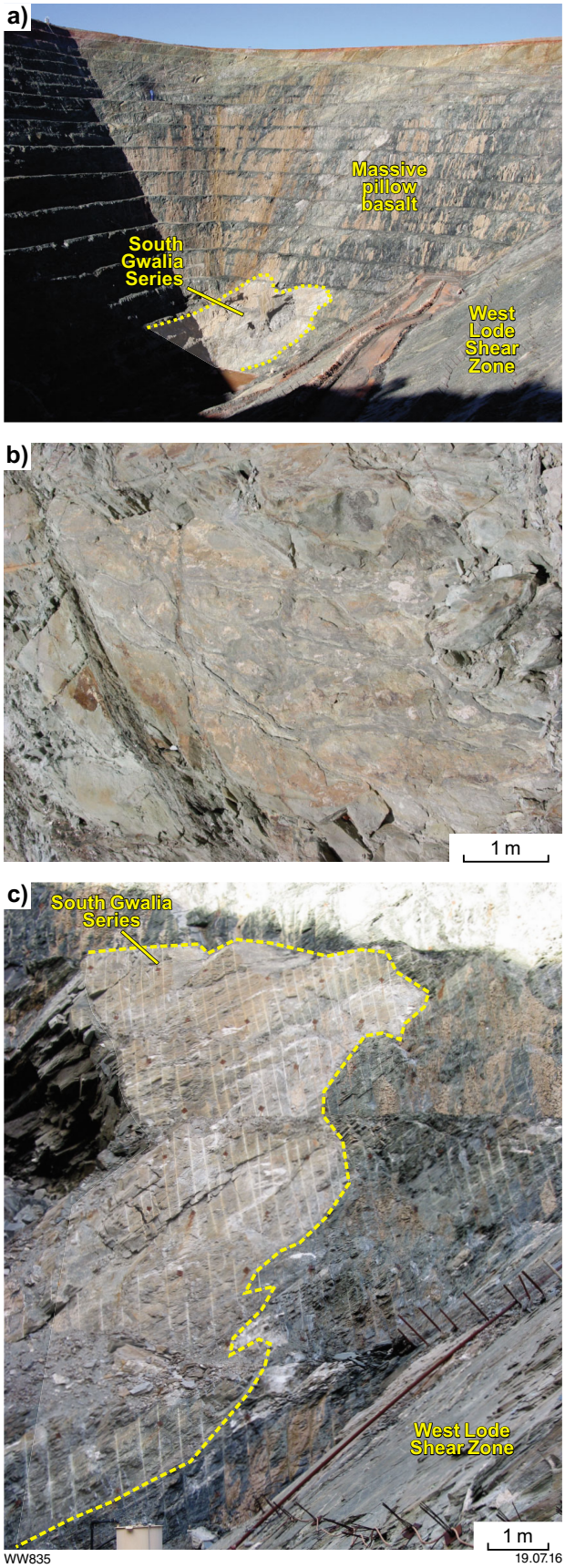

Similar controls are evident in shear-hosted deposits such as Marvel Loch in the Southern Cross district (Bloem et al., 1994; WK Witt, unpublished data). The Marvel Loch deposit comprises several orebodies (e.g. Sherwood, Contact, Undaunted, Exhibition, Boulder, New Lode; Fig. 3.33) that are hosted within a broad zone of shearing in the southern neck of a district-scale greenstone boudin (Targeting Criterion 2.13, Part 2 of this Atlas). High-grade quartz–diopside(–calcite, amphibole)–sulfide veins are folded and boudinaged within broad zones of ductile shearing and hydrothermal alteration. The axial planes of these intrafolial folds are parallel to the dominant shear fabric. Transverse and longitudinal cross sections through the Marvel Loch deposit illustrate the general form of the lodes, including the plunge, which is about 70° south (Fig. 3.33b–e) and colinear with the plunge of fold axes, boudins, mullions, and intersection lineations exposed in the openpit (Fig. 3.34).

At both Sons of Gwalia and Marvel Loch, the plunge and azimuth of lodes are very consistent within the deposit, and very persistent within individual ore shoots. These observations argue against the suggestion that sheath folds may control the location and geometry of the ore shoots (e.g. at Sons of Gwalia) because, in the case of sheath folds, a range of fold axis orientations should converge on the stretching direction (Alsop and Holdsworth, 1999). Other deposits, however, may well be controlled by sheath folds. For example, ore shoots in the Menzies district display a more variable plunge, from 20° to 40° south (Woodward, 1906), and are approximately colinear with stretching lineations (Witt, 1992a; Blewett and Czarnota, 2007; Morey et al., 2007a). Most asymmetric to symmetric fold axes in the Menzies area plunge about 20° south but the plunge is variable and includes some steeper examples (Morey et al., 2007a). The variation in fold plunges and colinearity of stretching lineations with the dominant fold plunge suggest the formation of sheath folds under extreme ductile deformation. These folds are a likely control on the plunge orientations of deposits and ore shoots in the Menzies district, including the Yunndaga deposit (see Targeting Criterion 3.5).

Figure 3.31. **Photos of openpit exposures, Sons of Gwalia mine, Leonora area, Eastern Goldfields Superterrane. a) View towards south wall of pit showing South Gwalia Series orebody as a domain of lighter-coloured hydrothermal alteration (outlined by dotted line) within chloritic schist. Despite the extremely high-strain fabric in the South Gwalia Series, massive pillow basalt is exposed in the south wall of the pit on the benches above. West wall of pit formed by West Lode Shear Zone. b) Closer view of massive pillow basalt exposed in benches above the South Gwalia Series orebody. c) Closer view of South Gwalia Series orebody shown in a). White quartz veins in the axial plane of the fold hinge are generally barren or low grade; high-grade veins in this view are indistinguishable from the enveloping sericite–ankerite–pyrite alteration.**

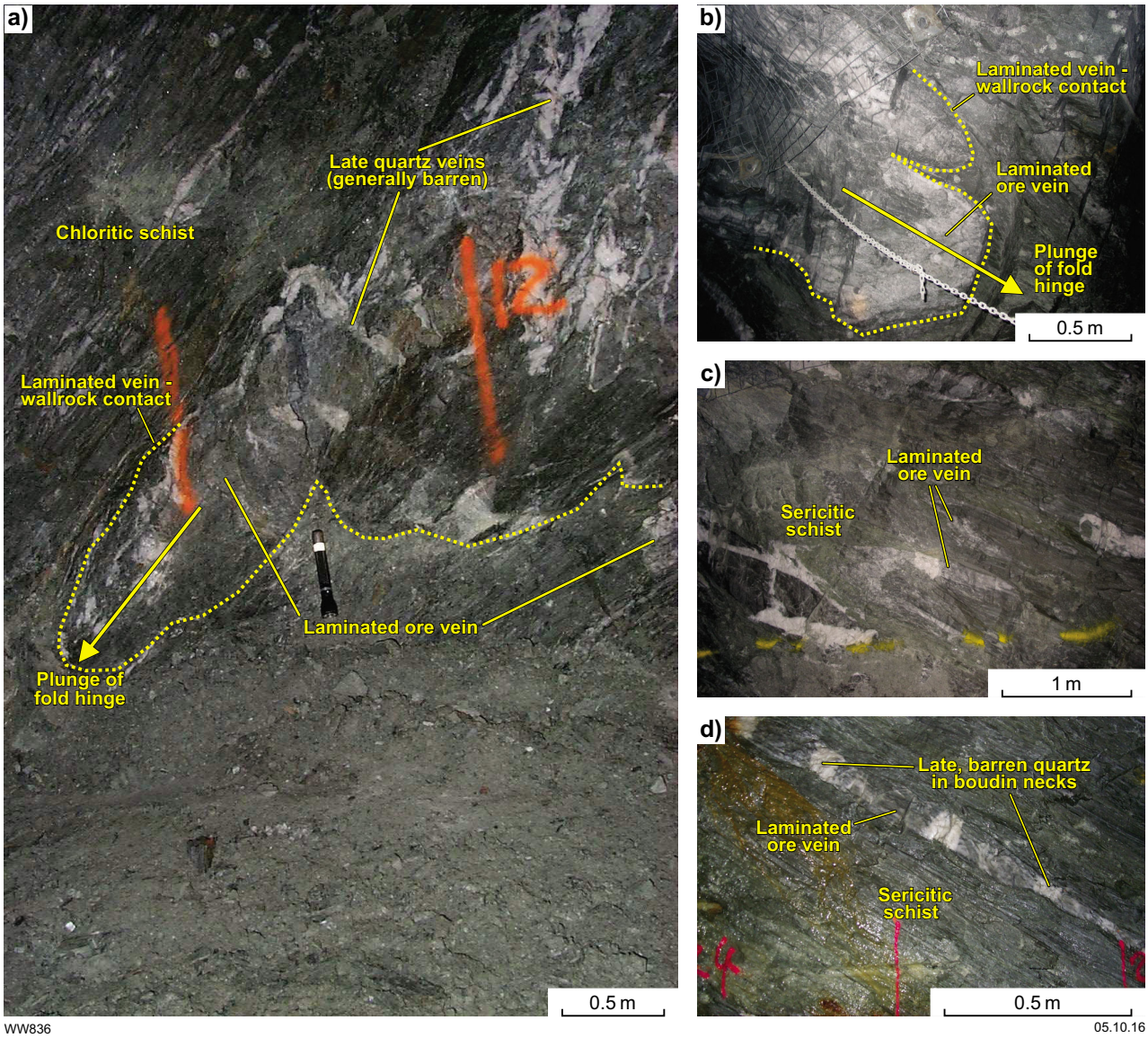

Figure 3.32. **Photos from Sons of Gwalia underground mine, Main Lode. a) Plunging fold defined by laminated ore vein enclosed in chloritic schist; the folded vein is overprinted by late-stage, largely barren white quartz. b) Folded ore vein and enclosing chloritic to sericitic schist. c) Folded ore veins in sericitic schist; lower grade to barren white quartz overprint grey ore veins and wallrock. d) Boudinaged laminated ore vein in sericitic schist; late-stage barren white quartz has been deposited in boudin necks.**

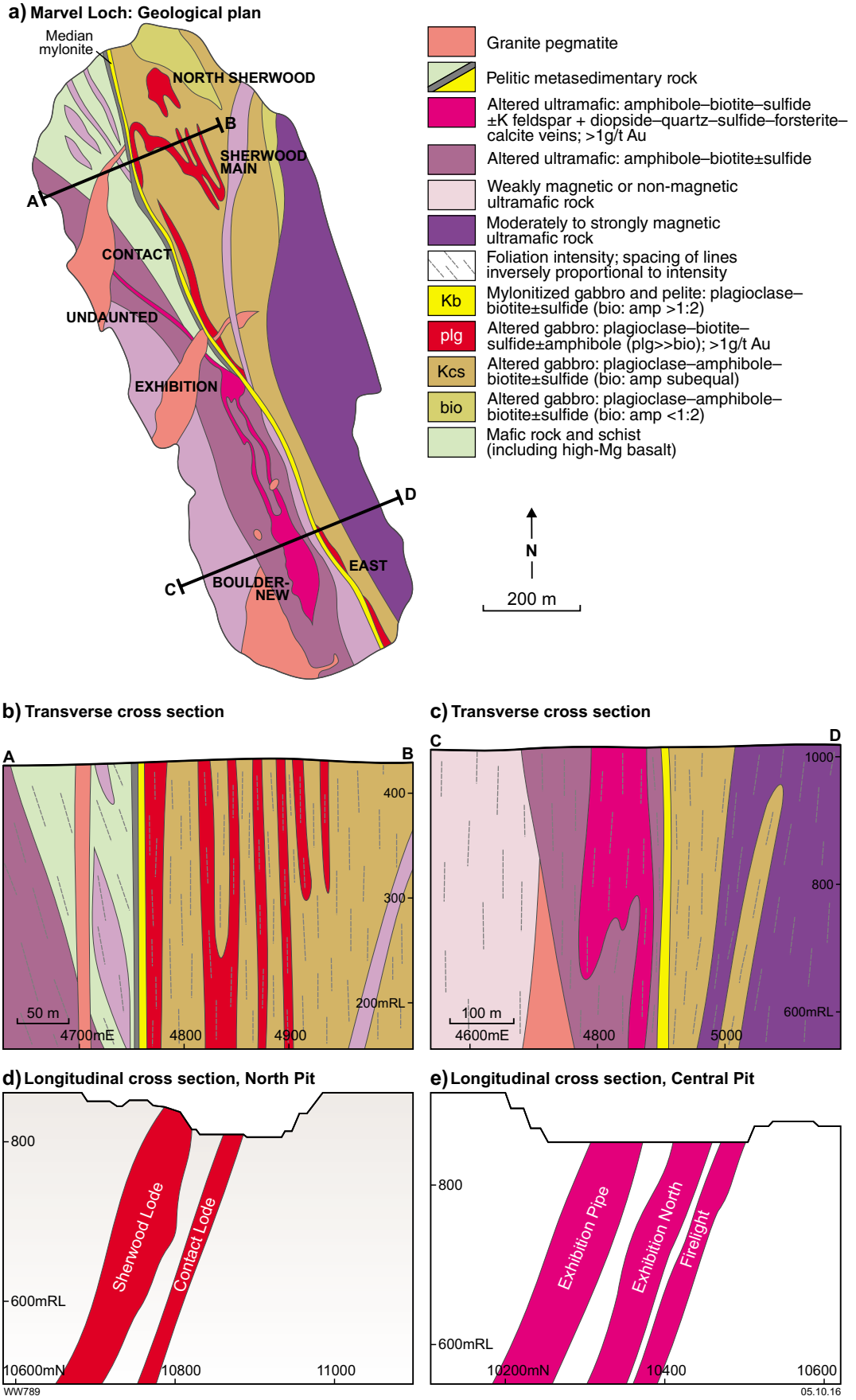

Figure 3.33. **Marvel Loch gold deposit, Southern Cross Domain of the Youanmi Terrane. a) openpit plan; b) and c) transverse cross sections A–B and C–D, respectively; d) and e) longitudinal cross sections of north and central pits, respectively.**

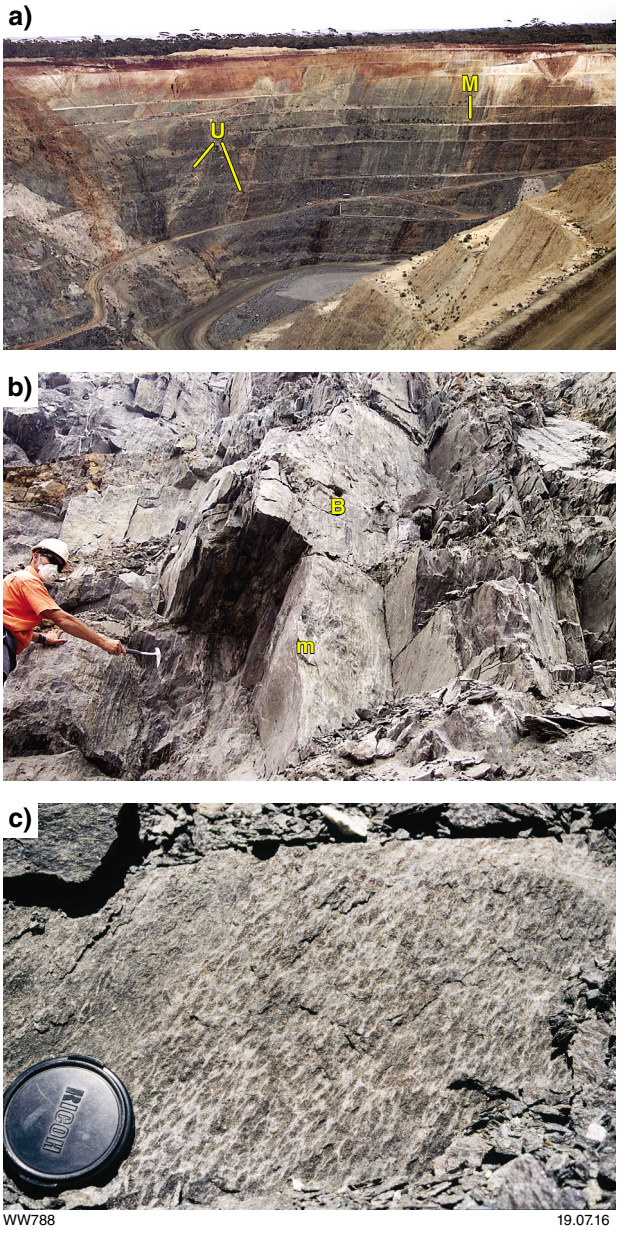

Figure 3.34. **Photos from Marvel Loch openpit. a) General view, looking northwest towards north and northwest walls of Undaunted pit showing boudins of ultramafic rock (U, pale grey) and mylonitic shear zone (M). b) Looking south-southwest at south wall of Exhibition pit illustrating south-plunging boudins (B) and mullions (m) in ultramafic unit. c) Steep south-plunging mineral lineation defined by aggregates of biotite, Exhibition pit.**

Deposits in which mineralized veins or lodes formed after, or at a late stage of, folding (class 2 above) are assigned to the following four subclasses.

- Subclass (i) deposits formed in jogs where a layer-parallel mineralized fault encounters a fold axis (e.g. Transvaal, Southern Cross district; Oroya shoot, Kalgoorlie) or an oblique fault crosses a fold axis.
- Subclass (ii) deposits formed in thickened fold hinges, typically defined by rheologically strong host rocks that have been isolated or partially isolated by folding and post-folding faults (e.g. Randalls, Copperhead, Golden Pig, Cornishman).
- Subclass (iii) deposits are bedding-conformable vein deposits formed in anticlinal hinges (i.e. saddle reefs).
- Subclass (iv) deposits are mineralized veins or shears with axial plane orientations and are formed in the attenuated limbs of folds and/or within fold closures.

The following paragraphs describe some examples from the Yilgarn Craton of the first and second sub-classes described above. There are few examples of subclasses (iii) and (iv) to draw upon for this discussion.

The association of gold mineralization with fault jogs created where a layer-parallel fault encounters a fold axis is exemplified by the Transvaal deposit in the Southern Cross district (Hagemann et al., 1998). Transvaal is the northernmost and best-endowed of several gold mines developed on two subparallel north-northwesterly striking, steeply east-dipping shears in the area (Fig. 3.35a). Most of these are openpit mines, but the Transvaal deposit has also been developed as an underground mine. The eastern mineralized shear is on or close to the contact between ultramafic and metasedimentary rocks south of the asymmetric fold. The western mineralized shear is within the metasedimentary unit, but may be the southern propagation of a shear zone on the same lithological contact, north of the asymmetric fold (Fig. 3.35a). To the south, the western mineralized shear appears to be localized on the contact between a thin internal psammitic unit and enveloping pelites. RD James (1995, unpublished internal company reports for Sons of Gwalia) reported, but did not describe in detail, a lineation in the pelitic metasedimentary unit that plunges 60° to 70° south. If this is an intersection lineation, similar to that observed at Marvel Loch, the steep plunge of the lineation is consistent with the mainly sinistral strike-slip displacement on the mineralized shear zones, as described by Keats (1991). As at Marvel Loch, the plunge of ore shoots in the Transvaal orebody (Fig. 3.36a) is colinear with the dominant observed linear fabric. Ultimately, this relationship may reflect thickened boudins of mineralized quartz-rich veins and folded gold-bearing veins within the mineralized shear. Ore shoots in the metasediment-hosted Mercury and Sunbeam deposits also have a prominent, steep south-plunging component, but the plunge orientations in these deposits vary greatly depending on the scale of observation (Fig. 3.36b,c), suggesting that there are more complex structural controls (not yet recognized) on ore shoot orientation.

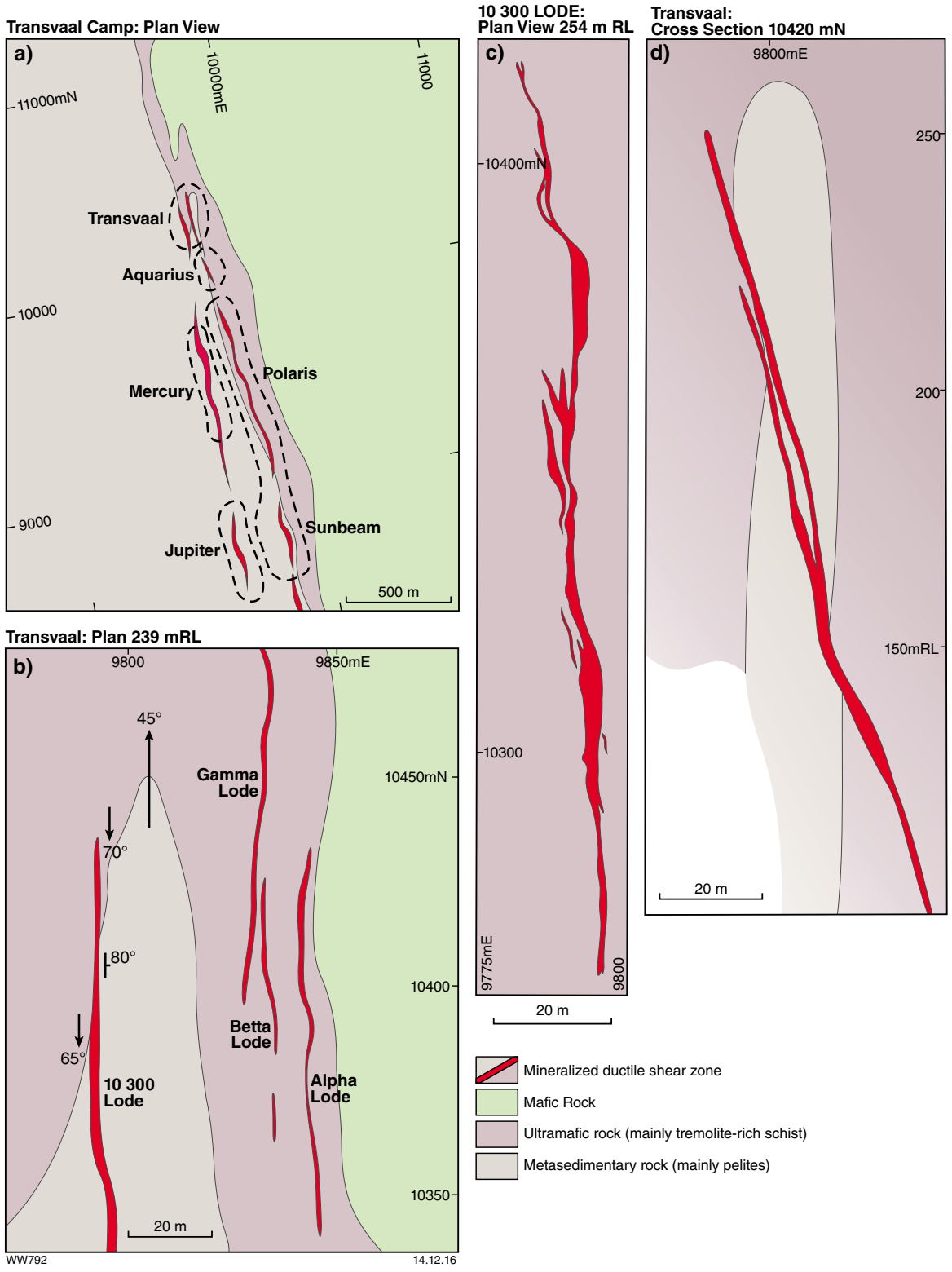

Figure 3.35. **Transvaal gold deposit, Southern Cross district, Youanmi Terrane. a) Geology of the Transvaal camp showing gold deposits. b) Enlarged map of the Transvaal deposit area. c) Transvaal 10 300 Lode, 254 m RL plan. d) Transvaal cross section 10 420N.**

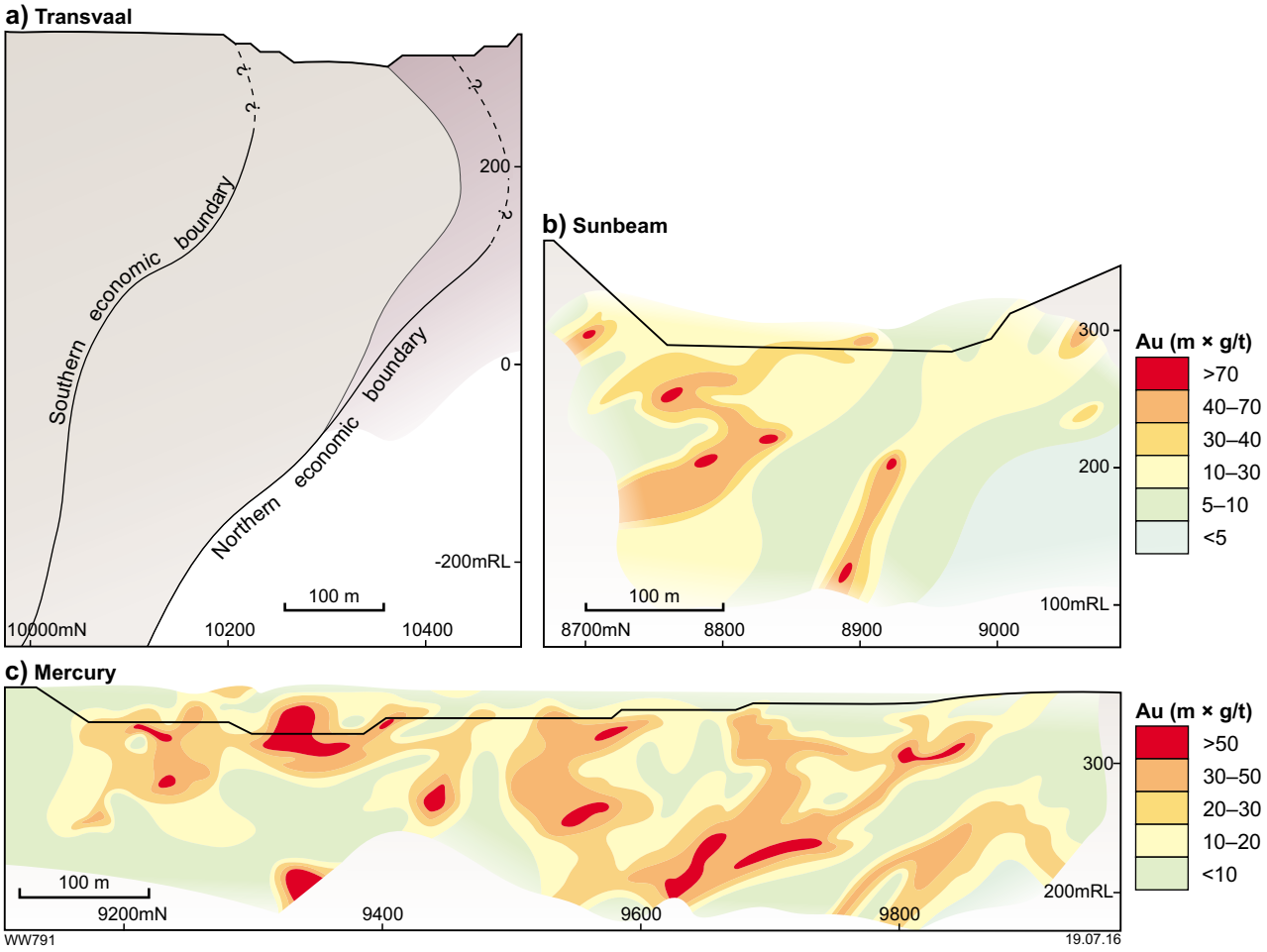

Figure 3.36. **Transvaal camp longitudinal cross sections. a) Transvaal orebody, showing limits of economic gold mineralization and steeply south-plunging orebody. b) Sunbeam orebody, showing steep south-plunging and shallow to moderate south-plunging ore shoots. c) Mercury orebody, showing complex array of ore shoots.**

The eastern and western shear zones at Transvaal converge northwards towards the S-shaped asymmetric fold (Fig. 3.35a). The Transvaal orebody at this location is about 150 m long and appears to terminate at around 200 m depth (Hagemann et al., 1998). The Transvaal pit and underground mine are in an extensional jog environment where the mineralized sinistral shear zone has jumped across the limbs of the asymmetric fold. The 10 300 lode is mainly on the ultramafic–metasedimentary rock contact and is the main source of gold ore. It has a complex geometry incorporating pronounced thickenings and bifurcations (Fig. 3.35c) and the ore envelope plunges steeply to the south (Fig. 3.36a). The dip of the 10 300 lode steepens slightly where it crosses the metasedimentary unit in the hinge of the asymmetric fold (Fig. 3.35d). On the eastern side of the fold axis there are several smaller lodes within the ultramafic unit, representing the eastern arm of the mineralized jog. Other south-plunging lodes, in deposits such as Sunbeam and Mercury (Fig. 3.35a), are also potentially controlled by thickened quartz vein boudins, but are less well-endowed, probably because they are farther from both the asymmetric fold and the extensional jog. It is worth noting that the plunges of the ore shoots are quite different from the plunge of the asymmetric fold (45° north) and, by implication, the fault jog. This observation might indicate insufficient exploration at depth, north of the Transvaal mine, or (more probably) a curved asymmetric fold axis that plunges south below 200 m depth (Fig. 3.36a).

Another very significant example, similar to Transvaal, is presented by the Oroya-style lodes at the Golden Mile, Kalgoorlie. The Oroya-style lodes are characterized by very high grades (up to 100 000 g/t Au) and oxidized hydrothermal alteration, including hematite and vanadian micas (Bateman and Hagemann, 2004). Shearing along an interflow sedimentary horizon jogs across minor asymmetric folds causing dilation and subsequent deposition of gold bonanza ore shoots that are controlled by the plunge of the fold axis (Swager, 1989; Bateman and Hagemann, 2004). A third, less well-endowed example is Twin Peaks (total resources of 71 000 oz, Saracen Mineral Holdings, media release and report to Australian Securities Exchange, October 2014), 100 km northeast of Kalgoorlie, where gold mineralization is associated with a fault jog that formed where a bedding-parallel fault encountered

a minor bedding flexure (open asymmetric fold) in a sequence of metasedimentary rocks (see Targeting Criterion 3.9).

East Lode at Wiluna illustrates a slight variation on the fault jog – fold axis association described under Targeting Criterion 3.2, whereby the fault jog has propagated vertically beyond the limits of the fold to which it is related (Fig. 3.11c). Jogs and fault bends on strike-slip faults that control mineralization in the Wiluna camp are transitional with depth to strike-slip folds with steeply plunging fold axes. For example, in the East Lode mine, displacement of the flow II basalt contact decreases from about 140 m at surface to effectively no displacement on the 1800-foot level. Drag folds adjacent to the East Lode Fault on the 1800-foot level and below control the steeply plunging geometry of the deep high-grade ore shoots in the East Lode deposit (Hagemann et al., 1992). This example from Wiluna may be a microcosm of the larger-scale variations with depth of controls on gold deposition that sees fault jogs prominent in the relatively shallow deposits of the Eastern Goldfields Superterrane and the dominance of folds and boudins in the deeper, higher metamorphic grade Southern Cross district of the Youanmi Terrane.

Most examples of gold deposits hosted by blocks of rheologically strong rock that have been isolated or partly isolated within weaker rock matrices by fault offsets (Targeting Criterion 3.6) formed in unfolded sections of greenstone belts. An equivalent example in the amphibolite-grade Southern Cross district is the Nevoria gold deposit, which is hosted by isolated blocks of banded iron-formation that have been offset across several north–south faults (Cullen et al., 1990). This has resulted in partial or complete isolation of the competent iron-formation host rock within weaker ultramafic and altered mafic schists. Generally, where folding is present, fold hinges are commonly thicker than fold limbs, which promotes the capacity for fracture of rheologically strong units in fold hinges under regional stress. Isolation of structurally thickened fold hinges in a weaker matrix may be effective in the development of large vein arrays, both in greenschist facies (e.g. Randalls) and amphibolite facies conditions. Several examples of gold mineralization in banded iron-formation host rocks from the Southern Cross district demonstrate the effectiveness of fold hinges in controlling selective fracture and consequent gold mineralization in high-grade metamorphic settings. Although oblique, offsetting faults may be present at some of these deposits (e.g. Golden Pig, Copperhead, Cornishman), their role is ambiguous, whereas the role of shallow to moderately plunging fold hinges is clear (e.g. Fig. 3.37a,b). The metamorphic grade of the host rocks of these deposits is estimated to be middle amphibolite facies (Bloem et al., 1994).

At Golden Pig (450 000 oz gold production; Nugus et al., 2003) and Cornishman (production + resources of 300 000 oz Au; Markwell, 2003), the banded iron-formation host rock forms a competent unit between weaker ultramafic schist and hydrothermally altered and subsequently metamorphosed mafic volcanic rocks (Figs 3.37a,b, and 3.38a,b). Regional east–west shortening and movement on north-northwesterly striking ductile shear zones created stress heterogeneity around thickened folded segments of iron-formation within predominantly weak schists. These competent iron-formation segments fractured under high fluid pressure and formed quartz–grunerite–clinopyroxene–pyrrhotite veins, which cut the folded mesobanding in the iron-formation (Fig. 3.38b,d,e) and host the bulk of the gold ore in these deposits. The distribution of the veins is strongly controlled by the thickened fold hinges. Thus, the ore shoots at Golden Pig and Cornishman plunge shallowly to the north and south, respectively, reflecting the plunge and azimuth of mesoscale fold axes in each case (e.g. Fig. 3.37c). Some of the gold in these deposits is hosted by the bounding shear zones (e.g. Taurus Lode at Golden Pig; Figs 3.37b and 3.38c), but this is subordinate to the gold resource in the iron-formation (Nugus et al., 2003). In contrast to the ore in iron-formation between shear zones, the shear-hosted Taurus mineralization plunges shallowly south-southwest, and is colinear with the dominant linear fabric in the Taurus shear zone, and is not necessarily hosted by iron-formation (Nugus et al., 2003).

At the northern end of the Southern Cross district, the Copperhead deposit is in upper greenschist to lower amphibolite facies greenstones (Mayers and Warriner, 1995; Mueller and McNaughton, 2000). Gold lodes are exposed in an erosional window of tightly folded mafic rocks and banded iron-formation under an overthrust sheet of barren amphibolite (Fig. 3.39a). The mafic rocks underwent hydrothermal sea-floor alteration and were subsequently metamorphosed to plagioclase–hornblende–biotite(–andalusite) and talc–ankerite(–chlorite, tremolite) assemblages (WK Witt, unpublished data). These constitute a rheologically weak unit within which thin units of rheologically strong banded iron-formation and massive (?exhalative) dolomite are interbedded or interleaved (Fig. 3.39a,b). The folded units are overprinted by steeply west-dipping, north-northwesterly striking shear zones (Fig. 3.39a,d). These shear zones are mineralized, but high-grade ore shoots are present only in relatively low-strain blocks between shear zones, particularly in banded iron-formation and dolomite units where hinge zones of early, overturned isoclinal folds are isolated between bounding shears (Fig. 3.39a,c,d). The folds plunge about 45° north-northwest, as do the high-grade ore shoots (Fig. 3.39d).

Saddle reefs (subclass (iii) above) are characteristic of the Victorian gold province of southeastern Australia (e.g. Cox et al., 1991), but there are few well-described equivalent examples in the Yilgarn Craton. The Wheel of Fortune deposit, in the central Lennonville mining centre of the Murchison Domain, is a possible example of a saddle reef (Watkins and Hickman, 1990). Shear zones with axial plane orientation (subclass (iv) above) are represented by Hoyle Pond in the Abitibi greenstone belt of Canada (Dinel et al., 2008). Possible examples of subclass (iv) deposits in the Yilgarn include Morning Star and Morning Star North in the Mount Magnet district of the Murchison Domain, where gold mineralization is in veins that align roughly with the axial plane of the Morning Star antiform (Wilson, 1990), as well as the Golconda and Eureka deposits in the Lake Austin mining centre, and deposits in the central Lennonville mining centre (Watkins and Hickman, 1990).

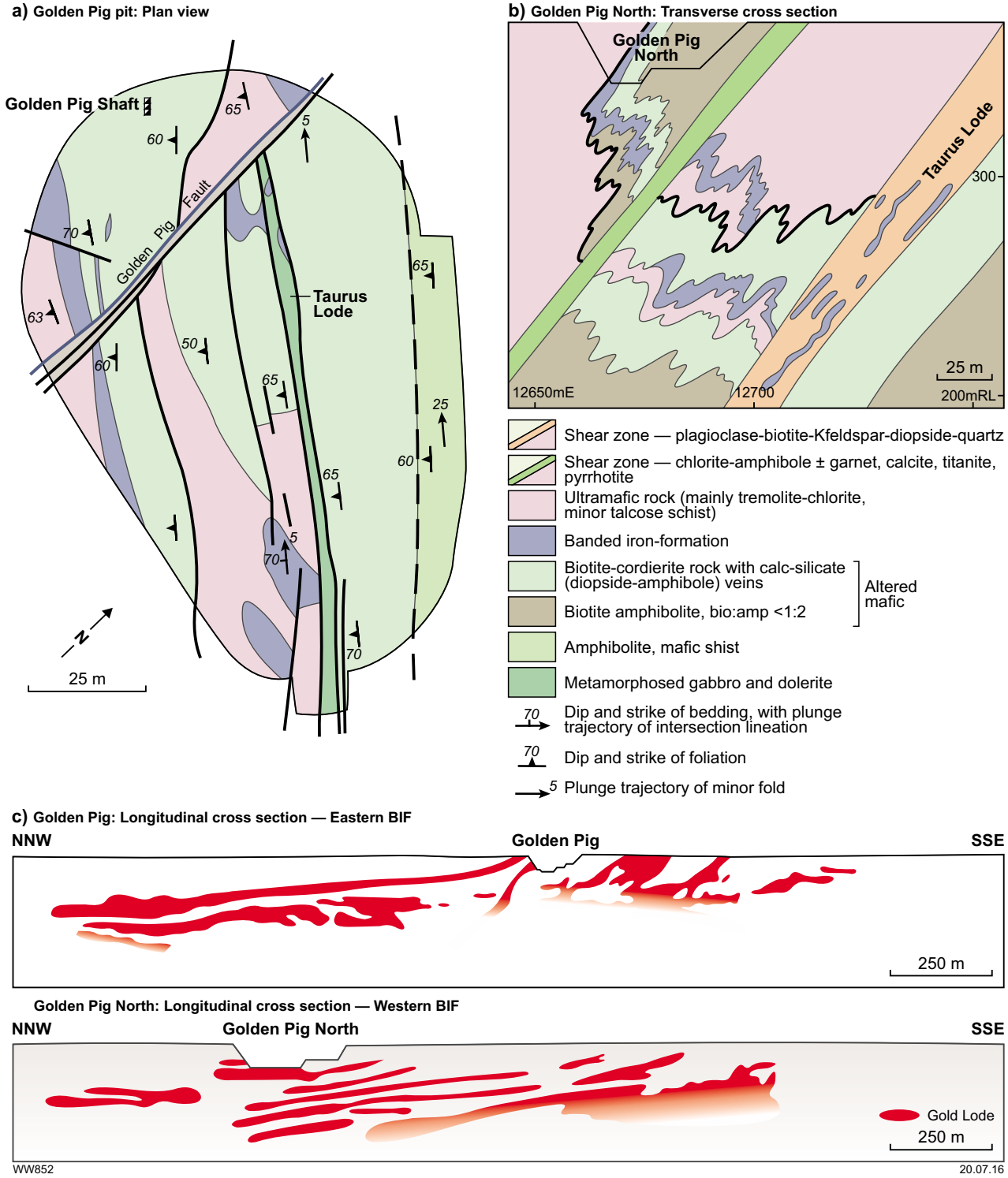

Figure 3.37. **Golden Pig gold deposit, Southern Cross district, Youanmi Terrane. a) Plan view, Golden Pig openpit. b) Transverse cross section, Golden Pig North, interpreted from resource drilling results. c) Longitudinal cross sections through the Golden Pig deposit; shallow northward plunge of ore shoots is colinear with the plunge of minor folds in the banded iron-formation host unit.**

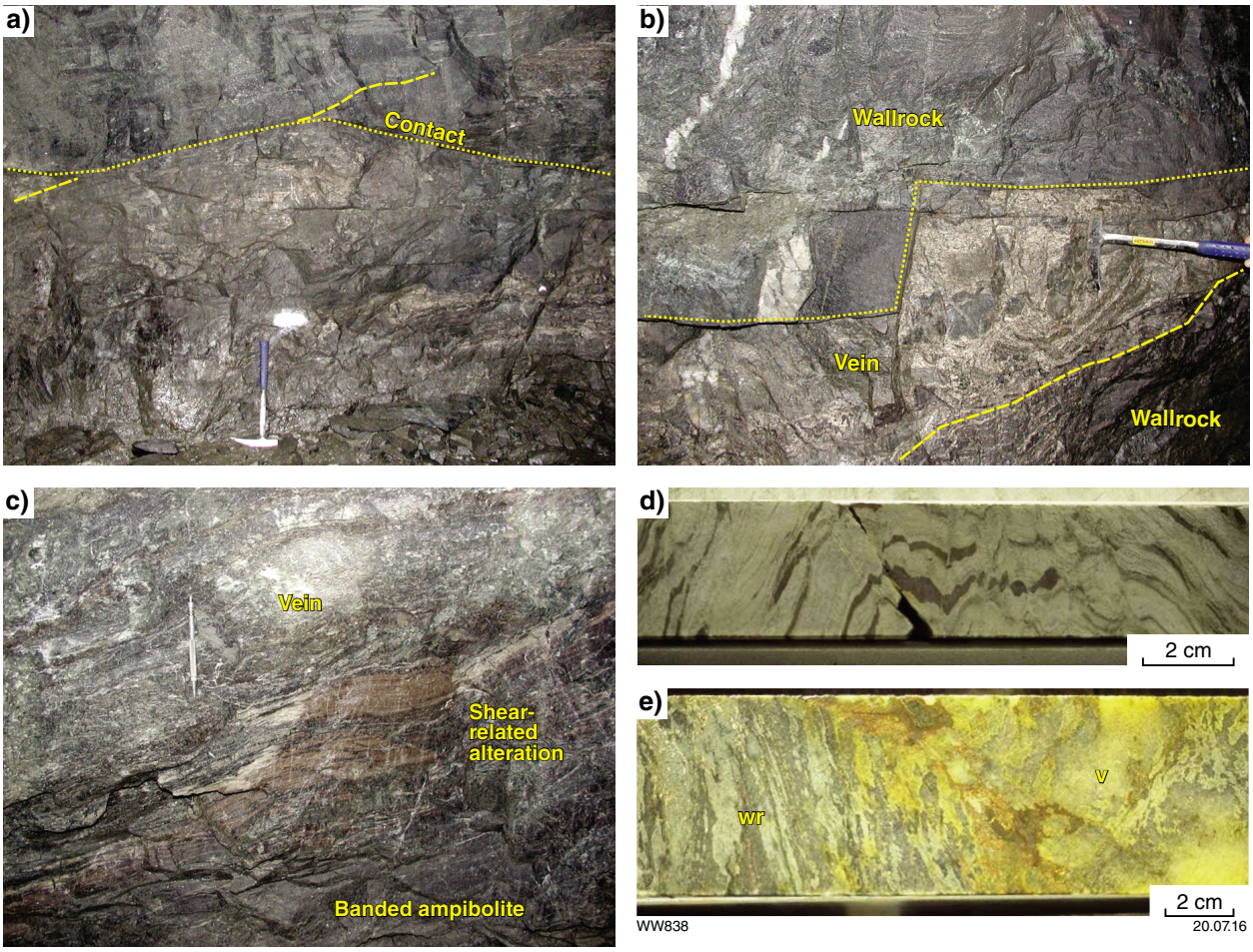

Figure 3.38. **Photos from Golden Pig (a to c) and Cornishman (d and e) mines. a) 'C' lode, level 7 decline, east wall; contact (subhorizontal apparent dip) between rheologically strong banded iron-formation (BIF) host rock (below) and rheologically weak altered mafic rock (above). Note gently undulating contact, possibly reflecting boudinage of BIF. Banding in both units is truncated by the contact (which dips away from the viewer), indicating shear movement on the contact. Banding in the hangingwall mafic unit reflects darker biotite–cordierite bands interspersed with lighter calc-silicate (diopside–amphibole) veins produced by metamorphism of sea-floor alteration of mafic rock and quartz-dolomite veins, respectively. b) 'C' lode, level 7 decline, east wall; metre-scale quartz–grunerite–clinopyroxene–pyrrhotite vein on BIF (below) – mafic rock (above) contact. Note blebby aggregates of quartz (white to grey) that identify these veins, which are otherwise mineralogically similar to hydrothermally altered iron-formation wallrock. c) 'C' lode, level 7 decline, west wall; vein and hydrothermal alteration in Taurus shear zone. The steeply dipping shear zone (apparent shallow dip) truncates folded BIF (not evident in photo, but see Figure 3.37b) and is in biotite–cordierite rock after pre-metamorphic hydrothermally altered mafic rock (lower right of photo, banded amphibolite in mine terminology). Upper half of photo shows coarse-grained diopside–calcite vein and biotite-rich lamellae of wallrock (brown). Shear-related alteration between the vein and banded amphibolite consists of pale brown K-feldspar–biotite–quartz, white plagioclase–quartz, dark green amphibole, and pale green diopside. d) Core CMD13, 206–207 m; mesoscopic folds (subhorizontal plunge) in unaltered BIF (quartz–grunerite–magnetite). e) Core CMD13, 217.8 m; quartz–grunerite–pyrrhotite vein (v, right) cuts mesobanding (wr, left) in iron-formation wallrock.**

Boudinage is closely related to folding, in that both processes are promoted at relatively high metamorphic grades; boudinage typically occurs on the limbs of folded competent layers. The constriction zones (bottlenecks) described under Targeting Criterion 3.4 are formed between boudins of intensely carbonated ultramafic rock and, more generally, the tips of boudins can be regarded as a specific type of bottleneck or constriction zone (cf. Targeting Criterion 2.13, Part 2 of this Atlas). Examples of gold deposits in which ore shoots are controlled, at least partly, by boudinage include New Celebration and Karonie in the Eastern Goldfields Superterrane, Marvel Loch in the Southern Cross Domain of the Youanmi Terrane, and Reedy in the Murchison Domain of the Youanmi Terrane. In the Hampton–Boulder deposit at New Celebration, which is hosted by the Boulder–Lefroy Fault, early boudinage of porphyry intrusions within mafic and ultramafic schist controlled the formation and location

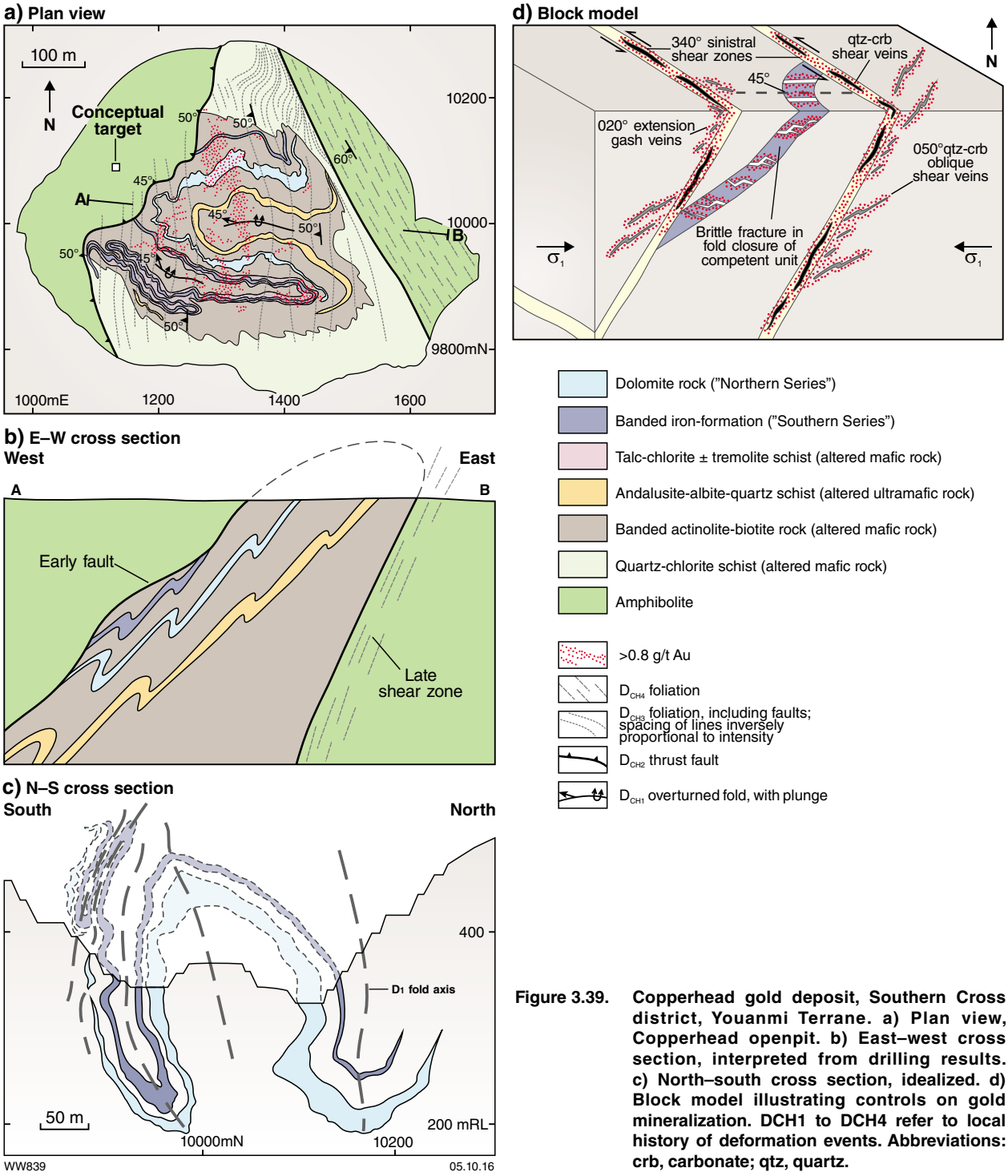

Figure 3.39. **Copperhead gold deposit, Southern Cross district, Youanmi Terrane. a) Plan view, Copperhead openpit. b) East–west cross section, interpreted from drilling results. c) North–south cross section, idealized. d) Block model illustrating controls on gold mineralization. DCH1 to DCH4 refer to local history of deformation events. Abbreviations: crb, carbonate; qtz, quartz.**

of late, fracture-controlled gold mineralization (Nichols and Hagemann, 2014). At Karonie, Roberts et al. (2004) described boudinaged calc-silicate alteration assemblages with coarse-grained pyroxene and pyrrhotite in the interboudin necks. At Reedy gold mine in the Murchison Domain, gold lodes plunge steeply south and are colinear with porphyry boudins and intrafolial fold axes (Henderson and Hill, 1990), similar to the relationships described at New Celebration.

Targeting Criterion 3.8: Low minimum stress anomalies produced by paleostress modelling

Paleostress modelling at district scale using the UDEC program and coupled deformation and fluid-flow modelling using FLAC3D software were described briefly under Targeting Criterion 2.14 in Part 2 of this Atlas. Deposit-scale stress modelling using UDEC software (Starfield and Cundell, 1998) was first applied to gold exploration at the Granny Smith deposit in the Laverton Tectonic Zone of the Eastern Goldfields Superterrane (Ojala et al., 1993; Holyland and Ojala, 1997). The Granny Smith gold deposit is on the eastern margin of the Granny Smith Granodiorite (Figs 3.40 and 3.41), one of the Mafic Group intrusions of Cassidy et al. (2002). Gold mineralization is associated with a reverse fault deformation zone that follows the eastern granite–greenstone contact where, assuming subhorizontal shortening, the relatively shallow dip of the contact favours simple shear and related fracturing (Ojala et al., 1993). The deformation zone hosts gold in metasedimentary country rock at Goanna, and in granodiorite, metasedimentary rock, and at the contact between them at Granny Smith and Windich (Ojala et al., 1993). Mineralization follows the contact between granodiorite and metasedimentary rock where the dip of the contact is <50°, and is hosted in granodiorite or metasedimentary rock where it is steeper (Fig. 3.40 inset).

Conjugate vein sets in the granodiorite allow estimation of the principal stress orientation at the time of gold mineralization; the orientation varies significantly with the form of the contact (Fig. 3.41). The estimated principal axis of paleostress is most variable where the contact is most irregular, and these sectors also coincide with the highest gold grades, implying focusing of the ore fluid where the form of the contact is irregular. Holyland and Ojala (1997) showed that the magnitude of the minimum stress axis is smallest where the dip of the contact between granodiorite and metasedimentary rock is relatively shallow and that there is a good correlation between these areas and high gold grade (Figs 3.41 and 3.42). These areas of relatively shallow dip promote contact dilation during reverse fault movement. Where the dip of the contact is relatively steep, it is 'misoriented' with respect to east–west (080°–260°) subhorizontal shortening, and mineralization is related to conjugate veins hosted by the rheologically stronger granodiorite, in accordance with the principles outlined by Oliver et al. (1990) and Ridley (1993). These areas where gold is hosted in granitic rocks correlate with broad zones of lower average gold grade (Fig. 3.40 inset).

Where gold mineralization is not controlled by steep faults and lithological contacts, stress modelling in cross section is preferable, as demonstrated by Mair et al. (2000). Mair et al. (2000) modelled stress across an east–west section through the upper part of the Sunrise Dam orebody. The main features of this geological cross section are:

- two subparallel shear zones that dip 25°–30° west-northwest
- a sequence of tight, asymmetrically folded intermediate volcaniclastic rocks with magnetite-rich interbeds, between the two shear zones
- a series of linking shears that cut the volcaniclastic sequence but merge into the bounding shear zones (Fig. 3.43a).

Gold is associated with disseminated pyrite and quartz–ankerite(–sericite) alteration in relatively shallow-dipping portions of the two subparallel shear zones and in brittle structures developed where linking shears cut the magnetite-rich beds (Mair et al., 2000). A subhorizontal east–west regional shortening direction was chosen for stress modelling by Mair et al. (2000) and, under these conditions, low minimum stress domains were shown to broadly correlate with gold mineralization (Fig. 3.43b). In detail, however, there appears to be a slight displacement between low minimum stress domains and areas where gold content is >0.1 g/t, and low minimum stress domains in the eastern part of the cross section appear to be poorly mineralized.

More-recent studies have indicated that gold was deposited at Sunrise Dam under variable stress orientations over a number of deformation stages and that a relatively small proportion of early stage gold was deposited during east–west shortening (Miller et al., 2007; Henson et al., 2010). Despite their inadequate assumptions about the principal stress direction at the time of gold mineralization, the stress modelling results of Mair et al. (2000) broadly substantiate the known distribution of gold (Fig. 3.43a,b). As discussed under Targeting Criterion 2.14 (Part 2 of this Atlas), small differences in the orientation of the principal stress direction (<25°) do not appear to produce major changes in the distribution of minimum stress anomalies resulting from UDEC stress modelling. The discrepancies between modelled low minimum stress and gold content of >0.1 g/t in the eastern part of the cross section may, however, be related to a more complex history of mineralization than envisaged by Mair et al (2000).

Despite the positive results of deposit-scale stress modelling at Granny Smith and Sunrise Dam, few similar studies have been published on Yilgarn Craton gold deposits. Several deposits that are either in or on the margins of granitic intrusions (e.g. Tarmoola and Porphyry in the Eastern Goldfields Superterrane) lend themselves to this sort of analysis. The dearth of such studies perhaps relates to perceived problems discussed under Targeting Criterion 2.14, such as the requirement for a detailed geological map, which typically requires an advanced stage of exploration. Nevertheless, there may be a role for stress modelling at all stages of exploration, including early-stage exploration where an imperfect geological map is based on aeromagnetic data interpretation.

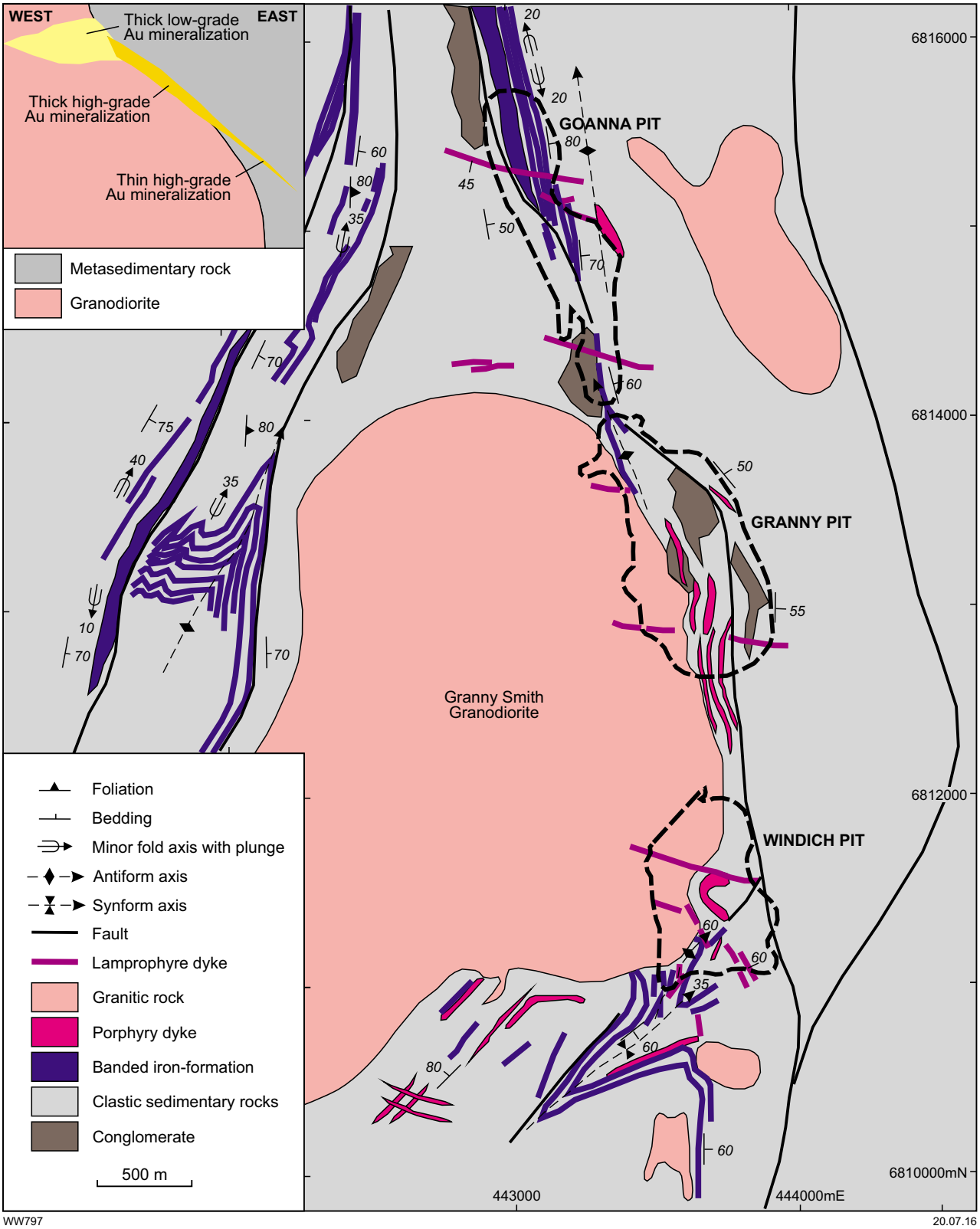

Figure 3.40. **Geological map showing the setting of the Granny Smith gold camp (after Holyland and Ojala, 1997). Inset: schematic cross section showing relationship of mineralization to dip of contact between granodiorite and metasedimentary rock.**

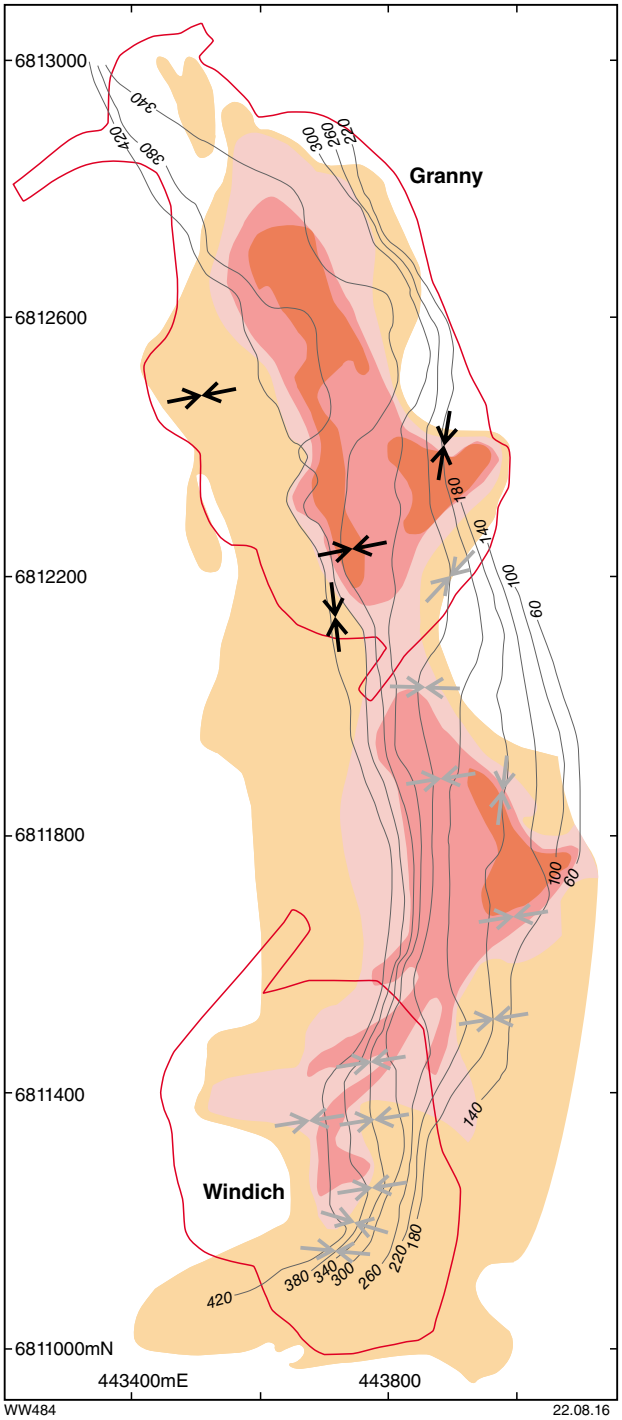

Figure 3.41. **Map showing relationship between gold mineralization and structural contours (metres above sea level) of the contact between granodiorite and metasedimentary country rock at Granny Smith deposit, Laverton district, Eastern Goldfields Superterrane (after Holyland and Ojala, 1997)**

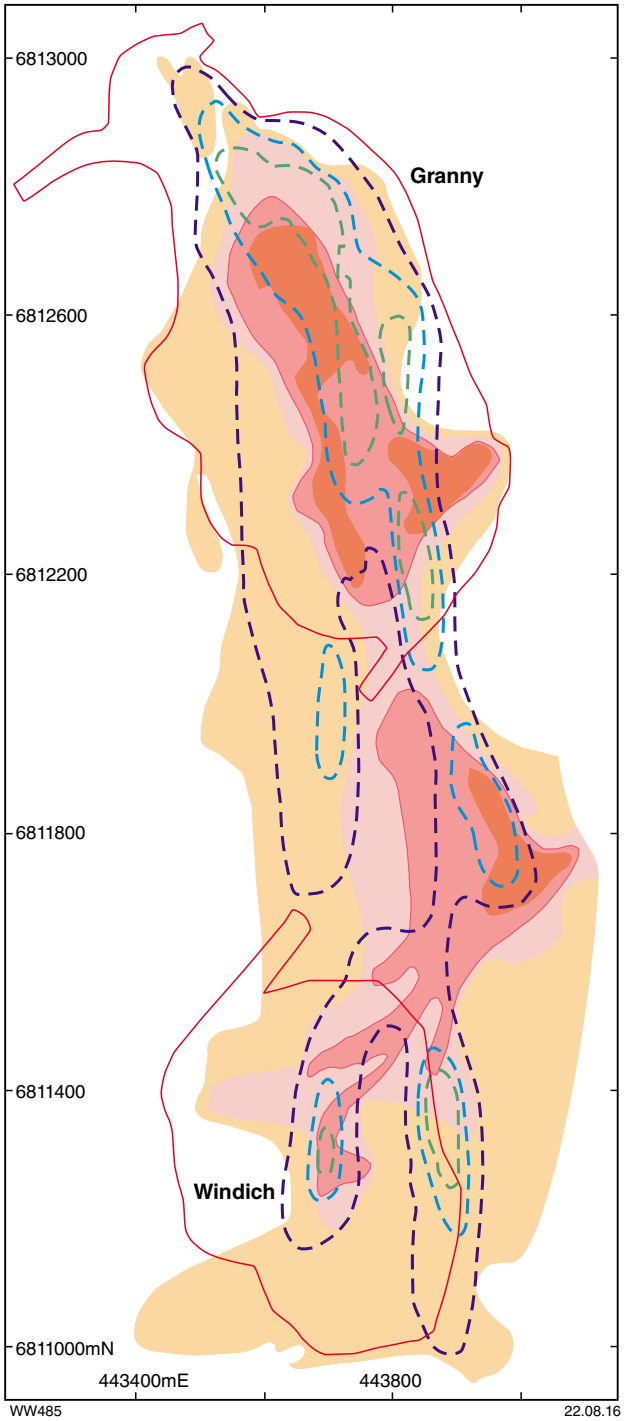

Figure 3.42. **Map showing relationship between gold mineralization and minimum principal stress at Granny Smith deposit, Laverton district, Eastern Goldfields Superterrane (after Holyland and Ojala, 1997)**

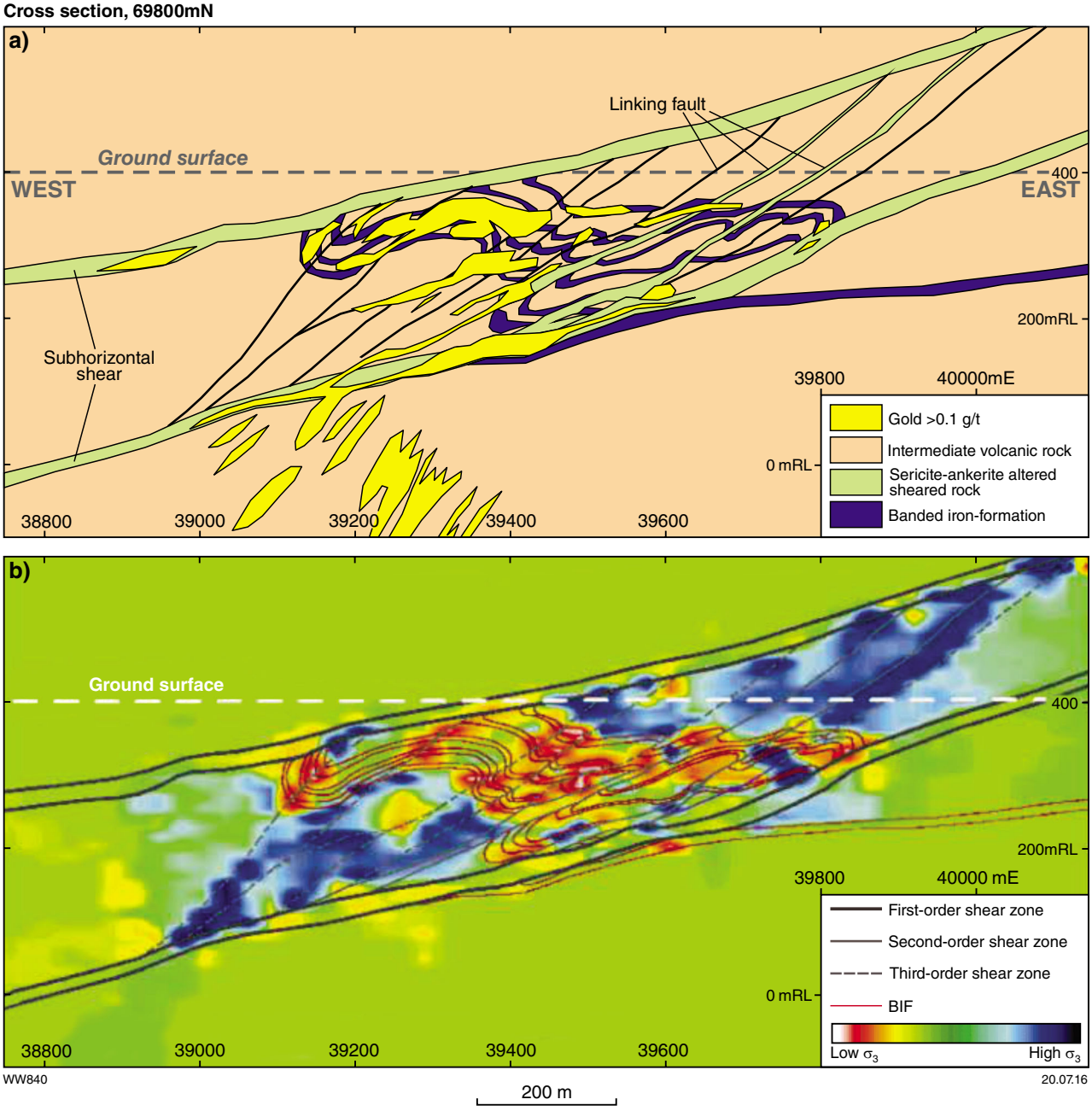

Figure 3.43. **Results of stress modelling at Sunrise Dam, Laverton district, Eastern Goldfields Superterrane (after Mair et al., 2000). a) Cross section showing geology and distribution of gold mineralization. b) Distribution of σ_3 resulting from stress modelling assuming subhorizontal east–west shortening illustrating correlation between gold mineralization and domains of low minimum stress (σ_3).**

Targeting Criterion 3.9: Geochemical dispersion (pathfinder elements)

Geochemical dispersion refers to variations in the abundances of major and trace elements, of stable isotope values, and of the magnitude of alteration indices in wallrocks surrounding mineralized veins, faults, or shear zones. To provide an effective exploration vector towards mineralization, variations in abundances of pathfinder elements and other proxies for gold should be characterized by:

- distinct variations in abundance or magnitude above background values, and
- broad dispersion beyond visible hydrothermal alteration (which can be recognized in the field and does not require costly multi-element geochemical analyses) and beyond anomalies defined by routinely analysed gold abundance.

These criteria are rarely fulfilled for gold deposits in the Yilgarn Craton, even though visible gold-related hydrothermal alteration halos are generally narrow relative to the controlling fluid conduits (veins, faults, shear zones). This is because geochemical dispersion halos are of similarly restricted extent and, in many cases, low-level gold abundance anomalies define dispersion as well as, or better than, pathfinder element (and other) anomalies. Further problems may arise where heterogeneity of the host rock sequence (e.g. a metasedimentary sequence) complicates establishment of background concentrations. This is a problem, for example, in the Agnew district (N. Thebaud, Centre for Exploration Targeting, pers. comm., August 2015).

In cases where only the first of the above criteria is met, geochemical dispersion may provide a vector to high-grade ore shoots within broad zones of hydrothermal alteration. This approach is most likely to be useful in an operating mine or during resource definition drilling programs, where the lateral extent of gold-related hydrothermal alteration is large relative to the scale of exploration. Even in these situations, the use of pathfinder elements, alteration indices, or stable isotopes is only cost effective if gold assays do not provide a similar vector.

Research into the utility of geochemical dispersion as an exploration tool for gold in the Yilgarn Craton has been hindered by the limitations described in the previous paragraphs. Nevertheless, there have been some notable contributions to this field and some indications of potential application to exploration at some deposits. Most notable amongst these contributions are the results of MERIWA Project 176 (Eilu and Mikucki, 1996). Some of the highlights of this Project were published in international geoscience journals, including Eilu and Mikucki (1998), Eilu et al. (1997), Eilu and Groves (2001), and Eilu et al. (2001). The discussion below of Targeting Criterion 3.9 is taken from these publications and is supplemented by the results of chemical dispersion analyses from Karari, Twin Peaks, and several other deposits in the Leonora and Southern Cross districts (WK Witt, unpublished data).

In analyses of geochemical dispersion it is important to set the limits of detection at appropriate levels to detect the concentration gradients between the deposit and the lowest or background levels distant from mineralization. For the elements investigated by Eilu and Mikucki (1996), these values are provided here in Table 3.2.

Deposits studied by MERIWA Project 176

MERIWA Project 176 investigated geochemical dispersion at five gold deposits in the Yilgarn Craton (Bulletin, Granny Smith, Kings Cross, Moyagee, and Twin Peaks). Background (anomaly threshold) values for the elements and alteration indices used by Eilu and Mikucki (1996) were determined at each mine site and are to some extent dependent on the dominant host rock (Table 3.3). Significant results from the five deposits are summarized below.

Bulletin deposit, Wiluna

Geochemical dispersion around the Bulletin lodes (Hagemann et al., 1992) was assessed by sampling core from seven diamond drillholes to generate two cross-sectional views through the gold ore system (Fig. 3.44a). Anomalous gold values extend only about 10 m beyond the ore zone (Fig. 3.44b). The most successful vectors at Bulletin are As and Sb, although all the analysed samples are above the concentration range for unaltered, unmineralized basalt, which suggests that regional As and Sb anomalies may extend beyond the area of investigation.

Within the Bulletin dataset, concentrations greater than local anomaly thresholds (set at 28 ppm for As and 2 ppm for Sb) extend up to 60 m from the Happy Jack – Bulletin shear zone, which hosts the Bulletin ore (Table 3.4, Fig. 3.44c,d). Furthermore, within the local anomaly, As and Sb concentrations define a gradient that can be used as a vector towards the ore (Fig. 3.44c,d). Other elements that define an anomaly that extends beyond the Happy Jack – Bulletin shear zone are Te and W. The W anomaly is of very restricted extent. The Te anomaly is more extensive than the local As and Sb anomalies but is defined only at very low concentrations (10 ppb). Eilu and Mikucki (1996) also reported that As, Sb, Te, and W anomalies within the Happy Jack shear zone extend for 100 m to more than 300 m along strike from the ore.

The results from Bulletin are particularly significant because the gold anomaly there does not extend much beyond the footwall of the Happy Jack – Bulletin shear zone in either of the two cross sections studied (Fig. 3.44b). On the other hand, distal chlorite–calcite alteration extends well beyond the Happy Jack – Bulletin shear zone, at least as far as the local As and Sb anomalies (Fig. 3.44c,d).

Table 3.2. Lower limits of detection recommended for pathfinder element analysis to detect geochemical dispersion around gold lodes (from Eilu and Mikucki, 1996)

Element	*Recommended detection limit, based on average contents of unaltered and unmineralized rocks*[(a)]	*Detection limit used by Eilu and Mikucki (1996)*
Silver (Ag)	0.01 ppm	0.01 ppm
Arsenic (As)	0.2–1 ppm	0.1–1 ppm
Gold (Au)	0.2–1 ppb	0.1 ppb
Boron (B)	1 ppm	
Bismuth (Bi)	0.01 ppm	0.01 ppm
Cadmium (Cd)	0.01–0.1 ppm	
Mercury (Hg)	3–5 ppb	
Molybdenum (Mo)	0.1 ppm	
Antimony (Sb)	0.01–0.05 ppm	0.01–0.05 ppm
Selenium (Se)	0.01 ppm	0.01–0.05 ppm
Tin (Sn)	0.3 ppm	
Tellurium (Te)	1–2 ppb	2 ppb
Tungsten (W)	0.1 ppm	0.1 ppm

NOTE: (a) Based on data compiled by Ringwood (1979), Hamlyn et al. (1985), Burrows and Spooner (1989), Perring et al. (1990), Nurmi et al (1991), Bornhorst et al. (1993), Rasilainen et al. (1993), and Eilu and Mikucki (1996)

Granny Smith, Laverton

The Granny Smith deposit is on the eastern contact of the Granny Smith Granodiorite with metasedimentary country rock (Ojala et al., 1993; Fig. 3.40). Eilu and Mikucki (1996) investigated pathfinder element distributions around Granny Smith Deeps gold lodes projected onto east–west cross section 11700N, using core samples from four diamond drillholes. The gold anomaly extends tens of metres into granodiorite and up to 30 m from ore in metasedimentary rock (Table 3.5).

Depending on the element concerned, dispersion of pathfinder elements at Granny Smith is of very restricted extent or non-existent in both granodiorite and metasedimentary rock. Only W and Te generate anomalies that extended more than 5 m from the zone of gold mineralization (broadly coincident with proximal sericite–pyrite alteration). The Te anomaly extends 2 to 60 m from the mineralized zone in granodiorite (>10 ppb) and 1 to 30 m in metasedimentary rock (>125 ppb). The W anomaly extends 1 to 60 m from the mineralized zone in granodiorite (>6 ppm) and 3 to 30 m in metasedimentary rock (>2.3 ppm). Even these anomalies do not extend beyond visible (dolomite and calcite–dolomite) alteration into unaltered protoliths. Furthermore, the gold anomaly extends for comparable or greater distances than those defined by Te and W (Fig. 3.45).

Kings Cross, Coolgardie

The Kings Cross deposit, in the Coolgardie district, is hosted by a north-northeasterly striking, steeply east-dipping brittle–ductile fault (the Kings Cross fault). Gold mineralization is associated with a quartz reef, 400 m long, that varies in thickness from <10 cm to 3 m and extends at least 250 m downdip (Knight et al., 1993). The Kings Cross deposit is distinct from other deposits studied by Eilu and Mikucki (1996) in that it is hosted by amphibolite facies greenstones and the proximal hydrothermal alteration of the mafic host rock is characterized by the presence of biotite. Hydrothermal alteration is of relatively restricted extent and is generally less than 10 m wide in the footwall and hangingwall of the lode. Eilu and Mikucki (1996) investigated pathfinder element dispersion by analysing samples from seven diamond drillholes projected onto an east–west cross section through the central part of the orebody, and a longitudinal section incorporating three of the holes (Fig. 3.46).

Gold dispersion is limited to the visible alteration zones in the Kings Cross fault. Beyond the fault, gold values are <10 ppb and mostly <5 ppb in unaltered rock, but increase (to a maximum of 230 ppb) in subsidiary subparallel shears in the hangingwall of the fault. Pathfinder elements Te, As, Sb, and W define anomalies that are of similar or greater extent than those defined by gold (Table 3.6).

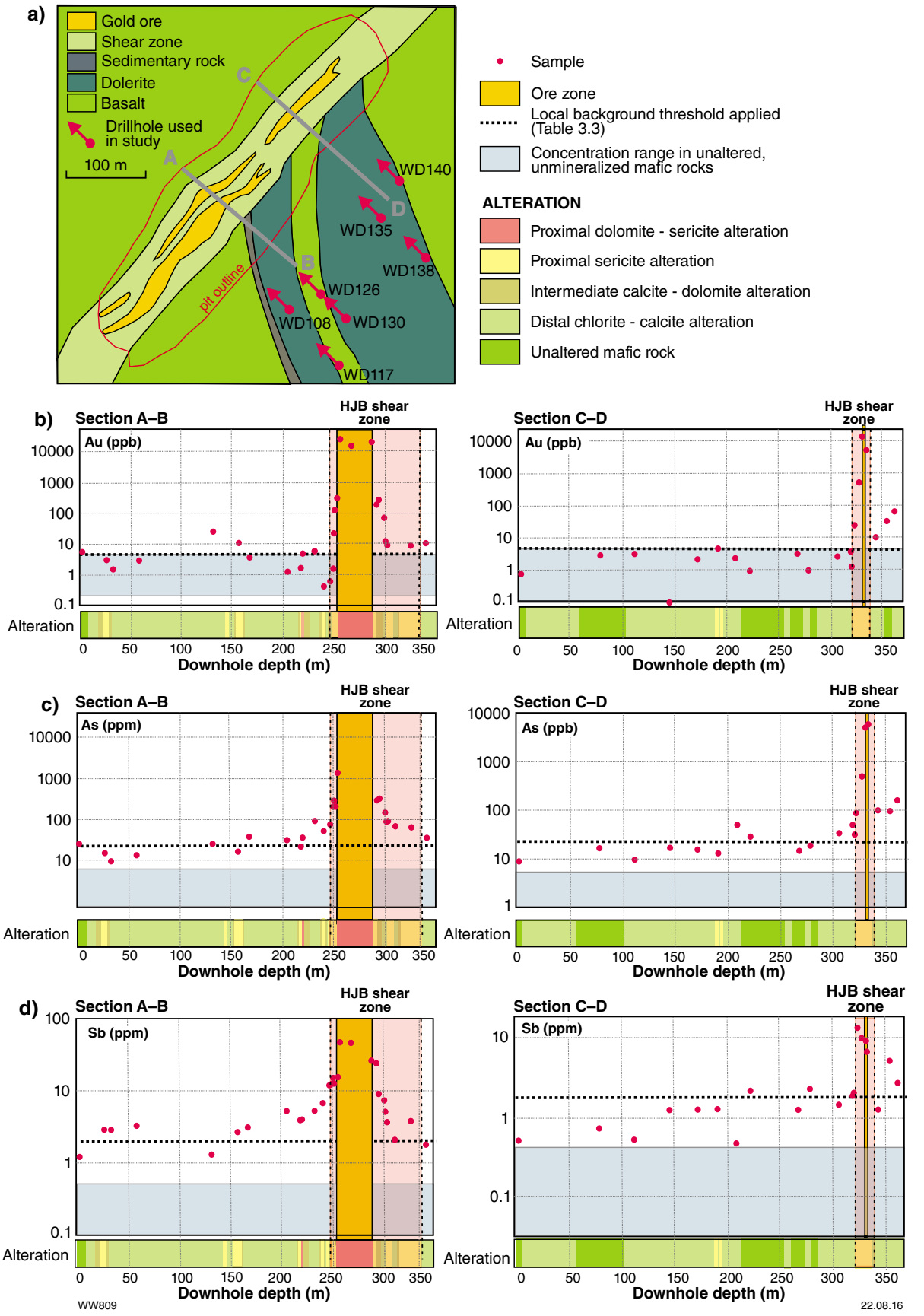

Figure 3.44. **Gold and pathfinder element dispersion at the Bulletin gold mine, Wiluna district, Eastern Goldfields Superterrane. a) Geological map showing locations of drillholes studied and of cross sections A–B and C–D. Distribution in cross sections A–B and C–D of b) Au (ppb), c) As (ppm), and d) Sb (ppm). HJB, (Happy Jack – Bulletin).**

Table 3.3. Background anomaly threshold values for pathfinder elements and alteration indices, from Eilu and Mikucki (1996)

	Granny Deeps		*Twin Peaks*	*Bulletin*	*Kings Cross*	*Moyagee*		*Average unmineralized*	
Pathfinder element	*Granodiorite*	*Sedimentary*	*Sedimentary*	*Basalt*	*Amphibolite*	*Komatiite*	*Porphyry*	*Igneous*	*Sedimentary*
Au (ppb)	8.5	2	2	6	5	6	6	0.5 to 4	2
Ag (ppm)	0.14	0.18	0.10	0.08	0.13	0.11	0.11	0.10 to 0.13	0.055 to 0.10
As (ppm)	5	40	6	28 (4)	4	5	5	1.0 to 5.0	4.0 to 6.0
Bi (ppm)	0.20	0.20	0.20					0.12 to 2.0	0.10 to 0.20
Sb (ppm)	0.9	1.0	0.8	2.0 (0.4)	0.9	0.45	0.45	0.03 to 0.22	1.10
Se (ppm)	0.10	1.0	0.17		0.30	0.15	0.15	0.05 to 0.17	0.05 to 0.20
Te (ppm)	0.010	0.125	0.050	0.010	0.037 (0.010)	0.010	0.010	≤0.010	0.050
W (ppm)	6.0	2.3	3.0	0.6	1.3	0.5	0.5	0.5 to 3.0	2.0 to 3.0
Alteration Index									
[Na/Al]mol	<0.63	<0.30	>0.30	0.85 to 1.15	0.16 to 0.25	0.3 to 0.5			
[3K/Al]mol	>0.030	0.015 to 0.026	0.85 to 1.15	<0.04	<0.04	<0.07			
[CO_2/Ca]mol	<0.4	<02.3		<0.30	<0.03	<0.20			
[CO_2/Ti]mol		<08.5	<08.0	<5.0	<0.5	<3.5			
[CO_2]mol/Zr	<1.3	<5.2	<9.0	<10	<1.0	<5.0			
[CO_2/(C+ Mg+Fe+0.75S)]mol						<0.05			
Y/Zr	<0.115	0.097 to 0.140		>0.34	>0.34	>0.24			
[1000*Y]/Ti		17 to 31		>24	>21	>23			

NOTE: Values in brackets are local regional thresholds where values derived from literature are too high, based on data from the deposit collected by Eilu and Mikucki (1996).

Table 3.4. Summary of pathfinder element data showing anomalies that extend beyond ore at Bulletin, Wiluna (Eilu and Mikucki, 1996)

Element	*Threshold*	*Extent of anomaly*		*Concentration gradient within anomaly*	
		From ore	*From Happy Jack – Bulletin shear zone*	*Beyond proximal alteration zone*	*Beyond Happy Jack – Bulletin shear zone*
Au	6 ppb	10 m	0 m		
Ag	0.08 ppm	0 to 10 m	0 m	None	None
As (local)	28 ppm	5 to 50 m	10 to 40 m	Common, 10 to 60 m	Common, 5 to 35 m
As (regional)	2 ppm	>150 m	>150 m		
Sb (local)	2 ppm	5 to 70 m	0 to 60 m	Common, 5 to 40 m	Common, 5 to 10 m
Sb (regional)	0.4 ppm	>150 m	>150 m		
Te	10 ppb	10 to 115 m	10 to 100 m	Common, 1 to 30 m	Local; 0 to 20 m
W	0.6 ppm	5 to 25 m	0 to 20 m	Common, 5 to 20 m	Local; 0 to 10 m

Table 3.5. Summary of pathfinder element data showing anomalies that extend beyond ore at Granny Smith, Laverton (Eilu and Mikucki, 1996)

Element	*Threshold*	*Extent of anomaly*		*Concentration gradient within anomaly*	
	Granodiorite/ metasedimentary rock	*From ore in granodiorite*	*From ore in metasedimentary rock*	*In granodiorite*	*In metasedimentary rock*
Au	8.5 ppb / 2 ppb	25 to >70 m	5 to 30 m		
Ag	0.14 ppm / 0.18 ppm	0 m	0 m	Local, 1 to 2 m	Local, 1 to 5 m
As	5 ppm / 40 ppm	0 m	0 to 5 m	None	Uncommon, 0 to 5 m
Sb	0.9 ppm / 1.0 ppm	0 m	0 to 5 m	Local, 0 to 5 m	Common, 2 to 10 m
Te	0.010 ppm / 0.125 ppm	2 to 60 m	1 to 30 m	Local, 0 to 10 m	Local, 0 to 5 m
W	6 ppm / 2.3 ppm	1 to 60 m	3 to 30 m	Local, 0 to 10 m	Common; 2 to 5 m

Table 3.6. Summary of pathfinder element data showing anomalies that extend beyond visible alteration in the Kings Cross fault at Kings Cross, Coolgardie (Eilu and Mikucki, 1996)

Element	*Threshold*	*Extent of anomaly from visible alteration*		*Concentration gradient within anomaly*	
		In unaltered wallrock only	*Incorporating hangingwall faults to the exclusion of intervening unaltered wallrock*	*Across strike*	*Along strike within fault*
Au	5 ppb	5 m	≥50 m	Negligible	Ill-defined
Te (local)	37 ppb	<10 m	<5 to >50 m	Possible, on a scale of 50 to 100 m	Not evident
Te (regional)	8 ppb	>90 m	>90 m		
As	4 ppm	<5 to >50 m	>50 m	Not evident	Possible, on a scale of 50 to 100 m
Sb	0.9 ppm	0 m[(a)]	0 m	Inconsistent	Not evident
W	1.3 ppm	≤5 m	>70 m	Not evident	Not evident

NOTE: (a) 0 m around Kings Cross fault but 5 to 20 m around some hangingwall faults. At a lower threshold of 0.5 ppm, an Sb anomaly extends for 20–50 m into the hangingwall of the Kings Cross fault (detection limit for Sb is 0.05 ppm; Eilu and Mikucki, 1996).

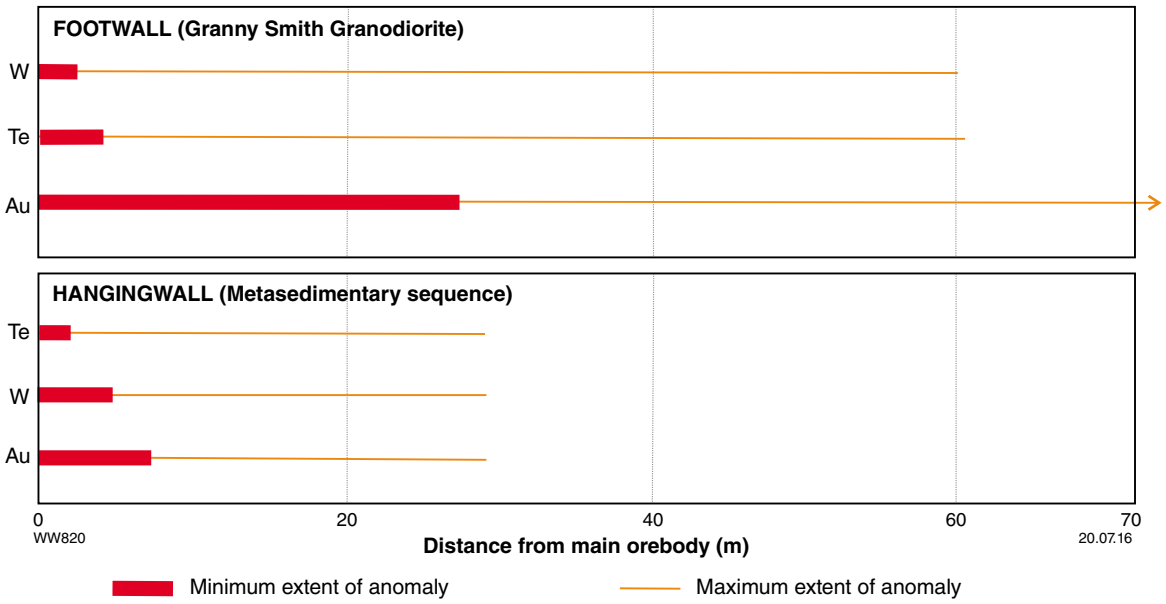

Figure 3.45. Extent of gold and pathfinder element (Te, W) anomalies from the orebody at Granny Smith (Deeps), Eastern Goldfields Superterrane (after Eilu and Mikucki, 1996)

The As and Te anomalies have mostly limited extent into unaltered wallrock in the hangingwall of the Kings Cross fault, but both elements are anomalous in subsidiary shears that are subparallel to the Kings Cross fault (Fig. 3.46). An along-strike concentration gradient for As within the Kings Cross Fault is also evident; this gradient provides a vector towards the thickest and highest grade part of the Kings Cross lode (Eilu and Mikucki, 1996). Antimony is not anomalous (>0.9 ppm) in unaltered amphibolite in the immediate hangingwall of the Kings Cross fault but does display some dispersion over distances of 5 to 20 m from some subparallel faults in the hangingwall (Eilu and Mikucki, 1996). Nevertheless, Sb provides a relatively consistent gradient extending from values >0.5 ppm proximal to the Kings Cross fault to <0.5 ppm at distances of up to 50 m from the ore (Fig. 3.46).

Moyagee, Murchison Domain

Eilu and Mikucki (1996) studied the Moyagee deposit, between Cue and Mount Magnet in the Murchison Domain, where gold mineralization is hosted by ultramafic (komatiite) rock and porphyry intrusions. Geochemical dispersion results are based on analyses of 126 RC drilling samples as no diamond cores were available at the time of their study (Fig. 3.47a).

Eilu and Mikucki (1996) recognized two distinct types of hydrothermal alteration in ultramafic rocks at Moyagee. Talcose alteration was found in relatively magnesian rocks (suites b, c; komatiite and Mg-rich basaltic komatiite), whereas talc-free alteration characterized less-magnesian rocks (suite a; most basaltic komatiite and some Mg-rich tholeiites). Eilu and Mikucki (1996) did not attempt to quarantine the data according to host rock, or talcose versus talc-free alteration type.

The centre of the shear zone is characterized by talc(–chlorite, dolomite, biotite) alteration with interleaved bands of biotite–dolomite–sericite alteration and there is a close spatial association of anomalous to ore-grade gold with porphyry intrusions and porphyry–ultramafic contacts (Fig. 3.47b). Gold anomalies (>6 ppb) extend for 10 m to more than 35 m from ore (defined as >1 ppm Au, but mostly coincident with talc-free biotite-bearing alteration), and do not extend beyond the visible hydrothermal alteration associated with the Lena shear zone (Fig. 3.47b; Table 3.7). Of the pathfinder elements studied, Te, W, Se, As, and Sb generated anomalies as large or larger than the gold anomaly, but only the Te and W anomalies extend beyond visible hydrothermal alteration associated with the Lena shear zone (Fig. 3.47c,d; Table 3.7). Within the shear zone, there are concentration gradients within anomalies, but they are generally limited to distances of about 20 m from ore (Eilu and Mikucki, 1996).

Figure 3.46. (opposite) Gold and pathfinder element dispersion, Kings Cross gold deposit, Coolgardie, Eastern Goldfields Superterrane (after Eilu and Mikucki, 1996). a) Hydrothermal alteration zoning projected onto east-southeast to west-northwest transverse cross section (20150E to 20200E; local grid) and onto longitudinal cross sections (tilted 60° W, in the plane of drilling) showing hydrothermal alteration zoning and dispersion of b) Au, c) Te, d) As, and e) Sb.

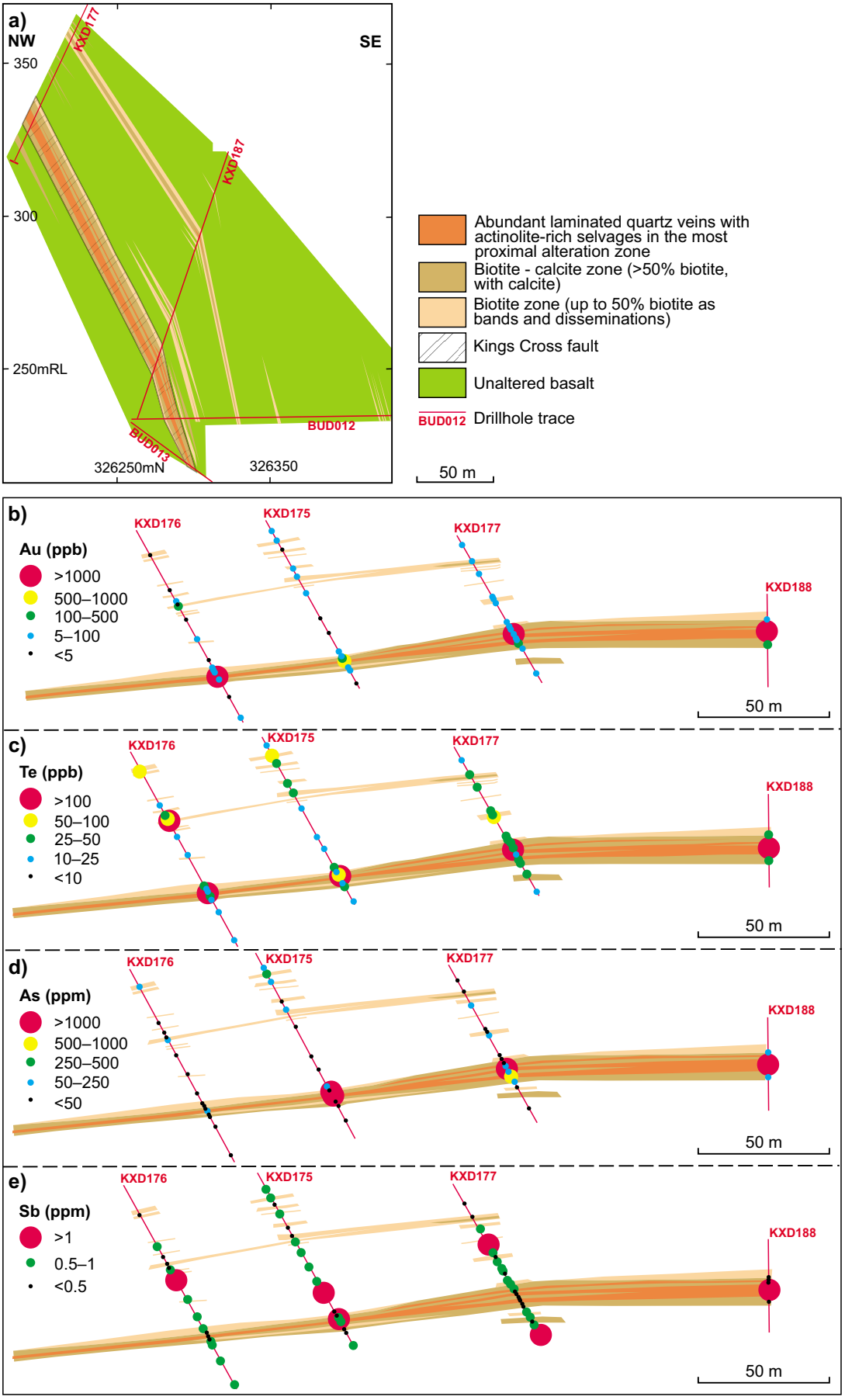
a)
NW
SE
350
300
250mRL
KXD177
KXD187
BUD012
BUD013
326250mN
326350
Abundant laminated quartz veins with actinolite-rich selvages in the most proximal alteration zone
Biotite - calcite zone (>50% biotite, with calcite)
Biotite zone (up to 50% biotite as bands and disseminations)
Kings Cross fault
Unaltered basalt
BUD012 Drillhole trace
50 m
b)
Au (ppb)
>1000
500–1000
100–500
5–100
<5
KXD176
KXD175
KXD177
KXD188
50 m
c)
Te (ppb)
>100
50–100
25–50
10–25
<10
d)
As (ppm)
>1000
500–1000
250–500
50–250
<50
e)
Sb (ppm)
>1
0.5–1
<0.5

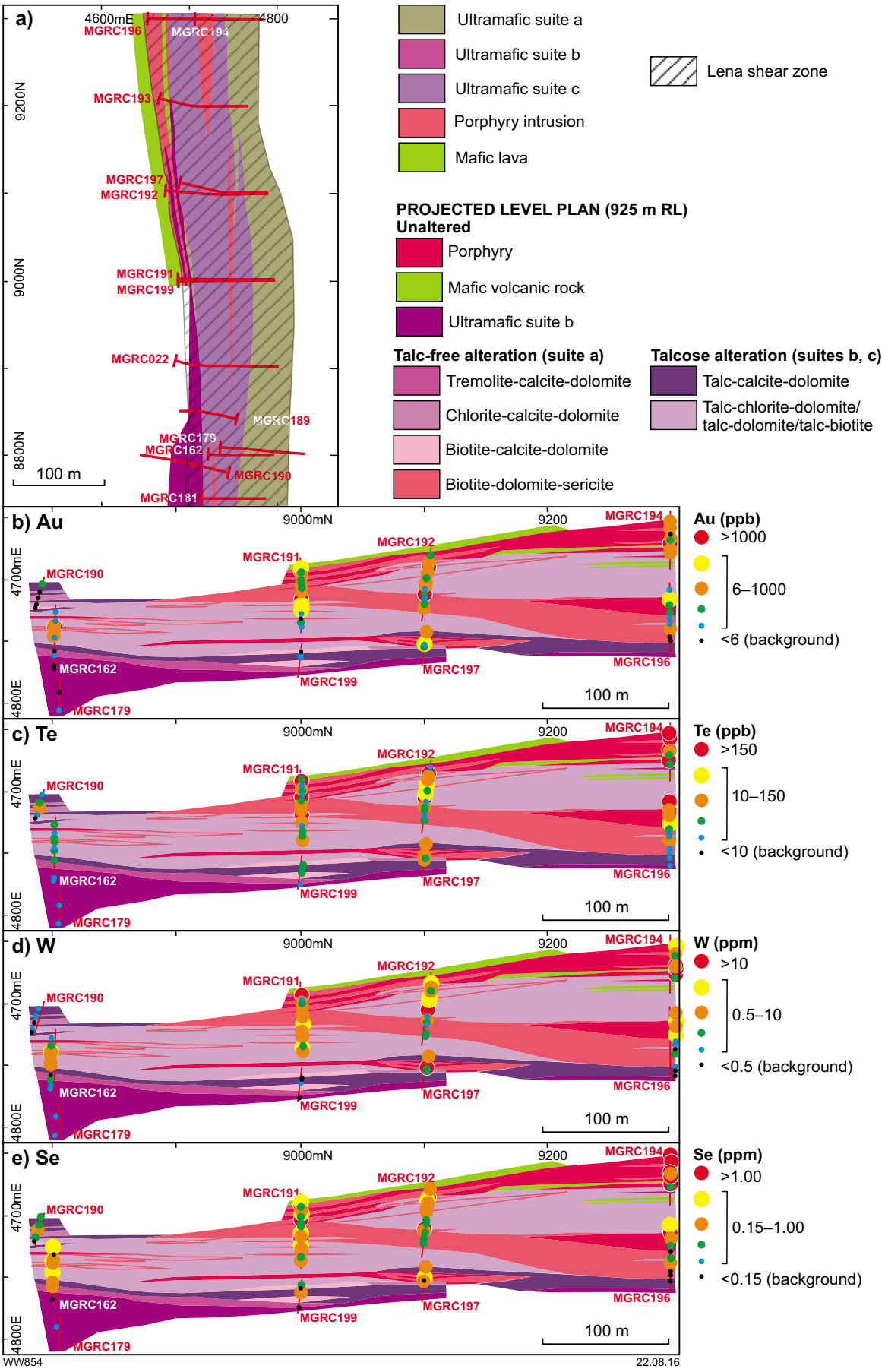
a)
4600mE
4800
9200N
9000N
8800N
MGRC196
MGRC194
MGRC193
MGRC197
MGRC192
MGRC191
MGRC199
MGRC022
MGRC189
MGRC179
MGRC162
MGRC190
MGRC181
100 m
Ultramafic suite a
Ultramafic suite b
Ultramafic suite c
Porphyry intrusion
Mafic lava
Lena shear zone
PROJECTED LEVEL PLAN (925 m RL)
Unaltered
Porphyry
Mafic volcanic rock
Ultramafic suite b
Talc-free alteration (suite a)
Tremolite-calcite-dolomite
Chlorite-calcite-dolomite
Biotite-calcite-dolomite
Biotite-dolomite-sericite
Talcose alteration (suites b, c)
Talc-calcite-dolomite
Talc-chlorite-dolomite/
talc-dolomite/talc-biotite
b) Au
c) Te
d) W
e) Se
9000mN
9200
4700mE
4800E
MGRC190
MGRC191
MGRC192
MGRC194
MGRC162
MGRC199
MGRC197
MGRC196
MGRC179
100 m
Au (ppb)
>1000
6–1000
<6 (background)
Te (ppb)
>150
10–150
<10 (background)
W (ppm)
>10
0.5–10
<0.5 (background)
Se (ppm)
>1.00
0.15–1.00
<0.15 (background)
WW854
22.08.16

Figure 3.47. (opposite) Gold and pathfinder element dispersion, Moyagee gold deposit, Murchison Domain, Youanmi Terrane (after Eilu and Mikucki, 1996). a) Simplified geological map (925 m RL, or about 75 m below the surface) of the Moyagee deposit showing traces of the drillholes studied. Gold and pathfinder element dispersion projected onto the 925 m RL level plan for b) Au, c) Te, d) W, and e) Se.

Twin Peaks, Carosue Dam camp

The Twin Peaks deposit is hosted in metasedimentary rock in the footwall of the Keith–Kilkenny Fault zone, about 100 km northeast of Kalgoorlie. Gold mineralization is related to a stockwork of quartz–ankerite–pyrite–arsenopyrite veins in strongly carbonate-altered feldspathic sandstone with minor argillic interbeds (Eilu and Mikucki, 1996; WK Witt, unpublished data). The stockwork of mineralized veins formed in a dilational jog where bedding-parallel faults encountered a minor bedding flexure with S-shaped asymmetry (Fig. 3.48). The resulting pipe-like orebody plunges 55° towards 084°. Hydrothermal alteration at Twin Peaks is characterized by distal calcite, intermediate dolomite (ankerite), and proximal white mica – dolomite (ankerite) zones. Pyrite and coarse (up to 4 mm) arsenopyrite characterize the intermediate dolomite and, more particularly, the proximal white mica – dolomite zones (Eilu and Mikucki, 1996). Eilu and Mikucki (1996) studied geochemical dispersion by sampling 11 diamond and RC drillholes, and projecting the data onto a southwest–northeast transverse cross section and a northwest–southeast inclined longitudinal cross section through the deposit.

Geochemical dispersion of pathfinder elements at Twin Peaks was also investigated by WK Witt (unpublished data) who delineated distal, intermediate, and proximal alteration zones, and collected samples from the pit floor and diamond cores through the orebody, and also undertook multi-element analyses (Au, As, Sb, Bi, Cu, Mo, Pb, Zn, Te, W) on grade-control samples from the 280 m RL of the Twin Peaks openpit.

Eilu and Mikucki (1996) found that anomalous gold values (>2 ppb) extend only 2 to 10 m across strike beyond ore in the proximal and intermediate zones of visible alteration (Fig. 3.49b). There are some local along-strike variations in abundance of Au and some pathfinder elements within those zones, over distances of more than 80 m, in which abundances decrease away from the contractional jog at the centre of the orebody (Fig. 3.50a). Eilu and Mikucki (1996) found that only As, W, and Ag were anomalous beyond the low level Au anomaly (>2 ppb; Table 3.8). They found that As provided the largest pathfinder element dispersion halo, extending up to 110 m into the distal calcite alteration zone and the unaltered hangingwall of the ore zone, at levels of 25 to 30 ppm (Fig. 3.49c). There is little or no lateral gradient in As concentration within this anomaly, but concentration gradients along strike within the mineralized zone reflect proximity to the jog at the centre of the orebody (Fig. 3.50b). Silver (>0.1 ppm) and tungsten (>3 ppm) display more restricted anomalies that extend only up to 30 m beyond the proximal alteration zone and rarely overlap unaltered rock (Fig. 3.49d). Both Ag and W, however, demonstrate along-strike concentration gradients within the mineralized fault and therefore show some potential as a strike-parallel vector to ore (Fig. 3.50c,d). Tellurium concentrations are somewhat erratic within the proximal and intermediate alteration zones, but are consistently in the 15 to 50 ppb range in the outer zone and in unaltered rock (Fig. 3.49e). Eilu and Mikucki (1996) interpreted this concentration range to be within the expected background range for sedimentary rocks and dismissed Te as a potential vector to ore. Given the positive Te results from Bronzewing (see below), the role of Te at Twin Peaks may be worthy of reassessment.

In support of the results of Eilu and Mikucki (1996), WK Witt (unpublished data) found a rapid decrease of gold concentration in grade-control samples from ore grade (>0.5 ppm Au) beyond the proximal alteration zone, and that ore-grade samples rarely extend the full breadth of the intermediate alteration zone (Fig. 3.51a). Tungsten, however, remains anomalous (>2.5 ppm) well into the distal calcite zone (Fig. 3.51b).

Table 3.7. Summary of pathfinder element data showing anomalies that extend beyond the ore at Moyagee, Murchison Domain (Eilu and Mikucki, 1996)

Element	*Threshold*	*Extent of anomaly*		*Concentration gradient within anomaly*	
		From ore	*From Lena shear zone*	*Beyond ore*	*Beyond Lena shear zone*
Au	6 ppb	10-35 m	0 m	Common, ≤5 m	
Ag	0.11 ppm	0 to 20 m	0 m	None	None
As	5 ppm	20 to 50 m	0 m	Locally, up to 20 m	None
Sb	0.45 ppm	1 to 20 m	0 m	Locally, up to 15 m	None
Te	10 ppb	>70 m	>50 m	Locally, up to 20 m	None
W	0.5 ppm	10 to >70 m	0 to >50 m	Locally, up to 20 m	None
Se	0.15 ppm	5 to 50 m	0 m	Locally, up to 20 m	None

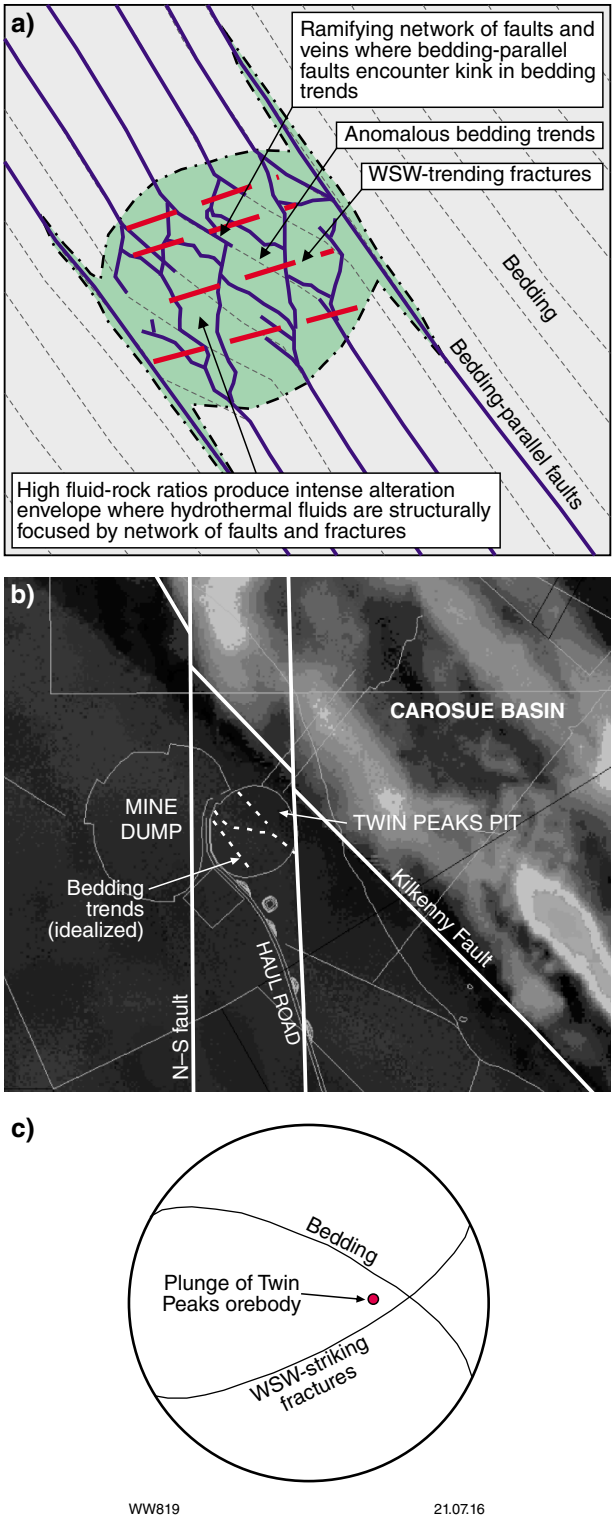

Figure 3.48. **Structural model for the Twin Peaks gold deposit, Carosue Dam district, Eastern Goldfields Superterrane (Witt, unpublished data). a) Schematic illustration of contractional jog where bedding-parallel faults encounter a Z-bend flexure in bedding. b) Aeromagnetic image showing interpreted faults and location of Twin Peaks deposit. c) Stereographic projection showing plunge of Twin Peaks orebody approximately coincident with the intersection between bedding and west-southwesterly striking fractures.**

More-precise analyses of gold in rock chip samples taken along the length and across the width of the Twin Peaks pit, and supported by samples from two diamond drillholes across mineralization, showed few samples with >10 ppb Au beyond the outer limit of the intermediate (dolomite) alteration zone (Fig. 3.52a). WK Witt (unpublished data) also found that anomalous As (>11 ppm) extends across, and locally beyond, the distal calcite alteration zone (Fig. 3.52b). It should be noted that the Twin Peaks deposit is within a district-scale As anomaly (>19 ppm As; Witt and Hammond, 2008) and that the low-level anomaly described by Eilu and Mikucki (1996) and Witt (herein) may therefore extend for several hundred metres along and across strike. It may, in fact, be difficult to distinguish a local As anomaly within the district-scale anomaly. Anomalous W (>2.5 ppm) is inconsistent within and beyond the distal calcite alteration zone (Fig. 3.52c). However, W defines the clearest concentration gradients along and across strike and thus provides a vector towards the high-grade centre of the orebody (Fig. 3.52c).

Other deposits in the Kalgoorlie and Kurnalpi Terranes

Bronzewing, Yandal belt

In basalt-hosted mineralization at Bronzewing, Eilu et al. (2001) found that Te at >44 ppb defined an anomaly that was similar in size and distribution to that of Au >4 ppb (Fig. 3.53a, c). However, at Te >6 ppb, which is equivalent to the average Te content of mafic igneous rocks (Koljonen, 1992), the Te anomaly extends beyond the limits of the study area (200 m from ore) and therefore far exceeds the footprint defined by anomalous gold (and all other pathfinder elements; Table 3.9). Gold correlates well with Te, Ag, W, and Sb, but poorly with As (Fig. 3.53d), which has a very low concentration (max. 11.9 ppm) at Bronzewing. Tungsten, Ag, Sb, Bi, and Te anomalies all spatially overlap the gold anomaly; the W (Fig. 3.53b), Sb, and Ag anomalies are of comparable size to the gold anomaly, but the Bi anomaly is much smaller. Because none of the anomalous elements exhibit concentration gradients within their anomalous areas, they all fail to provide an internal vector to ore (Eilu et al., 2001).

Karari, Carosue Dam camp

Karari is a sediment-hosted deposit on the contact with a monzonitic intrusion (Witt et al., 2009). It lies within the same district-scale, zoned hydrothermal alteration system as Twin Peaks, but in a more central part of the system that is relatively depleted in As (Witt and Hammond, 2008). Gold is mined from sediment-hosted albite-rich alteration zones within broader zones of potassic (biotite) alteration and is spatially associated with As and W (Witt et al., 2009; Fig. 3.54). WK Witt (unpublished data) investigated dispersion of multiple pathfinder elements by analysing grade-control samples on the 265 m RL of the Karari pit, rock chip samples from around the margins of the pit, and spaced samples from three diamond drillholes.

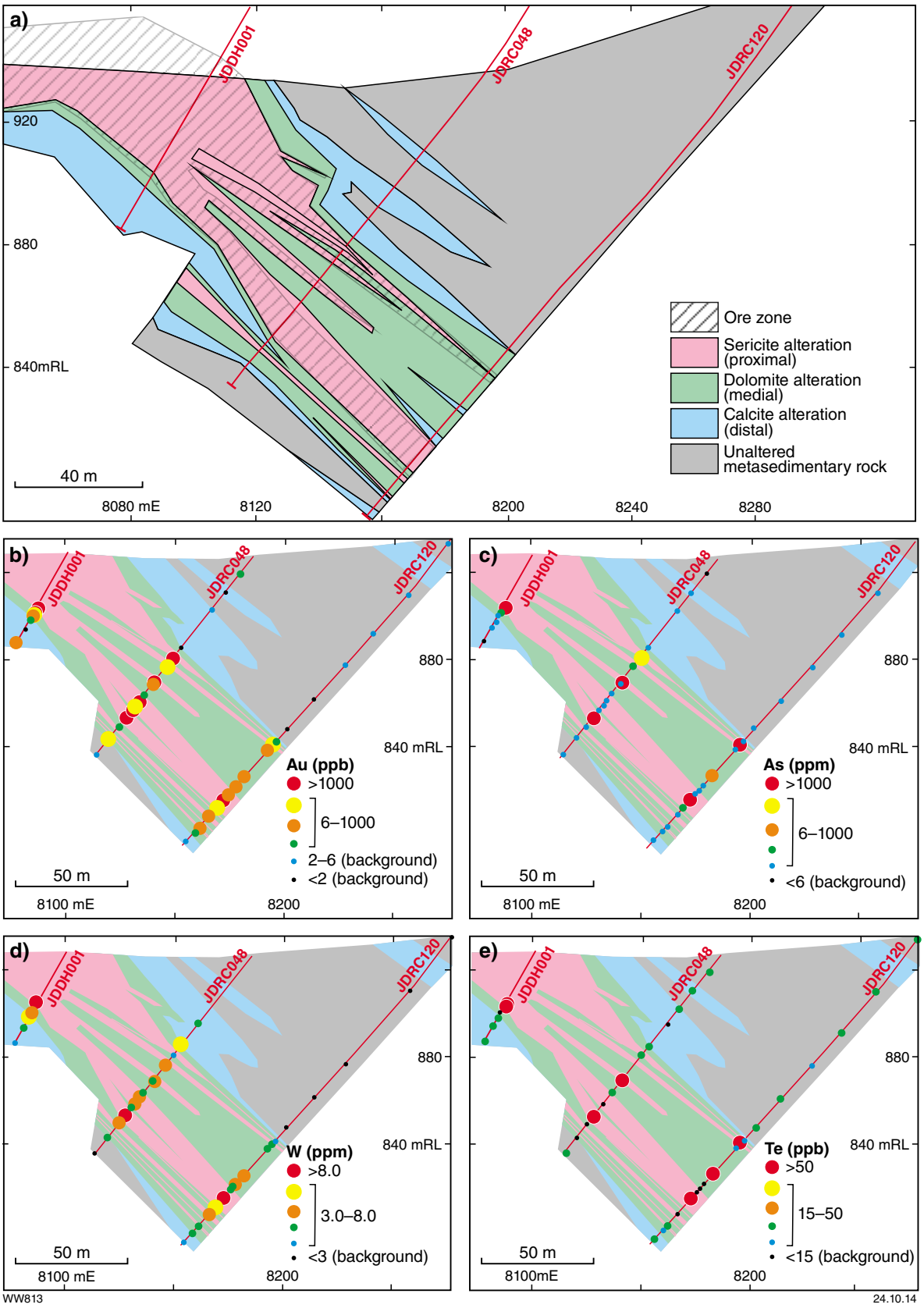

Figure 3.49. Gold and pathfinder element dispersion, Twin Peaks gold deposit (after Eilu and Mikucki, 1996). a) Southwest (left) – northeast (right) cross section showing distribution of hydrothermal alteration and ore zone (>1 g/t Au; diagonal lines overprint). Dispersion in cross section of b) Au, c) As, d) W, and e) Te. Coordinates refer to local mine grid.

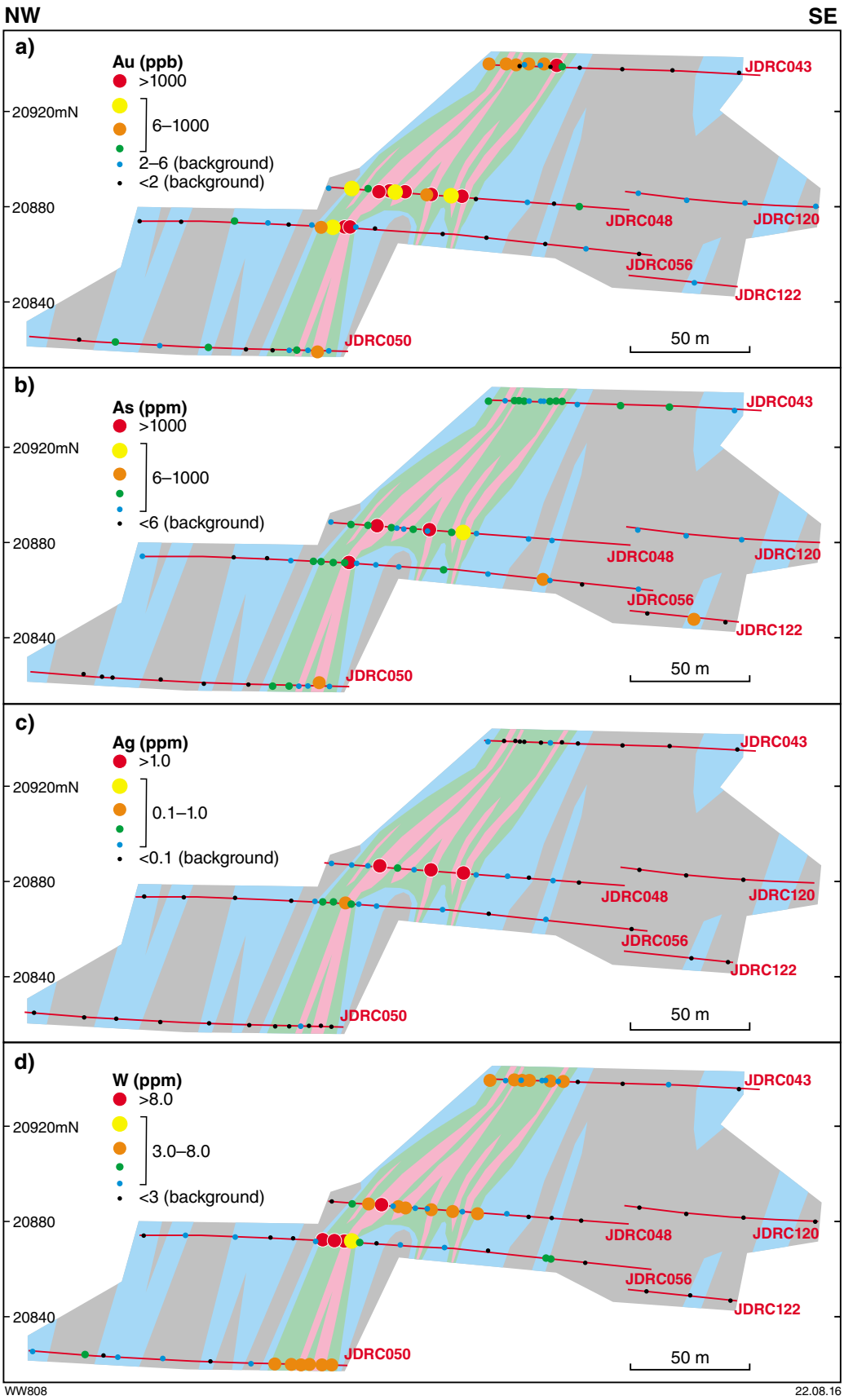

Figure 3.50. **Gold and pathfinder element dispersion on an inclined longitudinal cross section, Twin Peaks gold deposit (after Eilu and Mikucki, 1996). a) Au, b) As, c) Ag, and d) W. Coordinates refer to local mine grid. See Figure 3.49 for key to alteration zones.**

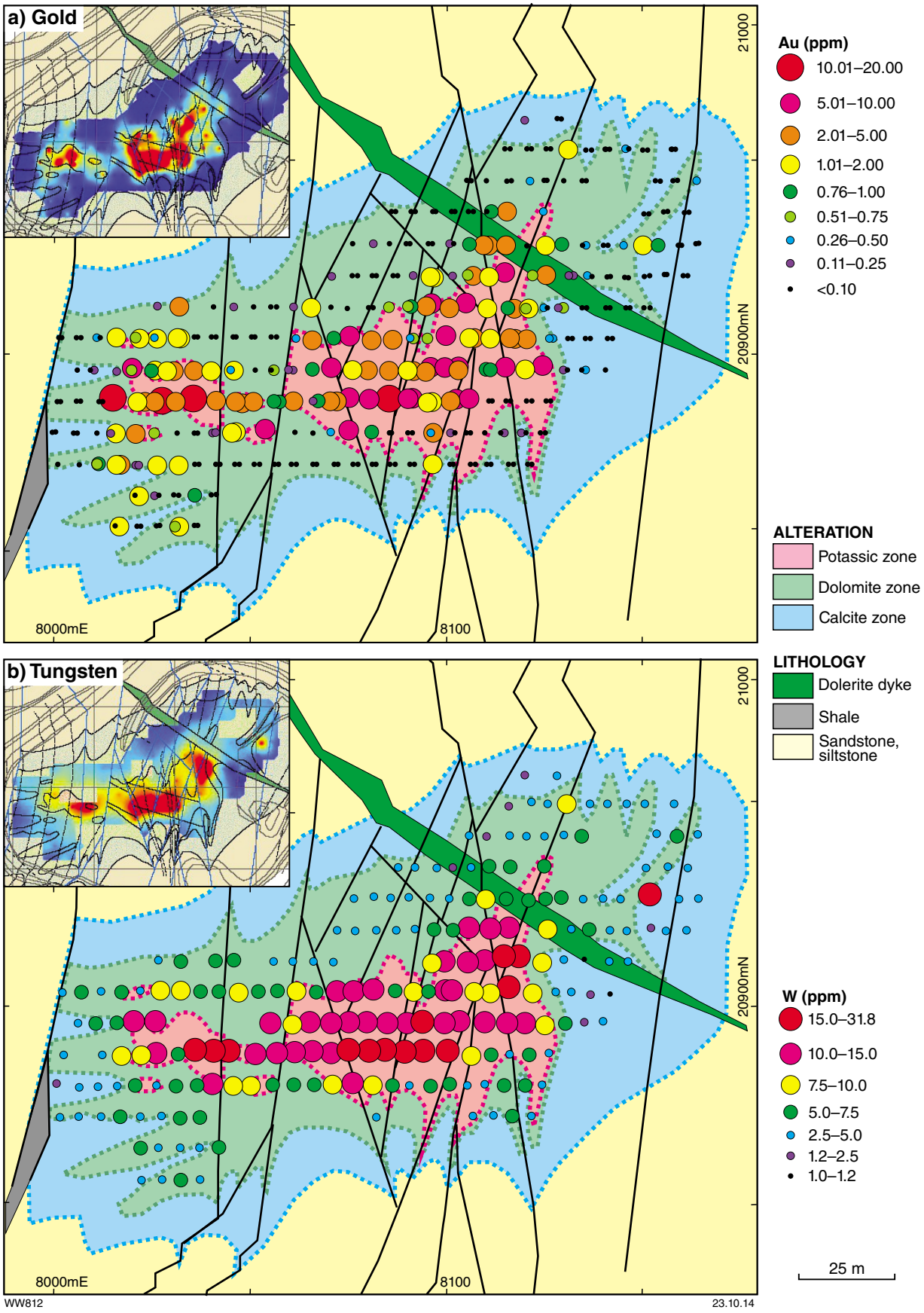

Figure 3.51. **Grade-control samples from 280 m RL, Twin Peaks gold deposit, overlain on alteration zones. a) Au, b) W. Insets are gridded data for Au and W. Coordinates refer to local mine grid.**

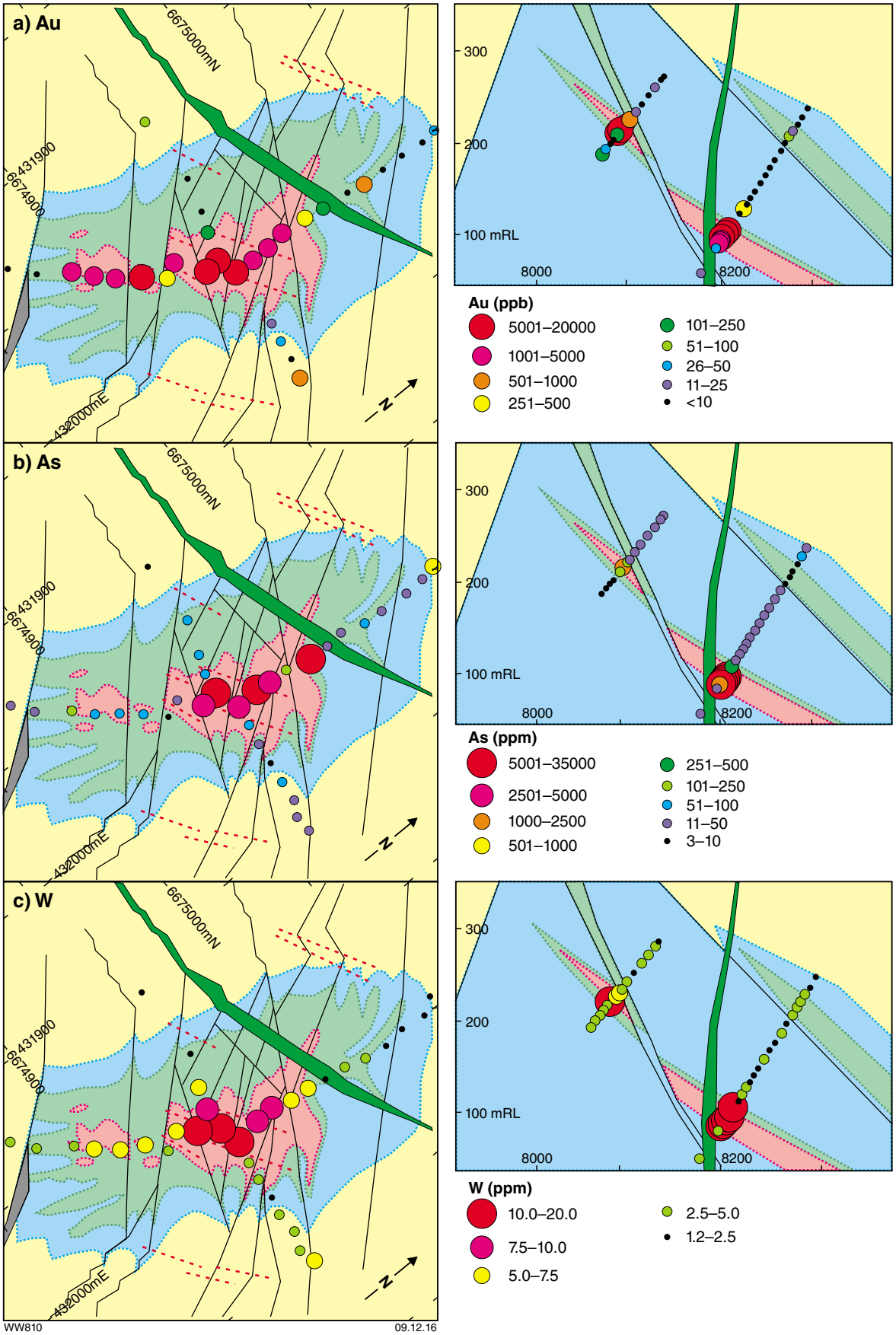

Figure 3.52. **Plan views (left) and cross sections (right), Twin Peaks gold deposit, showing distribution of gold and pathfinder elements in samples collected from the pit floor (plan) and from diamond drillholes (section). a) Au, b) As, and c) W. See Figure 3.51 for key to alteration zones. Coordinates refer to local mine grid.**

Table 3.8. Summary of pathfinder element data showing anomalies that extend beyond ore at Twin Peaks, Kurnalpi Terrane (Eilu and Mikucki, 1996)

Element	Threshold	Lateral extent of anomaly from ore		Concentration gradient within mineralized fault	
		Extent	Concentration gradient	Strike-parallel	Downdip
Au	2 ppb	2 to 10 m	Locally 0 to 10 m	Present, ≥80 m	Present, 50 m
As	6 ppm	20 to 110 m	Locally 5 to 30 m	Present, ≥80 m	Present, 50 m
Ag	0.10 ppm	0 to 20 m	Not present, 0 m	Present, ≥80 m	Present, 50 m
W	3 ppm	5 to 30 m	10 to 30 m	Present, ≥80 m	Present, ≥150 m
Te	50 ppb	0 m	Not present, 0 m	Present, ≥80 m	Not present, 0 m

Table 3.9. Summary of pathfinder element data showing anomalies that extend beyond ore at Bronzewing, Yandal greenstone belt (Eilu et al., 2001)

Element	Threshold	Extent of anomaly		Concentration gradient within anomaly
		From ore	From gold anomaly	
Au	4 ppb	1 to 80 m	0 m	Not recorded
Ag	0.16 ppm	0 to 40 m	0 m	Not recorded
Te (local)	44 ppb	0 to 20 m	0 m	Not recorded
Te (regional)	6 ppb	>200 m	>100 m	Not recorded
Sb	0.4 ppm	0 to 100 m	0 to 40 m	Not recorded
W	1.9 ppm	0 to 50 m	0 to 30 m	Not recorded

At the district-scale threshold of 3 ppm, W is anomalous throughout much of the pit, but is depleted in zones of muscovite alteration and in lamprophyre dykes interpreted to post-date mineralization (Witt et al., 2009; Fig. 3.54b). At a threshold of 5 ppm, As shows a similarly extensive footprint, but this anomaly is much smaller if a district-wide threshold of 19 ppm (Witt and Hammond, 2008) is employed. Most other pathfinder elements (including Ag, Bi, Mo, Cu, Te, Sb, Pb and Zn) are spatially associated with the adjacent monzonitic intrusion, which hosts weak Cu–Au mineralization.

Pit and diamond drillcore sample results are consistent with those of grade-control samples and show that there is a very sharp demarcation between ore in sodic alteration zones and gold at <50 ppb in adjacent potassic alteration zones and lamprophyre dykes. The results for rock chip and core samples support those of grade-control samples from the 265 m RL; they show that As (Fig. 3.55) and W (Fig. 3.56) are above 5 ppm and 3 ppm, respectively, throughout most of the sampled sections of the openpit, except in samples from muscovite alteration zones and lamprophyres.

Harbour Lights, Leonora camp

The Harbour Lights deposit is a complex, mineralized brittle–ductile shear zone close to the contact between the Raeside batholith (c. 2760 Ma) and greenstones of the Gwalia domain (Skwarnecki, 1989; Witt, 2001; Vearncombe, 1992). The mineralized shear zone is broadly centred on a contact between ultramafic and mafic units but encompasses thin units of intermediate intrusive rock (diorite) and interflow metasedimentary rock. All units are heavily modified by hydrothermal alteration and ductile deformation (Fig. 3.57). The somewhat stylized cross section in Figure 3.57 is based on geological mapping of the openpit and logging of selected diamond drillcore. The geochemical data shown are from exploration and mine development diamond and RC drillholes within a cross-sectional window through the centre of the orebody. Alteration of ultramafic rocks is dominated by hydrothermal biotite and dolomitic carbonate, but mafic units, some of which form relatively low-strain lithons within ultramafic schist, contain hydrothermal white mica rather than biotite. Fuchsitic mica is locally developed in metasedimentary interbeds and at mafic–ultramafic contacts. Sulfides are mainly pyrite and arsenopyrite.

Using the data of Skwarnecki (1989), Eilu et al. (1997) found that As and Sb were elevated over the entire 100 m width of the mineralized and hydrothermally altered shear zone. Despite relatively high detection limits, they showed that As remained in the 10 to 100 ppm range, and Sb in the 20 to 50 ppm range, for up to 40 m into the footwall of the deposit.

WK Witt (unpublished data) found that the mineralized shear zone was characterized by high As, W, Mo, Sb, and Bi contents, but that only As remained anomalous for more than about 10 m beyond the proximal zone of mica–carbonate alteration (Kb and bc in Fig. 3.57).

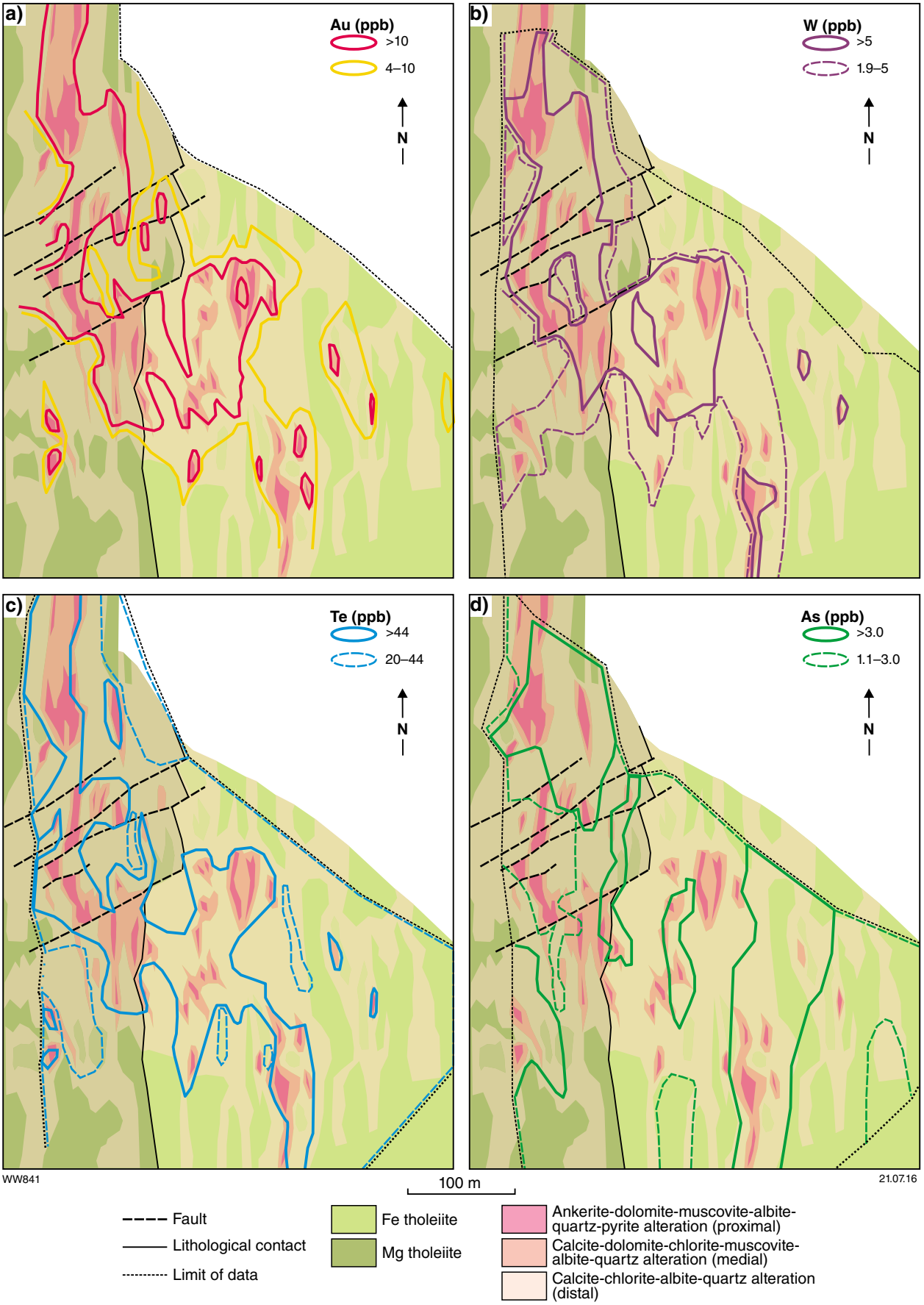

Figure 3.53. Gold and pathfinder element dispersion, Bronzewing gold deposit, Yandal district, Eastern Goldfields Superterrane (after Eilu et al., 2001). a) Au, b) W, c) Te, and d) As.

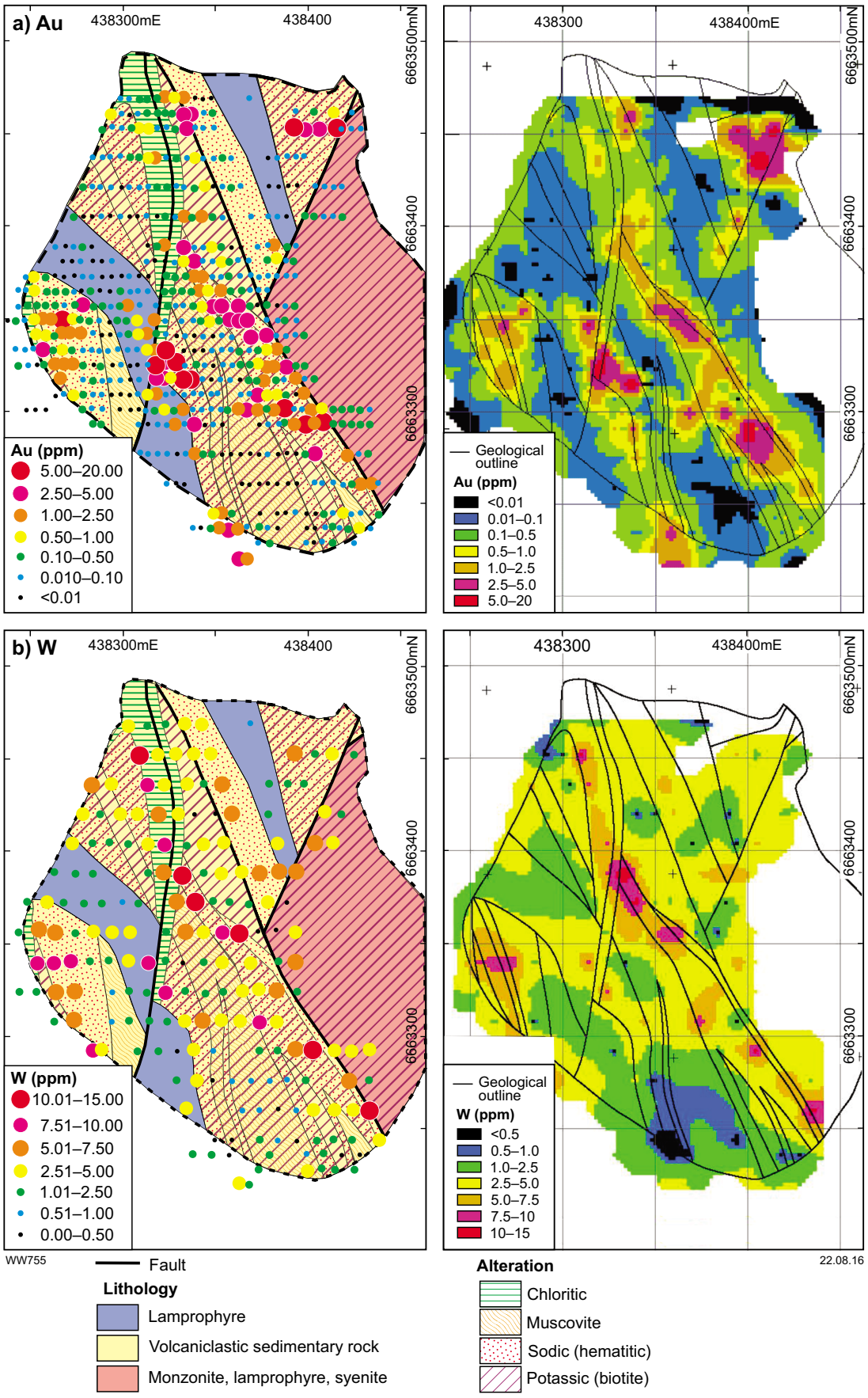

Figure 3.54. **Gold and pathfinder element distribution, Karari, Carosue Dam district, Eastern Goldfields Superterrane. Maps on left show abundances in grade-control samples collected from the 265 m RL; those on the right show the same data in a gridded format: a) Au and b) W.**

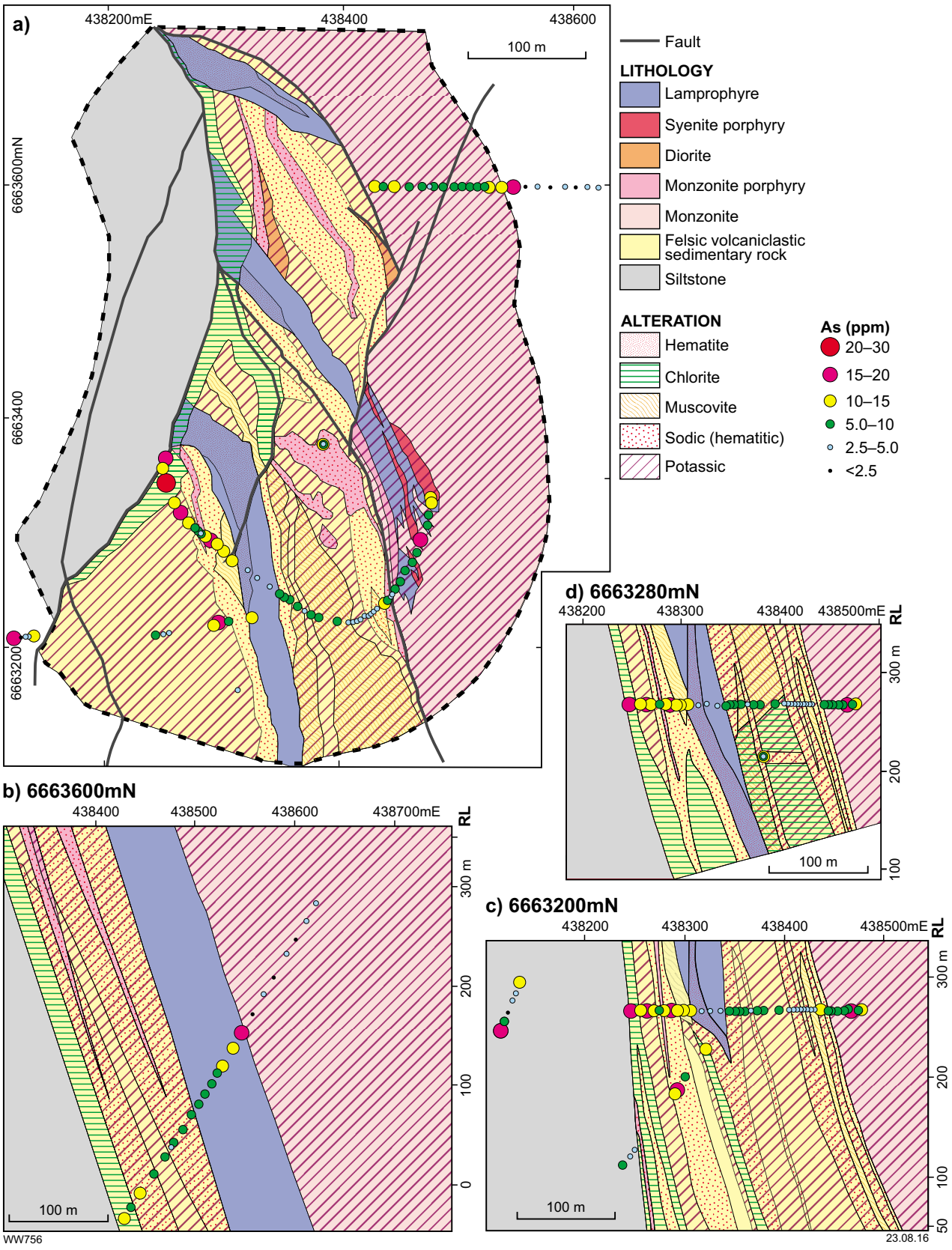

Figure 3.55. **Geological map and cross sections, Karari gold deposit, showing As abundance in samples collected from the openpit and selected drillcore. a) Plan view, b) cross section 6663600N, c) cross section 6663200N, d) cross section 6663280N.**

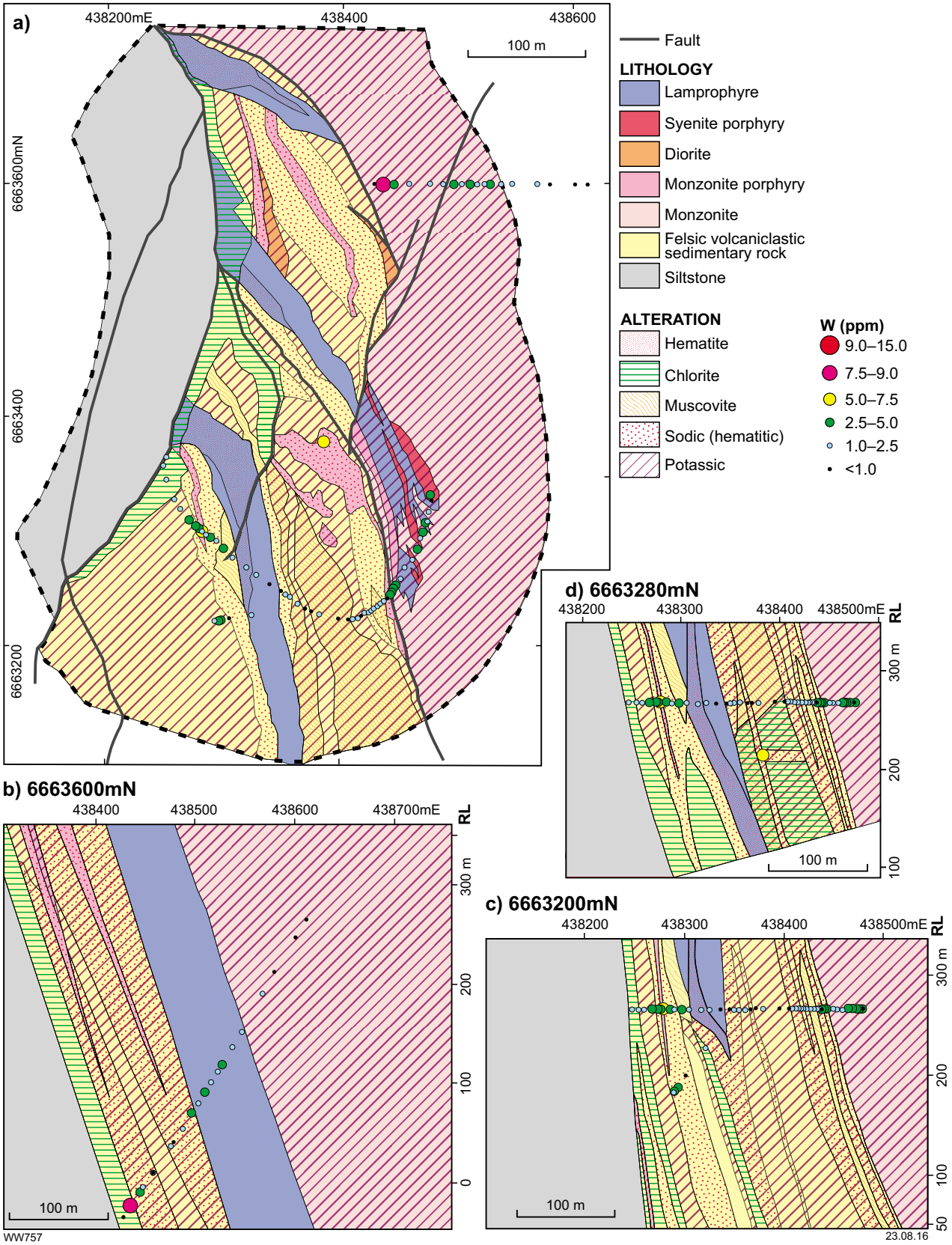

Figure 3.56. **Geological map and cross sections, Karari gold deposit, showing W abundance in samples collected from the openpit and selected drillcore. a) Plan view, b) cross section 6663600N, c) cross section 6663200N, d) cross section 6663280N.**

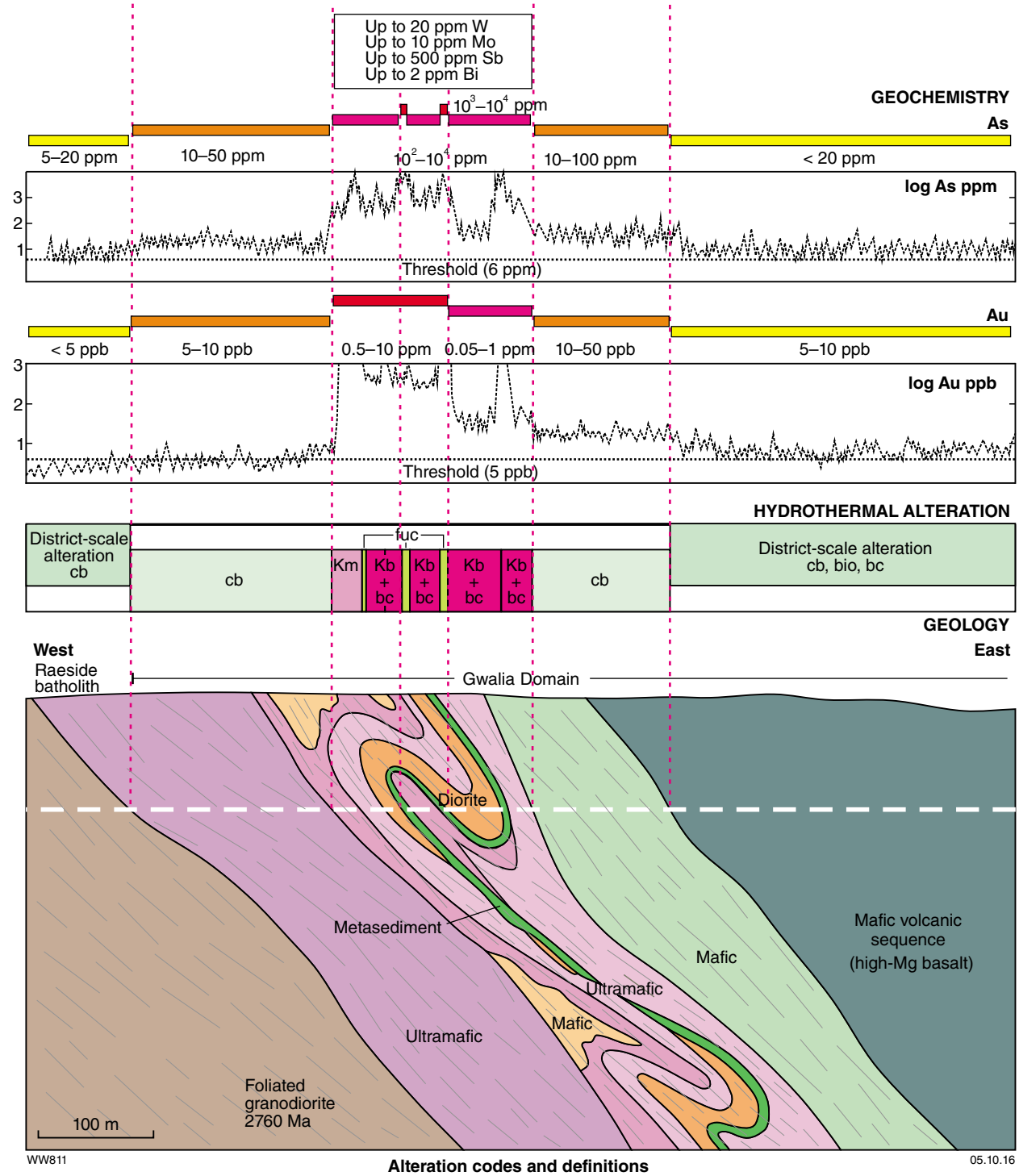

Alteration codes and definitions

PROXIMAL ALTERATION

- Fuchsite (fuc) — *Ultramafic and metasedimentary rock*
  Quartz-carbonate-muscovite (-fuchsite)-pyrite, arsenopyrite.
- Potassic (Km) — *Mafic rock*
  Quartz-carbonate-muscovite (locally fuchsitic)-pyrite, arsenopyrite.
- Potassic (Kb) — *Ultramafic rock*
  Carbonate-biotite-chlorite (+/– quartz, talc, pyrite)
  Biotite: chlorite >2:1

INTERMEDIATE ALTERATION

- Biotite-chlorite (bc) — *Ultramafic rock*
  Carbonate-chlorite-biotite (+/– talc, pyrite).
  Biotite: chlorite between 2:1 and 1:2
- Biotite-chlorite (bc) — *Mafic and diorite*
  Plagioclase-biotite-chlorite-carbonate (+/– pyrite).
  Biotite: chlorite between 2:1 and 1:2

DISTAL ALTERATION

- Carbonate (cb) — *Ultramafic rock*
  Carbonate-chlorite-talc.
- Carbonate (cb) — *Mafic rock*
  Chlorite-calcite-plagioclase.

Figure 3.57. Idealized cross section through Harbour Lights gold deposit, Leonora district, Eastern Goldfields Superterrane, showing hydrothermal alteration and distribution of gold and pathfinder elements

Both As (10 to 100 ppm) and Au (10 to 50 ppb) remain well above background in the hangingwall distal carbonate alteration zone. In the footwall, As remains anomalous (10 to 50 ppm) in the distal carbonate alteration zone, whereas gold decreases to threshold values (~5 ppb) within about 10 m of the proximal to intermediate alteration zones (Fig. 3.57). Arsenic also remains mildly anomalous in footwall granite of the Raeside batholith, whereas gold decreases to below the threshold value. Lower level As and Au anomalies characterize the district-scale alteration (equivalent to regional carbonate alteration plus pre-metamorphic alteration in Figure 2.119, Part 2 of this Atlas) of the Gwalia domain greenstones for distances of >400 m in the hangingwall of the deposit.

Figure 3.57 also shows how concentration gradients for Au in the footwall carbonate-altered ultramafic unit and hangingwall district-scale alteration provide a potential vector to mineralization. Contrastingly, the changes in As concentration are relatively sharp at these transitions and do not provide an internal vector. Arsenic does, however, provide a more distal vector in the footwall transition from carbonate-altered granodiorite to carbonate-altered ultramafic rock.

To summarize (Table 3.10), As provides a strong geochemical anomaly at Harbour Lights, which extends through the visible distal (carbonate) alteration zone. This anomaly also extends beyond the Au anomaly in the footwall carbonate alteration zone and, at lower abundance levels, into the footwall granite. A relatively subtle As and Au anomaly extends for several hundred metres into district-scale alteration in the hangingwall of the deposit, but the significance of this more extensive anomaly is uncertain; it may, in part, be related to a hydrothermal system unrelated to the Harbour Lights mineralization.

Tower Hill, Leonora camp

Tower Hill is 2 km south of Harbour Lights and similarly lies close to the margin of the Raeside batholith. At Tower Hill, the batholith has been intruded by later massive biotite monzogranite (c. 2750 Ma) and gold mineralization is associated with metre-scale, dismembered quartz reefs hosted by ultramafic rocks (Witt, 2001). The ultramafic rocks have been hydrothermally altered and now comprise proximal talc–carbonate–biotite–pyrite grading into distal talc–chlorite–carbonate schist (Figs 3.58 and 3.59). The hydrothermally altered wallrocks contain little gold and mining has focused on the quartz reefs. The easternmost of these, termed the hangingwall reef, contains much molybdenite, whereas bismuth minerals are common in the footwall reef (Schiller and Hannah, 1990; Witt, 2001).

Gold is anomalous throughout the proximal, potassic (biotite) alteration zone but dips below 5 ppb in the hangingwall, distal (carbonate) alteration zone and in the district-scale alteration zone separating Tower Hill from the exhalite horizon in the Mount George Shear Zone (Fig. 3.58). At a threshold of 5 ppb, Au remains anomalous over >150 m into the carbonate-altered footwall biotite monzogranite.

Pathfinder elements As, Sb, Bi, Mo, and W are elevated within the proximal, potassic (biotite) alteration zone, but none of these remain consistently elevated throughout the hangingwall distal carbonate alteration and district-scale alteration zones. Antimony is weakly anomalous at 0.5–5 ppm throughout most of the district-scale alteration, but is relatively depleted in the distal carbonate alteration zone. Arsenic concentrations are mostly below the anomaly threshold of 6 ppm, but show irregular spikes of up to about 100 ppm in the carbonate and district-scale alteration zones (Fig. 3.58). The reason for the As spikes is not known. The dispersion of As and Sb into the hangingwall at Tower Hill represents an anomalous zone of >600 m width beyond the gold anomaly. However, because the concentration of Sb is relatively depleted in the distal carbonate alteration zone, this dispersion appears to be related to the synvolcanic alteration below the Mount George exhalite horizon rather than the Tower Hill mineralization itself.

Gold (5–10 ppb), As (2–100 ppm), and Sb (1–5 ppm) are all continuously or intermittently anomalous for distances of about 200 m into the footwall of the deposit, where the Tower Hill Monzogranite has been overprinted by carbonate alteration (Table 3.11). Of these, Sb appears to show the most potential to define a broad but subtle anomaly in the footwall of the gold mineralization.

Table 3.10. Summary of pathfinder element data showing anomalies that extend beyond ore at Harbour Lights, Leonora district (WK Witt, unpublished)

Element	*Threshold*	*Extent of anomaly*			*Concentration gradient within anomaly beyond ore*
		From ore/proximal alteration	*From gold anomaly*	*From all visible gold-related alteration[b]*	
Au	10 ppb	110 m	0 m	0 m	Present over >100 m
Au	5 ppb	>400 m	0 m	>300 m	
As	10 ppm	110 m	0 m	0 m	Steps only
As	6 ppm	>400 m	0 m	>300 m	
As[a]	10 ppm	175 m	150 m	>50 m	Limited to transition between distal carbonate alteration and district-scale alteration

NOTES: (a) All entries refer to the deposit hangingwall, except this one, which is a footwall anomaly. (b) Excludes district-scale alteration in Figure 3.57.

Table 3.11. Summary of pathfinder element data showing anomalies that extend beyond ore at Tower Hill, Leonora district (WK Witt, unpublished)

Element	*Threshold*	*Extent of anomaly*			*Concentration gradient within anomaly beyond ore*
		From ore/proximal alteration	*From gold anomaly*	*From all visible gold-related alteration*	
Au	5 ppb	0 m	0 m	0 m	About 10 m
Au[(a)]	5 ppb	>150 m	0 m	>150 m	Not present
As[(b)]	6 ppm	0 m	0 m	0 m	Not present
Sb[(b)]	0.5 ppm	>400 m	>400 m	>300 m	Not present
Sb[(a)]	0.5 ppm	>175 m	>25m	>175 m	Concentration gradient at >1 ppm extends 200 m into the footwall

NOTES: (a) Footwall anomaly – hangingwall for all other entries. (b) Spikes of anomalous As concentrations extend >400 m into the hangingwall; hangingwall Sb is more continuously anomalous, but hangingwall As and Sb anomalies are probably not related to gold mineralization.

Gradients in the footwall Sb anomaly, and less clearly in the corresponding As anomaly, provide a vector towards the deposit. A narrow (~10 m) hangingwall vector is provided by Au, but not by As or Sb, which are possibly related to a relatively early (synvolcanic) period of hydrothermal alteration.

Deposits of the Southern Cross Domain*

Shear-hosted gold deposits

Geochemical data in the context of hydrothermal alteration zoning are presented for three shear-hosted deposits in the Southern Cross district: Marvel Loch, Yilgarn Star, and Transvaal. Unlike most of the deposits described above (Kings Cross excepted), these three deposits are in amphibolite facies greenstones, so the hydrothermal alteration they have undergone reflects correspondingly higher-temperature mineral assemblages. The hosting shear zones appear to have been more strongly ductile than the brittle to brittle–ductile host structures described above.

Marvel Loch

The Marvel Loch gold deposit comprises many separate lodes within a broad zone of ductile shearing that is centred on a mylonitized contact between mainly mafic (gabbroic) rocks to the east and mainly ultramafic rocks to the west (Fig. 3.33). The Sherwood, Contact, and East lodes are hosted by gabbroic rocks to the east of the 'median mylonite' (a local informal mining term), whereas the remaining lodes are hosted by ultramafic rocks to its west. In the mafic rocks, proximal plagioclase (plg) alteration lies within a broad zone of hydrothermal biotite (Kcs, bio) in which the proportion of biotite to amphibole decreases with distance from the lodes. In the ultramafic rocks, thin proximal zones of K-feldspar (Kfp) alteration are enveloped by much broader medial zones of potassic calc-silicate (Kcs) alteration and distal talcose (tlc) alteration zones (see Fig. 3.59 for key to alteration codes).

The most widely dispersed element at Marvel Loch is gold, which maintains anomalous values (10 to 100 ppb) for 30 m beyond the medial (Kcs) alteration zone in ultramafic host rocks, and (at >5 ppb) throughout the broad (several hundred metres wide) zone of medial alteration (Kcs) in mafic host rocks (Fig. 3.60). No pathfinder elements display the same extent of dispersion; As and Sb remain elevated to the outer limit of medial alteration in ultramafic rocks but fall below threshold values a few metres into the distal alteration (tlc) zone. In mafic rocks, As remains anomalous for 50 m beyond the proximal (plg) alteration, whereas Sb remains distinctly anomalous for only 25 m beyond the proximal alteration.

The Marvel Loch mineralization is within a several hundred metres wide zone of potassic alteration that is characterized by the presence of biotite and is more broadly developed in the mafic host rock sequence (Fig. 3.60). The average K content of mafic rocks is taken as 1160 ppm (Hart, 1971) and the extent of the K anomaly is about the same as that of the gold anomaly. The K anomaly is quite flat. Caesium (average concentration in tholeiitic basalt of 0.016 ppm; Hart, 1971), which commonly substitutes for K, defines an anomaly of similar extent but appears more sensitive to variations in hydrothermal alteration and Au content (Fig. 3.60). Nevertheless, dispersion of Au is greater than those of K and Cs.

Although neither gold, nor the pathfinder elements define anomalies larger than the hydrothermal biotite footprint, the gradual gradients of Au, As, and Sb provide vectors to ore in both the hangingwall and footwall of the deposit (Fig. 3.60; Table 3.12). Potassium displays a broad concentration gradient only in the footwall (west) of the deposit. In combination, the elements Au, As, and Sb provide effective step-wise vectors towards high-grade mineralization within the broad mafic-hosted medial alteration zone at Marvel Loch. The extent of the concentration gradient, which is found in the distal and outer medial alteration zones, is largest for gold, and decreases progressively through As and Sb.

* Based largely on unpublished work by WK Witt

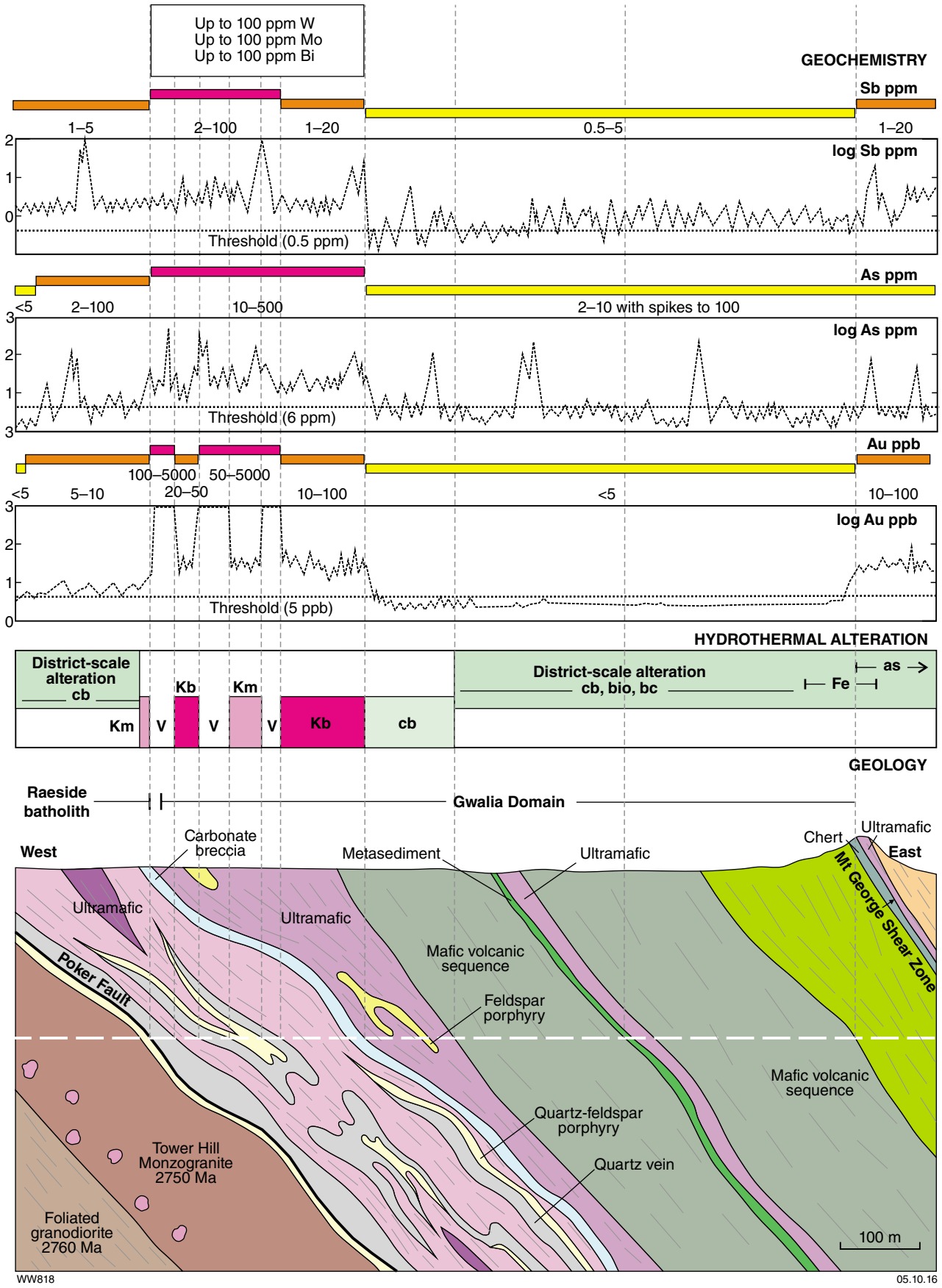

Figure 3.58. **Idealized cross section through Tower Hill gold deposit, Leonora district, Eastern Goldfields Superterrane, showing hydrothermal alteration and distribution of gold and pathfinder elements. See Figure 3.59 for explanation of alteration codes.**

Alteration codes and definitions

TOWER HILL (Figure 3.58)

PROXIMAL ALTERATION	DISTAL ALTERATION	REGIONAL ALTERATION
Potassic (Kb) — *Ultramafic rock* Talc-carbonate-biotite-pyrite (+/– retrograde chlorite). *Biotite: chlorite >2:1*	**Carbonate (cb)** — *Ultramafic rock* Chlorite-carbonate-talc.	**Carbonate (cb)** — *Mafic rock* Chlorite-carbonate (+/– plagioclase)
Potassic (Km) — *Felsic schist, porphyry, granite* Quartz-muscovite; minor calcite, chlorite, pyrite (replacement of biotite).		**Biotite (bio)** — *Mafic rock* Chlorite-carbonate-biotite (+/– plagioclase, sulfide). *Biotite: chlorite <1:2*
		Biotite–Chlorite (bc) — *Mafic rock* Chlorite-biotite-carbonate (+/– sulfide) *Subequal biotite and chlorite.*
		Ferrugionus (Fe) — *Mafic rock, sedimentary rock* Chlorite-magnetite (+/– siderite, pyrrhotite, quartz).
		Aluminosilicate (as) — *Mafic rock* Muscovite-carbonate-chlorite-quartz (+/– chloritoid, andalusite, sulfide).

MARVEL LOCH (Figure 3.60)

PROXIMAL ALTERATION	MEDIAL ALTERATION	DISTAL ALTERATION
Plagioclase (plg) — *Mafic rock* Plagioclase-biotite-sulfide *plg>>bio*	**Potassic/calc-silicate (Kcs)** — *Mafic rock* Plagioclase-biotite-amphibole ±sulfide bio*: amp <2:1 but >2:1* *(ie subequal)*	**Biotite (bio)** — *Mafic Rock* Plagioclase-amphibole-biotite±sulfide *bio:amp <1:2*
Potassic (Kb) — *Mafic rock* Plagioclase-biotite±sulfide bio*: amp >2:1*		**Calc-silicate (cs)** — *Mafic rock* Plagioclase-diopside±amphibole, sulfide
Potassic/calc-silicate (Kcs) +/– K-feldspar (Kfp) — *Ultramafic rock* K-feldspar-biotite-sulfide ±amphibole,diopside	**Potassic/calc-silicate (Kcs)** — *Ultramafic rock* Tremolitic amphibole-biotite±sulfide	**Talc (tlc)** — *Ultramafic rock* Tremolite-amphibole-talc±chlorite

YILGARN STAR (Figure 3.61 and 3.71)

PROXIMAL ALTERATION	DISTAL ALTERATION
Carbonate (cb) — *Ultramafic rock* Tremolite-actinolite-dioside-calcite-forsterite(±dolomite)-pyrrhotite	**Talc (tlc)** — *Ultramafic rock* Tremolite-actinolite-talc
Potassic (Kb) — *Metasedimentary rock* Quartz-biotite(±garnet)-pyrrhotite	
RETROGRESSIVE ALTERATION **Potassic (Km)** — *Metasedimentary rock* Quartz-muscovite-pyrrhotite	
PRE-METAMORPHIC ALTERATION **Potassic-magnesian (KMg)** — *Mafic rock* Quartz-biotite-cordierite (±garnet, plagioclase, pyrrhotite) with zoned calc-silicate (diopside-hornblende)veins	

GREAT VICTORIA (Figure 3.64)

	DISTAL ALTERATION
	Potassic (Km) — *Metasedimentary* rock Quartz-muscovite(±garnet, andalusite)
PRE-METAMORPHIC ALTERATION **Potassic-magnesian (KMg)** — *Mafic rock* Hornblende(±garnet, plagioclase,pyrrhotite) (Coarse, matted amphibole)	

WW842 05.10.16

Figure 3.59. Alteration codes and definitions used in Figures 3.58, 3.60, 3.61, 3.64, and 3.71.

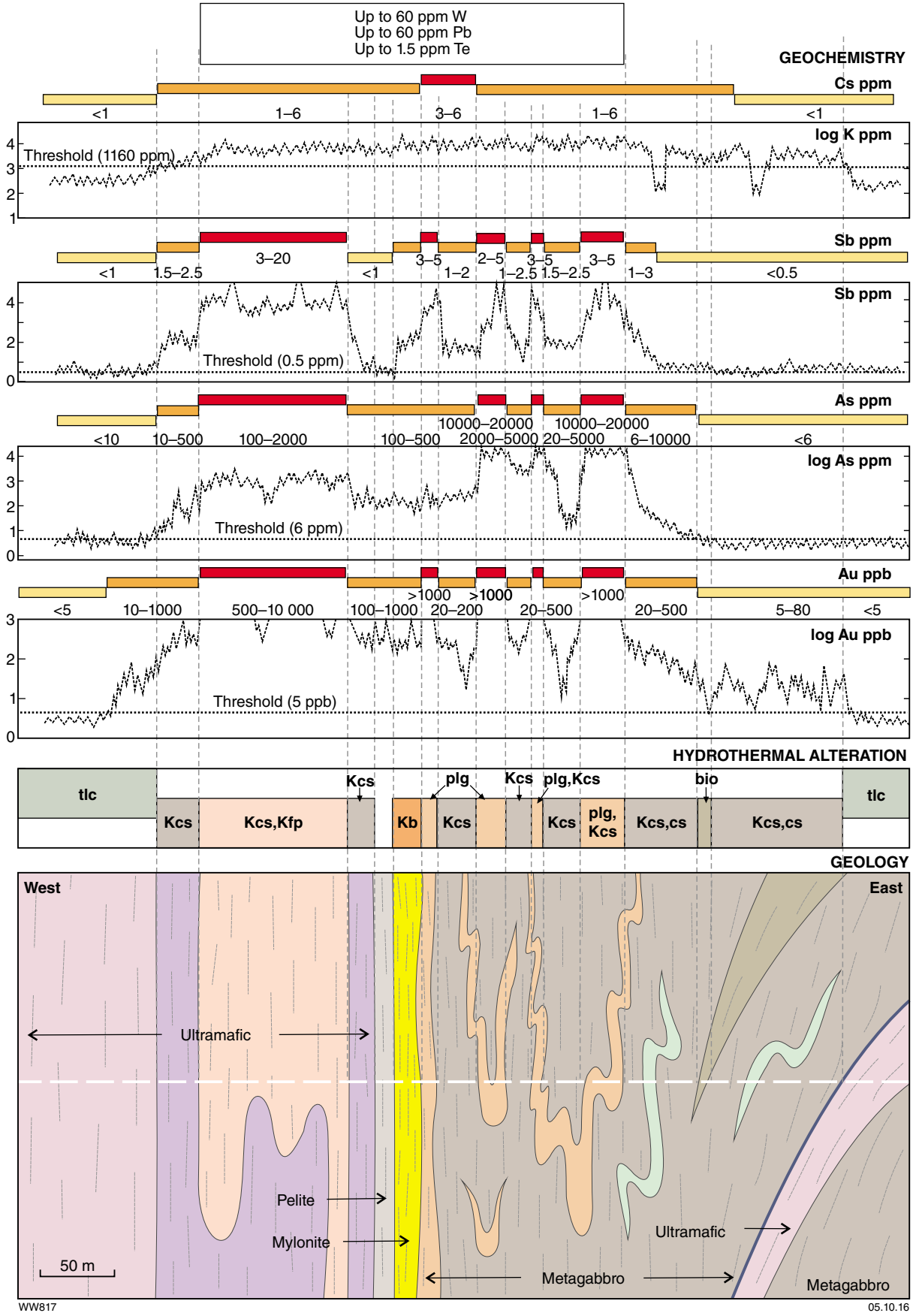

Figure 3.60. **Idealized cross section through Marvel Loch gold deposit, Southern Cross district, Youanmi Terrane, showing hydrothermal alteration and distribution of gold and pathfinder elements. See Figure 3.59 for explanation of alteration codes.**

Table 3.12. Summary of pathfinder element data showing anomalies that extend beyond ore at Marvel Loch, Southern Cross district (WK Witt, unpublished)

Element	Threshold	Extent of anomaly			Concentration gradient within anomaly beyond ore
		From ore/ proximal alteration	From gold anomaly	From all visible gold-related alteration	
Au (mafic)	5 ppb	>150 m	0 m	0 m	Present over 100 m
Au (ultramafic)	10 ppb	60 m	0 m	0 m	Present over 60 m
As (mafic)	6 ppm	50 m	0 m	0 m	Present over 50 m
As (ultramafic)	6 ppm	25 m	0 m	0 m	Present over 25 m
Sb (mafic)	0.5 ppm	25m	0 m	0 m	Present over 25 m
Sb (ultramafic)	0.5 ppm	25 m	0m	0 m	Not present
K (mafic)	1160 ppm	150 m	0 m	0 m	Not present
K (ultramafic)	1160 ppm	25 m	0 m	0 m	Weak gradient present
Cs (mafic)	1 ppm	75 m	0 m	0 m	Not present
Cs (ultramafic)	1 ppm	25 m	0 m	0 m	Not present

Yilgarn Star

Yilgarn Star is a shear-hosted gold deposit on the contact between ultramafic and metasedimentary rocks (Fig. 3.61). Proximal alteration related to pelitic metasediment-hosted gold-bearing veins (Herring Bone Lodes) contains hydrothermal biotite and pyrrhotite (Kb alteration), an assemblage that has been variably retrogressed to muscovite (Km alteration). The ultramafic-hosted Premier Lodes are auriferous veins that have a complex pyrrhotite-bearing proximal carbonate alteration assemblage (cb) and distal talcose (tlc) alteration (Fig. 3.59).

Gold is the most effective vectoring element at Yilgarn Star (Table 3.13). Although smooth gradients are not well-developed in the footwall, gold abundance changes in a series of steps, decreasing from peak values in the mineralized proximal alteration zones. For ultramafic host rocks, Au values above 50 ppb extend 10 to 20 m beyond the proximal alteration zone, through a further 15 m at values between 5 and 50 ppb, then falling to a local background level of <10 ppb (Fig. 3.61). In the metasedimentary hangingwall, there is a more gradual decrease in gold abundance with distance from the proximal alteration zone. Values >10 ppb extend 20 m beyond the proximal alteration zone, and values above 5 ppb extend a further 15 m.

Arsenic (>500 ppm) and antimony (>1.0 ppm) remain elevated for about 20 m into the distal (talc) alteration zone in ultramafic host rocks but do not extend more than a few metres beyond the proximal alteration zone in metasedimentary host rocks. Rubidium, which can be viewed as a geochemical proxy for potassium, is enriched (50–200 ppm) in the proximal alteration zone of the metasedimentary hangingwall and in the biotite-rich pre-metamorphic (KMg) alteration zone that separates the Premier and Herring Bone Lodes in the south of the deposit (Fig. 3.61). A weak but broad (>60 m) Rb concentration gradient in the metasedimentary hangingwall (35–125 ppm) may represent an exploration vector if the gradient is related to gold mineralization rather than pre-metamorphic KMg alteration. The proximal alteration zone in ultramafic rock is depleted in Rb, consistent with the low abundance of potassic minerals, but defines a weak enrichment halo (25–100 ppm) between 10 and 35 m into the footwall of the deposit. Zinc and tungsten are anomalous in the proximal alteration zone of the Premier Lodes but are also elevated in the pre-metamorphic (KMg) alteration zone; the origin of these anomalies is not clear.

Transvaal

Transvaal gold deposits are hosted by ductile shear zones that follow the contact between pelitic and psammitic metasedimentary units (Mercury-style lodes) and transect a folded contact between metasedimentary and ultramafic units (Polaris-style lodes)(see Fig. 3.35). Proximal alteration in metasedimentary rocks is similar to that at Yilgarn Star but proximal (amp) alteration in ultramafic rocks is dominated by tremolite–actinolite with variable biotite and pyrrhotite (Fig. 3.62), probably reflecting less-magnesian precursor ultramafic rocks at Transvaal.

Gold is an effective vector towards high-grade gold lodes in metasedimentary rocks at Transvaal, forming a concentration gradient (at >50 ppb) that extends 10 to 25 m beyond the proximal alteration zone within the footwall and the hangingwall (Fig. 3.62). A lower cutoff of 10 ppb Au produces a dispersion halo that extends about 70 m into the ultramafic and mafic hangingwall of Polaris-style lodes (Table 3.14). Concentrations remain at these elevated values in mafic rocks for at least 50 m beyond the distal ultramafic-hosted (Kcs) alteration zone. More restricted gradients in gold concentration constitute a vector to ore in ultramafic rock.

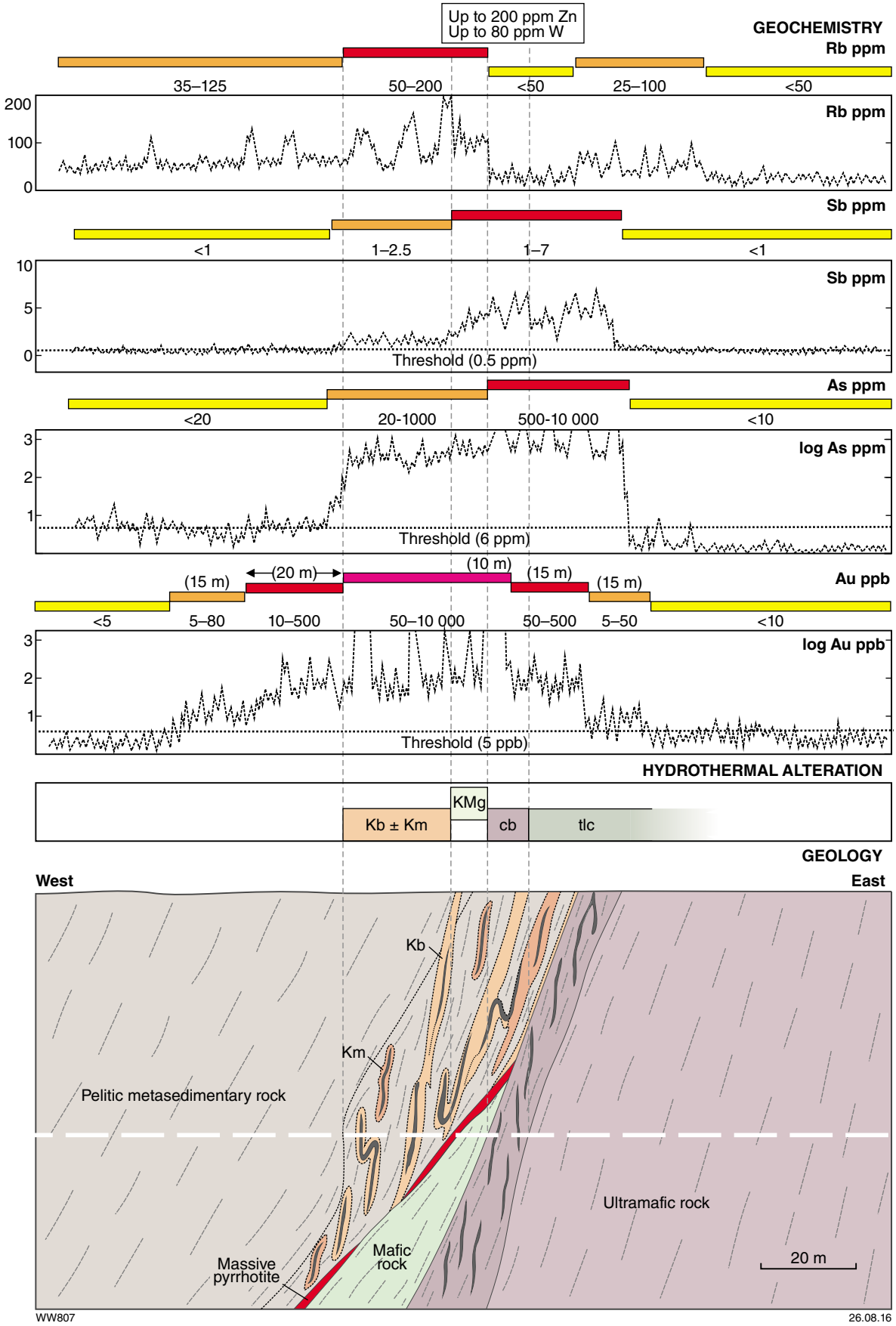

Figure 3.61. **Idealized cross section through Yilgarn Star gold deposit, Southern Cross district, Youanmi Terrane, showing hydrothermal alteration and distribution of gold and pathfinder elements. See Figure 3.59 for explanation of alteration codes.**

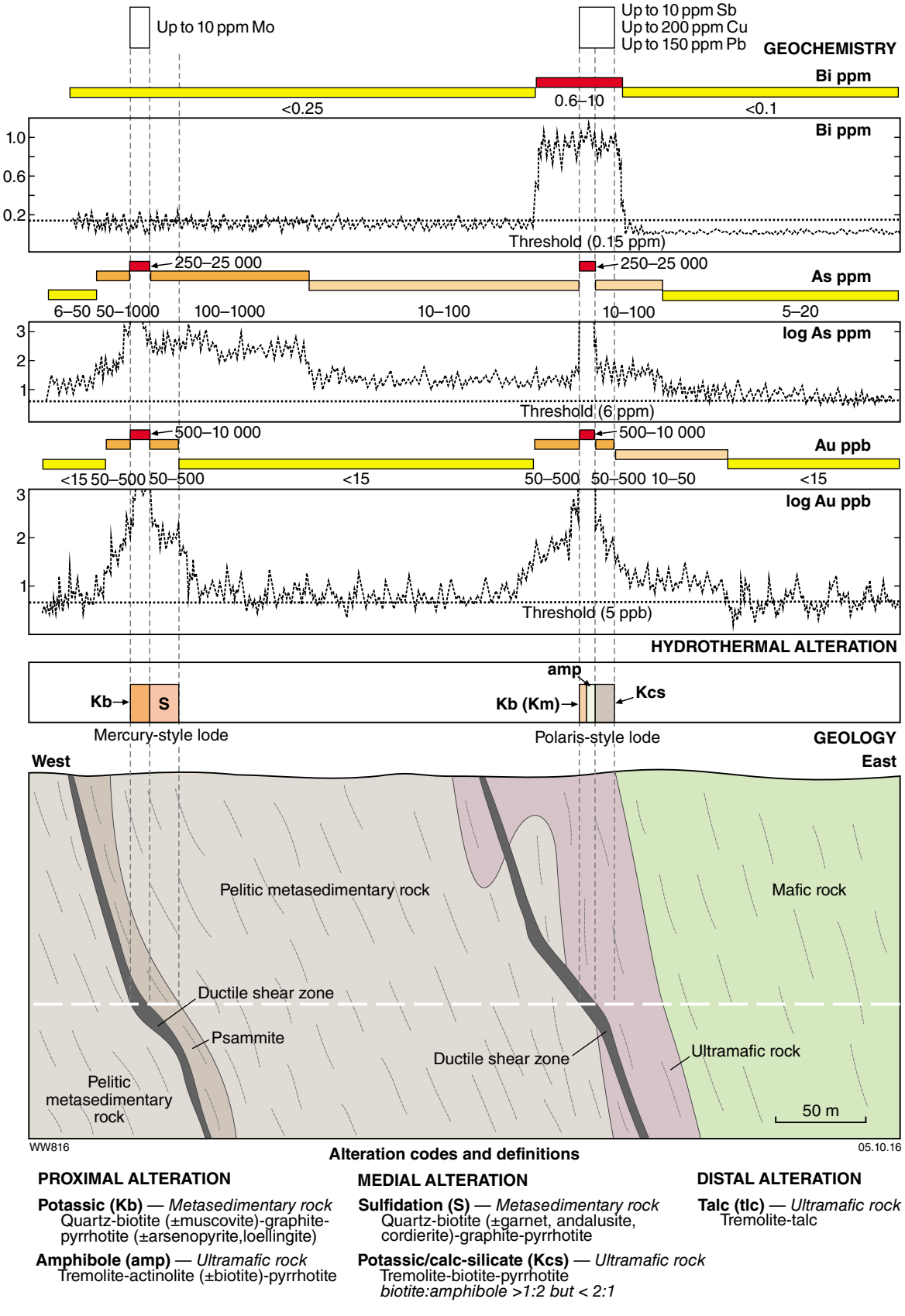

Alteration codes and definitions

PROXIMAL ALTERATION

Potassic (Kb) — *Metasedimentary rock*
Quartz-biotite (±muscovite)-graphite-pyrrhotite (±arsenopyrite,loellingite)

Amphibole (amp) — *Ultramafic rock*
Tremolite-actinolite (±biotite)-pyrrhotite

MEDIAL ALTERATION

Sulfidation (S) — *Metasedimentary rock*
Quartz-biotite (±garnet, andalusite, cordierite)-graphite-pyrrhotite

Potassic/calc-silicate (Kcs) — *Ultramafic rock*
Tremolite-biotite-pyrrhotite
biotite:amphibole >1:2 but < 2:1

DISTAL ALTERATION

Talc (tlc) — *Ultramafic rock*
Tremolite-talc

Figure 3.62. Idealized cross section through Transvaal gold deposit, Southern Cross district, Youanmi Terrane, showing hydrothermal alteration and distribution of gold and pathfinder elements

Table 3.13. Summary of pathfinder element data showing anomalies that extend beyond ore at Yilgarn Star, Southern Cross district (WK Witt, unpublished)

Element	Threshold	Extent of anomaly			Concentration gradient within anomaly beyond ore
		From ore/proximal alteration	From gold anomaly	From all visible gold-related alteration	
Au (sedimentary)[a]	5 ppb	35 m	0 m	35 m	Present over ~10 m
Au (ultramafic)	5 ppb	35 m	0 m	0 m	Steps, over 25 to 35 m
As (sedimentary)[a]	6 ppm	<5 m	0 m	<5 m	Not present
As (ultramafic)	500 ppm	20 m	0 m	0 m	Not present
Sb (sedimentary)[a]	0.5 ppm	0 m	0 m	0 m	Not present
Sb (ultramafic)	0.5 ppm	20 m	0m	0 m	Not present
Rb (sedimentary)[a]	50 ppm	>60 m	>25 m	>25 m	Not present
Rb (ultramafic)[b]	25 ppm	35 m	0 m	0 m	Not present

NOTES: (a) Sedimentary hangingwall includes thin wedge of KMg-altered mafic unit. (b) Rb anomaly is displaced 10 m into the hangingwall.

Table 3.14. Summary of pathfinder element data showing anomalies that extend beyond ore at Transvaal, Southern Cross district (WK Witt, unpublished)

Element	Threshold	Extent of anomaly			Concentration gradient within anomaly beyond ore
		From ore/proximal alteration	From gold anomaly	From all visible gold-related alteration	
Au (sedimentary)	50 ppb	10 to 25 m	0 m	10 to 25 m	Present over 10 to 25 m
Au (ultramafic/mafic)	10 ppb	70 m	0 m	>50 m	Present over ~10 m
As (sedimentary)[a]	100 ppm	90 m	65 to 80 m	65 to 80 m	Not present
As (ultramafic)	6 ppm	120 m	50 m	110 m	Present over 120 m
Bi (sedimentary)[b]	0.15 ppm	20 m	0 m	25 m	Not present
Bi (ultramafic)[b]	0.15 ppm	10 m	0m	5 m	Not present

NOTES: (a) Mercury-style lodes, hangingwall only; smaller dispersion halos in the footwall and around Polaris-style lodes. (b) Polaris-style lodes only

Arsenic remains at concentrations >100 ppm in the hangingwall of Mercury-style lodes for almost 90 m beyond the proximal alteration zone. This anomaly extends almost 70 m beyond the limits of visible alteration and the >50 ppb Au anomaly (Fig. 3.62). The anomaly in the footwall of the Mercury-style lodes is more restricted, but forms a gradient, falling to about 50 ppm As over 20 to 25 m. No such anomaly or gradient is present in the footwall of the Polaris-style lodes. Arsenic levels of 10–100 ppm form an anomaly in the ultramafic hangingwall of the Polaris-style lodes but also generate a low-level gradient, falling to a background value of 6 ppm As over 120 m (Fig. 3.62, Table 3.14).

Of the remaining pathfinder elements, Bi is the most effectively dispersed, extending beyond proximal alteration for 10 m into the ultramafic hangingwall and 20 m into the metasedimentary footwall of the Polaris-style lodes (Fig. 3.62; Table 3.14). Antimony, Cu, and Pb are anomalous within Polaris-style lodes but show very limited dispersion beyond the proximal zone of alteration. There is no Bi anomaly over the Mercury-style lodes but a weak Mo anomaly is present.

Gold deposits hosted in banded iron-formation

Gold deposits hosted by banded iron-formation in the Southern Cross district typically contain gold in late-stage quartz–pyrrhotite veins that cut folded mesobanding and related foliation (Fig. 2.101, Part 2 of this Atlas). The mineralized veins are associated with grunerite–clinopyroxene–pyrrhotite(–quartz) (cs) alteration of iron-formation wallrock. The footwall of the banded iron-formation is typically a biotite–cordierite–plagioclase assemblage representing metamorphosed sea-floor (KMg) alteration of mafic rock (see Witt and Hagemann, 2012). The hangingwall of the banded iron-formation is typically ultramafic schist (Fig. 3.63), although in some cases (e.g. Golden Pig) the banded iron-formation has been structurally emplaced within the altered mafic unit.

At mineralized sites, the folded and mineralized banded iron-formation is typically in the form of isolated blocks bound by strike-parallel (north-northwest) shear zones or oblique (northeast) faults (Fig. 3.63).

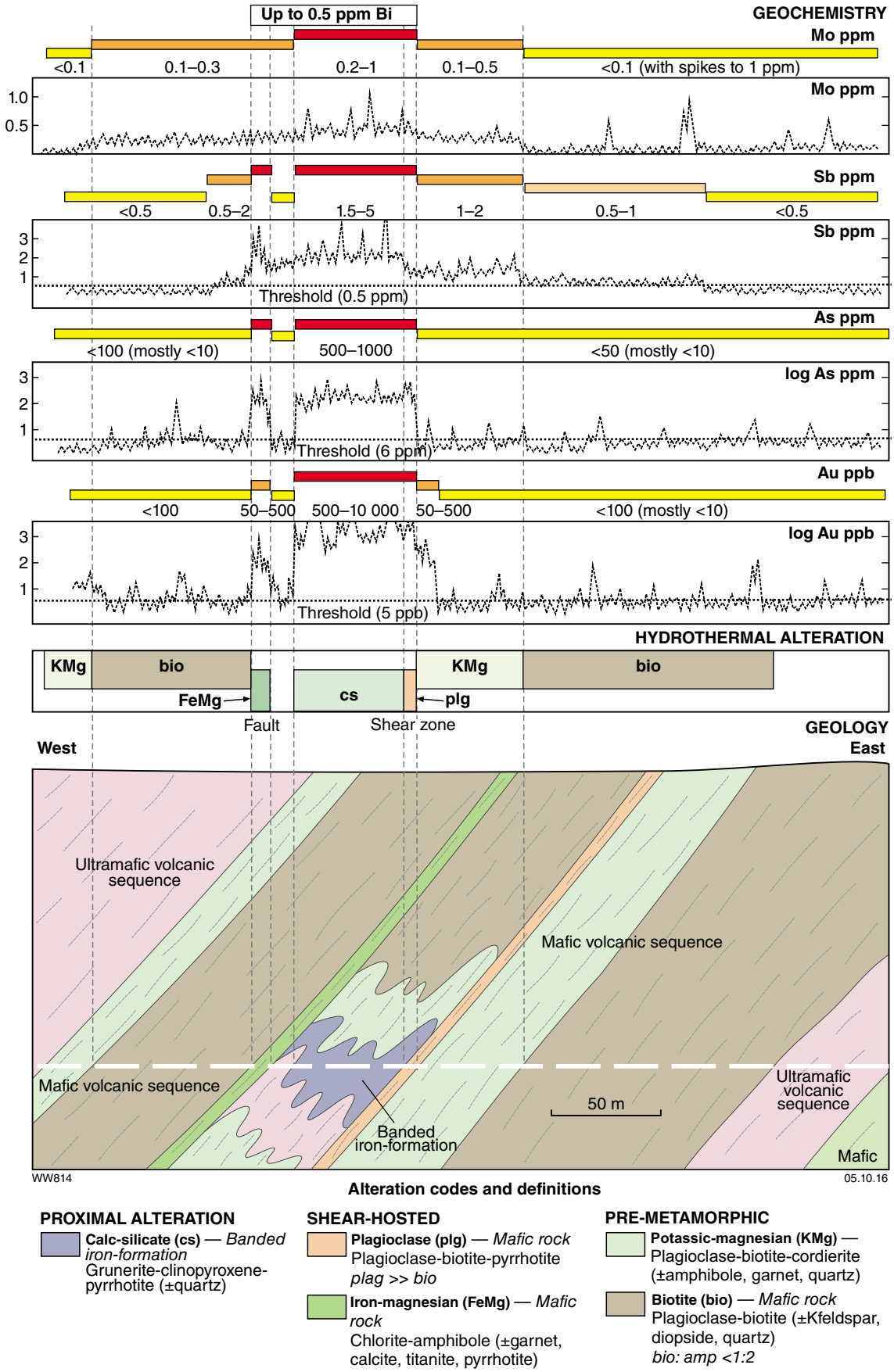

Figure 3.63. Idealized cross section through Golden Pig gold deposit, Southern Cross district, Youanmi Terrane, showing hydrothermal alteration and distribution of gold and pathfinder elements. Abbreviations: amp (amphibole), bio (biotite), plag (plagioclase).

Golden Pig

At the Golden Pig deposit, most pathfinder elements are anomalous within the fault-bound banded iron-formation block that hosts gold mineralization, but the Au anomaly extends at lower concentrations (50–500 ppb Au) across the bounding shear zones and a further 10 m into the altered and metamorphosed mafic footwall (Fig. 3.63). Beyond these limits, gold abundance is generally close to the threshold value (5 ppb), but is interrupted by higher abundance spikes of up to 10 ppb Au. The cutoff between the gold anomaly and the more distal background domain is sharp, providing little in the way of a vector towards ore.

Arsenic, Sb, Mo, and Bi remain anomalous in the banded iron-formation and bounding shear zones, but most of the boundaries between anomalous and background domains are sharp (Fig. 3.63). Broader, low-level anomalies with concentration gradients that provide potential vectors to ore are provided by Sb and Mo. Antimony remains elevated (0.5–2 ppm) for almost 150 m beyond the bounding shear zone in the footwall, and for about 20 m beyond the bounding shear zone in the hangingwall (Table 3.15). The Mo anomaly (0.1–0.5 ppm) extends almost 50 m into the footwall and (at 0.1–0.3 ppm) 90 m into the hangingwall, based on a low threshold of ~0.1 ppm Mo (Fig. 3.63).

In combination, Sb and Mo provide a low-level vector to mineralization that extends 90 m into the hangingwall and 140 m into the footwall of the Au anomaly. Although the central Sb and Mo anomalies are clearly related to gold mineralization, there is an element of uncertainty regarding the origin of the more extensive low-level anomalies. Neither extends beyond the KMg-altered mafic unit at Golden Pig. Therefore, it is not clear whether the low-level anomalies are a product of gold-related hydrothermal alteration or represent pre-existing sea-floor alteration. However, Sb and Mo are both more commonly associated with epigenetic gold mineralization than with gold-poor sea-floor hydrothermal systems (Eilu et al., 1997; Franklin et al., 2005; Galley et al., 2007), so it is more likely that the broad pathfinder element dispersion at Golden Pig is related to gold mineralization.

Great Victoria gold deposit

The Great Victoria gold deposit, 10 km southeast of Marvel Loch, shares some similarities with Golden Pig in that the host rock is an exhalative horizon and the structural setting is the hinge zone of an overturned anticline (Fig. 2.94, Part 2 of this Atlas). However, an unusual aspect of the Great Victoria deposit is that the host rock is a deformed and metamorphosed massive sulfide unit (interpreted as a sulfide facies variant of the banded iron-formation unit at Golden Pig and other localities in the Southern Cross area; see also Fig. 2.99). Gold is associated with deformed quartz–pyrrhotite(–amphibole) veins in the massive sulfide unit, which is dominated by pyrrhotite. The stratigraphic hangingwall to the massive sulfides is graphitic shale and, above that, a pelitic metasedimentary unit (Fig. 3.64). Distal calcite–pyrrhotite veins are found in the lower part of the hangingwall pelite. The stratigraphic footwall unit is mafic, and its upper part is composed of coarse-grained matted amphiboles with minor but variable amounts of biotite, diopside, and cordierite. The biotite-, diopside- and cordierite-bearing unit is interpreted as representative of metamorphosed sea-floor (KMg) alteration below the massive sulfide unit, comparable to the footwall alteration below the banded iron-formation at Golden Pig and Cornishman (see Witt and Hagemann, 2012). However, the dominance of matted amphibole suggests that there may also be a later component of gold-related (amp) alteration, comparable to that at Transvaal (Fig. 3.62).

The bulk of the gold at Great Victoria is associated with the massive sulfide unit, but grades are very inconsistent (Fig. 3.64), reflecting their association with centimetre- to metre-scale quartz–pyrrhotite(–amphibole) veins. Lower-grade gold (100–1000 ppb) is present over widths of about 45 m in the altered footwall mafic unit. A zone of anomalous gold (10–100 ppb) extends a further 10 m into the unaltered footwall mafic unit and 45 m across the black shale and zone of calcite–pyrrhotite veins in the hangingwall pelite. Concentration gradients at the margins of these anomalous gold zones provide potential vectors to ore. The quasi-symmetrical gold distribution around the massive sulfide unit suggests that the gold mineralization was not synvolcanic, but was introduced during regional deformation when strain was partitioned into the mafic–exhalite–black shale contact zone.

Arsenic distribution in the massive sulfide unit is irregular but shows an antithetic relationship with gold (Fig. 3.64), suggesting that the quartz–pyrrhotite(–amphibole) veins are As-poor, whereas the massive pyrrhotite wallrocks are relatively enriched in As. The distribution of As is asymmetric around the massive sulfide unit. Greater enrichment in the hangingwall might reflect higher background As for sedimentary rocks, but a concentration gradient of 25–125 ppm extends more than 40 m into the hangingwall before declining to background values of around 6 ppm, suggesting that the enrichment is related to gold mineralization. The As anomaly extends a further 20 m into the hangingwall and beyond the zone of calcite–pyrrhotite veins, but only at low concentrations (6–25 ppm). In the footwall, a subtle enrichment zone (5–15 ppm) is broadly coincident with the footwall altered mafic unit (Fig. 3.64). Antimony shows the broadest dispersion and has a symmetrical pattern that suggests a genetic relationship to gold mineralization. Though quite irregular, Sb enrichment (1.5–4 ppm) extends >75 m into the footwall and 45 m into the hangingwall (Table 3.16), falling below threshold levels only beyond the zone of calcite–pyrrhotite veins. The Sb concentration is still above the threshold of 0.5 ppm in unaltered metabasalt at a distance of 75 m from the massive sulfide unit, so that the extent of the footwall anomaly has not been defined. The Sb anomaly is more than 140 m across (about 120 m true width) and twice as broad in the footwall as in the hangingwall, where it has about the same extent as the Au anomaly (Fig. 3.64). A weak Sb concentration gradient in unaltered footwall mafic rocks provides a potential vector to ore.

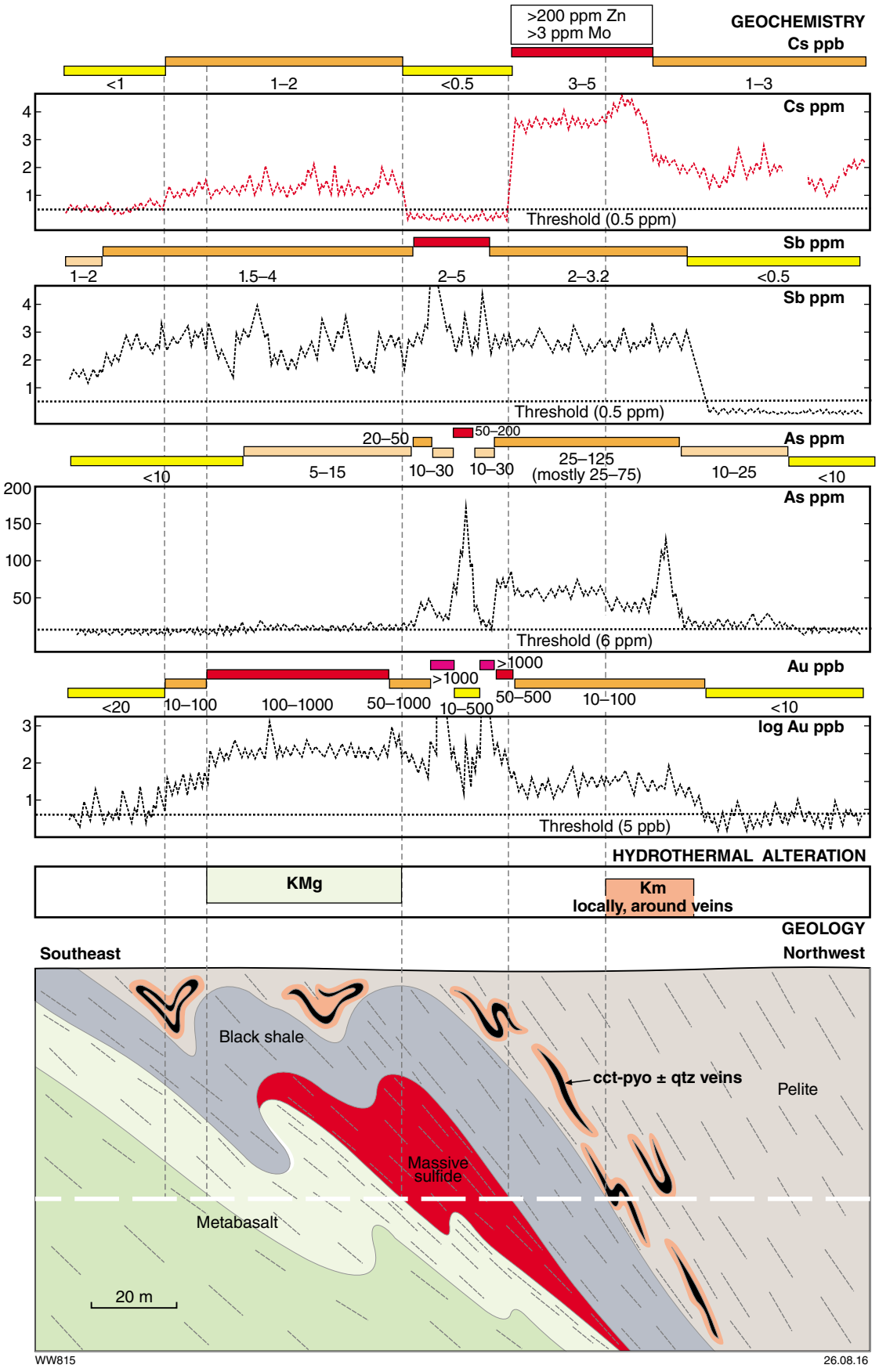

Figure 3.64. **Idealized cross section through Great Victoria gold deposit, Southern Cross district, Youanmi Terrane, showing hydrothermal alteration and distribution of gold and pathfinder elements. See Figure 3.59 for explanation of alteration codes. Abbreviations: cct (calcite), pyo (pyrrhotite), qtz (quartz).**

Table 3.15. Summary of pathfinder element data showing anomalies that extend beyond ore at Golden Pig, Southern Cross district (WK Witt, unpublished)

Element	Threshold	Extent of anomaly			Concentration gradient within anomaly beyond ore
		From ore/ proximal alteration	From gold anomaly	From all visible gold-related alteration	
Au (fw)	50 ppb	10 m	0 m	10 m	Not present
Au (hw)	50 ppb	20 m	0 m	0 m	Not present
As (fw)	6 ppm	0 m	0 m	0 m	Not present
As (hw)	6 ppm	20 m	0 m	0 m	Not present
Sb (fw)	0.5 ppm	150 m	140 m	150 m	Step-wise vector over 150 m
Sb (hw)	0.5 ppm	40 m	40m	40 m	Vector over about 20 m next to bounding shear zone
Mo (fw)	0.1 ppm	50 m	40 m	50 m	Over about 10 m at distal margin of anomaly
Mo (hw)	0.1 ppm	90 m	90 m	90 m	Over about 20 m at distal margin of anomaly

NOTES: fw, footwall; hw, hangingwall

Table 3.16. Summary of pathfinder element data showing anomalies that extend beyond ore at Great Victoria, Southern Cross district (WK Witt, unpublished)

Element	Threshold	Extent of anomaly			Concentration gradient within anomaly beyond ore
		From ore/proximal alteration	From gold anomaly	From all visible gold-related alteration[a]	
Au (fw)	10 ppb	55 m	0 m	55 m	Present over distal 10 m
Au (hw)	10 ppb	45 m	0 m	5 m	Not present
As (fw)	5 ppm	40 m	0 m	40 m	Not present
As (hw)	6 ppm	60 m	15 m	20 m	Steps
Sb (fw)[b]	1.5 ppm	>75 m	>25 m	>75 m	Present over distal >20 m
Sb (hw)	2 ppm	45 m	0 m	5 m	Not present
Cs (fw)	1 ppm	55 m	0 m	55 m	Weak over 60 m
Cs (hw)	3 ppm	35 m	0 m	0 m	Not present

NOTES: (a) Includes hanging wall calcite–pyrrhotite(–quartz) veins but excludes footwall KMg alteration. (b) The anomaly extends >80 m at a threshold of 0.5 ppm Sb. fw, footwall; hw, hangingwall

The Great Victoria deposit is associated with a broad alkali enrichment halo defined by K and Rb, but best defined by Cs (Table 3.16). The anomaly extends from the metasedimentary hangingwall into the (apparently) unaltered mafic footwall, and is probably related to metasomatic biotite. Although depleted in the massive sulfide unit, Cs is anomalous (1–2 ppm) for about 55 m into the footwall mafic unit, including 10 m beyond the KMg alteration zone (Fig. 3.64). It is uncertain whether this footwall Cs anomaly is related to gold ore fluid or to sea-floor alteration that pre-dates gold mineralization. Background Cs concentrations are relatively high in sedimentary rocks but there is a clear hangingwall anomaly (3–5 ppm) that extends through the graphitic shale and for another 10 m into the calcite–pyrrhotite vein zone of the hangingwall pelite before declining to values of around 2 ppm.

Zinc and Mo show similar distributions that contrast with those of gold and related pathfinder elements in that they are concentrated specifically in the graphitic (black) shale and its immediate hangingwall. These concentrations may have a sedimentary to diagenetic origin (Coveney and Nansheng, 1991; Lefebure and Coveney, 1995), unrelated to gold mineralization at Great Victoria.

Summary

The results of investigations into geochemical dispersion of gold and pathfinder elements at the deposits studied by Eilu and Mikucki (1996) and other deposits described above are summarized in Table 3.17.

Gold anomalies extend only a few tens of metres beyond the ore zone in most of these gold deposits. Exceptions that extend more than 50 m from the ore zone or proximal alteration assemblage include Granny Smith, Bronzewing, Harbour Lights, and Tower Hill in the Eastern Goldfields Superterrane, and Marvel Loch, Transvaal, and Great Victoria in the Southern Cross Domain of the Youanmi Terrane. The most extensive gold dispersion appears to be in deposits in districts dominated by ductile deformation and of relatively high metamorphic grade (e.g. Leonora

Table 3.17. Summary of gold and pathfinder element dispersion data showing anomalies in Yilgarn gold deposits

Deposit	*Au threshold*	*Lateral extent of Au anomaly*		*Lateral extent of pathfinder elements*	
		From ore/proximal alteration zone	*From all visible gold-related alteration*	*Beyond Au anomaly (anomaly threshold/ distance)[a]*	*Beyond all visible gold-related alteration (anomaly threshold/distance)*
Bulletin, Wiluna	6 ppb	10 m	0 m	As (>28 ppm/0-40 m), Sb (>2 ppm/0-60 m), W (>0.6 ppm/0-15 m), Te (>10 ppb/0-105 m)	
Granny Smith, Laverton	2 ppb (sedimentary); 8.5 ppb (granodiorite)	5 to 30 m (sedimentary); 25 to >70 m (granodiorite)	0 m		
Kings Cross, Coolgardie	5 ppb	5 m	0 m	As (>4 ppm/0->45 m), Sb (>0.9 ppm/5-20 m[b]), Te (>8 ppb/>85 m)	As (>4 ppm/0->45 m), Sb (>0.9 ppm/5-20 m[b]), Te (>8 ppb/>85 m)
Moyagee, Murchison	6 ppb	10 to 35 m	0 m	As (>5 ppm/10-15 m), Se (>0.15 ppm/0-15 m), W (>0.5 ppm/0->35 m), Te (>10 ppb/>35 m)	W (>0.5 ppm/0->50 m), Te (>10 ppb/>50 m)
Twin Peaks, Carosue Dam	2 ppb	2 to 10 m	0 m	Ag (>0.10 ppm/0-10 m), As (>6 ppm/20-110 m), W (>3 ppm/3-20 m)	As (>6 ppm/0-110 m); Te[c] (>15 ppb/10-110 m); W (>3 ppm/0-30 m)
Bronzewing, Yandal belt	4 ppb	1 to 80 m	0 m	Te (>6 ppb/>100 m), Sb (>0.4 ppm/0-40 m)	Te (>6 ppb/not established)
Karari, Carosue Dam	10 ppb (0.1 ppm)	10 to 20 m	0 m	As (5 ppm/20-120 m), W (>3 ppm/10-40 m)	
Harbour Lights, Leonora	10 ppb 5 ppb	110 m (hw only) >400 m (hw only)	0 m>300 m (hw only)	Footwall: As (>10 ppm/150 m)	Hangingwall: As (>6 ppm/>300 m)[d]
Tower Hill, Leonora	5 ppb	>150 m (fw only)	>150 m (fw only)	Footwall: Sb (>0.5 ppm/>25 m) Hangingwall: Sb (>0.5 ppm/>400 m)[d]	Footwall: Sb (>0.5ppm/>175 m) Hangingwall: Sb (>0.5 ppm/>300 m)[d]
Marvel Loch, Southern Cross	5 ppb(mafic) 10 ppb(ultramafic)	>150 m(mafic) 60 m(ultramafic)	0 m 0 m		
Yilgarn Star, Southern Cross	5 ppb(fw ultramafic) 5 ppb(hw sedimentary)	35 m(fw ultramafic) 35 m(hw sedimentary)	0 m (fw ultramafic) 35 m (hw sedimentary)	Rb (>25 ppm/10 m)(fw ultramafic) Rb (>50 ppm/>25 m)(hw sedimentary)	
Transvaal, Southern Cross	50 ppb(sedimentary) 10 ppb(ultramafic/mafic)	10-25 dimentary) 70m(ultramafic/mafic)	10 to 25 m(sedimentary) >20 m(ultramafic/mafic)	Metasedimentary: As (>100 ppm/65-80 m, Mercury hw; >6 ppm/25 m, Mercury fw) Ultramafic: As (>6 ppm/50 m, Polaris hw)	Metasedimentary: As (>100 ppm/>65-80 m, Mercury hw; >6 ppm/>45 m, Mercury fw); Bi (>0.15 ppm/25 m, Polaris fw)Ultramafic: As (>6 ppm/110m, Polaris hw); Bi (>0.15 ppm/5 m, Polaris hw)
Golden Pig, Southern Cross	50 ppb	10 m (fw) 20 m (hw)	10 m (fw) 0 m (hw)	Footwall: Sb (>0.5 ppm/140 m); Mo (>0.1 ppm/40 m) Hangingwall: Sb (>0.5 ppm/40 m); Mo (>0.1 ppm/90 m)	Footwall: Sb (>0.5 ppm/150 m); Mo (>0.1 ppm/50 m)Hangingwall: Sb (>0.5 ppm/40 m); Mo (>0.1 ppm/90 m)
Great Victoria, Southern Cross	10 ppb	55 m (fw) 45 m (hw)	55 m (fw) 5 m (hw)	Footwall: Sb (>1.5 ppm/>25 m	Footwall: As (>5 ppm/40 m); Sb (>1.5 ppm/>75 m; Cs (>1 ppm/55 m) Hangingwall: As (>6 ppm/20 m); Sb (>2 ppm/5 m)

NOTES: (a) Dispersion distance of pathfinder elements beyond the Au anomaly is estimated as the difference between dispersion distance beyond the ore zone less the gold dispersion (anomaly) distance beyond the ore zone. (b) The Sb anomaly (>0.9 ppm) at Kings Cross is not in the immediate hangingwall of the mineralized Kings Cross fault but is associated with subparallel hangingwall faults. At a lower threshold of 0.5 ppm, a Sb anomaly extends for 20-50 m into the hangingwall of the Kings Cross fault (detection limit for Sb is 0.05 ppm; Eilu and Mikucki, 1996). (c) The dispersion is only apparent using a background threshold of 15 ppb, in contradiction with the threshold of 50 ppb recommended by Eilu and Mikucki (1996). (d) Dispersion includes values in district-scale alteration, not necessarily related to gold mineralization.

and Southern Cross districts). Less commonly, gold anomalies extend beyond the limits of all visible gold-related alteration. Limited gold dispersion beyond gold-related visible alteration is again found mostly in districts dominated by ductile deformation, but even in these settings the gold anomalies do not extend beyond visible alteration related to hydrothermal events that pre-date gold mineralization (cf. Witt and Hagemann, 2012, 2013a,b).

Pathfinder element anomalies that extend the footprint of the deposit beyond low-level gold dispersion were identified at 12 out of 14 deposits; these elements are most commonly As, Sb, W, and Te. At Yilgarn Star, only Rb fulfils this role. Gold, As, and Sb are the elements that most commonly define a concentration gradient within the hydrothermal alteration envelope around gold lodes; this quality gives them the potential to be used as vectors to ore.

Pathfinder anomalies that extend beyond visible gold-related hydrothermal alteration, including distal alteration zones but excluding pre-metamorphic alteration, have been identified at nine of the 14 deposits (Table 3.17). Pathfinder elements that define these anomalies are As, Sb, W, and Te, and less commonly Mo, Rb, and Cs, although the reliability of W as a pathfinder element may be suspect in some cases because of the possibility of contamination during drilling or sample preparation. Detection of Te anomalies (in particular) requires low levels of detection which, at the time of the Eilu et al. (1997) study, were not readily available in Australian laboratories. However, most laboratories catering to the Australian mining and exploration community now offer detection limits in the range 0.01 to 0.05 ppm for inductively coupled plasma mass spectrometry (ICP-MS) analyses.

On the basis of the deposits investigated, it appears that pathfinder element dispersion beyond the limits of visible gold-related alteration is more extensive in deposits hosted by rocks of upper greenschist to upper amphibolite facies settings. The above analysis indicates that As and Sb, and possibly Te, are the most useful pathfinder elements for deposit-scale gold exploration and, although there are exceptions, the dispersion distances of As and Sb are limited to a few tens of metres beyond visible gold-related alteration and/or the gold anomaly (defined as >5 ppb). Gold, As, and Sb are the elements most likely to generate a concentration gradient and therefore provide a vector to ore within broader zones of hydrothermal alteration.

Targeting Criterion 3.10: Geochemical dispersion (alteration indices)

The sources of data used here for analysis of the use of alteration indices to target gold mineralization are largely those used in the preceding discussion of pathfinder elements at deposit scale (especially Eilu and Mikucki, 1996, 1998; Eilu et al., 1997, 2001; and WK Witt, unpublished data). The most widely applied alteration indices that have been devised for gold deposits, particularly orogenic gold deposits, include the carbonation index (Davies et al., 1990), the alkali indices (Kishida and Kerrich, 1987), and the rare alkali index (Heath and Campbell, 2004). This section of the Atlas begins with an explanation of these three indices, reviews the results of the application of the carbonate alteration and potassic alteration indices at several sites in the Yilgarn Craton, and then reviews the application of the rare alkali index in Yilgarn gold deposits, including the results of a new study of the Red October gold deposit in the Laverton district of the Eastern Goldfields Superterrane, which was completed as part of the project to produce this Atlas. Readers are referred to Targeting Criterion 3.9 for basic descriptions of the geology of the Yilgarn deposits discussed below, with the exception of Red October, which is described briefly within this section.

Carbonate alteration index

The carbonate alteration index monitors the extent to which a rock has been saturated with CO_2. The method presumes there is no graphite or organic carbon in the rock sample, a safe assumption for most gold deposits hosted by igneous rocks of the Yilgarn Craton. Where this presumption does not apply, carbon dioxide and organic carbon must be analysed separately. Carbon dioxide in hydrothermal fluid can combine with Ca, Fe, and Mg (and to less extent with Mn) to form a variety of carbonate minerals (e.g. magnesite, calcite, dolomite, ankerite, siderite). The capacity of a rock to form carbonate minerals is controlled by the abundances of CaO, FeO, and MgO in the rock. Thus, ultramafic rocks, which are characterized by high MgO content, can absorb large amounts of CO_2 from the fluid to form abundant Mg (±Ca) carbonates (e.g. dolomite, magnesite). Granitic rocks, in contrast, have low total Ca + Fe + Mg content and therefore have a lower capacity to form carbonate minerals through reactions with CO_2-bearing hydrothermal fluid (Kishida and Kerrich, 1987).

Davies et al. (1990) proposed the use of the molar CO_2/CaO ratio to monitor the degree of carbonate saturation in mafic rocks of the Timmins district in Canada. A molar CO_2/CaO ratio of 1 indicates that all of the Ca in a rock sample has combined with CO_2 to form calcite ($CaO.CO_2$). Samples with a molar ratio >1 contain dolomite ($CaO.MgO.2CO_2$) or ankerite ($CaO.FeO.2CO_2$). The molar CO_2/CaO ratio can be used as a carbonate alteration index for less mafic rocks (e.g. andesite, granite, most metasedimentary rocks) as well, but is unsuitable for ultramafic rocks and high-Mg volcanic rocks.

For ultramafic and other high-Mg rocks, Davies et al. (1990) proposed the use of the molar ratio CO_2/(CaO + FeO + MgO) to monitor the degree to which a sample was saturated in carbonate minerals such as dolomite. For sulfide-rich rocks, the index should be modified to allow for Fe accommodated in pyrite and other sulfides, such that a better carbonate alteration index is expressed as the molar ratio CO_2/(CaO + FeO + MgO – 0.5S) where pyrite (FeS_2) is the main sulfide. Where pyrrhotite (FeS) is the main sulfide, 1.0S is used in the denominator and, where pyrite and pyrrhotite abundance is approximately equal, 0.75S is used (Eilu et al., 1997; Eilu and Groves, 2001). Where arsenopyrite is a major sulfide component, As is incorporated into the index, as for the Bulletin example (discussed below). A molar ratio of one indicates that all of the Ca, Fe, and Mg have combined with CO_2 to form carbonate minerals such as ferroan dolomite.

Application of the carbonate alteration index at district scale in the Timmins district in the Abitibi subprovince of Canada (Fyon and Crockett, 1982) showed high degrees of carbonate saturation in major faults and shear zones (e.g. the Destor–Porcupine Fault) and large areas of strong carbonate alteration between faults. All but one significant gold deposit fell within areas of molar CO_2/CaO >1, but the study showed that these areas extend well beyond mineralization, and used trace element data (Au, As, Sb, B, Cu, Pb, Li) to distinguish barren carbonate alteration from gold-associated carbonate alteration (Fyon and Crockett, 1982).

To the author's knowledge, no comparable district-scale studies have been carried out in the Yilgarn Craton. Recently, however, other investigators at deposit scale (e.g. Eilu and Mikucki, 1996) have used molar quantities of an element instead of its oxide (e.g. Ca instead of CaO) in the denominator; this does not change the patterns defined by the index.

Alkali indices

The potassic alteration index (molar 3K/Al ratio, used to monitor the formation of muscovite) and the sodic alteration index (molar Na/Al ratio, used to monitor the formation of albite) were two alkali indices applied to the auriferous hydrothermal alteration system at the Kerr-Addison mine, Canada (Kishida and Kerrich, 1987). Muscovite (or a white mica that approximates muscovite in composition) and albite are common products of gold-related hydrothermal alteration in Yilgarn gold deposits and, alone or in combination, carry most of the alkalis in proximal alteration zones. Where all of the Al in a sample is in muscovite ($K_2O.3Al_2O_3.6SiO_2.2H_2O$), the molar ratio 3K/Al is 1. In relatively distal alteration zones where some Al is present in chlorite or albite, the molar ratio 3K/Al is <1. Ratios >1 reflect the presence of biotite ($K_2O.6(Mg,Fe)O.Al_2O_3.6SiO_2.2H_2O$) or K-feldspar ($K_2O.Al_2O_3.6SiO_2$), minerals that have potassic alteration indices as high as three. Therefore, the 3K/Al ratio is best-suited to deposits hosted by mafic to ultramafic rocks, particularly those in greenschist metamorphic environments where muscovite is the dominant proximal K-rich alteration mineral.

At Kerr-Addison, Kishida and Kerrich (1987) found a good correlation between elevated 3K/Al ratios (0.2 to 0.6) and mineralized zones of proximal carbonate–muscovite alteration, but no significant dispersion of this parameter beyond zones of visible gold-related alteration. Where all of the Al in a sample is present as albite ($Na_2O.Al_2O_3.6SiO_2$), the molar ratio Na/Al is 1. Relict or modified metamorphic albite is commonly present in distal alteration zones, but neoblastic hydrothermal albite is abundant in some proximal alteration zones of some deposits (e.g. Karari). In other deposits, muscovite replaces metamorphic albite in the proximal alteration zones, leading to a decrease in molar Na/Al, or to irregular patterns (e.g. Kerr-Addison deposit, Kishida and Kerrich, 1987). Consequently, the molar 3K/Al ratio is more commonly employed as an alteration index to target gold mineralization. However, the molar Na/Al ratio may have application in gold systems where proximal alteration is characterized by albitization (e.g. Karari, Witt et al., 2009; Centenary-style lodes at Darlot, Beardsmore and Gardner, 2003; and at New Holland, Ackroyd et al., 2001).

Rare alkali index

Heath (2003) and Heath and Campbell (2004) drew attention to the capacity for dispersion of alkali lithophile elements, such as Rb and Cs, beyond zones of visible potassic (sericite, muscovite, biotite) alteration around gold deposits hosted by mafic rocks at Kalgoorlie and St Ives. Sites investigated were the Golden Mile at Kalgoorlie, Victory at St Ives, and distal intersections of gold mineralization from south of Kalgoorlie and north-northwest of Victory. The authors developed a rare alkali index, equivalent to $([Rb + Cs]/Th)_N$. With this method, all element abundances are normalized to their corresponding mantle abundance (Sun and McDonough, 1989) to account for the order of magnitude difference between Cs abundances and Rb and Th abundances. The sum of normalized Rb and Cs abundances is divided by normalized Th to discount the effects of crustal contamination of the precursor magma, which has the potential to enrich alkali elements in unaltered basalt and komatiite (Barley, 1986; Arndt and Jenner, 1986).

Heath (2003) and Heath and Campbell (2004) showed that three aspects of the dispersion of alkali lithophile elements are important for gold exploration:

- Dispersion of alkali lithophile elements is best expressed by the ratio $([Rb + Cs]/Th)_N$.
- Elevated values (>5) of this parameter extend for tens to hundreds of metres beyond the visible proximal alteration halo around the gold lodes they studied.
- The width of dispersion is directly related to the size of the gold system.

Although the implications for gold exploration are clear, the technique does not appear to have been widely adopted by industry geologists exploring for gold in the Yilgarn Craton. This index was not developed at the time Eilu and co-workers completed their studies, so it has not been applied to those examples.

Application of carbonate alteration and potassic alteration indices

Bulletin deposit, Wiluna

Eilu and Mikucki (1996, 1998) applied carbonate alteration and alkali indices at the Bulletin deposit and found that both extended beyond the ore zone. The molar CO_2/Ca ratio was found to be the most effective index, extending for 10 to 80 m from the gold ore zone, which is confined to the proximal alteration zone (Eilu and Mikucki, 1996, 1998; Eilu and Groves, 2001). Against a nominated threshold value of 0.3, the molar CO_2/Ca anomaly extends 3 to 60 m beyond the Happy Jack shear zone, but the magnitude of the ratio appears to be controlled by distal (chlorite–calcite) alteration and the anomaly is not larger than the area of visible gold-related alteration (Fig. 3.65). The CO_2/[Ca + Fe + Mg – 0.5(S + As)] ratio defined a dispersion halo of similar extent (Eilu and Mikucki, 1996, 1998). The extents of the elevated carbonate alteration indices at Bulletin do not provide a significant advantage over pathfinder elements such as Te and (at regional thresholds) As and Sb (compare Tables 3.18 and 3.17, Targeting Criterion 3.9).

The spatial extent of the molar 3K/Al anomaly (>0.04) is relatively confined, extending 1 to 30 m beyond the ore zone. The magnitude of the ratio reflects the presence of sericite in proximal alteration assemblages and the anomaly does not encroach into intervals of distal alteration (Fig. 3.65, Table 3.18).

Granny Smith, Laverton

At Granny Smith, the molar CO_2/Ca ratio anomaly extends up to 60 m beyond the ore zone in granodiorite but no more than 5 m beyond it in metasedimentary rock. Eilu and Mikucki (1996) consider Ca to have been mobile in metasedimentary rocks at Granny Smith and, for this reason, recommend the Pearce Element Ratio (PER) CO_2/Zr as a more reliable indicator of carbonate alteration. The PER CO_2/Zr ratio produces qualitatively similar results to those of the molar CO_2/Ca ratio, but the PER CO_2/Zr anomaly is broader than those of any other index or pathfinder element around minor mineralized zones in the hangingwall, and there are larger PER CO_2/Zr gradients within the anomalies (Fig. 3.66). The hangingwall anomalies extend for up to 15 m from mineralization (up to 10 m beyond the Au anomaly) and 5 m away from visible alteration (Eilu and Mikucki, 1996; Table 3.18). The indices are therefore less-effective exploration tools than the gold anomaly (25 to >70 m dispersion in granodiorite, and 5 to 30 m in metasedimentary rock; Targeting Criterion 3.9). The gradients of carbonate saturation are of limited exploration value because they generally extend for ≤5 m from visible gold-related alteration.

There is no enhancement of the molar 3K/Al ratio or molar Na/Al ratio beyond the gold ore zone and gold-related visible alteration at Granny Smith in either metasedimentary rocks or granodiorite. Use of the Pearce Element Ratio (e.g. K/Zr, Na/Zr) does not provide anomalous areas of greater extent than those produced by these alkali indices (Eilu and Mikucki, 1996).

Table 3.18. Summary of carbonate and alkali alteration indices showing anomalies that extend beyond ore and beyond visible alteration at selected Yilgarn gold deposits (data from Eilu and Mikucki, 1996, 1998)

Deposit	*Au threshold*	*Lateral extent of Au anomaly*		*Lateral extent of alteration index anomalies*	
		From ore/proximal alteration zone	*From all visible gold-related alteration*	*Beyond Au anomaly[a]*	*Beyond all visible gold-related alteration*
Bulletin, Wiluna	6 ppb	10 to 20 m	0 m	mCO_2/Ca: 3 to 60 m (>0.3) m3K/Al: up to 20 m (>0.04) mNa/Al: up to 5 m (>0.25)	
Granny Smith, Laverton	2 ppb (metasedimentary); 8.5 ppb (granodiorite)	5 to 30m (metasedimentary); 25 to >70 m (granodiorite)	0 m	mCO_2/Ca: 1 to 35 m (>0.4) in granodiorite CO_2/Zr [PER]: up to 10 m	CO_2/Zr [PER]: up to 5 m
Kings Cross, Coolgardie	5 ppb	5 m	0 m	mCO_2/Ca: up to 20 m (>0.03) m3K/Al: up to 5 m (>0.04) mCO_2/Ca: up to 70 m (>0.03)[b] m3K/Al: up to 70 m (>0.04)[b]	mCO_2/Ca: up to 20 m (>0.03) m3K/Al: up to 5 m (>0.04) mCO_2/Ca: up to 70 m (>0.03)[b] m3K/Al: up to 70 m (>0.04)[b]
Moyagee, Murchison	6 ppb	10 to 35 m	0 m	mCO_2/(Ca+Fe+Mg-0.75S): 10 to 15 m (>0.05) m3K/Al: 5 to 15 m (>0.07) mNa/Al: up to 5 m (>0.3 to 0.5)	
Twin Peaks, Carosue Dam	2 ppb	2 to 10 m	0 m	CO_2/Ti [PER]: up to 80 m (>8)[c]	CO_2 (1 to 5%) >30 m beyond distal alteration zone[c]
Bronzewing, Yandal belt	4 ppb	1 to 80 m	0 m	mCO_2/CaO: up to 100 m (>0.3) m3K/Al: up to 40 m (>0.04)	
Yilgarn Star	5 ppb (metasedimentary) 5 ppb (ultramafic)	35 m (metasedimentary) 35 m (ultramafic)	35 m (metasedimentary) 0 m (ultramafic)	mCO_2/(Ca+Fe+Mg-0.75S): 20 m (>0.01); or 35 m (CO_2 >detection) m3K/Al: ?? undetermined distance from unknown lode (>0.1)	

NOTES: (a) Dispersion distance of pathfinder elements beyond the Au anomaly is estimated as the difference between dispersion distance beyond the ore zone less the gold dispersion (anomaly) distance beyond the ore zone. (b) Defined by considering only samples taken from the mineralized shear zone and subparallel shear zones and discounting samples taken from intervening domains of low strain and no hydrothermal alteration. (c) Carbonate index and CO_2 concentration dispersions at Twin Peaks are complicated by the presence of district-scale carbonate alteration (dolomite 'spots').

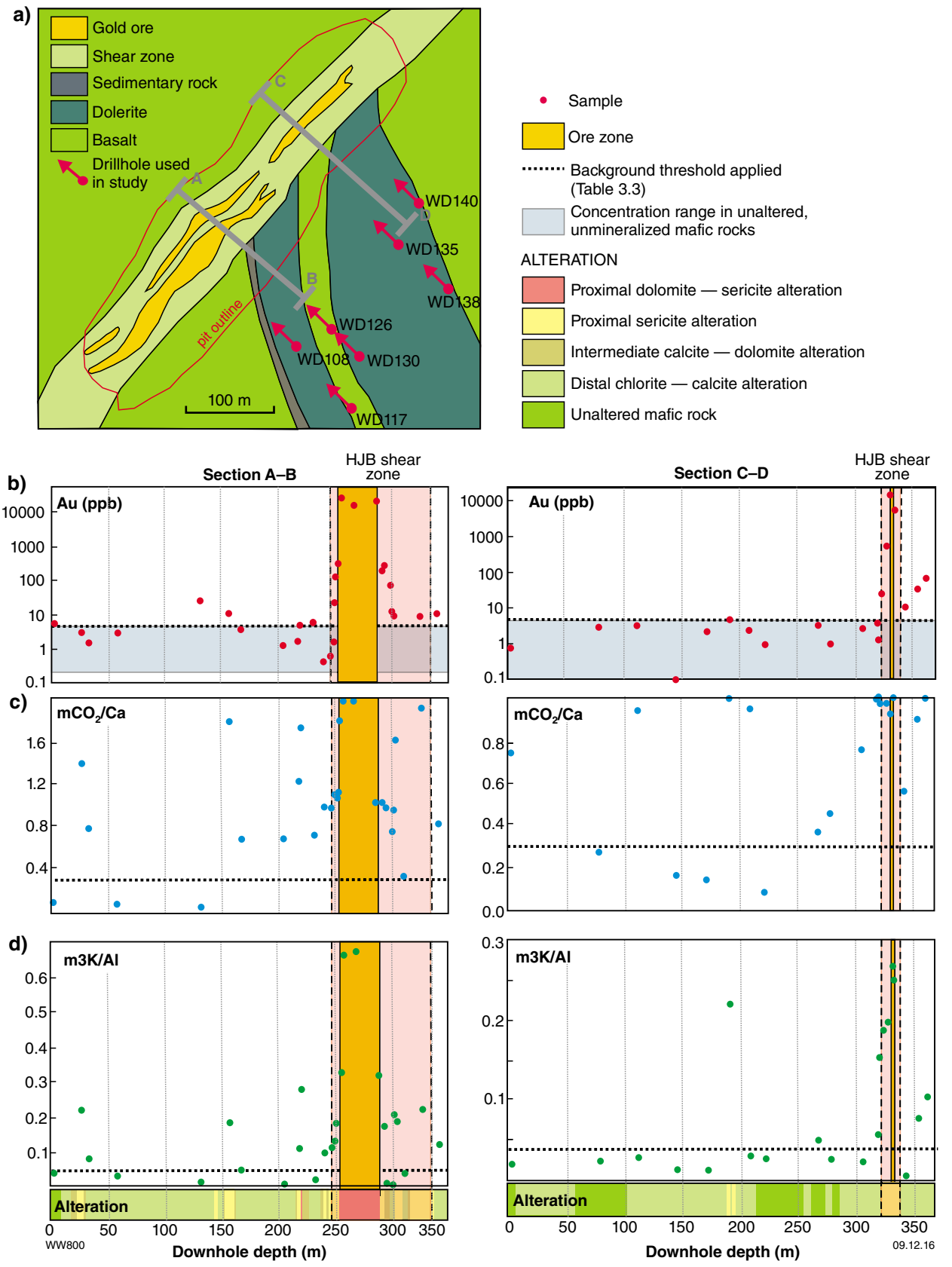

Figure 3.65. **Alteration indices at Bulletin gold deposit, Wiluna district, Eastern Goldfields Superterrane (from Eilu and Mikucki, 1996, 1998). a) Geological map of the Bulletin deposit. Dispersion along cross sections A–B and C–D of b) Au, c) carbonate alteration index mCO_2/Ca, and d) alkali index m3K/Al. HJB, (Happy Jack – Bulletin).**

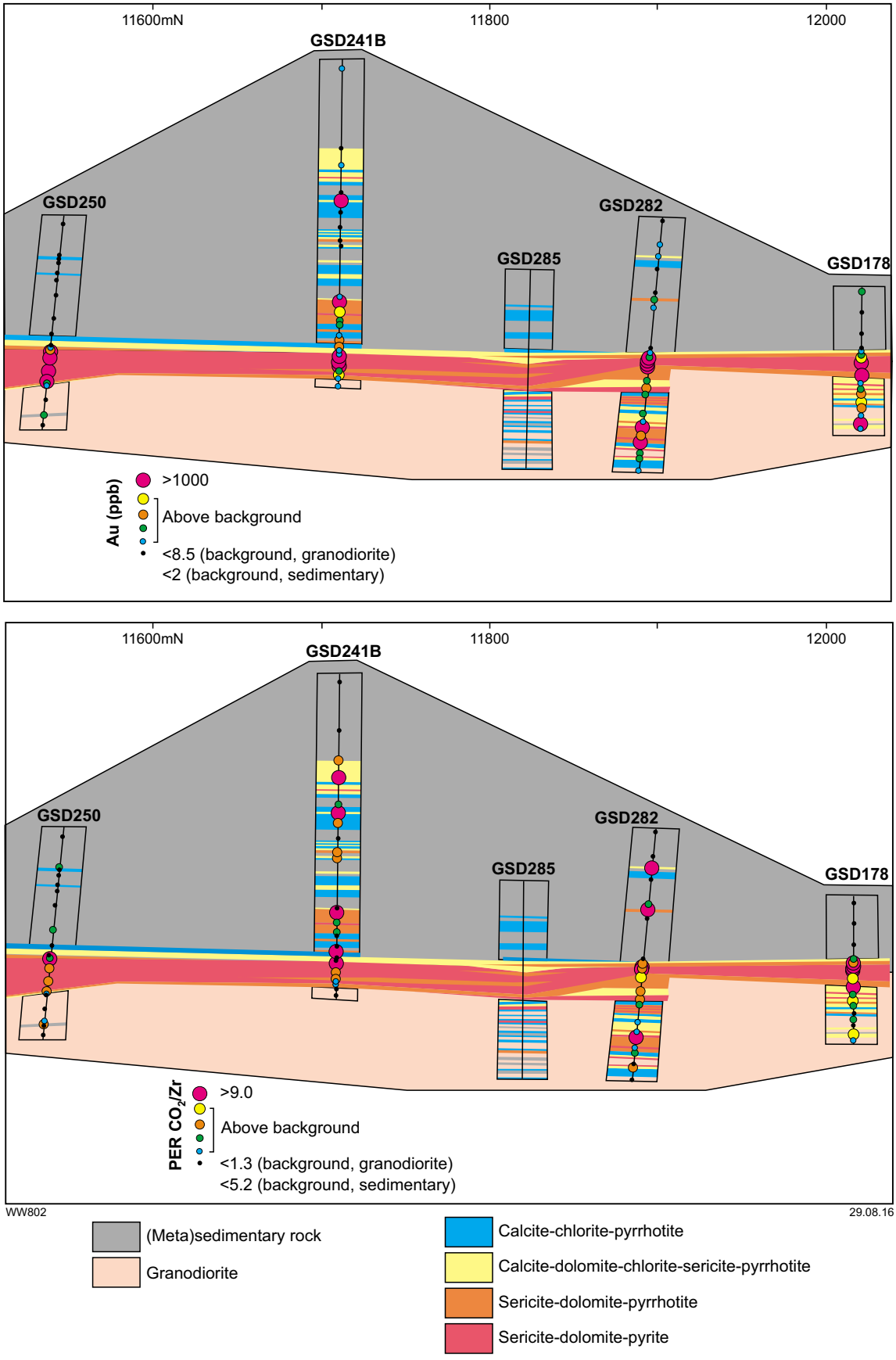

Figure 3.66. **Carbonate alteration index (PER CO_2/Zr) relative to gold dispersion, Granny Smith gold deposit, Laverton district, Eastern Goldfields Superterrane. Inclined longitudinal cross section (after Eilu and Mikucki, 1996) showing a) gold dispersion and b) PER CO_2/Zr. Coordinates refer to local mine grid.**

Kings Cross, Coolgardie

The application of carbonate alteration and alkali indices in upper greenschist to amphibolite facies settings is complicated by the stability of calcic plagioclase and amphiboles in rocks affected by gold-related hydrothermal alteration (Mueller and Groves, 1991; Witt, 1991; Witt et al., 1997). These phases compete for Ca and Al, thereby exaggerating the modal abundance of calcite and K-mica as measured by molar CO_2/Ca and 3K/Al ratios. Further complication is introduced by the presence of biotite, which tends to increase the molar 3K/Al ratio and lead to overestimation of muscovite abundance.

Nevertheless, at Kings Cross Eilu and Mikucki (1996) found that the molar 3K/Al ratio (>0.04) and the molar CO_2/Ca ratio (>0.03) define distinct anomalies throughout the Kings Cross Fault and that these anomalies extend for up to 5 m and 20 m, respectively, into unaltered wallrock around the fault (Fig. 3.67). If, on the other hand, only hydrothermally altered subparallel fault- and shear-hosted samples are considered, the extent of the anomalies increases to 70 m for both indices (Table 3.18). These anomalies are comparable to or better than those based on concentrations of gold and most pathfinder elements at Kings Cross (see Table 3.17, Targeting Criterion 3.9).

Moyagee, Murchison Domain

Gold mineralization hosted in ultramafic rocks at Moyagee in the Murchison Domain presents a low-level gold anomaly that extends 10 to 35 m from ore (Fig. 3.47; Eilu and Mikucki, 1996). The relatively magnesian host-rock association at Moyagee requires the carbonate alteration index to be expressed as molar CO_2/(Ca + Fe + Mg – 0.75S) rather than as molar CO_2/Ca. Anomalous molar 3K/Al (>0.07) and molar CO_2/(CaO + FeO + MgO – 0.75S) (>0.05) extend 5 to 50 m and 20 to 50 m, respectively, from ore and proximal alteration (Fig. 3.68). At Moyagee, anomalous molar Na/Al ratios (0.3 to 0.5) of ultramafic rocks (but not porphyry intrusions) also extend 10 to 40 m beyond ore (Eilu and Mikucki, 1996).

Gradients within the mineralized Lena shear zone are commonly defined by the carbonate alteration index, creating potential vectors to ore. None of the anomalous alteration indices extend beyond the visible alteration that characterizes the Lena shear zone. Although the carbonate alteration index is the most successful alteration index at Moyagee, the extent (dispersion) of the anomaly is not as large as those produced by the pathfinder elements Te and W (Table 3.17, section 3.9).

Twin Peaks, Carosue Dam camp

At Twin Peaks, Eilu and Mikucki (1996) found a low-level gold anomaly (>2 ppb) that extended 2 to 10 m, or intermittently for >120 m, from ore. The anomalous alkali alteration indices did not extend significantly beyond the ore-bearing proximal and medial alteration zones. The carbonate alteration index was assessed using the molar CO_2/Ti ratio to minimize the effects of variable pre-metasomatic sediment composition, and the anomaly was found to extend at molar CO_2/Ti ratios >8 for 0 to 80 m from ore. The anomaly is complicated by an extensive carbonate alteration halo that may pre-date gold mineralization and extends for more than 150 m from ore.

WK Witt (unpublished data) also found an extensive zone of CO_2 enrichment around the Twin Peaks gold deposit, with CO_2 content >1.0% (1 to 5%) extending more than 50 m from the proximal potassic alteration zone and for at least 30 m beyond the distal calcite alteration zone (Fig. 3.69). The calcite alteration zone was mapped on the basis of the reaction of samples with dilute HCl, so the presence of several percent CO_2 in samples beyond the calcite alteration zone suggests the presence there of dolomite rather than calcite. The CO_2 is most likely present in dolomite porphyroblasts or 'spots', which define the low-level, district-scale carbonate alteration; this may extend for hundreds of metres beyond the Twin Peaks deposit, though the outer limits of the alteration have not been defined.

Bronzewing, Yandal belt

The carbonate alteration index [molar CO_2/Ca and molar CO_2/(Ca + Fe + Mg – 0.75S)] anomalies at Bronzewing extend beyond all other alteration indices and pathfinder element anomalies, excepting the low-level (possibly regional) Te anomaly (Eilu et al., 2001). The carbonate alteration indices remain >0.3 and >0.11, respectively, for up to 100 m beyond ore, and up to 40 m beyond the gold anomaly (Fig. 3.70). At these levels though, the carbonate saturation anomaly does not extend beyond visible alteration. The alkali alteration index 3K/Al remains anomalous (>0.04) for up to 75 m beyond ore, and up to 30 m beyond the gold anomaly. The 3K/Al anomaly extends beyond the potassic alteration zone identified during field mapping and can potentially provide a signal indicating proximity to the proximal (potassic) alteration zone.

Yilgarn Star, Southern Cross greenstone belt

Both alkali (potassic) alteration (molar 3K/Al) and carbonate alteration [molar CO_2/(CaO + MgO + FeO)] indices have been applied at Yilgarn Star in the Southern Cross greenstone belt, Youanmi Terrane (Fig. 3.71). The presence of metamorphic biotite in the pelitic hangingwall sequence, and a wedge of sea-floor altered mafic rock between the pelite and the ultramafic footwall, gives rise to artificially high molar 3K/Al ratios that are probably not related to gold mineralization.

The potassic alteration index is very low in the mineralized ultramafic unit, which is consistent with the low abundances of K-mica and K-feldspar in the proximal carbonate alteration assemblage. A distal anomaly in ultramafic rock is defined by molar 3K/Al ratios between 0.1 and 0.5 between about 45 and 80 m from the mineralized contact (Table 3.18; Fig. 3.71). The source of this anomaly is unknown, but it may indicate a previously unrecognized, and deeper, en echelon lode in which biotite forms part of a medial alteration assemblage dominated by tremolite–actinolite and biotite (Kcs alteration; cf. Marvel Loch and Transvaal, Fig. 2.100, Part 2 of this Atlas).

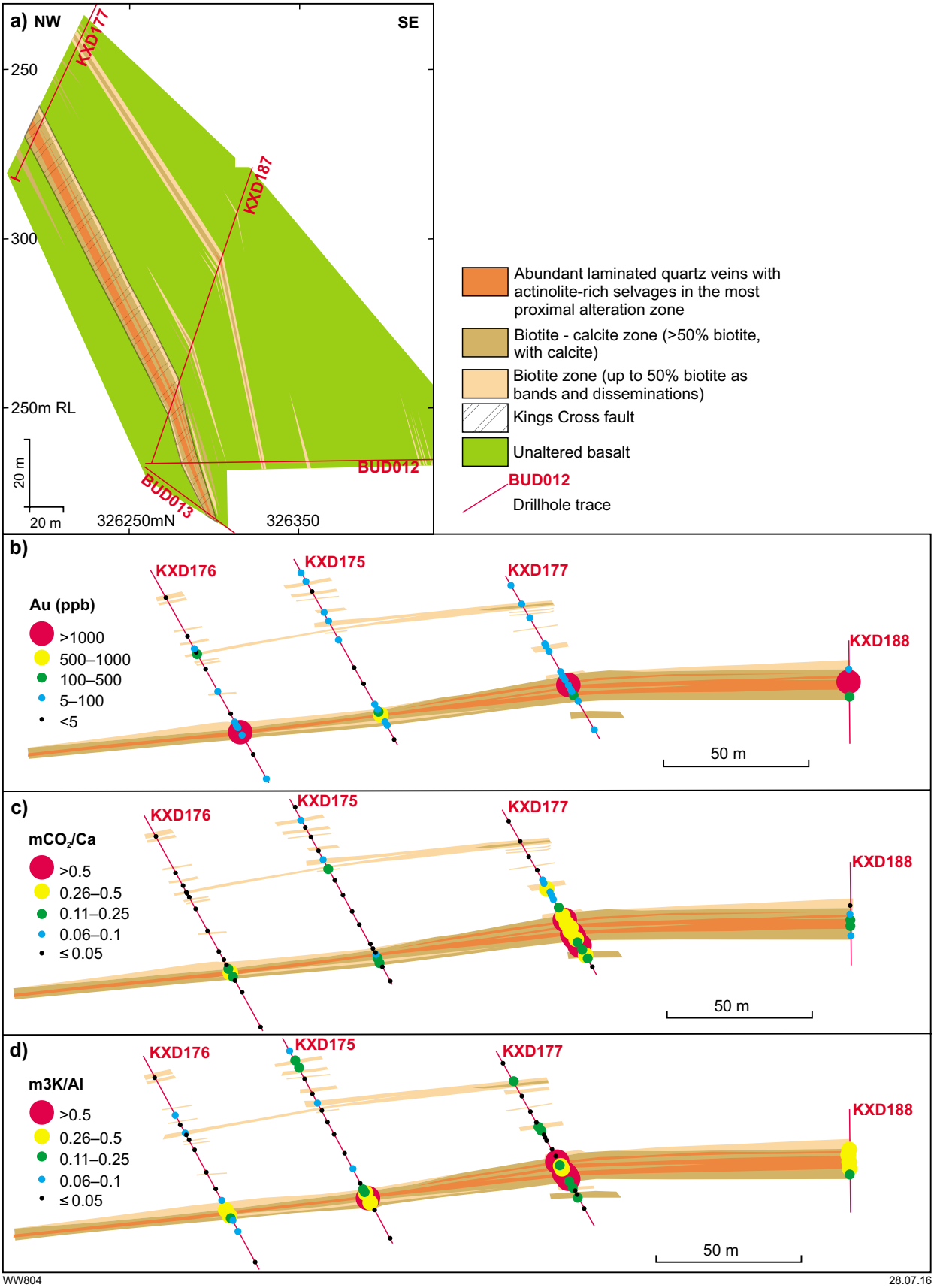

Figure 3.67. **Alteration indices, Kings Cross gold deposit, Coolgardie district, Eastern Goldfields Superterrane (after Eilu and Mikucki, 1996). a) Hydrothermal alteration zoning projected onto east-southeast transverse cross section 20150–20200E. Longitudinal cross sections (tilted 60°W, in the plane of drilling) showing hydrothermal alteration zoning, gold content, and alteration indices b) gold content, c) mCO_2/Ca, and d) m3K/Al. Coordinates refer to local mine grid.**

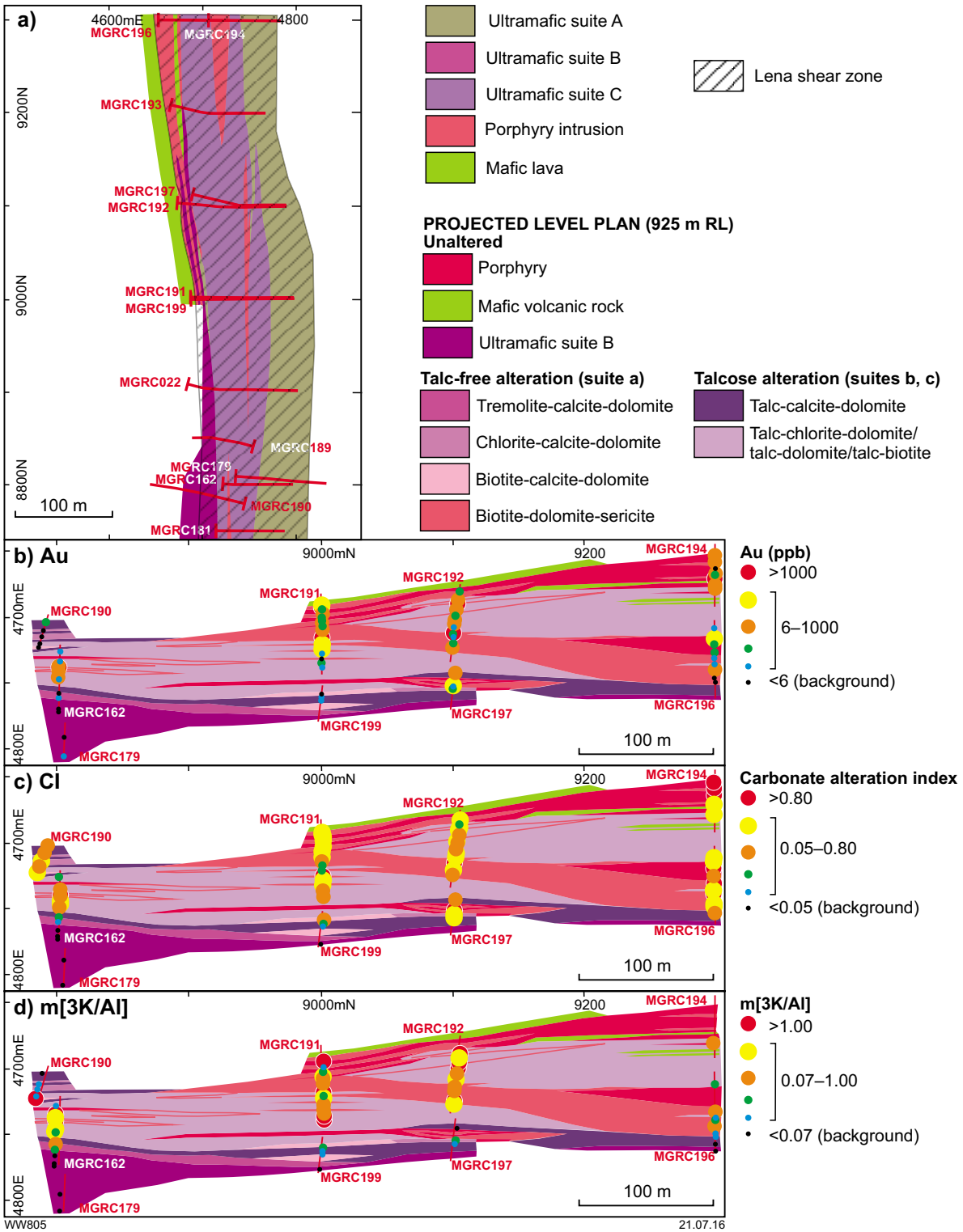

Figure 3.68. **Alteration indices, Moyagee gold deposit, Murchison Domain, Youanmi Terrane (after Eilu and Mikucki, 1996). a) Simplified geological map (925 m RL, or ~75 m below the surface) of the Moyagee deposit showing traces of the drillholes studied. Hydrothermal alteration zoning, gold content, and alteration indices projected onto the 925 m RL level plan. b) Gold content, c) $mCO_2/(Ca + Mg + Fe - 0.75S)$, and d) m3K/Al. Coordinates refer to local mine grid.**

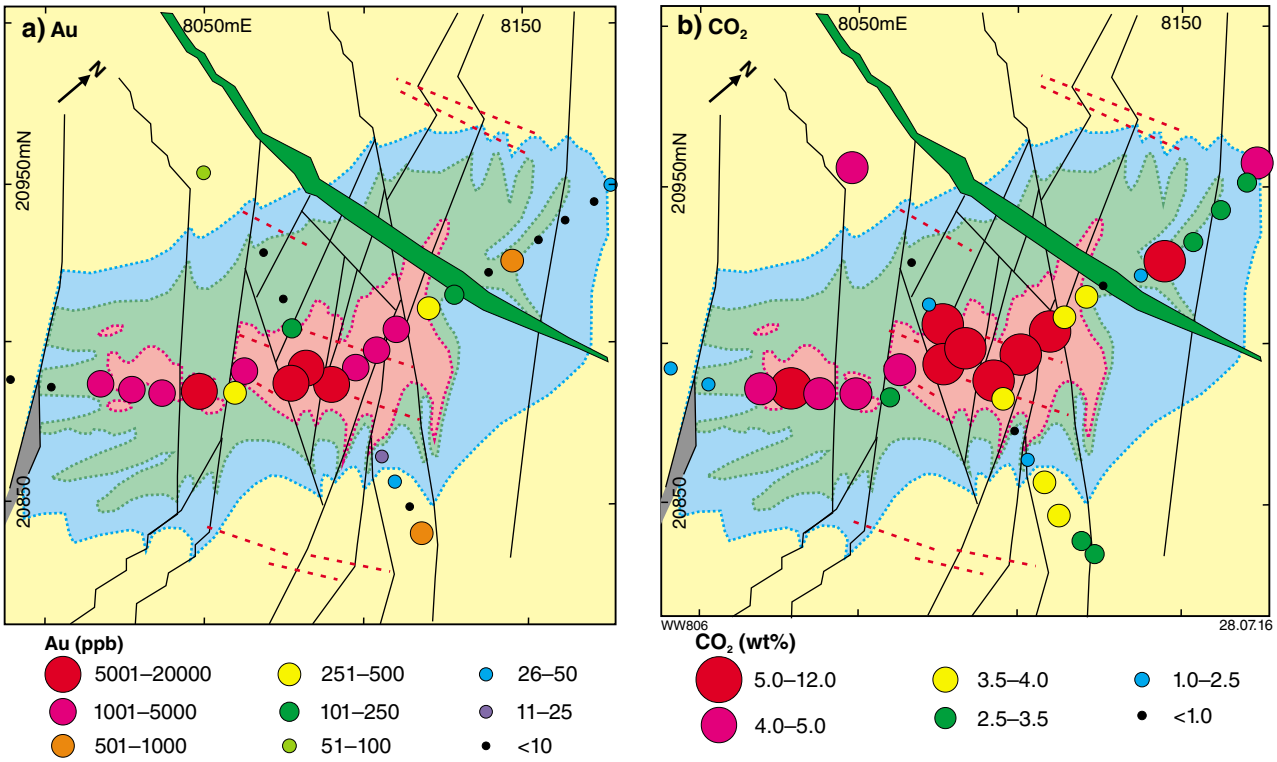

Figure 3.69. Hydrothermal alteration, Twin Peaks gold deposit, Carosue Dam district, Eastern Goldfields Superterrane, compared with a) gold content and b) CO_2 content. Alteration zones: distal calcite zone (blue), medial dolomite zone (green), proximal potassic zone (pink). Coordinates refer to local mine grid.

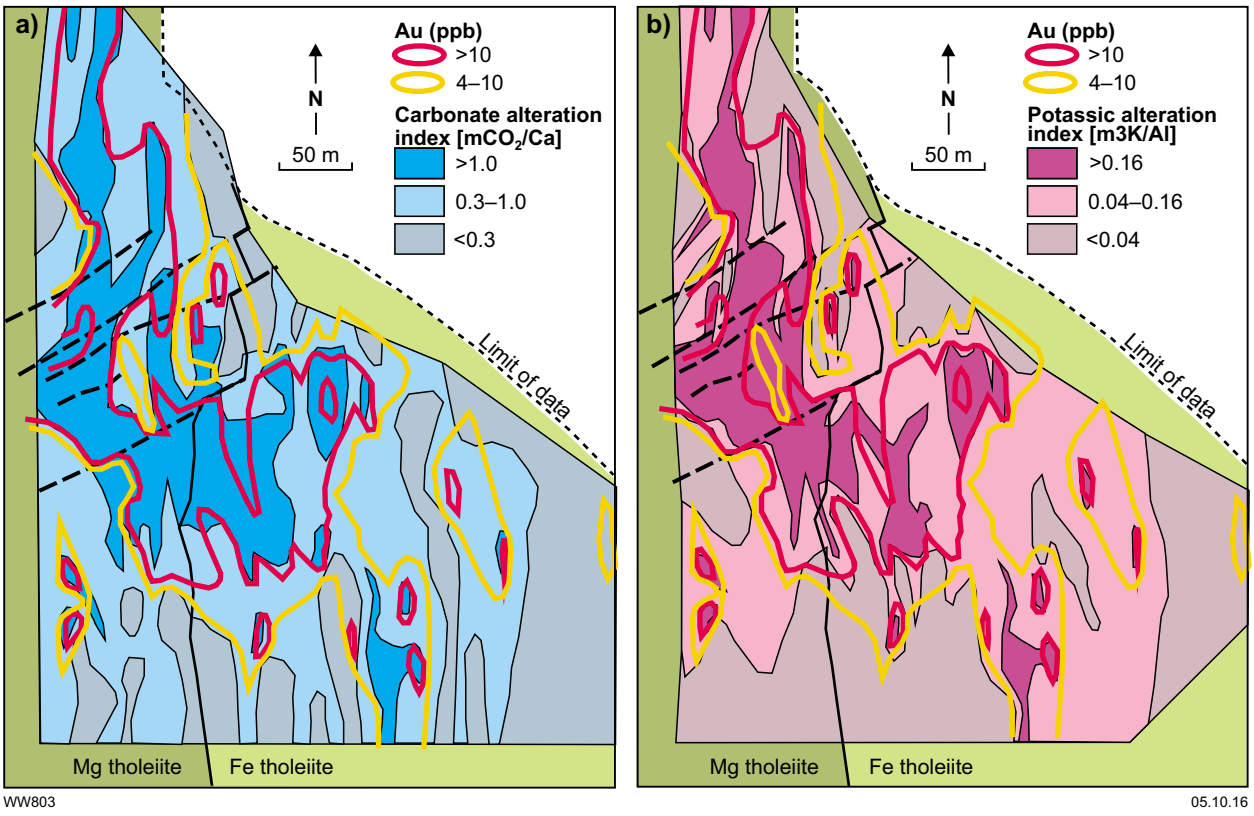

Figure 3.70. Gold content and alteration indices, Bronzewing gold deposit, Yandal district, Eastern Goldfields Superterrane (after Eilu et al., 2001). a) Au content and mCO_2/Ca, b) Au content and m3K/Al.

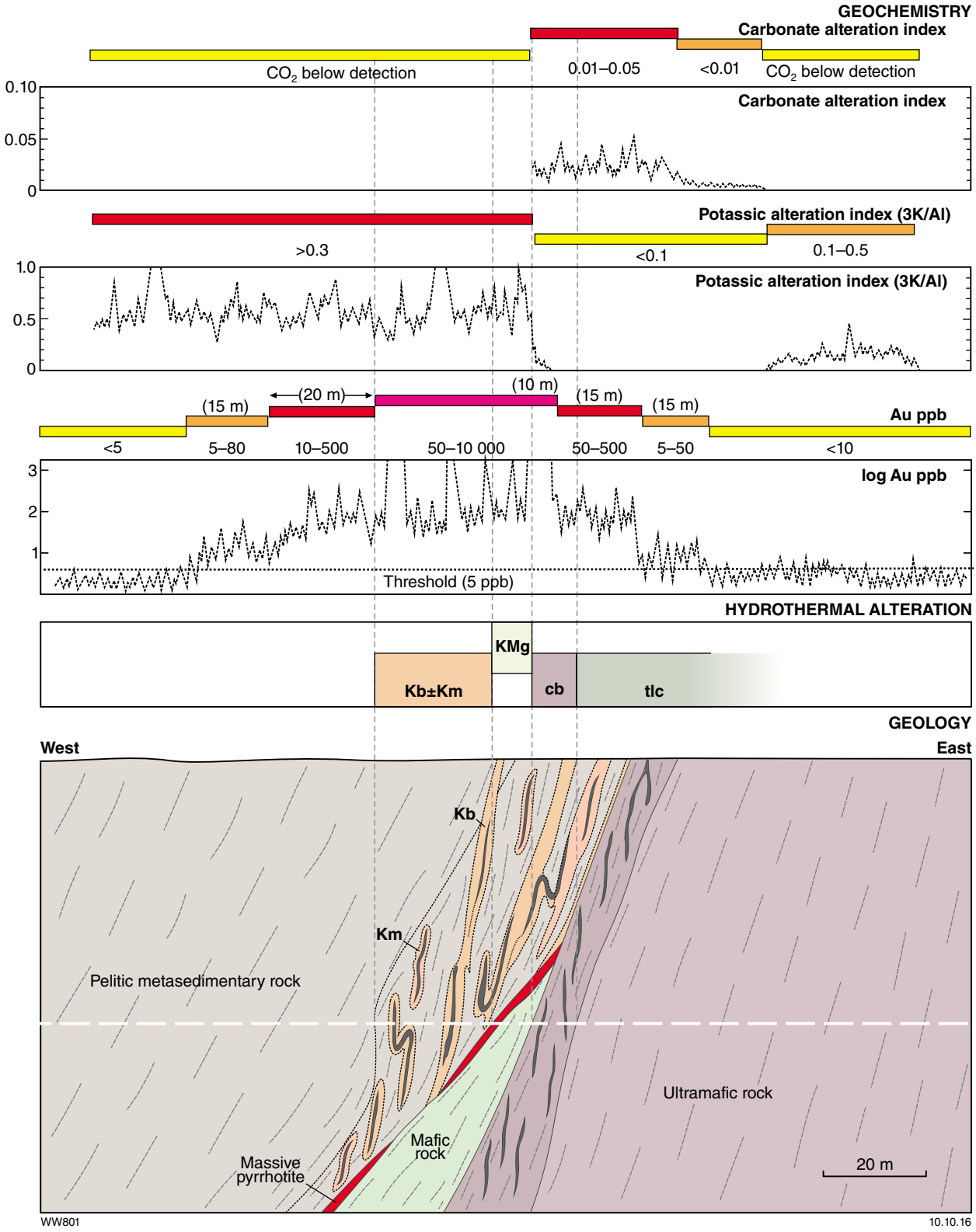

Figure 3.71. **Idealized cross section through Yilgarn Star gold deposit, Southern Cross district, Youanmi Terrane showing hydrothermal alteration and distribution of gold and alteration indices. See Figure 3.59 for explanation of alteration codes.**

The carbonate alteration index is close to zero (CO_2 below lower limit of detection) in the hangingwall pelites but anomalous (>0.01) in the mineralized ultramafic unit, reflecting differences in the proximal hydrothermal alteration in these two rock types. The carbonate alteration index anomaly (>0.01) extends about 20 m into the unmineralized distal alteration zone of the ultramafic footwall, but extends another 15 m if CO_2 detection is used as the cutoff. The lateral extent of the carbonate alteration index (>0.01) anomaly is similar to those of the As and Sb anomalies, but about 5 m short of the low-level (>5 ppb) gold anomaly (Fig. 3.61). Setting the cutoff at the detection level of CO_2, the carbonate alteration index anomaly extends 10 m beyond the low-level gold anomaly.

Application of rare alkali index

Red October, Laverton district

To assess the utility of the $([Rb + Cs]/Th)_N$ ratio as a tool for gold exploration at deposit scale, new whole-rock geochemical data were collected, in collaboration with Saracen Gold Mines Pty Ltd, from the Red October mine in the Laverton district of the Eastern Goldfields Superterrane.

The Red October gold deposit is hosted by a northeast-striking, moderately to steeply northwest-dipping fault that follows the contact between a hangingwall sequence of komatiite and high-Mg basalt and a footwall sequence of high-Mg and tholeiitic basalts (Fig. 3.72). A thin, discontinuous graphitic shale unit on this contact has been the focus of deformation, including zones of mylonitization and hydrothermal alteration. The proximal alteration assemblage is quartz–plagioclase–biotite–calcite–sulfide, but locally, where alteration is more intense, there is a quartz–muscovite–calcite–sulfide assemblage. Gold mineralization is in laminated and locally brecciated quartz–carbonate–sulfide veins and altered wallrocks that contain disseminated pyrite and arsenopyrite. Several hangingwall lodes, possibly representing north–south striking subvertical faults (Witt et al., in press), intersected locally by diamond drilling, also display quartz–plagioclase–biotite–calcite–sulfide alteration. A geological log of an early hole at Red October (ROD-2), logged in 1991 and published by Roberts et al. (2004), is shown in Figure 3.73.

This study of the rare alkali index at Red October is based on sampling of six diamond drillholes or diamond tails on reverse circulation precollars (RORD001 to RORD006) that were drilled into the hangingwall sequence during 2011 and terminated 20 to 50 m below the lode intersection (Fig. 3.72). To assess consistency of geological interpretation, two of the holes (RORD002 and RORD004) were logged by WK Witt (Figs 3.74 and 3.75) for comparison with logs compiled by Saracen geologists, who logged all six holes (Figs 3.76 to 3.81). Comparison of the two sets of logs for RORD002 and RORD004 showed them to be reasonably consistent. Duplicates of drillcore samples collected by Saracen for gold analysis were submitted to Genalysis Laboratory Services for analysis of Al, Cs, K, Rb, and Th. Because Saracen sampling is normally confined to zones of visible hydrothermal alteration, extra samples were collected by WK Witt in the hangingwall and footwall at nominal spacings of 1 m from 0 to 5 m beyond the lode, 5 m from 5 to 25 m beyond the lode, 10 m from 25 to 105 m beyond the lode, and 25 m at >105 m beyond the lode. Sample collection points were modified slightly to avoid fracture and fault zones in the hanging and footwalls, except in RORD004, where two hangingwall lodes were specifically targeted. Caesium, Rb, and Th were analysed by ICP-MS and Al and K by inductively coupled plasma atomic emission spectroscopy (ICP-OES) following four-acid digestion to dissolve refractory minerals such as monazite, thorite, and zircon. Full analytical results are provided in the Appendix.

Results of the Red October study are summarized in Figures 3.76 to 3.81 and Tables 3.19 and 3.20. In Table 3.19, the width of visible proximal alteration includes zones of potassic alteration (Km, Kb) and silicification (Si), even where logged as weak. Carbonate alteration dominated by calcite is classed as medial or distal alteration.

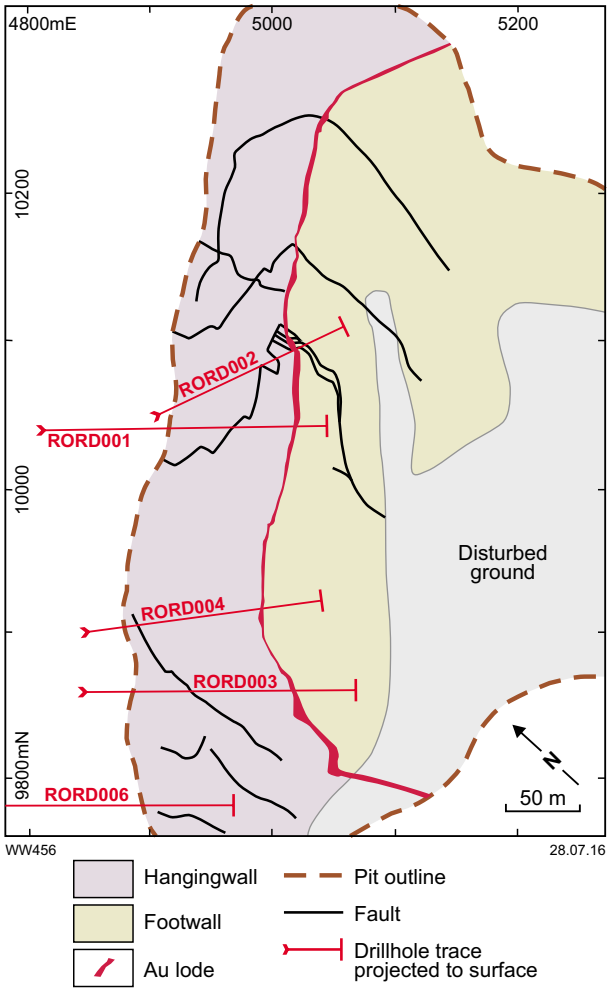

Notes: Collar for RORD006 lies just outside the map area. Collar and drill trace for RORD005 are approximately 50 m south of map area and directed grid east.

Figure 3.72. Geological map of the Red October openpit, Laverton district, Eastern Goldfields Superterrane, showing locations of drillholes used in this study

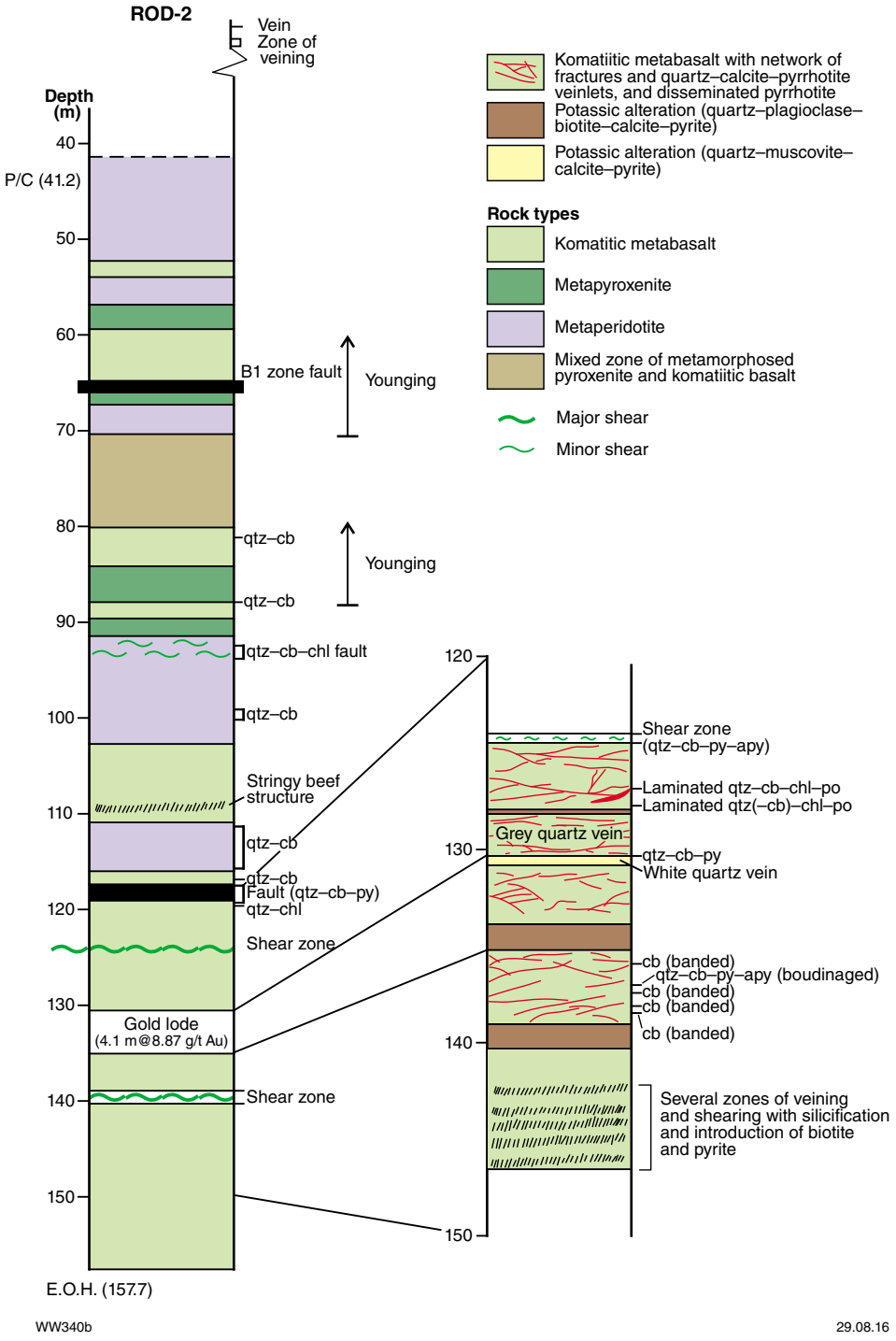

Figure 3.73. Detailed graphic log, ROD-2, Red October gold deposit (from Roberts et al., 2004). Abbreviations: Apy (arsenopyrite), cb (carbonate), chl (chlorite), po (pyrrhotite), py (pyrite), qtz (quartz).

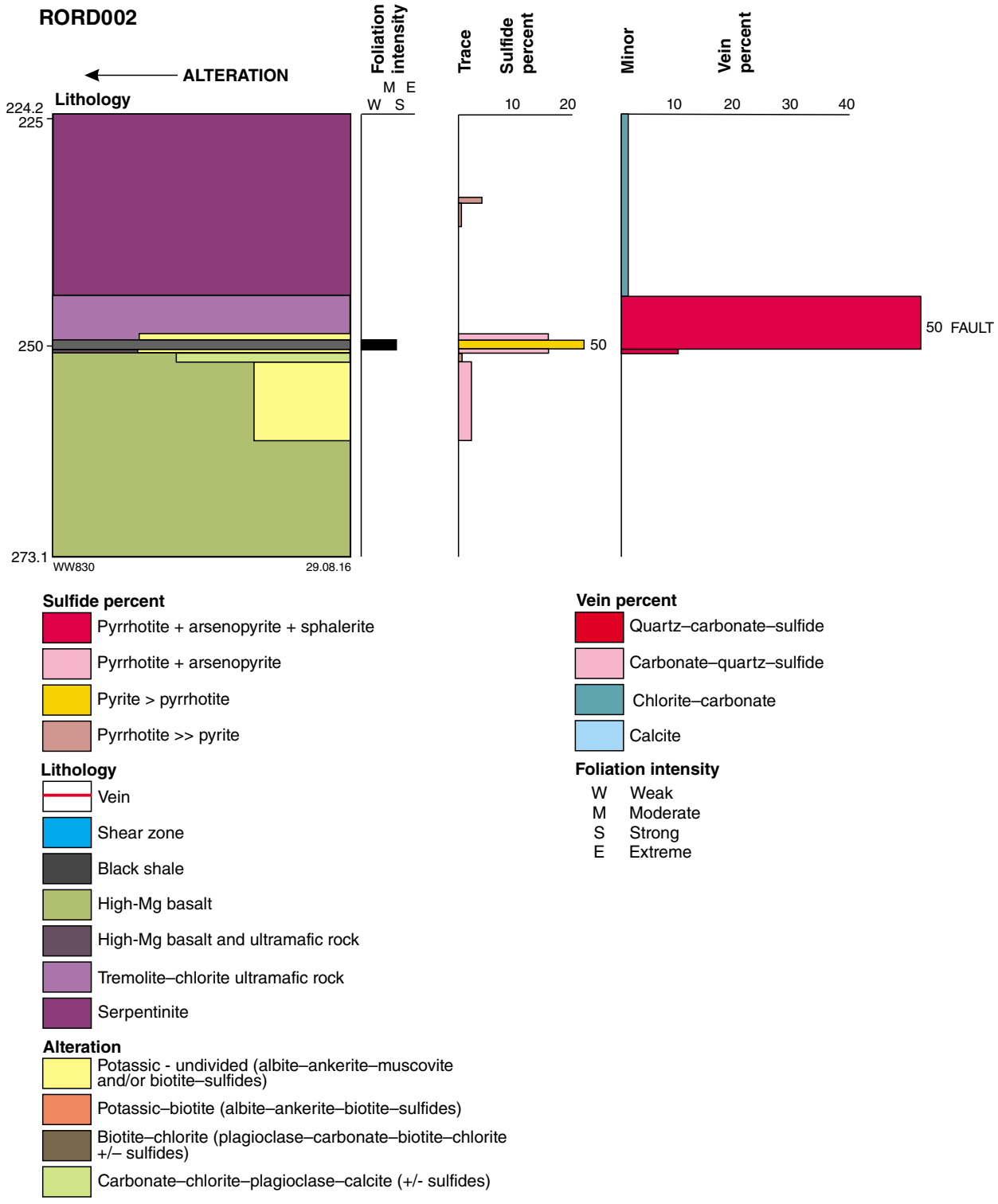

Figure 3.74. Graphic log, RORD002, Red October gold deposit, logged by WK Witt

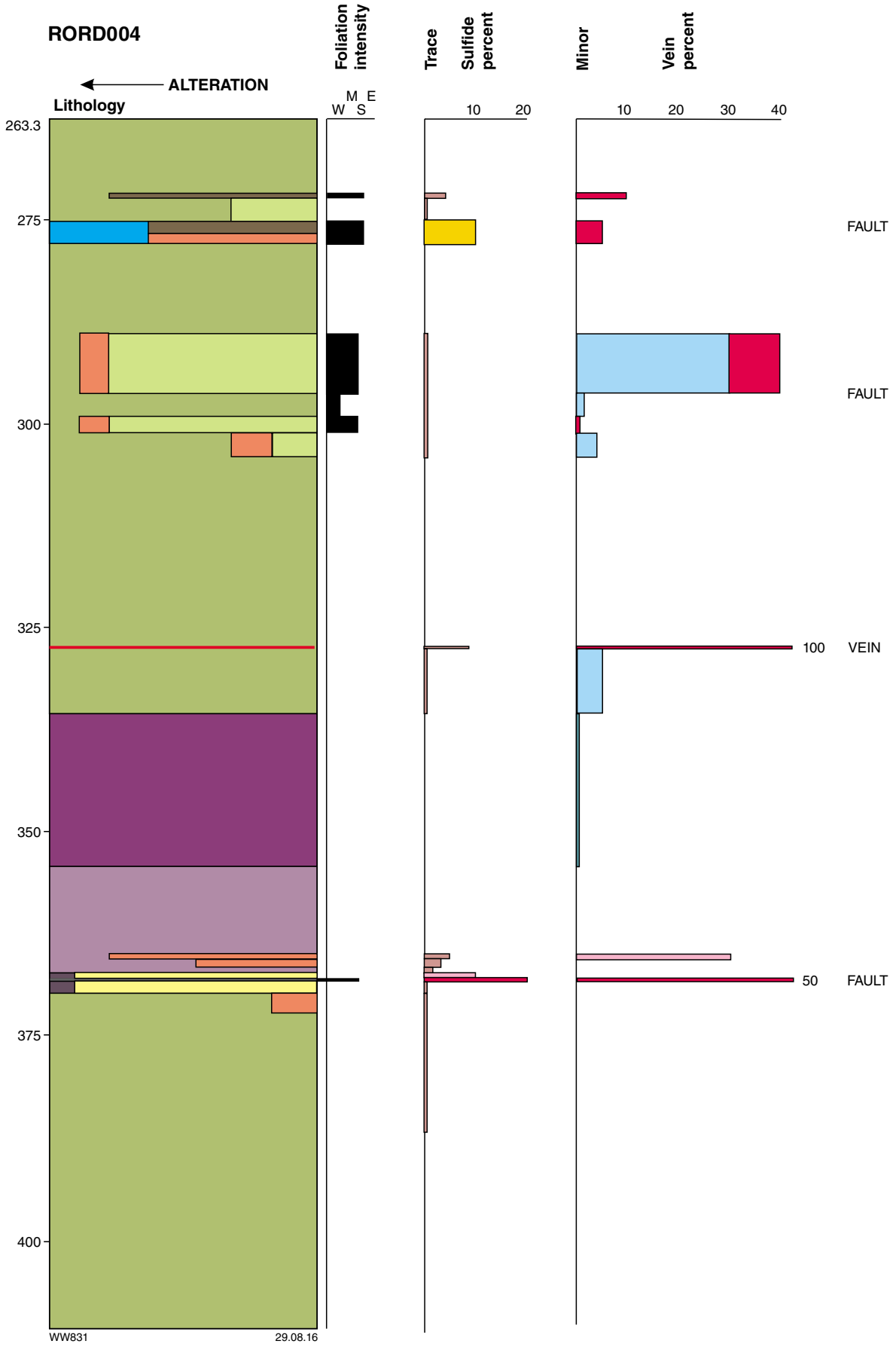

Figure 3.75. Graphic log, RORD004, Red October gold deposit, logged by WK Witt (see Fig. 3.74 for legend)

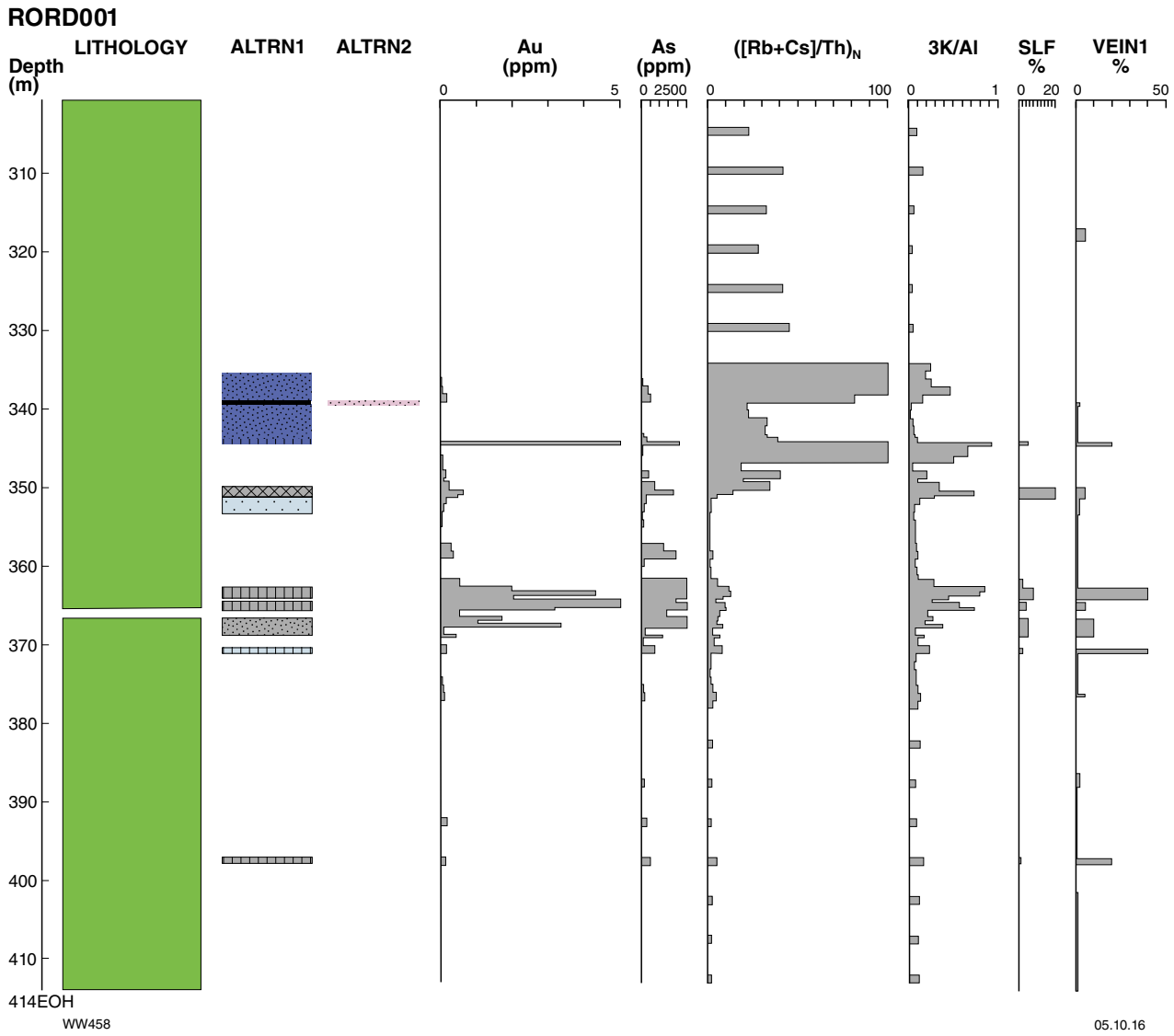

Figure 3.76. **Graphic log, RORD001, Red October gold deposit, logged by Saracen (see Figure 3.82 for legend). ALTRN1 (dominant alteration type), ALTRN2 (other alteration type), SLF% (percent sulfides), VEIN% (percent of dominant vein type).**

With the exception of RORD005 (a tail on an RC precollar for which no alkali data are available), all holes show a broad anomaly, defined by $([Rb + Cs]/Th)_N$ >5 (Heath and Campbell, 2004), which overlaps the lode and extends at least 45 m into the hangingwall and beyond the proximal zone of visible alteration. In both RORD001 and RORD002, the anomaly extends beyond medial to distal carbonate alteration. The complete width of the hangingwall anomaly is unknown for several holes because shallower, unweathered core samples were not available for analysis.

Most of the $([Rb + Cs]/Th)_N$ profiles display one or more peaks within the hangingwall sequence and in some cases the peak values over the lode are lower than those of the hangingwall peaks. Noting this, the narrow $([Rb + Cs]/Th)_N$ anomaly recorded over the lode in RORD005 may be a product of incomplete sampling of the profile, and may therefore be misleading. The broad but irregular $([Rb + Cs]/Th)_N$ anomalies in the hangingwall sequences in most holes are interpreted to reflect the presence of hangingwall lodes (subparallel shears or north–south faults), above the deformed lithological contact. In terms of visible alteration and gold assay data, these lodes appear to be least well-developed in holes intersecting the central part of the orebody (RORD001 and RORD002), but $([Rb + Cs]/Th)_N$ values in these holes clearly define the hangingwall anomaly related to these holes (Figs 3.76 and 3.77).

Hangingwall lodes are associated with hydrothermal alteration and some with anomalous gold (e.g. RORD004), but the $([Rb + Cs]/Th)_N$ anomaly in RORD004 still extends well beyond intervals of >0.1 ppm Au. A footwall $([Rb + Cs]/Th)_N$ anomaly is absent or very poorly developed in all holes. The reason for this is not

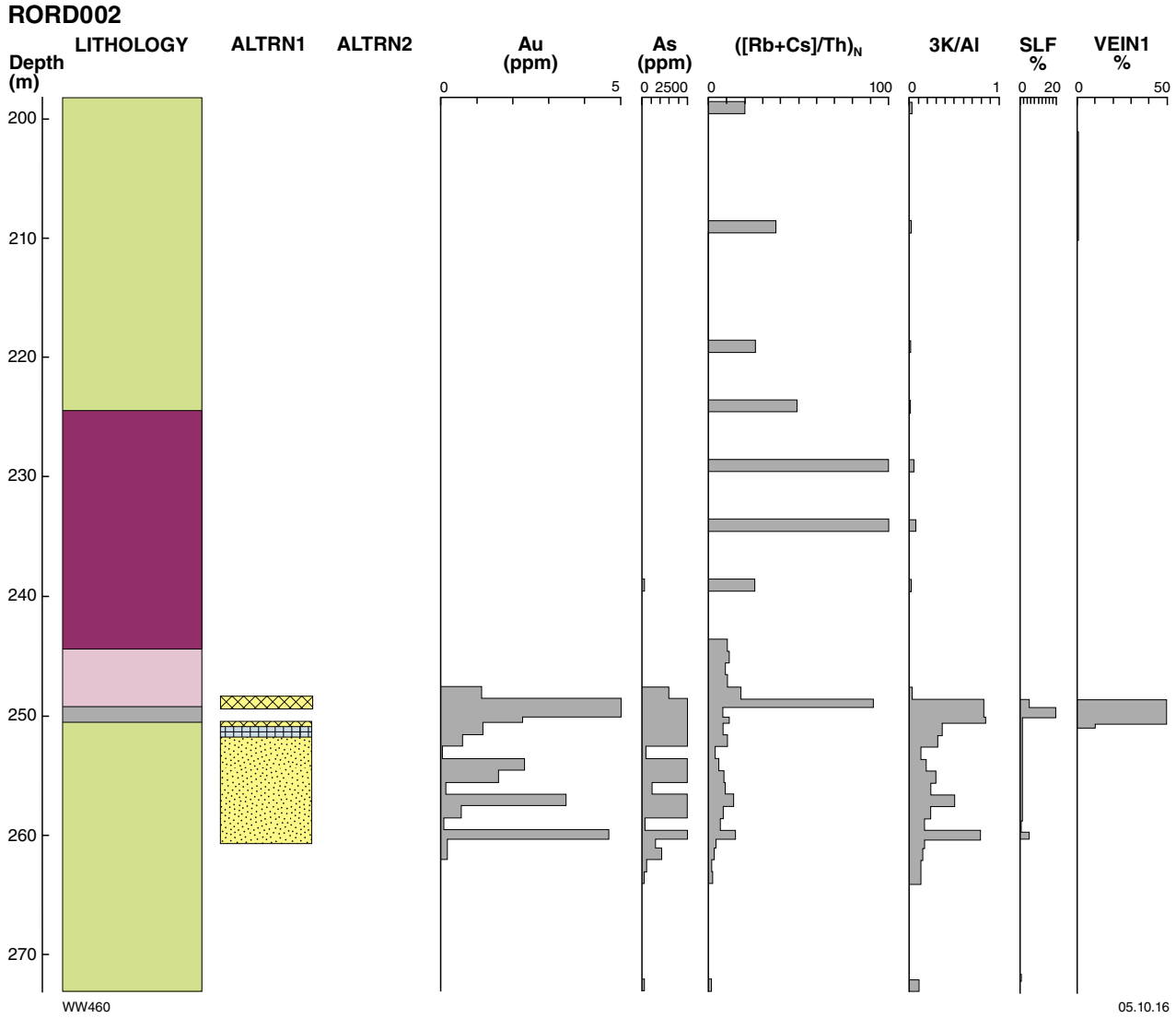

Figure 3.77. **Graphic log, RORD002, Red October gold deposit, logged by Saracen (see Figure 3.82 for legend). ALTRN1 (dominant alteration type), ALTRN2 (other alteration type), SLF% (percent sulfides), VEIN% (percent of dominant vein type).**

known. It is possible that the rare alkali index is more sensitive to the biotite and carbonate alteration observed in the hangingwall lodes, whereas alteration containing muscovite on the mineralized contact and footwall are better monitored using the molar 3K/Al alkali index. More research to investigate this possibility is warranted.

A threshold value of 0.15 was chosen for anomalous molar 3K/Al ratios, based on the results shown in Figures 3.76 to 3.81. With the exception of RORD005 (limited data), the extents of 3K/Al anomalies are more restricted than the $([Rb + Cs]/Th)_N$ anomalies and, although they highlight zones of visible hydrothermal alteration and gold mineralization, the anomalies do not generally extend more than a few metres beyond the limits of visible proximal to distal alteration (Table 3.20). In RORD001 and RORD002, for example, the 3K/Al anomalies do not extend into unaltered hangingwall rocks that are within the $([Rb + Cs]/Th)_N$ anomaly (Figs 3.76 and 3.77). An exception is the footwall anomaly in RORD006, where a broad 3K/Al anomaly encompasses several subordinate lodes in the hangingwall and footwall, each coincident with discrete $([Rb + Cs]/Th)_N$ anomalies (Fig. 3.81).

Discussion

The results of the Red October study support the conclusions of Heath and Campbell (2004) by showing broad dispersion of $([Rb + Cs]/Th)_N$, measured in tens of metres, beyond the gold lode and related visible alteration. Other examples of $([Rb + Cs]/Th)_N$ dispersion around gold lodes in the Eastern Goldfields Superterrane have been identified at Sons of Gwalia and Tower Hill in the Leonora district.

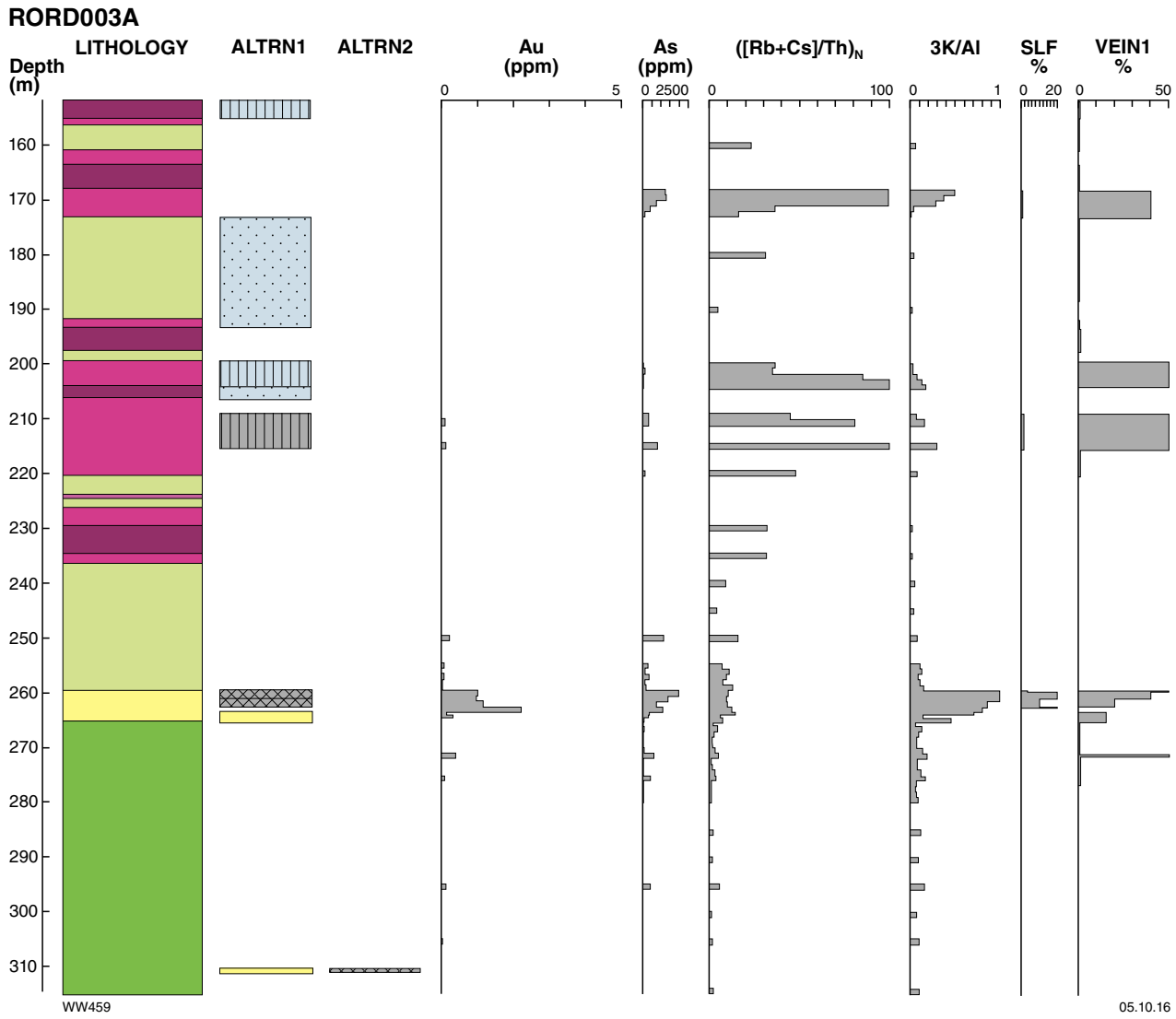

Figure 3.78. **Graphic log, RORD003A, Red October gold deposit, logged by Saracen (see Figure 3.82 for legend). ALTRN1 (dominant alteration type), ALTRN2 (other alteration type), SLF% (percent sulfides), VEIN% (percent of dominant vein type).**

Similar to the results from Red October, the $([Rb + Cs]/Th)_N$ ratio in ultramafic rocks at the Tower Hill deposit (Fig. 3.83a) is anomalous (>5) for distances of >100 m around the mineralized quartz veins, including about 50 m beyond the biotite alteration zone. Although somewhat irregular, the results from Tower Hill produce a gradient that illustrates how the $([Rb + Cs]/Th)_N$ ratio can be used as a vector towards a gold lode within broad volumes of hydrothermal (carbonate and biotite) alteration.

At Sons of Gwalia, the $([Rb + Cs]/Th)_N$, ratio is anomalous within the ore zone, but there is little dispersion beyond zones of proximal hydrothermal alteration (Fig. 3.83b–d). The situation there is further complicated by sea-floor hydrothermal (aluminosilicate) alteration in the footwall below the massive sulfide horizon, which clearly resulted in anomalous $([Rb + Cs]/Th)_N$ ratios in and beyond the limits of visible aluminosilicate alteration. The results from Sons of Gwalia show that caution should be applied when using $([Rb + Cs]/Th)_N$ ratios to target gold mineralization; false positives may arise from hydrothermal alteration not directly related to gold mineralization. It is worth noting, however, that at Sons of Gwalia the aluminosilicate alteration facies provides a vector towards the main lode (see Targeting Criterion 2.17, Part 2 of this Atlas). Perhaps the anomalous $([Rb + Cs]/Th)_N$ ratio associated with aluminosilicate alteration is a potential vector towards gold at Sons of Gwalia. In hole SGD3226, and perhaps in GWDD4A and GWDD7A (Fig. 3.83b–d), a sub-economic lode associated with weak hydrothermal muscovite between the Sons of Gwalia main lode and the massive sulfide horizon also displays anomalous $([Rb + Cs]/Th)_N$ ratios. In instances such as this, the $([Rb + Cs]/Th)_N$ ratio may highlight a potential lode that might otherwise be missed during exploration or, alternatively, could be used

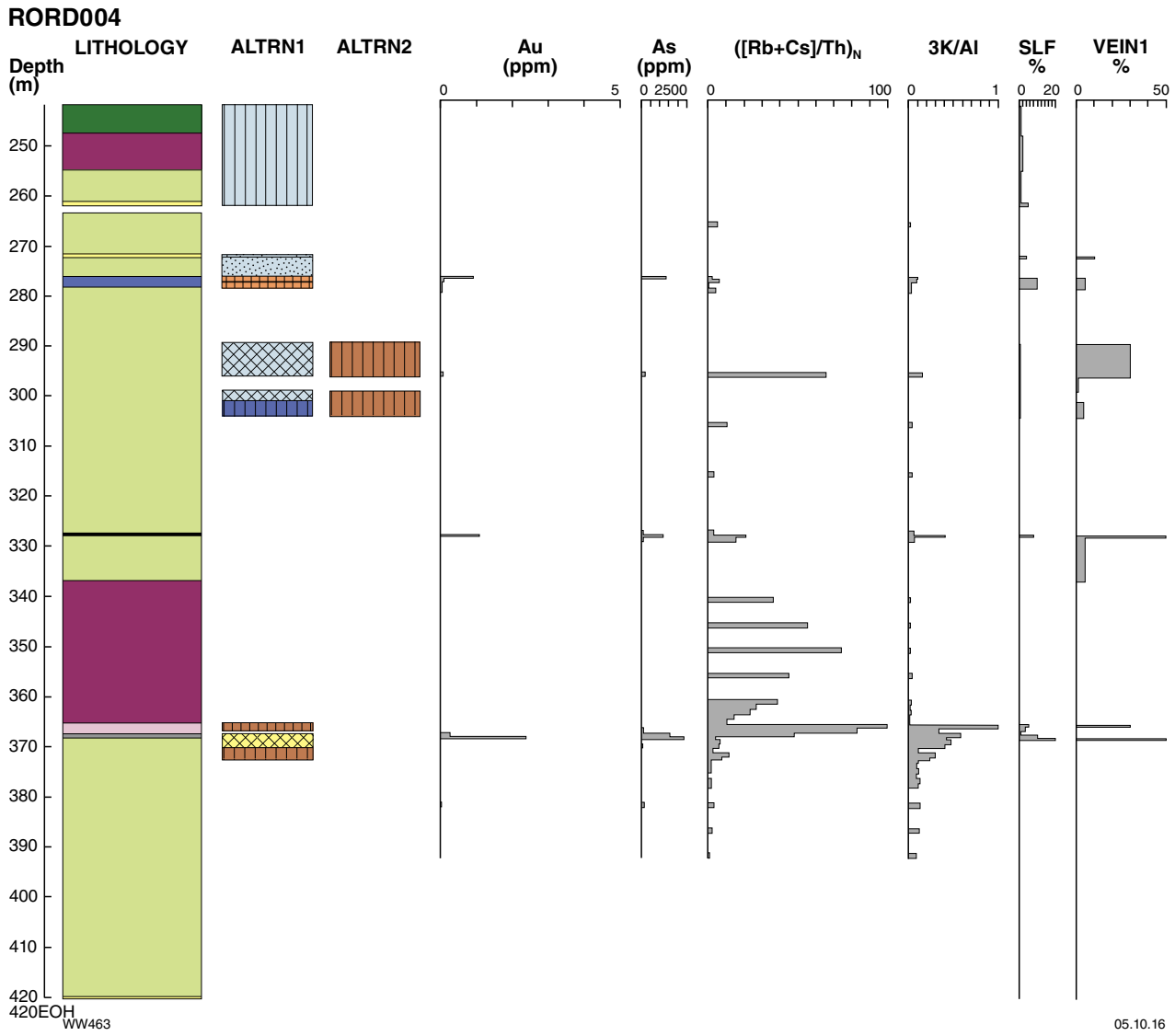

Figure 3.79. **Graphic log, RORD004, Red October gold deposit, logged by Saracen (see Figure 3.82 for legend). ALTRN1 (dominant alteration type), ALTRN2 (other alteration type), SLF% (percent sulfides), VEIN% (percent of dominant vein type).**

as a vector along strike or downdip towards higher-grade sections of the lode.

Summary

The carbonate alteration index is generally more useful than traditional alkali alteration indices (molar 3K/Al, molar Na/Al) for detecting the distal portions of gold-related hydrothermal systems. On the basis of the examples described above, traditional alkali alteration indices may, in some cases, extend beyond the proximal (K-mica-bearing) alteration zone and the low-level gold anomaly (e.g. Bronzewing), but they rarely extend beyond all visible gold-related alteration. The Kings Cross example shows that, where gold is present in relatively ductile structural settings, an alkali index anomaly may be defined by considering only samples taken from the host structure and subparallel shear zones, and ignoring those from intervening unstrained and unaltered rock.

Application of the molar 3K/Al index in the Southern Cross belt (e.g. Yilgarn Star), and probably some localities elsewhere in the Yilgarn Craton (e.g. Leonora), is complicated by the presence of pre-gold sea-floor alteration in footwall units to the mineralization. It is noteworthy that all examples where the anomalous molar 3K/Al index extends beyond the low-level gold anomaly are gold deposits hosted in mafic rocks. Mafic and ultramafic rocks have low background K contents, so the molar 3K/Al index may be less effective as a vector to gold mineralization in host rocks with higher background K concentrations, such as felsic rocks and metasedimentary rocks (e.g. Granny Smith, Twin Peaks).

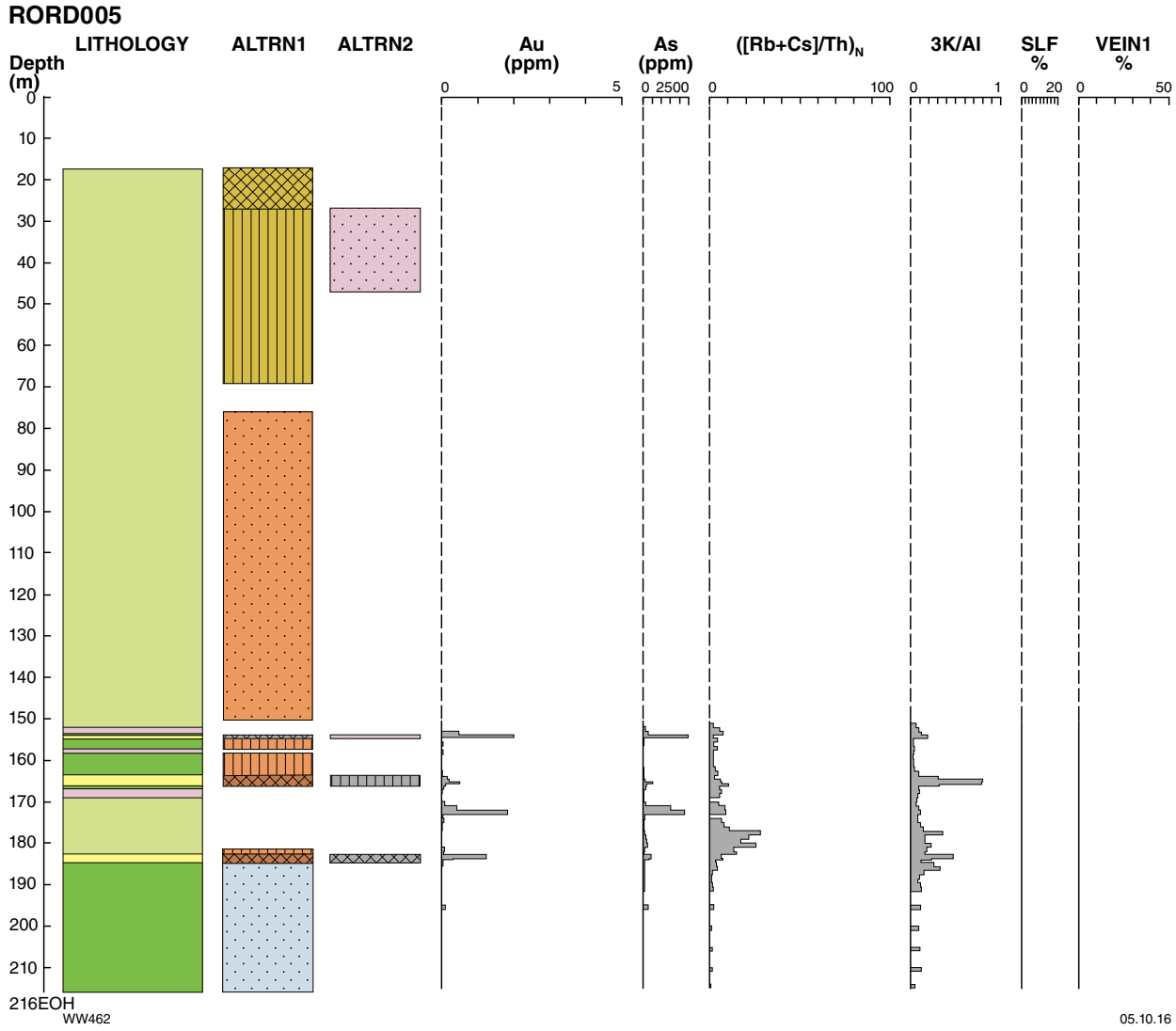

Figure 3.80. Graphic log, RORD005, Red October gold deposit, logged by Saracen (see Figure 3.82 for legend). ALTRN1 (dominant alteration type), ALTRN2 (other alteration type), SLF% (percent sulfides), VEIN% (percent of dominant vein type).

Anomalous carbonate alteration index values generally extend further from gold lodes than do the traditional alkali indices, in most cases for tens of metres beyond the low-level gold anomaly. The carbonate alteration index anomaly extends more than 5 m beyond visible alteration in only two of the studies described here (Kings Cross and Twin Peaks). At Twin Peaks, however, this anomaly reflects district-scale carbonation that may extend for hundreds of metres beyond the visible alteration in the form of dolomite spots (?porphyroblasts).

Use of the carbonate alteration index in gold exploration in the Yilgarn has been discouraged by the analytical costs involved. Analysis of CO_2 requires a separate sample preparation and analytical procedure. It cannot be added, relatively cheaply, to a list of pathfinder elements determined by ICP-MS or X-ray fluorescence techniques, for example. Furthermore, given that the carbonate saturation anomaly reflects the underlying carbonate alteration, the same outcome can usually be achieved using a bottle of dilute HCl, at minimal cost. In some cases, however, the carbonate alteration index may provide a vector within district-scale volumes of carbonate alteration. Based on district-scale studies in Canada, and the presence of extensive carbonate alteration in major shear zones of the Yilgarn Craton, similarly extensive carbonate alteration anomalies can also be anticipated in all gold deposits within regional shear zones (e.g. Paddington and New Celebration in the Eastern Goldfields Superterrane). These carbonate alteration zones are so extensive that they may not assist in the location of gold deposits within them without quantification in the form of carbonate alteration indices.

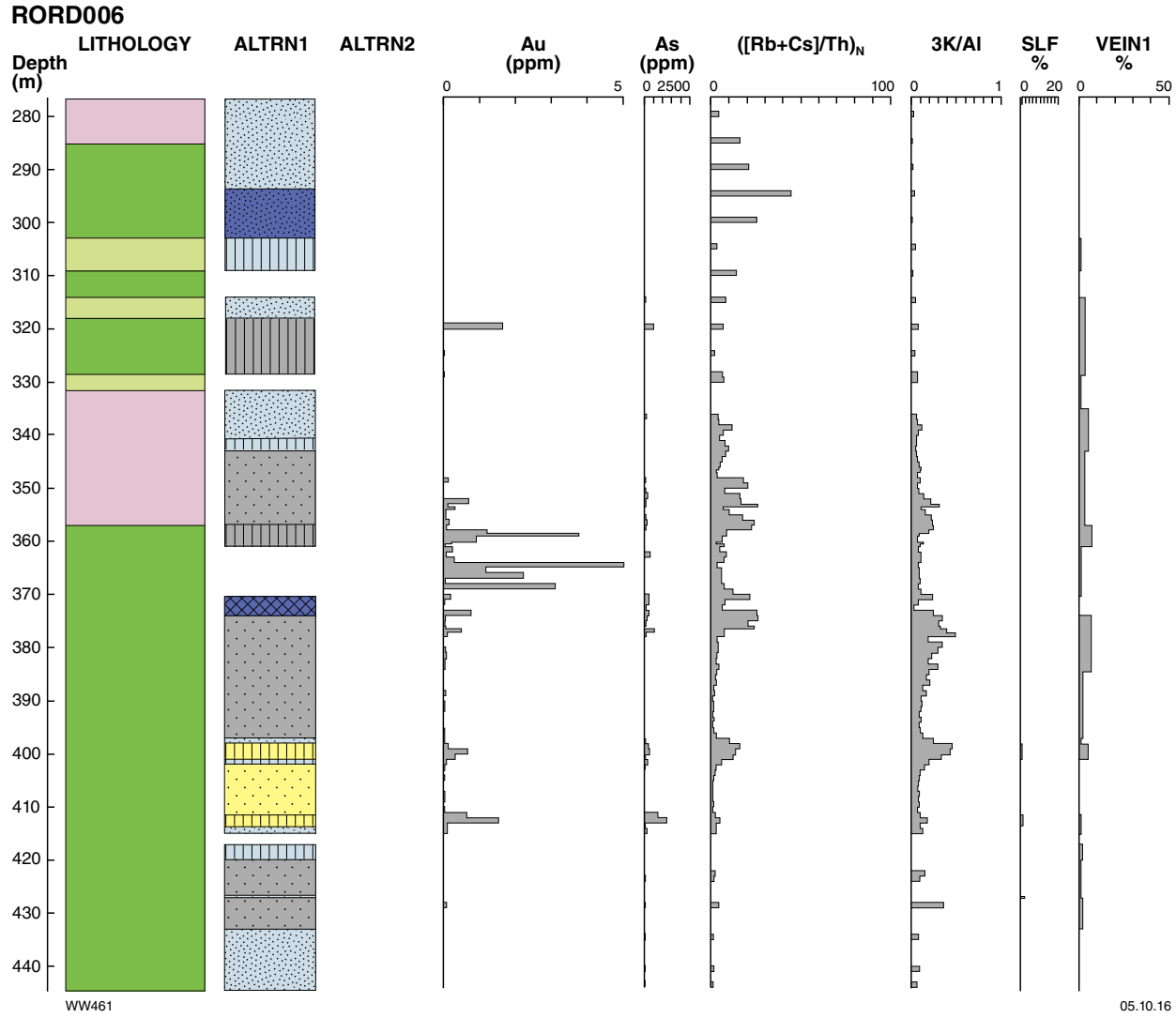

Figure 3.81. **Graphic log, RORD006, Red October gold deposit, logged by Saracen (see Figure 3.82 for legend). ALTRN1 (dominant alteration type), ALTRN2 (other alteration type), SLF% (percent sulfides), VEIN% (percent of dominant vein type).**

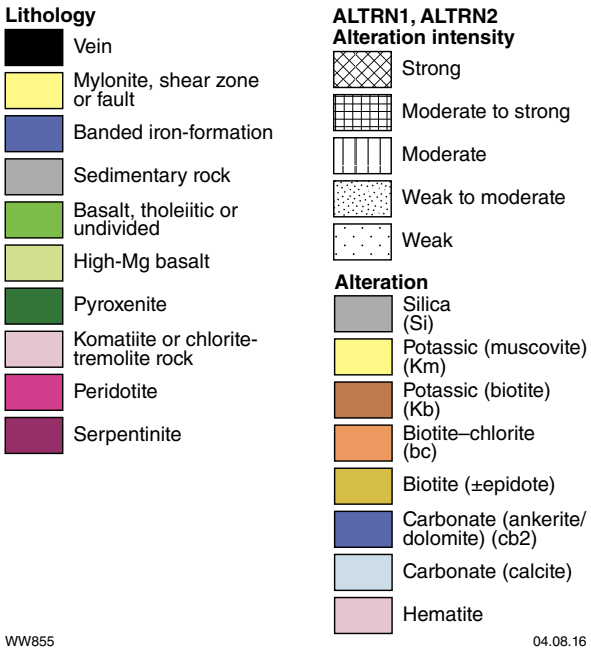

Figure 3.82. **Legend for Figures 3.76 to 3.81**

Table 3.19. Summary of ([Rb+Cs]/Th)$_N$ dispersion around the gold lode at Red October based on data from holes RORD001 to RORD006

		RORD					
	Extent (m)	*001*	*002*	*003A*	*004*	*005*	*006*
Lode	From	361.5	247.5	259.5	367.0	171	352
	To	367.7	260.3	263.5	368.2	184.0	369
Visible proximal alteration[(a)]	From	349.8	248.4	259.6	365.2	153.9	358
	To	368.8	260.5	265.2	372.4	184.6	374
	Type	Si (?Km)	Km	Si, Km	Km, Kb	Kb, bc	Si, cb2
([Cs+Rb]/Th)$_N$ anomaly[(b)]	From	<304	<198.5	<159.5	295.0	164.5	284.0
	To	371.0	260.3	265.4	367.7	184.0	378.0
	Width	>67.0	>61.8	>105.9	72.7	19.5	94.0
	Distance beyond all proximal alteration (hw)	>45.2	>49.9	>100.1	69.8	-10.6	74.0
	Distance beyond all proximal alteration (fw)	2.2	-0.2	0.2	-4.7	-0.6	4.0
Comments (below)		(1)		(2)		(3)	(4)

(1) Relatively depleted ([Cs+Rb]/Th)$_N$ within central lode

(2) Narrow silicified zone with ~0.1 ppm Au and hangingwall weak carbonate alteration zone broadly coincident with peak of ([Rb+Cs]/Th)$_N$ anomaly

(3) Very patchy lode; analytical data not available through most of hangingwall sequence

(4) Peak ([Cs+Rb]/Th)$_N$ value at ~295 m in hangingwall is coincident with zone of strong ankeritic carbonate alteration. A second ([Cs+Rb]/Th)$_N$ anomaly at ~400 m, in footwall of lode is coincident with subeconomic gold interval

NOTES: (a) See Fig. 3. 82 legend for key to alteration types. (b) Anomaly threshold set at 5.0 (Heath and Campbell, 2004). fw, footwall; hw, hangingwall

Table 3.20. Summary of 3K/Al dispersion around the gold lode at Red October based on data from holes RORD001 to RORD006

		RORD					
	Extent (m)	*001*	*002*	*003A*	*004*	*005*	*006*
Lode	From	361.5	247.5	259.5	367.0	171	352
	To	367.7	260.3	263.5	368.2	184.0	369
Proximal alteration[(a)]	From	349.8	248.4	259.6	365.2	153.9	358
	To	368.8	260.5	265.2	372.4	184.6	374
	Type	Si (?Km)	Km	Si, Km	Km, Kb	Kb, bc	Si, cb2
3K/Al anomaly[(b)]	From	334	248.5	257.5	365.3	163.8	351
	To	371	273	265.4	372.3	186.6	402
	Width	37	24.5	7.9	7.05	22.8	51
	Distance beyond all proximal alteration (hw)	15.8	0.1	2.1	-0.1	-9.9	7.0
	Distance beyond all proximal alteration (fw)	2.2	>12.5	0.2	-0.05	2.0	28.0
Comments (below)		(1)	(2)	(3)	(4)	(5)	(6)

(1) 3K/Al not depleted within central lode

(2) Final sample at 272–273 m has 3K/Al = 0.10 (probably close to footwall limit of 3K/Al anomaly)

(3) Two more anomalies in hangingwall but separated from the main anomaly and each other by intervals of 3K/Al <0.1

(4) Isolated anomalies in hangingwall

(5) Anomalous 3K/Al coincident with depleted ([Cs+Rb]/Th)$_N$ within central lode

(6) Broad 3K/Al anomaly encompasses Km alteration and Au >0.25 ppm in footwall of main lode

NOTES: (a) See Fig. 3.82 legend for key to alteration types. (b) Anomaly threshold taken as 0.15. fw, footwall; hw, hangingwall

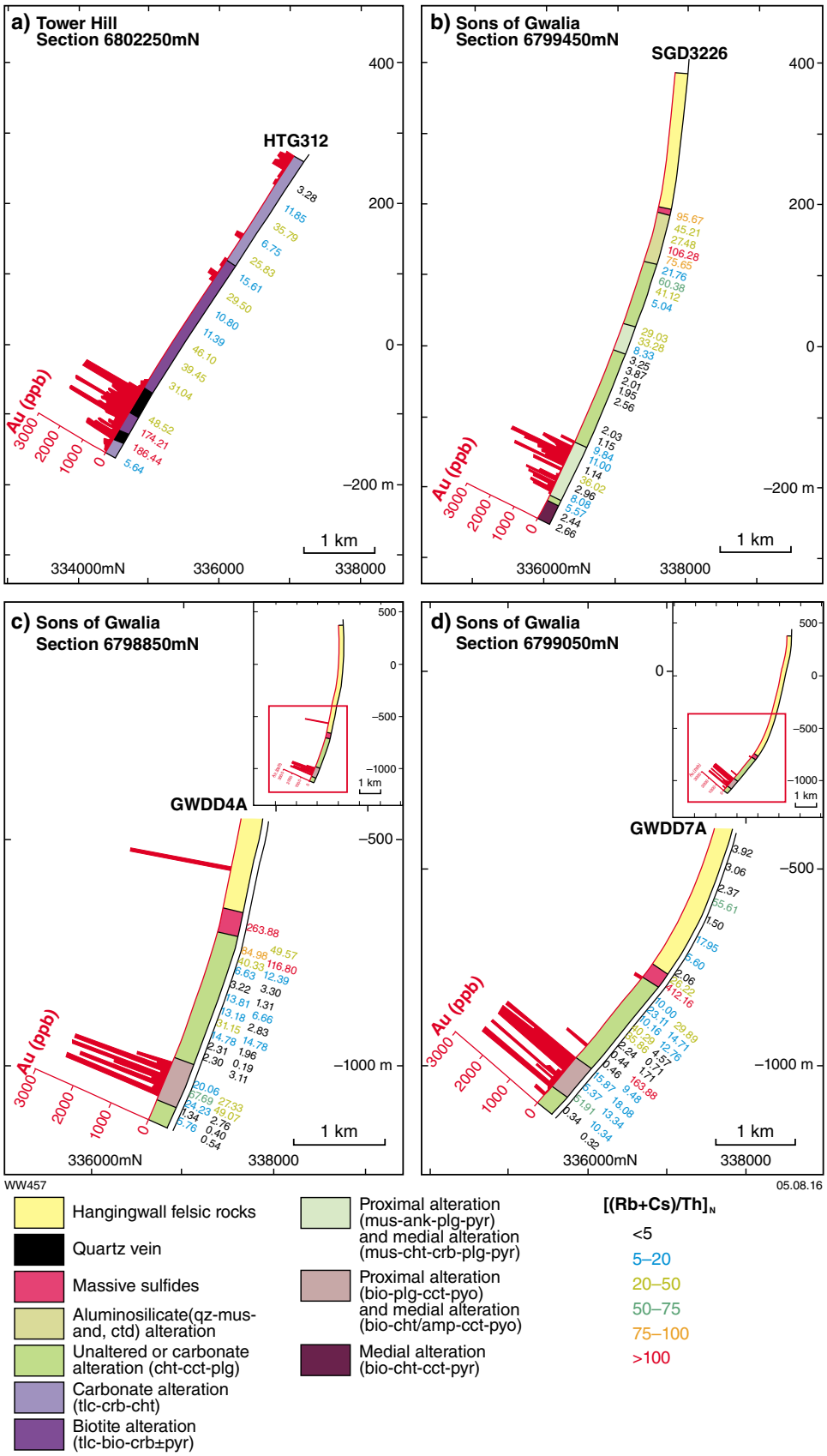

Figure 3.83. **Graphic drillhole logs from Tower Hill and Sons of Gwalia, Leonora district, Eastern Goldfields Superterrane, illustrating relations among hydrothermal alteration, gold content, and rare alkali index. a) RC hole HTG312, Tower Hill; b) diamond hole SGD3226, Sons of Gwalia; c) diamond hole GWDD4A, Gwalia Deeps; d) GWDD7A, Gwalia Deeps. Abbreviations: and (andalusite), ank (ankerite), bio (biotite), cct (calcite), cht (chlorite), crb (carbonate), ctd (chloritoid), mus (muscovite), plg (plagioclase), pyo (pyrrhotite), pyr (pyrite), tlc (talc).**

The $([Rb + Cs]/Th)_N$ rare alkali index is commonly anomalous over gold lodes and commonly extends for tens of metres beyond them. The anomaly invariably extends beyond the proximal alteration zone and, in some cases, beyond all visible gold-related alteration (e.g. Red October). In other cases (e.g. Tower Hill), where the gold lode is within a broad envelope of hydrothermal alteration, a gradient within the $([Rb + Cs]/Th)_N$ anomaly may provide a vector towards ore-grade mineralization (Fig. 3.83a). The rare alkali index is the most successful alteration index of those addressed here, though some cautionary comments are appropriate. Firstly, the examples used here are all hosted in mafic to ultramafic rocks in which the low background alkali content of the host rocks maximizes the effect of alkali metasomatism. Results from the granodiorite-hosted Pataz gold deposits in northern Peru suggest that the $([Rb + Cs]/Th)_N$ rare alkali index can be used in felsic rocks, but also suggest that both the magnitude and extent of the anomaly are much more restricted (Witt et al., 2014). Secondly, alkali metasomatism not related to gold mineralization (e.g. sea-floor alteration) can also produce a $([Rb + Cs]/Th)_N$ anomaly, which could act as a decoy for gold explorers (e.g. at Sons of Gwalia, Fig. 3.83b–d) unless the geochemical approach is applied within a well-understood geological context.

Targeting Criterion 3.11: Stable isotope dispersion

Stable isotopes of oxygen, carbon, and sulfur have been used to identify large-scale hydrothermal alteration cells in a number of settings, including syntectonic metamorphic-hydrothermal systems (Mount Isa), SEDEX deposits (McArthur River HYC), epithermal mineral districts (Drummond Basin), and Carlin-type deposits (Screamer) (Waring et al., 1998; Large et al., 2001; Barker et al., 2013). In most of these cases, whole-rock samples were analysed, although carbon and oxygen isotope analyses of carbonate mineral separates (e.g. dolomite from dolomitic shale at Mount Isa; Waring et al., 1998) and sulfur isotope analyses of groundwater (Andrew et al., 1994) have also proved useful. Generally, the hydrothermal signature is a depletion anomaly caused by the interaction of meteoric water with sedimentary host rocks. At Mount Isa, for example, a $\delta^{18}O$ anomaly (<16‰) extends over an area of 9 × 2 km around the copper orebody and is larger than any other geochemical expression of the hydrothermal system (Waring et al., 1998). At high fluid to rock ratios, extreme depletion of ^{18}O is accompanied by $\delta^{13}C$ depletion (<–5‰).

There have been several studies of stable isotope data related to orogenic gold deposits in general (Kerrich and Fryer, 1979; Jia et al., 2001) and to gold deposits of the Yilgarn Craton in particular (Golding and Wilson, 1983; Golding et al., 1990), but only limited application of stable isotope data in exploration for these types of deposits. The studies on Yilgarn gold deposits suggest that the large hydrothermal footprints described in the preceding paragraph are not present around lode gold deposits there. Nevertheless, only a limited amount of stable isotope data is available, partly because of reluctance within the exploration community to embrace the approach because

- stable isotope analyses are perceived as expensive
- timely reporting of results has been difficult to achieve
- access to specialist laboratories is needed.

This situation may change with the recent development of the off-axis integrated cavity output spectroscopy (OA-ICOS) analytical technique. This new method of analysis, which is becoming available through commercial laboratories, promises to provide rapid analysis of large numbers of samples, including the potential for analysis of samples in the field (Barker et al., 2013).

Whole-rock carbon and oxygen isotope studies of Yilgarn gold deposits

Most of the five deposits studied by Eilu and Mikucki (1996) presented evidence of a whole-rock $\delta^{13}C$ anomaly and some also demonstrated a whole-rock $\delta^{18}O$ anomaly, both of which were coincident with mineralization. The anomalies may be positive or negative, depending on the local background value. Eilu and Mikucki (1996) also observed that the anomalies are restricted in size (generally <20 m) and rarely, if ever, extend beyond the area of visibly altered rocks. They further observed that the largest $\delta^{18}O$ anomaly, at the Granny Deeps deposit (>1 Moz Au), extends at least 200 m into the metasedimentary hangingwall and suggested that the size of the $\delta^{18}O$ anomaly could be correlated with the size of the deposit. However, there is only a limited amount of data to support this contention. The results of the stable isotope dispersion studies of Eilu and Mikucki (1996) are described below and summarized in Table 3.21.

Bulletin deposit, Wiluna

At the Bulletin deposit, Wiluna district, Eastern Goldfields Superterrane, a negative $\delta^{13}C$ anomaly (<–4‰) is coincident with ore; it extends 15 to 30 m beyond ore, and 10 to 20 m beyond the Happy Jack shear zone (Fig. 3.84). Other intervals of proximal (sericite-bearing) alteration are similarly $\delta^{13}C$ depleted. Unaltered basalt and distal calcite-bearing alteration beyond the Happy Jack shear zone return $\delta^{13}C$ values of >–4‰.

Oxygen isotope data produced a depletion trend from values >10‰ 100 m from ore, decreasing to <9‰ over ore (Fig. 3.84). However, there are some reversals of the depletion trend within the 100 m interval and two samples within the ore zone have $\delta^{18}O$ of >10‰. A similar depletion halo was not found in a second drill section investigated at Bulletin by Eilu and Mikucki (1996). This inconsistency and the reversals in depletion trends shown in Fig 3.84 were attributed by Eilu and Mikucki (1996) to the size of the lode and variations in carbonate species (e.g. dolomite versus calcite).

Granny Smith, Laverton

At Granny Smith Deeps, Laverton district, Eastern Goldfields Superterrane, no $\delta^{13}C$ anomaly is recognized within the Granny Smith Granodiorite (Fig. 3.85). Eilu and Mikucki (1996) interpreted this observation to indicate that all the hydrothermal carbonate in the granodiorite, for a distance of 70 m from the gold lode, is related to the gold ore fluid. Although consistently lower than in the gold ore zone, $\delta^{13}C$ values within the metasedimentary unit are very erratic (Figs 3.85 and 3.86). Eilu and Mikucki (1996) attributed this irregular variation to inconsistent mixtures of carbonate derived from organic carbon (carbonate $\delta^{13}C$ = –46 to –15‰) and carbonate derived from sea-floor alteration (carbonate $\delta^{13}C$ close to –1‰).

The $\delta^{18}O$ depletion anomaly extends over 200 m or more in metasedimentary rock but produces no obvious anomaly or systematic gradient in granodiorite (Figs 3.85 and 3.86). In hole GSD241, the gradient within the sediment-hosted anomaly decreases towards the ore zone, from distal values of +14 to +17‰ to proximal values of +11‰ (Fig. 3.86). Eilu and Mikucki (1996) interpreted the $\delta^{18}O$ anomaly gradient to reflect progressive equilibration between metasedimentary rocks ($\delta^{18}O$ = +18 to +25‰) and a gold ore fluid with $\delta^{18}O$ of +11‰. This gradient is expressed over a very short distance in hole GSD282, however (Fig. 3.85).

Table 3.21. Summary of stable isotope dispersion data at selected Yilgarn gold deposits (Eilu and Mikucki, 1996)

Deposit	*Host rock*	*$\delta^{13}C$ (PDB)(‰)*		*$\delta^{18}O$ (SMOW)(‰)*		*Maximum extent of anomaly from ore (m)*	
		Background	*Ore*	*Background*	*Ore*	*$\delta^{13}C$*	*$\delta^{18}O$*
Bulletin, Wiluna	Basalt	-1 to -4	-5	+10 to +12l	+8.5 to +11	15 to 30	10 to 100
Granny Smith Deeps, Laverton	Granodiorite	-5 to -4	-4	+9 to +11	+11	>70[a]	No clear anomaly[a]
	Metasedimentary rock	-16 to -6	-4	>+14	+11	<5 to 10	>200
Kings Cross, Coolgardie	Basalt	-3 to -5	-7 to -6.5	+9 to +11	+9 to +11	5 to 20	0
Moyagee, Murchison	Ultramafic	-4 to -2[b]	-5 to -4	≤+9[b]	+11	20 to 50?	20 to 50?
Twin Peaks, Carosue Dam[c]	Metasedimentary rock	-8 to -7	-7.5	+11 to +14	≥+12.5	0?	0?

NOTES: (a) Area studied in the granodiorite (>70 m from ore) possibly did not extend beyond the area affected by gold-related hydrothermal carbonation. (b) At Moyagee, only one sample of unweathered unaltered rock with enough carbonate for reliable isotope analysis was identified, and the background ranges are partially based on trends within the shear zone (i.e. they do not represent unaltered rock). (c) At Twin Peaks, sample data are compromised by weathering. PDB, Pee Dee Belemnite standard; SMOW, Vienna Standard Mean Ocean Water

Kings Cross, Coolgardie

At Kings Cross, Eilu and Mikucki (1996) detected a subtle $\delta^{13}C$ depletion anomaly over the ore and extending into unaltered wallrock. This depletion with respect to distal (background) values was repeated in some small shears subparallel to the Kings Cross Fault and, in some cases, the depletion in subparallel shears was greater than that in the mineralized fault (Figs 3.87 and 3.88). A corresponding negative anomaly in the $\delta^{18}O$ data is evident over the mineralized shear zone in hole KXD187 (Fig. 3.88) but is subtle or non-existent in hole KXD177 (Fig. 3.87). In hole KXD177, the $\delta^{13}C$ depletion anomalies in subparallel shear zones are coincident with positive $\delta^{18}O$ anomalies, though this is less consistent in hole KXD187.

Moyagee, Murchison Terrane

Depletion of $\delta^{13}C$ and enrichment of $\delta^{18}O$ at Moyagee, Murchison Domain, is very subtle and cannot be regarded as an anomaly in the sense used for other deposits studied by Eilu and Mikucki (1996) because all samples are from within the mineralized shear zone (100 to 150 m wide).

Twin Peaks, Kurnalpi Terrane

Eilu and Mikucki (1996) reported that no $\delta^{13}C$ or $\delta^{18}O$ anomaly could be detected in a cross section through holes JDRC048 and JDRC120 at Twin Peaks. Data from another section, through holes JDRC018 and JDRC043, are considered to be affected by weathering and are therefore discounted.

Summary

There have been few studies investigating the presence, or extent, of stable isotope anomalies over and around gold deposits of the Yilgarn Craton. Results of the studies that have been carried out, using carbon and oxygen isotope data (Eilu and Mikucki, 1996), have yielded inconsistent results (Table 3.21). Based on the limited amount of available data, $\delta^{13}C$ more consistently produces an anomaly around the ore zone, but of very limited extent (generally <50 m), whereas $\delta^{18}O$ anomalies are less consistent, but more extensive in some cases.

The greatest potential for the use of stable isotopes as targeting tools for gold exploration appears to be the application of $\delta^{18}O$ to sediment-hosted deposits (e.g. Granny Smith Deeps). This potential arises from the relatively high $\delta^{18}O$ of unaltered siliciclastic sedimentary rocks (+10 to +22‰) relative to volcanic rocks, and the consequent contrast between background and hydrothermal alteration related to gold ore fluid (+9 to +12‰). However, more examples of oxygen isotope analyses in gold-related hydrothermal systems in metasedimentary rocks are required before the application of this approach to exploration can be established. As well as defining anomalies with respect to background values, $\delta^{18}O$ values describe a gradient that is a potential vector towards ore in some deposits (e.g. Bulletin, Granny Smith Deeps). The data from Twin Peaks emphasize the critical need for samples selected for stable isotope analysis to be fresh; even slight weathering can change the carbon and oxygen isotope values.

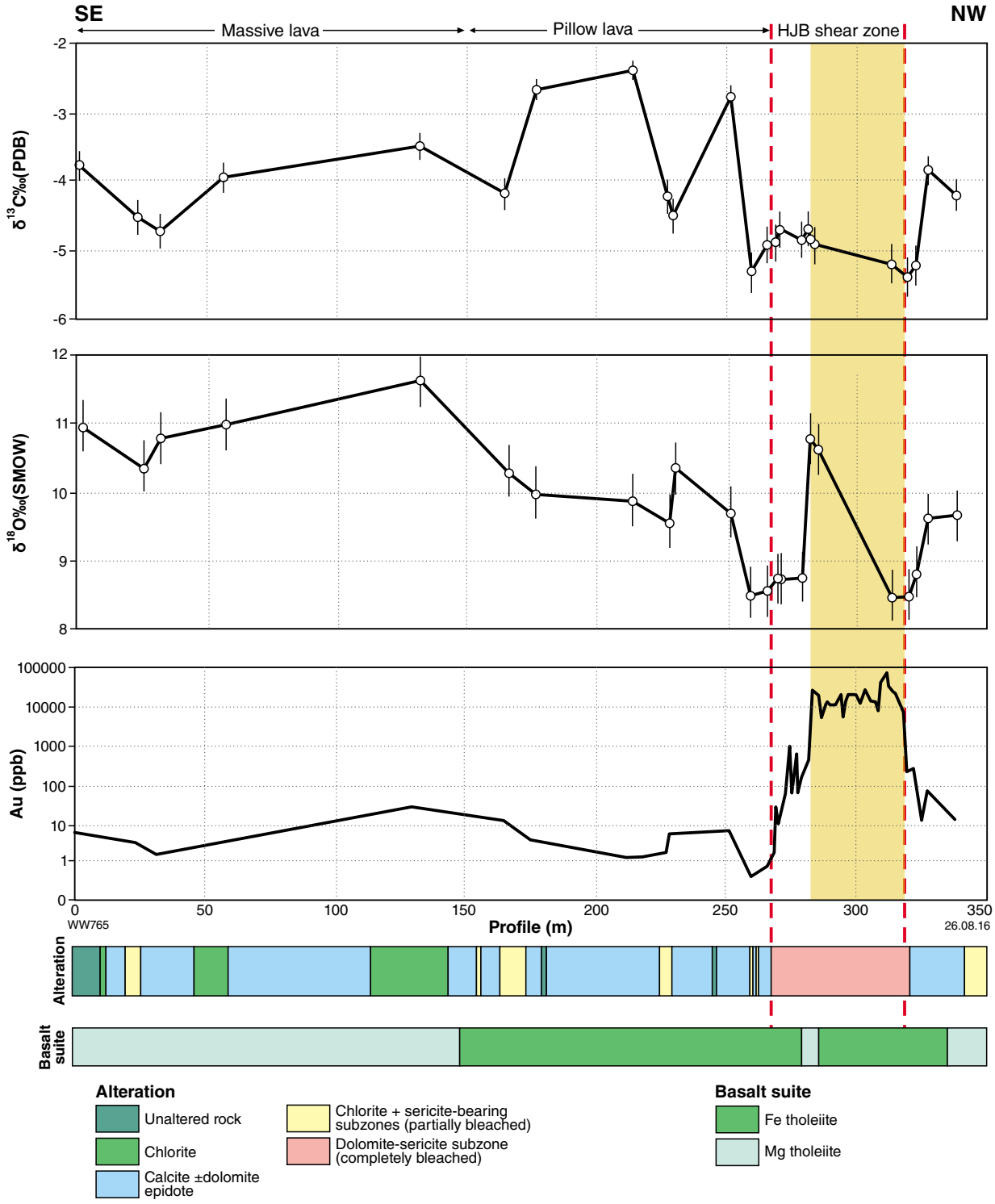

Figure 3.84. Stable isotope variations, Bulletin gold deposit, Wiluna district, Eastern Goldfields Superterrane (from Eilu and Mikucki, 1996). HJB (Happy Jack – Bulletin)

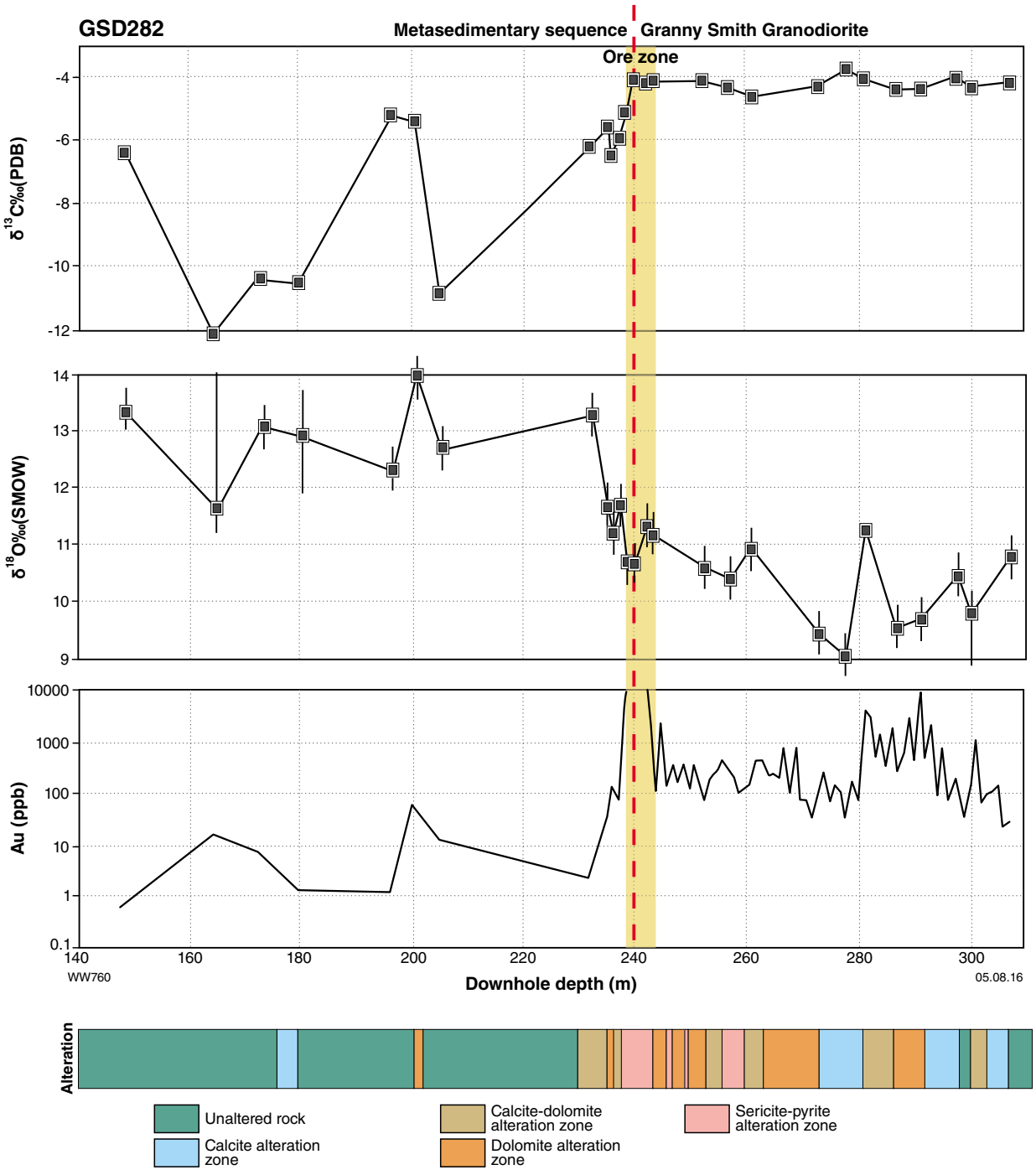

Figure 3.85. Stable isotope variations relative to hydrothermal alteration and gold, hole GSD282, Granny Smith gold deposit, Laverton district, Eastern Goldfields Superterrane (from Eilu and Mikucki, 1996)

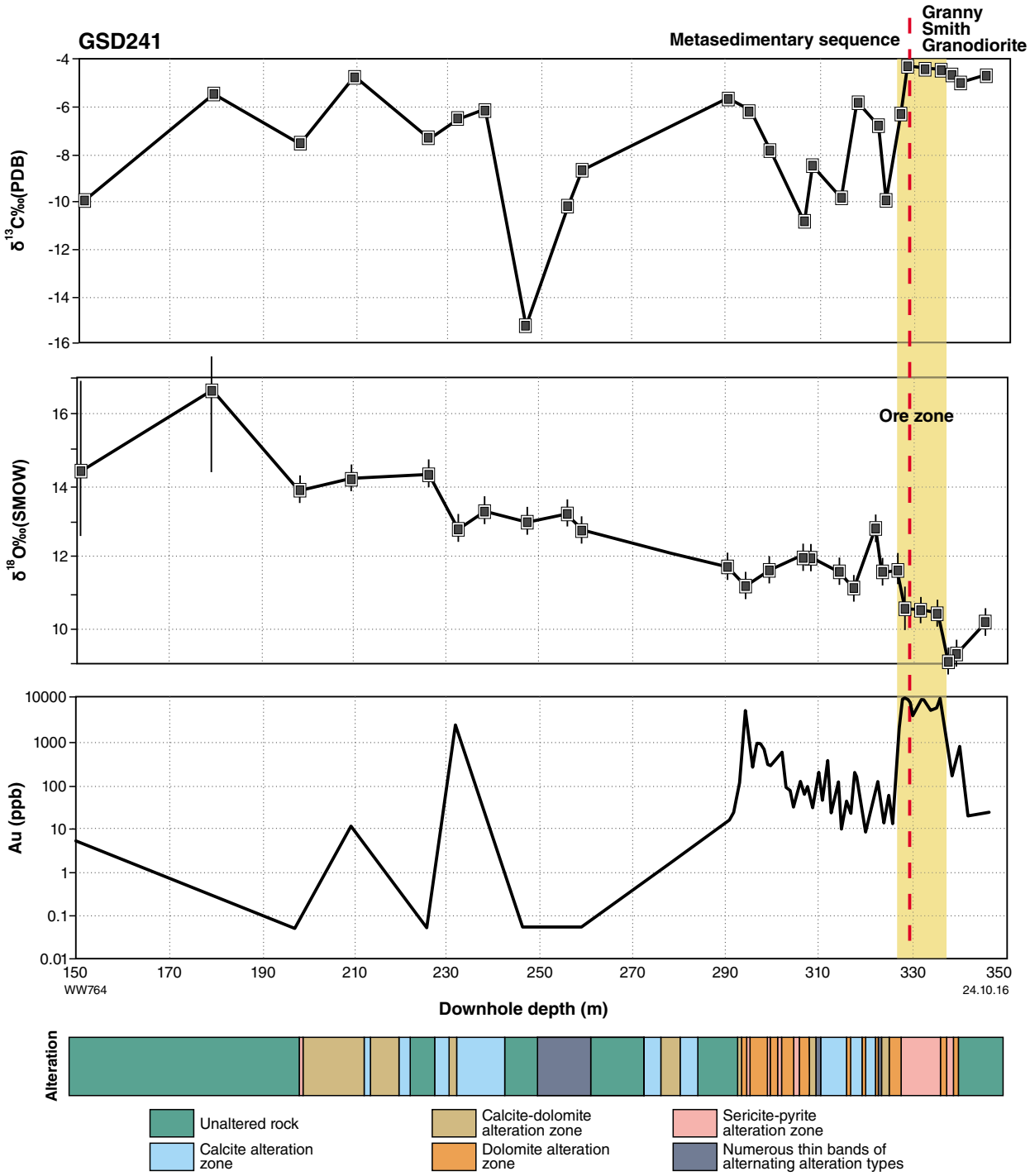

Figure 3.86. Stable isotope variations relative to hydrothermal alteration and gold, hole GSD241, Granny Smith gold deposit, Laverton district, Eastern Goldfields Superterrane (from Eilu and Mikucki, 1996)

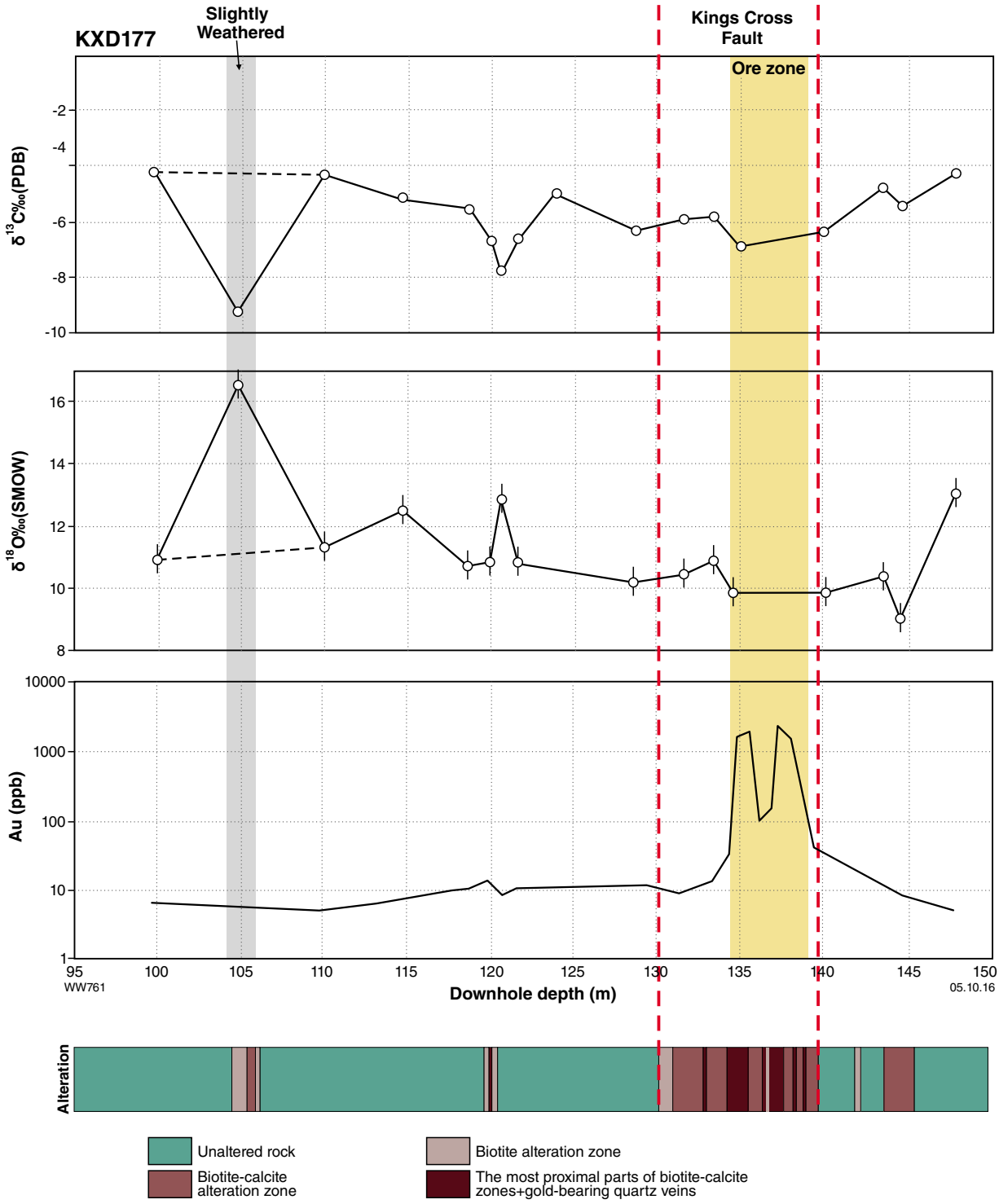

Figure 3.87. **Stable isotope variations relative to hydrothermal alteration and gold, hole KXD177, Kings Cross gold deposit, Coolgardie district, Eastern Goldfields Superterrane (from Eilu and Mikucki, 1996)**

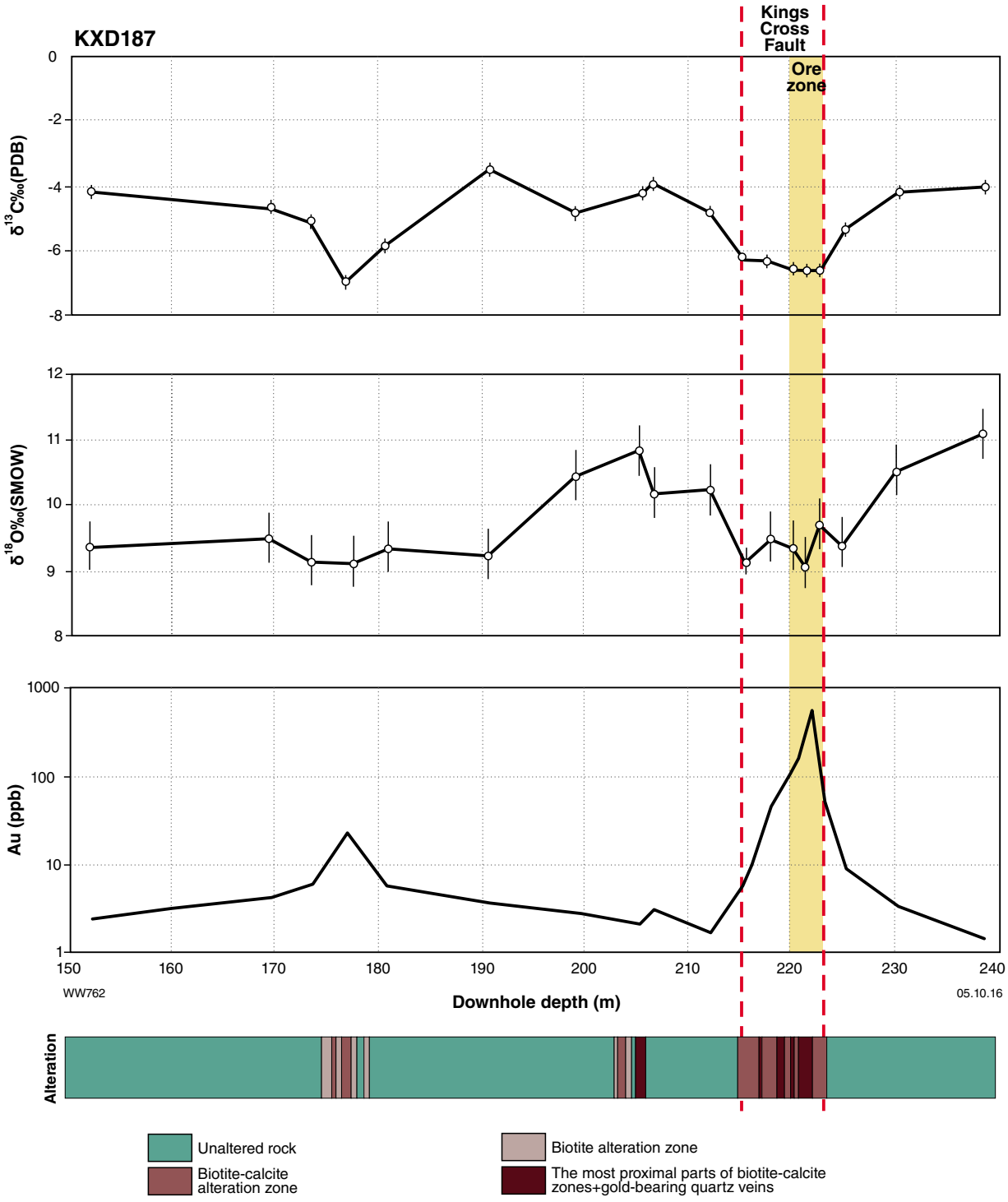

Figure 3.88. Stable isotope variations relative to hydrothermal alteration and gold, hole KXD187, Kings Cross gold deposit, Coolgardie district, Eastern Goldfields Superterrane (from Eilu and Mikucki, 1996)

Targeting Criterion 3.12: Spectral geology

with contributions from Tom Cudahy*, Carsten Laukamp*, and Lena Hancock

Spectral mapping in the SWIR and VNIR wavelength ranges

Airborne hyperspectral remote-sensing data in the short wavelength infrared (SWIR) and visible to near-infrared (VNIR) bands have been used to detect changes in the composition of white micas in alteration envelopes around some Fe-oxide copper–gold and volcanogenic massive sulfide deposits (Laukamp et al., 2011; van Ruitenbeek et al., 2012). Ground-based hyperspectral sensing data have been used to separate phengitic from muscovitic micas in hydrothermal alteration related to massive sulfides (Yang et al., 2011) and low-sulfidation epithermal gold deposits (Sonntag et al., 2012). In the Eastern Goldfields Superterrane, a number of studies have shown that white mica compositions also vary in alteration envelopes associated with Archaean gold deposits (Cudahy, 1997; Laukamp et al., 2010; Neumayr et al., 2007). In all of these deposit types, phengitic white micas are developed proximal to the mineralization. Recent models have attributed variations in white mica compositions to fluid redox properties (e.g. Walshe et al., 2006).

At deposit scale (Cudahy, 1997), and at district scale (Targeting Criterion 2.16, Part 2 of this Atlas), chlorite also shows compositional changes characterized by higher Fe or Mg contents in hydrothermal alteration cells spatially associated with Archean gold deposits. However, at deposit scale, chlorite composition may be influenced by the bulk composition of the host rock (e.g. mafic versus felsic) and may reflect partitioning of Fe between silicate minerals (e.g. chlorite) and co-existing sulfide minerals (e.g. Phillips and Groves, 1984). Other mineralogical parameters with potential application to gold exploration, such as amphibole and epidote abundance and composition, can also be derived from SWIR reflectance data (e.g. Roache et al., 2011; Laukamp et al., 2012), but these are less well established approaches and are not discussed in this section of the Atlas.

In this section, deposit-scale variations in spectral mineralogy, mainly concerning white mica abundance and composition, are described in two examples from the Eastern Goldfields Superterrane: the Golden Mile and Kanowna Belle deposits. The Golden Mile (67.3 Moz), at Kalgoorlie, is the largest gold deposit in the Yilgarn Craton and one of the largest orogenic gold deposits in the world (Goldfarb et al., 2005). This deposit was mapped using Advanced Spaceborne Thermal Emission and Reflection Radiometer (ASTER) satellite data in 1999 and using airborne hyperspectral survey (Hymapper) data in 1999 and 2004. Cudahy (1997) described the results of a lode-scale study at the Golden Mile using spectral data acquired with a hand-held instrument (PIMA, Spectral International Inc.). The Kanowna Belle deposit is another world-class gold orebody (5.8 Moz; Northern Star Resources website, August 2014) about 20 km northeast of the Golden Mile. This deposit was also covered by the 1999 ASTER and 2004 Hymapper surveys, and has also been studied in some detail using an automated Hylogger instrument (Quigley, 2005).

The Golden Mile

Gold mineralization in the Fimiston Superpit (the Golden Mile) is hosted by the Paringa Basalt and Fe-rich zones 8 and 7 of the Golden Mile Dolerite, a tholeiitic sill of ultramafic to intermediate composition that was intruded near the contact of the Paringa Basalt with the overlying metasedimentary Black Flag Group (Phillips, 1986; Bateman and Hagemann, 2004; Evans et al., 2006; Fig. 3.89). Two principal networks of mineralized faults, referred to as the Eastern Lode System and the Western Lode System, are separated by the north-northwesterly striking Golden Mile Fault. The age of the Golden Mile Dolerite is 2680 ± 9 Ma (SHRIMP U–Pb dating of zirconolite; Rasmussen et al., 2009). There is some disagreement about the age of the gold mineralization (Bateman and Hagemann, 2004; Rasmussen et al., 2009; Vielreicher et al., 2010; Bateman and Jones, 2015; Vielreicher et al., 2015), though this does not affect the spectral signature of the orebody that is the focus of this section.

Hydrothermal alteration is characterized by a 'regional' (kilometre scale), weakly carbonate-altered chlorite (chlorite–calcite) zone and a more local (100 m scale), intensely altered carbonate zone around auriferous pyritic zones that are 1 to 2 m thick (Phillips, 1986; Gauthier et al., 2007). The auriferous pyritic zones are characterized by intense white-mica alteration along narrow brittle to brittle–ductile faults and associated breccias and vein networks (Bateman and Hagemann, 2004). These mineralized structures have traditionally been subdivided into the main, caunter, cross, and easterly lode sets (Phillips, 1986; Boulter et al., 1987; Fig. 3.90). Phillips (1986) reported compositional variations of white mica in the pyritic alteration zone, ranging from muscovite to paragonite. No unambiguous correlation between wavelength position of the ~2200 nm absorption feature and Na/K ratio in white micas has yet been demonstrated, so variations of the Na/K ratio cannot be detected using spectral analysis.

1999 ASTER false-colour image

The 1999 ASTER false-colour image (Fig. 3.91a) shows the Kalgoorlie Superpit, the related mining facilities to the east and north of it, and the bordering settlements of the town of Kalgoorlie to the west. The AlOH abundance map derived from the same ASTER survey (Fig. 3.91b) shows that the relative abundance of white mica is distinctively enhanced along a north-northwest trend (outlined in red, Fig. 3.91a) that coincides with extensive

* CSIRO Centre for 3D Mineral Mapping, Western Australian Centre of Excellence, Australian Resources Research Centre, Kensington, WA 6151

white mica in the pyritic alteration zone of Main Lode in the Eastern Lode System (Fig. 3.90). Slightly lower levels of AlOH abundance in the southwestern part of the Superpit are interpreted to delineate pyritic alteration zones in the Western Lode System. The weak AlOH abundance anomalies to the north and east of Main Lode are attributed to contamination from ore transported from the Superpit to the ore treatment facilities.

The ASTER FeOH abundance map (Fig. 3.91c, and outlined in green on Fig. 3.91a) shows higher values in north-northwesterly trending zones to the east and west of the AlOH anomaly, effectively enveloping Main Lode. These ASTER FeOH anomalies are interpreted to represent the distal chlorite–calcite alteration zones of Phillips (1986). Distal chlorite alteration around the Western Lode System probably also contributed to the FeOH anomalies west of the Golden Mile Fault (Fig. 3.91a), but there is no anomaly west of the Western Lode System, possibly because chlorite has been destroyed or modified by weathering in the relatively shallow walls of the Superpit. Similarly, the full (kilometre scale) extent of the chlorite–calcite alteration zone is not evident in the ASTER data because basement exposures beyond the limits of the Superpit are few and strongly weathered.

The MgOH abundance map, (Fig. 3.91d) highlights the distribution of Mg-bearing silicates and Mg-bearing carbonates (e.g. dolomite, magnesian ankerite) and overlaps to a large extent with the distribution of chlorite indicated by elevated FeOH abundance (e.g. the northwest-trending zone east of Main Lode; Fig. 3.91c), as chlorite is one of the Mg-bearing silicates delineated by MgOH abundance. The extents of MgOH abundance anomalies that do not overlap FeOH abundance anomalies (outlined in yellow, Fig. 3.91a) are interpreted to indicate carbonate dominated alteration (the carbonate alteration zone of Phillips, 1986). The MgOH abundance probably indicates the presence of magnesian ankerite and magnesian siderite in the carbonate alteration zone; dolomite and magnesite are not present in the carbonate alteration zone of the Golden Mile (Phillips, 1986).

Figure 3.91a provides an overview of the dominant SWIR-active alteration phases in the Golden Mile. It indicates intensive white-mica alteration along the Main Lode and in the Western Lode System, partly overlapping with carbonate alteration and surrounded by chlorite alteration. This arrangement is consistent with the detailed alteration zoning around the Golden Mile lodes described by Phillips (1986) and demonstrates the type of SWIR signature that might be sought in district-scale ASTER data covering areas of good exposure. It also shows the potential for spectral data acquired with a hand-held instrument to be used to define deposit-scale vectors towards high-grade ore within large systems of hydrothermal alteration.

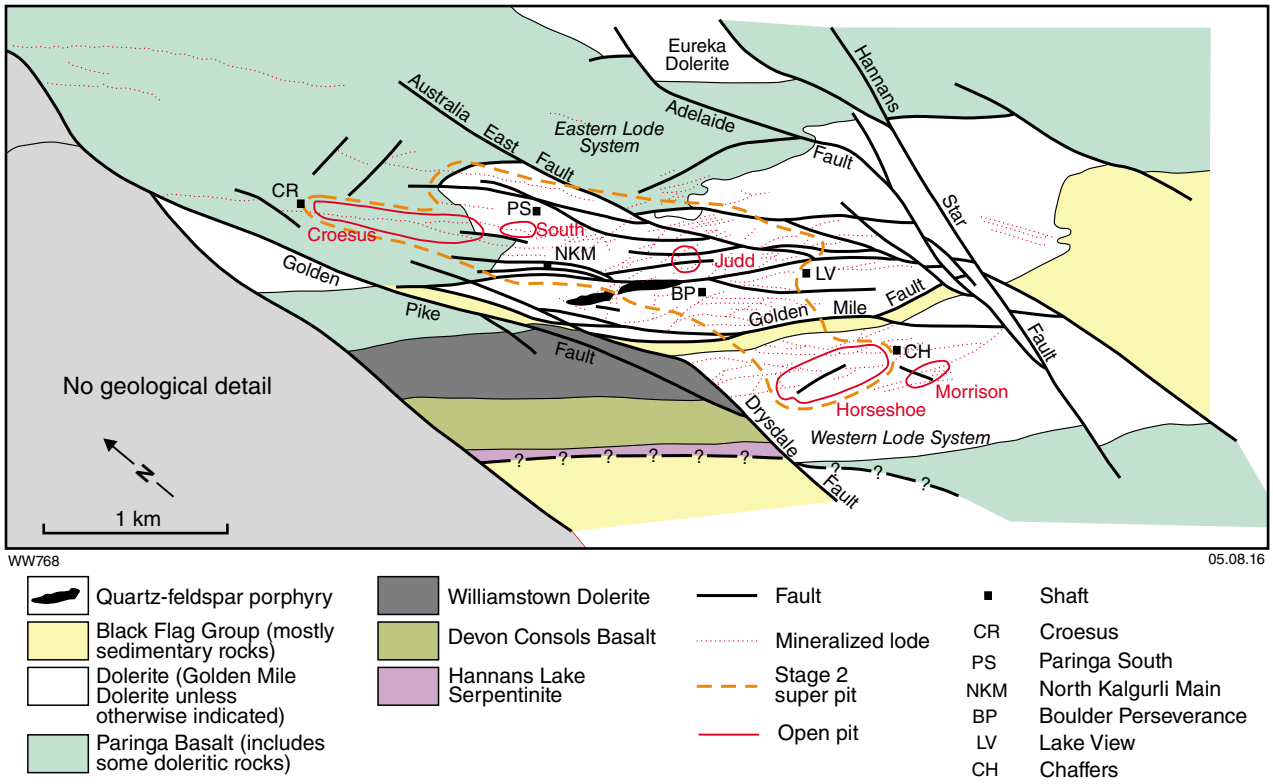

Figure 3.89. Geology of the Golden Mile, Kalgoorlie, Eastern Goldfields Superterrane (from Witt, 1992c). Note that the openpits shown have since been merged into the Golden Mile Superpit.

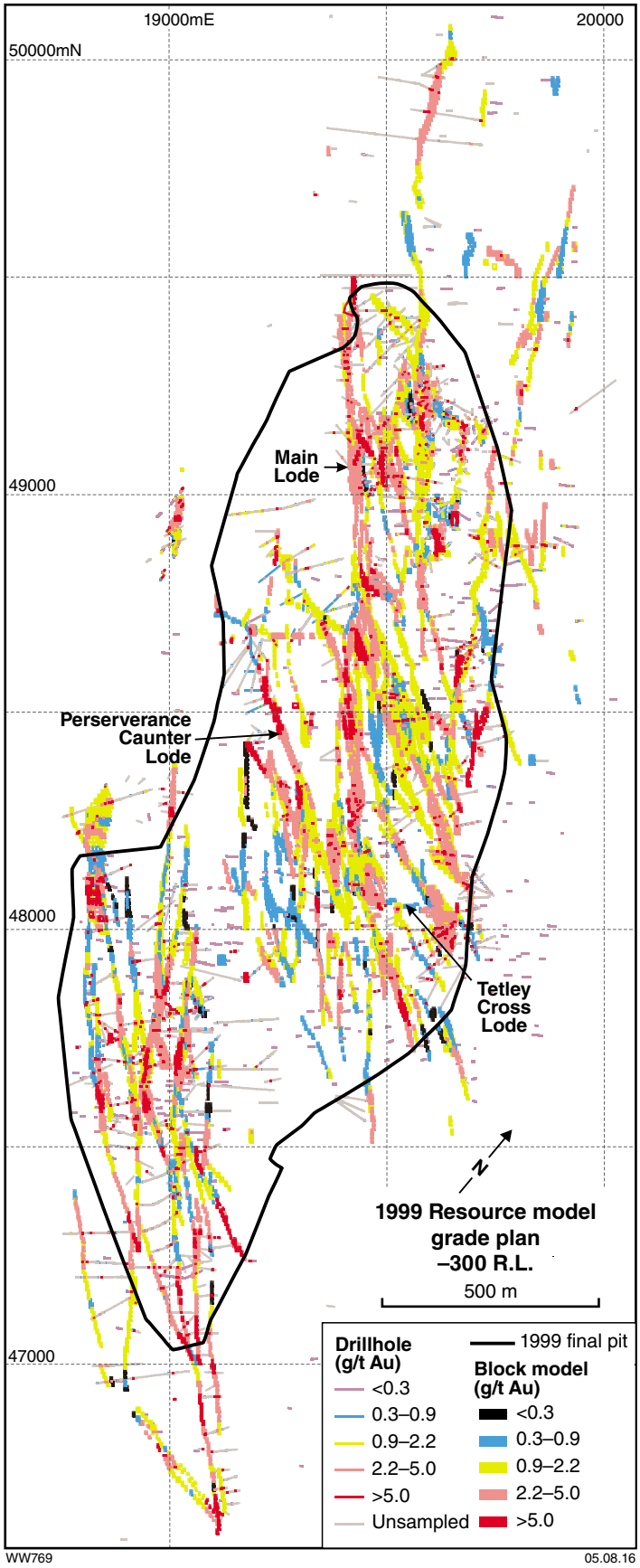

Figure 3.90. **Drillhole traces coloured by gold grade, Golden Mile Superpit, illustrating orientation of lodes (from Bateman and Hagemann, 2004). Coordinates refer to local mine grid.**

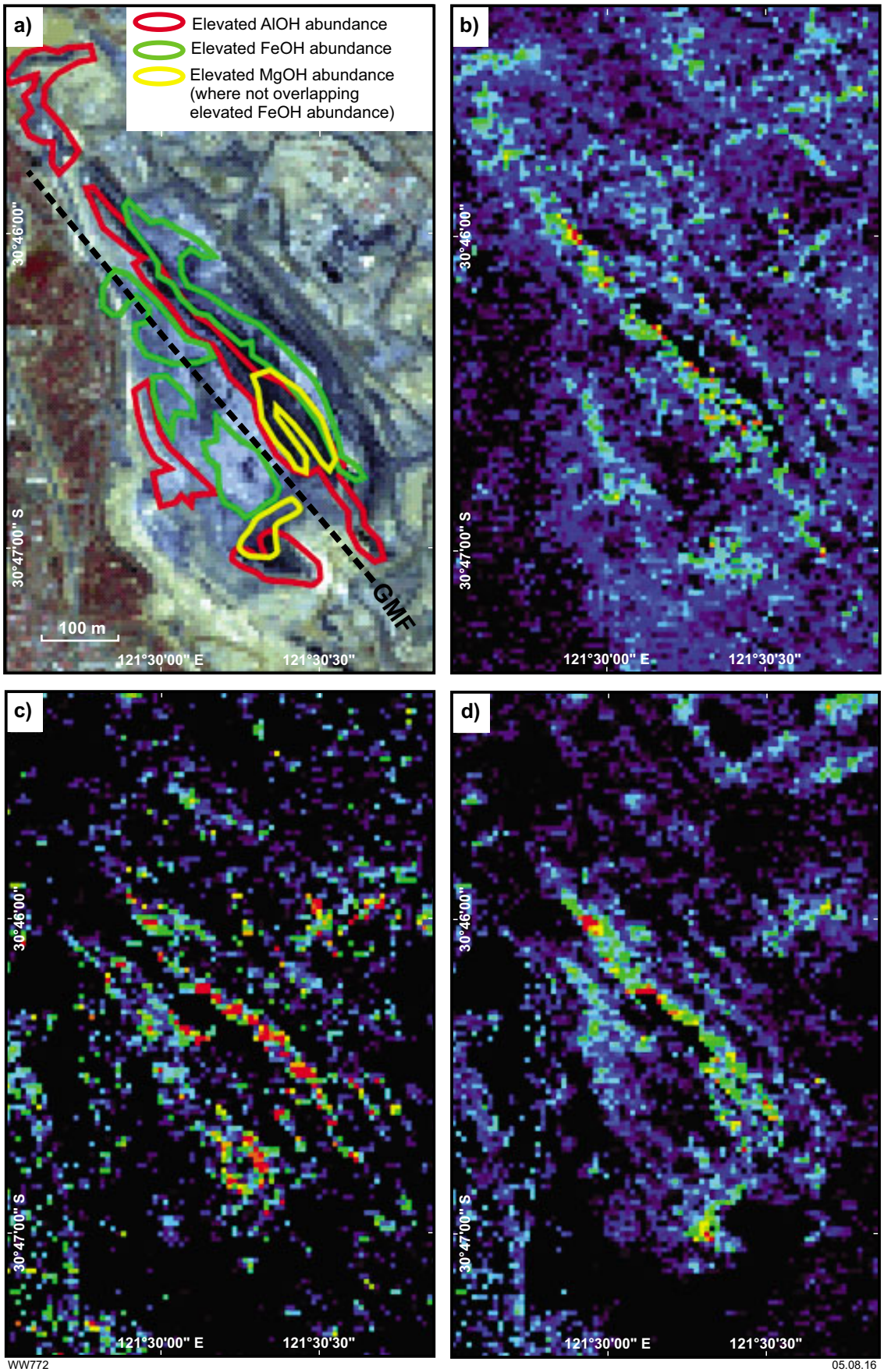

Figure 3.91. **ASTER images over the Golden Mile Superpit, Kalgoorlie. a) False colour with areas of elevated AlOH, FeOH, and MgOH abundances outlined; b) AlOH abundance; c) FeOH abundance; d) MgOH abundance. Warm colours indicate greater abundance than cool colours. GMF, Golden Mile Fault.**

Airborne hyperspectral data

Airborne hyperspectral (Hymapper) data were collected over areas that covered the Fimiston Superpit as it was in 1999 and 2004. Results from the 2004 survey were published by Cudahy et al. (2005). Figure 3.92 shows the different extents of the Golden Mile Superpit in 1999 and 2004. The resource model grade plan (Figs 3.90 and 3.92d) dates from 1999 and is derived from drillcore data.

The hyperspectral data shown in Figure 3.92 can be compared with results of a field study by Cudahy (1997), in which spectral data were collected from diamond core and blast hole pulps from the Birthday South orebody within the Eastern Lode System (Fig. 3.92d) by using a PIMA hand-held instrument. Cudahy (1997) found that distal chlorite, medial carbonate, and proximal pyritic alteration zones around the Birthday South caunter lode could be distinguished by using spectra that identified chlorite, white mica, and pyrite, respectively (Fig. 3.93). Cudahy (1997) also found that the Fe content of chlorite (measured using the wavelength of the 2250 nm absorption feature) increased, and the Al content of white mica (measured using the wavelength of the 2200 nm absorption feature) decreased, towards proximal alteration and high-grade gold ore, thus providing vectors to mineralization (Fig. 3.94). The white-mica vector extends over a distance of 30 to 150 m. Cudahy (1997) noted that the depth of the ~2200 nm absorption feature was not an effective gauge of white-mica abundance in proximal alteration zones, where abundant opaque minerals (mainly pyrite) obscured the white-mica response (Fig. 3.94g).

The abundance of AlOH-bearing phyllosilicate minerals (potentially including white mica and kaolin group minerals) derived from the 2004 airborne survey (Fig. 3.92b) only weakly identifies gold lodes. This may be because the white-mica response has been obscured by high modal pyrite, or the modal white mica content is low (3 to 8%, Cudahy, 1997), or the geology of the pit floor has become temporarily obscured by transported material (e.g. wind-blown sand or mud accumulated during rain). A strong response from benches to the east of the orebody (Fig. 3.92b) perhaps reflects a higher white-mica abundance in the carbonate alteration zones, though this has not been confirmed.

The white-mica composition map based on 2004 Hymapper data (Fig. 3.92c) shows longer wavelength positions of the 2200 nm feature (i.e. phengite) in the centre of the openpit, coincident with the network of Main Lode and caunter lodes (cf. Fig. 3.92d, which includes Birthday South). Long-wavelength white micas identified from airborne hyperspectral data acquired in 1999 (Fig. 3.92f) correlate well with the resource model grade plan (Fig. 3.92d); they successfully trace the Main Lode and a prominent caunter lode that intersects Main Lode from the southeast, and also identify the Western Lode System. Bateman and Hagemann (2004) postulated that the main ore shoots are typically at the intersections of lodes; the 1999 survey suggests that these intersections are associated with the longest wavelength (most phengitic) white mica.

Summary

The Golden Mile example shows the potential for airborne hyperspectral survey data to be used to identify phengite-rich areas that might represent proximal alteration around gold mineralization in areas where fresh or weathered basement rocks are exposed. However, as shown under Criterion 2.16 (Part 2 of this Atlas), phengitic white mica is also found in proximity to most felsic intrusions, including some that are not mineralized. Therefore, white-mica abundance and the associated ~2200 nm absorption wavelength should be used in combination with chlorite abundance and composition maps (and other tools such as pathfinder geochemistry and alteration indices) so that distal and proximal alteration zones can be identified.

ASTER data can also be used for this purpose, although the resolution of ASTER data is clearly inferior to that of hyperspectral data, and white mica and chlorite compositions cannot be extracted from ASTER spectra. Once the distal and proximal alteration zones have been distinguished, chlorite composition and white-mica composition can be used, sequentially or in tandem, to provide a vector towards high-grade ore if HyMapper data are available. If the resolution of available airborne spectral data is insufficient to achieve this end, or if drilling samples provide the only access to hydrothermally altered rocks, a hand-held PIMA instrument could be used to provide a vector towards ore within the hydrothermal alteration system.

Kanowna Belle

Gold mineralization at Kanowna Belle is hosted by metamorphosed intrusions and volcanosedimentary rocks on both sides of the steeply south-southeasterly dipping Fitzroy Fault (Fig. 3.2). The Fitzroy Structural Zone preserves a long history of deformation, beginning with ductile deformation and mylonitization after 2656 ± 10 Ma (Davis et al., 2010). The Kanowna Belle porphyry, which hosts about 70% of the mineralization at Kanowna Belle, was intruded into the Fitzroy Mylonite at 2655 ± 6 Ma (Ross et al., 2004), during this early ductile deformation event. Subsequent sinistral movement on the Fitzroy Fault caused brittle–ductile failure of the Kanowna Belle porphyry and the consequent formation of carbonate breccias and vein stockworks, siliceous breccias, quartz–carbonate–pyrite–sericite veinlets, and sheeted vein arrays, all of which contain gold (Davis et al., 2010).

During MERIWA study P373, an automated HyLogger instrument was used to collect hyperspectral reflectance data in the VNIR–SWIR range from 16 drillcores at the Kanowna Belle gold deposit (Fig. 3.95; Quigley, 2005). The most relevant data resulting from this study, from a gold exploration perspective, are the compositional variations in metasomatic and metamorphic white mica. Figures 3.96 and 3.97 provide a comparison of the wavelength of the white-mica ~2200 nm AlOH absorption feature and the white-mica species interpreted by The Spectral Assistant (TSA)* with various geological

* Automated spectral recognition software developed by the Commonwealth Scientific and Industrial Research Organisation (CSIRO Australia)

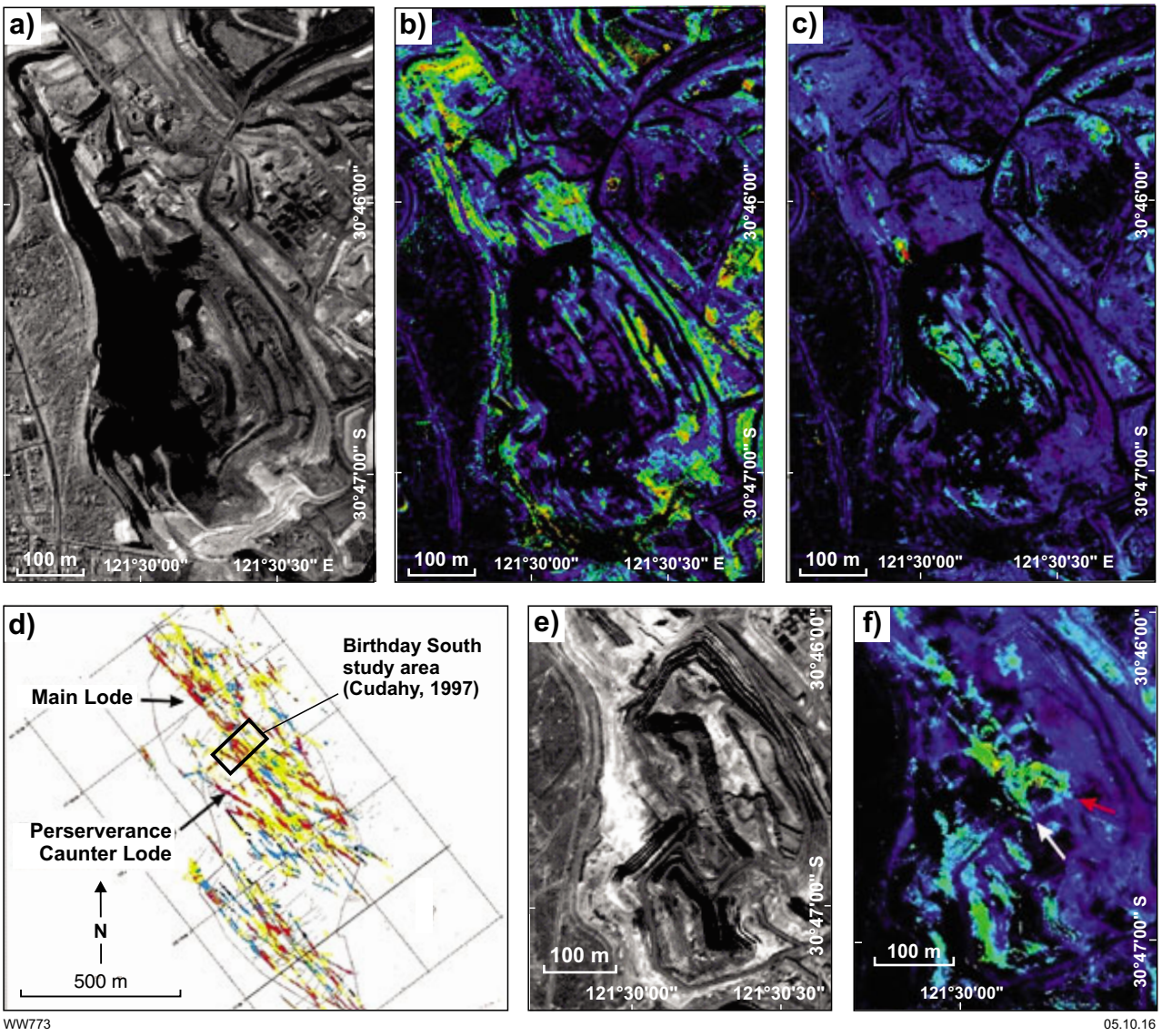

Figure 3.92. **Hyperspectral (Hymapper) data acquired over Golden Mile Superpit in 2004 (a, b, and c) and in 1999 (e and f). a) Albedo grey-scale image; b) AlOH abundance; c) white-mica composition based on wavelength of ~2200 nm AlOH absorption feature; d) drillhole traces coloured by gold grade (see Fig. 3.90 for more detail); e) Albedo grey-scale; f) white-mica composition derived as in c). In b, c, and f, warmer colours indicate higher white-mica abundance or more phengitic white mica. In f, white arrow indicates orientation of Main Lode and red arrow indicates orientation of Caunter Lodes.**

attributes (intrusions, hydrothermal alteration, nature and intensity of strain) logged conventionally by company geologists. To improve readability, the geological attributes in Figures 3.96 and 3.97 are shown in horizontal bar charts above each composite drillhole log. The main gold lodes are highlighted for each hole, excluding GVD095, which is 1 km north of Kanowna Belle.

The proximal alteration assemblage at Kanowna Belle has been described as an albite–sericite–carbonate–chlorite–hematite assemblage (Davis et al., 2010), or an albite–silica–pyrite assemblage (Quigley, 2005). This style of alteration is shown as albite–silica–sulfide alteration in strip logs in Figures 3.96 and 3.97. Proximal albite–silica–sulfide alteration is aspectral, but can generally be recognized by low white-mica absorption intensity in combination with reduced Fe^{2+} values for the whole-rock sample (Quigley, 2005). Abundant fluid inclusions in these alteration zones are associated with increased depth of the 1940 nm water absorption feature and reduced crystallinity of any white mica present (not shown in Figs 3.96 and 3.97; see Quigley (2005) for details).

The MERIWA study (Quigley, 2005) reported a change in white-mica composition ranging from distal paragonite (Al-rich, Fe/Mg poor) through muscovite to proximal phengite (Al-poor, Fe/Mg rich), based on the location of the diagnostic ~2200 nm AlOH absorption feature, and also reported that this compositional variation could be used as a vector to high-grade ore in many of the holes

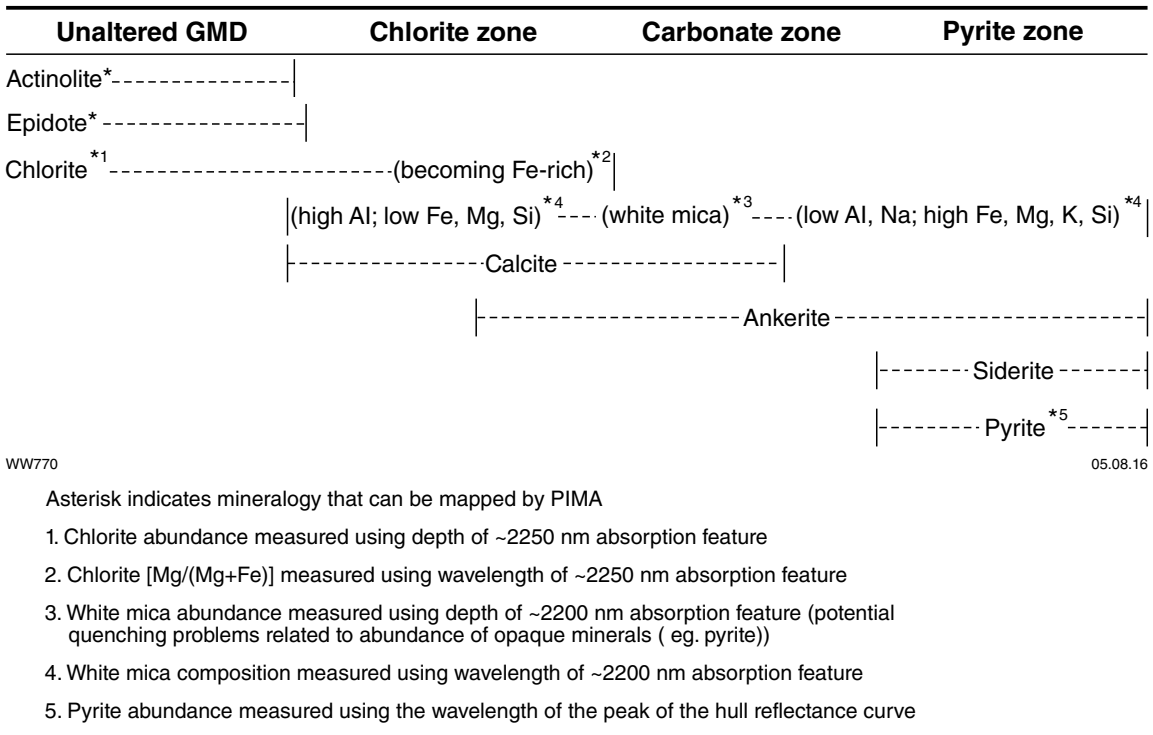

Figure 3.93. Summary of results of PIMA spectral study of the Birthday South lode, Golden Mile, relating spectral characteristics to hydrothermal alteration (Cudahy, 1997). GMD (Golden Mile Dolerite).

examined. Note, however, that the ability of the ~2200 nm AlOH absorption feature to identify paragonite has been questioned (see Targeting Criterion 2.16, Part 2 of this Atlas) and the vector should more correctly be described as a progressive increase in the location of the ~2200 nm AlOH absorption feature with proximity to ore.

Quigley (2005) found that gold mineralization in individual drillholes is commonly in zones of white-mica alteration with mixed phengite–muscovite characteristics, or on gradients between predominantly phengite and predominantly muscovite spectral signatures. Quigley (2005) also contended that the distribution of muscovite and phengite is not controlled by host rock lithology, and concluded that the association of mineralization with mixed phengite–muscovite spectral characteristics, or with gradients between phengite and muscovite, could be ascribed to mixing of oxidized (phengite-stable) and reduced (muscovite-stable) fluids. However, Quigley (2005) also noted that some gold mineralization was in phengite-only white-mica alteration zones.

Close examination of Figures 3.96 and 3.97 confirms that phengitic white mica is not restricted to felsic intrusions, but extends up to 80 m into the volcanosedimentary country rock, beyond porphyry (intrusive) contacts (e.g. holes GDD358 and KDU316). However, in most of the holes studied there is a fairly consistent spatial association of phengitic white mica with feldspar(–biotite) porphyries and, to less extent, with undivided felsic rocks. This association is stronger when comparing the distribution of porphyry intrusions with the wavelength of the ~2200 nm AlOH absorption feature rather than the white mica species assigned by TSA. The presence of phengitic white mica with a relatively long wavelength (>2210 nm) may extend for several tens of metres beyond the porphyry intersection, but the phengitic white mica intersection is consistently centred on one or other of these intrusions.

Not all porphyries contain predominantly phengitic white mica, but porphyry intersections that contain muscovite as the dominant white mica are generally coincident with zones of high strain, recorded variously as brittle–ductile fault, foliation, shearing, or mylonitization (Figs 3.96 and 3.97). Other muscovite-dominant intervals are adjacent to porphyry contacts where the competency contrast between the intrusion and metasedimentary country rock promotes the accumulation of strain. These observations suggest that phengitic mica is spatially associated with porphyry intrusions and that muscovitic mica is associated with faults and shear zones that are typically on the contacts of the porphyries or, less commonly, cut the relatively thin porphyry units within the high-strain Fitzroy Fault. This conclusion is consistent with those derived from district-scale spectral (PIMA) data (Targeting Criterion 2.16, Part 2 of this Atlas), where long-wavelength white mica is associated with felsic intrusions and short-wavelength white mica is distal from felsic intrusions and commonly associated with faults and shear zones.

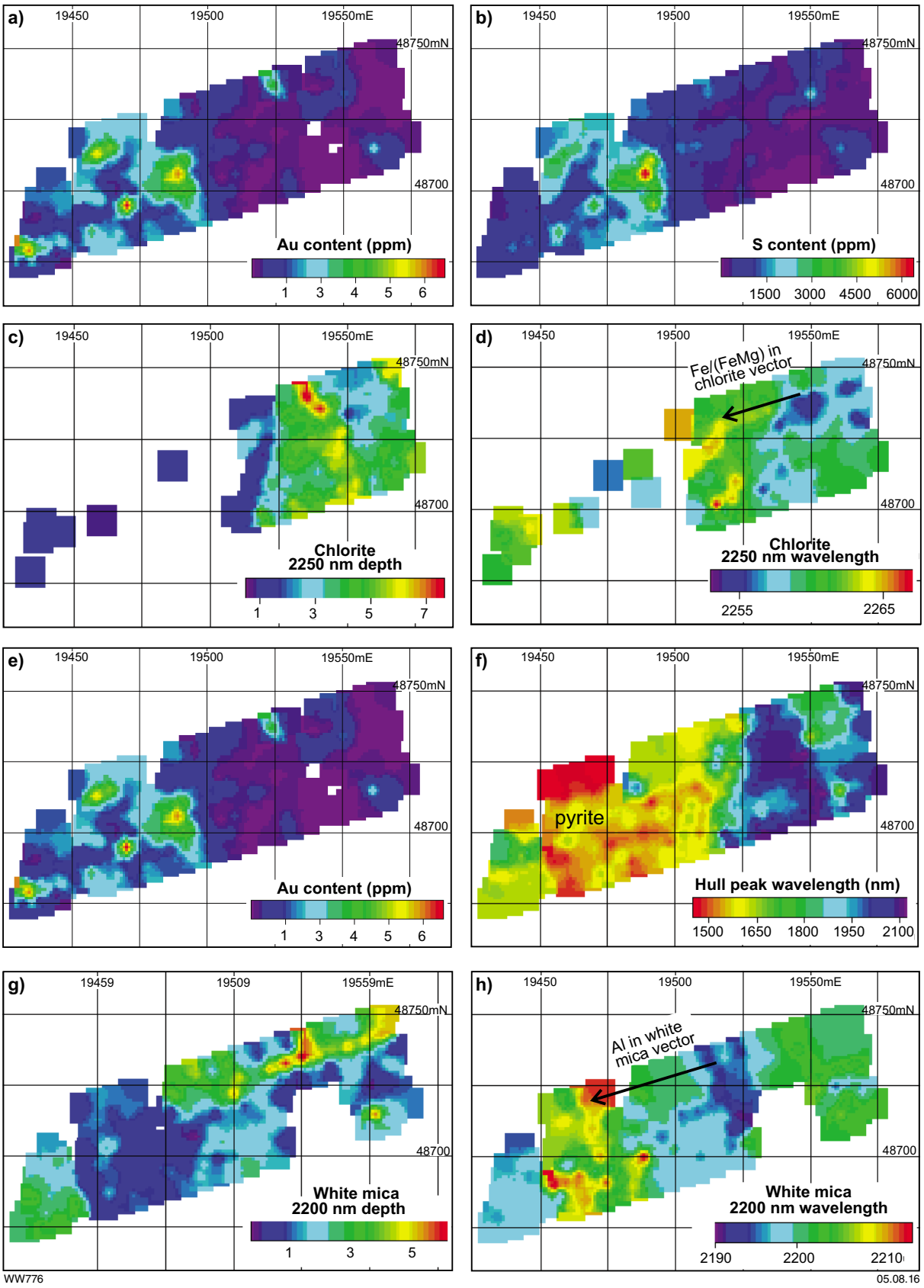

Figure 3.94. **Maps showing results of PIMA spectral study of the Birthday South lode, Golden Mile (Cudahy, 1997). a) Gold, b) sulfur, and c) chlorite abundances measured by depth of ~2250 nm absorption feature. d) Chlorite composition measured by wavelength of ~2250 nm absorption feature (longer wavelengths are relatively Fe-rich). e) Gold and f) pyrite abundances measured using the hull peak wavelength (Cudahy, 1997). g) White-mica abundance measured by the depth of ~2200 nm absorption feature. h) White-mica composition measured by wavelength of ~2200 nm absorption feature (longer wavelengths are relatively Al-poor and phengitic).**

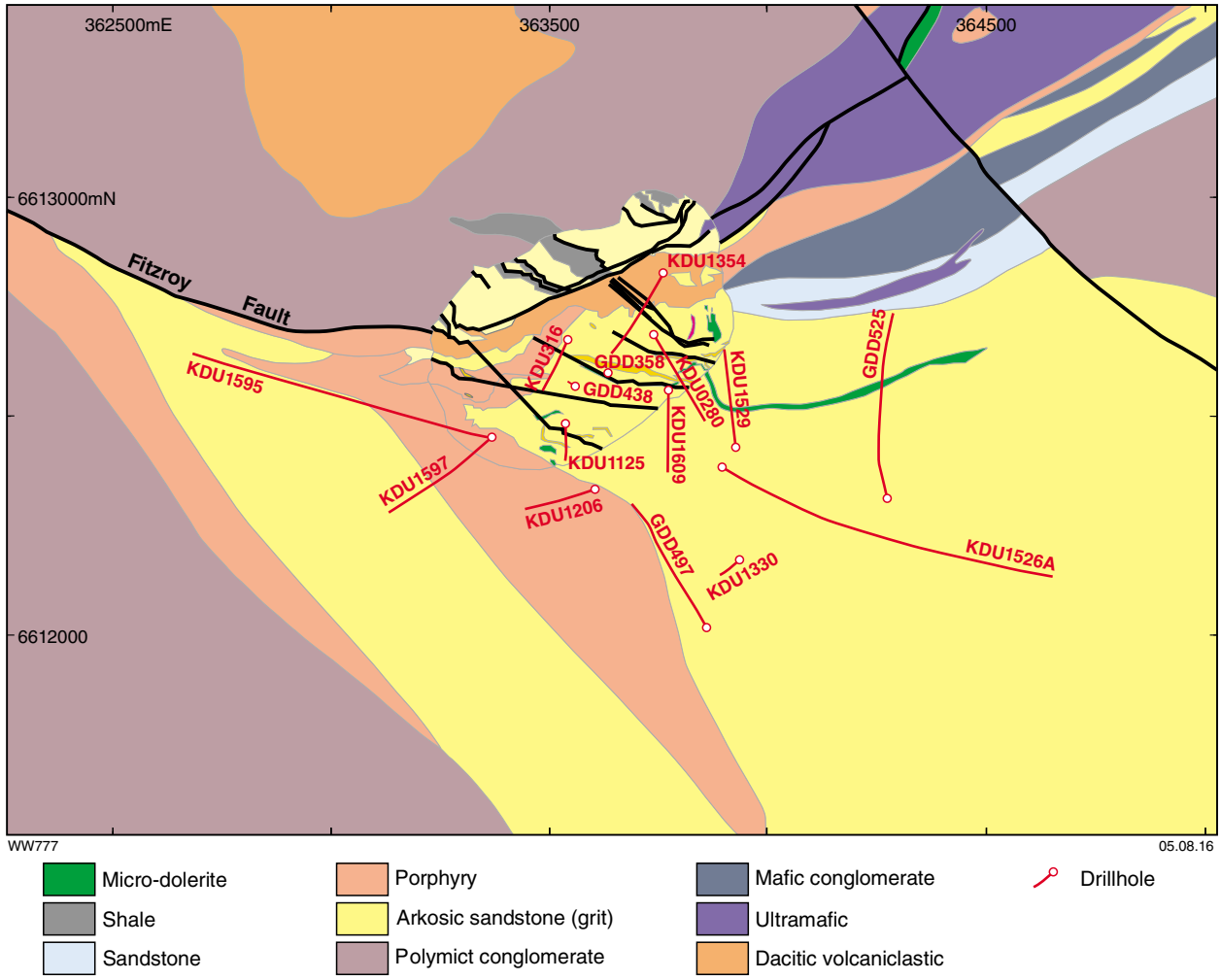

Figure 3.95. Geological setting of the Kanowna Belle gold deposit, Kanowna gold camp, Eastern Goldfields Superterrane, showing traces of diamond drillholes studied by Quigley (2005)

Other observations from Kanowna Belle are that dominant phengitic mica appears to be most common in sericite–carbonate alteration and albite–silica–sulfide alteration, whereas muscovite appears to be associated with chloritic alteration types (chlorite, chlorite–carbonate, and carbonate alteration, consistent with the results of the Cudahy (1997) study of the Birthday South lode at the Golden Mile), or in intervals logged as lacking alteration. Muscovitic white mica, therefore, is commonly dominant in intervals where white mica is less abundant, including intervals of deuteric alteration or metamorphic intervals that are not normally logged as hydrothermally altered, as well as in distal chloritic alteration zones associated with gold mineralization. This leads to the conclusion that phengitic white mica was initially developed in and around the Kanowna Belle porphyry, and muscovite replaced phengite in areas where the porphyry was subsequently overprinted by high-strain deformation. Muscovitic white mica is also dominant in the metasedimentary country rock, even where strain and/or alteration (chloritic or deuteric) is relatively weak.

Summary

Although high-grade gold intersections at Kanowna Belle are commonly in zones of white mica alteration with mixed phengite–muscovite characteristics, or on gradients between phengite and muscovite, some are well within phengitic alteration zones (e.g. hole GDD358), whereas others are within muscovite dominant zones (e.g. holes GDD438 and KDU1597). As discussed under Targeting Criterion 2.16 (Part 2 of this Atlas), the association of some gold with mixed phengite–muscovite intervals or transitional zones does not necessarily imply mixing of oxidized and reduced fluids as suggested by Quigley (2005). An alternative interpretation, consistent with district-scale observations, would attribute phengitic white mica to hydrothermal fluid derived from, or equilibrated with, felsic porphyry intrusions, and would attribute muscovite-rich intervals to unaltered metasedimentary rocks and hydrothermal activity related to overprinting high-strain zones.

The association of gold with mixed and transitional zones is entirely consistent with the conventional view that a gold ore fluid from a deep source was locally focused into zones of high strain on contacts between rheologically strong (porphyry intrusion) and rheologically weak (metasedimentary) geological units (e.g. Ojala et al., 1993; Ridley, 1993). Irrespective of debate concerning the origin of variations in the distribution of spectrally defined white-mica species, the key outcome of the study by Quigley (2005) is that these variations in white-mica composition, like those from the Golden Mile, can be used at deposit scale as a vector towards high-grade ore.

MERIWA study P373 Phase 3 (Quigley, 2006) was a follow-up study of the drillcore from Kanowna Belle that employed the TIR-Logger, an apparatus that automates the collection of hyperspectral reflectance measurements across most of the thermal infrared range (6000 to 14 000 nm) and therefore allows rapid and continuous collection of spectra that can be used to identify anhydrous minerals. This study focused on application of the TIR-Logger to identify variations in the abundance of quartz, albite, and carbonate minerals at Kanowna Belle. Although the results did not add significantly to the vectoring capacity demonstrated by the HyLogger (VNR–SWIR) study at Kanowna Belle discussed above, it showed that the TIR-Logger could be applied to analysis of hydrothermal alteration in amphibolite facies settings such as in the Southern Cross district. In these settings, the dominant minerals associated with gold mineralization are (in addition to biotite and amphibole) anhydrous minerals (feldspar, clinopyroxene, garnet) that are not detected by instruments that are limited to the VNIR–SWIR range.

Spectral mapping in the SWIR and TIR wavelength ranges

Southern Cross – Marvel Loch

Two styles of gold mineralization are recognized in the Southern Cross greenstone belt: shear-hosted Model 1 deposits in which mineralized veins are deformed (folded, boudinaged) within the ductile fabric of the shear zone, and relatively brittle Model 2 deposits comprising auriferous veins hosted by banded iron-formation (see Targeting Criterion 2.13, Part 2 of this Atlas, and Doublier, 2014).

In this section, new spectral data from representative diamond cores of both of these styles of mineralization are presented and compared with geological logs prepared by visual examination of the cores by WK Witt. The six cores of this study (Table 3.22) were analysed with the GSWA HyLogger-3, using SWIR and TIR spectrometers, at the GSWA Core Library in Perth in August 2012 (Hancock et al., 2013). Although no petrographic studies of thin sections have been carried out to cross-check the mineral phases identified by Hylogger-3, the geological logs presented here reflect the experience gained by WK Witt during field work and petrographic studies conducted in the Southern Cross district between 1997 and 2004.

The results of XRD analyses from hole GPD1464 at Golden Pig (provided by Dr Alison Dugdale of Curtin University) allow some assessment of the accuracy of the HyLogger data. Table 3.23 compares the modal mineralogy of ultramafic and mafic rocks in hole GPD1464, determined by TIR-Logger, with the results of XRD analyses provided by Dr Dugdale. Agreement between the two methods is generally good, although the TIR hyperspectral results cannot match the lower and more-precise levels of abundance reported by XRD analyses. There are also problems related to false identifications of cordierite by TSA (see below).

Model 1 deposits

Frasers

The Frasers mine, one of the oldest gold mines in the Southern Cross district, has exploited a Model 1 deposit at the northern end of the mega-boudin described under Targeting Criterion 2.13 (Part 2 of this Atlas). Total production from the mine to 1994 was a little over 3 Mt of ore at an average grade of 5.5 g/t Au, producing 16.5 t Au (N Taylor, in Witt et al., 1994). Since then, additional production has come from underground mining, though this has now ceased.

The mineralized shear zone at Frasers comprises mainly amphibolite-grade mafic to ultramafic metamorphic rocks and minor amounts of banded iron-formation (Dale and Thomas, 1990). The three main ore shoots (Sholls, Frasers, Greenstone) are within a shear zone of 30 to 80 m width. Metasomatic biotite, and calc-silicate veins, are widespread in the sheared mafic rocks. Most of the biotite is associated with cordierite and was probably formed during pre-metamorphic sea-floor (KMg) alteration (Witt and Hagemann, 2012). Metasomatic biotite, without cordierite, is also associated with the gold lodes, but this alteration can be difficult to distinguish visually from pre-metamorphic KMg alteration. Similarly, the auriferous quartz–carbonate–diopside–pyrrhotite veins are easily confused with pre-mineralization calc-silicate veins that were formed by metamorphism of quartz–carbonate veins, possibly related to sea-floor alteration.

Diamond core FMM397 intersected more than 100 m of variably sheared and hydrothermally altered mafic and ultramafic rocks (Fig. 3.99). The ultramafic rocks are weakly to moderately foliated, fine- to medium-grained tremolite–chlorite assemblages (Fig 3.100a), locally containing olivine porphyroblasts. The spectral log identifies Ca-amphibole and chlorite as dominant components in most ultramafic units, although the response to these minerals in the deeper ultramafic units is weaker than in associated mafic rocks. There is no feldspar response, which is part of the diagnostic set of spectral features for the ultramafic units. The TIR data identify olivine as the main component of the ultramafic unit between 66 and 71 m, suggesting this is a relatively magnesian unit, although metamorphic olivine was not identified visually.

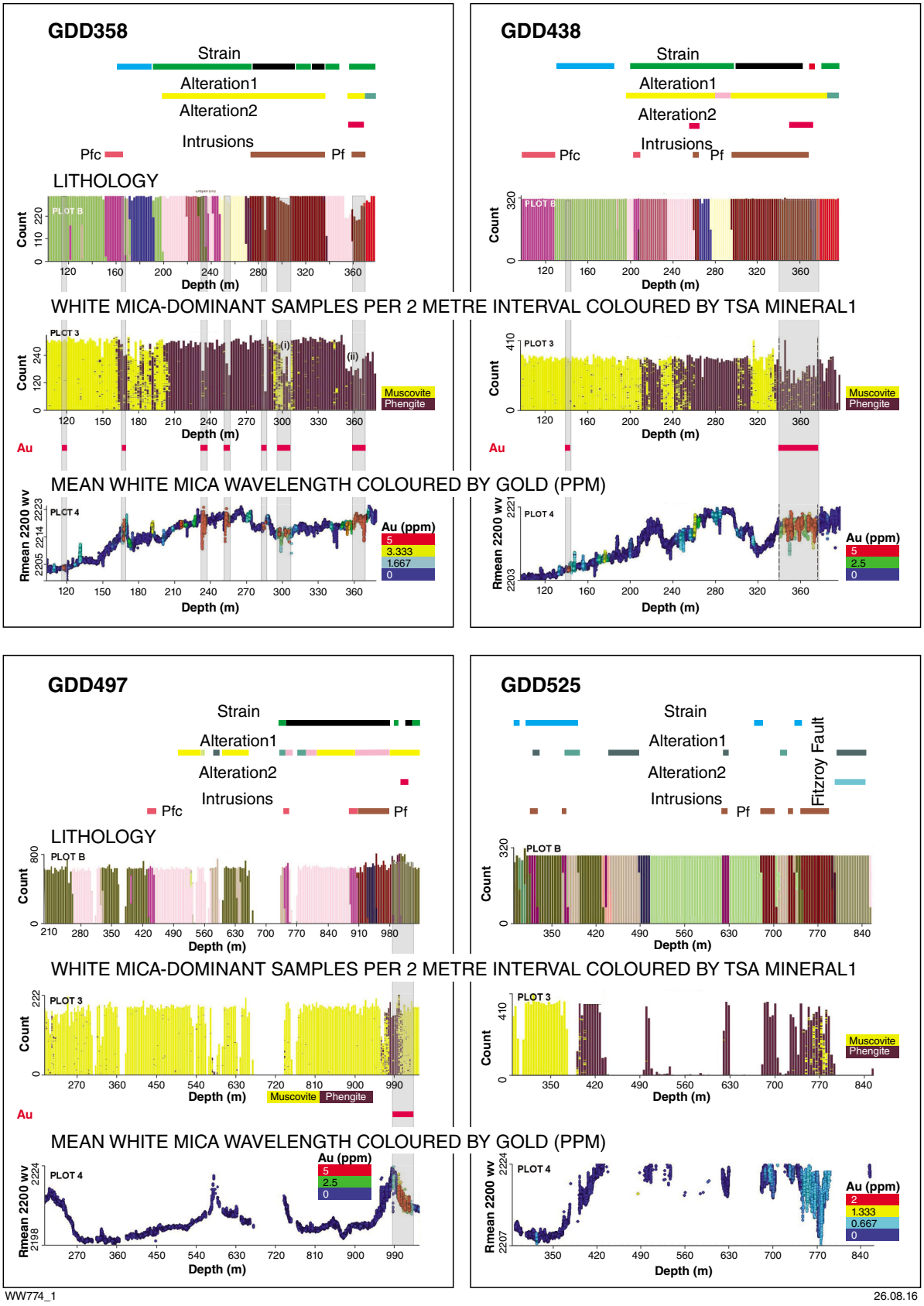

Figure 3.96. **Composite downhole logs, Kanowna Belle, relating spectrally determined white-mica composition to gold abundance and various geological features. Holes GDD358, 438, 497, 525; KDU280, 316, 1125, 1206. See Figure 3.98 for legend.**

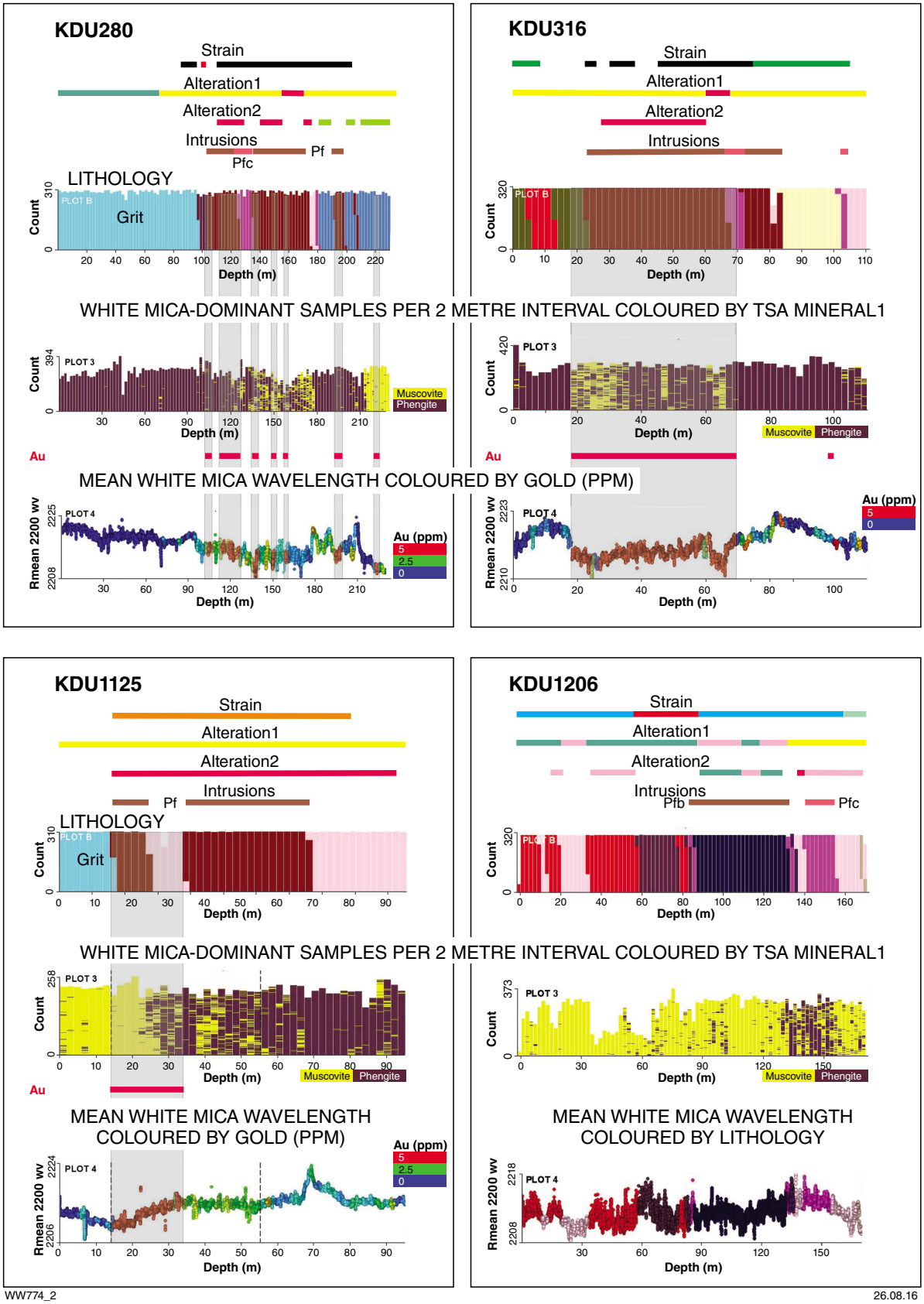

Figure 3.96. continued

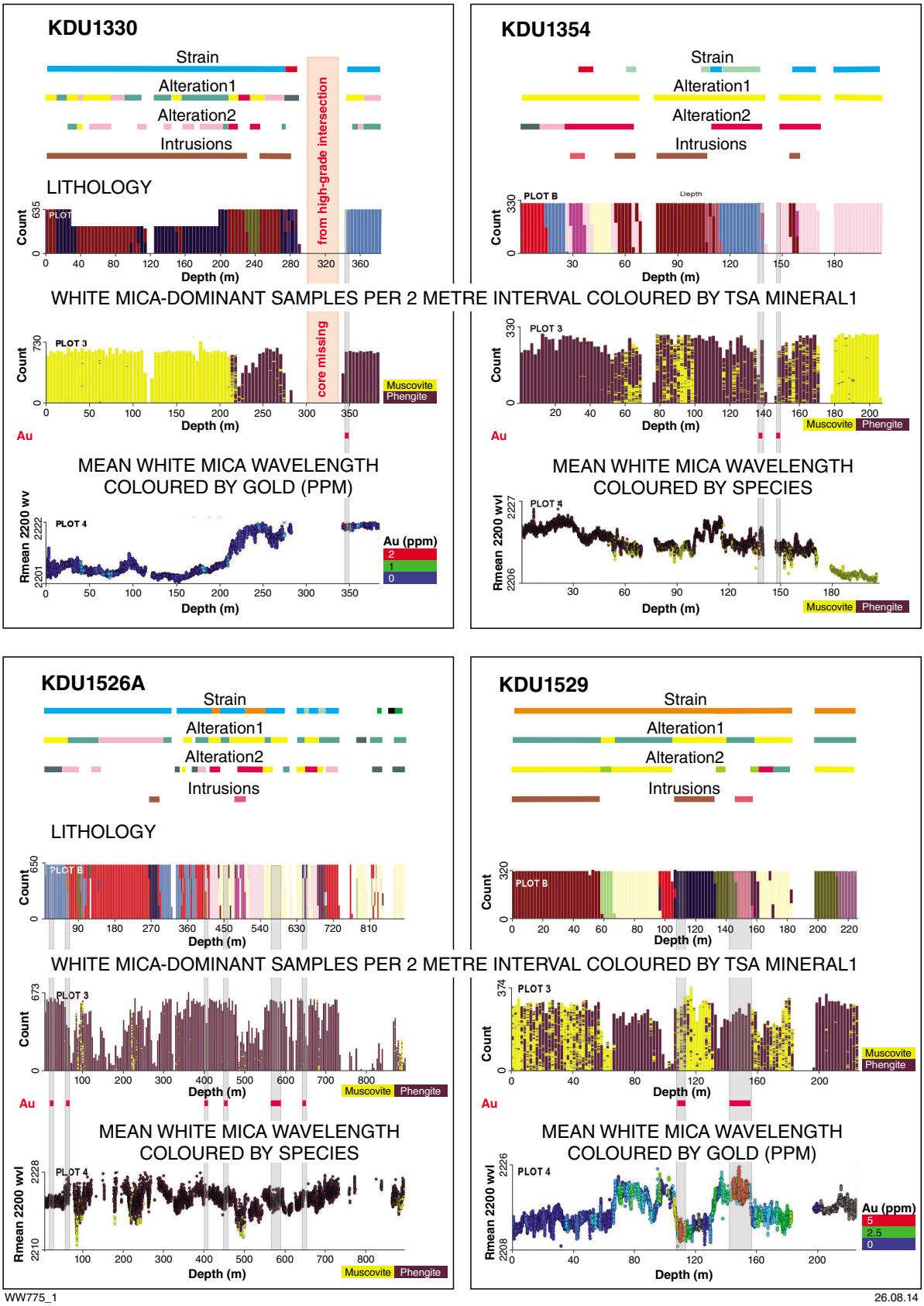

Figure 3.97. **Composite downhole logs, Kanowna Belle, relating spectrally determined white-mica composition to gold abundance and various geological features. Holes KDU1330, 1354 1526A, 1529, 1597, 1609, 1595. See Figure 3.98 for legend.**

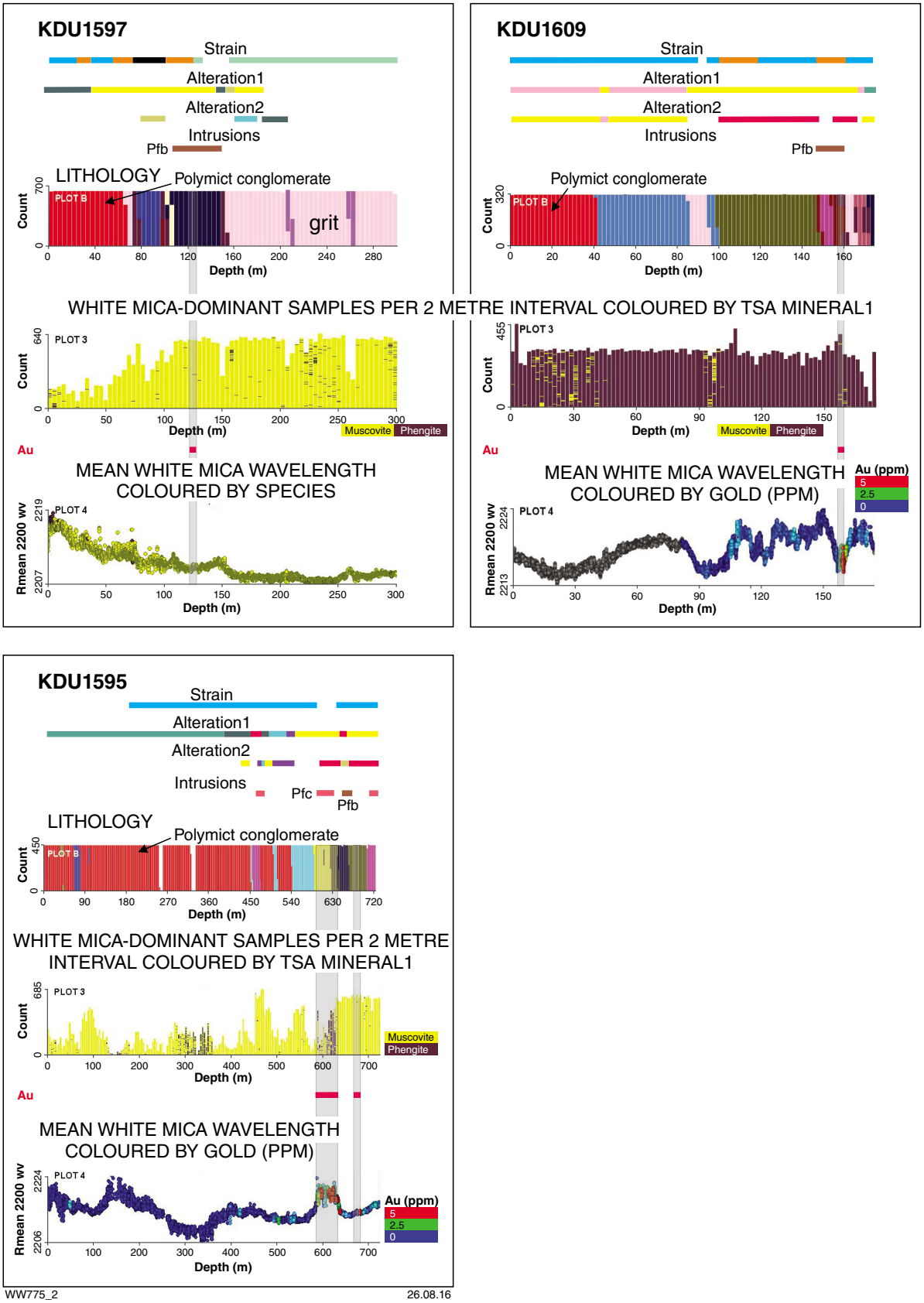

Figure 3.97. continued

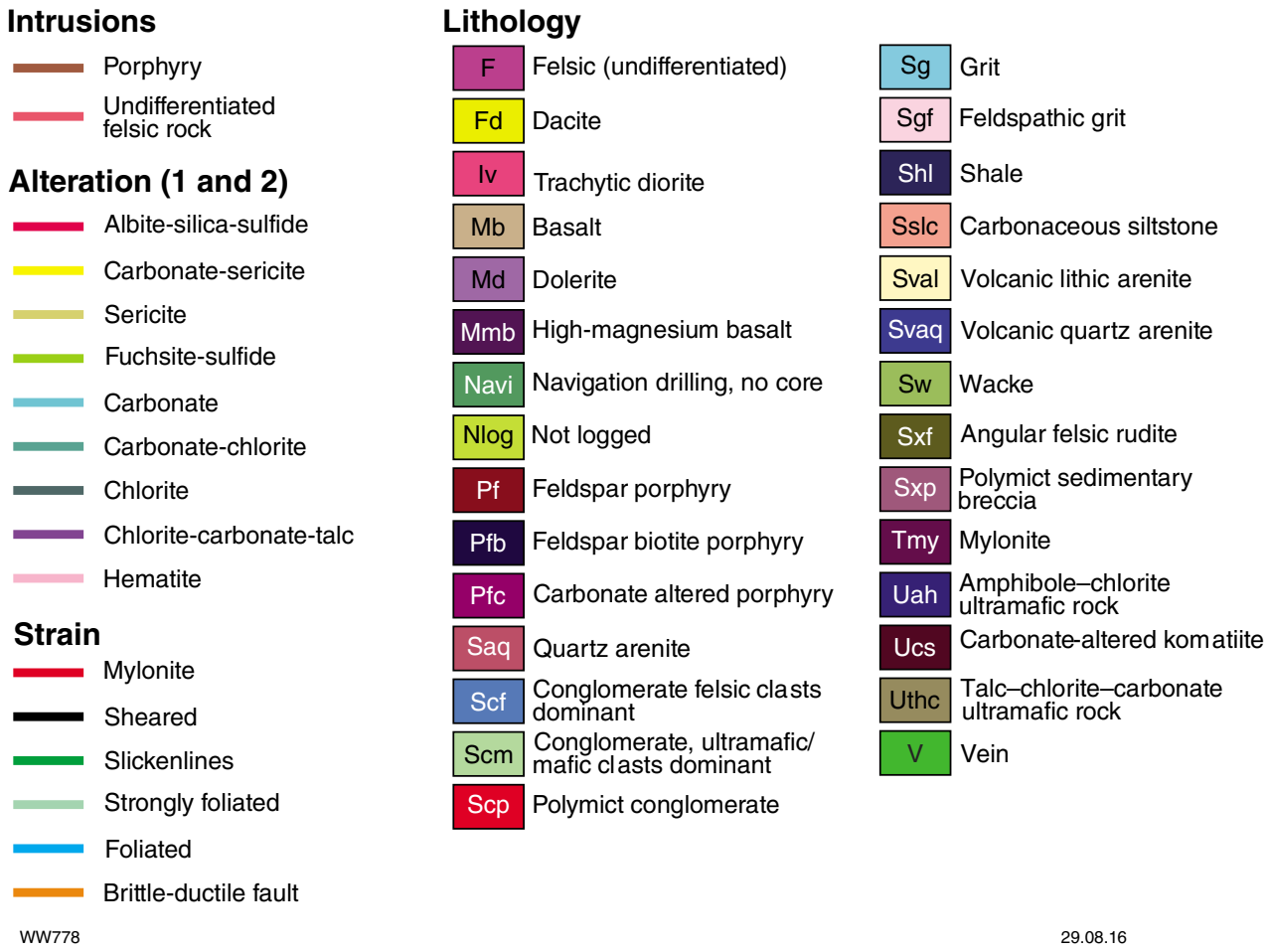

Figure 3.98. Legend for Figures 3.96 and 3.97

Table 3.22. Diamond cores from the Southern Cross district analysed by HyLogger-3 and reported in this volume

Hole[(a)]	*Deposit*	*Deposit type*	*Local grid east*	*Local grid north*	*Total depth (m)*
GPD1464	Golden Pig	Model 2	4731.8	14339.8	109.3
NVCD0102	Nevoria	Model 2	Unknown	Unknown	274.2
FMM397	Frasers (Southern Cross)	Model 1	Unknown	Unknown	106.7
OBRD067	O'Brien (Marvel Loch)	Model 1	Unknown	Unknown	282.2
UNRD331	Undaunted (Marvel Loch)	Model 1	Unknown	Unknown	80.1
FLRD052	Firelight (Marvel Loch)	Model 1	Unknown	Unknown	164.1

NOTE: (a) All holes are represented by diamond cores.

Table 3.23. Core GPD1464: Comparison of modal mineralogy determined by HyLogger-3 with that determined by XRD analyses[a]. Minerals recognized by both techniques are shown in bold type.

Depth (m)	*Lithology*	*XRD analysis (dominant minerals)[b]*	*XRD analysis (minor minerals)[c]*	*HyLogger-3 (dominant minerals)[f]*	*HyLogger-3 (minor minerals)[f]*
17.60 – 17.65	Ultramafic	**Chlorite (64.8)** **Tremolite–Actinolite[d] (28.7)** Magnetite (5.4)	Biotite Kaolinite Serpentine Diopside **Talc**	**Chlorite** **Actinolite**	**Talc**
29.29 – 29.15	Ultramafic	**Tremolite–Actinolite[d]** (34.5) **Chlorite (28.5)** Forsterite (14.1) **Serpentine (10.6)** Magnetite (8.5)	Epidote[e] Diopside Kaolinite Talc	**Amphibole** **Chlorite**	Forsterite **Serpentine**
41.20 – 41.31	Altered Mafic	**Magnesio-hornblende[d] (37.5)** **Albite (29.2)** **Quartz (12.6)** **Diopside (8.8)** **Chlorite (3.5)**	Titanite MuscoviteIlmenite Calcite Epidote **Biotite** Magnetite	**Hornblende** **Feldspar** (Oligoclase–andesine)	**Pyroxene[g]** **Quartz[h]** **Biotite[i]** **Chlorite**
48.0 – 58.0	Altered Mafic	**Magesio-hornblende[d] (79.2)** **Albite (11.1)** **Diopside (3.3)** Epidote[e] (2.9)	Talc **Biotite** **Siderite** **Chlorite**	Cordierite **Feldspar** (Andesine–labradorite) **Biotite**(i) **Amphibole**	**Pyroxene[g]** **Carbonate** Quartz[h] Olivine **Chlorite**
59.50 – 59.60	Ultramafic	**Tremolite–Actinolite[d] (37.6)** **Chlorite (30.7)** Biotite (12.1) Titanite (6.9) Quartz (5.1) **Talc (3.2)**	Calcite	Cordierite[j] **Chlorite** **Amphibole**	**Talc**

NOTES:
(a) XRD data supplied by Dr A Dugdale (Curtin University)
(b) Dominant minerals >2.5%; modal abundance determined by XRD in parentheses
(c) Minor minerals listed in order of abundance, as determined by XRD analysis
(d) Tremolite–actinolite and magnesio-hornblende not distinguished by XRD, but, where amphibole is indicated, the species has been assigned according to bulk-rock composition
(e) Epidote includes clinozoisite
(f) Dominant minerals defined as Count% >10; NOTE that Dominant and Minor HyLogger-3 minerals are not listed in order of abundance
(g) HyLogger-3 recognizes pyroxene, but where it is in mafic to ultramafic rocks it is probably diopside, consistent with field observations and published analyses of other mafic rocks of the Southern Cross district (e.g. Mueller, 1997)
(h) Reported by HyLogger-3 as silica but presumed to have detected quartz
(i) Reported by HyLogger-3 as dark mica but presumed to have detected biotite
(j) Detection of cordierite in ultramafic rock by HyLogger-3 is inconsistent with XRD data and petrographic observations of ultramafic rocks elsewhere in the Southern Cross greenstone belt, and may be erroneous. Alternatively, the identification of cordierite may be correct, in which case the host rock may be altered mafic rock logged erroneously as ultramafic rock.

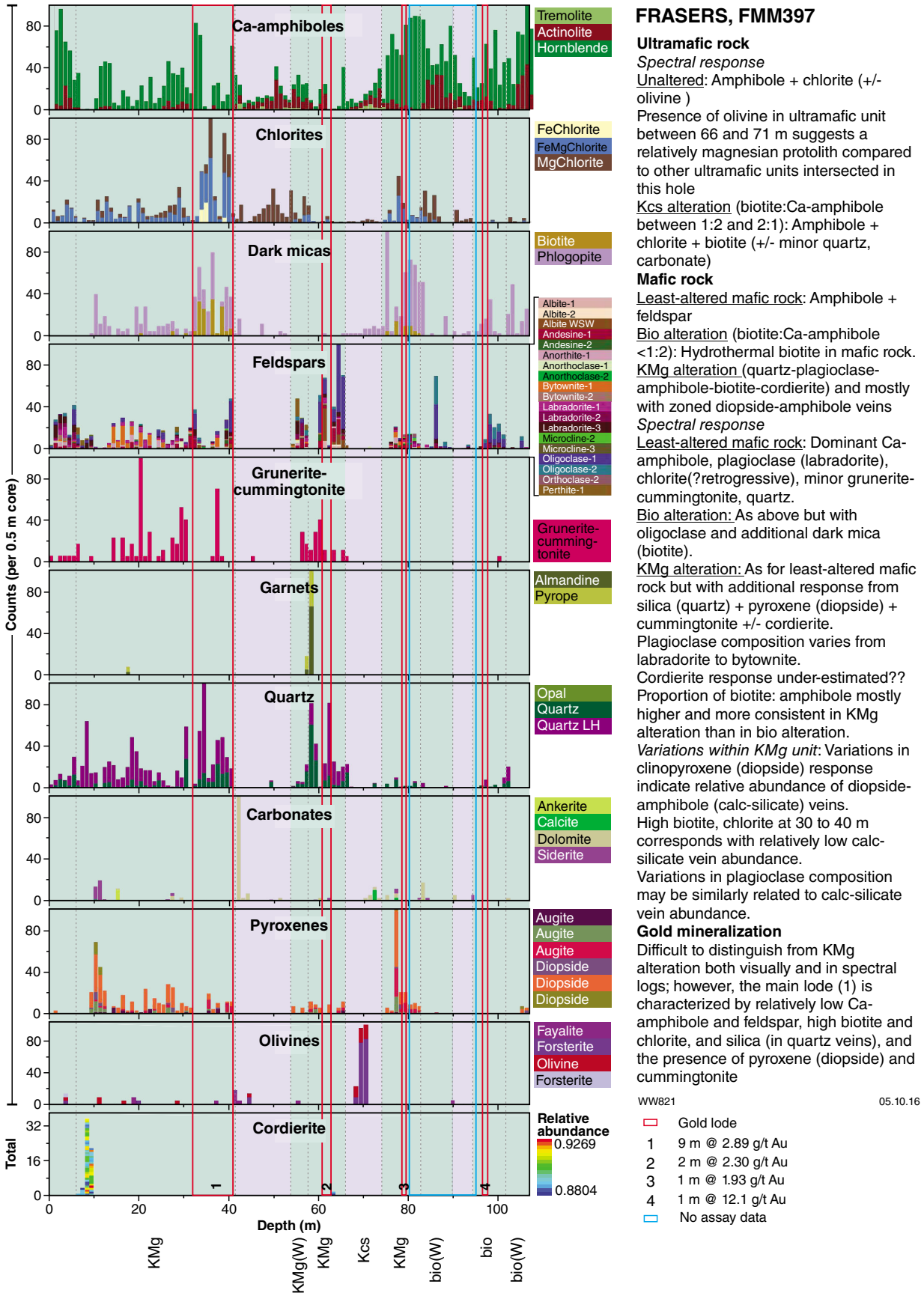

FRASERS, FMM397

Ultramafic rock

Spectral response

Unaltered: Amphibole + chlorite (+/- olivine)

Presence of olivine in ultramafic unit between 66 and 71 m suggests a relatively magnesian protolith compared to other ultramafic units intersected in this hole

Kcs alteration (biotite:Ca-amphibole between 1:2 and 2:1): Amphibole + chlorite + biotite (+/- minor quartz, carbonate)

Mafic rock

Least-altered mafic rock: Amphibole + feldspar

Bio alteration (biotite:Ca-amphibole <1:2): Hydrothermal biotite in mafic rock.

KMg alteration (quartz-plagioclase-amphibole-biotite-cordierite) and mostly with zoned diopside-amphibole veins

Spectral response

Least-altered mafic rock: Dominant Ca-amphibole, plagioclase (labradorite), chlorite(?retrogressive), minor grunerite-cummingtonite, quartz.

Bio alteration: As above but with oligoclase and additional dark mica (biotite).

KMg alteration: As for least-altered mafic rock but with additional response from silica (quartz) + pyroxene (diopside) + cummingtonite +/- cordierite.

Plagioclase composition varies from labradorite to bytownite.

Cordierite response under-estimated??

Proportion of biotite: amphibole mostly higher and more consistent in KMg alteration than in bio alteration.

Variations within KMg unit: Variations in clinopyroxene (diopside) response indicate relative abundance of diopside-amphibole (calc-silicate) veins.

High biotite, chlorite at 30 to 40 m corresponds with relatively low calc-silicate vein abundance.

Variations in plagioclase composition may be similarly related to calc-silicate vein abundance.

Gold mineralization

Difficult to distinguish from KMg alteration both visually and in spectral logs; however, the main lode (1) is characterized by relatively low Ca-amphibole and feldspar, high biotite and chlorite, and silica (in quartz veins), and the presence of pyroxene (diopside) and cummingtonite

WW821 05.10.16

Gold lode
1 9 m @ 2.89 g/t Au
2 2 m @ 2.30 g/t Au
3 1 m @ 1.93 g/t Au
4 1 m @ 12.1 g/t Au
No assay data

Figure 3.99. Spectral log showing auriferous intersections and annotations indicating rock types and associated hydrothermal alteration (at base of graphic log), core FMM397, Frasers gold deposit, Southern Cross district, Youanmi Terrane. Green intervals denote mafic rock; purple intervals denote ultramafic rock. See text and Figure 3.100 for key to alteration types.(W) indicates weak alteration.

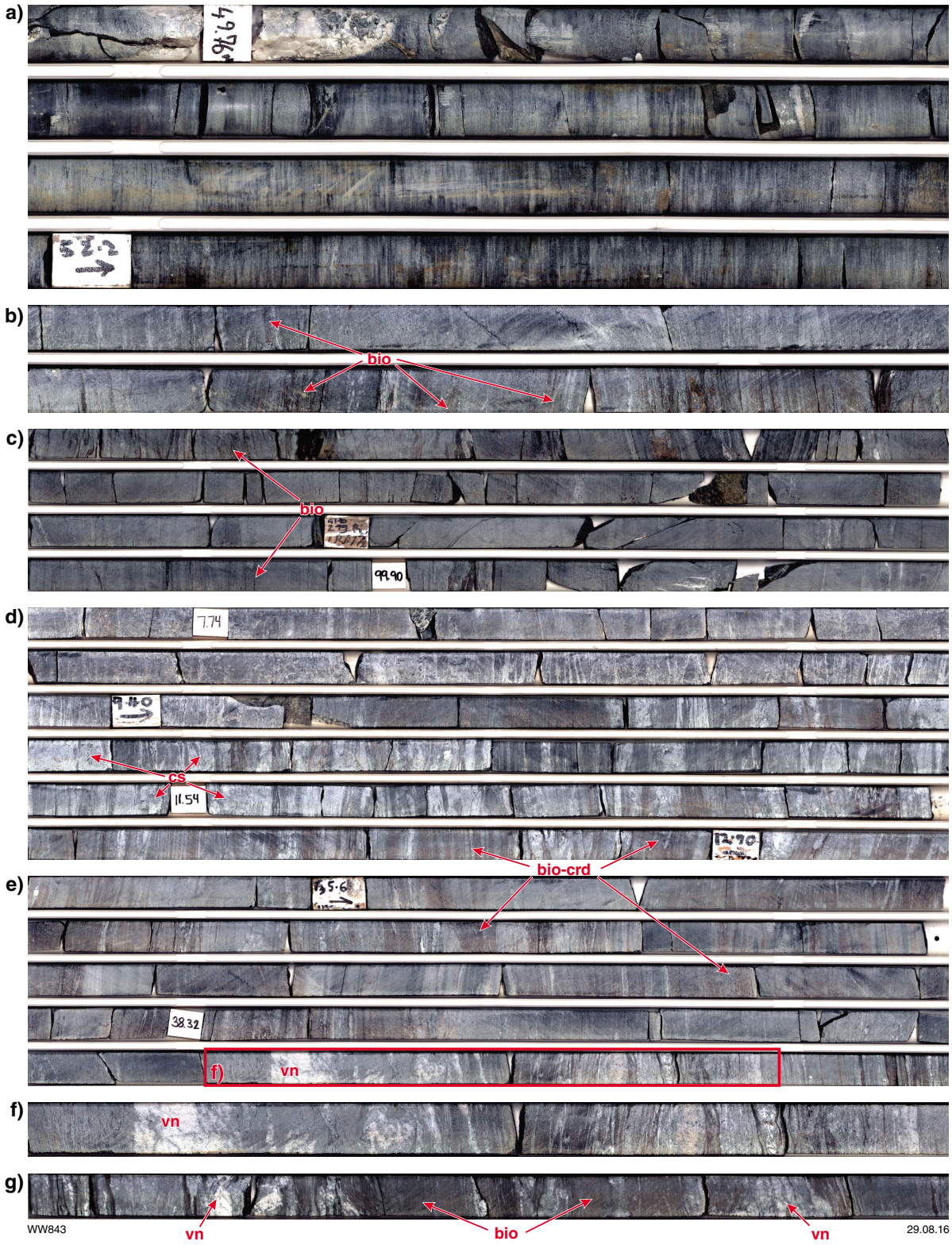

Figure 3.100. Core photos illustrating features of FMM397 referred to in the text. a) 49.7–52.6 m, ultramafic unit of fine- to medium-grained tremolitic amphibole and chlorite. b) 74–75 m, ultramafic unit with Kcs alteration (overall biotite:amphibole >1:2 but <2:1), showing bands of biotite (bio). c) 96.5–100.4 m, mafic unit with bio-alteration (overall biotite:amphibole <1:2), showing bands of biotite (bio). d) 7.5–13.1 m, mafic unit with KMg alteration (biotite–cordierite, bio-crd) and numerous deformed calc-silicate veins (cs). e) 35.3–39.6 m, mafic unit with KMg alteration (biotite–cordierite) and few calc-silicate veins; auriferous quartz–carbonate–diopside–pyrrhotite veins (vn) are present in the lower row of core (outlined in red and shown in more detail in panel f); some biotite in the wallrocks may be related to the gold veins but is hard to distinguish from biotite formed during the earlier KMg alteration. f) Detail of quartz–carbonate–diopside–pyrrhotite veins identified by red outline in panel e. g) 40.0–40.8 m, quartz–carbonate–diopside–pyrrhotite veins (vn) and biotite-rich wallrocks (bio) from intersection of core with main lode.

Potassic calc-silicate (Kcs) alteration of the ultramafic unit between 71 and 75 m (Fig 3.100b) is identified mainly by the additional dark mica (biotite) response, but also by weak silica (quartz) and carbonate responses (Fig. 3.99). Diopside bands and veins, though locally present in the ultramafic units, are not recognized by TSA analysis of TIR spectra.

The least-altered mafic unit in core FMM397, intersected between 0 and 5 m, is defined by spectra that identify Ca-amphibole (hornblende) and feldspar (mainly labradorite) as major components (Fig. 3.99), though chlorite, cummingtonite, and silica (quartz) are also identified. Chlorite is probably retrogressive after Ca-amphibole and silica is present as deformed quartz(–carbonate) veinlets. Biotite alteration (biotite:Ca-amphibole <1:2) in the mafic unit towards the bottom of the hole (Fig. 3.100c) is identified spectrally as a response to dark mica(–silica, chlorite), without major changes in other spectra (e.g. Ca-amphibole), although there is an apparent shift in the composition of feldspar from labradorite to oligoclase (Fig. 3.101a).

The more strongly altered mafic rocks (sea-floor KMg alteration; Fig. 3.100d,e) produce a stronger dark mica (biotite) response and plagioclase compositions as calcic as bytownite (Fig. 3.101a), together with a moderate to strong pyroxene (diopside) response and variable silica (quartz), grunerite–cummingtonite, and carbonate responses.

The pyroxene response in KMg-altered mafic units reflects the presence of numerous diopside-rich calc-silicate bands (Fig. 3.100d) that are interpreted to be metamorphosed dolomite-bearing veins. The bytownite interval between 10 and 25 m coincides with elevated cummingtonite and quartz responses but relatively low pyroxene abundance. This suggests that Ca may be partitioned into diopside veins at the expense of plagioclase. The more calcic plagioclase compositions of the relatively pyroxene-poor intervals may reflect loss of Na during sea-floor hydrothermal alteration (Franklin et al., 1981; Lydon, 1984).

The grunerite–cummingtonite spectral response in KMg-altered rocks (Fig. 3.99) is probably caused by cummingtonite, which commonly forms a narrow halo of colourless acicular amphibole around the dark-green hornblende and light-green diopside in deformed calc-silicate (metamorphosed carbonate-bearing) veins. Cordierite, normally a major component of KMg alteration in the Southern Cross district (Witt and Hagemann, 2012), is identified spectrally only at the top of the first and thickest mafic unit in core FMM397 (Fig. 3.99). Minor amounts of olivine are also indicated in some units, though previous petrographic studies of this type of alteration (Barker, 1998; Bodycoat, 1999) did not identify olivine, so the TSA identification is interpreted to be erroneous. The spectral response to biotite is relatively subdued in the KMg-altered mafic unit between 53 and 66 m, consistent with visual observations that indicate the presence of biotite, but at lower abundance than in similar units shallower in the hole.

Figure 3.101. (opposite) Detailed TIR feldspar spectra from diamond cores: a) FMM397, Frasers; b)UNRD331,Sherwoodlodes(Undaunted),Marvel Loch; c) OBRD067, O'Brien lode, Marvel Loch; d) FLRD052, Firelight lode, Marvel Loch. Green intervals denote mafic rock; purple intervals denote ultramafic rock; yellow interval denotes metasedimentary rock; grey interval denotes shear zone; pink intervals denote pegmatite. Alteration abbreviations: amp (amphibole), bio (biotite), Kcs (potassic-calcsilicate), KMg (potassic-magnesian), plg (plagioclase). (W) indicates weak alteration.

Gold lodes at Frasers (N Taylor, in Witt et al., 1994) are associated with quartz veins that are either conformable with (Frasers ore shoot) or discordant to (Sholls ore shoot) the shear fabric in mafic–ultramafic greenstones, or in banded iron-formation (Greenstone ore shoot). The best gold intersection in core FMM397 is between 32 and 41 m (9 m at 2.89 g/t Au) on the contact between KMg-altered mafic rock and an ultramafic unit (Fig. 3.99). This interval of core contains several quartz–carbonate–diopside–pyrrhotite veins, particularly at the higher grade margins of the interval (Fig. 3.100e–g). Although biotite is perhaps more abundant in the wallrocks around these veins, it is difficult (in the absence of veins) to visually distinguish this alteration from KMg alteration (Fig. 3.100e). However, the spectral log shows a relative decrease in the abundance of Ca-amphibole and feldspar (particularly towards the centre of the interval) and a corresponding increase in the abundances of silica (quartz), dark mica (biotite), cummingtonite, and chlorite within the lode (Fig. 3.99). These features are less evident in the thinner lodes marked 2, 3, and 4 in Figure 3.99.

Marvel Loch

Marvel Loch, the largest production centre in the Southern Cross district, is about 35 km south-southeast of Southern Cross township. Historic underground mining of gold from a number of shafts was succeeded in 1981 by openpit mining that incorporated most of the historic lodes, and later by a return to underground mining below the pit floor. Total production has been estimated at more than 2.5 Moz of gold (S Shenton, in Doublier, 2014). The district-scale geological setting of the deposit is shown in Figure 2.125 (Part 2 of this Atlas). The Marvel Loch deposit is described briefly under Targeting Criterion 3.7 (map and cross sections in Fig. 3.33). More detailed descriptions of the ultramafic-hosted Savage lode at the southern end of Marvel Loch (Rolley and Baxter, 1990) are provided by Mueller (1991) and Mueller et al. (1991).

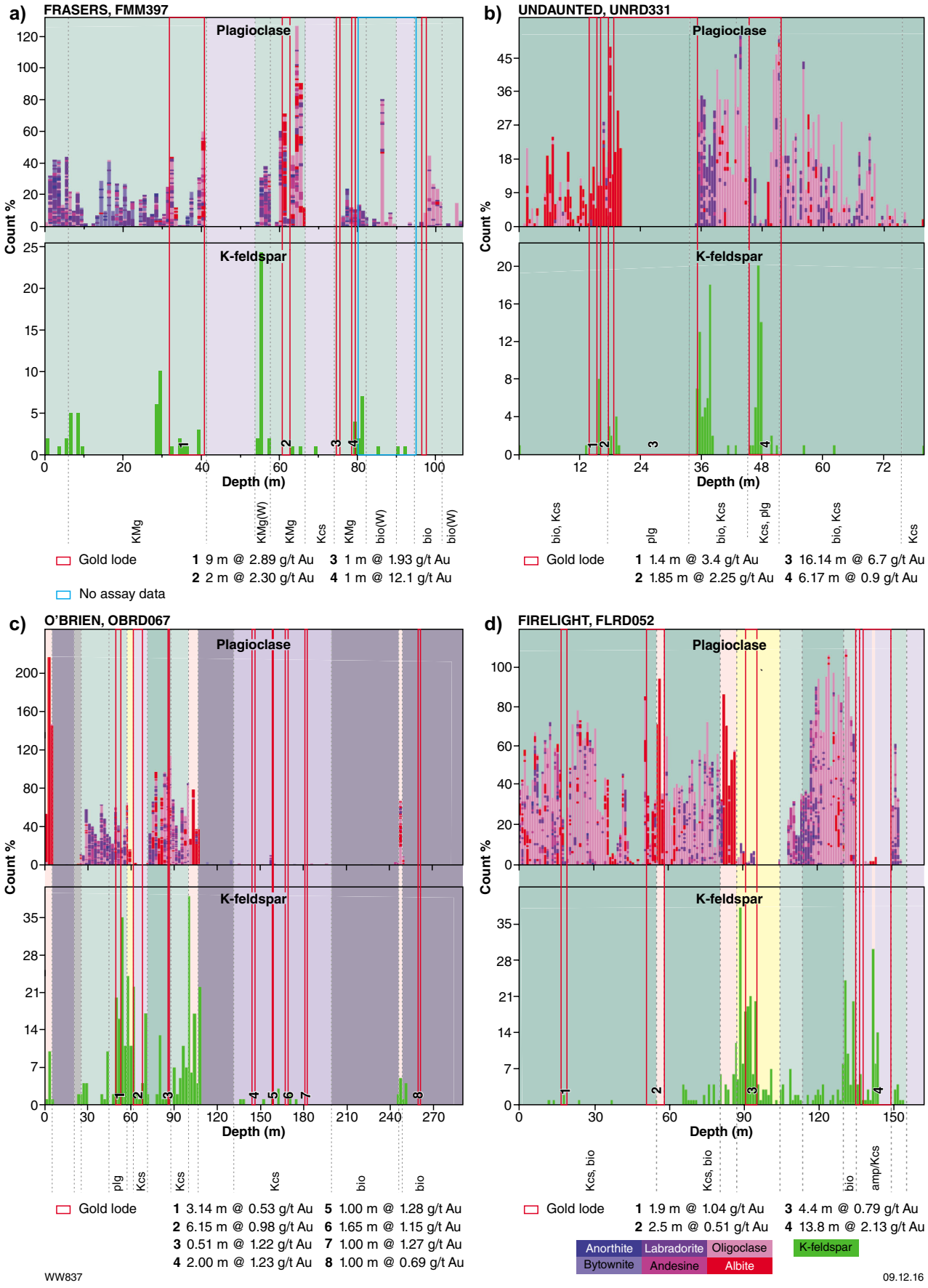
a)
FRASERS, FMM397
Plagioclase
K-feldspar
Count %
Depth (m)
KMg
KMg(W)
KMg
Kcs
KMg
bio(W)
bio
bio(W)
Gold lode
No assay data
1 9 m @ 2.89 g/t Au
2 2 m @ 2.30 g/t Au
3 1 m @ 1.93 g/t Au
4 1 m @ 12.1 g/t Au
b)
UNDAUNTED, UNRD331
Plagioclase
K-feldspar
Count %
Depth (m)
bio, Kcs
plg
bio, Kcs
Kcs, plg
bio, Kcs
Kcs
Gold lode
1 1.4 m @ 3.4 g/t Au
2 1.85 m @ 2.25 g/t Au
3 16.14 m @ 6.7 g/t Au
4 6.17 m @ 0.9 g/t Au
c)
O'BRIEN, OBRD067
Plagioclase
K-feldspar
Count %
Depth (m)
plg
Kcs
Kcs
Kcs
bio
bio
Gold lode
1 3.14 m @ 0.53 g/t Au
2 6.15 m @ 0.98 g/t Au
3 0.51 m @ 1.22 g/t Au
4 2.00 m @ 1.23 g/t Au
5 1.00 m @ 1.28 g/t Au
6 1.65 m @ 1.15 g/t Au
7 1.00 m @ 1.27 g/t Au
8 1.00 m @ 0.69 g/t Au
WW837
d)
FIRELIGHT, FLRD052
Plagioclase
K-feldspar
Count %
Depth (m)
Kcs, bio
Kcs, bio
bio
amp/Kcs
Gold lode
1 1.9 m @ 1.04 g/t Au
2 2.5 m @ 0.51 g/t Au
3 4.4 m @ 0.79 g/t Au
4 13.8 m @ 2.13 g/t Au
Anorthite
Labradorite
Oligoclase
Bytownite
Andesine
Albite
K-feldspar
09.12.16

Three diamond cores were analysed in the SWIR and TIR spectral ranges using the GSWA HyLogger-3 instrument; the results are described below. The cores were collared in the Undaunted, O'Brien, and Firelight areas of the Marvel Loch underground mine and, in combination, represent the main styles of mineralization at Marvel Loch (Fig. 3.102). Hole UNRD331, collared in the Undaunted development, was drilled eastwards to intersect ~80 m of deformed gabbro and the Sherwood lode to the east of the 'median mylonite' (Fig. 3.33). Hole OBRD067 was collared in the O'Brien development and intersected mafic to ultramafic rock on the west side of the 'median mylonite'. Hole FLRD052 was collared in gabbroic rocks in the Firelight development and was drilled westwards, across the 'median mylonite' into mafic–ultramafic rocks.

Sherwood lodes (UNRD331)

The Sherwood lodes, hosted by metagabbro on the eastern side of the 'median mylonite' (Fig. 3.33), were intersected by core UNRD331. Throughout the intersection, the metagabbro in the core displays variable hydrothermal biotite, classified as distal (bio) alteration (biotite:amphibole <1:2) and medial Kcs (biotite:amphibole between 1:2 and 2:1) alteration (Fig. 3.103a,b). Alteration proximal to lodes is classified as plagioclase alteration (plagioclase abundance >> biotite with or without minor amounts of amphibole), is characterized by a bleached appearance, and is commonly sulfide bearing (Fig. 3.103d,e). These proximal alteration zones occur within Kcs alteration envelopes in all the gold lodes indicated in Figure 3.104, but are too thin to show individually, except for a thick zone of plagioclase alteration associated with the thickest and highest grade lode (18–34 m depth). A diopside–plagioclase assemblage that overprints the pervasive foliation in medial and distal alteration zones is termed calc-silicate (cs) alteration (Fig. 3.103c); the relationship between calc-silicate alteration and gold mineralization is uncertain, and individual calc-silicate alteration zones are too small to show individually in Figure 3.104.

The spectral signature of the distal and medial hydrothermal alteration zones around the gabbro-hosted Sherwood lodes is best reflected in the relative heights of Ca-amphibole and dark-mica/chlorite peaks; these two mineral groups show an inverse relationship within zones of bio and Kcs alteration (Fig. 3.104). Chlorite is more commonly detected than dark mica in these alteration zones and, if this spectral identification is correct, the chlorite is probably retrogressive after biotite (dark mica). However, chlorite was not recognized visually in the core, and the spectra for biotite and chlorite are very similar, so biotite may have been misidentified as chlorite by TSA. The strong silica response throughout the hole, except for the mineralized zone between 18 and 34 m, cannot be reconciled with visual inspection of the core.

Proximal alteration around the main gold intersection, between 18 and 34 m, is not well characterized by the spectral data, perhaps because the dark quarter core analysed (Fig. 3.103e) generated a weak spectral signal that was difficult for TSA to interpret. The spectral data for this interval of plagioclase alteration is characterized by variable but locally high Ca-amphibole abundance and weak to zero feldspar, quartz, dark mica, and chlorite (Fig. 3.104), characteristics that are not compatible with visual observations of the core (Fig. 3.103e). A strong spectral response to sulfates (oxidized sulfides) appears to be the feature that best characterizes this proximal alteration zone, although there is also a broadly inverse relation between spectral Ca-amphibole abundance and gold grades (Fig. 3.104). Predominantly albitic plagioclase in the interval from 14 to 20 m suggests that the metasomatic plagioclase in the main gold intersection may be relatively sodic (Fig. 3.101b).

The less weathered, lower grade gold lode between 45 and 52 m contains relatively minor plagioclase alteration within dominant Kcs alteration, and this interval is defined spectrally by enhanced dark mica and chlorite at the expense of Ca-amphibole and feldspar responses, but low sulfate abundance (Fig. 3.104). High pyroxene abundance between 35 and 39 m in core UNRD331, appears to track the distribution of calc-silicate alteration, in contrast to other Southern Cross drillholes, where a weaker pyroxene response identifies diopside-bearing veins. Feldspar in calc-silicate alteration intervals is relatively calcic (labradorite, as opposed to oligoclase in bio and Kcs alteration zones; Fig. 3.101b).

Although feldspar was not detected in the proximal plagioclase alteration zone between 18 and 34 m, feldspar spectra provide the most useful vector to mineralization in core UNRD331. The feldspar composition changes from labradorite to oligoclase at around 39 m, 3 m beyond a 0.3 g/t Au cutoff and a further 2 m beyond the plagioclase alteration zone (Fig. 3.104). This change in feldspar composition appears to correlate with the presence of calc-silicate alteration (identified by the pyroxene spectra) and may not be directly related to gold mineralization. However, the feldspar spectra between 35 and 39 m also contain an indication that plagioclase is accompanied by minor amounts of K-feldspar (microcline, orthoclase, anorthoclase). The plagioclase compositional gradient on the uphole side of the high-grade lode (18–34 m) may have been obscured by weathering, but does show the presence of minor amounts of K-feldspar adjacent to the proximal alteration zone. The presence of K-feldspar (microcline) is also indicated within the lower grade lode (45–52 m), although there is no vector outside the lode in this case (Fig. 3.101b).

A second potential vector is provided by the distribution of spectrally identified pyroxene (Fig. 3.104). More work is warranted to confirm pyroxene abundance as a vector in the Sherwood lodes because it is partly controlled by calc-silicate alteration which, although readily detected visually, has not been widely recognized at Marvel Loch and its genetic relationship to gold mineralization, if any, is not well understood.

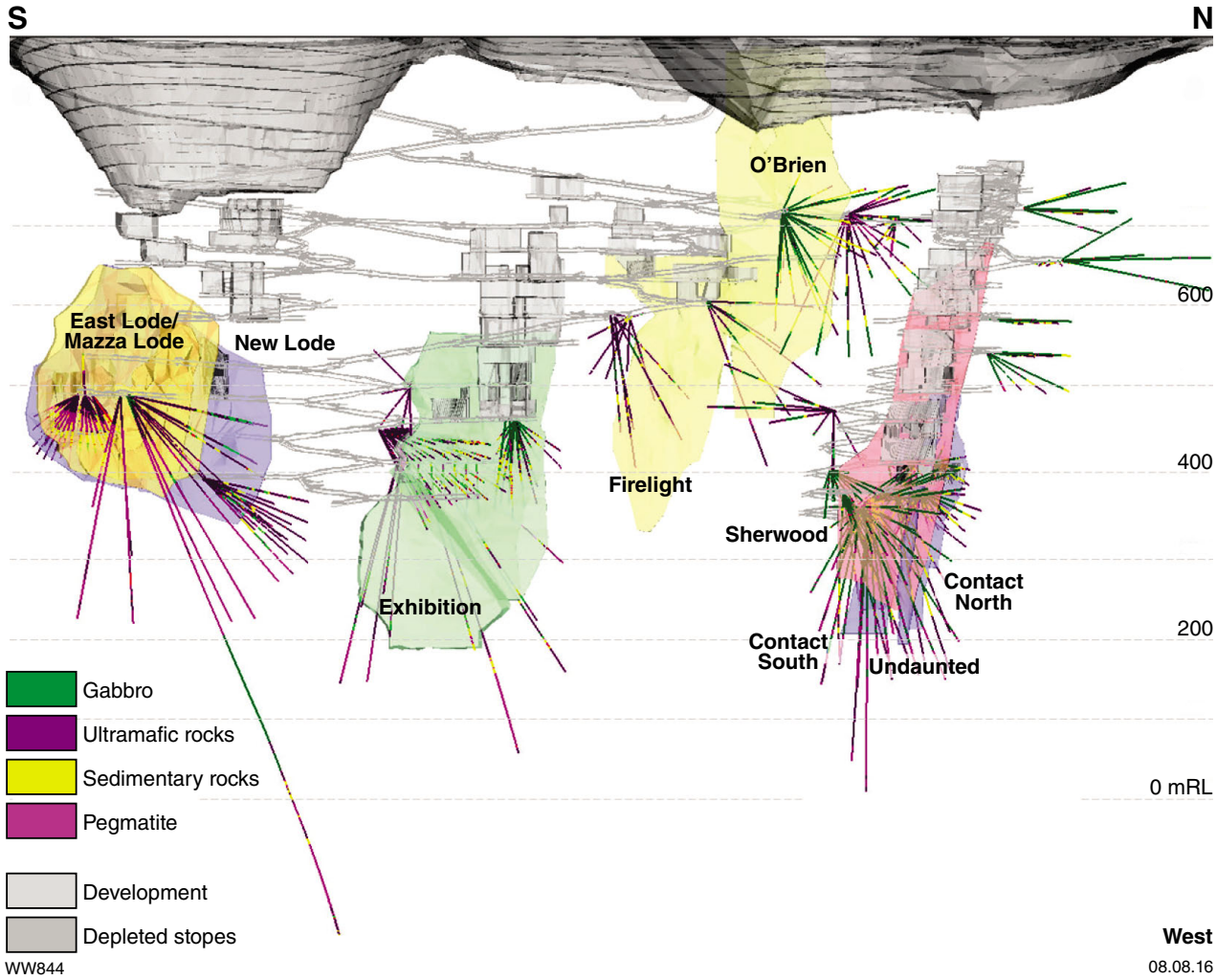

Figure 3.102. Longitudinal cross section through a 3D model at Marvel Loch showing the depth extent of openpits, underground development, and stopes, and the positions and shapes of orebodies (from Doublier, 2014). Note that the assignation of sedimentary host rocks for the Firelight and O'Brien lodes is considered erroneous; the orebodies are hosted by altered mafic and ultramafic rocks as shown in Figures 3.105 to 3.108.

Exhibition-style lodes (OBRD067)

Drillhole OBRD067 in the O'Brien development (Fig. 3.105) passed through a thin metasedimentary unit at about 60 m downhole and then intersected another 200 m of mainly ultramafic rock that hosts gold in lodes equivalent to the Exhibition and Boulder–New lodes (Fig. 3.33). Gold mineralization was also intersected in mafic and ultramafic rocks adjacent to the metasedimentary unit (equated with the 'median mylonite'), which may be equivalent to the Contact Lodes (Fig. 3.102), although the prominent quartz vein in the Contact Lodes is not present in this hole.

The distal and medial alteration assemblages in ultramafic rocks at Marvel Loch are similar to those in metagabbro and are given the same codes (bio, Kcs). Differences include lower feldspar content, a more tremolitic composition of amphiboles, and a more phlogopitic composition of biotite in altered ultramafic rock (Fig. 3.106d,f). Furthermore, the inner medial (Kcs) alteration zone commonly hosts the bulk of economic gold mineralization (Fig. 3.106d). Proximal alteration zones are generally thinner (or absent), and can be assigned to two categories. Amphibole (amp) alteration is defined by matted amphiboles, typically less tremolitic than in the medial zone, with minor amounts of biotite and sulfides. Proximal K-feldspar (Kfp) alteration is distinguished as containing a major component of microcline feldspar that can usually be recognized by its salmon pink colour.

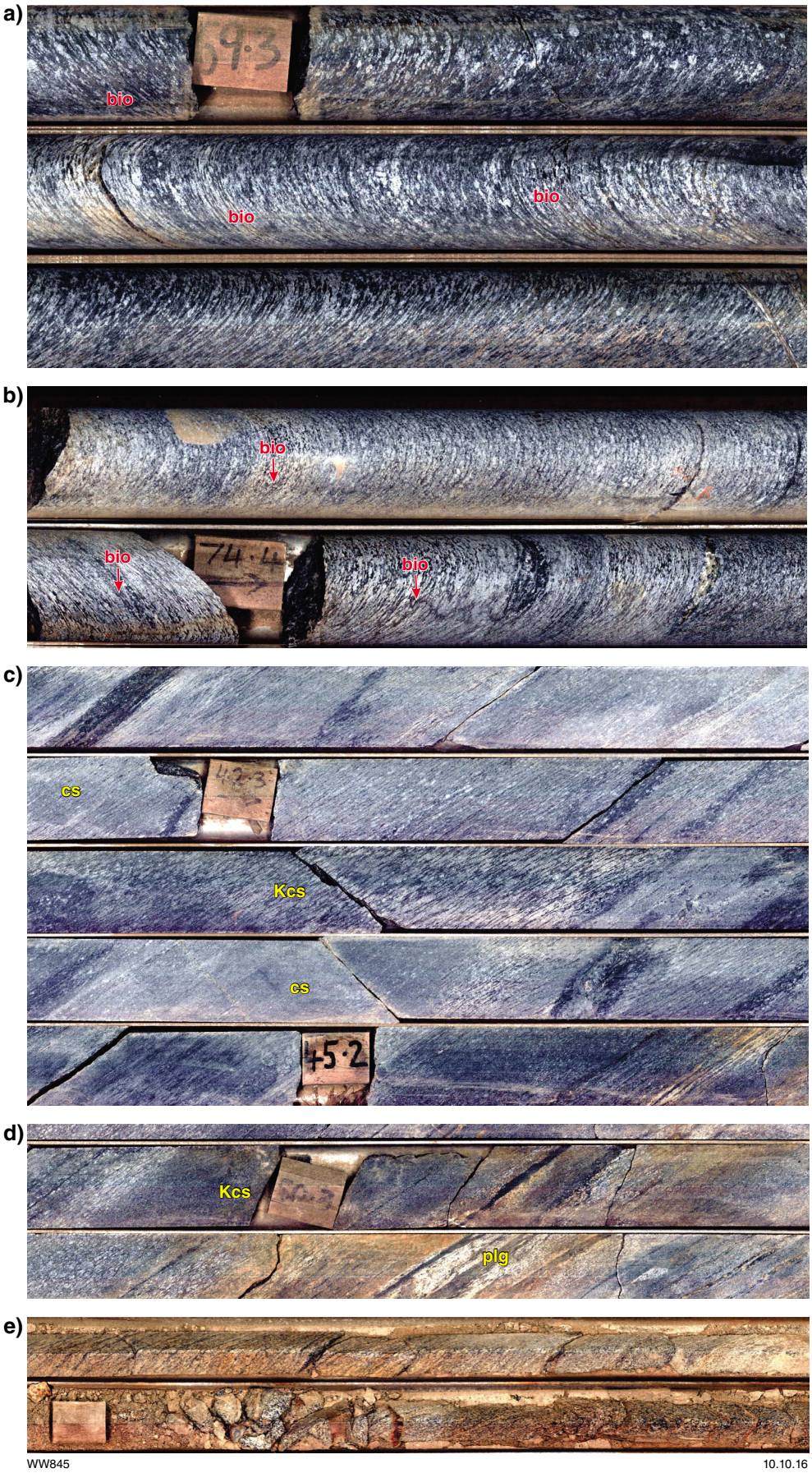
a)
bio
bio
bio
b)
bio
bio
bio
c)
cs
Kcs
cs
d)
Kcs
plg
e)
WW845
10.10.16

Figure 3.103. (opposite) Core photos showing hydrothermal alteration of metagabbro associated with Sherwood lodes (UNRD331). a) ~60 m, distal (bio) alteration (biotite:amphibole <1:2), strongly foliated. b) ~74 m, medial (Kcs) alteration with subequal biotite and amphibole (proportions between 1:2 and 2:1), strongly foliated. c) 41–45 m: patchy calc-silicate (cs) alteration overprinting Kcs alteration; note destruction of foliation and pale apple-green colour caused by the presence of fine- to medium-grained diopside in calc-silicate (diopside + plagioclase) alteration zones. d) ~50 m, bands of plagioclase (plg) alteration within broader zone of Kcs alteration. e) 25–26 m, plagioclase (plg) alteration in which plagioclase is the dominant mineral, accompanied by smaller amounts of biotite and minor to no amphibole. Alteration codes shown in yellow; mineral codes (bio) shown in red.

Except in mineralized zones, ultramafic rocks are identified spectrally by strong serpentine and olivine responses and weak chlorite responses in the absence of feldspar and quartz (Fig. 3.105). The spectral identification of olivine in relatively magnesian units (serpentinite) corresponds to the presence of columnar, neoblastic (metamorphic) olivine grains, including porphyroblasts. The strongest olivine response, in the upper part of the hole, correlates with low tremolite (Ca-amphibole) and chlorite responses and identifies a metamorphosed high-Mg ultramafic rock that contains a high proportion of (partly serpentinized) metamorphic olivine (Fig. 3.106a–c). Serpentine spectra indicate olivine-bearing rocks with partial retrogressive serpentinization of metamorphic olivine (Fig. 3.105). Units logged as serpentinite also yield a spectral response for garnet (not shown in Fig. 3.105), but there is no visual evidence in the core to support this identification, which is considered erroneous.

Intervals of hydrothermally altered ultramafic rock, in which the olivine response is weak to absent, yield stronger Ca-amphibole (tremolite) and chlorite responses, and are less magnesian. Distal (bio) to medial (Kcs) hydrothermal alteration of the ultramafic units in core OBRD067 are identified spectrally as dark mica and variations in the relative strength of dark mica and Ca-amphibole responses (Fig. 3.105). Some hydrothermal biotite is related to proximity to pegmatite intrusions rather than gold mineralization.

Two types of mafic unit were intersected in hole OBRD067. The first, medium-grained, foliated amphibolite (e.g. 25–45 m), is identified spectrally by the dominance of Ca-amphibole and feldspar (oligoclase–labradorite; Fig. 3.105). Quartz, not identified visually but indicated by the TIR data, may be a result of hydrothermal alteration associated with the 'median mylonite' and associated gold mineralization, as it would not normally be expected in metamorphosed mafic rock. Potassic calc-silicate (Kcs) alteration of the mafic unit at 90–100 m (Fig. 3.106g) is characterized by elevated dark mica and chlorite responses at the expense of Ca-amphibole responses in Hylogger spectra (Fig. 3.105). The second mafic rock type is massive to banded metadolerite, which is similarly characterized by spectral identification of Ca-amphibole and feldspar (albite–oligoclase), and (?retrograde) chlorite. Some quartz is also identified, again possibly a result of hydrothermal alteration.

The thin sedimentary unit ('median mylonite') at ~60 m was logged as quartz–biotite–feldspar–sillimanite schist with sulfide-rich bands (Fig. 3.106h). Quartz, dark mica, and feldspar (microcline and albite) are identified as major components by the HyLogger data, as are white mica and cordierite (Fig. 3.105). Sillimanite was not detected by HyLogger spectrometers, but was possibly erroneously identified as white mica. Similarly, cordierite identified by HyLogger may be misidentified white mica. The spectra for cordierite, sillimanite, and paragonite are all very similar. Pegmatite intrusions are uniquely distinguished by HyLogger identification of major white mica, quartz, and feldspar (albite–microcline) responses in the absence of Ca-amphibole responses (Figs 3.105 and 3.101c).

Thin zones of ultramafic-hosted gold mineralization between 140 and 200 m depth are within broad intervals of elevated, spectrally determined pyroxene and carbonate (Fig. 3.105). The pyroxene (diopside veins) is readily identified visually (Fig. 3.106e,f), but the semi-quantitative data generated by HyLogger provide a vector that extends 10 to 20 m beyond the ore (defined here as >0.5 g/t Au). This vector also extends about 10 m beyond the elevated gold halo (defined as >0.10 g/t Au). Carbonate abundance provides a similar vector to ultramafic-hosted mineralization, but less effective than pyroxene abundance. Mafic- and ultramafic-hosted gold mineralization between 50 and 90 m is spectrally much less distinctive, lacking carbonate and pyroxene responses. The low-grade mafic-hosted mineralization at 50–53 m (Ore zone 1 in Fig. 3.105), associated with plagioclase alteration (Fig. 3.106i), does not show a uniquely strong presence of feldspar. However, the broad zone of mineralization between 50 and 90 m is indicated by the presence of microcline in addition to plagioclase feldspar spectra representing variable compositions between albite and labradorite (Fig. 3.101c).

Exhibition-style lodes (FLRD052)

Drillhole FLRD052 in the Firelight development passed through a thin metasedimentary unit, interpreted to represent the 'median mylonite', between about 88 and 105 m downhole (Fig. 3.107). The main gold mineralization is hosted by ultramafic rock between 135 and 148.8 m, but several other lower-grade zones of mineralization were intersected in and above the metasedimentary unit. The ultramafic-hosted lode is equivalent in style to the Exhibition and Boulder–New lodes (Fig. 3.33). Hydrothermal alteration associated with gold mineralization in mafic and ultramafic rocks is consistent with those described above from other holes at Marvel Loch.

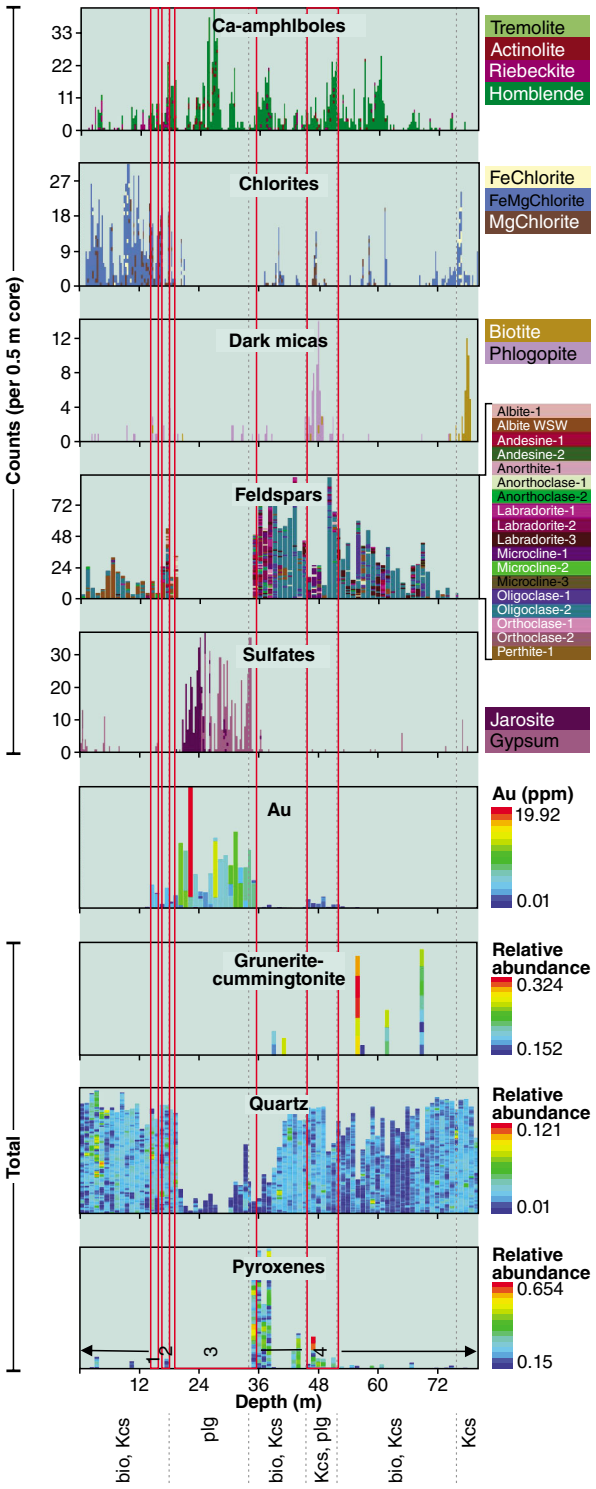

SHERWOOD, UNRD331

Mafic rock – Gabbro

Least-altered gabbro: No unaltered gabbro preserved in core but mineralogy would be dominated by amphibole and feldspar with minor Fe-Ti oxides and possibly minor quartz.

bio alteration - biotite:amphibole <1:2

Kcs alteration - biotite:amphibole between 1:2 and 2:1

Spectral response

Dominant quartz, amphibole, and feldspar with variable but minor dark mica (biotite) and chlorite reflecting strength of alteration. Chlorite (?retrogressive after amphibole, biotite or biotite misidentified by TSA) also locally abundant. Quartz over-represented by spectra. Variations within Mg-Kcs unit: Highest biotite between 45 and 49 m, also below 76 m; both intervals coincident with low chlorite. Biotite in Kcs alteration zones visually more abundant than indicated by spectra but perhaps TSA misidentifies some biotite as chlorite.

Gold mineralization

Visual identification of core obscured by weathering of sulfides but plg alteration appears dominant from 18 to 34 m and minor from 45 to 52 m.

Spectral response

High-grade (18–34 m): Major sulfate with low amphibole, chlorite, quartz, feldspar (no pyroxene or carbonate, little biotite).

NOTE: The spectral data from this mineralized zone do not match field observations - spectral response compromised by weathering and quarter core.

Low- to moderate-grade (45–52 m): Biotite in Kcs alteration zones appears visually more abundant than indicated by spectra but perhaps TSA misidentifies some biotite as chlorite.

Vectors

Feldspars: Presence of K-feldspar spectra proximal or within gold lodes 1 to 4. Change in plagioclase composition from oligoclase to labradorite over >5 m proximal to high-grade lode at 39–35 m weathering and quarter core. This vector is not readily recognized visually.

Pyroxene: An increase in pyroxene abundance towards the high-grade lode, from 39 to 35 m is attributed to calc-silicate alteration. A similar vector towards the low-grade lode (4) may be present between 42 and 45 m. These pyroxene vectors are not evident on the alternative contacts of either lode and are not recognized more generally within the Sherwood lode system.

WW825 05.10.16

Gold lodes

1	1.4 m @ 3.4 g/t Au	3	16.14 m @ 6.7 g/t Au
2	1.85 m @ 2.25 g/t Au	4	6.17 m @ 0.9 g/t Au

Figure 3.104. Spectral log showing auriferous intersections and annotations indicating rock types and associated hydrothermal alteration (at base of graphic log), core UNRD331, Sherwood lodes, Marvel Loch gold deposit, Southern Cross district, Youanmi Terrane. Note that the entire core is metagabbro (coloured green). See text and Figure 3.103 for key to alteration types.

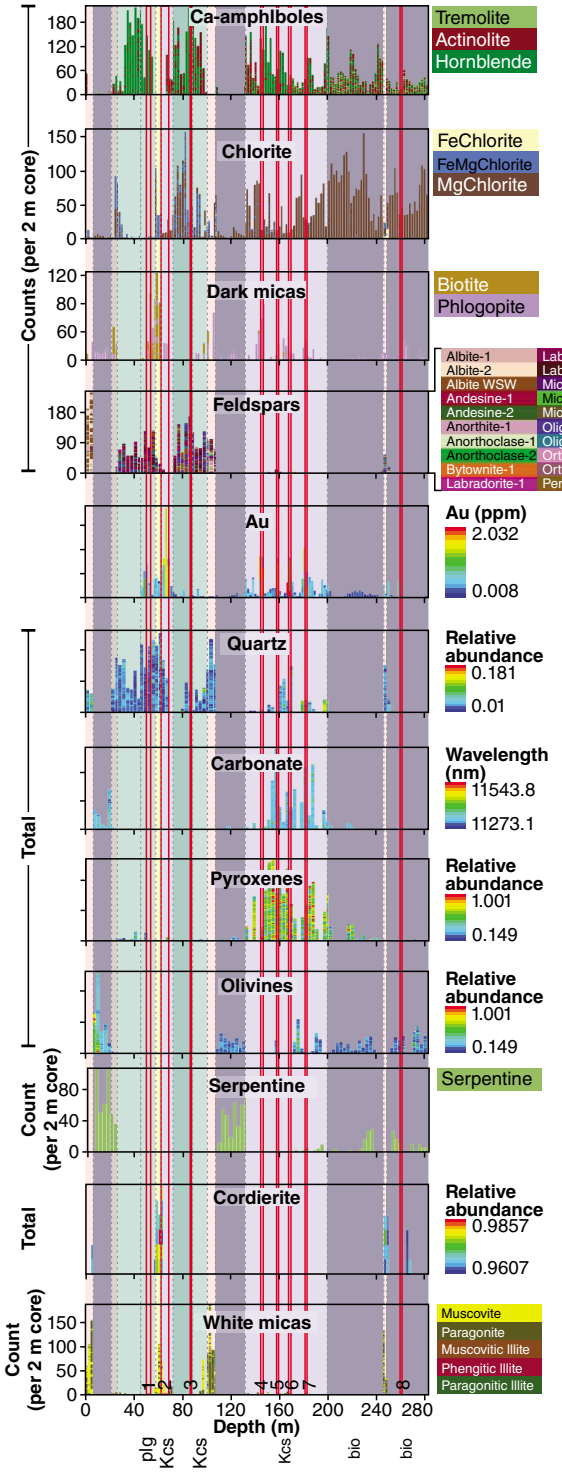

O'BRIEN, OBRD067

Ultramafic rock – Serpentinite

Least-altered ultramafic: Various combinations of talc, Ca-amphibole (tremolite) and metamorphic olivine partly retrogressed to serpentine. Tremolite absent in unaltered very magnesian ultramafics.

Spectral response

Dominant olivine, serpentine, and garnet with weak to moderate Ca-amphibole, biotite, biotite/chlorite, carbonate in MgO-rich units; garnet identification erroneous; quartz and feldspar absent.

Kcs and bio alteration: biotite: amphibole between 1:2 and 2:1, and <1:2, respectively.

Spectral response

Biotite and chlorite, in addition to Ca-amphibole.

Dark mica in serpentinite at 7–20 m not recognized visually.

Gold-related Kcs alteration at ~140–200 m associated with unique broad zone of quartz, pyroxene and carbonate (TIR) enrichment; mineralization at 50–90 m correlates with a broad halo of quartz enrichment.

Barren shear zone

Talcy, biotite-rich (Kb) alteration on sheared contact between serpentinite and mafic rock.

Spectral response

High quartz, biotite and chlorite at expense of Ca-amphibole (talc not identified).

Mafic rock – Amphibolite

Least-altered mafic: Medium-grained foliated amphibolite (?metagabbro).

Spectral response

Dominant Ca-amphibole, feldspar (oligoclase-labradorite) and quartz; quartz not identified visually.

Kcs alteration (90–101.5 m): biotite: amphibole between 1:2 and 2:1

Spectral response

Reflected in progressive increase in dark mica signal at expense of Ca-amphibole.

Mafic rock – Dolerite

Least-altered dolerite: Massive to banded, medium-grained metadolerite

Spectral response

Dominant Ca-amphibole, chlorite, and feldspar (albite-oligoclase); inverse relationship between (?retrograde) chlorite and Ca-amphibole.

Sediment – Median Mylonite?

Quartz-biotite-sillimanite-feldspar schist with sulfide-rich bands.

Spectral response

Dominant quartz, dark mica, white mica, cordierite with less feldspar (microcline) and chlorite; Ca-amphibole absent; sillimanite not identified but abundant cordierite (not identified visually) detected.

Pegmatite

Coarse-grained quartz, feldspar.

Spectral response

Dominant quartz and feldspar (albite and microcline); strong white mica; Ca-amphibole, chlorite, pyroxene, garnet, olivine low to absent. Cordierite is a misidentification.

WW824 05.10.16

Gold lode

1	3.14 m @ 0.53 g/t Au	5	1.00 m @ 1.28 g/t Au
2	6.15 m @ 0.98 g/t Au	6	1.65 m @ 1.15 g/t Au
3	0.51 m @ 1.22 g/t Au	7	1.00 m @ 1.27 g/t Au
4	2.00 m @ 1.23 g/t Au	8	1.00 m @ 0.69 g/t Au

Figure 3.105. Spectral log showing auriferous intersections and annotations indicating rock types and associated hydrothermal alteration (at base of graphic log), core OBRD067, O'Brien lodes, Marvel Loch gold deposit, Southern Cross district, Youanmi Terrane. Green intervals denote undivided mafic rock; dark green interval denotes dolerite; purple intervals denote undivided ultramafic rocks; dark purple intervals denote serpentinite; yellow interval denotes metasedimentary rock; pink interval denotes pegmatite; grey interval denotes shear zone. See text and Figure 3.106 for key to alteration types.

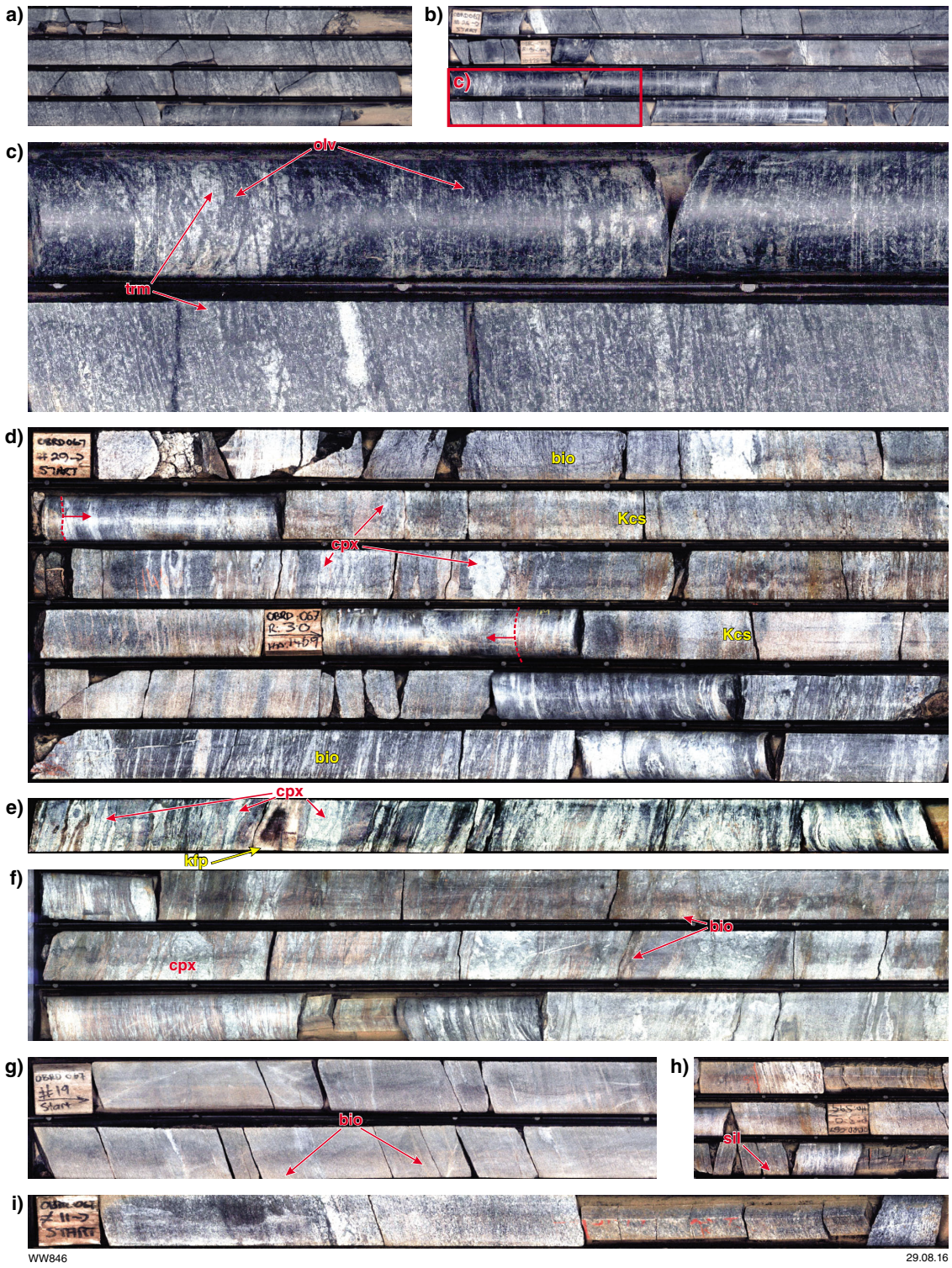

Figure 3.106. Core photos from OBRD067 showing unaltered and altered rock types. a) 109.5–112.5 m, foliated high-Mg ultramafic unit with abundant metamorphic olivine (black, partly serpentinized) and interstitial tremolitic amphibole and talc. b) 127.9–131.5 m, as for panel a. c) Enlargement of area outlined in red in panel b, highlighting metamorphic olivine (dark, olv) and interstitial areas dominated by tremolitic amphibole (pale, trm). d) 144–149.3 m, hydrothermally altered ultramafic unit subdivided into bio and Kcs alteration reflecting the proportions of biotite and amphibole; upper and lower boundaries of >0.5 g/t Au ore zone indicated by broken red lines and red arrows. e) 159.1–160 m, 1.28 g/t Au interval showing Kcs alteration and abundant diopside veins (cpx); a possible thin proximal zone of Kfp alteration is indicated. f) 168–170.7 m, 1.15 g/t Au interval showing Kcs alteration and diopside veins (cpx); thin zones of proximal Kfp alteration may also be present but are difficult to distinguish in the photo from hydrothermal biotite (bio). g) 92.4–93.5 m, mafic unit showing Kcs alteration defined by hydrothermal biotite (bio). h) Metasedimentary unit, indicating sillimanite (white flecks, sil). i) 51–52 m, mafic-hosted, low-grade mineralization characterized by weak plagioclase alteration (bleaching). Alteration codes shown in yellow; mineral codes shown in red.

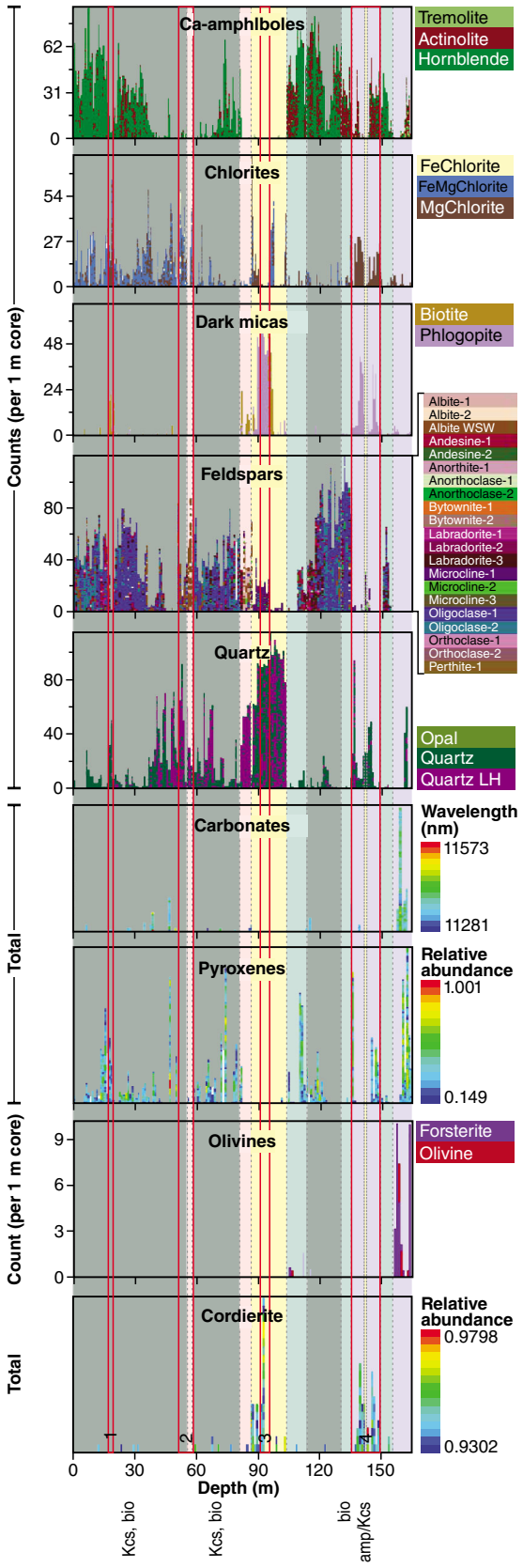

FIRELIGHT, FLRD052

Ultramafic rock

Least-altered high-Mg ultramafic: Talc-forsterite metamorphic assemblage below 154.5 m; cut by quartz-diopside vein at 160.6–161.6 m.

Spectral response

Unique dominant olivine in high-Mg unit; also minor chlorite; strong pyroxene, carbonate, Ca-amphibole (tremolite) and quartz abundance coincident with quartz-pyroxene vein.

Amp/Kcs alteration: Proximal amphibole alteration (matted amphiboles dominant) and medial Kcs alteration (biotite and amphibole subequal).

Spectral response

Strong amphibole and dark mica + (?retrogressive) chlorite response in absence of significant feldspar (except in thin pegmatite intrusion); also variable but inversely correlated silica and pyroxene peaks, reflecting quartz and diopside veins, respectively. Strong cordierite response is suspect.

Amp alteration volumetrically minor; not differentiated.

Mafic schist – ?metabasalt

Least-altered mafic schist: Medium-grained, foliated amphibole and feldspar, and bands of diopside.

Spectral response

Dominant Ca-amphibole and feldspar (oligoclase-andesine) with minor chlorite; quartz and pyroxene identify quartz and diopside veins, respectively.

Bio alteration: minor biotite (biotite:amphibole <1:2)

Spectral response

Weak chlorite response (?retrogressed biotite)

Mafic rock – Meta-dolerite

Least-altered meta-dolerite: Medium-grained, foliated amphibole - plagioclase assemblage.

Spectral response

Strong Ca-amphibole and feldspar (oligoclase-labradorite) response; pyroxene and quartz responses of variable intensity relate to diopside- and quartz-rich veins, respectively.

Mafic rock – Meta-gabbro

Kcs, bio alteration: Foliated, medium- to coarse-grained amphibole - plagioclase - biotite assemblage with variable abundance of diopside veins and calc-silicate alteration.

Proportion of biotite: amphibole varies from <1:2 (bio) to within the range 1:2 to 2:1 (Kcs).

Spectral response

Dominant Ca-amphibole, feldspar (oligoclase–albite), and chlorite; biotite response weak (probably misidentified as chlorite).

Antithetic relationship between chlorite and silica versus Ca-amphibole consistent with interpretation of hydrothermal biotite and quartz (the latter not recognized visually).

Variable pyroxene abundance generally correlates with cm-scale diopside-rich veins or calc-silicate (diopside - plagioclase) alteration.

Sediment

Banded to foliated quartz-biotite-sillimanite-feldspar rock with sulfide-rich bands.

Spectral response

Very strong quartz response, with strong but variable dark mica, chlorite, and weaker feldspar (K-feldspar); carbonate, Ca-amphibole, pyroxene weak to absent; cordierite response in upper part of unit is probably erroneous.

Pegmatite

Coarse-grained quartz, feldspar ± biotite and/or muscovite.

Spectral response

Dominant quartz and feldspar (albite and microcline); strong white mica (not shown); dark mica and chlorite weak to absent.

WW822 05.10.16

Gold lode

1 1.9 m @ 1.04 g/t Au
2 2.5 m @ 0.51 g/t Au
3 4.4 m @ 0.79 g/t Au
4 13.8 m @ 2.13 g/t Au

Figure 3.107. Spectral log showing auriferous intersections and annotations indicating rock types and associated hydrothermal alteration, core FLRD052, Firelight lodes, Marvel Loch gold deposit, Southern Cross district, Youanmi Terrane. Green intervals denote undivided mafic rock; dark green intervals denote gabbro or dolerite; purple intervals denote undivided ultramafic rocks; yellow interval denotes metasedimentary rock; pink intervals denote pegmatite. See text and Figure 3.108 for key to alteration types.

a)

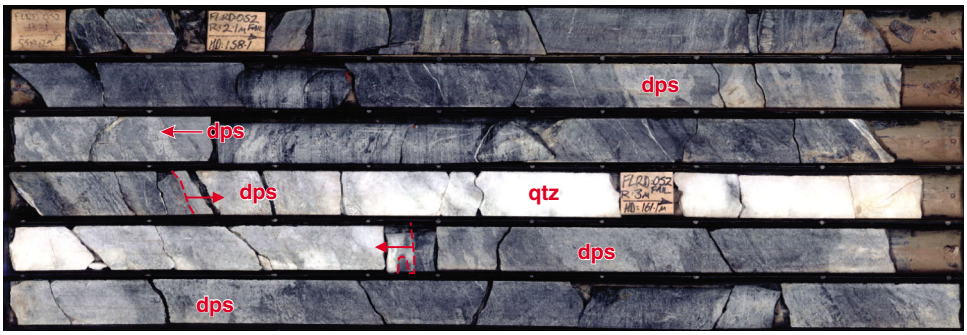

b)

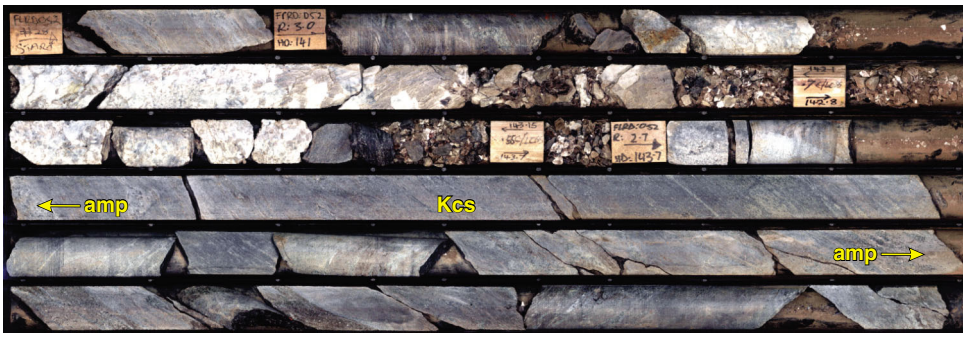

c)

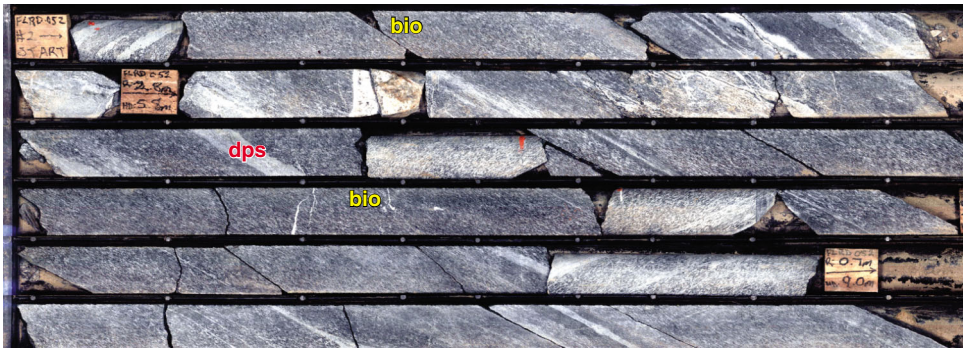

d)

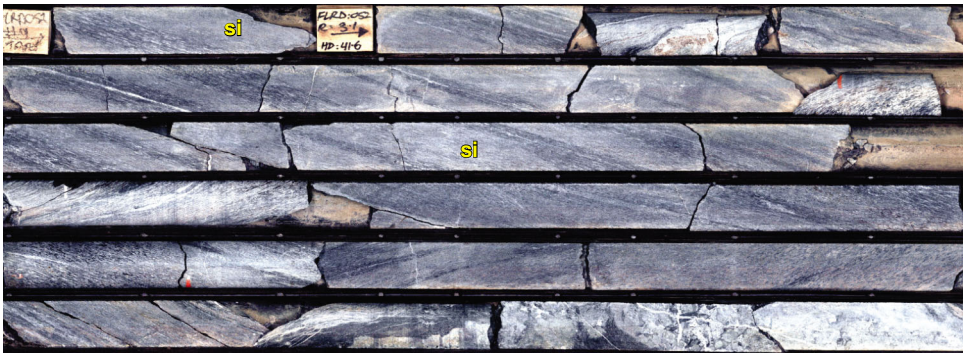

e)

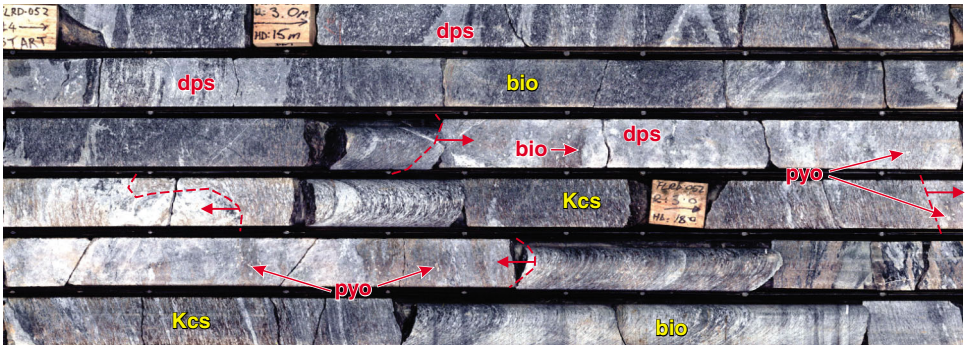

WW847 29.08.16

Figure 3.108. (opposite) Core photos illustrating features of FLRD052 (Firelight) referred to in the text. a) 158–163 m, high-Mg ultramafic unit comprising metamorphic olivine (forsterite), tremolitic amphibole, and talc; a quartz (qtz)–diopside (dps) vein between 160.6 and 161.6 m is indicated, as are several diopside-only veins (dps) above and below. b) 140.6–146.6 m, ultramafic unit with Kcs alteration (overall bio:amp >1:2 but <2:1) cut by pegmatite dyke; note narrow bands of proximal amphibole (amp) alteration characterized as matted, coarse-grained amphiboles. c) 5.9–9.9 m, foliated metagabbroic unit with biotite (bio) alteration (overall bio:amp <1:2) and cut by centimetre-scale diopside-rich veins (dps). d) 41.4–46.7 m, strongly foliated metagabbroic unit with zones of silicification (si). e) 14.8–20.1 m, auriferous quartz–biotite–carbonate–diopside–pyrrhotite (pyo) veins (delineated by red broken lines and arrows) within bio and Kcs alteration of metagabbroic unit; note the diopside-rich veins (dps) above the auriferous vein. Alteration codes shown in yellow and mineral codes shown in red.

As was the case in hole OBRD067 (O'Brien development), high-Mg ultramafic rock intersected at the bottom of the hole is characterized by metamorphic olivine (forsterite), tremolitic amphibole, and talc. A large quartz–diopside vein is present between 160.6 and 161.6 m, and diopside-rich, quartz-poor veins, up to about 10 cm across, are present for almost a metre either side of the quartz–diopside vein (Fig. 3.108a). Spectrally, the unaltered ultramafic unit is defined by strong olivine and tremolitic Ca-amphibole responses; the quartz–diopside vein is distinguished by peaks in pyroxene, carbonate, and quartz abundance, at the expense of olivine (Fig. 3.107). The main ore zone, between 135 and 150 m (4 in Fig. 3.107), is potassic calc-silicate (Kcs) altered with thin intervals of amphibole-rich (amp) alteration, and is cut by a thin pegmatite intrusion at 142 m (Fig. 3.108b). Amphibole in Kcs alteration zones is tremolitic, whereas that in amphibole alteration zones appears less magnesian (?hornblende, ?actinolite). The spectral signature of the Kcs alteration zones combines actinolitic Ca-amphibole, chlorite, dark mica (biotite), and cordierite with variable quartz (in quartz-dominant veins) and pyroxene (in diopside-dominant veins) (Fig. 3.107). The presence of cordierite could not be confirmed visually and is almost certainly an erroneous TSA identification.

The only vector to this ore zone, determined from HyLogger spectral data, is a progressive increase in the strength of K-feldspar spectra with proximity to ore from 120 m (15 m into the hangingwall), and from 155 m (6 m into the footwall; Fig. 3.101d). This vector appears to be independent of the thin pegmatite dyke at 145 m (within the lode).

Mafic rocks below the metasedimentary unit are foliated, fine- to medium-grained, amphibole-rich rocks containing some pale-green diopsidic bands and are probably metamorphosed high-Mg basalt. They are lithologically similar to medium-grained foliated mafic schist in hole OBRD067 (O'Brien) and are similarly defined by a spectral signature comprising predominant Ca-amphibole with variable feldspar (oligoclase–labradorite; Fig. 3.101d) and minor amounts of chlorite. Variable but mostly minor spectra reported as quartz are visible in the core as minor quartz veins. Minor spectra reported as pyroxene are visible in the core as diopside veins or bands of calc-silicate alteration. Spectra for the metadolerite unit are dominated by Ca-amphibole and plagioclase (oligoclase–labradorite). Below the dolerite unit, bands of metasomatic biotite (bio alteration) in mafic schist are recorded by TSA only as minor amounts of chlorite (Fig. 3.107), probably a misidentification of biotite.

Above the metasedimentary unit, the gabbroic unit is coarse-grained and similar to that seen in hole UNRD331 (Undaunted; Fig. 3.103). The varying hydrothermal biotite content of this unit was logged as bio and Kcs alteration (Fig. 3.108c); however, for the most part, biotite appears to have been misreported by TSA as chlorite (Fig. 3.107). The diminished abundance of Ca-amphibole spectra, coincident with elevated quartz, provides a possible vector for tens of metres around the low-grade gold lode and pegmatite at about 60 m depth. This silica-rich interval coincides with increased strain intensity and bleaching (interpreted as silicification; Fig. 3.108d). Pyroxene peaks are more irregularly distributed through the gabbro unit and are probably a response to mostly barren calc-silicate (diopside) alteration and veins (Fig. 3.108c). The gold lode at about 18 m is, however, coincident with a unique combination of pyroxene, quartz, dark mica, and chlorite peaks matched by only minor peaks for feldspar and Ca-amphibole (Fig. 3.107). This spectral combination maps a large (metre-scale) calc-silicate vein containing coarse disseminated pyrrhotite (Fig. 3.108e). Any gradients that might be used as a vector to ore in the lode at 18 m are very steep and of limited width. The gradients in mineral abundance around the low-grade interval at 60 m are much broader, but might be related to deformation and pegmatite emplacement as much as to gold deposition. There are no evident vectors defined by plagioclase or K-feldspar spectra for these shallower gold lodes.

The metasedimentary unit ('median mylonite') is a quartz–biotite–chlorite–sulfide (mainly pyrrhotite) unit containing abundant feldspar and, below 97 m, sillimanite. TSA records dominant quartz and dark mica but does not appear to recognize the sillimanite. The identification of cordierite could not be confirmed petrographically and may be erroneous. Feldspar is recorded as microcline (Fig. 3.101d). Pegmatites are recorded by HyLogger as quartz, feldspar (albite), and white mica (not shown in Fig. 3.107) with or without dark mica. A broad halo of spectrally identified K-feldspar around the metasediment-hosted lode is similar to that around the deeper gold lode, but the association is complicated by the strong presence of K-feldspar in the metasedimentary unit.

Model 2 deposits

Golden Pig

The Golden Pig deposit (~0.5 Moz Au) is about 1 km northwest of Southern Cross township. The geology of the Golden Pig gold mine was described by Nugus et al. (2003) and is also discussed under Targeting Criterion 3.7.

Diamond hole GPD1464 at Golden Pig intersected 38 m of ultramafic rock followed by a thin banded iron-formation (BIF-1; Fig. 3.109 inset) and then more than 40 m of altered mafic rock, before intersecting the target unit, the banded iron-formation (BIF-2) that hosts J Lode (Fig. 3.109). Hole GPD1464 intersected 2.9 m at 24.55 g/t Au and 1.35 m at 22.14 g/t Au, both in BIF-2a. The three intersections of iron-formation can be interpreted as a single folded unit (Fig. 3.109 inset). The thick mafic unit that forms the footwall to the banded iron-formation is characterized by sea-floor alteration of varying intensity, which has been metamorphosed to a biotite–cordierite assemblage (KMg alteration; Witt and Hagemann, 2012). There is a thin but richly auriferous intersection of 1.9 m at 34.04 g/t Au (67.6–69.5 m) within the altered mafic unit, about 15 m below (uphole from) the BIF-2 footwall contact (Fig. 3.109).

The banded iron-formation intersections in hole GPD1464 are recognized in the HyLogger spectra as strong responses to silica (quartz) with little or no feldspar (Fig. 3.109). Only the footwall mafic unit (locally) contains as much quartz as the iron-formations, but these quartz-rich intervals in the mafic unit are accompanied by spectra indicating the presence of Ca-amphibole, chlorite, dark mica and feldspar. The definitive iron-formation TIR signature is well demonstrated by BIF-1, which is a typical, but poorly mineralized, quartz–grunerite–magnetite banded iron-formation (Fig. 3.110a–c). A poor response to grunerite–cummingtonite in BIF-2 is accounted for by interference from pyrrhotite, which is more abundant in BIF-2 than in BIF-1 (Fig. 3.110d–g). Pyrrhotite-rich core intervals generate peaks in the TIR Background Offset (height of background curve, equivalent to a blank sample) and this parameter can be used to identify sulfide-rich intervals, though not all of these are auriferous.

Another major, but inconsistent, response to banded iron-formation is identified as pyroxene by TSA (Fig. 3.109). Visual observations of the core reveal that pyroxene is locally present as coarse-grained quartz–pyrrhotite–clinopyroxene (hedenbergite) veins and possibly also as replacement clinopyroxene in adjacent wallrocks (Fig. 3.110d–g). In the Southern Cross district, these quartz–pyrrhotite–clinopyroxene veins in banded iron-formation are typically associated with ore-grade gold, and the strong response of pyroxene from BIF-2a, coincident with the main lode development, supports this observation. Quartz–pyrrhotite–clinopyroxene veins are less well developed in the weakly mineralized BIF-2b (Fig. 110g), accounting for the poor pyroxene spectral response. Although quartz–clinopyroxene veins are present in BIF-1 (Fig. 110a), they are clinopyroxene rich and sulfide poor, so they are poorly mineralized (best intersection of 0.34 g/t Au) and the grunerite spectral response is not suppressed in the BIF-1 unit.

The ultramafic hangingwall unit in hole GPD1464 is predominantly tremolite(–chlorite) rock, but can be subdivided into ultramafic rocks that contain olivine and those that do not (Fig. 3.109). The presence and absence of metamorphic olivine (Fig. 111a–c) probably reflects the MgO content (B-zones and A-zones of the original komatiitic flows; Arndt et al., 1977; Perring et al., 1995). The recognition of B-zones and A-zones allows individual komatiite flows to be recognized (Fig. 111a). The broader-scale downhole increase in the abundance of amoeboid olivine porphyroblasts above BIF-1 (Fig. 3.109) suggests that the younging direction is uphole, consistent with the district-wide hangingwall position of the ultramafic unit with respect to the banded iron-formation. Local retrogression of metamorphic olivine to talc and serpentine complicates the spectral definition of komatiite B-zones and A-zones at the scale of individual komatiite flows, but there is sufficient preservation of olivine in core GPD1464 to determine the younging direction in the compound flow sequence, and this is evident in the spectral log (Fig. 3.109).

The footwall mafic unit displays evidence for strong pre-metamorphic (sea-floor) hydrothermal (KMg) alteration. Although not studied in detail at Golden Pig, the footwall mafic unit at several other localities in the Southern Cross greenstone belt contains moderate to abundant modal biotite and cordierite (Witt and Hagemann, 2012). Immobile element data demonstrate that these rocks were originally mafic and developed their present peraluminous composition through pre-metamorphic leaching of Ca and Na and enrichment of K and Si (Barker, 1998; Bodycoat, 1999). The altered mafic rocks in core GPD1464 vary from foliated and banded biotite-amphibolite (e.g. 40–50 m; Fig. 3.111d–f) to lighter-coloured grey-green rocks in which cordierite is relatively abundant (e.g. 50–65 m; Fig. 3.111g–i). Banding throughout the footwall mafic unit, as at other localities, is defined by deformed calc-silicate veins that are typically zoned from diopside-rich centres (dps in Fig. 3.111g) to hornblende-rich margins. The veins are interpreted as metamorphosed, barren dolomite–quartz veins, probably formed coeval with sea-floor alteration.

The footwall mafic unit is defined by spectra that identify the co-occurrence of Ca-amphibole, plagioclase, dark mica (biotite), chlorite (probably misidentified biotite), and quartz. Cordierite and pyroxene (diopside in calc-silicate veins) may also be present but in varying abundance (Fig. 3.109). The thin gold lode hosted by the footwall mafic unit (67.6–69.5 m) is a very pyrrhotite-rich interval (Figure 3.112a,b) in which the main spectral responses are identified as carbonate and silica (quartz). The unit was logged as banded iron-formation by mine geologists, but the spectral signal for quartz is weak and there is little evidence of meso-banding in core photos (Fig. 3.112a,b).

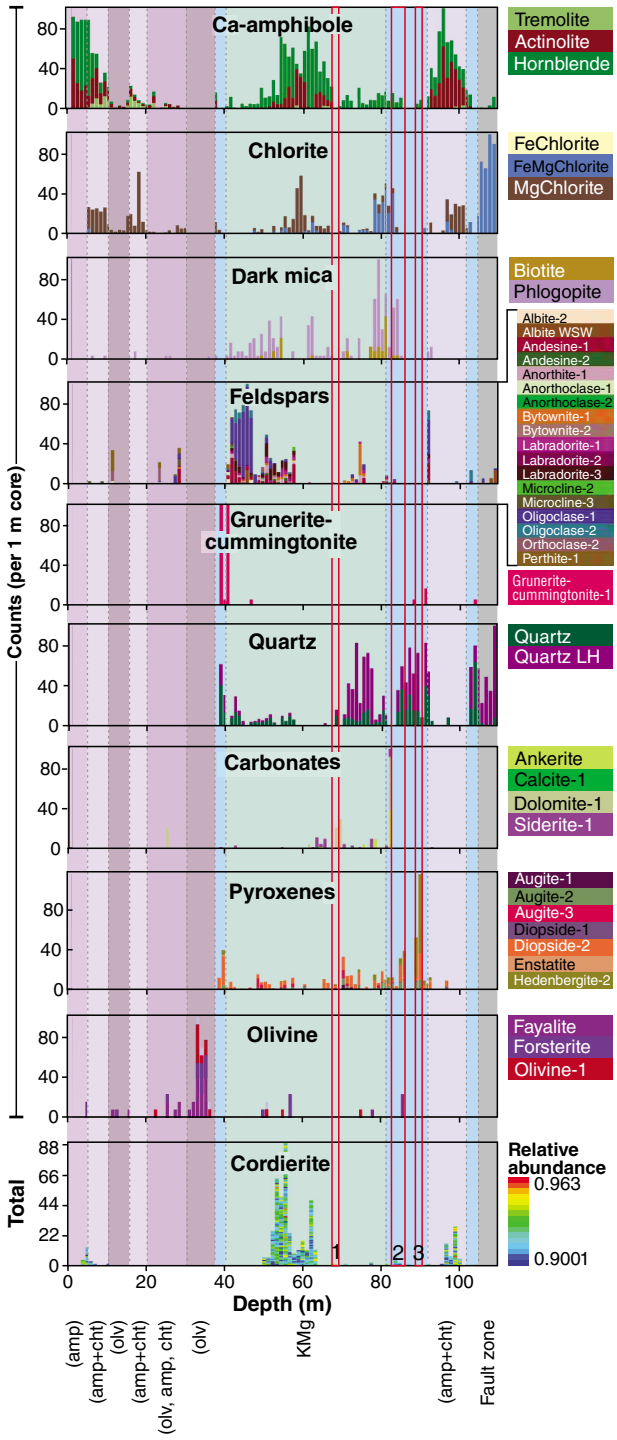

GOLDEN PIG GPD1464

Banded iron-formation
Spectral response
Silica (quartz) +/- grunerite-cummingtonite (+/- clinpoyroxene)
Ca-amphible and feldspars low abundance to absent
NOTE: Pyroxene occurs in BIF-hosted quartz-hedenbergite+/-pyrrhotite veins and, where sulfide-rich, carry most of the gold mineralization.

Ultramafic rock
Spectral response
Most magnesian: Olivine (+/- amphibole, chlorite)
Less magnesian: Amphibole + chlorite
Least magnesian?: Amphibole only
Down-hole variations from 0 to 37.5 m probably reflect komatiite magma fractionation and indicates up-hole younging.

Mafic rock
All mafic rocks in this hole are altered - mainly KMg alteration (quartz-plagioclase-amphibole-biotite-cordierite) and mostly contain zoned diopside-amphibole (calc-silicate) veins
Spectral response
Silica (quartz) + plagioclase + amphibole + biotite (+/- cordierite, chlorite, pyroxene)
Variations within unit: increasing quartz and biotite, and deceasing amphibole and cordierite abundance with increasing proximity to BIF units, interpreted as increasing strength of K-Si metasomatism.
Variations in clinopyroxene (diopside) response indicate relative abundance of calc-silicate veins.

Cordierite signal at <10 m and between BIF-2a and BIF-2b suspect - not generally observed in Southern Cross ultramafic rocks.
Garnet identification (not shown) in ultramafic units definitely misleading - no field recognition of garnet in ultramafic rocks and not recognized in core photos. Similarly, the identification of minor olivine in the footwall mafic unit is also considered erroneous.

Gold mineralization: Broad gradients in strength of silica (quartz) and dark mica (biotite), inversely proportional to Ca-amphibole and chlorite, provide a broad vector to BIF-hosted lodes, with stronger signal adjacent to better lode in fold hinge. Vector provided by metamorphosed sea-floor alteration in footwall basalt.

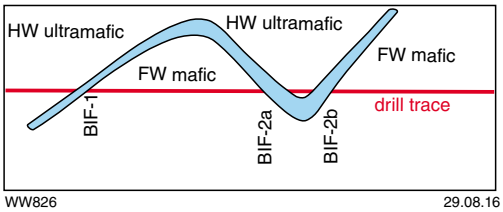

Gold lode
1 1.9 m @ 34.04 g/t Au
2 2.9 m @ 24.55 g/t Au
3 1.35 m @ 22.14 g/t Au
J Lode

Figure 3.109. Spectral log showing auriferous intersections and annotations indicating rock types and associated hydrothermal alteration (at base of graphic log), core GPD1464, Golden Pig gold deposit, Southern Cross district, Youanmi Terrane. Green intervals denote undivided mafic rock; shades of purple intervals denote various metamorphic assemblages in ultramafic rocks (amp, amphibole; cht, chlorite; olv, olivine); blue intervals denote banded iron-formation; grey interval denotes shear zone. See text and Figure 3.110 for key to alteration types. Inset diagram at bottom right is an interpretation relating three BIF intersections to the same folded unit; HW and FW indicate hangingwall and footwall, respectively.

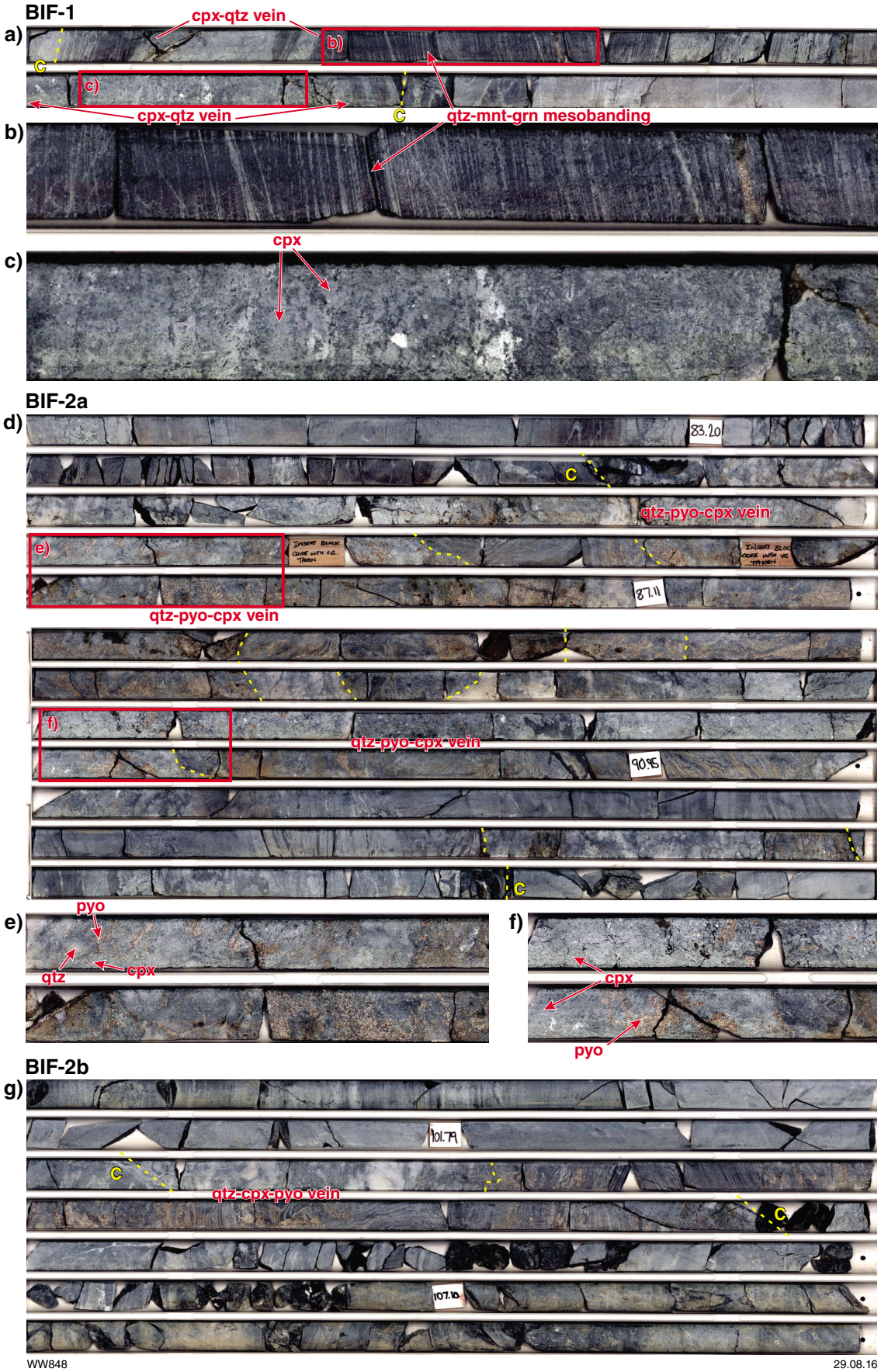
BIF-1
a)
cpx-qtz vein
b)
c)
C
cpx-qtz vein
C
qtz-mnt-grn mesobanding
b)
cpx
c)
BIF-2a
d)
83.20
C
qtz-pyo-cpx vein
e)
87.11
qtz-pyo-cpx vein
f)
qtz-pyo-cpx vein
90.95
C
e)
pyo
qtz
cpx
f)
cpx
pyo
BIF-2b
g)
101.79
C
qtz-cpx-pyo vein
C
107.10
WW848
29.08.16

Figure 3.110. (opposite) Photos of core in banded iron-formation units, core GPD1464, Golden Pig gold deposit. a) 38–40 m, complete intersection of BIF-1 with contacts shown as broken yellow lines and marked C; sulfide-poor clinopyroxene (hedenbergite)–quartz veins indicated; locations of panels b and c outlined in red. b) Detail of quartz–magnetite–grunerite mesobanding in BIF-1. c) Detail of quartz–clinopyroxene vein showing coarse-grained hedenbergite. d) 82.5–94 m, complete intersection of BIF-2a with contacts shown as broken yellow lines marked C; pyrrhotite-rich quartz–sulfide–clinopyroxene (hedenbergite) veins indicated and delineated with unlabelled broken yellow lines; locations of panels e and f outlined in red. e) Detail of quartz–sulfide–clinopyroxene (hedenbergite) vein. f) Detail of quartz–sulfide–clinopyroxene (hedenbergite) vein. g) 100.5–108.5 m (note ~1.5 m of missing core), complete intersection of BIF-2b with contacts shown as broken yellow lines marked C; note sulfide-poor quartz–clinopyroxene (hedenbergite)–sulfide vein on upper contact of BIF-2b (lower contact of vein marked by unlabelled broken yellow line). Abbreviations: cpx (clinopyroxene), grn (grunerite), mnt (magnetite), pyo (pyrrhotite), qtz (quartz).

On the other hand, the mineralized interval is followed by several metres of altered mafic rock with abundant calc-silicate veins (Fig. 3.112a,c). This mineralization is interpreted here as shear-hosted mineralization, similar to that in the Taurus Lode (Fig. 3.37; Nugus et al., 2003).

There are some potential vectors to the mineralized banded iron-formation in the altered footwall mafic unit. Based on the interpretation that BIF-1 and BIF-2 represent the same unit (BIF-1 on an attenuated fold limb and BIF-2 on a thickened fold hinge of the same unit), the abundances of quartz (over ~10 m) and then biotite and chlorite (over ~5 m) increase sequentially (at the expense of Ca-amphibole) from lode 1 towards the footwall contact of the mineralized BIF-2a, located in a fold hinge (Fig. 3.109).

Abundant cordierite at deeper stratigraphic levels within the footwall mafic unit defines an intermediate vector between proximal quartz–biotite/chlorite and distal amphibole–plagioclase (unaltered amphibolite, without cordierite, biotite, silica) assemblages. However, incorrect TSA identification of cordierite in some other holes from Southern Cross (OBRD067, FLRD052, see above) requires that the significance of this mineral at Golden Pig should be viewed with some caution. The cordierite-rich interval reported by TSA is broadly coincident with a change of the plagioclase composition from mainly oligoclase to more calcic compositions (andesine to bytownite; Fig. 3.113a).

It is important to understand that these footwall vectors are not directly related to the gold mineralization event; rather, they are related to pre-metamorphic sea-floor alteration. They nevertheless allow the explorer to target the iron-formation host rock, and the thicker fold hinges. This may be useful in structurally complex areas such as Golden Pig, where the target banded iron-formation has been dismembered and segmented (Nugus et al., 2003). Based on TIR spectral results, mineralized banded iron-formation is coincident with abundant pyroxene (diopside or hedenbergite in veins), but barren diopside-bearing veins are also present at Golden Pig, which means that the presence of pyroxene alone is insufficient to define a gold lode. Pyrrhotite abundance in association with pyroxene-bearing veins is a more reliable indicator of gold mineralization and is readily identified in the field, but may also be identified spectrally by the relatively high background offset and suppression of the grunerite response.

Nevoria

Nevoria gold deposit (~0.8 Moz Au) is about 10 km southeast of Marvel Loch and 40 km southeast of Southern Cross township. The geology of the Nevoria gold mine has been described by Cullen et al. (1990) and Mueller (1997). The mine sequence is similar to that at Golden Pig, except that the banded iron-formation that hosts gold mineralization is a few tens of metres below the mafic–ultramafic contact (Mueller, 1997; Fig. 3.114). The iron-formation defines open folds (D_3 of Witt et al., 2001a) with north-striking axial planes and fold axes that plunge 60° to 75° east. The iron-formation is also offset by northeast-striking sinistral faults, and ore shoots appear to be controlled by the combined effect of thickened fold hinges and short strike lengths of iron-formation isolated between the northeast-striking faults (Fig. 3.114).

Diamond hole NVCD0102 (Fig. 3.115) intersected banded iron-formation at 184–198 m (BIF-1) and at 233–272 m (BIF-2). The hangingwall (above BIF-2) comprises fine-grained tremolitic amphibole and chlorite rock interpreted as metamorphosed low-Mg komatiite and high-Mg basalt. Thin units of similar rock are (?tectonically) interleaved with BIF-2. A hangingwall tholeiitic mafic unit equivalent to that shown in Figure 3.114 could not be distinguished in the NVCD0102 core. Pegmatite dykes are present in the hangingwall sequence, and another obscures the BIF-2 footwall contact.

Gold is found mainly in BIF-1 (16.2 m at 1.71 g/t Au) and BIF-2 (28.8 m at 2.98 g/t Au, excluding interleaved mafic–ultramafic units). There were relatively narrow (1.0 to 1.5 m) intersections of high-grade ore (9.5 to 21.9 g/t Au) on the lower contacts of BIF-2 against each of the two internal ultramafic units and against the footwall pegmatite (Fig. 3.115). The mafic footwall unit was not intersected in NVCD0102. However, dolerite units, possibly equivalent to the late intrusions shown in Figure 3.114, were intersected in the hangingwall.

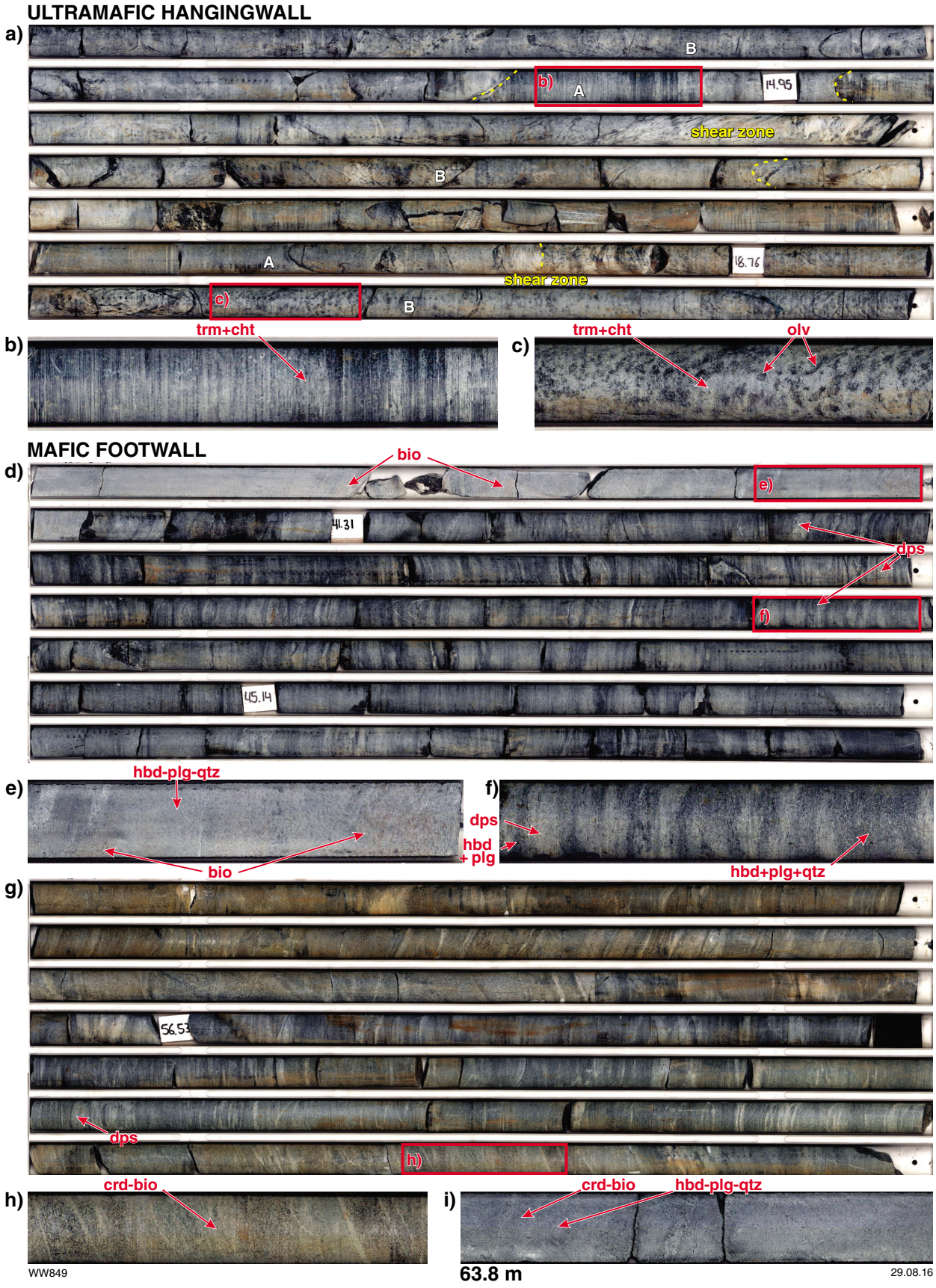
ULTRAMAFIC HANGINGWALL
a)
B
b)
A
14.95
shear zone
B
A
18.76
shear zone
c)
B
b)
trm+cht
c)
trm+cht
olv
MAFIC FOOTWALL
d)
bio
e)
41.31
dps
f)
45.14
e)
hbd-plg-qtz
bio
f)
dps
hbd
+ plg
hbd+plg+qtz
g)
56.53
dps
h)
h)
crd-bio
i)
crd-bio
hbd-plg-qtz
WW849
63.8 m
29.08.16

Figure 3.111. Photos of core in ultramafic hangingwall and mafic footwall units, core GPD1464, Golden Pig gold deposit. a) 13.2–19.9 m, section of hangingwall ultramafic rock showing relatively low-MgO tremolite–chlorite rock (A-zones), and relatively high-MgO rock (B-zones) containing amoeboid olivine porphyroblasts. Approximate contacts between A- and B-zones shown as broken yellow lines. Locations of panels b and c outlined in red. b) Detail of low-MgO tremolite–chlorite rock. c) Detail of high-MgO ultramafic rock with olivine porphyroblasts. d) 40–46.8 m, section of mafic footwall unit dominated by biotite amphibolite. Locations of panels e and f outlined in red. e) Detail of mafic unit showing metasomatic biotite. f) Detail of altered mafic unit showing deformed calc-silicate (diopside) veins. g) 53.6–60.2 m, altered footwall mafic unit that contains cordierite and biotite; location of panel h outlined in red. h) Detail of banded biotite–cordierite altered mafic footwall unit. i) 63.8 m, cut surface of biotite–cordierite altered mafic footwall unit. Abbreviations: bio (biotite), cht (chlorite), crd (cordierite), dps (diopside), hbd (hornblende), olv (olivine), plg (plagioclase), qtz (quartz), trm (tremolite).

As was the case at Golden Pig, the banded iron-formation units are recognized in the HyLogger spectra as strong responses to silica (quartz) and, most distinctively, grunerite–cummingtonite (Fig. 3.115). Minor grunerite–cummingtonite is also found in the magnesian unit separating BIF-1 and BIF-2. However, in this case, there is an antithetic relationship with quartz. The origin of the grunerite–cummingtonite response in this magnesian unit could not be determined from visual inspection of core, but may reflect the presence of minor amounts of cummingtonite, which is common in metabasic rocks in the Southern Cross district. In the BIF units, grunerite can be formed by isochemical hydrous metamorphic reaction between magnetite and quartz, but much of the grunerite in the Nevoria BIFs (and other BIFs in the Southern Cross district) overprints quartz–magnetite mesobanding (Fig. 3.116a–e). The reaction is magnetite-destructive, and is probably the result of metasomatic addition of hydrothermal SiO_2 and H_2O during the gold mineralization process.

Other significant minerals in mineralized banded iron-formation identified by TSA are pyroxene, dark mica, and carbonate (Fig. 3.115). As might be anticipated, spectral responses of feldspar, chlorite, and Ca-amphibole are absent or poor in the banded iron-formation. As was the case in the Golden Pig core (GPD1464), some pyroxene is present in quartz–pyrrhotite–clinopyroxene (hedenbergite) veins, but in NVCD0102 most of the pyroxene is in the form of bedding-parallel to transgressive replacement bands (Fig. 3.116a,d,e). Dark mica (biotite) within the BIF-1 and BIF-2 intervals is associated with contact-related shear zones containing disseminated pyrrhotite and quartz–carbonate–pyrrhotite veins, both in the BIF and the interleaved magnesian units (Fig. 3.116f). TSA misidentified much of the biotite as chlorite in these shear zones, though the shear zones can still be identified by the spectral identification of dark mica (Fig. 3.115). Carbonate is present mainly as late-stage veins and replacement, typically associated with biotite-bearing shear zones. Garnet is identified by TSA in most BIF units, but is not observed in the core (Fig. 3.116) and is almost certainly a misidentification.

The high-Mg to ultramafic unit that forms the hangingwall to BIF-2 in core NVCD0102 is intersected in two main intervals, and comprises fine- to medium-grained amphibole and chlorite (Fig. 3.116f). The uppermost interval (above 120 m) also contains minor amounts of biotite (weak Kcs alteration). The spectral response in both units is dominated by Ca-amphibole and chlorite (Fig. 3.115). In the uppermost unit, the presence of feldspar (oligoclase–labradorite) suggests a high-Mg basalt composition, in contrast to the feldspar-free, more magnesian ultramafic composition of the unit between 200 and 233 m. Chlorite is antithetically related to Ca-amphibole and feldspar; the more chloritic rocks possibly have more magnesian bulk compositions. The white mica, carbonate, and quartz responses in mafic to ultramafic rocks are highly variable and appear to be related to alteration in shear zones and around late-stage quartz and pegmatite veins (e.g. there is a thin pegmatite unit between 222 and 226 m that is too small to show in Fig. 3.115). The dark mica, pyroxene, and grunerite–cummingtonite responses are weak to absent in these units, despite the field observation of biotite in the uppermost unit. Chlorite identified by TSA probably includes metasomatic biotite (misidentified) as well as metamorphic chlorite.

Late intrusions of dolerite are composed of medium-grained plagioclase and amphibole. The spectral response is dominated by Ca-amphibole, feldspar (oligoclase), and chlorite (Fig. 3.113). Ca-amphibole is identified by TSA as predominantly hornblende, in contrast to the actinolitic composition of Ca-amphibole in more magnesian unit above 120 m. Chlorite may be at least partly a retrogressive phase after Ca-amphibole. Minor quartz and carbonate responses, especially between 170 and 180 m, are possibly related to late-stage quartz(–carbonate) veins observed in the core. Coarse- to very coarse-grained granite pegmatite dykes intrude BIF-2 and the hangingwall sequence. The spectral response of the pegmatite is predominantly quartz, feldspar (albite, microcline), and white mica (Figs 3.115 and 3.113b). Although quartz generates a more consistently strong response than the other minerals, the presence of alkali feldspar (albite, K-feldspar), especially in combination with the strong white-mica response, is distinctive. The presence of cordierite in pegmatite intrusions, inconsistently indicated by the spectra, is not supported by field observation or petrography, and is considered erroneous.

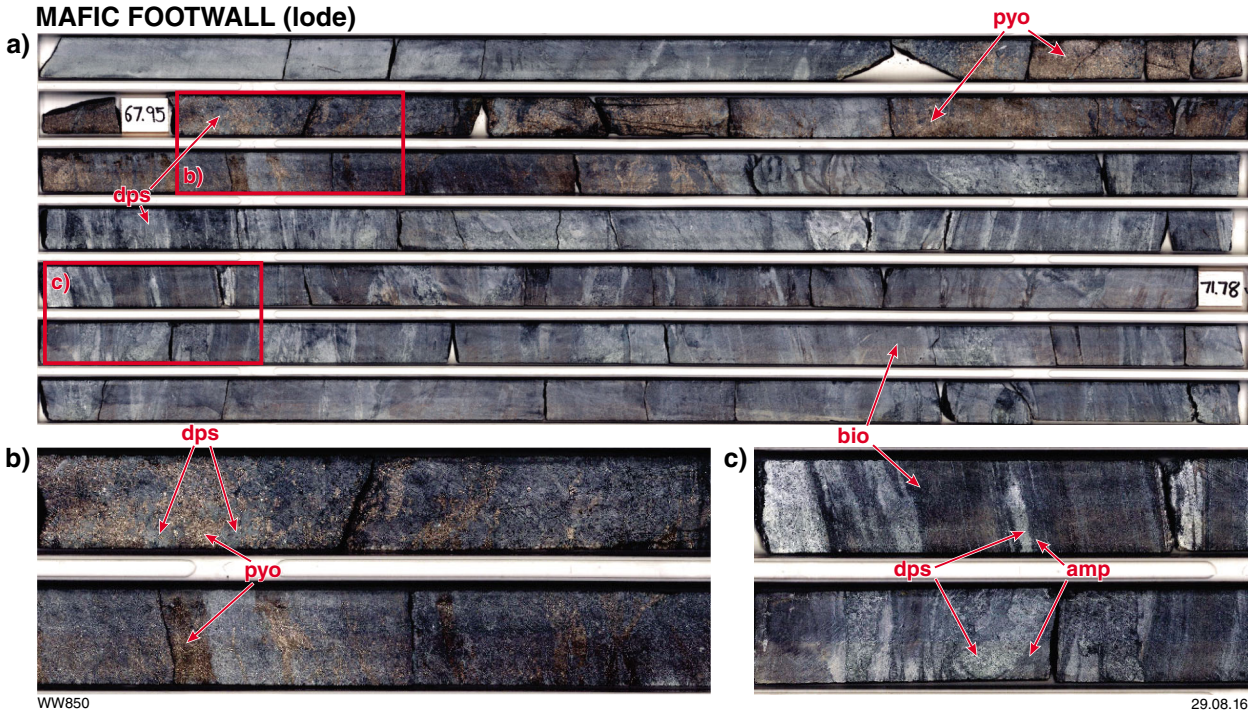

Figure 3.112. **Photos of core in mafic footwall units, core GPD1464, Golden Pig gold deposit. a) 66.9–73.7 m, section of mafic footwall unit hosting 1.9 m at 34.04 g/t Au (pyrrhotite-rich section) and underlying shear zone indicated by numerous calc-silicate veins (dps). Locations of panels b and c outlined in red. b) Detail of mafic-hosted pyrrhotite-rich lode. c) Detail of altered (biotite-rich) mafic and calc-silicate (diopside)-rich veins in shear zone. Abbreviations: amp (amphibole), bio (biotite), dps (diopside), pyo (pyrrhotite).**

Potential vectors to target BIF-hosted gold mineralization at Nevoria include the distributions of carbonate, chlorite, and Ca-amphibole. For example, there is a progressive increase in carbonate abundance towards the BIF-1 (footwall) contact at ~200 m (Fig. 3.115) that is probably related to hydrothermal alteration in the shear zone separating BIF-1 from mafic–ultramafic rock. The increase in carbonate abundance can be recognized over a distance of >20 m into the footwall and about 10 m into the hangingwall of the contact shear zone. There is no comparable shear zone or spectral response to carbonate on the hangingwall (uphole) contact of BIF-1, which is not defined by a shear zone. The potential vector on the footwall contact is not evident from visual inspection of the core. A decrease in Ca-amphibole and chlorite abundance towards the uphole contact of BIF-2 is compensated for by increased white mica abundance (Fig. 3.115). This latter trend is probably related to pegmatite emplacement rather than gold mineralization.

Summary of Southern Cross – Marvel Loch HyLogger results

Despite apparent erroneous identification of some minerals, such as cordierite and garnet, and the probable misidentification of some biotite as chlorite, it is possible to use HyLogger SWIR and TIR data in combination with TSA software to identify the most common rock types in the Southern Cross district. Diagnostic combinations of minerals identified from the HyLogger spectral data are shown in Table 3.24. Identification is complicated where calc-silicate (diopside) veins are present, but this problem can be minimized by virtue of the simple visual recognition of the veins in drillcore.

The more common alteration types in mafic and ultramafic units in the Southern Cross district are generally distinguished by the addition of dark mica to the minerals reported by TSA, though metasomatic biotite may be reported as chlorite in some cases (Tables 3.25 and 3.26). Proximity to mafic- and ultramafic-hosted lodes can be correlated with decreasing Ca-amphibole and increasing biotite/chlorite abundance, but Hylogger spectra do not consistently record these trends. Large auriferous veins can be recognized spectrally in mafic rocks by a combination of quartz and pyroxene (diopside) with or without dark mica (biotite) and carbonate. This combination of spectrally defined vein minerals is similar to that of metamorphosed sea-floor (KMg) alteration, but the latter can be distinguished by the more consistent presence of feldspar, particularly where the feldspar has relatively calcic composition (andesine–bytownite). In ultramafic rocks, large auriferous veins are defined by pyroxene (diopside) with or without Ca-amphibole, cummingtonite, quartz, and carbonate (Table 3.25). In some cases (though not encountered in

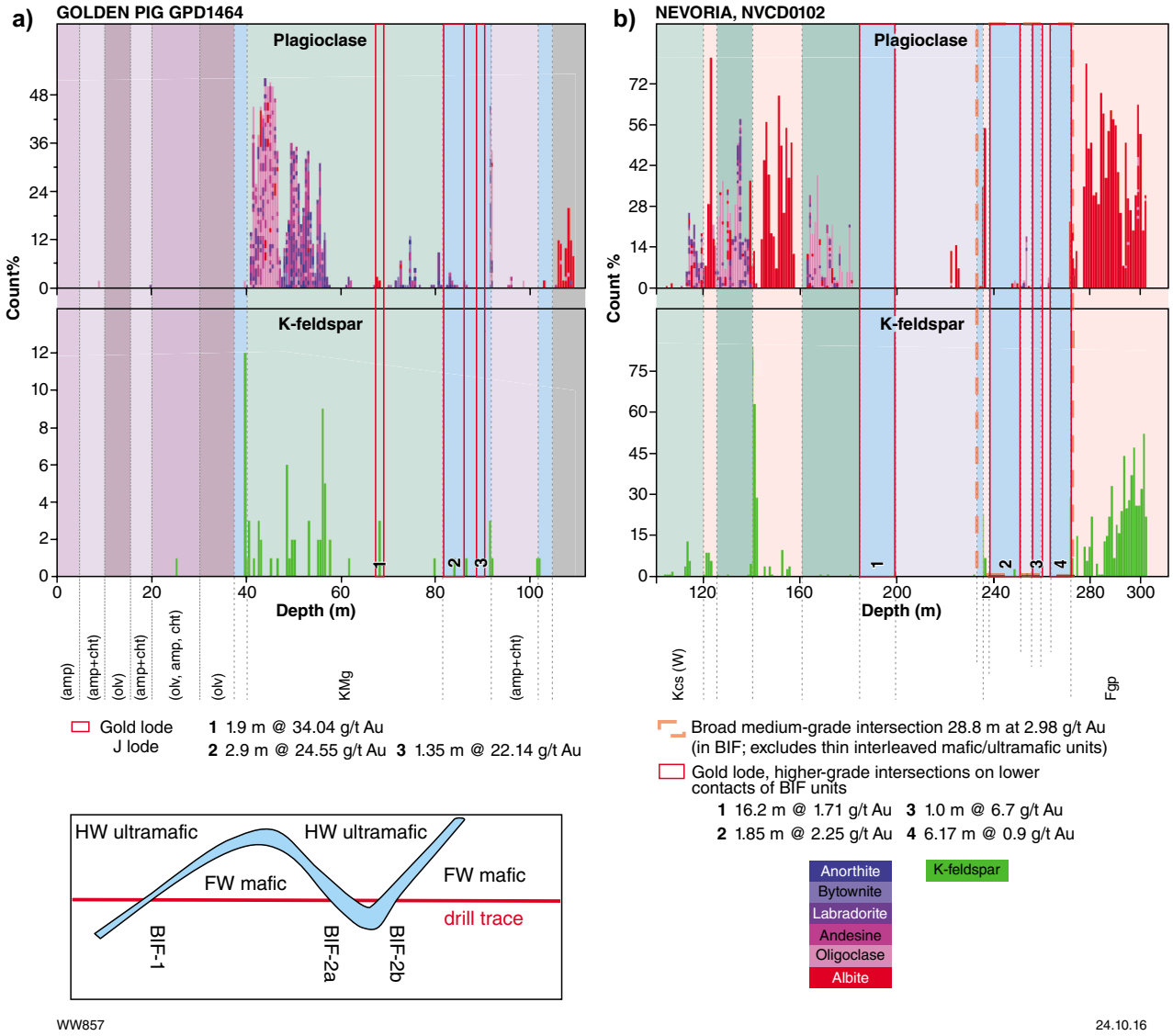

Figure 3.113. **Detailed TIR feldspar spectra from diamond cores: a) GPD1464, Golden Pig; b) NVCD0102, Nevoria. Lithological abbreviations: Green intervals denote undivided mafic rock; dark green intervals denote dolerite; shades of purple intervals denote various metamorphic assemblages in ultramafic rocks (amp, amphibole; cht, chlorite; olv, olivine); blue intervals denote banded iron-formation; pink intervals denote pegmatite; grey interval denotes shear zone. Alteration abbreviations: amp (amphibole), bio (biotite), Kcs (potassic-calcsilicate), KMg (potassic-magnesian), plg (plagioclase). (W) indicates weak alteration. HW and FW indicate hangingwall and footwall, respectively.**

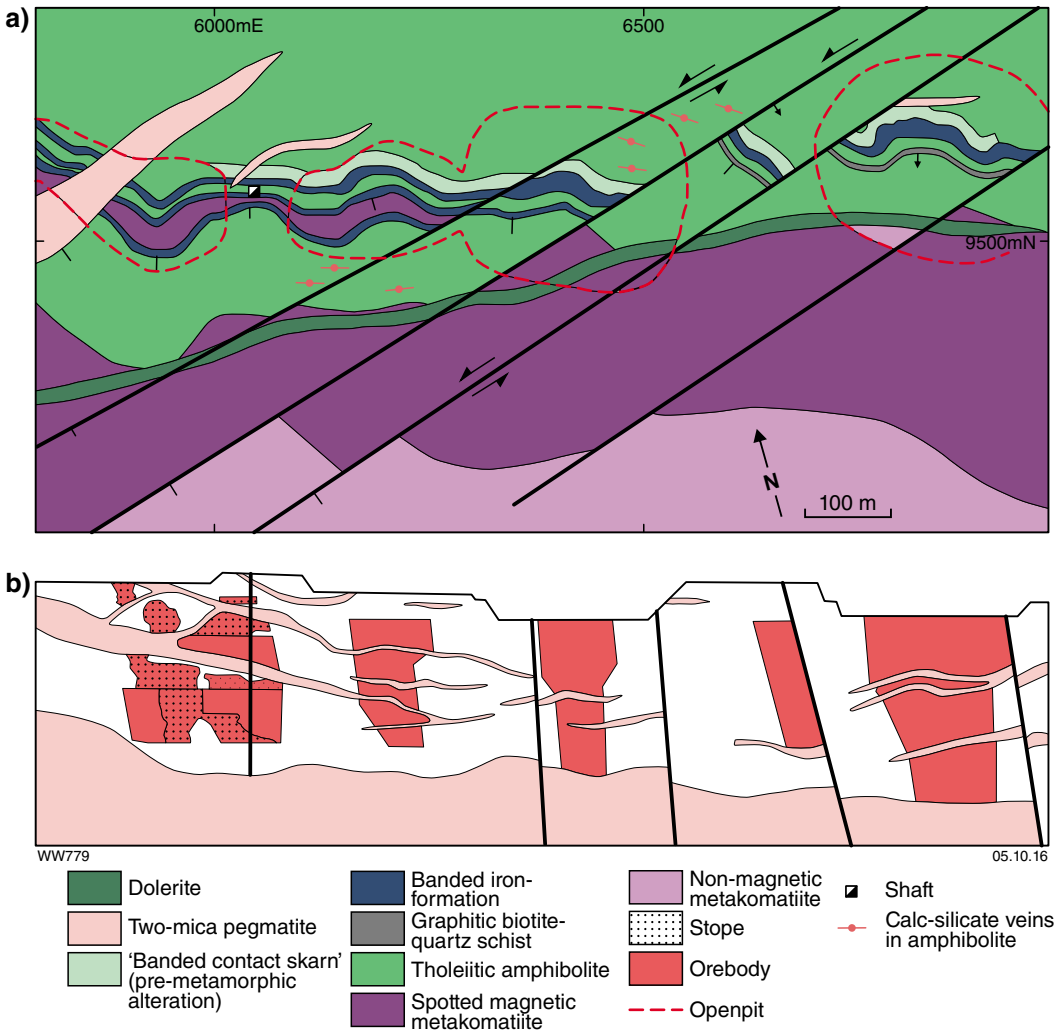

Figure 3.114. Nevoria gold deposit, Southern Cross district, Youanmi Terrane (after Mueller, 1997). a) Geological map; b) longitudinal cross section (9555N, local mine grid) showing mine workings and areas of stoping.

this study), ultramafic-hosted auriferous veins contain forsterite–calcite aggregates (e.g. at Yilgarn Star) that should be detected by the TIR spectrometer. There is little to distinguish unaltered banded iron-formation from altered and mineralized iron-formation in the spectra from Golden Pig and Nevoria (Table 3.27). However, abundant pyrrhotite in mineralized iron-formation might be detected as elevated background offset and suppression of grunerite spectra, or as sulfates where even weak oxidation has occurred (Fig. 3.104).

A number of vectors towards gold mineralization have been recognized in the spectral data, though not all of these are consistently demonstrated for all gold lodes. The most consistent and useful vector appears to be provided by the composition of feldspars in mineralized mafic and ultramafic units (Figs 3.101 and 3.113; Tables 3.25 and 3.26). K-feldspar is present in many of the mafic- and ultramafic-hosted lodes, though it is not always easy to identify visually, and K-feldspar is detected by TSA for ten to several tens of metres beyond the mineralized proximal alteration zone in several of the holes that intersected shear-hosted lodes.

Data from UNRD331 (Undaunted, Marvel Loch) suggest that patchy calc-silicate alteration, defined spectrally by essential pyroxene and feldspar (labradorite), may provide another vector, of similar dimensions, around the Sherwood lodes at Marvel Loch. At Golden Pig, proximity to mineralized banded iron-formation can be gauged by decreases in the abundances of Ca-amphibole and feldspar and sequential increases in the abundances of quartz, followed by dark mica (or chlorite) that might reflect either deformation of the iron-formation contacts or the strength of pre-metamorphic sea-floor alteration. These trends are usually not easily recognized visually. K-feldspar does not appear to be an important component of, or vector towards, gold mineralization in banded iron-formation.

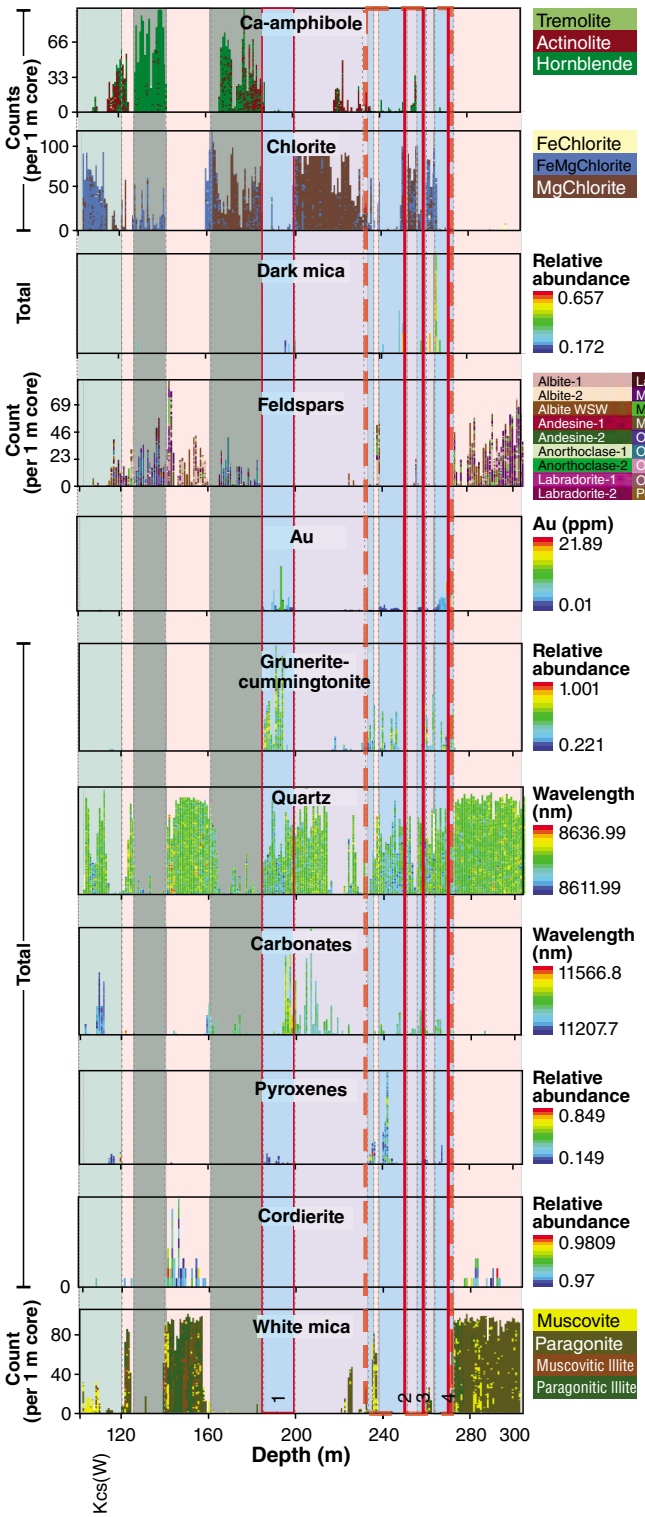

NVCD0102

Banded iron-formation

Banded quartz-grunerite+/-magnetite;quartz-carbonate-pyrrhotite veins;

Spectral response

Dominant quartz and grunerite; variable pyroxene (hedenbergite), carbonate, dark mica (biotite). Percent grunerite-cummingtonite (metasomatic) increases towards mineralized shear vein at 197.5–198 m. Ca-amphibole, feldspar, white mica, chlorite low to absent.

NOTE: The identification of garnet in mineralized BIF is most likely an error as no garnet was identified visually.

Dolerite

Medium-grained amphibole and feldspar

Spectral response

Dominant Ca-amphibole, chlorite and feldspar (oligoclase); no biotite, white mica, pyroxene; subtle veining highlighted by minor to moderate quartz and carbonate response between 170 and 180 m.

Ultramafic/high-Mg basalt

Fine-grained tremolitic amphibole and chlorite, and minor biotite; locally with late-stage quartz veining and related white mica alteration.

Spectral response

Dominant Ca-amphibole and chlorite; feldspar, white mica, pyroxene low to absent. Quartz, carbonate and white mica related to late-stage quartz and pegmatite veins and related alteration.

Pegmatite

Very coarse-grained quartz and feldspar.

Spectral response

Dominant quartz, feldspar (albite, microcline) and white mica; also cordierite (likely error); all other minerals low to absent.

Vectors to mineralization

Carbonate: A gradual increase in carbonate abundance over >20 m (from 225 to the ore zone at 200 m).

Ca-amphibole: Possible decrease in Ca-amphibole abundance over >10 m (from 173 to ore zone at 184 m).

Neither of these vectors are readily recognized visually.

WW823 05.10.16

Gold lode

Broad medium-grade intersection
28.8 m at 2.98 g/t Au (in BIF; excludes thin interleaved mafic/ultramafic units)

High-grade intersections on lower contacts of BIF units

1 16.2 m at 1.71 g/t Au
2 0.9 m at 21.9 g/t Au
3 1.0 m at 9.14 g't Au
4 1.55 m at 16.1 g/t Au

Figure 3.115. Spectral log showing auriferous intersections and annotations indicating rock types and associated hydrothermal alteration (at base of graphic log), NVCD0102, Nevoria gold deposit, Southern Cross district, Youanmi Terrane. Green intervals denote metamorphosed high-Mg basalt; dark green intervals denote dolerite; purple intervals denote metamorphosed high-Mg basalt to ultramafic rock; blue intervals denote banded iron-formation; pink intervals denote pegmatite. See text and Figure 3.116 for key to alteration types. (W) indicates weak alteration.

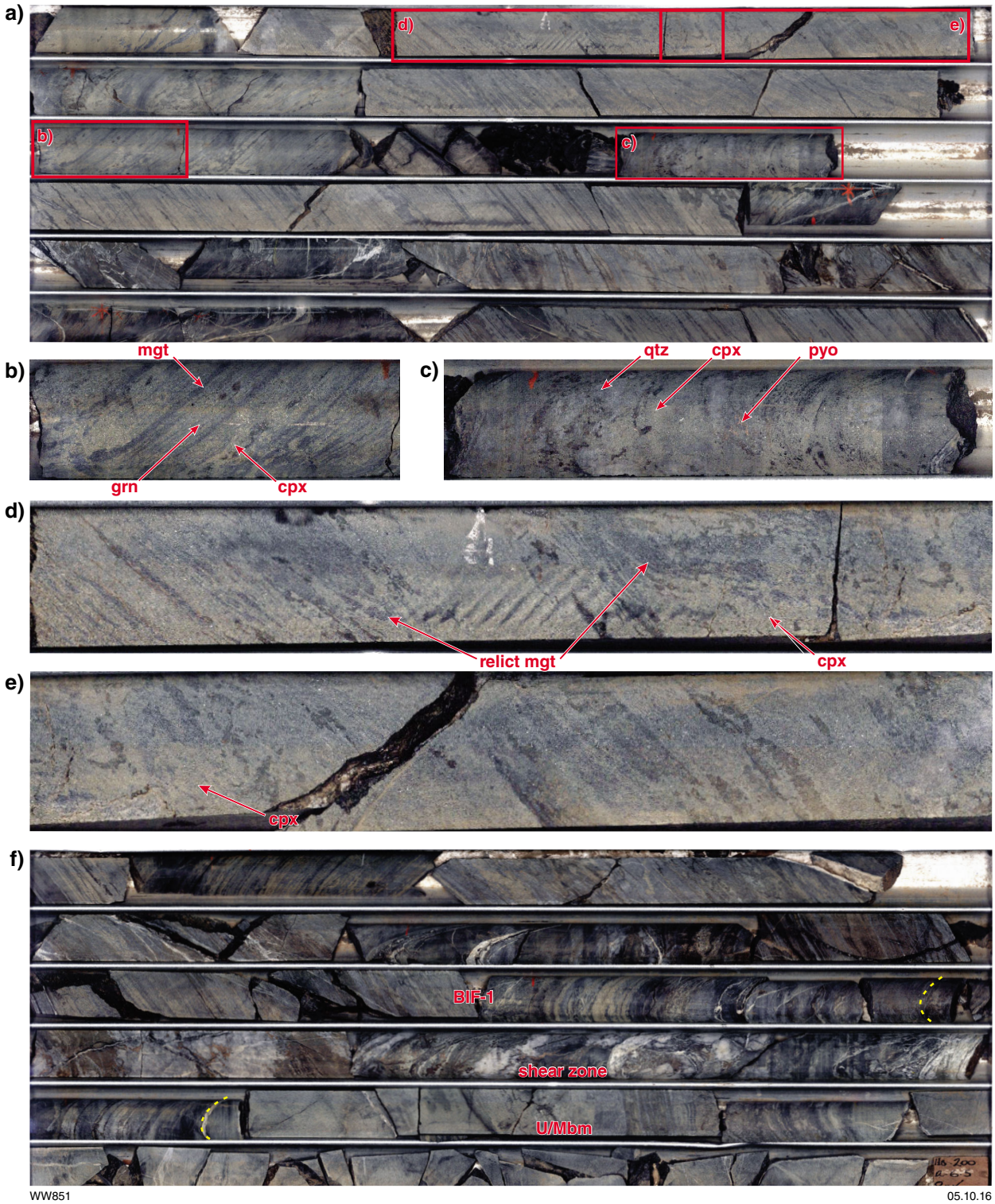

Figure 3.116. Core photos illustrating features of core NVCD0102, Nevoria gold deposit, referred to in the text. a) 189.5–194 m, BIF-1 showing folded quartz–magnetite mesobanding overprinted by grunerite and clinopyroxene (hedenbergite). Red outlines mark core shown in detail in following panels. b) Detail of quartz–magnetite–grunerite mesobanding in BIF-1. c) Detail of quartz–clinopyroxene vein showing coarse-grained hedenbergite (cpx). d) Detail of massive grunerite and clinopyroxene overprinting quartz–magnetite mesobanding; note metasomatic destruction of folds defined by mesobanding. e) Detail of massive grunerite and clinopyroxene overprinting quartz–magnetite mesobanding; note metasomatic destruction of folds defined by mesobanding, particularly in vicinity of fold hinge (near label cpx). f) 194.6–199.8 m, quartz–carbonate–pyrrhotite vein and biotite alteration in shear zone on footwall contact of BIF-1; broken yellow lines mark margins of shear zone. Abbreviations: cpx (clinopyroxene), grn (grunerite), mgt (magnetite), pyo (pyrrhotite), qtz (quartz), U/Mbm (ultramafic to high-Mg basalt).

Table 3.24. Summary of SWIR/TIR spectral characterization of unaltered rock types, Southern Cross

HyLogger spectral identification[a]	*High-Mg ultramafic*	*Low-Mg ultramafic*	*Mafic*	*Meta-dolerite/ gabbro*	*Meta-sedimentary*	*Banded iron-formation*	*Pegmatite*
Olivine							
Grunerite–cummingtonite							
Feldspar			Olig-lab	Olig-lab	K-feldspar		Alb-K-feldspar
Quartz				Vn			
Garnet							
Pyroxene	Vn	Vn	Vn	Vn		Vn	
Carbonate							
Cordierite					X		X
Ca-amphibole							
Chlorite			Retro		Retro		
Dark mica							
White mica							
Serpentine							

NOTES: (a) Grey cells identified by TIR spectrometer; white cells identified by SWIR spectrometer

Red, essential; Pink, common but not essential; Black, absence or very low abundance is part of spectral definition; White, not part of spectral definition; Vn, only as (quartz or diopside) veins; X, cordierite possibly a misidentification of paragonitic white mica.

Retro: Possibly retrograde after biotite but dark mica (biotite) and chlorite have very similar spectra and it is likely that some metasomatic biotite has commonly been misidentified as chlorite

Alb (albite), olig (oligoclase), lab (labradorite)

Table 3.25. Summary of SWIR/TIR spectral characterization of altered ultramafic rock types, Southern Cross (see Fig. 3.59 for definition of alteration types)

HyLogger spectral identification[a]	*Unaltered (low-Mg)*	*bio*	*Kcs*	*amp*	*Kfp*	*Au veins*
Olivine						(b)
Grunerite-cummingtonite						
Feldspar			K-feldspar		K-feldspar	
Quartz			Vn[d]			
Garnet						
Pyroxene			Vn			
Carbonate						
Cordierite						
Ca-amphibole						
Chlorite		(c)	(c)	(c)		
Dark mica						
White mica						

NOTES: (a) Grey cells identified by TIR spectrometer; white cells identified by SWIR spectrometer. (b) Olivine may be present as forsterite–calcite intergrowths.
(c) Dark mica (biotite) is commonly misidentified as chlorite. (d) Source of quartz in Undaunted hole UNRD331 is uncertain but may reflect weak silicification

Red, essential; Pink, common but not essential; Black, absence or very low abundance is part of the spectral definition; White, not part of spectral definition; Vn, only as (quartz or diopside) veins

Table 3.26. Summary of SWIR/TIR spectral characterisation of altered mafic rock types, Southern Cross (see Fig. 3.59 for definition of alteration types)

HyLogger spectral identification[a]	*Unaltered*	*bio*	*Kcs*	*Plg*[d]	*Au veins*	*cs*	*KMg*
Olivine							
Grunerite–cummingtonite							
Feldspar	Olig-lab	Olig	Olig	Alb-lab and K-feldspar		Lab	Olig-byt
Quartz		(c)	(c)				
Garnet							
Pyroxene	Vn	Vn	Vn				Vn
Carbonate							
Cordierite							
Ca-amphibole							
Chlorite		(b)	(b)				
Dark mica					(b)		
White mica							

NOTES: (a) Grey cells identified by TIR spectrometer; white cells identified by SWIR spectrometer. (b) Note that dark mica (biotite) is commonly mis-identified as chlorite. (c) The strong quartz response throughout most of UNRD331 cannot be reconciled with field observations but may reflect weak silicification because quartz is readily detected at even a few modal percent by the TIR spectrometer. The strong relative depletion in the mineralized plagioclase alteration zone of UNRD331 may be significant but could just be a symptom of the overall weak spectral response to quarter core. (d) Proximal plagioclase alteration in UNRD331 is poorly characterized by HyLogger data, probably because the quarter core in this interval does not provide a suitable sample for analysis.

Red, essential; Pink, common but not essential; Black, absence or very low abundance is part of the spectral definition; White, not part of spectral definition; Vn, only as diopside veins.

Alb (albite), olig (oligoclase), lab (labradorite), byt (bytownite)

Table 3.27. Summary of SWIR/TIR spectral characterization of mineralized banded iron-formation, Southern Cross

HyLogger spectral identification[a]	*Unaltered*	*Mineralized*
Olivine		
Grunerite–cummingtonite		
Feldspar		
Quartz		
Garnet		
Pyroxene	Vn	Vn
Carbonate		
Cordierite		
Ca-amphibole		
Chlorite		
Dark mica		
White mica		

NOTES: (a) Grey cells identified by TIR spectrometer; white cells identified by SWIR spectrometer.

Red, essential; Pink, common but not essential; Black, absence or very low abundance is part of the spectral definition; White, not part of spectral definition; Vn, only as diopside in veins

Summary and conclusions

In comparison with recent research directed towards predictive exploration at global to camp scales, there has been very little work done in this field at deposit scale. During the 1980s and 1990s, research at individual gold deposits focused on descriptive and genetic models, but applications of these studies to predictive exploration were few. The scarcity of deposit-scale predictive exploration studies can be attributed partly to the unavailability of the datasets required to undertake them, either because the data have not been collected at the mine site or because any such data has not been made available to researchers (or subsequently published). Consequently, the major advances achieved at global to camp scale in the past decade or two have not been matched at deposit scale. This is a serious shortcoming, considering the imperative for mine management to discover new ore shoots in order to extend mine life.

As a consequence of the shortage of deposit-scale datasets or predictive studies, Part 3 of the Yilgarn Gold Exploration Targeting Atlas is dominated by empirical, qualitative reports or observations, with relatively few of the quantitative or qualitative analyses of large datasets that were presented in Parts 1 and 2 of the Atlas. The deposit-scale predictive exploration criteria presented here in Part 3 of the Atlas can be divided into two major classes: structural criteria (where a heavy emphasis is placed on prediction of unknown ore), and geochemical and mineralogical criteria (where direct detection of undiscovered ore is emphasised).

Structural criteria

Virtually all gold deposits of the Yilgarn Craton display an essential component of structural control, and most of these are related to faults or shear zones, particularly in sub-greenschist to lower amphibolite facies metamorphic settings. Many well-documented deposits are controlled by

- intersections of faults or shear zones (e.g. Jundee–Nimary, Bronzewing, Golden Cities)
- intersections of faults or shear zones with particular lithological units (Mount Charlotte, Santa Claus, Nevoria)
- fault bends and fault jogs (Defiance and Revenge, Norseman, Wiluna).

Fault bends and fault jogs are particularly common controls on deposits and ore shoots within them. Some of these fault bends and jogs are controlled by intersections between faults, or between faults and specific lithological units, even though many published descriptions emphasize the intersection rather than the jog. Not all fault intersections are fault jogs, however, and the common feature of the three structural settings listed above is that they all provide an increase in rock permeability that promotes focused flow of ore fluid.

Less common or less well-established structural controls on gold mineralization at deposit scale are hydraulic seals (Enterprise, Sunrise Dam) and bottlenecks (Robinsons). Hydraulic seals impede the upward movement of over-pressured ore fluid, leading to high fluid pressure and high fluid to rock ratios immediately beneath the hydraulic seal. As is the case for regional-scale bottlenecks (Part 1 of this Atlas), deposit-scale bottlenecks represent an environment where dismemberment and displacement of greenstones create favourable conditions for rock fracture and dilation, and thereby focus the flow of ore fluid. In all cases, rock dilation may result in unmixing (effervescence) of ore fluid and the consequent deposition of gold; in others the high fluid to rock ratio may cause precipitation of gold through fluid–rock chemical reaction.

The common element in the structural targeting criteria is rock fracture and focused fluid flow (high fluid to rock ratios). The role of rheology and rheological gradients is paramount in promoting rock fracture and focused fluid flow. For example, fault intersections in rheologically weak units, such as ultramafic or pelitic schists, are more likely to be accommodated by ductile deformation than by rock fracture. Fault intersections with specific lithological units are most commonly mineralized where the lithological unit is rheologically strong (e.g. dolerite, porphyry, banded iron-formation), thus promoting brittle fracture. Fault bends and fault jogs are mostly formed where a fault intersects a contact between units of contrasting rheological strength. Hydraulic seals form where rheologically weak units overlie rheologically strong units, and bottlenecks typically form where rheologically weak units are confined between rheologically strong units. Thus, the common property that is important for all of the structural targeting criteria described here is rock rheology and, in particular, steep rheological gradients. This statement is reinforced by the observation that most faults that control gold mineralization are on contacts between lithological units of contrasting rheological strengths.

Hronsky (2014) emphasized rock rheology as the single most important criterion that controls the development of gold mineralization and ore shoots, to the exclusion of traditional structural analysis. This is because conventional kinematic analysis of stress-related deformation commonly fails to predict the locations of ore shoots, especially in complex gold deposits, such as Lancefield in the Laverton district. The probable reason for this failure is that high fluid pressure generates an escape path (from an over-pressurised source to, and beyond, the gold deposit environment) of its own making, which is heavily dependent on the rheological architecture of the deposit environment and overwhelms the imposed stress field. A good example of this is the Homestead deposit, Mount Pleasant, where ore shoots within the Homestead Shear Structure are defined by laminated quartz veins that formed on contacts between rheologically strong carbonate(–quartz) replacement units within a matrix of rheologically weak chloritic schist. These mineralized contacts are oriented approximately north–south, at a high angle to the regional- and district-scale direction of maximum stress (σ_1). Conventional kinematic analysis would predict these contacts to be compressional rather than dilational. However, the rheological gradient represented by the intra-fault lithological contacts provided the least resistant pathway for a deeply sourced,

over-pressured ore fluid with consequent formation of gold-bearing laminated quartz veins oriented at a high angle to σ_1.

At deeper crustal levels, represented by higher metamorphic grade settings, many of the same structural controls can be recognized, including fault or shear zone control (e.g. all model 1 deposits in the Southern Cross district), fault jogs (e.g. Transvaal), and fault – lithological unit intersections (Nevoria). However, in these deeper, hotter environments, fold hinges and boudins take on an important additional role. These controls are best represented at district scale by the concentration of model 1 deposits in the necks of mega-boudins and smaller boudins in the Southern Cross district (Targeting Criterion 2.13, Part 2 of this Atlas). Although not discussed at length in this report, deposit-scale boudins may exercise some control on the location and plunge of ultramafic-hosted ore shoots at Marvel Loch. Boudin necks represent low-stress environments where rock dilation and fluid focusing are promoted by ascending over-pressured fluids. The role of rock rheology is again significant because a boudin represents a rheologically strong unit within a rheologically weak matrix.

Fold hinges are also very important controls on ore shoot formation in mid- to upper-amphibolite facies metamorphic settings. These controls are diverse in form (Fig. 3.29), but all depend on the rheological properties of geological units in the mine environment. Preferential fracture of thickened fold hinges is most likely in rheologically strong units such as banded iron-formation (e.g. Golden Pig, Cornishman). Similarly, dilation of folded contacts in fold hinges is most likely where the contacts separate lithological units of contrasting rheological strength. Examples of gold mineralization in layer-parallel shears or faults that encounter a parasitic fold hinge are known in both low-grade (e.g. Oroya shoot at Kalgoorlie, Twin Peaks) and high-grade (e.g. Transvaal) metamorphic settings. In these cases, the fault is typically controlled by a lithological contact between units of considerably different rheological strength, and a jog develops where this fault encounters a folded contact. Jogs are sometimes created where an oblique fault intersects a fold axis, but this is most likely to occur where the fault intersects a rheologically strong lithological unit. In all of these cases, the plunge of the ore shoot is predicted to be colinear with the plunge of fold axes. This is also true where pre-existing mineralization has been folded during progressive or later deformation (e.g. Sons of Gwalia).

The foregoing review emphasizes the primary importance of rock rheology in controlling the structures that control gold mineralization at deposit scale, and the formation of high-grade ore shoots within such deposits. Clearly, a good geological map of a gold deposit and the immediate mine environment is an essential prerequisite for effective prediction of new ore shoots, or of extensions of known ore shoots; that mapping should incorporate the rheological properties of each geological unit and structural unit (e.g. faults, shear zones). Hydrothermal alteration is an essential component of geological mapping because alteration can profoundly change the rheological properties of a lithological unit. Table 2.4 (Part 2 of this Atlas) provides a starting point for the assignment of rheological properties to rocks on the basis of lithology; however, other sources might be helpful, or measurements of rock strength of samples taken from mine sites. To date, this approach has rarely been used at mine sites.

Some geophysical techniques may provide faster, but less precise, methods of mapping the relative rheological strengths of rocks at and around gold deposits; this approach has the added advantage that survey data can be acquired some distance beyond the areas of mine development that can be accessed for conventional geological mapping. These include seismic surveys (Turner et al., 2014), and various electrical methods such as induced polarization (IP), electromagnetic (EM), magnetotelluric, and subaudio magnetics (SAMS) surveys. The application of all of these methods is discussed by Dentith and Mudge (2014).

Paleostress mapping also has some potential for prediction of the location of undiscovered ore shoots, but depends on the availability of a reliable geological map. By the time a reliable map has been compiled by conventional means (on the basis of exploration and mine development drilling), there is normally some indication of any undiscovered ore shoots in drillhole assay data. If the practical problems that come with conducting electrical surveys in operating mines can be overcome, application of paleostress mapping to a geological and rheological map generated by a combination of mine development mapping and geophysical methods has the potential to identify undiscovered ore shoots in areas beyond the mine development.

Geochemical and mineralogical criteria

Delineation of the ore fluid conduit using geological mapping and/or geophysical techniques can be supplemented using geochemistry and mineralogy to directly detect the conduit (Fig. 3.117). Geochemical studies at several Yilgarn gold deposits have shown very limited dispersion of pathfinder elements and most alteration indices beyond the gold lode. In most cases, dispersion of pathfinder elements does not extend beyond the visible alteration halo and, in even fewer instances, beyond the low-level gold anomaly (a few tens of metres for most deposits). The extent of geochemical dispersion appears to be greater in deposits dominated by ductile deformation that are normally found in relatively high metamorphic grade settings (e.g. Leonora, Southern Cross). Most of these studies emphasize dispersion orthogonal to the ore fluid conduit, but pathfinder elements and alteration indices that display the greatest orthogonal dispersion should also be dispersed the greatest distance along the strike of the conduit, beyond a known ore shoot. These will be the most effective parameters to apply to the discovery of new ore shoots within the ore fluid conduit (Fig. 3.117).

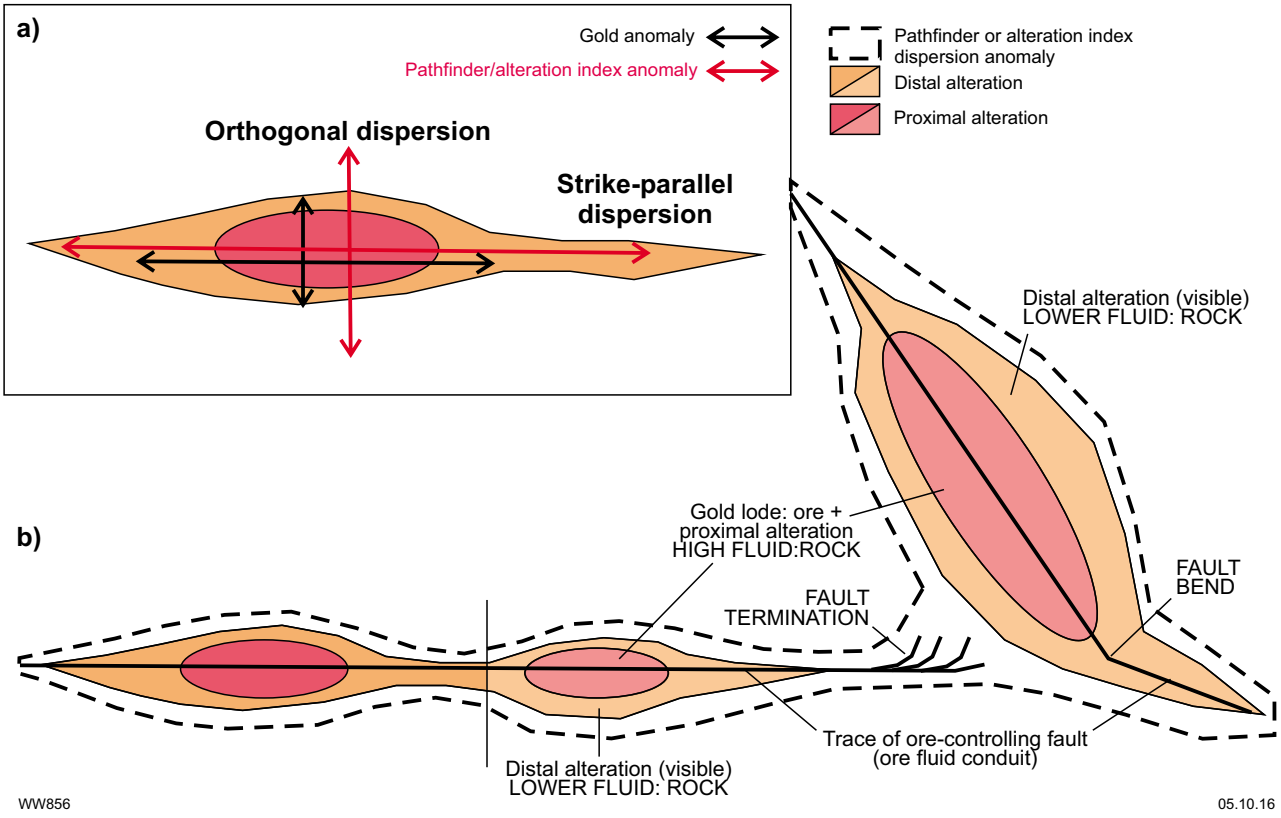

Figure 3.117. Schematic diagram (plan view) illustrating the use of geochemical dispersion around a known ore shoot to delineate an ore fluid conduit linking to other unknown ore shoots. a) Original known ore shoot. b) Relationship of known ore shoot to ore conduit and unknown ore shoots.

The most widely dispersed pathfinder elements are As, Sb, W, and Te, but Au, As, and Sb are probably the most useful elements because they most commonly generate orthogonal concentration gradients within the visible gold-related alteration halo that provide vectors towards ore. By inference, these will also be the most useful elements for tracing an ore fluid conduit between ore shoots. Such vectors are also useful in large areas of hydrothermal alteration (potentially including alteration not directly related to gold mineralization) characterized by widespread anomalous but low-grade gold concentrations. Although the dispersion of pathfinder elements may be of limited extent at most Yilgarn gold deposits, the application of As, Sb, Mo, Bi, and W analyses at deposit scale may still be useful to locate intrusions and zones of structural deformation (cf. district-scale, Targeting Criterion 2.19). No results of deposit-scale investigations of this nature have yet been published. Periodic addition of these five elements to grade-control and development samples would not add greatly to the costs of gold production. This approach, but including immobile elements such as Ti, Al, Zr, Sc, Th, and Cr could be particularly useful if complex structural and hydrothermal overprinting has obscured lithological identification.

The application of stable (C and O) isotope analyses to a few Yilgarn gold deposits has been investigated in an attempt to identify large-scale hydrothermal alteration cells. The results have generally been disappointing, with the exception of the Granny Smith Deeps deposit where $\delta^{18}O$ depletion of metasedimentary host rocks ($\delta^{18}O$ of +18 to +25‰) to values of +11‰ generated an anomaly extending over 200 m from the ore. The success of the ^{18}O study at Granny Smith is probably critically dependent on the high $\delta^{18}O$ values of the metasedimentary host rocks that host the Granny Smith Granodiorite. Similar studies have been successful in some Carlin-style gold deposits hosted in metasedimentary rocks in Nevada, USA (Barker et al., 2013). Volcanic-hosted gold deposits are less likely to generate significant $\delta^{18}O$ depletion anomalies.

Given the limited extents of pathfinder element and stable isotope anomalies around most gold deposits, any gold-related geochemical parameter that extends beyond visible hydrothermal alteration is a valuable tool for the mine geologist seeking new ore shoots. The best known alteration indices are the carbonate alteration index, the alkali alteration indices, and the more recently proposed rare alkali index. Application of the carbon alteration index in the Yilgarn is not common, principally because of the extra analytical cost involved in acquiring CO_2 concentrations. The alkali alteration indices (molar 3K/Al, molar Na/Al) have been trialled at several Yilgarn gold deposits but have rarely been found to extend beyond the visible alteration halo.

The rare alkali index ($[Rb + Cs]/Th)_N$ of Heath and Campbell (2004) has been applied at several Yilgarn gold deposits, including a recent study at Red October that was completed as part of the project to produce this Atlas. This index consistently remains anomalous beyond the visible gold-related alteration at all deposits where it has been applied (Kalgoorlie, St Ives, Tower Hill, Sons of Gwalia). In most of the Red October drillholes sampled, the rare alkali index anomaly extends at least 45 m beyond visible alteration in the hangingwall of the gold lode.

A relatively new technique with application to gold exploration at camp to deposit scale exploits characteristic mineral spectra generated in the VNIR–SWIR range by airborne surveys, automated loggers, or hand-held instruments. Early studies of airborne spectral (ASTER and HyMapper) data at Kalgoorlie have shown their potential for recognition of zoned gold-related hydrothermal alteration in well-exposed terrains, of which there are few in the Yilgarn Craton. Spectral data generated by automated HyLogger analysis of drillcore are potentially more useful in the Yilgarn. One such study, at Kanowna Belle, illustrates the application of this type of data to delineate oxidized and reduced hydrothermal domains, which can be applied in a similar way to that described for district-scale spectral data (Targeting Criterion 2.16, Part 2 of this Atlas).

VNIR–SWIR data have application in settings of low metamorphic grade, where hydrous alteration minerals are common, but the newly developed TIR capacity of HyLogger allows spectral identification of anhydrous minerals such as garnet, pyroxenes, carbonates, and feldspars, with potential application to gold exploration in high-grade metamorphic settings such as in the Southern Cross district. Drillcores from several gold deposits in the Southern Cross district have been analysed by HyLogger (with TIR spectrometer operating) and the results presented here under Targeting Criterion 3.12. Although there have been instances where automated TSA analysis of HyLogger spectral data misidentified some minerals, most of the common rock types in the Southern Cross belt can be defined using HyLogger spectral output and, in some cases, intervals of mineralization can be identified by a characteristic combination of quartz, pyroxene, and biotite/chlorite spectra that is not shared by any of the common unaltered rock types. However, spectral identification of mineralization may be complicated by spatially associated (sea-floor) hydrothermal alteration, which generates similar combinations of spectra.

Analysis of the HyLogger data from Southern Cross also identified some vectors to gold mineralization, including decreasing strength of Ca-amphibole spectra and sequentially increasing strength of peaks identifying quartz, followed by biotite/chlorite in the sea-floor altered footwall to (model 2) deposits hosted by banded iron-formation. In some cases these vectors extend for tens of metres into the footwall or hangingwall of the gold lode. Although sea-floor alteration, which pre-dates gold mineralization, can be visually recognized in drillcore, HyLogger data reports semi-quantitative variations in these mineral abundances over several tens of metres, which can be difficult to duplicate by traditional core logging. For (model 1) shear-hosted deposits, the vector with the most potential appears to be changes of feldspar composition proximal to ore. In particular, the appearance of minor amounts of K-feldspar in and around the gold lodes is well documented by Hylogger data but can be difficult to recognize in the field.

Acknowledgements

Personnel at Saracen Gold Mines Pty Ltd (Phil Hartofilis, Tim Laneyrie) are thanked for their cooperation and collaboration in application of the rare alkali index to samples from Red October gold mine. The author wishes to acknowledge the support of management at Sons of Gwalia Ltd, where several of the case studies presented in this volume originated. Similarly, Norton Goldfields Ltd (particularly Peter Ruzicka) is thanked for permission to present results of geological mapping and sampling at Homestead, Havana, and Robinsons mines. Shaun Magner of Norton Goldfields Ltd provided intelligent guidance and good company during regular visits to the Homestead underground mine. Dr Alison Dugdale, Curtin University, is thanked for making available XRD analytical results from Golden Pig core GPD1464. The majority of figures in all three volumes of this Atlas were drafted by Joyce Peng at the Department of Mines and Petroleum. The work of Carol Scarfe in drafting many of the figures for the Leonora and Southern Cross regions is acknowledged with thanks. The authors of the discussion of Targeting Criterion 3.12 thank the Western Australian Government for their support of the activities of the Western Australian Centre of Excellence for 3D Mineral Mapping <http://c3dmm.csiro.au>. The C3DMM team and CSIRO's Mineral and Environmental Sensing group are thanked for making the ASTER data for Western Australia available. External peer reviews by Gerard Tripp and Nico Thebaud contributed to many improvements of the original manuscript.

References

Ackroyd, BJ, Hagemann, SG, Neumayr, P, Ingle, LJ, Inwood, NA and Smolonogov, S 2001, Hydrothermal alteration and gold mineralization at the sandstone-hosted New Holland gold deposit, Agnew-Lawlers gold camp, Western Australia, *in* World-class gold camps and deposits in the eastern Yilgarn craton, Western Australia, with special emphasis on the Eastern Goldfields Province *edited by* SG Hagemann, P Neumayr and WK Witt: Geological Survey of Western Australia, Record 2001/17, p. 99–125.

Alsop, GI and Holdsworth, RE 1999, Vergence and facing patterns in large-scale sheath folds: Journal of Structural Geology, v. 21, p. 1335–1349.

Anand, RR and Butt, CRM 2010, A guide for mineral exploration through the regolith in the Yilgarn Craton, Western Australia: Australian Journal of Earth Sciences, v. 57, p. 1015–1114.

Andrew, AS, Carr, GR, Giblin, AM, Whitford, DJ, Anderson, JA and Drown, CG 1994, Exploration for concealed mineralisation: multi-isotopic studies of groundwaters, AMIRA Project P338, Hydrogeochemistry of the Meninnie Dam Prospect, South Australia: CSIRO Division of Exploration and Mining, North Ryde, NSW, Restricted Investigation Report 11R.

Arnold, R, Gordon, C and Lloyd, C 1995, Nevoria, *in* Southern Cross Greenstone Belt, Geology and Gold Mines *compiled by* PJ Schwebel: Geoconferences (WA) Inc. Extended Abstracts Volume, p. 97–102.

Arndt, NT and Jenner, GA 1986, Crustally contaminated komatiites and basalts from Kambalda, Western Australia: Chemical Geology, v. 56, p. 229–255.

Arndt, NT, Naldrett, AJ and Pyke, DR 1977, Komatiitic and iron-rich tholeiitic lavas of Munro Township, northeast Ontario: Journal of Petrology, v. 18, p. 319–369.

Baggott, MS 2006, A refined model for the magmatic, tectonometamorphic and hydrothermal evolution of the Leonora District, Eastern Goldfields Province, Yilgarn Craton, Western Australia: University of Western Australia, Perth, PhD thesis (unpublished).

Baker, T, Bertelli, M, Blenkinsop, T, Cleverly, JS, McLellan, J, Nugus, M and Gillen, D 2010, P-T-X conditions of fluids in the Sunrise Dam gold deposit, Western Australia, and implications for the interplay between deformation and fluids: Economic Geology, v. 105, p. 873–894.

Barker, C 1998, Alteration systematics of the "Triple O" and "Double O" gold deposits, Southern Cross, Western Australia: University of Western Australia, Perth, Graduate Diploma Dissertation, (unpublished).

Barker, SL, Dipple, GM, Hickey, KA, Lepore, WA and Vaughan, JR 2013, Applying stable isotopes to mineral exploration: teaching an old dog new tricks: Economic Geology, v. 108, p. 1–9.

Barley, ME 1986, Incompatible-element enrichment in Archean basalts: a consequence of contamination by older sialic crust rather than mantle heterogeneity: Geology, v. 14, p. 9475950.

Barnett, CT and Williams, PM 2012, A radical approach to exploration: let the data speak for themselves: SEG Newsletter, v. 90, p. 1–17.

Bateman, RJ and Hagemann, SG 2004, Gold mineralisation throughout about 45 Ma of Archaean orogenesis: protracted flux of gold in the Golden Mile, Yilgarn Craton, Western Australia: Mineralium Deposita, v. 39, p. 536–559.

Bateman, RJ and Jones, S 2015, Discussion: The timing of gold mineralization across the eastern Yilgarn Craton using U-Pb geochronology of hydrothermal phosphate minerals: Mineralium Deposita, v. 50, p. 885–888.

Beardsmore, TJ and Gardner, Y 2003, Darlot gold deposit, Yandal gold province, Yilgarn Craton, Western Australia: CSIRO Explore, v. 1, p. 173–219.

Blewett, RS and Czarnota, K 2007, Diversity of structurally-controlled gold through time and space of the central Eastern Goldfields Superterrane – a field guide: Geological Survey of Western Australia, Record 2007/19, 65p.

Blewett, RS, Czarnota, K and Henson, PA 2010, Structural-event framework for the eastern Yilgarn Craton, Western Australia, and its implications for orogenic gold: Precambrian Research, v. 183, p. 203–229.

Bloem, EJM, Dalstra, HJ, Groves, DI and Ridley, JR 1994, Metamorphic and structural setting of Archaean amphibolite-hosted gold deposits near Southern Cross, Southern Cross Province, Western Australia: Ore Geology Reviews, v. 9, p. 183–208.

Bodycoat, F 1999, The nature and genesis of alteration and mineralisation at the Yilgarn Star gold deposit, Southern Cross Province, Western Australia: University of Western Australia, Perth, BSc (Hons) thesis (unpublished).

Bornhorst, TJ, Rasilainen, K and Nurmi, PA 1993, Geochemical character of lithological units in the late Archaean Hattu schist belt, Ilomantsi, eastern Finland, *in* Geological Development, Gold Mineralization and Exploration Methods in the late Archaean Hattu Schist Belt, Ilomantsi, eastern Finland *edited by* P Nurmi and P Sorjonen-Ward: Geological Survey of Finland, Special Paper 17, p. 133–145.

Boulter, CA, Fotios, MG and Phillips, GN 1987, The Golden Mile, Kalgoorlie: a giant gold deposit localized in ductile shear zones by structurally induced infiltration of an auriferous fluid: Economic Geology, v. 82, p. 1661–1678.

Bromley, GJ 1990, Galtee More Gold Deposits, *in* Geology of the Mineral Deposits of Australia and Papua New Guinea *edited by* FE Hughes: Australasian Institute of Mining and Metallurgy, p. 243–247.

Burrows, DR and Spooner, ETC 1989, Relationships between Archean gold quartz vein-shear zone mineralization and igneous intrusions in the Val d'Or and Timmins areas, Abitibi subprovince, Canada: Economic Geology, Monograph 6, p. 424–444.

Campbell, JD 1990, Hidden Gold, the Central Norseman Story: Australasian Institute of Mining and Metallurgy, Monograph 16, 68p.

Cassidy, KF and Bennet, JM 1993, Gold mineralisation at the Lady Bountiful mine, Western Australia: An example of a granitoid-hosted Archaean lode gold deposit: Mineralium Deposita, v. 28, p. 388–408.

Cassidy, KF, Champion, DC, Krapez, B, Barley, ME, Brown, SJA, Blewett, RS, Groenewald, PB and Tyler, IM 2006, A revised geological framework for the Yilgarn Craton: Geological Survey of Western Australia, Record 2006/8, 14p.

Cassidy, KF, Champion, DC, McNaughton, NJ, Fletcher, IR, Whitaker, AJ, Bastrakova, IV and Budd, AR 2002, Characterisation and metallogenic significance of Archaean granitoids of the Yilgarn craton, Western Australia: MERIWA Report 222, 514p.

Cassidy, KF, Groves, DI and McNaughton, NJ 1998, Late-Archean granitoid-hosted lode-gold deposits, Yilgarn Craton, Western Australia: Deposit characteristics, crustal architecture and implications for ore genesis: Ore Geology Reviews, v. 13, p. 65–102.

Clark, ME, Carmichael, DM, Hodgson, CJ and Fu, M 1989, Wallrock alteration, Victory gold mine, Kambalda, Western Australia: processes and P-T-X(CO_2) conditions of metasomatism, *in* The Geology of Gold Deposits: the perspective in 1988 *edited by* RR Keays, WRH Ramsay and DI Groves: Economic Geology, Monograph 6, p. 445–456.

Connolly, HJC 1936, A contour method of revealing some ore structures: Economic Geology, v. 31, p. 259–271.

Coveney, RM Jr and Nansheng, C 1991, Ni-Mo-PGE-Au-rich ores in Chinese black shales and speculations on possible analogues in the United States: Mineralium Deposita, v. 26, p. 83–88.

Cox, SF and Ruming, K 2004, The St Ives mesothermal gold system, Western Australia – a case of golden aftershocks?: Journal of Structural Geology, v. 26, p. 1109–1125.

Cox, SF, Wall, VJ, Etheridge, MA and Potter, TF 1991, Deformational and metamorphic processes in the formation of mesothermal vein-hosted gold deposits – examples from the Lachlan Fold Belt in central Victoria, Australia: Ore Geology Reviews, v. 6, p. 391–423.

Cudahy, T 1997, Geometry of the spectral-mineralogical alteration halo at Birthday South, Fimiston Gold Deposit, Western Australia: CSIRO Exploration and Mining Report, 421R, 69p.

Cudahy, T, Caccetta, M, Cornelius, A, Hewson, R, Wells, M, Skwarnecki, M, Halley, S, Hausknecht, P, Mason, P and Quigley, M 2005, Regolith, Geology and Alteration Mineral Maps from New Generation Airborne and Satellite Remote Sensing Technologies: MERIWA Report No. 252, 114p (incl. Appendices).

Cullen, I, Jones, M and Baxter, JL 1990, Nevoria gold deposits, *in* Geology of the Mineral Deposits of Australia and Papua New Guinea *edited by* FE Hughes: Australian Institute of Mining and Metallurgy, Monograph 14, p. 301–305.

Czarnota, K, Champion, DC, Goscombe, B, Blewett, RS, Cassidy, KF, Henson, PA and Groenewald, PB 2010, Geodynamics of the eastern Yilgarn Craton: Precambrian Research, v. 183, p. 175–202.

Dale, GR and Thomas, BD 1990, Fraser gold deposit, Southern Cross, *in* Geology of the Mineral Deposits of Australia and Papua New Guinea: Australian Institute of Mining and Metallurgy, Monograph 14, p. 287–288.

Davies, JF, Whitehead, RES, Huang, J and Nawaratne, S 1990, A comparison of progressive hydrothermal carbonate alteration in Archean metabasalts and metaperidotites: Mineralium Deposita, v. 25, p. 65–72.

Davis, BK, Blewett, RS, Squire, R, Champion, DC and Henson, PA 2010, Granite-cored domes and gold mineralisation: Architectural and geodynamic controls around the Archaean Scotia–Kanowna Dome, Kalgoorlie Terrane, Western Australia: Precambrian Research, v. 183, p. 316–337.

Davis, BK, Hickey, KA and Rose, S 2001, Superposition of gold mineralisation on pre-existing carbonate alteration: structural evidence from the Mulgarrie gold deposit, Yilgarn Craton: Australian Journal of Earth Sciences, 48, p. 131–149.

Dentith, M, and Mudge, A 2014, Geophysics for the Mineral Exploration Geoscientist: Cambridge University Press, 454p.

Dinel, E, Fowler, AD, Ayer, J, Still, A, Tylee, K and Barr, E 2008, Lithogeochemical and stratigraphic controls on gold mineralization within the metavolcanic rocks of the Hoyle Pond mine, Timmins, Ontario: Economic Geology, v. 103, p. 1341–1363.

Doublier, MP 2014, Geological setting of mineral deposits in the Southern Cross district – a field guide: Geological Survey of Western Australia, Record 2013/11, 62p.

Duuring, P, Hagemann, SG, Cassidy, KF and Johnson, CA 2004, Hydrothermal alteration, ore fluid characteristics and gold depositional processes along a trondhjemite – komatiite contact at Tarmoola, Western Australia: Economic Geology, v. 99, p. 423–451.

Duuring, P, Hagemann, SG and Groves, DI 2000, Structural setting, hydrothermal alteration and gold mineralization at the Archaean syenite-hosted Jupiter deposit, Yilgarn craton, Western Australia: Mineralium Deposita, v. 35, p. 402–421.

Eilu, P and Groves, DI 2001, Primary alteration and geochemical dispersion haloes of Archaean orogenic gold deposits in the Yilgarn craton: the pre-weathering scenario: Geochemistry, Exploration, Environment, Analysis, v. 1, p. 183–200.

Eilu, P and Mikucki, EJ 1996, Primary geochemical and isotope dispersion in Archaean lode-gold systems: Assessment of alteration indices for use in district- and mine-scale exploration (MERIWA Project M243): MERIWA Report 176, Volumes I to VI.

Eilu, P and Mikucki, EJ 1998, Alteration and primary geochemical dispersion associated with the Bulletin lode-gold deposit, Wiluna, Western Australia: Journal of Geochemical Exploration, v. 63, p. 73–103.

Eilu, P, Mikucki, EJ and Dugdale, AL 2001, Alteration zoning and primary geochemical dispersion at the Bronzewing lode-gold deposit, Western Australia: Mineralium Deposita, v. 36, p. 13–31.

Eilu, P, Mikucki, EJ and Groves, DI 1997, Wallrock alteration and primary geochemical dispersion in lode-gold exploration. SGA Short Course Series, Volume 1, 65p.

Evans, KA, Phillips, GN, Powell, R 2006, Rock-buffering of auriferous fluids in altered rocks associated with the Golden Mile-style mineralization, Kalgoorlie Gold Field, Western Australia: Economic Geology, v. 101, p. 805–817.

Finucane, KJ 1965, Ore distribution and lode structures in the Kalgoorlie goldfield, *in* Geology of Australian Ore Deposits (2nd edition) *edited by* J McAndrew: Eighth Commonwealth Mining and Metallurgical Congress, Australia and New Zealand, Publication 1, p. 80–86.

Franklin, JM, Gibson, HL, Jonasson, IR, and Galley, AG 2005, Volcanogenic massive sulphide deposits: Economic Geology 100th Anniversary Volume, p. 523–560.

Franklin, JM, Sangster, DF and Lydon, JW 1981, Volcanic-associated massive sulphide deposits: Economic Geology 75th Anniversary Volume, p. 485–627.

Fyon, JA and Crockett, JH 1982, Gold exploration in the Timmins district using field and lithogeochemical characteristics of carbonate alteration zones: Canadian Institute of Mining and Metallurgy, Special Volume 24, p. 113–129.

Galley, AG, Hannington, MD and Jonasson, IR 2007, Volcanogenic massive sulphide deposits, *in* Mineral Deposits of Canada *edited by* WD Goodfellow: Geological Association of Canada, Mineral Deposits Division, Special Publication 5, p. 141–161.

Gardner, Y, Hagemann, SG and Hay, R 2001, Gold mineralization at the Darlot–Centenary gold mine, southern Yandal greenstone belt, Eastern Goldfields Province, Western Australia: evidence for diverse mineralization styles and hydrothermal alteration types, *in* World-class gold camps and deposits in the eastern Yilgarn Craton, Western Australia, with special emphasis on the Eastern Goldfields Province *edited by* SG Hagemann, P Neumayr and WK Witt: Geological Survey of Western Australia, Record 2001/17, p. 127–150.

Gauthier, L, Hagemann, S, Robert, F 2007, The geological setting of the Golden Mile gold deposit, Kalgoorlie, WA, *in* Proceedings of Geoconferences (WA) Inc Kalgoorlie '07 Conference *edited by* FP Bierlein and CM Knox-Robinson: Geoscience Australia Record 2007/14, p. 181–185.

Goldfarb, RJ, Baker, T, Dube, B, Groves, DI, Hart, CJR and Gosselin, P 2005, Distribution, character and genesis of gold deposits in metamorphic terranes: Economic Geology 100th Anniversary Volume, p. 407–450.

Golding, SD, Clark, ME, Keele, RA, Wilson, AF and Keays, RR 1990, Geochemistry of Archaean epigenetic gold deposits in the Eastern Goldfields Province, Western Australia: Geology Department and University Extension, University of Western Australia, Publication 23, p. 141–176.

Golding, SD and Wilson, AF 1983, Geochemical and stable isotope studies of the No. 4 lode, Kalgoorlie, Western Australia: Economic Geology, 78, 438–450.

Griffin, TJ 2007, The exploration potential of the Yilgarn Craton: The obvious and not so obvious, *in* Proceedings of Geoconferences (WA) Inc Kalgoorlie '07 Conference *edited by* FP Bierlein and CM Knox-Robinson: Geoscience Australia Record 2007/14, p. 235–237.

Groves, DI, Goldfarb, RJ, Knox-Robinson, CM, Ojala, J, Gardoll, S, Yun, GY and Holyland, P 2000, Late-kinematic timing of gold deposits and significance for computer-based exploration techniques with emphasis on the Yilgarn Block, Western Australia: Ore Geology Reviews, v. 17, p. 1–38.

Guj, P, Fallon, M, McCuaig, TC and Fagan, R 2011, A time-series audit of Zipf's Law as a measure of terrane endowment and maturity in mineral exploration: Economic Geology, v. 106, p. 241–259.

Hagemann, SG, Brown, PE, Ridley, JR, Stern, P and Fournelle, J 1998, Ore petrology, chemistry and timing of electrum in the Archean hypozonal Transvaal lode gold deposit, Western Australia: Economic Geology, v. 93, p. 271–291.

Hagemann, SG, Groves, DI, Ridley, JR and Vearncombe, JR 1992, The Archean lode gold deposits at Wiluna, Western Australia: high-level brittle-style mineralization in a strike-slip regime: Economic Geology, v. 87, p. 1022–1053.

Hall, G 2007, Exploration success in the Yilgarn Craton: Insights from the Placer Dome experience – the need for integrated research, *in* Proceedings of Geoconferences (WA) Inc. Kalgoorlie '07 Conference *edited by* FP Bierlein and CM Knox-Robinson: Geoscience Australia, Record 2007/14, p. 199–202.

Hamlyn, PR, Keays, RR, Cameron, WE, Crawford, AJ and Waldron, HM 1985, Precious metals in magnesian low-Ti lavas: implications for metallogenesis and sulphur saturation in primary magmas: Geochimica et Cosmochimica Acta, v. 49, 1797–1811.

Hancock, EA, Green, AA, Huntington, JF, Schodlok, MC and Whitbourn, LB 2013, HyLogger-3: Implications of adding thermal-infrared sensing: Geological Survey of Western Australia, Record 2013/3, 24p.

Harding, TP 1985, Seismic characteristics and identification of negative flower structures, positive flower structures, and positive structural inversion: AAPG Bulletin, v. 69, p. 582–600.

Harrison, N, Bailey, A, Shaw, JD, Peterson, GN and Allen, CA 1990, Ora Banda gold deposits, *in* The Geology of Mineral Deposits of Australia and Papua New Guinea *edited by* FE Hughes: Australasian Institute of Mining and Metallurgy, Monograph 14, p. 389-394.

Hart, SR 1971, K, Rb, Cs, Sr and Ba contents and Sr isotope ratios of ocean floor basalts: Philosophical Transactions of the Royal Society of London, A268, p. 573–587.

Heath, CJ 2003, Fluid flow at the giant Golden Mile deposit, Kalgoorlie, Western Australia: Australian National University, PhD thesis, 182p. (unpublished).

Heath, CJ and Campbell, IH 2004, A new geochemical technique for gold exploration: alkali element mobility associated with gold mineralization in the West Australian goldfields: Economic Geology, v. 99, p. 313–324.

Henderson, RG and Hill, LV 1990, Reedy Gold Deposits, Meekatharra, *in* Geology of Mineral Deposits of Australia and Papua New Guinea *edited by* FE Hughes: Australasian Institute of Mining and Metallurgy, Monograph 14, p. 205–209.

Henson, PA, Blewett, RS, Roy, IG, Miller, JM and Czarnota, K 2010, 4D architecture and tectonic evolution of the Laverton region, eastern Yilgarn craton, Western Australia: Precambrian Research, v. 183, p. 338–355.

Hicks, JD 1990, Golden Crown gold deposit, *in* Geology of the Mineral Deposits of Australia and Papua New Guinea *edited by* FE Hughes: Australasian Institute of Mining and Metallurgy, Monograph 14, p. 217–220.

Holyland, PW and Ojala, VJ 1997, Computer aided structural targeting: two and three dimensional stress mapping: Australian Journal of Earth Sciences, v. 4, p. 421–432.

Hronsky, JMA 2014, Advances from traditional ore deposit models: AIG Symposium, Perth, Western Australia, August 2014, Controls on high-grade gold ore shoots: towards a new paradigm, Abstract and Powerpoint presentation (https://www.youtube.com/watch?v=KIfu6alX19w&feature=youtu.be).

Hronsky, JMA and Groves, DI 2008, Science of targeting: definition, strategies, targeting and performance measurement: Australian Journal of Earth Sciences, v. 55, p. 3–12.

Hronsky, JMA, Groves, DI, Loucks, RR and Begg, GC 2012, A unified model for gold mineralisation in accretionary orogens and implications for regional-scale exploration targeting methods: Mineralium Deposita, v. 47, p. 339–358.

Jia, K, Ly, X and Kerrich, R 2001, Stable isotope (O, H, S, C, and N) systematics of quartz vein systems in the turbidite-hosted Central and North Deborah gold deposits of the Bendigo gold field, central Victoria, Australia: constraints on the origin of ore-forming fluids. Economic Geology, v. 96, p. 705–721.

Jones, S 2014, Contrasting structural styles of gold deposits in the Leonora Domain: evidence for early gold deposition, Eastern Goldfields, Western Australia: Australian Journal of Earth Sciences, v. 61, p. 881–917.

Keats, W 1991, Geology and gold mines of the Bullfinch – Parker Range region, Southern Cross Province, Western Australia: Geological Survey of Western Australia, Report 28, 44p.

Kenworthy, S, Hagemann, SG and Chanter, SC 2001, Structural control and mineralization style of the quartz reef-hosted Golden Age gold mine, Wiluna greenstone belt, Yilgarn craton, *in* World-class Gold Camps and Deposits in the eastern Yilgarn Craton, Western Australia, with special emphasis on the Eastern Goldfields Province *edited by* SG Hagemann, P Neumayr and WK Witt: Geological Survey of Western Australia, Record 2001/17, p. 177–196.

Kerrich, R and Fryer, BJ 1979, Archaean precious-metal hydrothermal systems, Dome Mine, Abitibi Greenstone Belt: II REE and oxygen isotope relations: Canadian Journal of Earth Sciences, v. 16, p. 440–458.

Kishida, A and Kerrich, R 1987, Hydrothermal alteration zoning and gold concentration at the Kerr-Addison Archean lode gold deposit, Kirkland Lake, Ontario: Economic Geology, v. 82, p. 649–690.

Knight, JT, Groves, DI and Ridley, JR 1993, The Coolgardie Goldfield, Western Australia: district-scale controls on an Archean gold camp in an amphibolite facies terrane: Mineralium Deposita, v. 28, p. 436–456.

Knox-Robinson, CM 2000, Vectorial fuzzy logic: a novel technique for enhanced mineral prospectivity mapping, with reference to the orogenic gold mineralisation potential of the Kalgoorlie Terrane, Western Australia: Australian Journal of Earth Sciences, v. 47, p. 929–941.

Kohler, E, Dong, G, Maclean, D and Beilby, G 2000, Shear zone-hosted gold mineralisation, Jundee–Nimary goldfield, Yandal belt, *in* Yandal Greenstone Belt *edited by* GN Phillips and R Anand: Australian Institute of Geoscientists, Bulletin 32, p. 219–232.

Koljonen, T 1992, Results of mapping, *in* The Geochemical Atlas of Finland, Part 2: Geological Survey of Finland, Espoo, p. 107–137.

Krcmarov, R, Beardsmore, TJ, King, J, Kellett, R and Hay, R 2000, Geology, regolith, mineralisation and mining of the Darlot-Centenary gold deposit, Yandal belt, *in* Yandal Greenstone Belt *edited by* GN Phillips and R Anand: Australian Institute of Geoscientists, Bulletin 32, p. 351–372.

Large, RR, Bull, SW and Winefield, PR 2001, Carbon and oxygen isotope halo in carbonates related to the McArthur River (HYC) Zn-Pb-Ag deposit, north Australia: Implications for sedimentation, ore genesis, and mineral exploration: Economic Geology, v. 96, p. 1567–1593.

Laukamp, C, Cudahy, T and Murdie, R 2010, Hyperspectral remote mapping of Archaean lithologies and hydrothermal alteration mineralogy in the Eastern Goldfields Superterrane, Australia, *in* 2010 Australian Earth Science Convention 2010, Earth Systems: change, sustainability, vulnerability: Geological Society of Australia, Abstract No 98, p. 79–80.

Laukamp, C, Cudahy, T, Thomas, M, Jones, M, Cleverley, J, Oliver, N 2011, Hydrothermal mineral alteration patterns in the Mount Isa Inlier revealed by airborne hyperspectral data: Australian Journal of Earth Sciences, v. 58, p. 917–936.

Laukamp, C, Termin, KA, Pejcic, B, Haest, M, Cudahy, T 2012, Vibrational spectroscopy of calcic amphiboles – Applications for exploration and mining: European Journal of Mineralogy, v. 24, p. 863–878.

Lefebure, DV and Coveney, RM Jr 1995, Shale-hosted Ni-Zn-Mo-PGE, *in* Selected British Columbia Mineral Deposit Profiles, Volume 1 *edited by* DV Lefebure and GE Ray: British Columbia Ministry of Energy, Mines and Petroleum Resources, p. 45–47.

Lydon, JW 1984, Ore deposit models-8. Volcanogenic massive sulphide deposits, Part I, A descriptive model: Geoscience Canada, v. 11, p. 195–202.

Mair, JL, Ojala, V, Salier, BP, Groves, DI and Brown, SM 2000, Application of stress mapping in cross section to understanding ore geometry, predicting ore zones and developing drilling strategies: Australian Journal of Earth Sciences, v. 47, p. 895–912.

Markwell, TS 2003, Cornishman gold deposit, Southern Cross Mining District, WA, *in* Regolith Expressions of Australian Ore Systems *compiled by* CRM Butt, M Cornelius, KM Scott and IDM Robertson, CRC_LEME Thematic Volume, 3p.

Mayers, BJ and Warriner, S 1995, Copperhead gold mine, *in* Southern Cross Greenstone Belt, Geology and Gold Mines, Extended Abstracts, *compiled by* PJ Schwebel: Geoconferences (WA) Inc. Extended Abstracts Volume, p. 45–48.

McCuaig, TM, Beresford, S and Hronsky, J 2010, Translating the mineral systems approach into an effective exploration targeting system: Ore Geology Reviews, v. 38, p. 128–138.

McGrath, AG and Davison, I 1995, Damage zone geometry around fault tips: Journal of Structural Geology, v. 17, p. 1011–1024.

Micklethwaite, S and Cox, SF 2004, Fault-segment rupture, aftershock-zone fluid flow, and mineralization: Geology, v. 32, p. 813–816.

Miller, J, Nugus, M and Henson, P 2007, Importance of structural targeting: Case studies from the Eastern Goldfields Superterrane, *in* Proceedings of Geoconferences (WA) Inc Kalgoorlie '07 Conference, Kalgoorlie, Western Australia *edited by* FP Bierlein and CM Knox-Robinson: Geological Survey of Western Australia, Record 2007/14, p. 209–213.

Morey, AA, Weinberg, RF, Bierlein, FP and Davidson, GJ 2007a, Gold deposits of the Bardoc Tectonic Zone: a distinct style of orogenic gold in the Archaean Eastern Goldfields Province, Yilgarn Craton, Western Australia: Australian Journal of Earth Sciences, v. 54, p. 783–800.

Morey, AA, Weinberg, RF and Bierlein, FP 2007b, The structural controls of gold mineralisation within the Bardoc Tectonic Zone, Eastern Goldfields Province, Western Australia: implications for gold endowment in shear systems: Mineralium Deposita, v. 42, p. 583–600.

Mueller, AG 1991, The Savage Lode magnesian skarn in the Marvel Loch gold-silver mine, Southern Cross greenstone belt, Western Australia: Part 1. Structural setting, petrography and geochemistry: Canadian Journal of Earth Sciences, v. 28, p. 659–685.

Mueller, AG 1997, The Nevoria gold skarn deposit in Archean iron-formation, Southern Cross greenstone belt, Western Australia: Part I. Tectonic setting, petrography and classification: Economic Geology, v. 92, p. 181–209.

Mueller, AG and Groves, DI 1991, The classification of Western Australian greenstone-hosted gold deposits according to wallrock-alteration mineral assemblage: Ore Geology Reviews, v. 6, p. 291–331.

Mueller, AG, Groves, DI and Delor, CP 1991, The Savage Lode magnesian skarn in the Marvel Loch gold-silver mine, Southern Cross greenstone belt, Western Australia: Part 2: Pressure-temperature estimates and constraints on fluid sources: Canadian Journal of Earth Sciences, v. 28, p. 686–705.

Mueller, AG and McNaughton, NJ 2000, U-Pb ages constraining batholiths emplacement, contact metamorphism and the formation of gold and W-Mo skarns in the Southern Cross area, Yilgarn craton, Western Australia: Economic Geology, v. 95, p. 1231–1257.

Neumayr, P, Walshe, JL, Petersen, K, Young, C, Roache, A and Halley, S 2007, Redox boundaries in gold deposits of the Eastern Goldfields, Yilgarn, WA – mapping a critical genetic parameter?, *in* Proceedings of Geoconferences (WA) Inc Kalgoorlie '07 Conference *edited by* FP Bierlein and CM Knox-Robinson: Geoscience Australia, Record 2007/14, p. 176–180.

Newton, PGN, Smith, B, Bolger, C and Holmes, R 1998, Randalls gold deposits, *in* Geology of Australian and Papua New Guinea Mineral Deposits *edited by* DA Berkman and DH McKenzie: Australasian Institute of Mining and Metallurgy, Monograph 22, p. 225–232.

Nguyen, PT, Cox, SF, Harris, LB and Powell, CMcA 1998, Fault valve behaviour in optimally oriented shear zones: an example at the Revenge gold mine, Kambalda, Western Australia: Journal of Structural Geology, v. 20, p. 1625–1640.

Nichols, SJ and Hagemann, SG 2014, Structural and hydrothermal alteration evidence for two gold mineralisation events at the New Celebration gold deposits in Western Australia: Australian Journal of Earth Sciences, v. 61, 113–141.

Norris, N 1990, New Celebration gold deposits, *in* Geology of the Mineral Deposits of Australia and Papua New Guinea *edited by* FE Hughes: Australasian Institute of Mining and Metallurgy, Monograph 14, p. 449–454.

Nugus, MJ, Blenkinsop, TG, Dominy, SC and Robson, S 2003, Enigmatic kinematics resolved in the Taurus Shear Zone, Golden Pig Gold Mine, Southern Cross, Western Australia – Resource implications: Australasian Institute of Mining and Metallurgy, Fifth International Mining Geology Conference, Conference Proceedings, p. 171–179.

Nurmi, P, Lestinen, P and Niskavaara, H 1991, Geochemical characteristics of mesothermal gold deposits in the Fennoscandian Shield, and a comparison with selected Canadian and Australian deposits: Bulletin of the Geological Survey of Finland, 351, 101p.

Ojala, VJ, Ridley, JR Groves, DI and Hall, GC 1993, The Granny Smith gold deposit: the role of heterogeneous stress distribution at an irregular granitoid contact in a greenschist facies terrane: Mineralium Deposita, v. 28, p. 408–419.

Oliver, NHS, Valenta, RK and Wall, VJ 1990, The effect of heterogeneous stress and strain on metamorphic fluid flow, Mary Kathleen, Australia, and a model for large-scale fluid circulation: Journal of Metamorphic Geology, v. 8, p. 311–331.

Peacock, DCP 1991, Displacement and segment linkage in strike-slip fault zones: Journal of Structural Geology, v. 9, p. 1025–1035.

Perring, CS, Barnes, SJ and Hill, RET 1995, The physical volcanology of Archaean komatiite sequences from Forrestania, Southern Cross Province, Western Australia: Lithos, v. 34, p. 189–207.

Perring, CS, Groves, DI and Shellabear, JN 1990, Ore geochemistry, *in* Gold Deposits of the Archaean Yilgarn Block, Western Australia: nature, genesis and exploration guides *edited by* SE Ho, DI Groves and JM Bennett. University of Western Australia, Department of Geology and University Extension Service, Publication 20, p. 93–101.

Phillips, GN, 1986, Geology and alteration in the Golden Mile, Kalgoorlie: Economic Geology, v. 81. P. 779-808.

Phillips, GN and Groves, DI 1983, The nature of Archaean gold bearing fluids as deduced from gold deposits of Western Australia: Journal of the Geological Society of Australia, v. 30, p. 25–40.

Phillips, GN and Groves, DI 1984, Fluid access and fluid–wallrock interaction in the genesis of the Archean gold–quartz vein deposit at Hunt mine, Kambalda, Western Australia, *in* Gold '82 – The Geology, Geochemistry and Genesis of Gold Deposits *edited by* RP Foster: Geological Society of Zimbabwe, Special Publication 1, AA Balkema, p. 389-416.

Phillips, GN, Vearncombe, JR, Blucher, I and Rak, D 2000, Bronzewing gold deposit – 1998 perspective, *in* Yandal Greenstone Belt *edited by* GN Phillips and R Anand: Australian Institute of Geoscientists, Bulletin 32, p. 283–298.

Quigley, ME 2005, Mineralogical interpretation of VNIR–SWIR Hylogger data, Kanowna Belle gold mine, Eastern Goldfields, WA: MERIWA Project 373, Phase 1, 163p.

Quigley, ME 2006, Mineralogical interpretation of TIR-Logger data, Kanowna Belle mine, Eastern Goldfields, WA: MERIWA Project 373, Phase 3, 68p.

Rasilainen, K, Nurmi, PA and Bornhorst, TJ 1993, Rock geochemical implications for gold exploration in the late Archean Hattu schist belt, Ilomantsi, eastern Finland, *in* Geological Development, Gold Mineralization and Exploration Methods in the Late Archean Hattu schist belt, Ilomantsi, eastern Finland *edited by* P Nurmi and P Sorjonen-Ward: Geological Survey of Finland, Special Paper 17, p. 353–362.

Rasmussen, B, Mueller, AG and Fletcher, IR 2009, Zirconolite and xenotime U-Pb age constraints on the emplacement of the Golden Mile Dolerite sill and gold mineralisation at the Mt Charlotte mine, Eastern Goldfields Province, Yilgarn craton, Western Australia: Contributions to Mineralogy and Petrology, v. 157, p. 559–572.

Ridley, JR 1993, The relations between mean rock stress and fluid flow in the crust: with reference to vein- and lode-style gold deposits: Ore Geology Reviews, v. 8, p. 23–37.

Ridley, JR and Mengler, F 2000, Lithological and structural controls on the form and setting of vein stockwork orebodies at the Mount Charlotte gold deposit, Kalgoorlie: Economic Geology, v. 95, p. 85–98.

Ringwood, AE 1979, Origin of the Earth and Moon. Springer-Verlag, New York, 295p.

Roache, TJ, Walshe, JL, Huntington, JF, Quigley, MA, Yang, K, Bil, BW, Blake, KL and Hyvarinen, T 2011, Epidote-clinozoisite as a hyperspectral tool in exploration for Archean gold: Australian Journal of Earth Sciences, v. 58, p. 813–822.

Robert, F and Brown, AC 1986, Archean gold-bearing quartz veins at the Sigma mine, Abitibi greenstone belt, Quebec, Parts 1 and 2: Economic Geology, v. 81, p. 578–592 and p. 593–616.

Roberts, FI, Witt, WK and Westaway, J 2004, Gold mineralization in the Edjudina–Kanowna region, Eastern Goldfields, Western Australia: Geological Survey of Western Australia, Report 90.

Rolley, PJ and Baxter, JL 1990, Marvel Loch gold deposit, *in* Geology of the Mineral Deposits of Australia and Papua New Guinea *edited by* FE Hughes: Australasian Institute of Mining and Metallurgy, Monograph 14, p. 297–300.

Ross, AA, Barley, ME, Brown, SJA, McNaughton, NJ, Ridley, JR and Fletcher, IR 2004, Young porphyries, old zircons: new constraints on the timing of deformation and gold mineralisation in the Eastern Goldfields from SHRIMP U-Pb zircon dating at the Kanowna Belle mine, Western Australia: Precambrian Research, v. 128, p. 105–142.

Salier, BP, Groves, DI, McNaughton, NJ and Fletcher, IR 2004, The world class Wallaby gold deposit, Laverton, Western Australia: an orogenic-style overprint on a magmatic-hydrothermal magnetite-calcite alteration pipe?: Mineralium Deposita, v. 39, p. 473–494.

Salier, BP, Groves, DI, McNaughton, NJ and Fletcher, IR 2005, Geochronological and stable isotope evidence for widespread orogenic gold mineralization from a deep-seated fluid source at ca 2.65 Ga in the Laverton gold province, Western Australia: Economic Geology, v. 100, p. 1363–1388.

Schiller, JC and Hannah, JP 1990, Tower Hill gold deposit, *in* Geology of the Mineral Deposits of Australia and Papua New Guinea *edited by* FE Hughes: Australasian Institute of Mining and Metallurgy, Monograph 14, p. 349–352.

Sibson, RH 1990, Rupture nucleation on unfavourably oriented faults: Bulletin of the Seismological Society of America, v. 80, p. 1580–1604.

Skwarnecki, MS 1989, Alteration and deformation in a shear zone hosting gold mineralization at Harbour Lights, Leonora, Western Australia, *in* Advances in Understanding Precambrian Gold Deposits, Volume II *edited by* SE Ho and DI Groves: Geology Department and University Extension, University of Western Australia, Publication 12, p. 111–130.

Smith, AB 2000, Structural controls and wallrock alteration across the greenschist-amphibolite facies transition at Sons of Gwalia gold deposit, Leonora, Western Australia: University of Western Australia, PhD thesis (unpublished).

Sonntag, I, Laukamp, C and Hagemann, SG 2012, Low potassium hydrothermal alteration in low sulfidation epithermal systems, an example from the Co-O mine, Philippines: Ore Geology Reviews, v. 45, p. 47–60.

Starfield, AM and Cundell, PA 1988, Towards a methodology for rock mechanics modelling: International Journal of Rock Mechanics Science and Geomechanics Abstracts, v. 25.3, p. 99–106.

Sun, SS and McDonough, WF 1989, Chemical and isotopic systematics of oceanic basalts: implications for mantle composition processes: Geological Society Special Publication 42, p. 313–345.

Swager, CP 1989, Structure of Kalgoorlie greenstones – regional deformation history and implications for the structural setting of the Golden Mile gold deposits: Geological Survey of Western Australia, Report 25, p. 59–84.

Tattum, CM 1953, Geology of the Sons of Gwalia goldmine, *in* Geology of Australian Ore Deposits, Volume 1 *edited by* AB Edwards: Australasian Institute of Mining and Metallurgy, Melbourne, p. 208–214.

Thomas, A, Johnson, K and MacGeehan, PJ 1990, Norseman gold deposits, *in* Geology of the Mineral Deposits of Australia and Papua New Guinea *edited by* FE Hughes: Australasian Institute of Mining and Metallurgy, Monograph 14, p. 493–504.

Thompson, MJ, Watchorn, RB, Bonwick, CM, Frewin, MO, Goodgame, VR, Pyle, MJ and MacGeehan, PJ 1990, Gold deposits of the Hill 50 gold mine NL at Mount Magnet, *in* Geology of the Mineral Deposits of Australia and Papua New Guinea *edited by* FE Hughes: Australian Institute of Mining and Metallurgy, Monograph 14, p. 221–242.

Tripp, GI 1998, Structural analysis of gold mines in the Siberia – Ora Banda – Mt Pleasant mining district: Centaur Mining and Exploration Limited (unpublished report OB-372), March, 1998, 33p.

Tripp, G 2013, Structural and stratigraphic controls on hydrothermal alteration and gold mineralisation, North Kalgoorlie District, Western Australia: James Cook University of North Queensland, Townsville, PhD thesis (unpublished).

Tripp, GI and Vearncombe, JR 2004, Fault/fracture density and mineralization: a contouring method for targeting in gold exploration: Journal of Structural Geology, v. 26, p. 1087–1108.

Turner, G. and HISEIS Staff 2014, Finding gold – time for a seismic shift in exploration thinking: Australian Institute of Geoscientists Gold14 Symposium, Kalgoorlie, Western Australia, Abstracts Volume, p. 134–136.

van Ruitenbeek, FJ, Cudahy, TJ, van der Meer, FD and Hale, M 2012, Characterization of the hydrothermal systems associated with Archean VMS-mineralization at Panorama, Western Australia, using hyperspectral, geochemical and geothermometric data: Ore Geology Reviews, v. 45, p. 33–46.

Vearncombe, JR 1992, Archaean gold mineralisation in a normal-motion shear zone at Harbour Lights, Leonora, Western Australia: Mineralium Deposita, v. 27, p. 182–191.

Vearncombe, JR 1998, Shear zones, fault networks and Archean gold: Geology, v. 26, p. 855–858.

Vearncombe, J and Vearncombe, S 1999, The spatial distribution of mineralization: applications of Fry analysis: Economic Geology, v. 94, p. 475–486.

Vielreicher, RM, Groves, DI, Ridley, JR and McNaughton, NJ 1994, A replacement origin for the BIF-hosted gold deposit at Mt Morgans, Yilgarn Block, Western Australia: Ore Geology Reviews, v. 9, p. 325–347.

Vielreicher, NM, Groves, DI and McNaughton, NJ 2015, Reply to Discussion: The timing of gold mineralization across the eastern Yilgarn Craton using U-Pb geochronology of hydrothermal phosphate minerals: Mineralium Deposita, v. 50, p. 889–894.

Vielreicher, NM, Groves, DI, Snee, LW, Fletcher, IR and McNaughton, NJ 2010, Broad synchroneity of three gold mineralization styles in the Kalgoorlie Gold Field: SHRIMP U-Pb and Ar/Ar geochronological evidence: Economic Geology, v. 105, p. 187–227.

Walshe, J, Neumayr, P and Petersen, K 2006, Scale-integrated architectural and geodynamic controls on alteration and geochemistry of gold systems in the Eastern Goldfields Province, Yilgarn craton: MERIWA Report 256, 290p.

Waring, CL, Andrew, AS and Ewers, GR 1998, Use of O, C, and S stable isotopes in regional mineral exploration: AGSO Journal of Australian Geology and Geophysics, v. 17, p. 301–313.

Warren, JD, Thebaud, N, Miller, JM and Micklethwaite, S 2015, Distinguishing between local versus regional extension as a control on orogenic gold mineralisation: The new 2.4 Moz Castle Hill Camp, WA: Precambrian Research, v. 269, p. 242–260.

Watkins, KP and Hickman, AA 1990, Geological evolution and mineralization of the Murchison Province, Western Australia: Geological Survey of Western Australia, Bulletin 137, 252p plus appendices.

Weinberg, RF and Vanderborgh, P 2008, Extension and gold mineralization in the Archean Kalgoorlie Terrane, Yilgarn craton: Precambrian Research, v. 161, p. 77–88.

Williams, PR, Nesbit, RW and Etheridge, MA 1989, Shear zones, gold mineralization and structural history in the Leonora district, Eastern Goldfields Province, Western Australia: Australian Journal of Earth Sciences, v. 36, p. 383–403.

Wilson, AC 1990, North Morning Star (Parkinson Pit) Gold Deposit, Mount Magnet, *in* Geology of the Mineral Deposits of Australia and Papua New Guinea *edited by* FE Hughes: Australian Institute of Mining and Metallurgy, Monograph 14, p. 249–253.

Witt, WK 1990, Geology of the Bardoc 1:100 000 sheet: Geological Survey of Western Australia, Explanatory Notes Series, 50p.

Witt, WK 1991, Regional metamorphic controls on alteration associated with gold mineralization in the Eastern Goldfields province, Western Australia: Implications for the timing and origin of Archean lode-gold deposits: Geology, v. 19, p. 982–985.

Witt, WK 1992a, Gold deposits of the Menzies and Broad Arrow areas, Western Australia: Part 1 of a systematic study of gold mines of the Menzies–Kambalda region: Geological Survey of Western Australia, Record 1992/15, 159p.

Witt, WK 1992b, Gold deposits of the Mount Pleasant – Ora Banda areas, Western Australia: Part 2 of a systematic study of gold mines of the Menzies–Kambalda region: Geological Survey of Western Australia, Record 1992/14, 104p.

Witt, WK 1992c, Gold deposits of the Kalgoorlie–Kambalda – St Ives areas, Western Australia: Part 3 of a systematic study of gold mines of the Menzies–Kambalda region: Geological Survey of Western Australia, Record 1992/15, 108p.

Witt, WK 1993a, Gold mineralization in the Menzies–Kambalda region, Eastern Goldfields, Western Australia: Geological Survey of Western Australia, Report 39, 165p.

Witt, WK 1993b, Lithological and structural controls on gold mineralization in the Archaean Menzies–Kambalda area, Western Australia: Australian Journal of Earth Sciences, v. 40, p. 65–86.

Witt, WK 2001, Tower Hill gold deposit, Western Australia: an atypical, multiply deformed, Archaean gold-quartz vein deposit: Australian Journal of Earth Sciences, v. 48, p. 81–99.

Witt, WK, Drabble, M and Bodycoat, FM 2001, Yilgarn Star gold deposit, Southern Cross greenstone belt, Western Australia: geological setting and characteristics of an amphibolite-facies orogenic gold deposit, *in* World-class gold camps and deposits in the eastern Yilgarn Craton, Western Australia, with special emphasis on the Eastern Goldfields Province *edited by* SG Hagemann, P Neumayr, and WK Witt: Geological Survey of Western Australia, Record 2001/17, p. 456–462.

Witt, WK, Ford, A, Hanrahan, B and Mamuse, A 2013, Regional-scale targeting for gold in the Yilgarn Craton: Part 1 of the Yilgarn Gold Exploration Targeting Atlas: Geological Survey of Western Australia, Report 125, 131p.

Witt, WK, Ford, A and Hanrahan, B 2015a, District-scale targeting for gold in the Yilgarn Craton: Part 2 of the Yilgarn Gold Exploration Targeting Atlas: Geological Survey of Western Australia, Report 132, 277p.

Witt, WK, Groves, DI and Ho, SE 1994, Ore Deposits of the Eastern Goldfields, Western Australia: Geological Society of Australia (WA Division), Excursion Guidebook No 8, 80p.

Witt, WK and Hagemann, SG 2012, Synvolcanic hydrothermal alteration in Yilgarn Craton greenstones: Centre for Exploration Targeting Newsletter, v. 22 (December 2012), p. 28–39.

Witt, WK and Hagemann, SG 2013a, Intrusion-related hydrothermal alteration in the Yilgarn Craton, Part 1: Centre for Exploration Targeting Newsletter, v. 23 (March 2013), p. 1–14.

Witt, WK and Hagemann, SG 2013b, Intrusion-related hydrothermal alteration in the Yilgarn Craton, Part 2: Centre for Exploration Targeting Newsletter, v. 24 (June 2013), p. 1–13.

Witt, WK, Hagemann, SG and Cassidy, KF, 2015b, A proposed revision of the orogenic gold class, based on multiple ore fluid compositions inferred from proximal alteration: Society for Geology Applied to Mineral Deposits Conference, Nancy, France, Abstracts.

Witt, WK, Hagemann, SG and Miller, JMcL 2012, Lode gold mineralization: Tectonic and structural controls, from continental- to deposit-scale: Australian Institute of Geoscientists, Structural Geology and Resources Symposium 2012, Kalgoorlie, Western Australia, Abstracts p.176–179.

Witt, WK, Hagemann, SG, Ojala, J, Laukamp, C, Vennemann, T, Villanes, C and Nykanen, V 2014, Multiple methods for regional- to mine-scale targeting, Pataz gold field, northern Peru: Australian Journal of Earth Sciences, v. 61, p. 43–58.

Witt, WK and Hammond, DP 2008, Archean gold mineralisation in an intrusion-related, geochemically zoned, district-scale alteration system in the Carosue Basin, Western Australia: Economic Geology, v. 103, p. 445–454.

Witt, WK, Knight, JT and Mikucki, EM 1997, A synmetamorphic lateral fluid flow model for gold mineralization in the Archaean southern Kalgoorlie and Norseman Terranes, Western Australia: Economic Geology, v. 92, p. 407–437.

Witt, WK, Laneyrie, T and Gates, K, in press, Red October gold deposit, *in* Australian Ore Deposits: Australasian Institute of Mining and Metallurgy, Monograph.

Witt, WK, Mason, DR and Hammond, DP 2009, Archaean Karari gold deposit, Eastern Goldfields Province, a monzonite-associated disseminated gold deposit: Australian Journal of Earth Sciences, v, 56, p. 1061–1086.

Woodward, HP 1906, Auriferous Deposits and Mines of Menzies, North Coolgardie Goldfield: Geological Survey of Western Australia, Bulletin 22, 104p.

Yang, K, Huntington, JF, Gemmell, JB and Scott, KM 2011, Variations in composition and abundance of white mica in the hydrothermal alteration system at Hellyer, Tasmania, as revealed by infrared reflectance spectroscopy: Journal of Geochemical Exploration, v. 108, p. 143–156.

Zhou, T, Phillips, GN, Denn, S and Burke, S 2003, Woodcutters goldfield: gold in an Archaean granite, Kalgoorlie, Western Australia: Australian Journal of Earth Sciences, v. 50, p. 553–569.

Appendix

Results of whole-rock geochemical analyses from the Red October mine

Genalysis Job number	Hole ID	Sample ID	Depth (m)		Au	Au (repeat analysis)	Al	As	Cs	K	Rb	Th
			From	To				(ppm)				
1206.0 / 1104238	RORD002	141692	198.5	199.5	X		21806	X	1.92	263	2.57	0.27
1206.0 / 1104238	RORD002	141693	208.5	209.5	X		19426	X	2.12	221	2.57	0.16
1206.0 / 1104238	RORD002	141694	218.5	219.5	X		21871	26	1.38	147	2.03	0.15
1206.0 / 1104238	RORD002	141695	223.5	224.5	X		21147	X	2.28	132	2.4	0.13
1206.0 / 1104238	RORD002	141696	228.5	229.5	X		23103	X	4.94	516	6.83	0.13
1206.0 / 1104238	RORD002	141697	233.5	234.5	X		24460	X	6.02	770	9.02	0.15
1206.0 / 1104238	RORD002	141698	238.5	239.5	0.011		22171	62	1.04	219	2.26	0.12
1206.0 / 1104238	RORD002	141699	243.5	244.5	0.008		35757	X	0.74	89	0.96	0.2
1206.0 / 1104238	RORD002	141700	244.5	245.5	0.012		33312	X	0.74	63	0.81	0.18
1206.0 / 1104238	RORD002	141701	245.5	246.5	0.005		36059	X	0.69	64	0.66	0.2
1206.0 / 1104238	RORD002	141702	246.5	247.5	0.007		36808	X	0.76	130	0.95	0.2
1206.0 / 1104238	RORD002	141703	247.5	248.5	1.106		41804	1461	1.42	572	3.01	0.23
1206.0 / 1104238	RORD002	141704	248.5	249.2	39.965	35.85	43172	31043	4.49	17256	68.67	0.23
1206.0 / 1104238	RORD002	141706	249.2	250.0	13.63	12.4	34226	4092	1.38	13632	47.64	1.21
1206.0 / 1104238	RORD002	141707	250.0	250.5	2.282		52319	7002	2.39	21423	78.65	1.44
1206.0 / 1104238	RORD002	141708	250.5	251.5	1.168		61440	5728	3.11	10801	43.58	1.74
1206.0 / 1104238	RORD002	141709	251.5	252.5	0.61		66355	2676	5.06	9950	43.54	1.86
1206.0 / 1104238	RORD002	141710	252.5	253.5	0.035		68017	173	1.91	4064	15.44	1.9
1206.0 / 1104238	RORD002	141711	253.5	254.5	2.313		67504	5434	2.82	6249	24.42	1.88
1206.0 / 1104238	RORD002	141712	254.5	255.5	1.602		69034	4300	4.41	9745	41.65	1.99
1206.0 / 1104238	RORD002	141713	255.5	256.5	0.121		63206	533	4.21	7355	35.32	1.79
1206.0 / 1104238	RORD002	141714	256.5	257.5	3.482	3.28	62648	14425	5.74	15034	67.32	1.75
1206.0 / 1104238	RORD002	141715	257.5	258.5	0.579		62447	2627	3.93	6989	33.41	1.79
1206.0 / 1104238	RORD002	141716	258.5	259.5	0.076		64991	138	3.23	5235	24.6	1.84
1206.0 / 1104238	RORD002	141717	259.5	260.3	4.692	4.93	55787	23579	4.42	21197	84.58	1.52
1206.0 / 1104238	RORD002	141718	260.3	261	0.188		67212	719	2.15	5452	22.04	2.04
1206.0 / 1104238	RORD002	141719	261	262	0.187		67009	1083	1.39	4634	17.52	1.91
1206.0 / 1104238	RORD002	141720	262	263	0.041		67420	235	0.68	4193	12.6	1.91

NOTE: X = below detection limit

Genalysis Job number	Hole ID	Sample ID	Depth (m)		Au	Au (repeat analysis)	Al	As	Cs	K	Rb	Th
			From	To	(ppm)							
1206.0 / 1104238	RORD002	141721	263	264	0.017		71168	76	1.03	4372	15.55	1.99
1206.0 / 1104238	RORD002	141722	272	273	0.016		67565	70	0.6	3355	9.47	1.85
1206.0 / 1104238	RORD004	141723	242	243	X		35642	15	4.38	1434	7.83	0.22
1206.0 / 1104238	RORD004	141724	265	266	0.005		52087	X	0.54	565	0.68	0.28
1206.0 / 1104238	RORD004	141726	275.9	276.35	0.913		34371	1371	1.09	1654	4.85	1.33
1206.0 / 1104238	RORD004	141727	276.35	277	0.095		53193	X	1.26	2310	5.26	0.61
1206.0 / 1104238	RORD004	141728	277	278.1	0.049		47106	X	0.4	737	1.64	2.03
1206.0 / 1104238	RORD004	141729	278.1	279.1	0.046		57406	14	0.5	1027	2.06	0.35
1206.0 / 1104238	RORD004	141730	295	296	0.078		49384	202	6.17	3730	15.3	0.28
1206.0 / 1104238	RORD004	141731	305	306	X		50748	X	0.95	946	2.54	0.27
1206.0 / 1104238	RORD004	141732	315	316	X		55877	X	0.29	978	1.03	0.29
1206.0 / 1104238	RORD004	141733	326.6	327.6	X		53848	76	0.26	1499	1.98	0.29
1206.0 / 1104238	RORD004	141734	327.6	328	1.081		26341	1210	3.47	5195	18.32	0.55
1206.0 / 1104238	RORD004	141735	328	329	X		54169	106	1.45	1645	5.11	0.29
1206.0 / 1104238	RORD004	141736	340	341	X		20903	14	1.26	196	2.11	0.1
1206.0 / 1104238	RORD004	141737	345	346	X		22521	X	2.56	278	3.2	0.13
1206.0 / 1104238	RORD004	141738	350	351	X		24365	X	3.43	260	3.84	0.13
1206.0 / 1104238	RORD004	141739	355	356	X		30675	X	3.14	551	5.39	0.2
1206.0 / 1104238	RORD004	141740	360.3	361.3	X		30122	X	2.12	437	4.3	0.16
1206.0 / 1104238	RORD004	141741	361.3	362.3	0.009		29072	23	1.36	359	3.34	0.15
1206.0 / 1104238	RORD004	141742	362.3	363.3	0.01		34142	17	1.33	459	3.58	0.17
1206.0 / 1104238	RORD004	141743	363.3	364.3	X		36858	15	0.97	265	1.79	0.19
1206.0 / 1104238	RORD004	141744	364.3	365.3	X		38016	X	0.76	116	1.04	0.2
1206.0 / 1104238	RORD004	141745	365.3	366	0.013		31472	32	16.62	20366	109.34	0.16
1206.0 / 1104238	RORD004	141746	366	367	0.013		36589	123	4.63	5958	25.85	0.19
1206.0 / 1104238	RORD004	141747	367	367.75	0.271		46754	1584	2.16	13042	47.02	0.25
1206.0 / 1104238	RORD004	141748	367.75	368.25	2.383	2.31	23106	2346	0.58	4772	15.88	0.85
1206.0 / 1104238	RORD004	141749	368.25	369.25	X		55230	40	1.74	12524	43	1.5
1206.0 / 1104238	RORD004	141750	369.25	370	X		59748	57	1.55	11606	40.53	1.56
1206.0 / 1104238	RORD004	141751	370	370.9	0.009		65620	X	1.13	3550	14.65	1.8

NOTE: X = below detection limit

Genalysis Job number	Hole ID	Sample ID	Depth (m)		Au	Au (repeat analysis)	Al	As	Cs	K	Rb	Th
			From	To				(ppm)				
1206.0 / 1104238	RORD004	141752	370.9	371.9	X		58113	X	5.42	8401	38.91	1.64
1206.0 / 1104238	RORD004	141753	371.9	372.35	0.008		57561	X	3.33	6769	28.4	1.58
1206.0 / 1104238	RORD004	141754	372.35	373	X		63487	X	0.84	3316	8.55	1.81
1206.0 / 1104238	RORD004	141756	373	374	X		67777	X	1.01	3149	8.57	1.87
1206.0 / 1104238	RORD004	141757	374	375	X		68552	X	0.81	3556	10.93	1.86
1206.0 / 1104238	RORD004	141758	375	376	0.007		66199	21	0.75	2967	9.06	1.92
1206.0 / 1104238	RORD004	141759	376	377	X		65563	X	0.75	4271	12.65	1.79
1206.0 / 1104238	RORD004	141760	377	378	X		67523	X	0.82	3506	10.74	1.99
1206.0 / 1104238	RORD004	141761	381	382	0.023		66747	160	1.92	4302	17.51	2.02
1206.0 / 1104238	RORD004	141762	386	387	X		68235	X	0.95	3806	14.62	1.95
1206.0 / 1104238	RORD004	141763	391	392	X		66319	X	0.35	2715	8.53	1.83
1206.0 / 1104788	RORD001	141764	304	305	X		17918	0.8	1.7	837	5.47	0.23
1206.0 / 1104788	RORD001	141765	309	310	X		18081	X	1.6	1407	8.64	0.13
1206.0 / 1104788	RORD001	141766	314	315	X		18398	X	1.2	558	2.94	0.11
1206.0 / 1104788	RORD001	141767	319	320	X		18612	X	1.05	371	2.04	0.11
1206.0 / 1104788	RORD001	141768	324	325	X		19303	X	1.6	350	2.3	0.11
1206.0 / 1104788	RORD001	141769	329	330	X		20274	X	2.03	490	3.52	0.13
1206.0 / 1104788	RORD001	141770	334	335	X		25592	9	8.5	2986	20.49	0.14
1206.0 / 1104788	RORD001	141771	335	336	X		21196	14.3	5.39	1884	12.63	0.12
1206.0 / 1104788	RORD001	141772	336	337	0.008		16976	43.2	5.08	2052	11.92	0.09
1206.0 / 1104788	RORD001	141773	337	338	0.033		18636	359.6	9.17	4125	23.27	0.11
1206.0 / 1104788	RORD001	141774	338	339	0.151		17088	501.4	3.26	1276	8.46	0.12
1206.0 / 1104788	RORD001	141776	339	340	0.016		18737	57.1	0.68	211	1.08	0.09
1206.0 / 1104788	RORD001	141777	340	341	X		22737	30.9	0.94	209	1.35	0.12
1206.0 / 1104788	RORD001	141778	341	342	X		26841	3.2	1.67	529	3.53	0.15
1206.0 / 1104788	RORD001	141779	342	343.1	X		28912	14.2	1.7	676	3.87	0.16
1206.0 / 1104788	RORD001	141780	343.1	343.5	0.011		27437	66.2	1.73	822	4.58	0.16
1206.0 / 1104788	RORD001	141781	343.5	344.08	0.018		32917	281.7	2.61	1546	8.47	0.21
1206.0 / 1104788	RORD001	141782	344.08	344.54	10.897	10.19	26604	2082.3	12.91	11764	57.13	0.16
1206.0 / 1104788	RORD001	141783	344.54	345.9	0.013		39909	40.2	8.69	12577	82.39	0.2

NOTE: X = below detection limit

Genalysis Job number	Hole ID	Sample ID	Depth (m)		Au	Au (repeat analysis)	Al	As	Cs	K	Rb	Th
			From	To	(ppm)							
1206.0 / 1104788	RORD001	141784	345.9	346.75	0.05		48342	15.9	8.08	11606	75.01	0.24
1206.0 / 1104788	RORD001	141785	346.75	347.75	0.059		38916	33.3	1.37	838	3.77	0.22
1206.0 / 1104788	RORD001	141786	347.75	348.75	0.144		33651	390.6	2.39	3226	13.19	0.2
1206.0 / 1104788	RORD001	141787	348.75	349.15	0.068		36246	36.8	1.24	1828	6.43	0.21
1206.0 / 1104788	RORD001	141788	349.15	350.3	0.224		46341	726.3	2.6	7574	28.46	0.31
1206.0 / 1104788	RORD001	141789	350.3	350.85	0.629		39029	1740.9	1.66	13714	47.13	0.77
1206.0 / 1104788	RORD001	141790	350.85	351.25	0.479		64149	213.2	1.33	8813	29.21	1.56
1206.0 / 1104788	RORD001	141791	351.25	352	0.148		45517	201.7	0.44	2601	7.71	1.31
1206.0 / 1104788	RORD001	141792	352	353	0.071		60461	127.3	0.62	1841	6.21	1.72
1206.0 / 1104788	RORD001	141793	353	354	0.023		70377	20.7	0.42	1811	3.59	1.99
1206.0 / 1104788	RORD001	141794	354	355	0.024		69698	60	0.51	2475	5.55	1.93
1206.0 / 1104788	RORD001	141795	355	356	X		69081	16	0.44	2571	5.76	2
1206.0 / 1104788	RORD001	141796	356	357	0.011		68832	14.8	0.48	2538	5.5	2
1206.0 / 1104788	RORD001	141797	357	358	0.27		68727	1209.4	0.61	2733	6.34	1.97
1206.0 / 1104788	RORD001	141798	358	359	0.343		68709	1880.7	1.28	3508	11.34	1.98
1206.0 / 1104788	RORD001	141799	359	360	0.009		70107	129.8	0.49	2565	6.73	1.98
1206.0 / 1104788	RORD001	141800	360	361	0.014		67963	49.5	0.57	3102	8.98	1.87
1206.0 / 1104788	RORD001	141801	361	361.5	X		67263	35.5	0.62	3163	8.08	1.86
1206.0 / 1104788	RORD001	141802	361.5	362.5	0.508		61071	2498.5	1.84	8306	30.16	1.71
1206.0 / 1104788	RORD001	141803	362.5	363.08	1.968		56517	29815.9	3.14	23186	81.65	1.66
1206.0 / 1104788	RORD001	141804	363.08	363.7	4.298		35306	19198	2.3	13524	50.37	1.06
1206.0 / 1104788	RORD001	141806	363.7	364.1	2.012		64512	11889.8	3.65	13777	48.76	1.94
1206.0 / 1104788	RORD001	141807	364.1	364.5	16.806	14.06	67123	1897.3	1.6	8324	29.45	1.87
1206.0 / 1104788	RORD001	141808	364.5	365.2	14.744	13.97	61650	11645.8	3.32	16730	59.56	1.77
1206.0 / 1104788	RORD001	141809	365.2	365.5	3.167		52412	14218.9	2.25	18584	68.7	1.51
1206.0 / 1104788	RORD001	141810	365.5	366.3	0.516		70236	1422.7	3.36	7195	29.08	2.02
1206.0 / 1104788	RORD001	141811	366.3	366.8	1.708		62901	6728.6	2.25	8095	30.03	1.84
1206.0 / 1104788	RORD001	141812	366.8	367.25	1.022		65707	2862	2.35	5657	21.52	1.83
1206.0 / 1104788	RORD001	141813	367.25	367.7	3.342		52696	11411.1	2.62	9487	36.73	1.54
1206.0 / 1104788	RORD001	141814	367.7	368.65	0.067		68855	156.9	1.44	2572	8.06	1.95
1206.0 / 1104788	RORD001	141815	368.65	369	0.411		49277	1150.5	2.49	4124	16.85	1.38

NOTE: X = below detection limit

Genalysis Job number	Hole ID	Sample ID	Depth (m)		Au	Au (repeat analysis)	Al	As	Cs	K	Rb	Th
			From	To				(ppm)				
1206.0 / 1104788	RORD001	141816	369	370	0.017		69144	51.7	1.96	3262	11.03	1.95
1206.0 / 1104788	RORD001	141817	370	371	0.154		57592	740.5	3.63	6283	26.29	1.69
1206.0 / 1104788	RORD001	141818	371	372	0.011		71934	13.9	0.92	2743	7.43	1.95
1206.0 / 1104788	RORD001	141819	372	373	0.017		70817	36.3	0.93	2140	5.93	1.94
1206.0 / 1104788	RORD001	141820	373	374	0.016		70229	16.2	0.61	2724	6.57	2.09
1206.0 / 1104788	RORD001	141821	374	375	0.025		68148	14.7	0.94	2816	9.01	2.07
1206.0 / 1104788	RORD001	141822	375	376	0.041		65825	86.8	1.39	3098	11.63	1.91
1206.0 / 1104788	RORD001	141823	376	377	0.075		64203	102	2.32	4204	18.67	1.89
1206.0 / 1104788	RORD001	141824	377	378	0.015		69127	6.8	1.38	3396	12.49	2
1206.0 / 1104788	RORD001	141826	382	383	0.007		66406	20.1	1.2	4003	13.04	1.89
1206.0 / 1104788	RORD001	141827	387	388	0.016		67568	125.6	0.9	2501	8.34	1.92
1206.0 / 1104788	RORD001	141828	392	393	0.181		69920	289.5	0.79	2767	6.93	2.06
1206.0 / 1104788	RORD001	141829	397	398	0.133		50804	450.7	1.81	4054	17.16	1.46
1206.0 / 1104788	RORD001	141830	402	403	X		66820	6.6	0.99	3512	10.98	1.94
1206.0 / 1104788	RORD001	141831	407	408	X		67860	5.4	0.99	3349	11.4	1.96
1206.0 / 1104788	RORD001	141832	412	413	X		69319	3.8	0.85	3706	11.58	1.98
1206.0 / 1104788	RORD003A	141833	159.5	160.5	X		50416	3	2.16	1800	6	0.28
1206.0 / 1104788	RORD003A	141834	168	169	0.037		27391	1304.8	10.21	6654	31.94	0.17
1206.0 / 1104788	RORD003A	141835	169	170	0.036		26356	1357.8	7.39	4930	23.22	0.15
1206.0 / 1104788	RORD003A	141836	170	171	0.021		29996	805.3	6.86	4303	21.3	0.15
1206.0 / 1104788	RORD003A	141837	171	172	0.012		33839	466.1	2.3	798	4.05	0.18
1206.0 / 1104788	RORD003A	141838	172	173	0.022		36578	151.6	1.68	345	5.58	0.31
1206.0 / 1104788	RORD003A	141839	179.5	180.5	X		42901	5.4	2.64	941	3.81	0.24
1206.0 / 1104788	RORD003A	141840	189.5	190.5	X		52153	1.7	0.48	718	0.68	0.29
1206.0 / 1104788	RORD003A	141841	199.7	200.7	0.013		41980	38.5	3.37	676	4.22	0.26
1206.0 / 1104788	RORD003A	141842	200.7	201.7	0.012		37591	146.6	2.63	542	2.8	0.21
1206.0 / 1104788	RORD003A	141843	201.7	202.7	X		24018	26.6	3.58	917	5.55	0.12
1206.0 / 1104788	RORD003A	141844	202.7	203.7	0.01		26286	25.7	5.32	1653	11.34	0.14
1206.0 / 1104788	RORD003A	141845	203.7	204.5	0.009		28426	26.4	6.47	2413	16.01	0.16
1206.0 / 1104788	RORD003A	141846	209	210	0.027		34005	304.3	3.23	1146	6.65	0.21

NOTE: X = below detection limit

Genalysis Job number	Hole ID	Sample ID	Depth (m)		Au	Au (repeat analysis)	Al	As	Cs	K	Rb	Th
			From	To	(ppm)							
1206.0 / 1104788	RORD003A	141847	210	211.3	0.116		43250	327.5	5.85	3301	16.68	0.22
1206.0 / 1104788	RORD003A	141848	214.4	215.5	0.128		34318	803.8	8.16	4878	25.91	0.16
1206.0 / 1104788	RORD003A	141849	219.5	220.5	0.018		34256	119.2	2.84	1242	7.81	0.18
1206.0 / 1104788	RORD003A	141850	229.5	230.5	X		28994	5.2	1.95	269	1.6	0.17
1206.0 / 1104788	RORD003A	141851	234.5	235.5	X		30585	13.8	2.17	265	1.64	0.19
1206.0 / 1104788	RORD003A	141852	239.5	240.5	X		53679	19.3	0.84	1210	3.08	0.3
1206.0 / 1104788	RORD003A	141853	244.5	245.5	X		53282	6.4	0.41	955	1.18	0.3
1206.0 / 1104788	RORD003A	141854	249.5	250.5	0.226		46783	1153.6	1.33	1739	6.1	0.28
1206.0 / 1104788	RORD003A	141856	254.5	255.5	0.085		49330	283.1	0.45	2639	4.81	0.27
1206.0 / 1104788	RORD003A	141857	255.5	256.5	0.012		52819	126.8	0.76	3394	8.69	0.29
1206.0 / 1104788	RORD003A	141858	256.5	257.5	0.081		53246	336.8	0.78	2312	5.39	0.3
1206.0 / 1104788	RORD003A	141859	257.5	258.5	0.037		56705	115.5	0.49	2979	6.5	0.3
1206.0 / 1104788	RORD003A	141860	258.5	259.5	0.038		49755	172.1	0.79	3475	10.52	0.27
1206.0 / 1104788	RORD003A	141861	259.5	260.5	1		56228	1970.9	2.48	27133	103.1	1.99
1206.0 / 1104788	RORD003A	141862	260.5	261.5	0.977		25035	1393	1.06	13080	46.99	1
1206.0 / 1104788	RORD003A	141863	261.5	262.5	1.165		19223	768.4	1.08	7949	32.78	0.73
1206.0 / 1104788	RORD003A	141864	262.5	263.5	2.224		31979	1084.3	3.19	12409	53.09	1.26
1206.0 / 1104788	RORD003A	141865	263.5	264	0.152		44411	370.4	3.74	15091	60.03	1.26
1206.0 / 1104788	RORD003A	141866	264	264.5	0.317		15987	324.6	1.47	1118	5.86	0.76
1206.0 / 1104788	RORD003A	141867	264.5	265.4	0.015		57282	57.1	1.94	12428	48.04	1.62
1206.0 / 1104788	RORD003A	141868	265.4	266	0.014		56438	29.2	0.82	1725	9.05	1.58
1206.0 / 1104788	RORD003A	141869	266	267	0.008		71285	52.5	2.51	4407	20.37	2.08
1206.0 / 1104788	RORD003A	141870	267	268	0.006		66129	15	1.18	3073	10.38	1.93
1206.0 / 1104788	RORD003A	141871	268	269	X		68152	9	0.83	2551	7.11	1.99
1206.0 / 1104788	RORD003A	141872	269	270	0.005		73027	8.8	1.05	2602	7.47	2.16
1206.0 / 1104788	RORD003A	141873	270	271	0.007		53112	91.9	1.14	3617	12.14	1.48
1206.0 / 1104788	RORD003A	141874	271	272	0.406		59938	602.7	2.16	5415	21.51	1.78
1206.0 / 1104788	RORD003A	141876	272	273	0.009		68897	8.5	0.47	2778	7.08	1.92
1206.0 / 1104788	RORD003A	141877	273	274	0.018		68118	16.2	0.76	2507	6.85	1.96
1206.0 / 1104788	RORD003A	141878	274	275.2	X		62582	6.2	1.33	3576	12.86	1.79
1206.0 / 1104788	RORD003A	141879	275.2	276	0.092		68118	434.5	1.76	5481	20.7	1.97

NOTE: X = below detection limit

Genalysis Job number	Hole ID	Sample ID	Depth (m)		Au	Au (repeat analysis)	Al	As	Cs	K	Rb	Th
			From	To				(ppm)				
1206.0 / 1104788	RORD003A	141880	276	277	X		71917	9.1	0.49	2418	7.1	2.1
1206.0 / 1104788	RORD003A	141881	277	278	0.007		71188	5.5	0.31	2189	5.91	2.04
1206.0 / 1104788	RORD003A	141882	278	279	0.007		67665	16.5	0.42	2229	6.06	1.86
1206.0 / 1104788	RORD003A	141883	279	280	0.01		68421	43.4	0.52	2818	9.43	1.93
1206.0 / 1104788	RORD003A	141884	285	286	0.012		71581	2.2	0.75	3979	14.22	2.07
1206.0 / 1104788	RORD003A	141885	290	291	X		70651	5.5	0.5	2929	9.04	1.97
1206.0 / 1104788	RORD003A	141886	295	296	0.116		70202	387.3	2.59	5175	24.54	1.97
1206.0 / 1104788	RORD003A	141887	300	301	0.008		69679	10	0.39	2147	5.21	1.85
1206.0 / 1104788	RORD003A	141888	305	306	0.015		71149	13.1	0.5	3430	11.51	1.91
1206.0 / 1104788	RORD003A	141889	314	315	0.011		65643	14.3	0.68	2989	9.95	1.84
1206.0 / 1105727	RORD005	141890	151	152	0.008		56433	17.7	0.19	1757	4.16	0.47
1206.0 / 1105727	RORD005	141891	152	153	X		50439	133.3	0.39	2258	6.1	0.34
1206.0 / 1105727	RORD005	141892	153	153.8	0.49		48886	303.5	0.65	2764	9.52	0.39
1206.0 / 1105727	RORD005	141893	153.8	154.5	2	1.99	18691	2892	0.44	1724	6.76	0.93
1206.0 / 1105727	RORD005	141894	154.5	155.5	0.018		51572	35.9	0.42	822	1.4	0.3
1206.0 / 1105727	RORD005	141895	155.5	156.5	0.033		56025	59.9	0.23	933	1.09	0.32
1206.0 / 1105727	RORD005	141896	156.5	157.5	X		58305	15	0.35	1334	2.68	0.32
1206.0 / 1105727	RORD005	141897	157.5	158.5	0.053		58373	12	0.22	1087	1.16	0.33
1206.0 / 1105727	RORD005	141898	158.5	159.5	X		59584	7.1	0.17	866	0.88	0.31
1206.0 / 1105727	RORD005	141899	159.5	160.5	X		56638	9.6	0.19	798	1.05	0.3
1206.0 / 1105727	RORD005	141900	160.5	161.5	X		53915	10.8	0.17	951	1.18	0.3
1206.0 / 1105727	RORD005	141901	161.5	162.5	X		50811	23.1	0.2	1162	2.11	0.27
1206.0 / 1105727	RORD005	141902	162.5	163.5	0.03		54391	42.7	0.23	2382	6.4	0.31
1206.0 / 1105727	RORD005	141903	163.5	163.82	0.005		54052	22.8	0.33	2180	8.05	0.72
1206.0 / 1105727	RORD005	141904	163.82	164.5	0.158		31540	50.2	0.67	4785	21.65	1.91
1206.0 / 1105727	RORD005	141906	164.5	165.05	0.222		30157	104.5	0.98	11724	46.95	1.47
1206.0 / 1105727	RORD005	141907	165.05	165.65	0.5		11047	550.8	0.37	4236	18.24	0.5
1206.0 / 1105727	RORD005	141908	165.65	166.25	0.107		11386	163.9	0.28	1759	7.76	0.17
1206.0 / 1105727	RORD005	141909	166.25	167	0.058		52377	152.5	0.28	2286	6.85	0.3

NOTE: X = below detection limit

Genalysis Job number	Hole ID	Sample ID	Depth (m)		Au	Au (repeat analysis)	Al	As	Cs	K	Rb	Th
			From	To				(ppm)				
1206.0 / 1105727	RORD005	141910	167	168	0.015		59114	40.8	0.36	2800	8.69	0.32
1206.0 / 1105727	RORD005	141911	168	169	X		61278	32.5	0.35	2449	6.91	0.33
1206.0 / 1105727	RORD005	141912	169	170	0.009		55767	38.7	0.3	2029	5.05	0.31
1206.0 / 1105727	RORD005	141913	170	171	0.103		55922	107	0.34	1805	4.97	0.31
1206.0 / 1105727	RORD005	141914	171	172	0.431		54488	1527	0.47	2435	9.51	0.29
1206.0 / 1105727	RORD005	141915	172	173	1.841	1.78	57763	2310.4	0.5	3118	10.33	0.3
1206.0 / 1105727	RORD005	141916	173	174	0.038		55071	106.7	0.23	2098	5.52	0.29
1206.0 / 1105727	RORD005	141917	174	175	0.063		55327	51.9	0.41	2258	7.23	0.31
1206.0 / 1105727	RORD005	141918	175	176	0.007		56410	35.9	0.43	3069	9.03	0.3
1206.0 / 1105727	RORD005	141919	176	177	0.021		54309	45.2	0.57	3653	13.56	0.31
1206.0 / 1105727	RORD005	141920	177	178	X		45606	93.5	0.92	7793	34.26	0.25
1206.0 / 1105727	RORD005	141921	178	179	X		40433	157.3	1.16	3177	14.16	0.23
1206.0 / 1105727	RORD005	141922	179	180	0.008		44222	171.3	0.68	3535	14.81	0.22
1206.0 / 1105727	RORD005	141923	180	181	X		43946	201.1	1.09	4936	22.75	0.23
1206.0 / 1105727	RORD005	141924	181	182	0.075		46644	69.5	0.75	4112	19.36	0.34
1206.0 / 1105727	RORD005	141926	182	182.7	0.064		51371	59	0.75	3968	18.29	0.3
1206.0 / 1105727	RORD005	141927	182.7	183.7	1.233	1.28	24147	418.9	0.96	5517	27.47	0.97
1206.0 / 1105727	RORD005	141928	183.7	184.05	0.324		52108	343.6	2.78	5792	29.03	1.58
1206.0 / 1105727	RORD005	141929	184.05	184.6	0.025		55167	77	1.28	3042	14.18	1.61
1206.0 / 1105727	RORD005	141930	184.6	185.6	0.041		62547	22.7	0.89	7757	31.56	1.76
1206.0 / 1105727	RORD005	141931	185.6	186.6	0.005		63382	7.6	0.86	10060	35.5	1.73
1206.0 / 1105727	RORD005	141932	186.6	187.6	X		71483	18.8	0.4	5037	16.28	2.02
1206.0 / 1105727	RORD005	141933	187.6	188.6	0.018		70278	8.2	0.27	3403	10.55	2.03
1206.0 / 1105727	RORD005	141934	188.6	189.6	0.01		61244	10.6	0.29	2401	6.9	1.74
1206.0 / 1105727	RORD005	141935	189.6	190.6	0.019		70135	37.4	0.56	3649	11.55	1.98
1206.0 / 1105727	RORD005	141936	190.6	191.6	0.007		68251	39.9	0.6	3954	13.33	1.93
1206.0 / 1105727	RORD005	141937	195	196	0.1		67132	232.1	1.17	3677	12.55	1.91
1206.0 / 1105727	RORD005	141938	200	201	0.012		70361	13.6	0.41	3105	9.37	2.05
1206.0 / 1105727	RORD005	141939	205	206	0.014		66883	13.5	0.41	3243	9.46	1.86
1206.0 / 1105727	RORD005	141940	210	211	0.005		70490	7.9	0.45	4019	13.15	2.04
1206.0 / 1105727	RORD005	141941	214	215	X		69685	5.6	0.19	1690	4.03	1.95

NOTE: X = below detection limit

Genalysis Job number	Hole ID	Sample ID	Depth (m)		Au	Au (repeat analysis)	Al	As	Cs	K	Rb	Th
			From	To	(ppm)							
1206.0 / 1105727	RORD006	141942	279	280	X		54691	9.6	0.49	698	0.82	0.33
1206.0 / 1105727	RORD006	141943	284	285	X		36191	0.8	1.24	241	0.99	0.21
1206.0 / 1105727	RORD006	141944	289	290	X		36354	1	1.41	415	2.06	0.19
1206.0 / 1105727	RORD006	141945	294	295	X		24584	20.3	2.03	447	3.14	0.13
1206.0 / 1105727	RORD006	141946	299	300	X		32488	3	1.57	183	1.13	0.17
1206.0 / 1105727	RORD006	141947	304	305	X		54388	0.6	0.28	1146	1.48	0.3
1206.0 / 1105727	RORD006	141948	309	310	X		38253	0.8	0.91	412	1.86	0.19
1206.0 / 1105727	RORD006	141949	314	315	X		43649	62.3	0.63	961	2.25	0.24
1206.0 / 1105727	RORD006	141950	319	320	1.64		54768	472.8	0.45	2071	5.68	0.3
1206.0 / 1105727	RORD006	141951	324	325	0.01		52434	3.3	0.14	1093	1.24	0.28
1206.0 / 1105727	RORD006	141952	328	329	0.024		50543	9.8	0.52	1844	5.1	0.32
1206.0 / 1105727	RORD006	141953	329	330	X		55226	3.3	0.57	1935	4.61	0.31
1206.0 / 1105727	RORD006	141954	336	337	0.015		46835	54.4	0.36	1424	3.08	0.34
1206.0 / 1105727	RORD006	141956	337	338	0.011		56263	18.1	0.32	1904	4.06	0.3
1206.0 / 1105727	RORD006	141957	338	339	0.013		54618	23.3	0.82	3045	9.95	0.3
1206.0 / 1105727	RORD006	141958	339	340	X		56081	14.1	0.59	2200	5.56	0.32
1206.0 / 1105727	RORD006	141959	340	341	0.01		55189	16.8	0.37	1663	3.68	0.29
1206.0 / 1105727	RORD006	141960	341	342	X		54377	8.2	0.63	1586	4.46	0.29
1206.0 / 1105727	RORD006	141961	342	343	X		51025	39.1	0.79	1312	3.89	0.27
1206.0 / 1105727	RORD006	141962	343	344	X		48152	16.7	0.67	1325	3.68	0.27
1206.0 / 1105727	RORD006	141963	344	345	0.005		54398	29.6	0.52	1813	4.41	0.3
1206.0 / 1105727	RORD006	141964	345	346.12	0.005		50686	33.2	0.31	2010	5.29	0.29
1206.0 / 1105727	RORD006	141965	346.12	346.6	0.005		30418	19.2	0.51	1559	6.13	0.48
1206.0 / 1105727	RORD006	141966	346.6	347	X		50037	41	0.53	2397	7.83	0.87
1206.0 / 1105727	RORD006	141967	347	348	0.005		55512	20.8	0.26	1667	3.43	0.34
1206.0 / 1105727	RORD006	141968	348	349	0.123		55874	55.4	1.51	2567	10.7	0.3
1206.0 / 1105727	RORD006	141969	349	350	X		53044	31.2	1.95	1711	7.35	0.3
1206.0 / 1105727	RORD006	141970	350	351	0.005		52087	71	0.57	2064	5.53	0.28
1206.0 / 1105727	RORD006	141971	351	352	0.005		46398	177.9	0.9	3035	11.03	0.24
1206.0 / 1105727	RORD006	141972	352	353	0.677		45768	65.3	0.7	4791	18.47	0.26

NOTE: X = below detection limit

Genalysis Job number	Hole ID	Sample ID	Depth (m)		Au	Au (repeat analysis)	Al	As	Cs	K	Rb	Th
			From	To	(ppm)							
1206.0 / 1105727	RORD006	141973	353	353.6	0.101		49915	66.9	1.07	7445	33.19	0.28
1206.0 / 1105727	RORD006	141974	353.6	354	0.296		44206	28.3	0.53	2373	8.8	0.37
1206.0 / 1105727	RORD006	141976	354	355	0.056		45941	41.1	0.49	3480	12.2	0.29
1206.0 / 1105727	RORD006	141977	355	356	0.061		53997	103.5	0.97	5713	23.14	0.32
1206.0 / 1105727	RORD006	141978	356	357	0.157		46364	144	1.05	5178	21.99	0.24
1206.0 / 1105727	RORD006	141979	357	357.9	0.064		54516	116	1.15	6506	27.47	0.3
1206.0 / 1105727	RORD006	141980	357.9	358.62	1.216		32164	19.2	0.93	2971	13.02	0.47
1206.0 / 1105727	RORD006	141981	358.62	359	3.777	3.39	47011	20.4	0.72	1935	5.72	0.31
1206.0 / 1105727	RORD006	141982	359	360.2	0.908		54038	23.4	0.49	1658	3.63	0.28
1206.0 / 1105727	RORD006	141983	360.2	360.6	0.226		32431	12.4	0.46	2050	7.78	0.76
1206.0 / 1105727	RORD006	141984	360.6	361	0.019		54303	49	0.42	2406	7.2	0.29
1206.0 / 1105727	RORD006	141985	361	362	0.249		54665	32.5	0.3	2047	4.5	0.31
1206.0 / 1105727	RORD006	141986	362	363	0.078		52321	314.2	0.55	2598	6.99	0.28
1206.0 / 1105727	RORD006	141987	363	364	0.289		49761	21.3	0.41	2573	6	0.26
1206.0 / 1105727	RORD006	141988	364	365	9.853	9.41	52997	17.5	0.36	2027	3.96	0.43
1206.0 / 1105727	RORD006	141989	365	366	1.193		52673	25.5	0.42	2178	4.42	0.3
1206.0 / 1105727	RORD006	141990	366	367	2.224		54907	16.3	0.39	2307	5.51	0.3
1206.0 / 1105727	RORD006	141991	367	368	0.036		55952	20.1	0.4	2548	6.52	0.33
1206.0 / 1105727	RORD006	141992	368	369	3.108	3.45	57405	16	0.58	2249	6.07	0.32
1206.0 / 1105727	RORD006	141993	369	370	0.018		53325	18.4	0.84	2646	8.26	0.28
1206.0 / 1105727	RORD006	141994	370	371	0.193		41852	262.1	0.86	4630	18.51	0.22
1206.0 / 1105727	RORD006	141995	371	372	0.025		38297	250	0.38	1448	4.46	0.21
1206.0 / 1105727	RORD006	141996	372	373	0.014		40226	72.1	0.43	473	0.95	0.21
1206.0 / 1105727	RORD006	141997	373	374	0.768		42866	231.4	1.09	4977	20.08	0.22
1206.0 / 1105727	RORD006	141998	374	375	0.043		47336	166	1.02	7684	29.83	0.26
1206.0 / 1105727	RORD006	141999	375	376	0.039		52143	93.8	0.8	7522	31.29	0.31
1206.0 / 1105727	RORD006	142000	376	376.5	0.054		53378	25.5	0.82	8381	37.28	0.3
1206.0 / 1105727	RORD006	142001	376.5	377.2	0.482		27112	545.3	0.63	5091	21.76	0.65
1206.0 / 1105727	RORD006	142002	377.2	378	0.091		75720	88	2.02	17902	73.87	2.17
1206.0 / 1105727	RORD006	142003	378	379	0.013		65468	20.2	1.07	5748	22.43	1.83
1206.0 / 1105727	RORD006	142004	379	380	0.011		49134	31.1	0.63	8037	24.25	1.4

NOTE: X = below detection limit

Genalysis Job number	Hole ID	Sample ID	Depth (m)		Au	Au (repeat analysis)	Al	As	Cs	K	Rb	Th
			From	To				(ppm)				
1206.0 / 1105727	RORD006	142006	380	381	0.031		61209	14.5	0.91	8731	34.55	1.8
1206.0 / 1105727	RORD006	142007	381	382	0.041		65472	5.7	0.95	7195	31	1.97
1206.0 / 1105727	RORD006	142008	382	383	0.038		67464	9.4	0.81	6126	23.41	1.93
1206.0 / 1105727	RORD006	142009	383	384	0.018		64387	4.3	0.98	9160	40.06	1.89
1206.0 / 1105727	RORD006	142010	384	385	0.013		64097	2.6	0.97	5919	23.25	1.84
1206.0 / 1105727	RORD006	142011	385	386	0.011		66065	3.1	0.55	5250	18.5	1.91
1206.0 / 1105727	RORD006	142012	386	387	X		59158	3.3	0.62	5706	21.16	1.67
1206.0 / 1105727	RORD006	142013	387	388	X		70446	4.2	0.51	4378	15.36	2.01
1206.0 / 1105727	RORD006	142014	388	389	0.052		70294	3.7	0.44	5666	18.02	2
1206.0 / 1105727	RORD006	142015	389	390	0.005		60162	3	0.33	2960	5.96	1.67
1206.0 / 1105727	RORD006	142016	390	391	0.019		67418	3.5	0.4	3820	10.4	1.94
1206.0 / 1105727	RORD006	142017	391	392	0.025		68576	3.3	0.43	3388	9.34	1.92
1206.0 / 1105727	RORD006	142018	392	393	X		68348	3.5	0.32	2967	8	1.99
1206.0 / 1105727	RORD006	142019	393	394	X		68355	4.9	0.34	3490	10.22	1.97
1206.0 / 1105727	RORD006	142020	394	395	0.005		68843	3.9	0.4	2877	7.21	1.97
1206.0 / 1105727	RORD006	142021	395	396	0.015		68158	4.4	0.42	3052	8.56	2.03
1206.0 / 1105727	RORD006	142022	396	397	0.015		64031	23.7	1.3	3795	16.45	1.88
1206.0 / 1105727	RORD006	142023	397	398	0.029		69381	55.9	5.39	8294	47.05	1.99
1206.0 / 1105727	RORD006	142024	398	399	0.122		46936	195	5.11	10333	52.83	1.3
1206.0 / 1105727	RORD006	142026	399	400.08	0.657		57467	256	4.63	12053	61.91	1.54
1206.0 / 1105727	RORD006	142027	400.08	401	0.325		60618	79.1	6.22	9629	53.15	1.96
1206.0 / 1105727	RORD006	142028	401	402	0.074		57348	172.8	2.45	5264	25.4	1.68
1206.0 / 1105727	RORD006	142029	402	403	0.025		65895	46.6	1.06	4581	18.7	1.89
1206.0 / 1105727	RORD006	142030	403	404	0.01		71749	14.2	0.6	3403	11.47	1.96
1206.0 / 1105727	RORD006	142031	404	405	0.023		64811	6.7	0.5	2767	8.35	1.82
1206.0 / 1105727	RORD006	142032	405	406	X		68356	3.7	0.47	2385	5.94	2.09
1206.0 / 1105727	RORD006	142033	406	407	X		67177	3.8	0.4	2105	4.93	1.94
1206.0 / 1105727	RORD006	142034	407	408	0.015		66926	4.7	0.34	2640	7.4	1.91
1206.0 / 1105727	RORD006	142035	408	409	0.016		69244	7.6	0.36	2514	6.76	1.99
1206.0 / 1105727	RORD006	142036	409	410	0.014		68740	7.8	0.52	2893	8.64	1.98
1206.0 / 1105727	RORD006	142037	410	411	0.029		66796	8.6	0.32	2049	4.86	1.97

NOTE: X = below detection limit

Genalysis Job number	*Hole ID*	*Sample ID*	*Depth (m)*		*Au*	*Au (repeat analysis)*	*Al*	*As*	*Cs*	*K*	*Rb*	*Th*
			From	*To*				*(ppm)*				
1206.0 / 1105727	RORD006	142038	411	412	0.625		70216	746.1	1.16	3081	9.94	2.08
1206.0 / 1105727	RORD006	142039	412	413	1.516	1.6	49399	1243	1.83	4142	19.17	1.51
1206.0 / 1105727	RORD006	142040	413	414	0.083		67221	61.6	1.45	3219	11.6	2.04
1206.0 / 1105727	RORD006	142041	414	415	0.079		62325	84	1.11	3764	13.8	1.81
1206.0 / 1105727	RORD006	142042	422	423	0.026		64331	15	0.75	4761	15.77	1.84
1206.0 / 1105727	RORD006	142043	423	424	0.013		61848	45.9	0.74	2889	8.53	1.75
1206.0 / 1105727	RORD006	142044	428	429	0.089		64566	19.6	1.06	11048	42.06	1.82
1206.0 / 1105727	RORD006	142045	434	435	0.012		68375	5.8	0.59	2658	6.78	2
1206.0 / 1105727	RORD006	142046	440	441	X		70175	2	0.78	3006	8.78	1.95
1206.0 / 1105727	RORD006	142047	443	444	X		69150	3.6	0.6	1951	5.32	1.96
1206.0 / 1105727	ROD118	142048	280	281	X		55600	26.9	0.22	1344	1.58	0.34
1206.0 / 1105727	ROD118	142049	281	282	0.005		56573	26.8	0.33	1216	1.41	0.34
1206.0 / 1105727	ROD118	142050	282	282.37	0.074		50628	39.8	0.37	1404	1.94	0.28
1206.0 / 1105727	ROD118	142051	282.37	283	X		50190	59	0.33	1149	1.78	0.31
1206.0 / 1105727	ROD118	142052	283	283.38	X		51087	120.7	0.38	2343	4.93	0.3
1206.0 / 1105727	ROD118	142053	283.38	284	7.318	7.42	42150	2612.4	2.98	11913	43.15	1.37
1206.0 / 1105727	ROD118	142054	284	284.63	0.942		25108	2308.8	1.54	6973	28.45	1.14
1206.0 / 1105727	ROD118	142056	284.63	286	0.094		51946	352.6	1.61	3550	12.97	0.31

NOTE: X = below detection limit

The Yilgarn Gold Exploration Targeting Atlas, a collaborative project between the Geological Survey of Western Australia, the Centre for Exploration Targeting and several industry groups, is a three-part project of which this is the third part. In Part 3 (deposit-scale targeting), 12 deposit-scale targeting criteria for gold in the Yilgarn Craton are described and assessed.
In contrast to Parts 1 and 2, Part 3 relies mostly on qualitative studies and published results because the deposit-scale datasets required to generate quantitative spatial analyses were not available to the project. Targeting criteria assessed include eight related to structural controls on ore bodies and high-grade ore shoots within them, three related to geochemical dispersion around ore, and one based on the mineralogical aspects of hydrothermal alteration associated with gold mineralization.

For the Yilgarn Craton, this study documents strong structural controls on the distribution of gold. These controls include well-established criteria, such as fault intersections, fault bends and jogs, and intersections of faults with rheologically favourable geological units. The rheological architecture of the deposit and its environs is of paramount importance because it controls the escape path of over-pressured fluids at or below the brittle–ductile transition. This important aspect can 'over-ride' the local stress conditions leading to formation of ore shoots at locations not predicted by conventional stress analysis. Geochemical dispersion around gold lodes is generally very restricted, limiting the effectiveness of this approach to mine-scale exploration. However, the relatively recent development of the rare alkali index shows potential for tracking the path of the gold ore fluid beyond the limits established by conventional pathfinder element, alteration index and stable isotope halos. Spectral mineralogical analysis at the mine scale can be applied to resolve different hydrothermal events and to vector towards gold ore, in a similar manner to that at the district-scale (see Part 2 of this Atlas).

Further details of geological products and maps produced by the Geological Survey of Western Australia are available from:

Information Centre
Department of Mines and Petroleum
100 Plain Street
EAST PERTH WA 6004
Phone: (08) 9222 3459 Fax: (08) 9222 3444

www.dmp.wa.gov.au/GSWApublications